2005

Evaluation of the transverse load capacity of block stoppings for mine ventilation control

Thomas M. Barczak
West Virginia University

EVALUATION OF THE TRANSVERSE LOAD CAPACITY OF BLOCK STOPPINGS FOR MINE VENTILATION CONTROL

Thomas M. Barczak

Dissertation submitted to the
College of Engineering and Mineral Resources
at West Virginia University
in partial fulfillment of the requirements of

Doctor of Philosophy
in
Mining Engineering

Syd S. Peng, Ph.D., Chair
Keith A. Heasley, Ph.D.
Yi Luo, Ph.D.
Stephen C. Tadolini, Ph.D.
Yunqing Zhang, Ph.D.

Department of Mining Engineering

Morgantown, West Virginia
2005

Keywords: Stoppings, Transverse Load, Ventilation

Evaluation of the Transverse Load Capacity of Block Stoppings for Mine Ventilation Control

Thomas M. Barczak

ABSTRACT

The transverse loading requirement for stoppings as specified in the current Code of Federal Regulations is 39 psf. This measure is based on physical testing of a freestanding wall in accordance with ASTM E 72 specifications, where the dominant parameter is the tensile strength of the sealant. A new protocol based on arching has been developed to determine the true transverse load capacity of stoppings. Arching is achieved by the restraint of the stopping against the mine roof and floor, whereby compressive forces are developed within the wall. A laboratory procedure using the NIOSH Mine Roof Simulator (MRS) to simulate rigid-arching of stoppings was developed and verified through full-scale in-mine tests. Using this protocol, a systematic study of the design parameters that affect arching capability in block stoppings was conducted. The study included a theoretical assessment of arching and development of design formulations that can accurately define the transverse load capacity of various stopping constructions under various loading conditions. This approach should lead to a safer mine environment by matching the transverse load capabilities of the stopping design to the requirements in the mine to ensure proper ventilation control is maintained.

DEDICATION

I dedicate this dissertation to my God Father, John Waddella, who realized the value of an education and encouraged me during my high school years to go on to college. He was and always will be my “best buddy”.

ACKNOWLEDGEMENTS

The author wishes to thank those who have contributed to the preparation and completion of this dissertation. A debt of gratitude is owed to Dr. Syd S. Peng for encouraging me to continue my education and guidance in my studies at West Virginia University. Special appreciation is also given to the members of my advisory and examination committee: Dr. Keith Heasley, Dr. Yi Luo, Dr. Stephen Tadolini, and Dr. Yunqing Zhang for their guidance and supervision.

The author also wishes to extend his deepest gratitude to Mr. David F. Gearhart and Mr. Timothy J. Batchler. Dave has been a colleague for the past 20 years and we have worked together on numerous projects during that time. Dave has been instrumental in conducting tests in both the Mine Roof Simulator and Experimental Coal Mine in support of this dissertation. I also thank Dave for imparting his overall experience in testing of large-scale structures and insights into the procedures developed for this study. Tim also contributed to this effort by operating the Mine Roof Simulator and processing raw data for many of the experiments that were done in support of this dissertation. I would also like to acknowledge Lisa Burke, a colleague at NIOSH who recently completed her Masters Thesis at Virginia Tech on numerical modeling of stopping walls for axial loading induced by roof-to-floor closure of the mine opening. Lisa and I shared many discussions regarding the mechanics of the loading behavior of a stopping wall, which helped me tremendously in pursuing my goals in this dissertation.

I must also express my gratitude to Dr. Gerald L. Finfinger, an old friend and long time colleague, who after twenty years of prodding finally convinced me to do this.

I would also like to thank my fellow students, who accepted me as one of them even though I was nearly 30 years older than most of them. I must also give my sincerest thanks to Karen Centofanti, who was a tremendous help to this “non traditional” student, who was lost most of the time in knowing where to go, who to see, and what to do in the administrative requirements of my schooling.

Finally, I express my deepest appreciation to my family, my wife Peggy and daughters Sarah and Nora, for putting up with me while I was studying at home in the evenings and on weekends and for their overall support in allowing me to achieve this goal at their expense.

TABLE OF CONTENTS

Page

Page

Page

Page

LIST OF FIGURES

Page

Page

LIST OF TABLES

ABBREVIATIONS OF UNITS

psf – pounds per square foot

psi – pounds per square inch

lbs – pounds

kips – measure of force equating to 1,000 pounds

in – inch

ft – feet

mils – thousandths of an inch

pct – percent

sq ft – square feet

cu ft – cubic feet

in^2 – square inches

ft^2 – square feet

water gage, in – inches of water gage where 1 psi equals 27.5 inches of water gage

CHAPTER 1: INTRODUCTION

An effective ventilation system requires a ventilation plan that is not only sound in design, but also well implemented during both mine development and subsequent production stages. Ventilation stoppings control ventilation throughout an underground mine and are an integral part of the ventilation system. Operating longwalls in the United States (U.S.) alone require an estimated 21,600 new stoppings each year, and mines using room-and-pillar mining methods will require another 66,000 stoppings (Tien, 1996). With an average cost of $600 - $800 per stopping, total costs could easily exceed $90 million per year for the coal industry (Tien, 1996).

Stoppings are designed primarily to withstand air pressure differentials generated by the mine fan that exert transverse loading against the high-pressure side or face of the stopping. These pressures, typically measured in inches of water gage, are generally less than 7 inches of water in the working sections of the mine, equating to approximately 0.25 psi. The pressure increases as the proximity to the mine fan increases. Near the mouth of a bleeder fan, the pressure can exceed 1 psi, which exerts considerable force against the stopping. Air blasts from roof falls can generate localized areas of higher pressure that can destroy stoppings. Seals, with a minimum transverse load capacity of 20 psi, are designed to contain explosions, but stoppings also play a role in maintaining ventilation during an explosion. Australia, for example, requires a 5 psi transverse load capacity for permanent stoppings used in main roadways and near sealed areas (Gillies et al., 2001). This is done, in part, to prevent widespread damage to the ventilation system in the event that an explosion does occur.

Unlike seals, which are required to pass full-scale testing to ensure their transverse load capacity, there are no full-scale tests required for stoppings to determine their load capacity. The current Code of Federal Regulations (CFR) requirement is to test 4x8-ft sections of freestanding walls (CFR Part 75.333 Ventilation Controls, 1996). This test inadequately determines the transverse load capacity of stopping constructions since in the mine the walls are restrained by the mine roof and floor, and pillar ribs. This restraint allows for significantly greater transverse loading capability by taking advantage of the compressive forces that are generated as the wall arches between the mine roof and floor. As a result, the true transverse load capacities of mine ventilation stoppings are not known.

Recently, a new generation of lightweight blocks has been developed for mine ventilation stopping constructions. While stoppings utilizing these blocks have all passed the current CFR criteria, it is believed that their true transverse load capacity varies considerably. This is because the material strength of the block types vary by as much of an order of magnitude, and the material strength of the blocks correlates to the arching capability of the restrained wall in the mine during transverse loading. Without such knowledge, the design of mine ventilation systems using these lighter-weight, but lower-capacity, alternative constructions can be misleading, potentially exposing the mine to inadequate ventilation control under some circumstances.

The objective of this dissertation is to develop a new protocol to examine the transverse load capacity of block stopping constructions and use this protocol to evaluate transverse load capacities of various stopping constructions under arching conditions. Using the unique biaxial loading capabilities of the National Institute for Occupational Safety and Health's (NIOSH) Mine Roof Simulator (MRS), arching conditions for stoppings are simulated in the laboratory, using a single or multiple column of block to predict the transverse load capacity of an entire stopping. Verification of the procedure has been done through full-scale testing of stoppings in a pressure chamber in the NIOSH Experimental Coal Mine and in the underground Longwall Gallery at the NIOSH Lake Lynn facility. A complete systematic study of the various design parameters that affect the capability of a stopping to develop transverse loading under arching conditions was conducted. From this study, predictive models were developed and compared against laboratory testing results. The outcome of the dissertation is a complete set of design formulations for eight different block material constructions and generic design formulations that provide transverse load capacity approximations for standard concrete, cellular concrete, and low strength concrete block materials.

CHAPTER 2: REVIEW OF LITERATURE

Masonry structures have been utilized dating back to building of pyramids and other structures 10,000 years ago. Modern masonry type structures using cementitious materials date back over a 100 years. As a result of this long history, considerable research has been

conducted on masonry structures. Masonry as a general term involves clay brick or concrete block structures where the unit blocks are mortared together at the joints to form a more continuous structure. Most mine ventilation stoppings are walls constructed from concrete blocks and therefore fit this classification, except that stoppings in recent times are dry-stacked as opposed to having mortared joints. In this regard, the research to support this dissertation is considered an extension of what has previously been done in this general area.

A comprehensive assessment of masonry design is found in a book authored by Drysdale, et al. (1994) entitled "Masonry Structures: Behavior and Design". Transverse loading due to wind pressure has been analyzed for walls spanning vertically between lateral supports along the top and bottom edges of the wall face. In two dimensions, this condition equates to a simply supported beam. The flexural strength of such walls is determined by the tensile strength of the mortared joints, generally at the mid span of the wall. The current U.S. CFR requirements for transverse loading of stoppings (CFR Part 75.333 Ventilation Controls, 1996) are an extension of this flexural analysis, except the CFR assumes dry-stacked block construction for mine ventilation stoppings, which therefore have no tensile strength. The CFR requires testing of freestanding walls with sealant applied to the low-pressure face of the wall to provide the tensile strength necessary to resist the moment induced by the transverse pressure.

Drysdale also addresses the impact of axial loading on the wall. For a dry-stacked wall, axial loading can significantly increase the transverse load capacity by resisting the bending moment induced by the transverse load. In this sense, the axial load can take the place of the lack of tensile strength in these dry-stacked configurations. This is why ground pressures acting on a stopping wall will greatly increase their transverse load capacity. Drysdale also describes a unity equation for combined axial and transverse loading of walls. The unity equation 2.1 is present in some masonry codes and requires that the combined compressive stresses from axial loading and bending must be limited to the material strength to achieve proper design under these conditions.

$$\frac{f_a}{F_a} + \frac{f_b}{F_b} = 1 \qquad \textbf{(2.1)}$$

Where f_a, f_b = compressive stresses due to applied axial load and bending, respectively, and

F_a, F_b = allowable axial and bending compressive stresses, respectively.

The loading mechanism being addressed in this dissertation involves arching of the wall structure. Drysdale also devotes a section of the book to the arching of walls. Generally, arching can be described as bridging between two rigid abutments as opposed to unrestrained end conditions. Studies into the arching behavior of masonry date back to 1951. The Armour Research Foundation, in conjunction with work sponsored by the U.S. Air Force and technically monitored by the Special Studies Office of the Installation Division, Air Material Command, first reported on an investigation of the arching theory. At this time, arching was a radical departure from conventional beam deflection theory that was typically used to evaluate the resistance of masonry walls to wind-generated or some other form of lateral loading.

McDowell has reported on this work in a paper published in the Proceedings of the American Society for Civil Engineers (McDowell et al., 1956). This was the first comprehensive paper published in a trade journal on this subject. McDowell showed that arching can be used to explain the significantly higher lateral loads that brick beams are capable of withstanding than conventional bending analysis would allow. In conventional bending analysis, beams strengths relative to lateral loading are controlled by the tensile properties of the material. This works well for steel beams since steel has a high tensile strength. Conversely, the tensile strength of concrete is generally about one tenth of its compressive strength, so masonry structures cannot depend solely on the tensile strength of the construction material to resist bending or provide for large lateral loading of wall structures.

McDowell proposed that a three-hinge arch is formed and that the resistance of the wall to lateral loading is due entirely to the tendency of the masonry to crush at the mid span and end supports due to the arching action. The masonry material is assumed to be unable to withstand tensile stress. McDowell describes the transverse loading of a wall as follows. Immediately upon loading, cracks develop on the tension side at the ends and center of the span. Initially, these cracks extend to the centerline of the beam (wall). During subsequent motion, it is assumed that each half of the wall remains rigid and rotates about an end and

where the two half walls meet at the center of the wall. The resistance to this motion comes about through a force couple set up at the ends and center due to crushing of the masonry at these positions. The rotation continues until the resisting couple vanishes (i.e., the material fails) or the load is removed.

McDowell also reported on a series of tests conducted at the Massachusetts Institute of Technology where 17 brick beams were tested under fixed-end conditions (Massachusetts Institute of Technology, 1954). These tests were consistent with the arching theory. The ultimate lateral strength of the beams was shown to correlate to the compressive strength of the material. The transverse load capacity was six times greater than what a simply supported beam analysis predicts.

Anderson (1984) examined the theory of arching in more detail by comparing the behavior of masonry walls during the initial loading prior to cracking of the wall and post-cracking behavior of the wall. He concluded that the load required to cause cracking of a wall with rigid abutments can be three times greater than a wall without arching restraint. He also concluded that the ultimate (post-cracking) transverse load capacity of a wall with abutments was three to nine times more than the pre-cracking load. Anderson showed the significance of the stiffness of the abutments in a theoretical analysis of arching and concluded that reducing the stiffness of the abutments will allow greater wall deflections to occur; and a theoretical limit of stability exists where the deflection is too large to generate an arching thrust. Anderson developed an equation relating the arching thrust to the transverse load. This relationship is used in this dissertation with modified coefficients to account for the physical characteristics of mine ventilation stoppings.

$$q_{lat} = \frac{f_k}{\gamma_m} \times \left(\frac{t}{L} \right)^2 \qquad \textbf{(2.2)}$$

Where q_{lat} = design lateral strength per unit area of wall, psi,

f_k = characteristic compressive strength of the masonry, psi,

γ_m = material safety factor,

t = wall thickness, in, and

L = span of the wall, in.

Through these and related efforts, arching has been recognized as a valid loading mechanism and design consideration for walls bridging rigid abutments. The British Codes of Practice (British Standards Institution, 1978) first recognized arching as a design mechanism in 1978. Curiously, arching is not recognized in the U.S. Masonry Designers Guide (Masonry Designer's Guide: Based on Building Code Requirements for Masonry Structures (ACI 530-92/ASCE, 5-92/TMS 402-92) and Specifications for Masonry Structures (ACI 530.1-92/ASCE 6-93/TMS 602-92)). The design formula specified for arching in the British Codes of Practice is of the same form as that developed by Anderson (equation 2.2). Close contact between the wall and the end abutments must be maintained for these criteria to be applicable in the British code. For vertical spanning walls, such as a wall spanning between a floor and roof, the design code requires that the dead weight vertical load be sufficient to sustain the arching. This work forms the basis for the rigid-arching assessment of stopping walls pursued in this dissertation.

The U.S. Bureau of Mines also conducted research on stopping behavior dating back to the 1960's (Kawenski and Mitchell, 1966). The emphasis of this work was primarily on the leakage of stoppings as a result of structural damage from either transverse loading or by ground movements. Fundamental construction techniques were examined and although full-scale tests of transverse loading were conducted, a study into the loading mechanics was not done during this period.

Recently, the concept of arching has also been applied to seal behavior (Sapko, et al., 2003). Tests conducted on seals in a hydrostatic chamber indicated that arching is occurring across the width of the seal, in this case the restraint provided by the pillar ribs. Initial tests showed good agreement of the ultimate transverse loading pressure of the seal to the arching mechanics described in equation 2.2. Research continues in this area to develop scaling factors for various materials and seal thicknesses.

CHAPTER 3: CURRENT CFR CRITERIA FOR STOPPINGS

Part 75.333 Ventilation Controls of the CFR requires that permanent ventilation control structures and mine stoppings for underground coal mines be constructed in a traditionally accepted method. Materials that have been tested and shown to have greater or equal strength than traditionally accepted in-mine control structures must be used. While this is somewhat vague, the statute goes on to specify that alternative stopping technologies be tested in accordance with ASTM E 72-80, "Standard Methods of Conducting Strength Tests of Panels for Building Construction", Section 12 – Transverse Loading – Specimen Vertical (ASTM Designation E 72-80, 1981).

3.1 ASTM E 72 TEST SPECIFICATIONS

The procedure requires testing of a nominal 4-ft-wide section of wall of a height equal to the mining height where the stopping will be used. Hence, for an 8-ft mining height, a 4x8-ft section of wall would be tested. The wall is to be constructed in the manner it will be used in the mine, including the application of sealant when specified. The test apparatus is shown in the diagram illustrated in figure 3-1. Figure 3-2 shows a wall section being placed into the reaction frame for ASTM E 72 testing at a commercial laboratory (Professional Services Industries) in Pittsburgh, PA. As seen from these figures, the freestanding wall is tested in a vertical orientation. The wall is placed on a steel channel which rests on a cylindrical roller (figure 3-3a) to *prevent restrained end conditions*. The axis of the roller is parallel to the face of the wall, allowing rotation to occur without restraint, as the wall is deformed from the application of transverse pressure. Two reaction rollers and contact plates positioned at the top and bottom of the wall allow the wall to deflect under the application of transverse pressure from the opposite face (figure 3-3b). Again, rollers are utilized *to prevent longitudinal restraint* as the wall deflects. Transverse pressure is applied across the width of the wall through a steel contact plate at quarter-height points of the wall. Rollers in the form of a steel pipe are again used to transfer load from a central I-beam through the contact plates, again to *prevent any rotational restraint* from occurring. As the load is applied, it is required that the load be recorded as a function of the displacement at the mid-span of the wall height. The maximum load normalized to the square foot area of the wall is then

defined as the transverse pressure capacity for the wall. It is also required that three separate walls be tested. The average transverse pressure capacity from these three tests must exceed 39 psf to comply with the CFR statute.

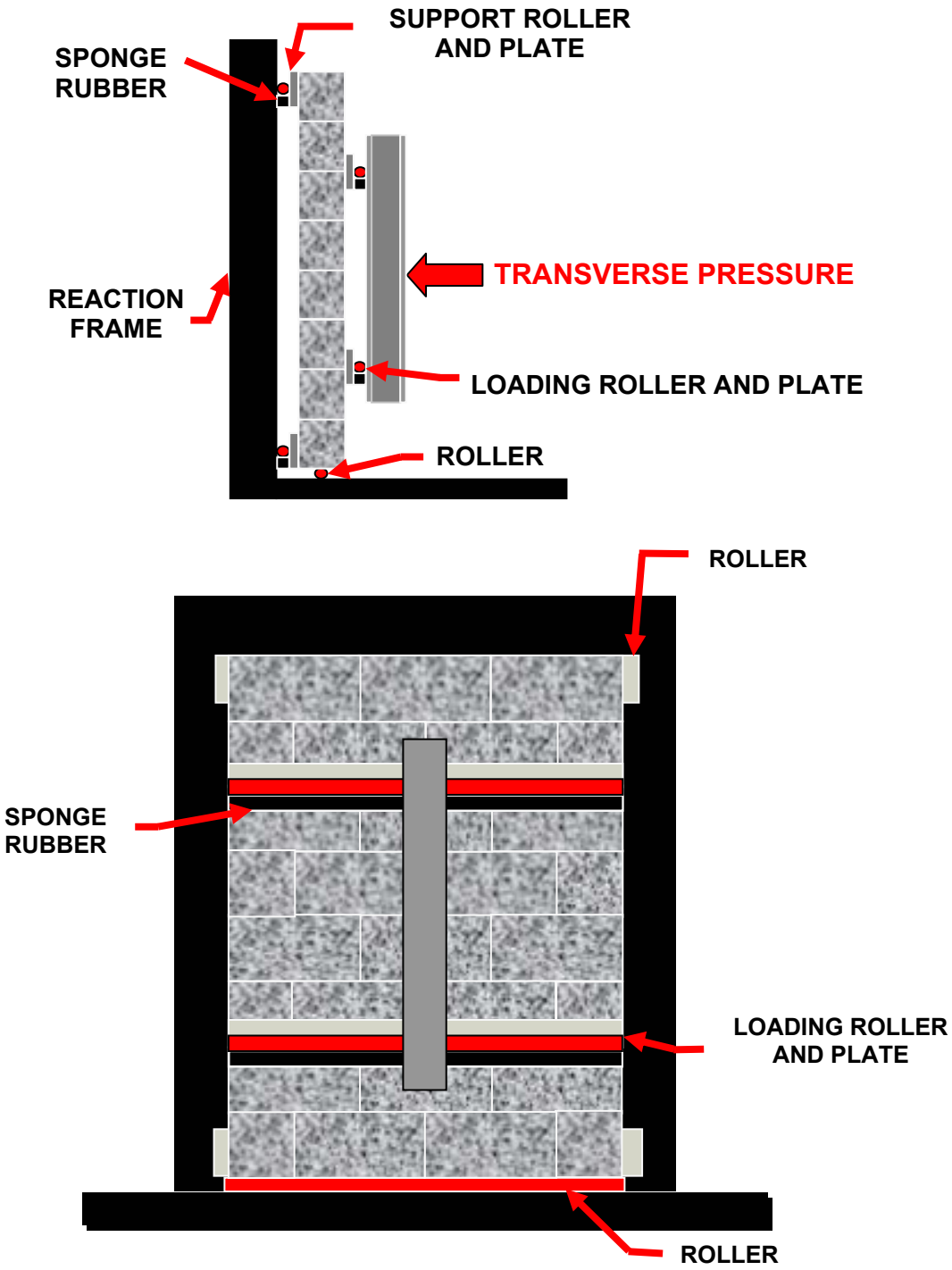

Figure 3-1. Diagram of test apparatus for transverse pressure testing of stoppings in accordance with ASTM E 72 specifications.

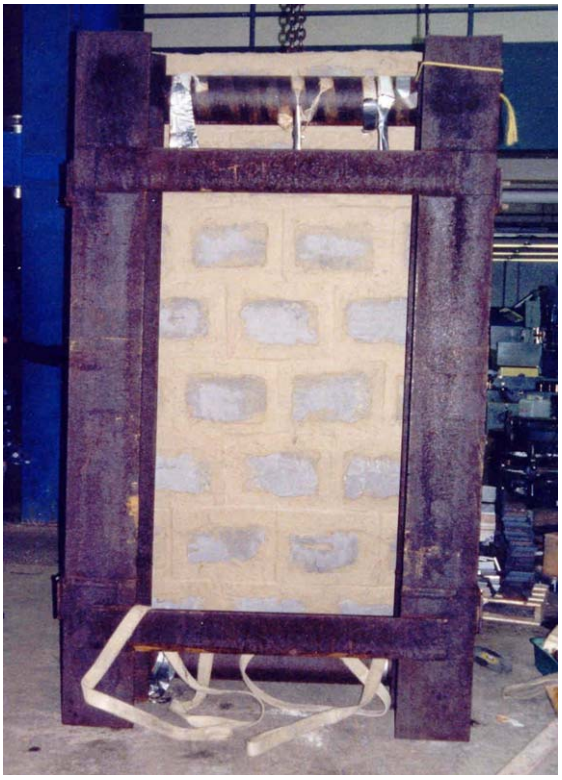

Figure 3-2. A 4 x 8 ft section of wall being placed into reaction frame for ASTM E 72 testing.

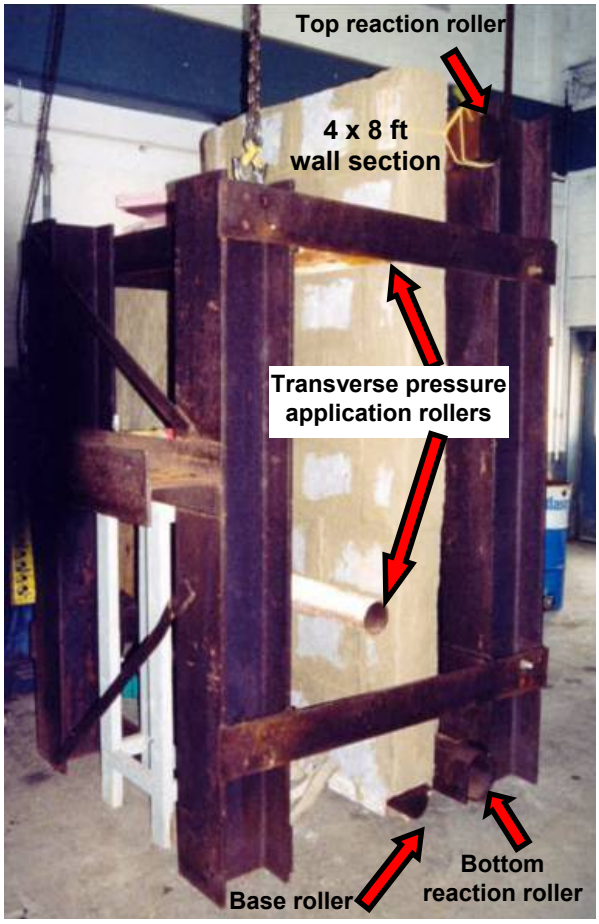

Figure 3-3a. A 4 x 8 ft section of wall positioned in the reaction frame for ASTM E 72 transverse pressure testing.

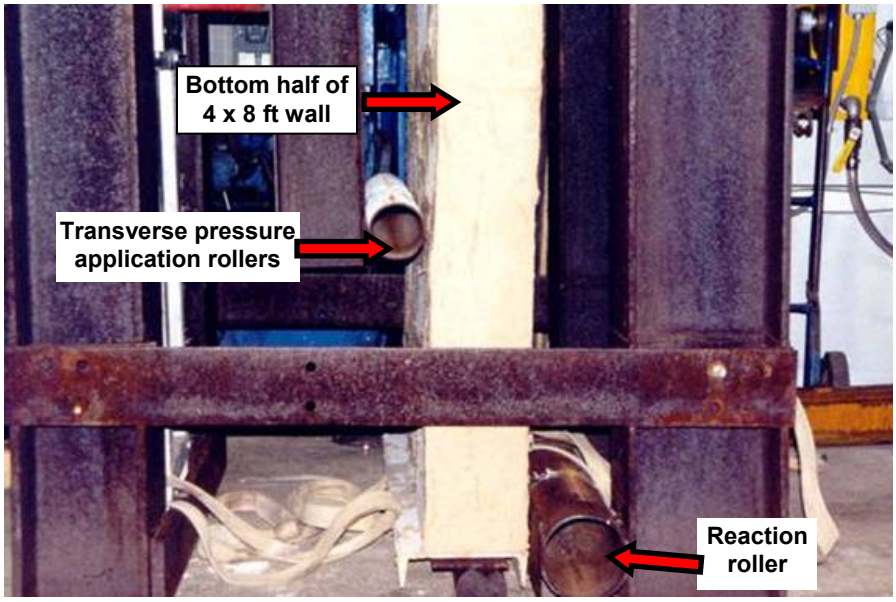

Figure 3-3b. Close up view of sections of pipe used as reaction roller to avoid rotational restraint as the wall deflects from application of transverse pressure.

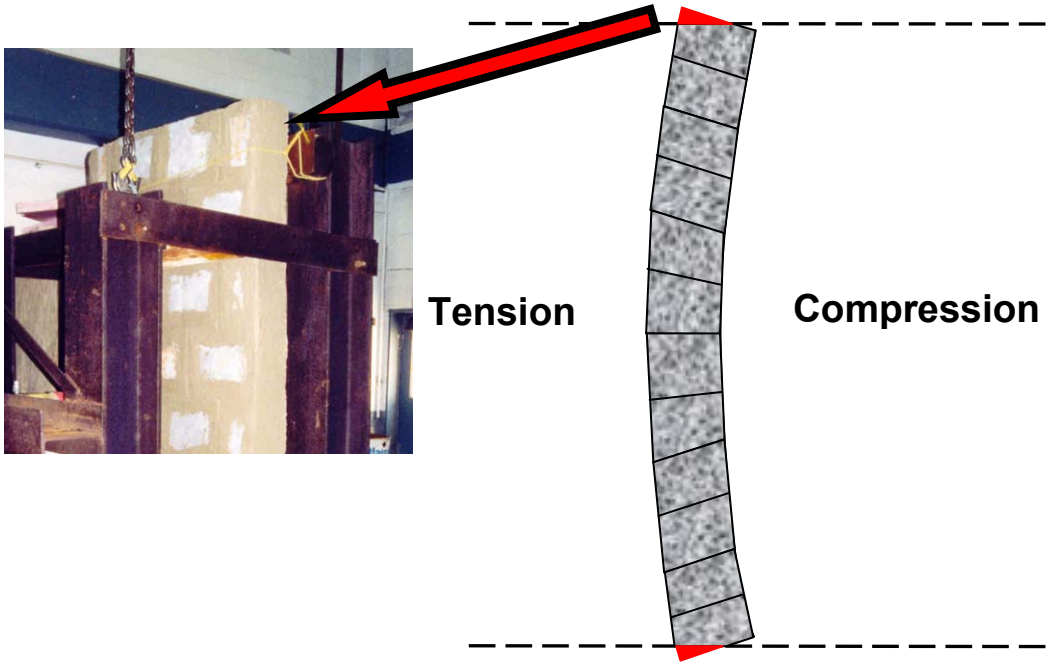

Figure 3-4. The wall is not restrained vertically in this free-standing test condition.

3.2 INADEQUACIES OF CURRENT CFR SPECIFICATIONS

Examination of the mechanics of the wall response to transverse pressure reveals the inadequacies of the CFR test procedure. First, it is seen that great care is taken to ensure that there is no longitudinal restraint provided to the wall as the load is applied. Essentially, the wall is considered freestanding and unrestrained from vertical movement as it bends from the application of transverse pressure (figure 3-4). The objective of the test is to evaluate the flexural strength of the wall. Any structure that is subject to bending produces tensile stresses on one side of the structure and compressive stresses on the opposite side of the structure (figure 3-4). Typically, the tensile strength of the material, being weaker than the compressive strength, controls the capability of the structure to withstand loads that produce bending. Concrete has relatively little tensile strength, but a *dry-stacked* block stopping has no effective tensile strength since the joints are not bonded. Theoretically, the transverse pressure capacity of a freestanding, dry-stacked stopping would be provided only from the weight of the block, which acts to provide a superimposed vertical load on the structure. Even the heaviest blocks would not provide enough axial loading to meet the 39-psf criteria in the CFR.

The tensile strength is actually provided by the application of sealant to the face of the wall. This brings up a few more points of discussion. First, this is obviously not the primary function of the sealant. As such, there was little information available about the tensile strengths of sealants prior to this research, and in fact, evaluating or knowing the strength of the sealant is not part of CFR test requirement. Since the sealant under these conditions is providing the major contribution to the transverse pressure capacity of the dry-stacked block stopping, the placement of the sealant is also critical to the test results. In order for the sealant to be effective in controlling the transverse pressure, it must be applied to the face opposite the load application, i.e., the low-pressure side of the stopping in the mine environment. If the ventilation could be reversed either intentionally or unintentionally, then the sealant should be applied to both sides of the stopping under these criteria. Since several sealants are available each with different material properties, then the stopping should only be certified with a specific sealant as used in the test. Furthermore, for a given sealant, the thickness of the sealant contributes significantly to the effective tensile strength and resulting transverse pressure capacity of the wall. How thick the sealant is applied in the test program compared to the thickness normally applied to such stoppings in the mine is another issue of concern. The test program should exclude abnormally thick sealant applications.

In conclusion, the current CFR requirements using ASTM E 72 specifications for evaluating stopping walls is nothing more than a test of the sealant tensile strength. Observations made in this research, and those reported by MSHA in the approval and certification of stoppings, indicate that inconsistent results can be achieved with these sealant-related test procedures. As described above, the test procedure is predicated on a freestanding wall arrangement, which for dry-stacked stopping constructions requires the sealant to control the transverse pressure. The only other factor influencing the transverse pressure capability is the height of the wall, and this factor is frequently ignored, as an 8-ft test height is a standard height used in ASTM E 72 testing. The physical and material properties of the block are irrelevant in this test procedure. This process will allow any block type to be used providing the sealant can sufficiently adhere to the block to provide the required tensile strength across the block joints.

CHAPTER 4: ARCH LOADING MECHANISM

In the mine, stopping walls are not freestanding structures as assumed in the ASTM E 72 test standard used to define the current CFR criteria. Stoppings, as constructed in the mine, bridge the distance between the mine floor and the mine roof and are typically wedged in place at the roof interface to provide a tight fit during installation. They also span the full entry width, butted against the pillars on both sides. Hence, if the mine stoppings are restrained by the mine roof and floor and pillars, this restraint allows for a completely different loading mechanism to occur, namely arching.

4.1 PHYSICAL DESCRIPTION OF ARCHING

Arching is the mechanism that occurs when the elongation of the tension face of the stopping due to the rotation of the wall as it bends under the application of transverse pressure is prevented by the contact abutments of the mine roof and floor. This arching of the wall produces a thrust that acts at the mine roof and floor interface, and produces compressive forces within the wall that can dramatically increase the transverse pressure capacity of the wall compared to a freestanding condition. An examination of the wall as it bends from the transverse pressure further explains how arching works. Initially, the ends of the wall are in full contact with the mine roof and floor and the individual horizontal joints between the courses of block are in full contact with each other. As the transverse pressure increases, the wall will begin to bend. Associated with the bending will be the opening of the joint along the mid-height span of the wall (location of the maximum positive moment), and opening of the joints between the top and bottom block at the roof and floor interface (location of the maximum negative moment). A three-hinged arch is formed where the external moment caused by the transverse pressure (ρ x $L^2/8$) is resisted by the internal force couple (P x r), where r is defined as the width of the arch and P is the thrust generated by the arching. This condition is illustrated in the diagram in figure 4-1, and expressed mathematically by equations 4.1 and 4.2. As shown in the figure, crush zones occur at the three hinge points.

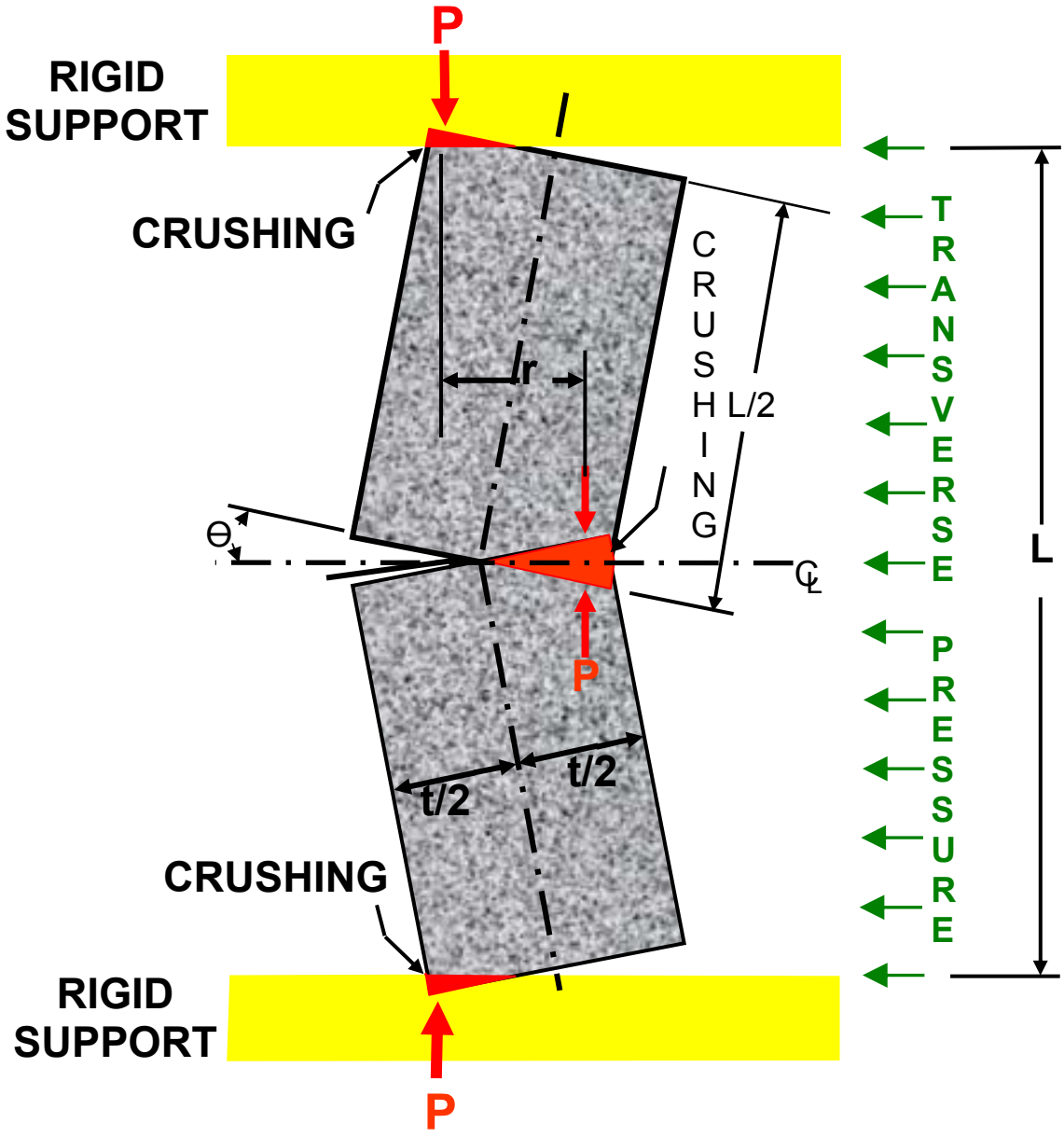

Figure 4-1. Illustration of rigid arching of a wall structure.

$$\frac{\rho \times L^2}{8} = P \times r \tag{4.1}$$

$$\rho = \frac{8 \times P \times r}{L^2} \tag{4.2}$$

Where ρ = transverse pressure, psi,

L = height of the wall, in,

P = resultant thrust force at the hinge points, lbs per in of wall width, and

r = width of the arch, in.

In this analysis, the compressive forces will control the transverse pressure capacity. Hence, the compressive strength of the block material becomes the dominant control parameter in defining the transverse pressure capacity. Lower strength blocks will have less transverse pressure capacity than higher strength blocks. This is a significant departure from the dominance of the sealant in controlling the transverse pressure capacity in the current CFR testing requirement. Under arching conditions, the contribution of the sealant to the transverse pressure capacity would be insignificant for all but the very weakest block materials used for stopping construction.

4.2 SIMULATING ARCHING THROUGH BIAXIAL LOADING IN THE MINE ROOF SIMULATOR

It is apparent from the preceding analysis that an assessment of the true transverse pressure capacity of a mine ventilation stopping cannot be attained by a freestanding wall evaluation. Arching has been shown to be an accepted loading mechanism for masonry design for walls that are restrained by high stiffness abutments. A ventilation stopping bridging between the mine roof and floor satisfies this condition. However, full-scale testing of mine ventilation stoppings in an actual underground mine is difficult and time consuming to conduct. In order to determine the transverse pressure capacity of a stopping underground,

either a hydrostatic pressure chamber is required to develop the controlled loading or an explosive charge is needed to create the loading much like seals are currently tested.

Likewise, there are only a few facilities where full-scale laboratory tests of such large structures can be conducted. Laboratory testing of partial masonry beams by other researchers have been successfully conducted, although these too have been relatively limited in scope, requiring specialized reaction frames and fixtures to accomplish rudimentary tests. As the theory indicates, the thrust forces involved in rigid arching of wall structures can be substantial (over 100 tons of abutment loading for a 4-ft wide wall). This requires robust fixtures to preserve the low yielding or rigid abutment conditions. NIOSH has a unique load frame that is designed to simulate the behavior of rock masses for underground mining operations. It is called the Mine Roof Simulator (MRS). This unique facility provides an ideal framework in which to conduct rigid-arch testing of stopping walls.

4.2.1 Description of the Mine Roof Simulator

A photograph of this unique machine is shown in figure 4-2. A detailed description of the load frame is provided in Appendix A. The platen size measures 20 x 20 ft, and with a maximum vertical opening of 16 ft, the MRS can accommodate full-scale stopping constructions, as shown in figure 4-3, where a compressive load is being applied to a stopping wall to measure its capacity relative to roof loading. The MRS is capable of providing controlled biaxial loading in the vertical and one horizontal axis. Up to 3 million lbs of vertical force can be applied through a 24-in stroke of the lower platen and 1.6 million lbs of horizontal force through a 16-in stroke of the lower platen. The loads or displacements in these two axes can be applied individually or simultaneously if desired. The biaxial capabilities of the load frame are used to simulate transverse loading of stoppings. A test protocol using half-wall sections of the stopping to evaluate its transverse loading behavior is described in the next section.

Figure 4-2. NIOSH Mine Roof Simulator load frame.

Figure 4-3. Full-scale mine ventilation stopping wall being tested in the NIOSH Mine Roof Simulator.

4.2.2 Test Protocol For Simulating Arching

In order to simulate arching, a half-height section of a stopping wall is placed in the load frame in a typical vertical orientation, as it would be in the mine. The upper platen position is adjusted to the height of the block column and is hydraulically clamped to maintain its position. The vertical position of the lower platen is commanded to remain constant. Hence, the fixed vertical positions of the upper and lower platen allow them to act as rigid restraints. The lower platen is then moved horizontally at a constant velocity of 0.5 inches/minute, causing the wall to rotate (figure 4-4). As the base of the wall is forced to move horizontally, hinge points and deformation zones are created at the ends of the wall on opposite sides, consistent with the arch loading mechanism. The horizontal force applied by the MRS to the base of the half-wall is measured. This force is equivalent to the transverse load acting on a stopping wall. The transverse pressure is computed by normalizing the resultant of this force over the area of the wall to determine the transverse pressure capacity for comparison to the current CFR requirements.

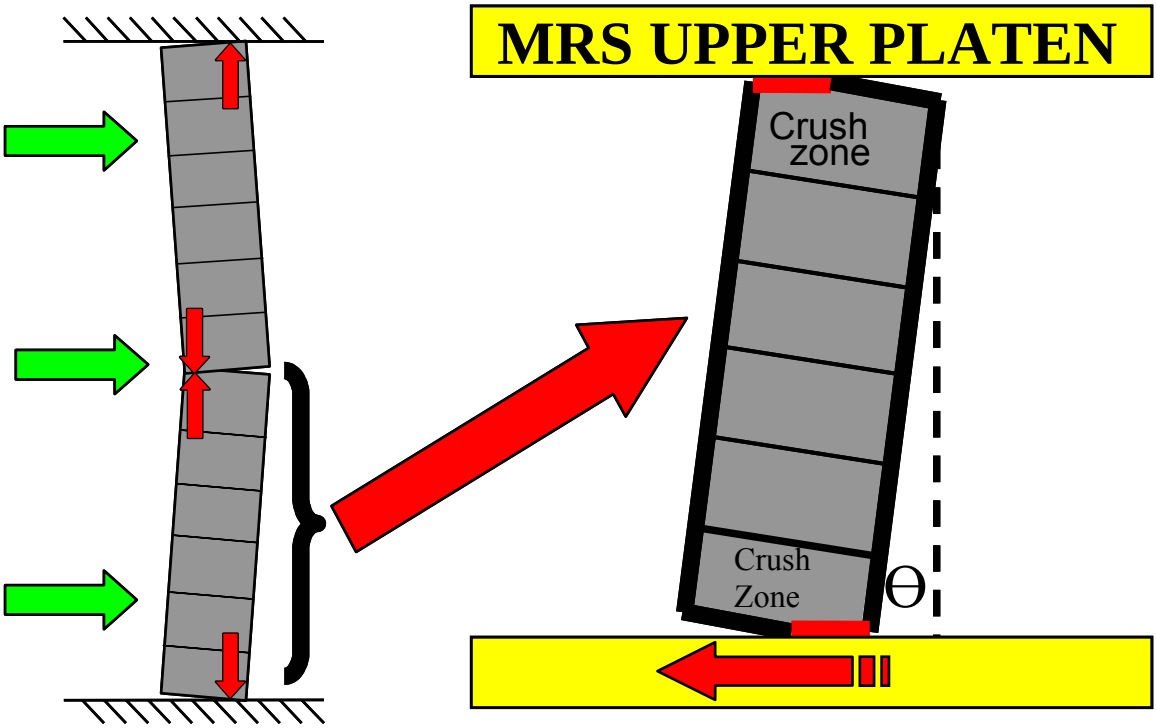

Figure 4-4. Diagram illustrating the simulation of rigid arching on a half-wall section of a stopping by biaxial testing in the NIOSH Mine Roof Simulator.

In order to measure the applied horizontal loading more accurately than the capabilities of the MRS which use the large actuator pressures to measure the loading, an arrangement using load cells was employed which can independently record the horizontal load at a higher resolution. Figure 4-5 illustrates the testing apparatus. A single or triple column of block, equal in height to half the full-scale installation height is constructed on the rolling platform. The rolling platform is a two-in-thick steel plate that is secured to four 32-ton-capacity crawler units (figure 4-6). A load measuring reaction fixture is located adjacent to the crawler assembly. Two bolts are secured into the lower platen, which has inserts on a 20 x 20-in grid to accommodate bolt placements. The bolts serve as the rigid horizontal restraint against which transverse pressure of the block column is generated. A two-in-thick metal plate is then used to bridge the gap between the two bolts. Two, 20-kip load cells are then placed in front of the reaction plate to accurately measure the horizontal load (figure 4-7). These have a calibration accuracy of 0.1 pct, meaning they can measure the transverse load to an accuracy of 20 lbs. The load cells laid horizontally on the platen have a threaded bar extending from them to provide contact with the stopping block's rolling platform. Two machined nuts at the end of the threaded bar provide some minor adjustments to ensure that proper contact is established with the block platform before the test commences.

Although the apparatus was designed to test a column up to three blocks wide, it was concluded from shakedown testing that a single column of block would provide the most consistent results for standard masonry block materials. Block dimensional tolerances can cause variations in the height of the wall across a three-block arrangement (figure 4-8) for dry-stacked block constructions that are being evaluated in this study. Since the MRS is acting as a rigid restraint, any differential in the height of the wall will produce non-uniform loading of the wall from block-to-block across the width of the wall. By using a single column of block, a uniform height can be more easily achieved to provide uniform loading and results that are more consistent. Three block wide half-walls were utilized for the lower modulus block materials where the block tolerances were not as critical.

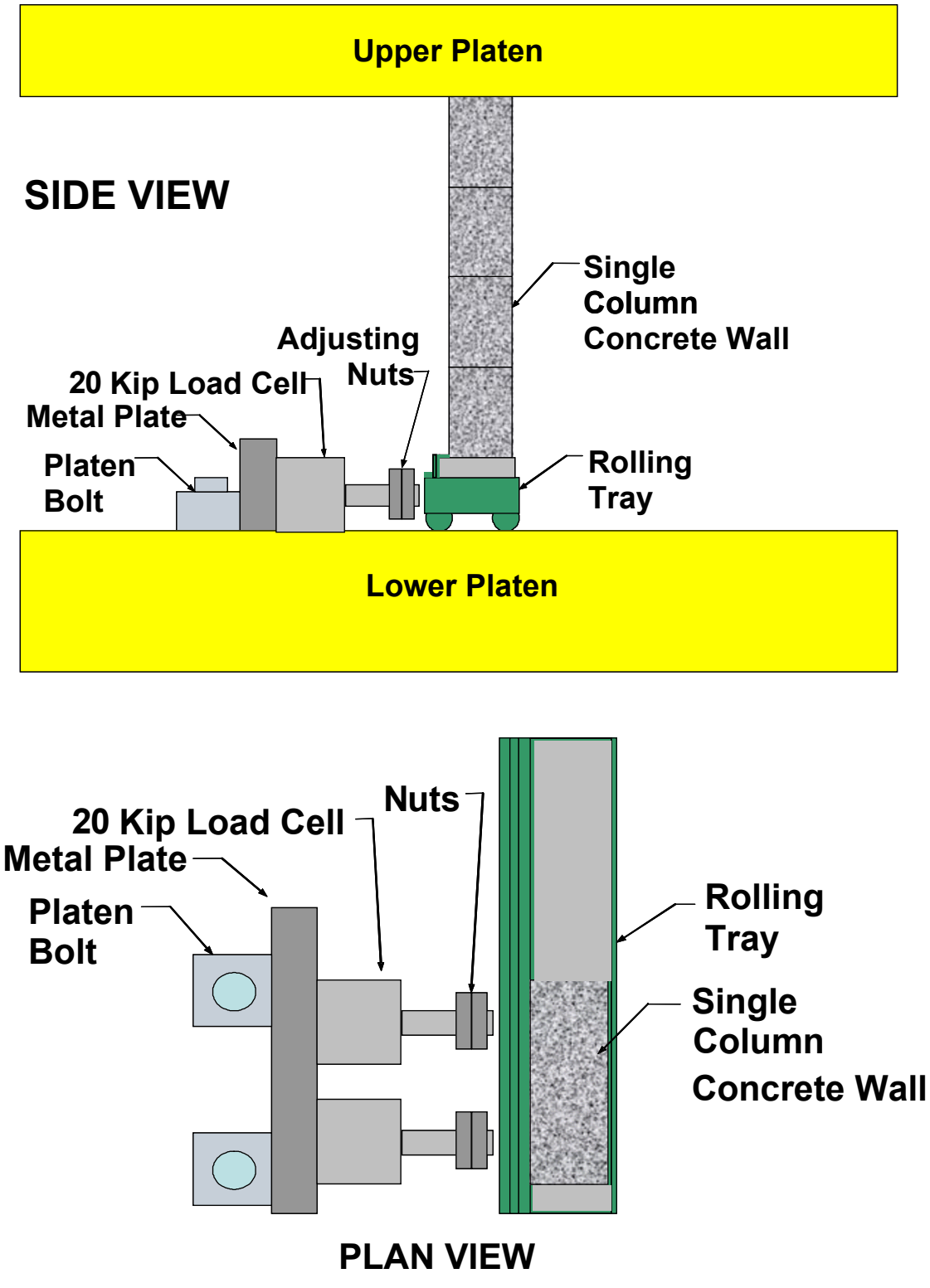

Figure 4-5. Apparatus used to conduct half-wall rigid-arching tests of stopping walls in the NIOSH Mine Roof Simulator.

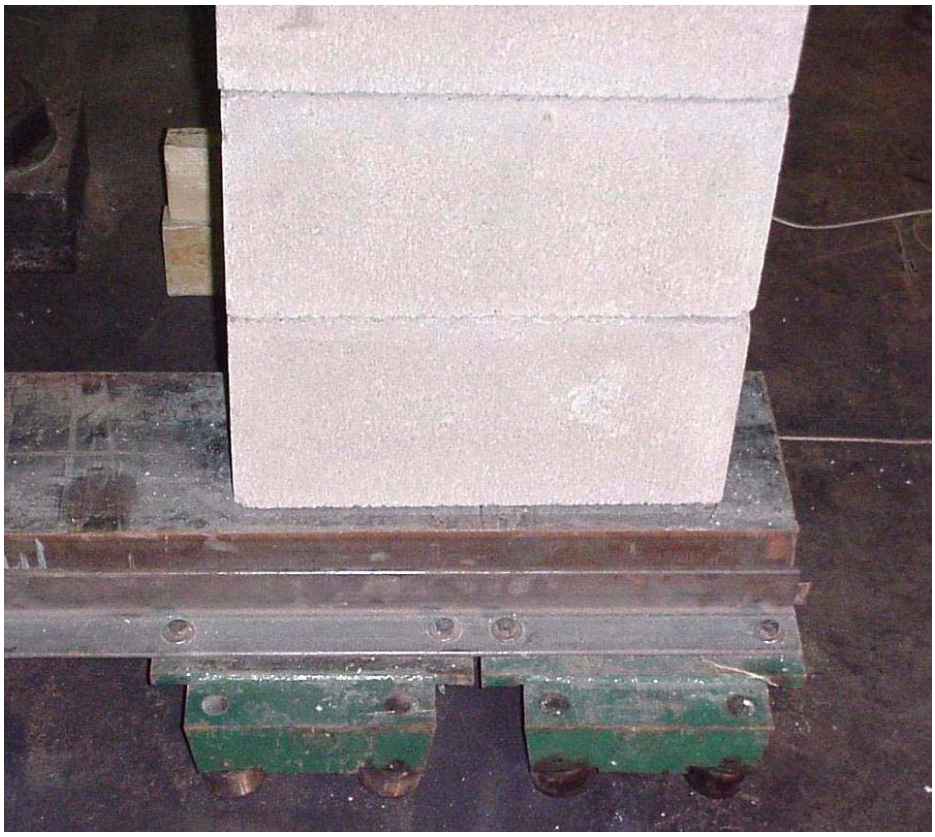

Figure 4-6. Block column rests on rolling platform to allow load cells to measure lateral loading.

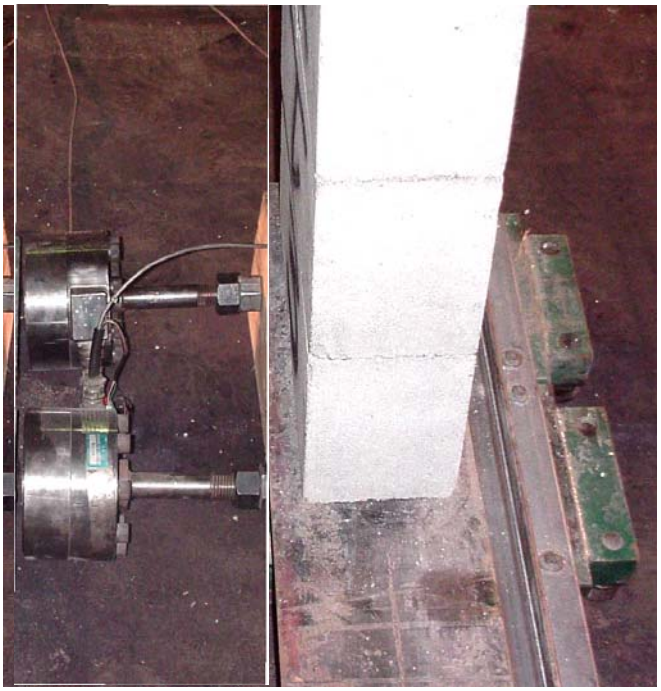

Figure 4-7. Load cells used to accurately measure horizontal loading.

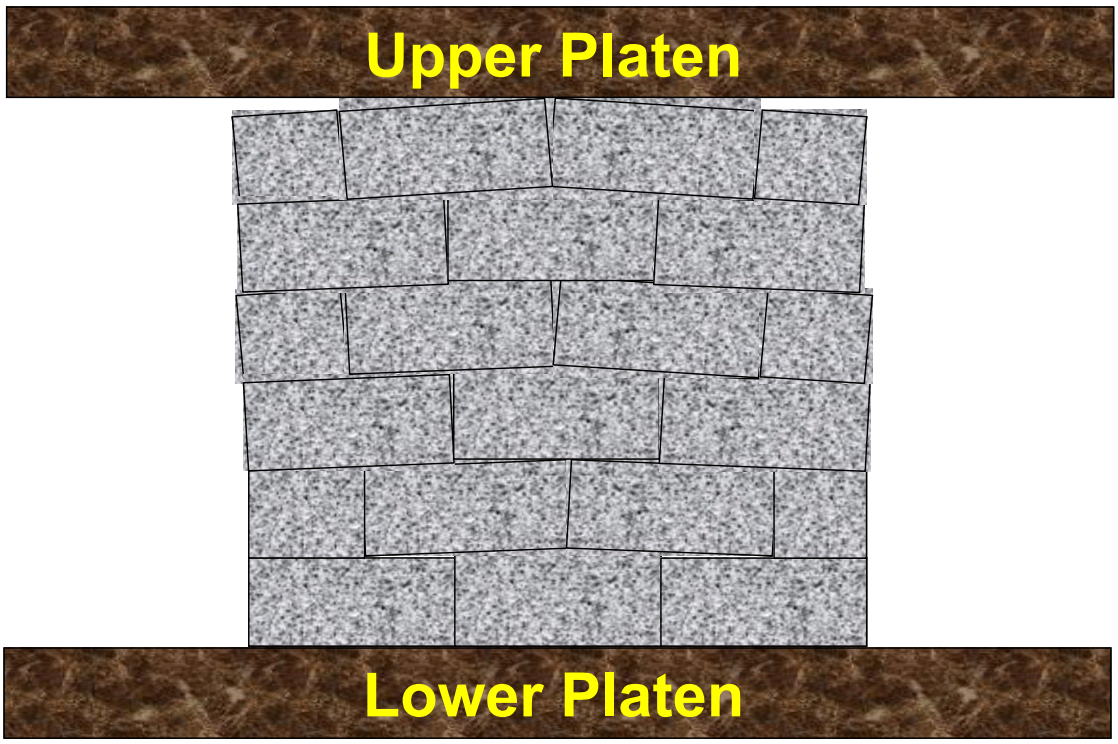

Figure 4-8. Illustration of how block dimensional tolerances can cause localized loading on a three-block-wide wall (not to scale).

4.2.3 Transverse Pressure Determinations From MRS Half-Wall Testing

Two examples of transverse pressure tests conducted on two different types of concrete block are shown in figures 4-9a and 4-9b. Both tests consisted of a single column of block, stacked four blocks high with the narrow side contact between blocks. The first test (4-9a) is a half wall constructed from a lightweight block manufactured by Kingsway Technology from autoclaved concrete. Air pockets introduced into the concrete mix (figure 4-9c) result in the low material density. This block measures 5.875 x 8.375 x 17.250 inches with a density of 42.5 lbs/cu ft resulting in a unit block weight of approximately 21 lbs. Tests conducted on an individual block indicated that the compressive strength was 546 psi (figure 4-10). This type of block is being used by some mines because of its lighter weight to reduce material handling injuries associated with stopping construction. The second wall was constructed from block made by Klondike Block and Masonry Supplies, Inc., from conventional Portland cement, sand, and aggregate material. This block measured 5.625 x 7.500 x 15.625 inches with a material density of 109.7 lbs/cu ft and a unit weight of

approximately 45 lbs. This block has a compressive strength of 1,330 psi as shown in figure 4-11.

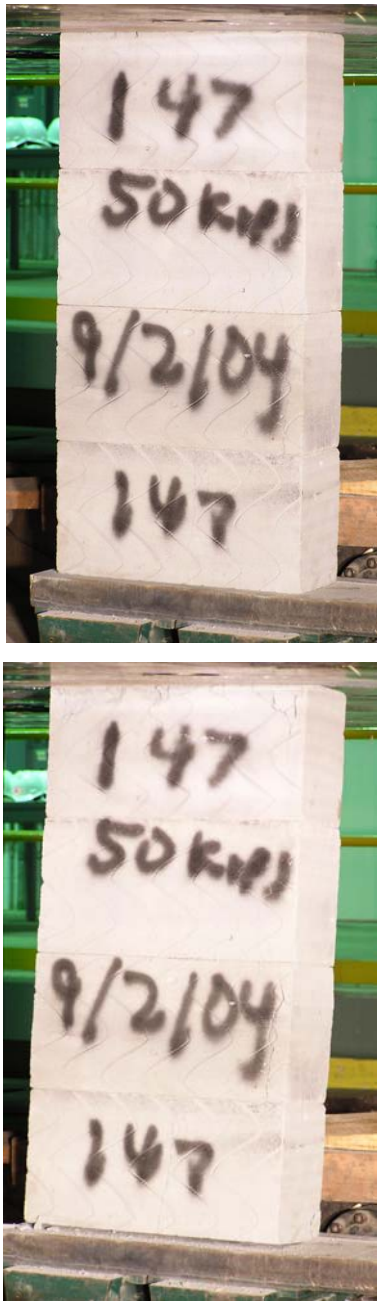

Figure 4-9a. Test of a half-wall made from lightweight block (546-psi compressive strength).

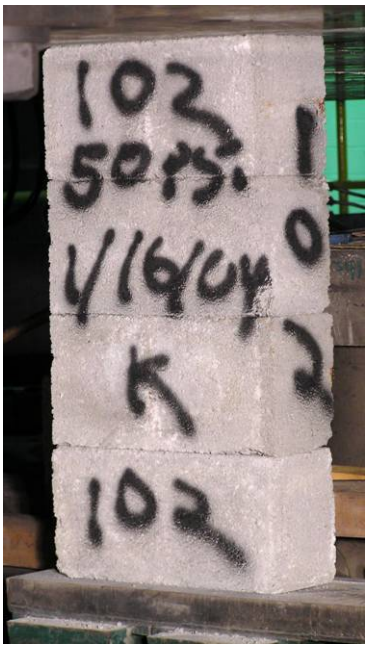

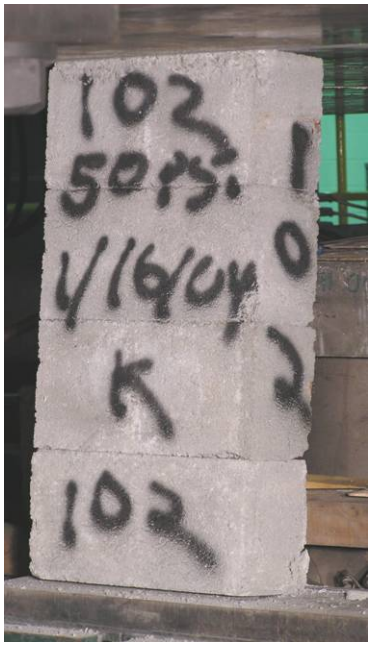

Figure 4-9b. Test of a half-wall made from conventional concrete block (1,330-psi compressive strength).

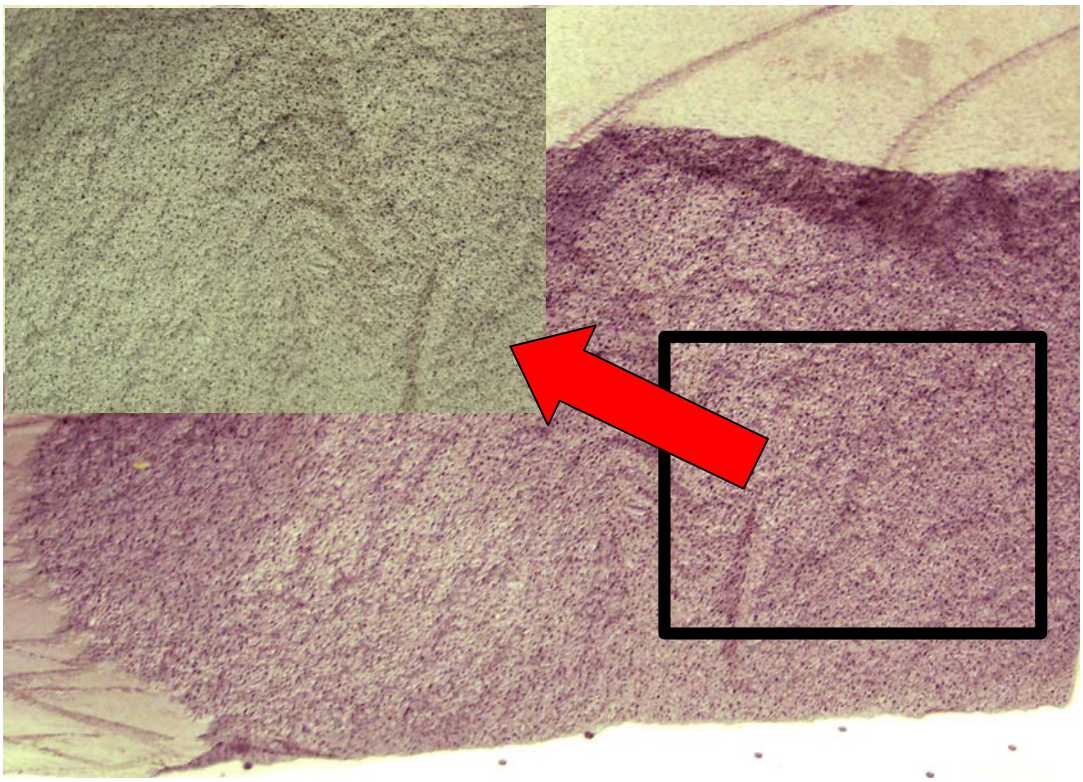

Figure 4-9c. Close up view of Kingsway, autoclaved, concrete block shows air pockets in the block structure.

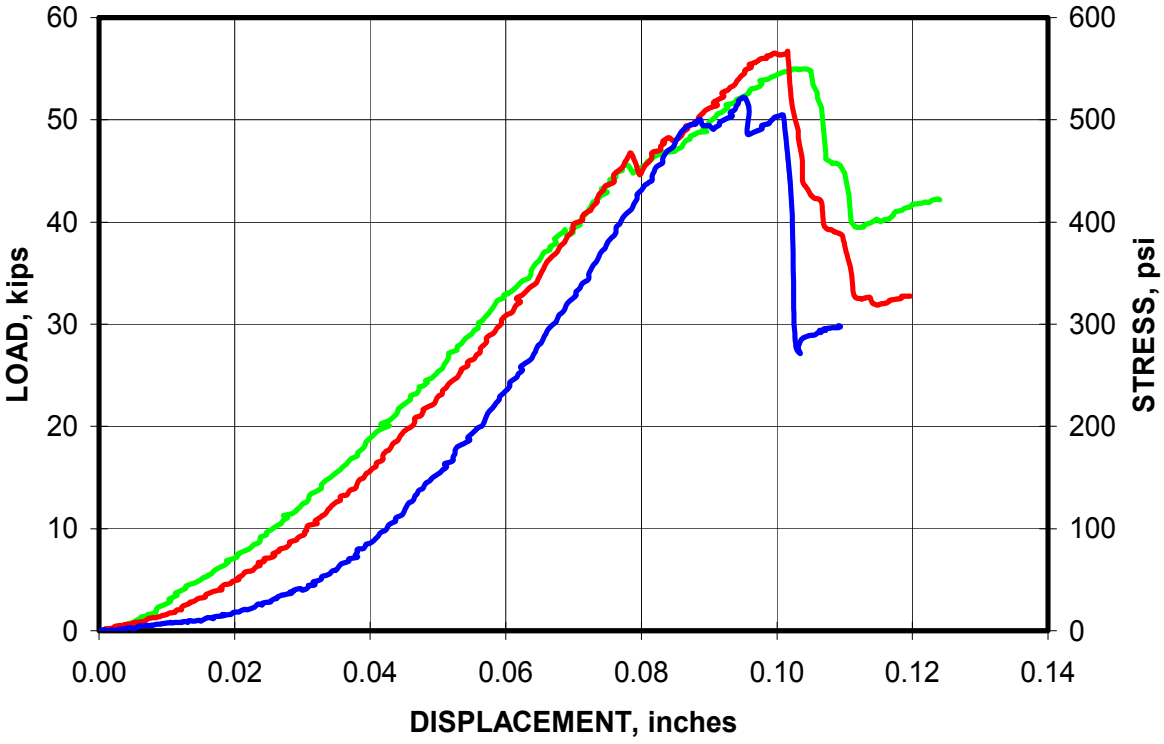

Figure 4-10. Compressive strength test data for Kingsway block.

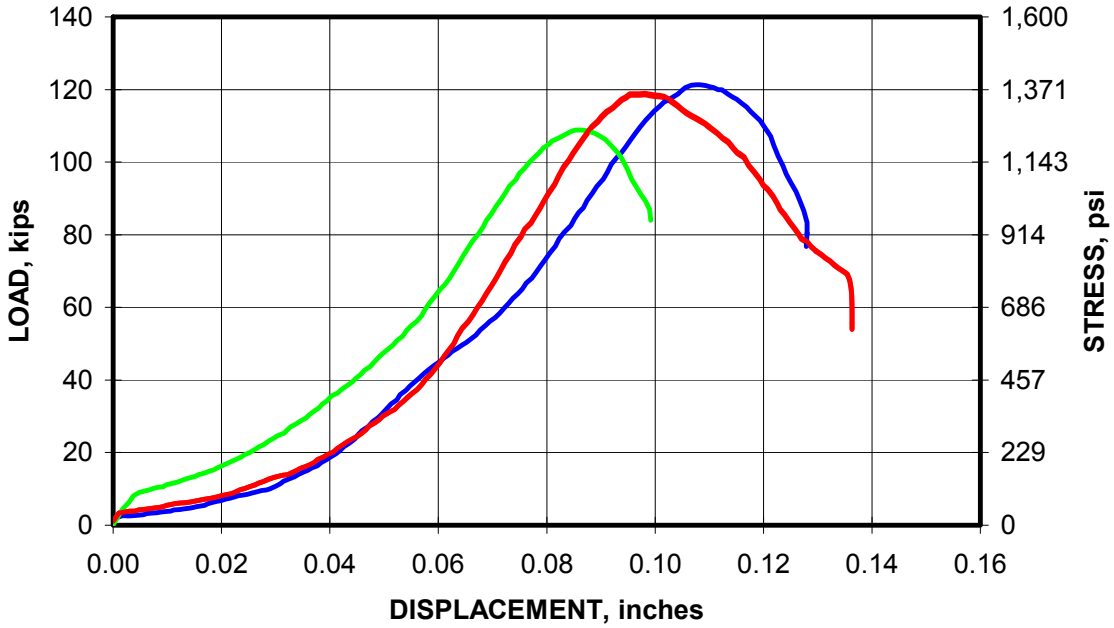

Figure 4-11. Compressive strength test data for conventional concrete block.

Figure 4-12 documents the half-wall rigid arching test results for the lightweight (Kingsway) block. The graph plots the applied lateral load provided by the load frame to produce the controlled lateral displacement of the wall. The graph shows that the lateral load increases with increasing lateral displacement up to the peak load, which in this test was approximately 1,675 lbs occurring at 0.74 inches of lateral displacement. It is also seen from figure 4-12 that the thrust reaction load measured by the load frame, since the vertical opening of the platens is held constant, also increases as the lateral loading increases. This is consistent with arching theory. The measured vertical force is equivalent to the arching force or thrust (P).

The applied lateral load can then be normalized to the area of the wall to provide a transverse pressure capacity measured in pounds per square foot or psf. The arching mechanics require that the force acting at the based of wall be doubled to properly distribute this load as a uniform force over the entire wall. For the example shown in figure 4-12, the four-course, single-block column was 17.25 inches wide by 33.50 inches high providing an area of 577.88 in^2 or 4.01 ft^2. Multiplying the lateral load from the test (1,675 lbs) by 2 and dividing this force by the area provides a transverse pressure capacity of 834 psf. This is an order of magnitude higher than the 39 psf required by the current CFR criteria based on a freestanding wall analysis.

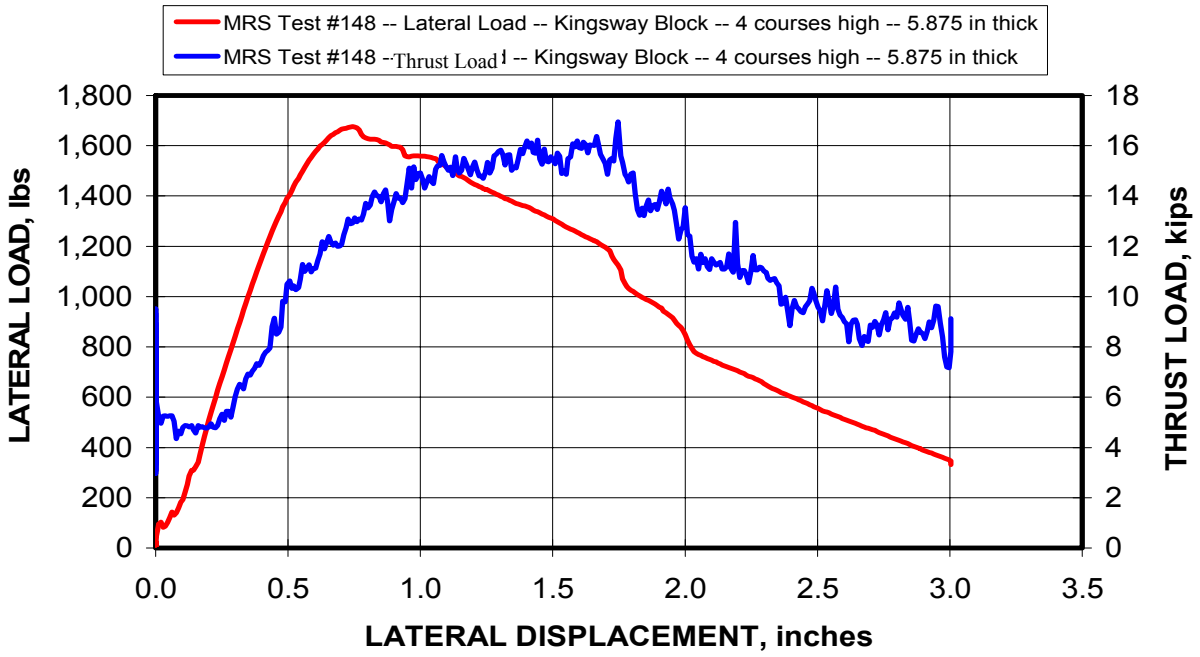

Figure 4-12. Half-wall rigid-arching tests conducted in the Mine Roof Simulator on the Kingsway lightweight block.

Figure 4-13 shows the test results from the second example using conventional concrete block, or conventional masonry units (CMU) as they are sometimes called. This block has a compressive strength of 1,330 psi or about 2.5 times that of the autoclaved block tested in the first example. As seen in figure 4-13, the peak lateral load acting on this wall was 3,855 lbs occurring at a lateral displacement of 1.02 in. This equates to a transverse pressure of 2,134 psf or 2.56 times that of the autoclaved block used in the previous test. It is noted that the difference in lateral load capacity between the lightweight and the conventional block is consistent with the difference in material strength. This provides additional validation for the application of arching theory to stopping wall behavior. Again, it is noted that this transverse pressure is two orders of magnitude higher than current 39-psf allowance under the CFR.

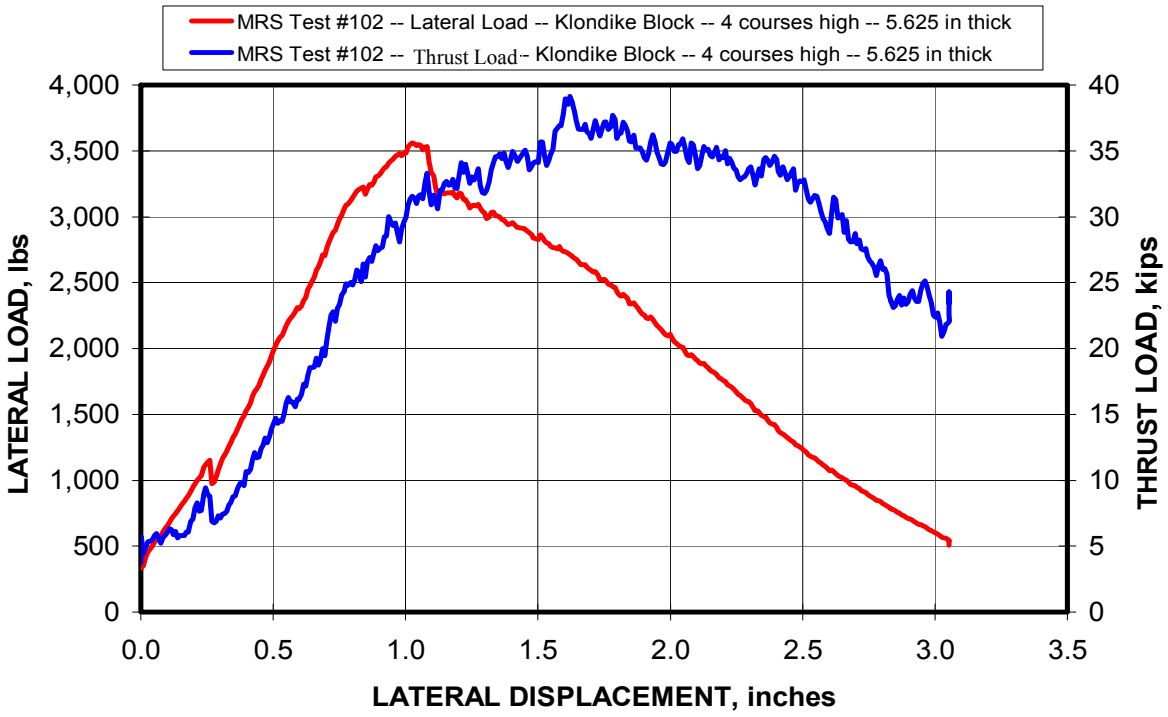

Figure 4-13. Half-wall rigid-arching tests conducted in the Mine Roof Simulator on conventional concrete block.

4.3 VALIDATION OF EXPERIMENTAL DESIGN METHODOLOGY AND ARCHING BEHAVIOR

In order to confirm that arching was the proper loading mechanism controlling the transverse pressure capacity of mine ventilation stoppings and to verify the MRS half-wall rigid-arching testing protocol, a few full-scale tests of stopping walls were also conducted. These tests were conducted in the NIOSH Experimental Coal Mine at the Pittsburgh Research Laboratory. Test data was also analyzed from explosion testing of full-scale stoppings at the NIOSH Lake Lynn Laboratory.

4.3.1 NIOSH PRL Experimental Coal Mine Tests

The Experimental Coal Mine is an abandoned coal mine that has been used as an underground laboratory for conducting various research experiments by NIOSH researchers. The mine has been part of the Bureau of Mines since 1910 and is now owned by NIOSH. It is located on site at the Pittsburgh Research Laboratory near Bruceton, PA.

An air pressure chamber was constructed in one of the crosscuts in the mine to provide a facility for static loading of mine ventilation stoppings. The crosscut measures approximately 16 ft in width with about an 80-in height. A barrier wall was constructed from mortared high strength solid concrete blocks. The barrier is 16 in thick. An access door, air intake port, and data acquisition lead wire ports were installed during construction of the barrier. A stopping wall is then constructed approximately 3-ft from the barrier wall. A concrete pad was formed on the floor of the crosscut to provide a flat foundation for constructing the stopping wall. The pillar ribs were also squared up, again to facilitate the stopping wall construction in order to minimize air leakage that might occur along this interface.

Two full-scale wall tests were conducted in the NIOSH Experimental Coal Mine. The first test utilized the lightweight autoclaved blocks that were used in the first example presented for the MRS rigid-arching tests. The second test was a wall constructed from the conventional solid concrete aggregate block that was utilized in the second MRS rigid-arching test. This was done so that a direct comparison to these tests could be made.

Photos of the remains of the stopping after the full-scale mine test of the lightweight block stopping are shown in figures 4-14 and 4-15. It is seen in these figures that the bottom and top course of block stayed in place after the wall was blown out. This is most likely because the bottom course was grouted in place to provide a level and secure foundation to build the wall. Likewise, cement grout was squeezed into the voids on top of the wall between and around the wooden wedges to stop air leaks, and this secured the top block to the shotcreted roof in the Experimental Coal Mine. This suggests that the functional wall height relative to the arching length may have been the eight courses of block between the top and bottom layer as denoted in figure 4-14.

Figure 4-14. Photo after the wall was destroyed from the transverse loading. Researcher is standing next to the displacement transducers used to measure the wall deflection.

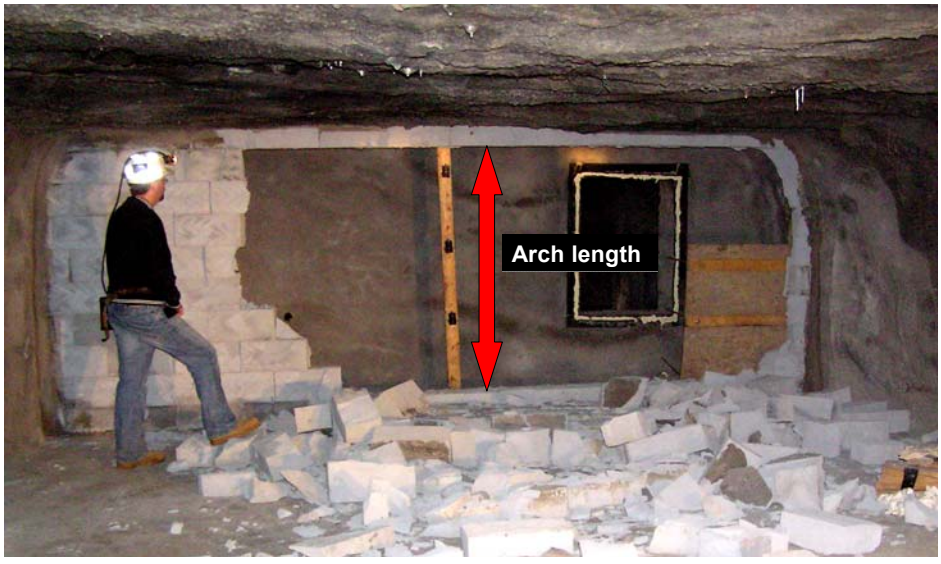

Figure 4-15. Arch height shown to occur between top and bottom layer of block that were grouted (cemented) in place in this particular test.

The results of the lightweight autoclaved block MRS tests in comparison to the full-scale mine test are shown in figure 4-16. As seen in the figure, the 5-course-high, single-column, half-wall rigid-arching test conducted in the MRS more closely predicted the full-scale wall behavior in the mine than the 4-course-high, half-wall test. The peak transverse pressure was 834 psf for the 4-course-high, half-wall and 462 psf for the 5-course-high, half-wall MRS test compared to 400 psf for the full-scale mine test. If it is assumed that the arching length did occur over the 8-course height, this suggests that the wall failed prematurely in the full-scale mine test compared to the laboratory test, perhaps from a lower block strength than was achieved in the laboratory test or due to differences in the boundary conditions.

Figure 4-17 compares the full-scale mine test with all the MRS half-wall tests correlating the term $f_c \times (t/L)^2$, where f_c is the compressive strength of the concrete block, t is the wall thickness, and L is the full wall height. The underlying assumption in this analysis is that the arch thrust is limited by the compressive strength of the material. The MRS laboratory tests are based on the unit block compressive strength of 546 psi. Two cases are presented for the full-scale mine test, one where the compressive strength is derived from testing a single block (546 psi unit block compressive strength) using the full construction height of 10 courses, and the other where the strength is derived from a column of 4 to 6 blocks (342 psi column compressive strength) and using the apparent 8-course arching height. As seen in this figure, both these measures place the full-scale mine test for the $f_c \times (t/L)^2$ correlation close to the MRS laboratory tests data, but the lower strength (column measure) provides the best correlation of the full-scale mine test to the half-wall MRS tests.

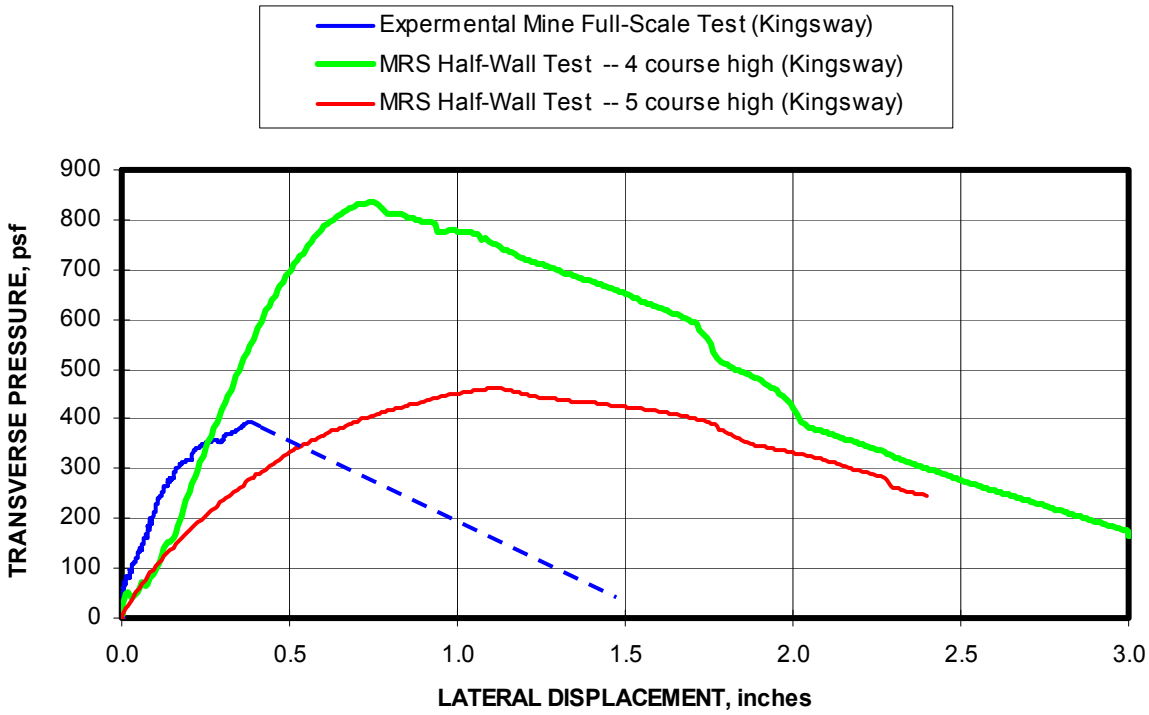

Figure 4-16. Comparison of half-wall rigid-arch test in the MRS to the full-scale stopping wall test in the NIOSH Experimental Coal Mine for the Kingsway block.

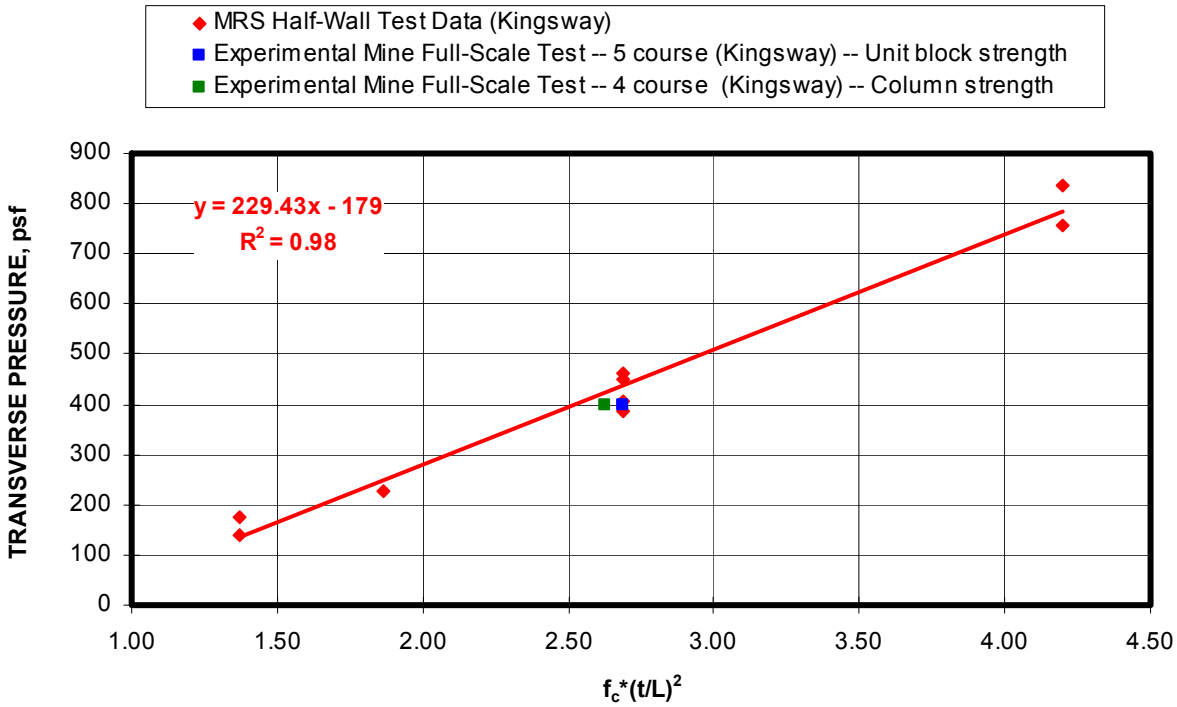

Figure 4-17. Comparison of full-scale mine test with Kingsway block with the MRS half-wall tests.

Photos of the remains of the full-scale stopping test with the conventional Klondike block are shown in figures 4-18 and 4-19. The wall was constructed with 10 courses of block. Figure 4-18 shows the arching length occurred between the mine roof and bottom course of block, equating to 9 courses of block in this case. Figure 4-19 shows a close up view of the base of the wall illustrating the rotation of the wall and formation of the bottom hinge of the arch. This is proof of the arching mechanism.

The comparisons of the MRS half-wall rigid-arching test to the full-scale mine test for the walls constructed from the conventional Portland cement, sand, and aggregate block manufactured by Klondike are shown in figure 4-20. The graph shown both a 4-course-high and a 6-course-high half-wall test in the MRS as well as a projected 5-course-high result in comparison to the measured full-scale mine test. Since the wall appeared to arch over a 9-course height, there is not a direct comparison to a MRS laboratory test, but the projected 5-course-high half-wall test fits the mine response reasonably well with a peak transverse pressure of 1,200 psf compared to the 975 psf for the full-scale mine test. If the lateral displacement is considered, the full-scale mine test at failure falls nicely in between the four and six course high MRS half-wall response.

A comparison of the full-scale mine test to the regression trend line developed from the suite of MRS tests showing the correlation of the transverse pressure to the $f_c \times (t/L)^2$ term is shown in figure 4-21. As with the lightweight block test presented in the previous example, here again it is seen that the full-scale test was very close to the MRS trend line and is slightly better when the column strength is considered with the shorter wall height compared to the unit block strength with the higher wall height.

Figure 4-18. Photo showing conventional (Klondike) wall after full-scale test in the Experimental Coal Mine noting the arch length between the top and bottom course of block.

Figure 4-19. Close up view of the base of the conventional (Klondike) block wall showing the rotation of the wall and formation of the bottom hinge of the arch.

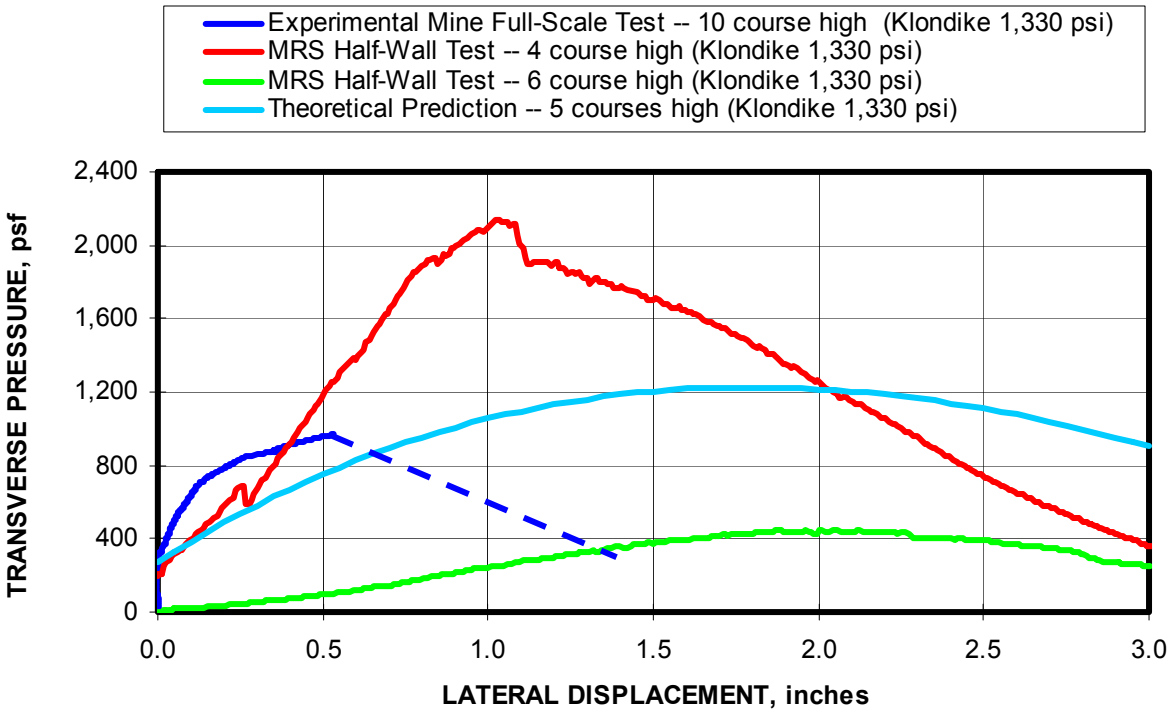

Figure 4-20. Comparison of half-wall rigid-arch test in the MRS to the full-scale stopping wall test in the NIOSH Experimental Coal Mine for the Klondike block.

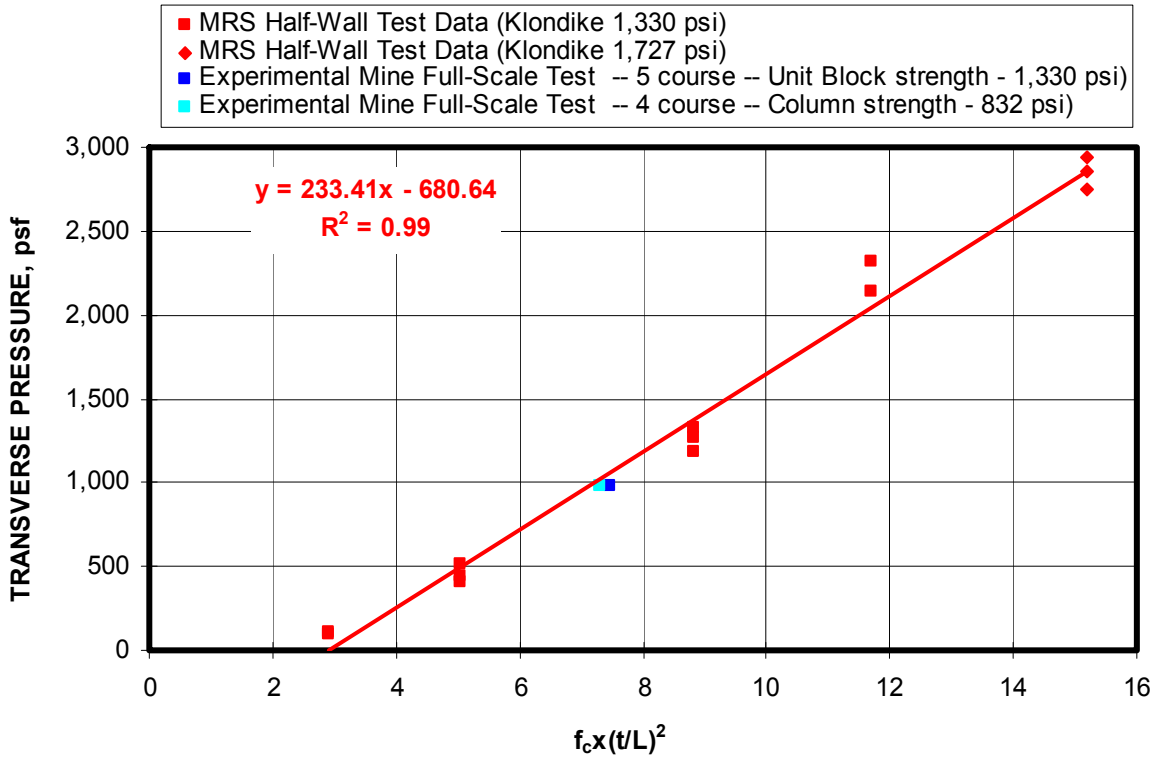

Figure 4-21. Comparison of full-scale mine test of Klondike conventional block with the MRS half-wall regression trend line and suite of MRS tests.

4.3.2 NIOSH Lake Lynn Laboratory Tests

A series of tests were conducted at the NIOSH Lake Lynn Laboratory at the request of the Mine Safety and Health Administration (MSHA) to evaluate the effects of explosions on mine ventilation stoppings as part of NIOSH's research on the prevention and mitigation of gas/dust explosions. These tests also provided additional data to validate the transverse pressure capacity of stoppings

The test protocol consisted of constructing stoppings in the crosscuts between the C and B-drifts of the Lake Lynn Longwall Gallery, and progressively increasing the intensity of gas/dust explosions to induce sufficient air pressures to cause transverse pressure failures of the stoppings. Both hollow-core and solid concrete block stoppings were evaluated in this study. The hollow-core block had an average material compressive strength of 1,456 psi and the solid block an average compressive strength of 1,900 psi. The stopping walls constructed in the crosscuts were 12 courses high (7.5 ft), 6-inches thick, and approximately 20 ft in length. Pressure transducers were used to measure both the static and dynamic pressure at the stoppings resulting from the explosive charge.

The results of the explosion tests at the Lake Lynn Laboratory indicated that the transverse pressure capacity of the dry-stacked, hollow core stopping was 490 psf and 821 psf for the solid, dry-stacked concrete block stopping. Since neither of these particular blocks was available for testing at the MRS, a direct comparison to MRS half-wall tests could not be made. However, by computing the term $f_c \times (t/L)^2$, a comparison can be made to overall MRS test results. Two cases are considered: (1) arching over the full wall height (12 courses) and (2) arching over 10 courses. For a nominal block height of 8 inches, this produces arch heights (L) equal to 96 and 80 inches, respectively. These results are depicted in figure 4-22. Here again, there is good agreement between the MRS laboratory tests and the full-scale mine tests, and the correlations are more accurate when the lower (column) strength is used in the analysis.

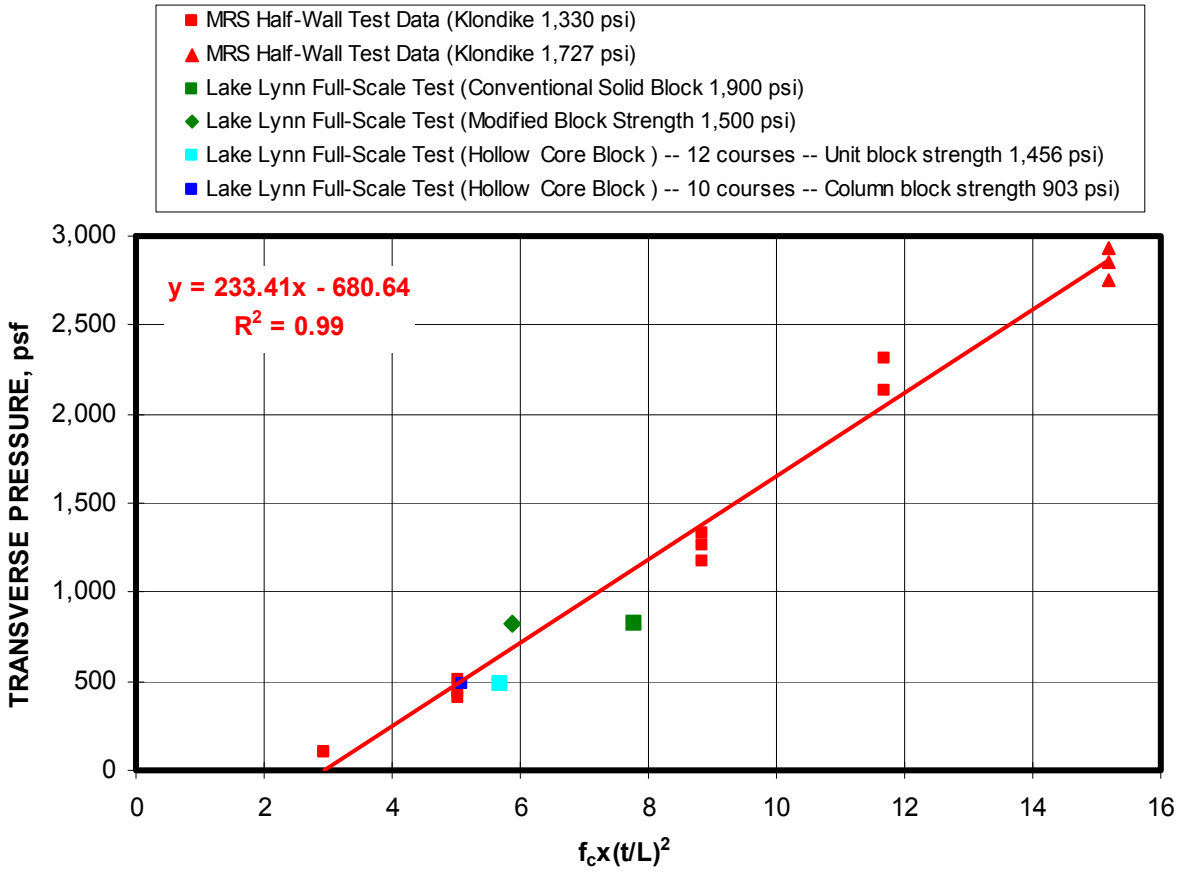

Figure 4-22. Comparison of Lake Lynn full-scale stopping tests with the MRS rigid arching tests.

CHAPTER 5: DEVELOPMENT OF GENERAL TRANSVERSE LOAD DESIGN EQUATION FROM ARCHING MECHANICS

Figure 5-1 is used to re-examine the half-wall mechanics. Here the arching thrust (P) is shown to act on two ends of the wall at a distance of one-tenth the wall thickness from the end of the wall. The lateral force (HF) is shown to act at the ends of wall in accordance with the MRS laboratory protocol for conducting half-wall test using the biaxial capabilities of the simulator. This force will be used to compute the transverse load capacity of the stopping. Equation 5-1 is formed by summing moments about the top left corner of the wall as illustrated in figure 5-1.

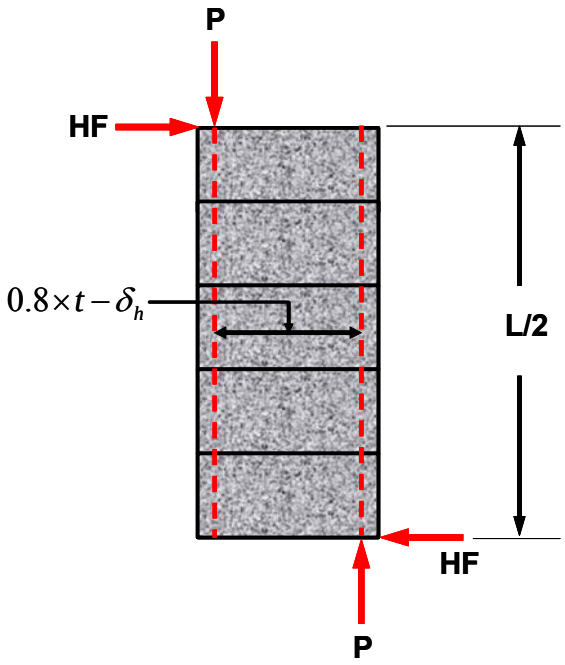

Figure 5-1. Half-wall statics showing the width of the arching thrust varies as a function of the wall displacement.

$$P\times\left(0.8\times t-\delta_h\right)=HF\times L/2 \qquad \textbf{(5.1)}$$

Where P = arching thrust, lbs,
t = thickness of the wall, in,
δ_h = lateral displacement of wall at the mid span, in,
HF = horizontal force measured at based of half-wall, lbs, and
L/2 = half-wall height, in.

This equation is then solved for the horizontal force, which is a measured parameter in the MRS laboratory testing and is used to verify the test data with the arching mechanics theory.

$$HF=\frac{P\times\left(0.8\times t-\delta_h\right)}{L/2} \qquad \textbf{(5.2)}$$

In order to transform the measured horizontal force into transverse pressure that would be acting on a full-scale stopping, the resultant horizontal force must be repositioned to the middle of wall to represent the resultant transverse load of a uniform load acting against the face of a stopping. This transposition to the middle of wall requires the force be increased by a factor of two to satisfy moment equilibrium requirements as expressed in equation 5.1 (see figure 5-2).

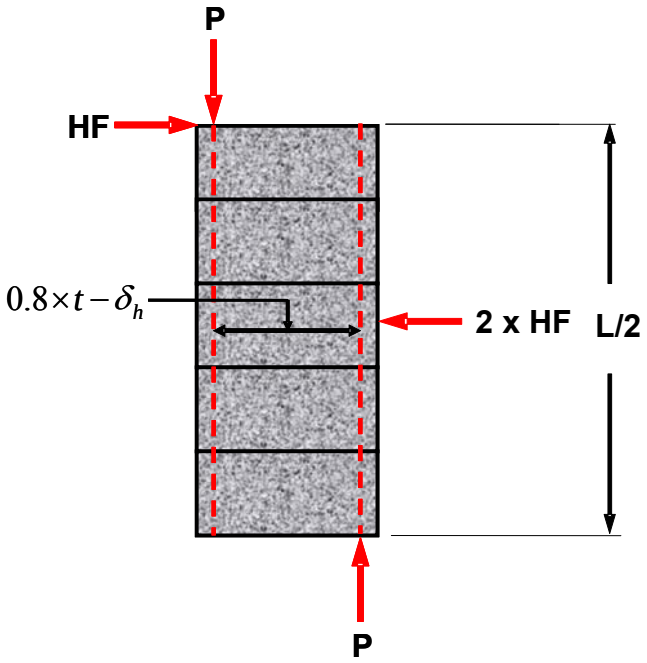

Figure 5-2. Repositioning of the horizontal force to equate to the resultant force acting against a full-scale stopping wall.

The transverse load per unit area is computed by dividing the horizontal force acting on the half-wall by the area of the wall (equation 5.3).

$$\rho = \frac{2\times HF}{w\times L/2}\times 144 \qquad \textbf{(5.3)}$$

Where ρ = transverse load, psf,

HF = horizontal force measured at base of wall in laboratory half-wall tests, lbs,

w = width of the wall, in, and

L/2 = half-wall height, in.

Substituting the horizontal force (HF) from equation 5.2 into equation 5.3 yields an expression for the transverse load as a function of the lateral displacement of the wall.

$$\rho = \frac{2\times\dfrac{P\times(0.8\times t-\delta_h)}{L/2}}{w\times L/2}\times 144 = \frac{2\times P\times(0.8\times t-\delta_h)}{w\times(L/2)^2}\times 144 \qquad \textbf{(5.4)}$$

Where ρ = transverse load, psf,

P = arching thrust, lbs,

δ_h = lateral displacement of wall at the mid span, in,

w = width of the wall, in, and

L/2 = half-wall height, in.

A more generalized approach to finding a solution to computing the transverse pressure can be found by integrating the transverse load over the area of the wall as illustrated in figure 5-3 to equate the maximum bending moment from the transverse pressure to the moment produced by the arch thrust. The maximum bending moment assuming a uniformly distributed load produced by the transverse pressure can be found from equation 5.5. The moment equilibrium requirements expressed in equation 5.1 can then be expressed as equation 5.6.

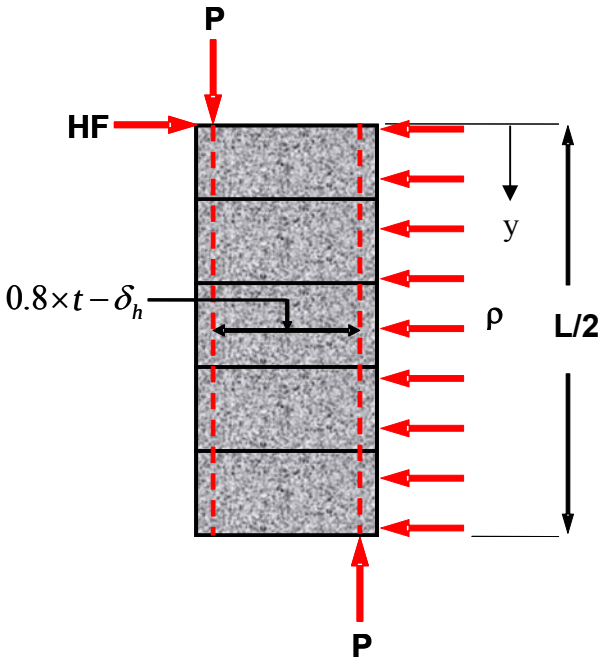

Figure 5-3. Displaying transverse pressure acting on half-wall.

$$\int_0^{L/2} w \times y \times \rho \times dy = w \times \frac{y^2}{2} \times \rho \Big|_0^{L/2} = \frac{w \times L^2}{8} \times \rho \qquad \textbf{(5.5)}$$

$$P \times (0.8 \times t - \delta_h) = \frac{w \times L^2}{8} \times \rho \qquad \textbf{(5.6)}$$

Equation 5.6 can then be solved for the transverse pressure (ρ) as shown in equation 5.7, providing the same solution derived in equation 5.4.

$$\rho = \frac{8 \times P \times (0.8 \times t - \delta_h)}{w \times L^2} = \frac{2 \times P \times (0.8 \times t - \delta_h)}{w \times (L/2)^2} \qquad \textbf{(5.7)}$$

Taking moments about the bottom right corner of the half-wall (see figure 5-3), reveals the relationship expressed in equation 5.8, which can be solved for the horizontal force (HF) as shown in equation 5.9 as a function of the wall width (w), wall height (L), and the transverse pressure (ρ).

$$HF \times (L/2) = \frac{w \times L^2}{8} \times \rho \quad \textbf{(5.8)}$$

$$HF = \frac{w \times L}{4} \times \rho \quad \textbf{(5.9)}$$

CHAPTER 6: THEORETICAL ASSESSMENT OF FACTORS THAT AFFECT THE TRANSVERSE PRESSURE

As seen in the previous theoretical analysis of the arching mechanics, several parameters affect the transverse pressure of mine ventilation stoppings under arch loading conditions. An assessment of these parameters is made to further understand their significance.

6.1 WALL HEIGHT

An increase in wall height causes a reduction in the transverse load capacity of a mine ventilation stopping. The physical description of arching described in section 4.1 of Chapter 4 shows that wall height is a critical parameter in controlling the transverse load capacity of a stopping. The moment equilibrium equation 5.1 shows that the horizontal force moment arm is much larger than the thrust moment arm due to the wall height. Equation 5.4 shows that the transverse pressure varies inversely with the square of the half-wall height because of the moment equilibrium requirements. Hence, wall height will have a big impact on the transverse load capacity.

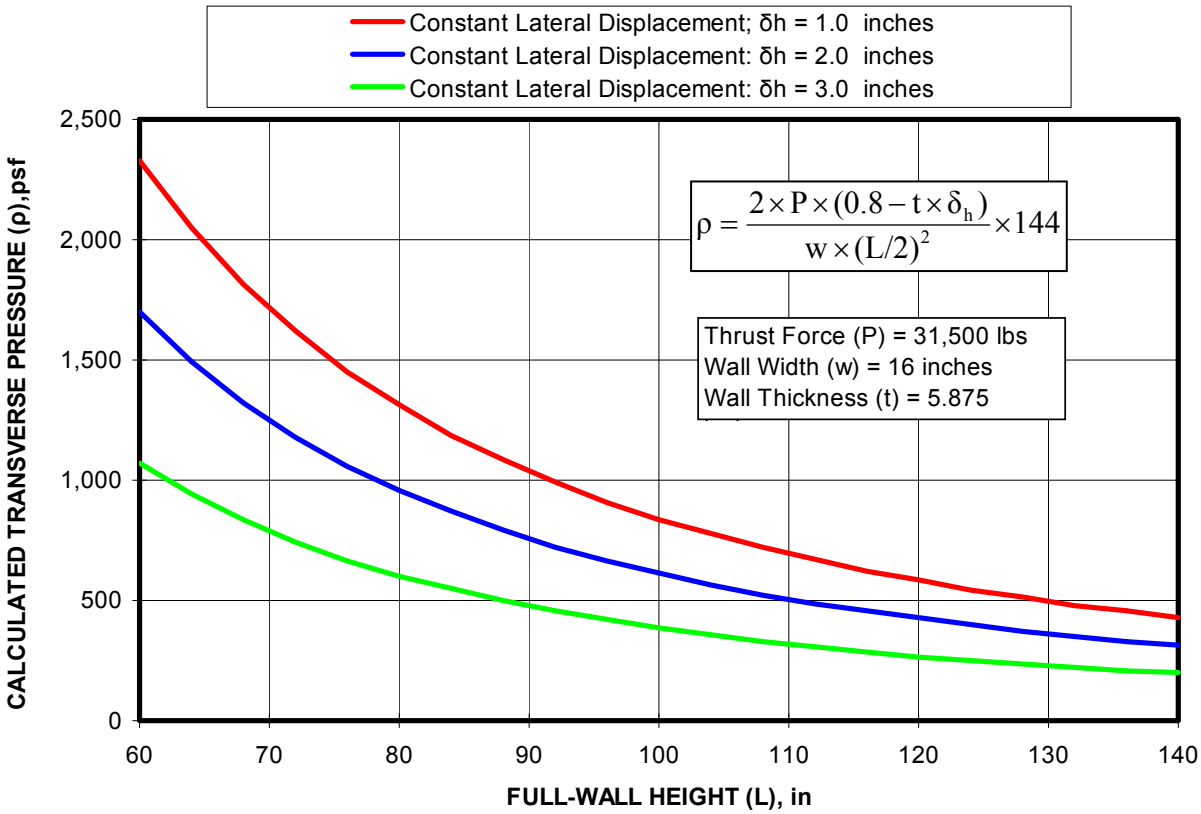

Figure 6-1. Impact of wall height on transverse load capacity.

Figure 6-1 depicts the transverse pressure as a function of wall height for lateral wall displacements of 1, 2, and 3 inches. The wall thickness in this example is a 5.875 inches and a constant arching thrust force of 31,500 lbs was acting on a single block column measuring 16 inches in width. As seen in this figure, the impact of wall height will be greater for shorter wall heights and becomes less of a factor as the wall height increases. For example, increasing the wall height from 60 to 96 inches decreases the transverse pressure by 61%; whereas, increasing the wall height from 96 to 120 inches reduces the transverse load capacity by 36%.

6.2 WALL THICKNESS

Equation 5.4 shows that the transverse load capacity is directly related to the thickness of the wall. Ultimately, the thickness of the wall determines the arch thrust moment arm, which is the distance between the resultant thrust hinge points as shown in figure 5-1 and represented by the factor (0.8 x t - δ_h). The impact of wall thickness on a 90-inch wall height is shown in figure 6-2 for lateral wall displacements of 1, 2, and 3 inches. Increasing the wall thickness from six to 8 inches, representative of a common block geometry, increases the transverse load capacity from 784 to 1,232 psf at a lateral displacement of 2 inches, an increase of 57%.

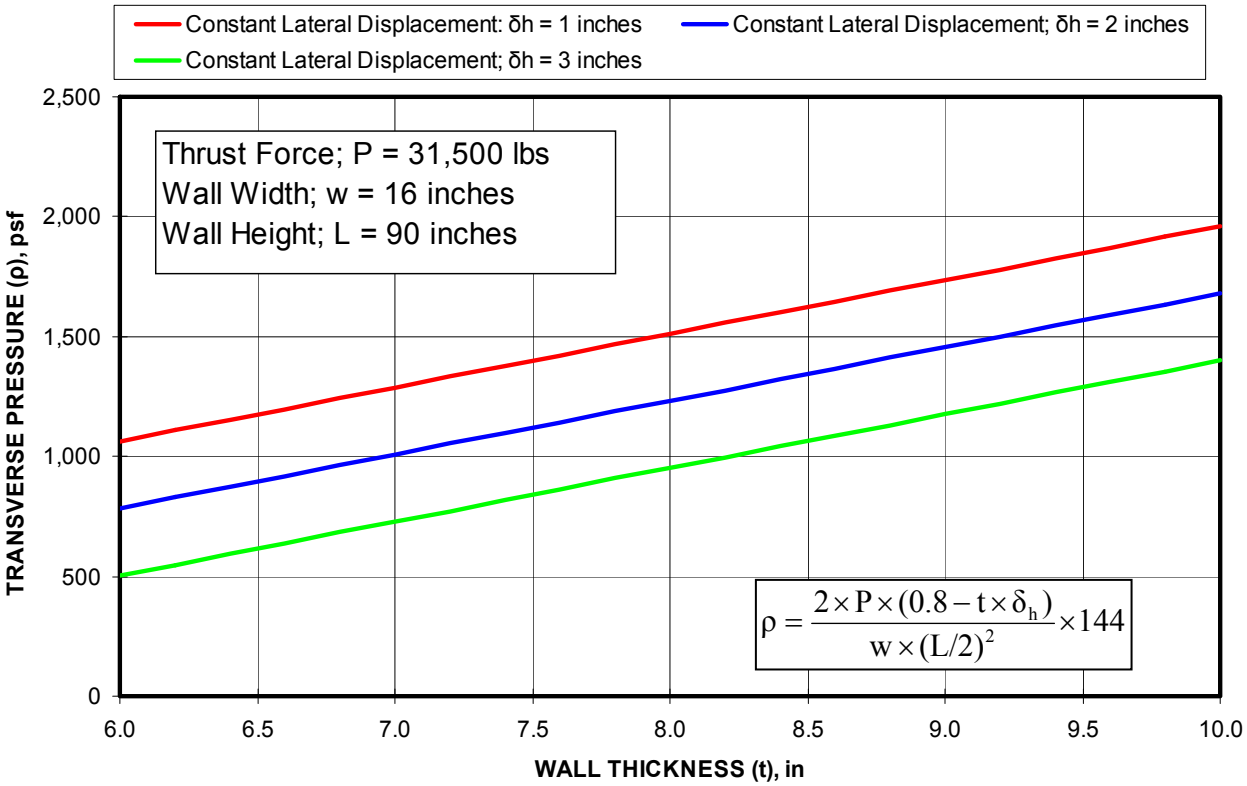

Figure 6-2. Impact of wall thickness on transverse load capacity.

6.3 WALL WIDTH

Equation 5.4 implies that the transverse pressure acting on a wall is also inversely related to the width of the wall, the width being analogous to the entry width. However, the arching thrust as shown here is the total thrust acting on the full width of the wall. The width factor is included only to normalize the thrust to a unit width, which is necessary to calculate the transverse pressure acting on the wall. In other words, the arching thrust cannot be considered a constant unless the wall width is also a constant. Hence, the wall width does not affect the transverse pressure capability of the stopping.

Physically, the reason why the width of the wall is not important is that the blocks are dry-stacked. If the joints of the block courses were mortared or laterally confined, then the arch may form along the width of the wall since this is typically the long axis in comparison to the height of the wall. However, since the blocks are dry-stacked, the joints have no tensile strength, and the arch is formed from the mine floor to the mine roof instead of from coal pillar to coal pillar, as is generally the case in seal behavior.

6.4 ARCH THRUST

Examination of equation 5.4 shows that the transverse capacity of a stopping wall is directly related to the arching thrust (P). The higher the arch thrust, the larger the transverse load capacity will be. If the arch thrust doubles, the transverse load capacity of the stopping will also double. Therefore, the compressive arch thrust force is the key to the how much transverse capacity a stopping of a given geometry can develop. The development of the arching thrust depends on several factors, including the geometry of the wall (i.e. height and thickness). But it is primarily determined by the material properties of the block and boundary stiffness of the roof and floor, both of which control how much lateral displacement of the wall will occur as the transverse pressure is applied to the face of the stopping. Understanding the development and role of the arching thrust requires a reexamination of the arching mechanics.

Transverse pressure applied to the face of the stopping will cause a three-hinge arch to form and lateral displacement of the middle hinge point with respect to the roof or floor hinge point. The lateral displacement causes an extension of the tension face of the stopping, which is resisted by the mine roof and floor and hinge point at the center section of the wall

(see figure 4-1). These reactions produce the thrust forces. How much thrust force is developed depends primarily on the stiffness of the wall structure and the mine roof and floor. The stiffness of the half-wall can be expressed as a function of the elastic modulus of the wall (see equation 6.1).

$$k = \frac{A \times E}{L/2} \qquad \textbf{(6.1)}$$

Where k = stiffness, lbs/in,
A = axial loading area of the wall, in^2,
E = elastic modulus, psi, and
L/2 = half-wall height, in.

Axial (vertical) loading is produced by the arching thrust. The deformation in the hinge zones is a function of the thrust force. Hence, the stiffness of the wall can be expressed as a function of the arching thrust and the deformation in the hinge zones (equation 6.2).

$$k = \frac{P}{2y} \qquad \textbf{(6.2)}$$

Where k = stiffness, lbs/in,
P = thrust force, lbs, and
y = deformation in each of the two hinge zones on the half-wall section, in.

Combining equation 6.1 and 6.2 yields the following expression.

$$\frac{A \times E}{L/2} = \frac{P}{2y} \qquad \textbf{(6.3)}$$

Where A = axial loading area of the wall, in^2,
E = elastic modulus, psi,
L/2 = half-wall height, in,
P = thrust force, lbs, and
y = deformation in each of two hinge zones on half-wall section, in.

This equation can them be solved for the arching thrust.

$$P = \frac{2 \times A \times E \times y}{L/2} \qquad \textbf{(6.4)}$$

Where P = thrust force, lbs,

A = axial loading area of the wall, in^2,

E = elastic modulus, psi,

y = deformation in each of two hinge zones on half-wall section, in, and

L = full wall height, in.

The area, modulus, and height of the wall are all known parameters, but the deformation of the hinge areas needs to be calculated. An examination of the arching mechanics and formation of the three-hinge arch shows that the deformation of the hinge areas is geometrically related to the lateral displacement. The diagram shown in figure 4-1 shows the three-hinge arch formed from the application of transverse pressure. As seen in the diagram, the shaded red areas at the hinge zones represent sections of the wall that must deform in order for the lateral displacement to occur. An expression that relates the hinge zone deformation (y) to the lateral displacement (δ_h) can be determined by analyzing the geometry of the wall configuration shown in figure 6-3. The distance between the rigid roof and floor abutments represents the construction height of the stopping (L). The half-wall height is represented as L/2, which as shown in the diagram is half the construction height and is the distance between the two hinge zone planes formed at end of the wall and the mid span. The hinge zone deformation (y) is shown as the extension of the wall beyond the abutment that would occur if the abutment was not there. Although it is illustrated in this manner, the "y" distance actually represents the shortening of the tension side of the wall due to the deformation of the hinge zone by the arching thrust that is acting against the rigid abutment.

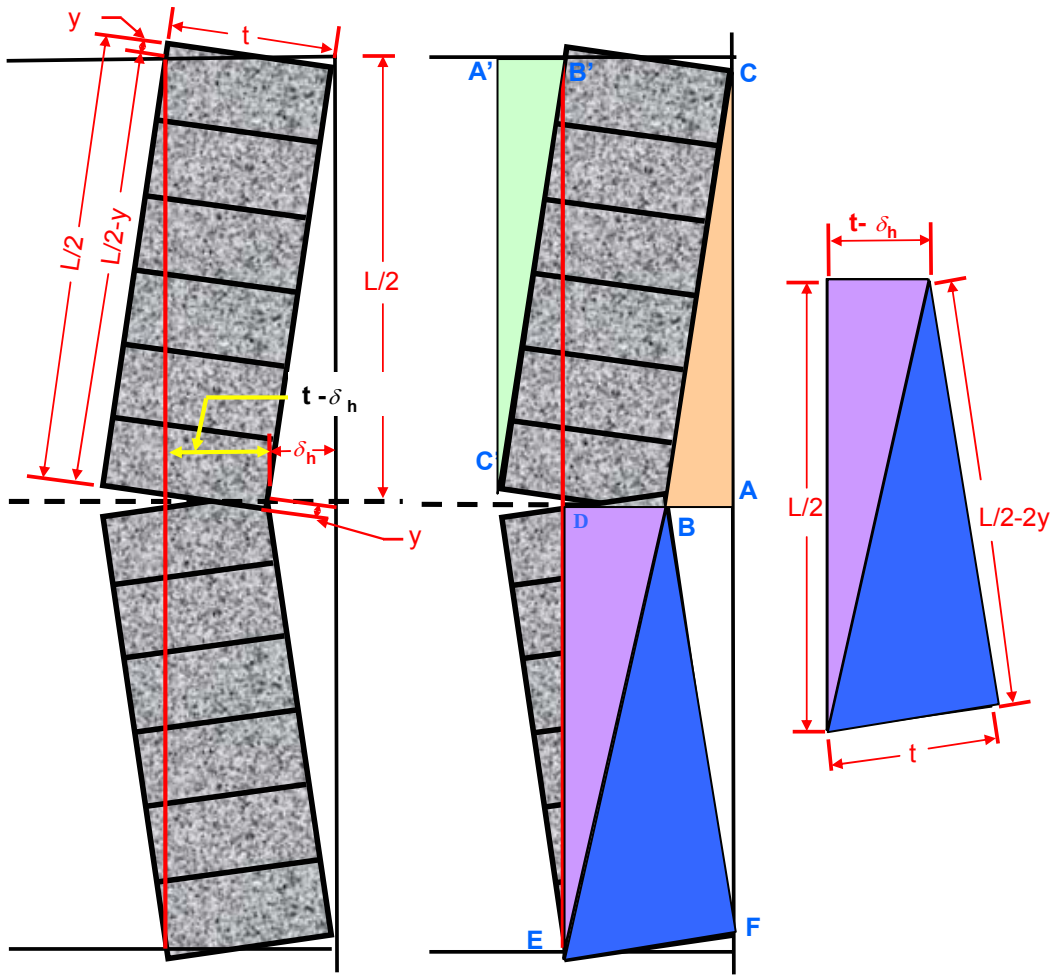

Figure 6-3. Diagram of wall geometry as a function of the lateral displacement.

First, examine triangle ABC (beige-shaded triangle) that is formed by the lateral displacement of the wall. The lateral displacement is equal to the side AB in this triangle. By similarity, examining triangle A′, B′, C′ (green-shaded triangle), it is seen that A′B′ also equals the lateral displacement of the wall. Now consider the purple-shaded triangle labeled BDE. Examining the geometry shows that the side BD is equal to the wall thickness (t) minus the lateral displacement (δ_h). The length of side DE is equal to the half-wall length (L/2). Using the rule that the length of the hypotenuse squared is equal to the sum of the squared lengths of the other two sides of a triangle, the following relationship can be developed.

$$\left(\frac{L}{2}\right)^2 + (t - \delta_h)^2 = \overline{BE}^2 \qquad \textbf{(6.5)}$$

Next, examine the blue-shaded triangle BEF that shares the same hypotenuse as the purple-shaded triangle BDE. The length FE is equal to the thickness (t) of the wall. Examining the geometry of the wall shows that BF is equal to the half-wall length (L/2) minus the deformation of each crush zone (y). Using the same rule as applied above, the following relationship is developed for triangle BEF.

$$\left(\frac{L}{2} - 2y\right)^2 + t^2 = \overline{BE}^2 \qquad \textbf{(6.6)}$$

Equations 6.5 and 6.6 can be combined to form equation 6.7.

$$\left(\frac{L}{2}\right)^2 + (t - \delta_h)^2 = \left(\frac{L}{2} - 2y\right)^2 + t^2 \qquad \textbf{(6.7)}$$

Equation 6.7 can then be solved for the hinge area deformation using the quadratic equation ($y = ax^2 + bx + c$), once the terms are computed and simplified as shown in equation 6.9. Equation 6.10 is the solution used to determine the hinge area deformation (y) if the lateral displacement (δ_h) is known for a particular wall thickness (t) and wall height (L).

$$\left(\frac{L}{2}\right)^2 + t^2 - 2 \times t \times \delta_h + {\delta_h}^2 = \left(\frac{L}{2}\right)^2 - 2 \times \frac{L}{2} \times 2y + (2y)^2 + t^2 \qquad \textbf{(6.8)}$$

$${\delta_h}^2 - 2 \times t \times \delta_h + 2 \times L \times y - 4 \times y^2 = 0 \qquad \textbf{(6.9)}$$

$$4 \times (y)^2 - 2 \times L \times (y) + \left[2 \times t \times \delta_h - \delta_h^2\right] = 0$$

Quadratic equation solultion $\quad \mathbf{y} = \dfrac{-b \pm \sqrt{b^2 - 4 \times a \times c}}{2 \times a}$

$$y = \frac{2 \times L \pm \sqrt{4 \times L^2 - 32 \times t \times \delta_h + 16 \times \delta_h^2}}{8} \qquad \textbf{(6.10)}$$

Figure 6-4 shows the thrust force developed as a function of lateral displacement for wall stiffness of 80, 120, and 160 kips/in based on an elastic modulus of 40,000, 60,000 and 80,000 psi, respectfully. As seen from this theoretical analysis, the arch thrust increases proportionally with increasing material modulus. From this, it can be deduced that the resulting transverse pressure will also increase proportionally with the arching thrust. The chart shows that the arching thrust will continue to increase with lateral displacement since there is no limit on the material strength in this example. If the arch thrust is limited to the compressive strength of the material, the arch thrust will not continue to increase, and as such, will limit the transverse load capacity of the stopping.

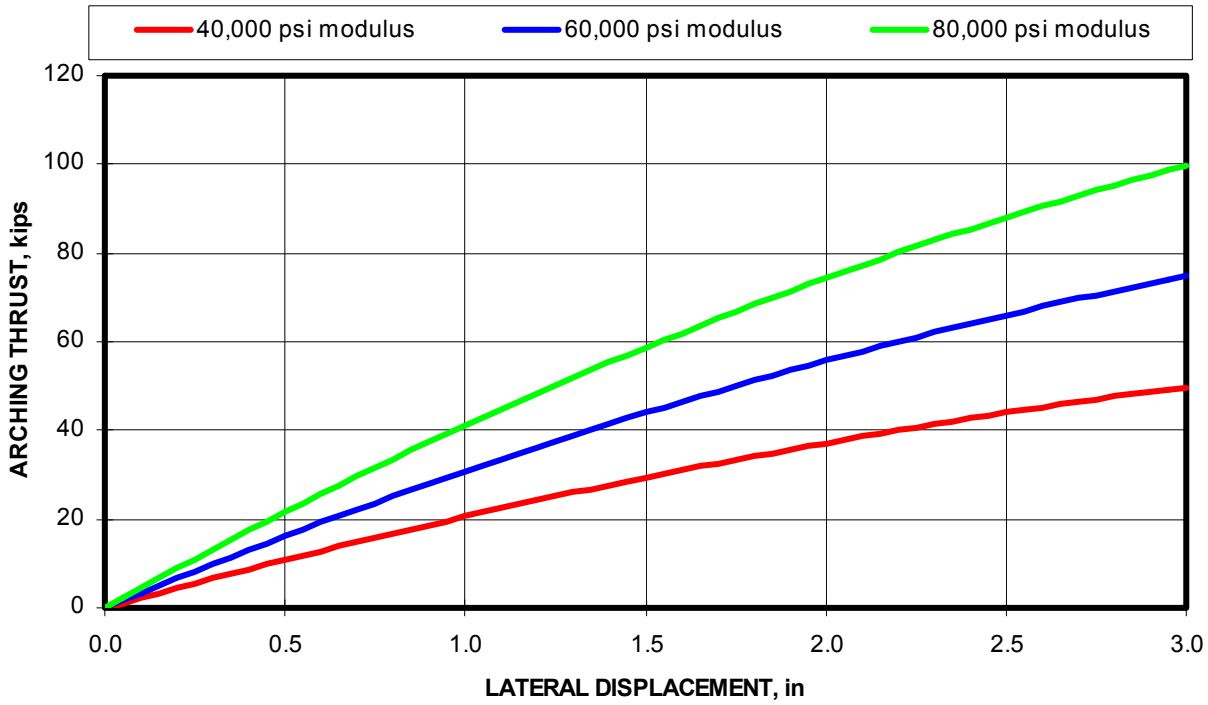

Figure 6-4. Impact of wall stiffness on transverse load capacity.

6.5 LATERAL DISPLACEMENT

The lateral displacement also plays a big role in determining the transverse capacity of a block stopping. The diagram in figure 6-5 illustrates the change in wall geometry due to lateral displacement. As seen in figure 6-5, the width of the arch, represented by the distance between the resultant thrust forces and mathematically expressed as $0.8 \times t - \delta_h$, will decrease as the lateral deflection of the wall increases. The decrease in the width of the arch will cause a proportional decrease in the transverse load capacity of the wall, since the force couple produced by the arch thrust will decrease.

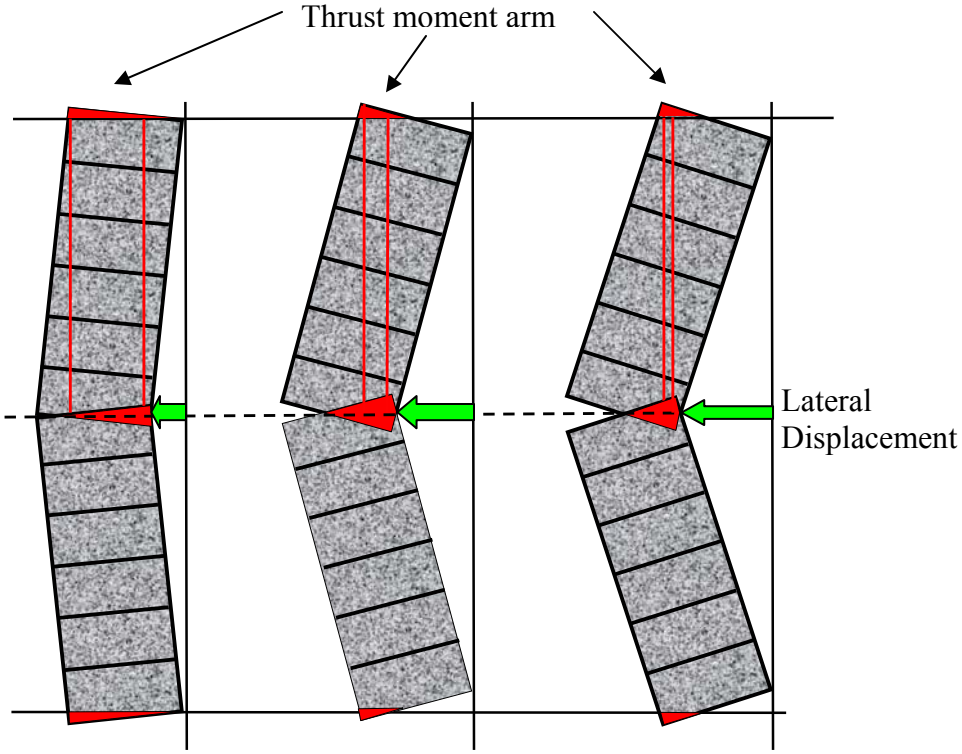

Figure 6-5. Diagram showing that lateral displacement of the stopping reduces the arch width.

Figure 6-6 illustrates a hypothetical example of the impact of the lateral displacement of the wall on the transverse load capacity. In this example, a constant arching thrust of 31,500 lbs, representative of the thrust acting per unit block width, is considered. The wall thickness is 6 inches. Half-wall heights (L/2) of 30, 45, and 60 inches are considered. The theoretical transverse pressure is calculated from equation 5.4.

As shown in this figure, the transverse pressure decreases with increasing lateral displacement of the wall. The decreasing slope of the curves as the half-wall height increases indicates that the lateral displacement will have a greater magnitude in reducing the transverse pressure for shorter walls than it will for taller walls. For example, an increase in the lateral displacement from 1 to 2 inches, theoretically will cause a decrease in the transverse pressure on a 30-in half-wall height from 2,400 psf to 1,750 psf, a decrease 650 psf. However, for a 60-in half-wall height, the transverse pressure would decrease from approximately 600 psf to 440 psf, a decrease of 160 psf. Expressed as a percentage, the transverse pressure is decreased by approximately 27 pct for all three wall heights when the lateral displacement is increased from 1 to 2 inches.

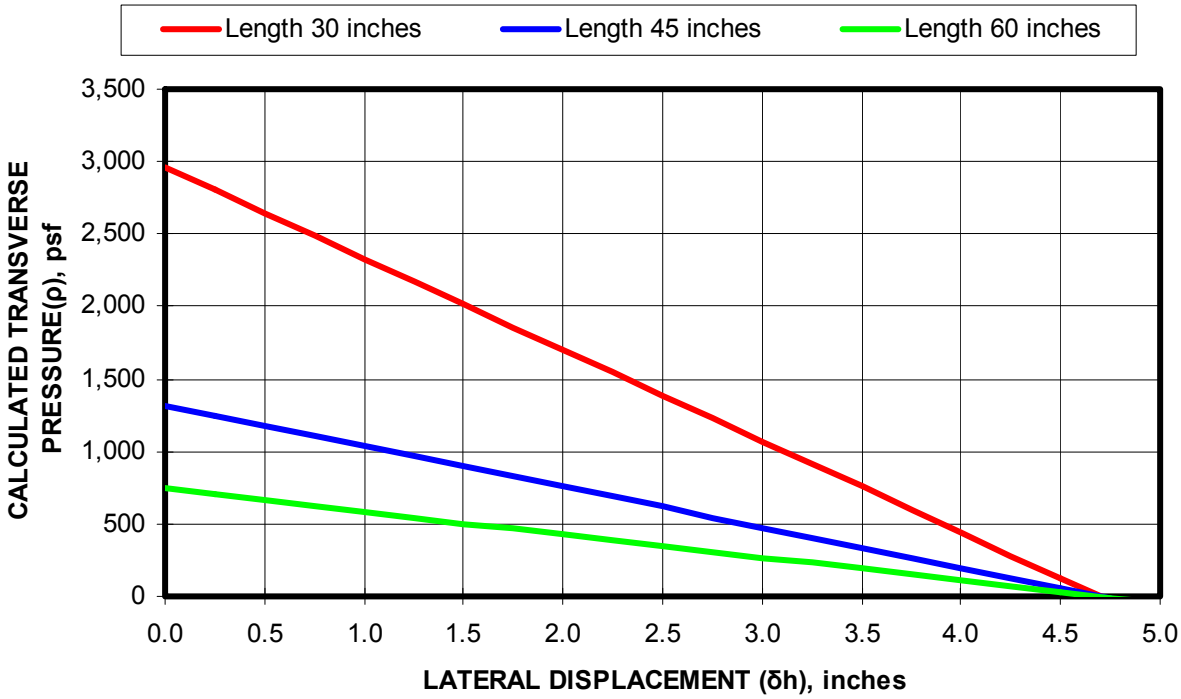

Figure 6-6. Hypothetical example of the impact of lateral displacement on the transverse load capacity of stoppings of various half-wall heights.

Further examination of the chart in figure 6-6 indicates that the transverse pressure will continue to decrease until the arch width is reduced to zero. For the 6-inch wall thickness used in the example considered in figure 6-6, this will occur at lateral displacement of 4.8 inches, given the initial assumption that the resulting thrust force is acting at distance one-tenth of wall thickness from the end of the block. This maximum lateral displacement can be

considered as a limit of stability, beyond which the wall cannot sustain an arching thrust. This concept was illustrated graphically in figure 6-5, which showed how the arch width decreased as the lateral displacement increased.

6.6 COMPRESSIVE STRENGTH AND MATERIAL MODULUS

The compressive strength and the elastic modulus of the block play important roles in defining the transverse load capacity of a mine ventilation stopping. In order to understand the impact of these parameters, the arching mechanics need to be fully understood. As previously indicated, the arching thrust limits the capability of the wall to sustain transverse pressure. The transverse load capacity of a stopping wall is limited even if the material strength has not been exceeded, because the rotation of the wall impacts the development of the arching thrust and moment equilibrium requires that the force couple developed with the arching thrust and the transverse pressure must balance. As was shown in figure 6-4, the arch thrust as a function of the lateral wall displacement will be larger for higher modulus materials than it will be for lower modulus materials. As a result, the transverse load capacity will be greater for higher modulus materials for a wall of a given geometry (thickness and height).

A theoretical example is shown in figure 6-7. In this example, three modulus values are considered: (1) 40,000 psi, (2) 60,000 psi, and (3) 80,000 psi. The peak transverse pressure occurs at 2 inches of lateral displacement for all three walls, since this is determined by the wall thickness and height. However, the peak transverse pressure for the 80,000-psi modulus material is twice that of the 40,000-psi modulus wall construction, since the transverse pressure is directly related to the material modulus. Is this example, the compressive strength of the block does not affect the transverse load capacity, only the mechanics of the arch formation is considered. Figure 6-8 shows what the outcome would be if it assumed that the 40,000-psi modulus wall reached the full strength of the block at the peak transverse pressure, and this same block strength was assumed for the other two wall constructions with the 60,000 and 80,000-psi modulus materials. It is seen that although the block strength limits the transverse load capacity of the 60,000 and 80,000-psi modulus walls, the transverse load capacity continues to be greater for the higher modulus walls.

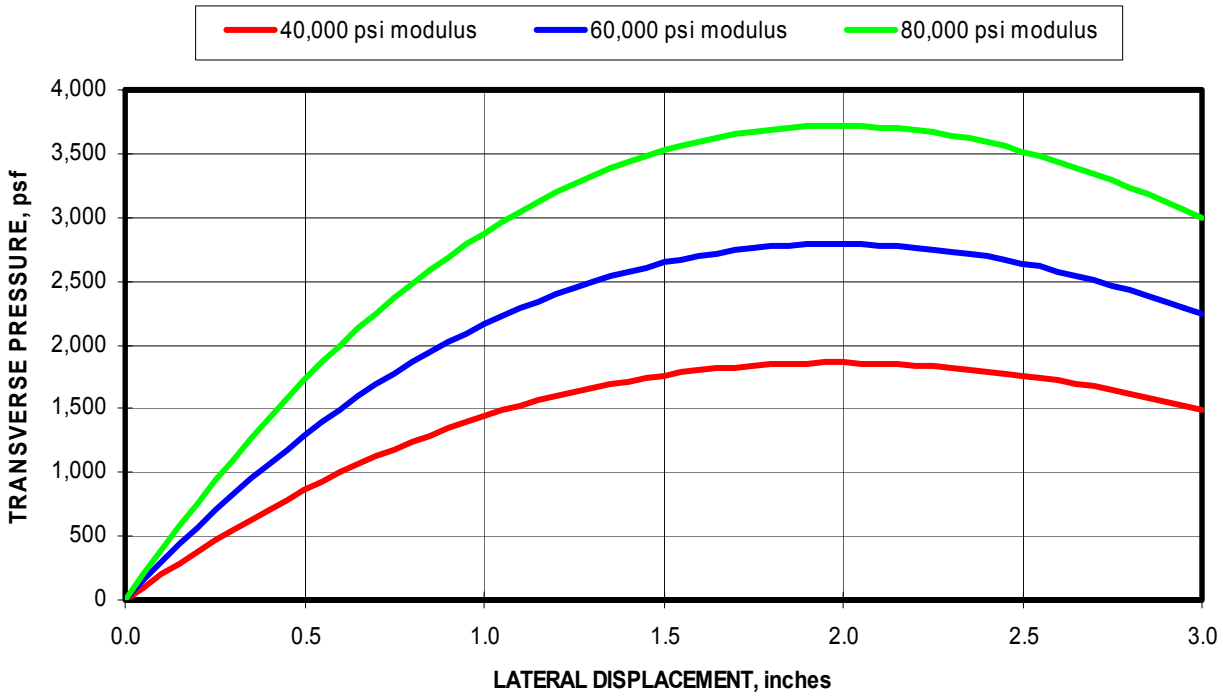

Figure 6-7. The transverse load capacity of a stopping is directly related to the material modulus of the block from which the stopping is constructed.

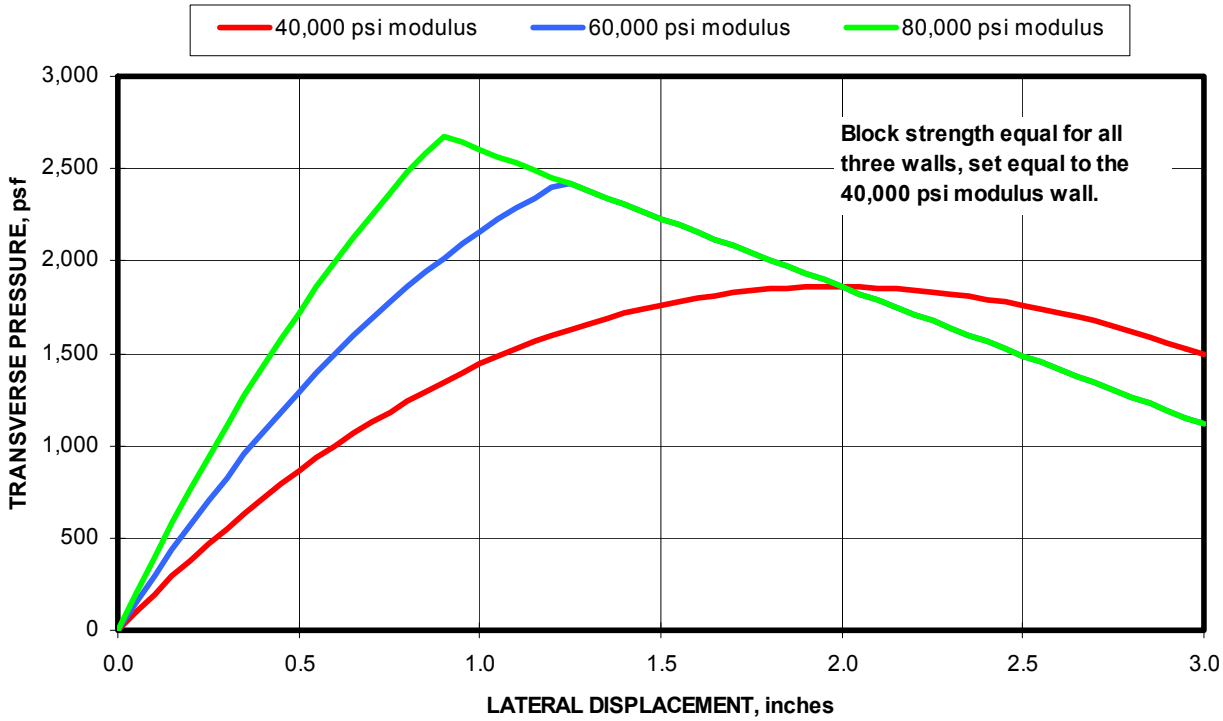

Figure 6-8. Chart shows transverse load capacity if all block had the same compressive strength.

Figure 6-9 illustrates the required the block strength if the peak transverse pressure were equal for all three walls. As seen in the chart in this theoretical example, the block strength would be equal to a 2,066 psi for the lowest modulus block (40,000 psi), 1,396 psi for the 60,000-psi modulus block, and 1,310 psi for the 80,000-psi modulus block. Following this analysis, it can be seen that there is an optimum block strength that is needed to ensure that the full transverse pressure potential is realized. However, it is also seen that this optimum strength increases with increasing material modulus. For this theoretical example, the optimum strength would be approximately 2,000 psi for the low modulus (40,000 psi) material, but it would double to 4,000 psi for the high modulus (80,000 psi) material. Beyond this, the transverse pressure will be controlled by the arching mechanics and the benefit of the higher block strength will not be realized in the transverse pressure development of the stopping. Following this logic, it can also be seen that it is theoretically possible for a lower strength block to provide more transverse load capacity than a higher strength block, if the modulus of the higher strength block is sufficiently lower than that of the lower strength block. While this is unlikely for block of similar materials, it may occur for blocks fabricated from dissimilar materials.

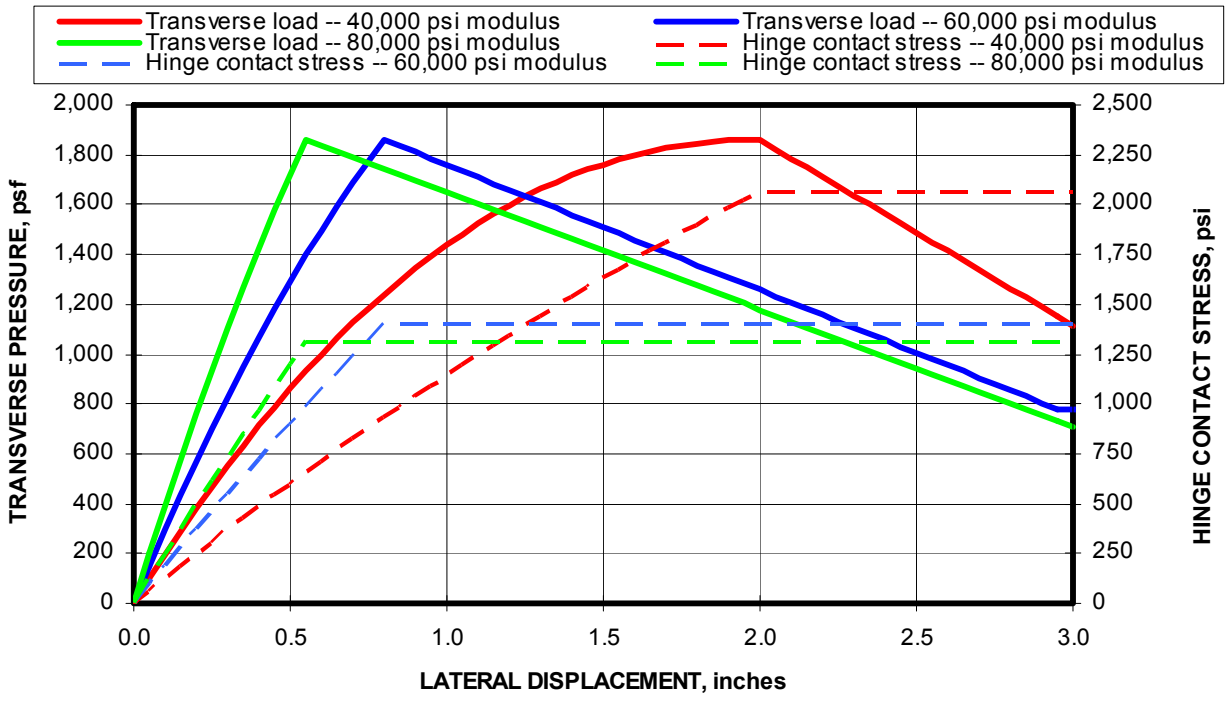

Figure 6-9. Dashed lines show the required block strength to provide the same transverse load capacity for all three walls.

6.7 OTHER FACTORS THAT IMPACT THE TRANSVERSE LOAD CAPACITY OF A STOPPING

Other factors that may impact the transverse load capacity of a stopping include: (1) stiffness of the abutments, (2) use of strain softening materials within the wall to absorb ground deformation, (3) compressive loading of the wall from ground pressures, (4) use of wedges to tighten the wall against the mine roof during construction, and (5) use of prestressing devices such as grout bags to seal the perimeter around the stopping.

6.7.1 Impact of Abutment Stiffness

Up to this point, the analysis has assumed a rigid arching condition whereby the abutments are assumed not to deform. Under rigid arching conditions, as shown in the previous analysis, the lateral displacement of the wall is controlled by the stiffness and elastic response of the block wall. It was shown that the transverse load capacity will decreases as the block modulus decreases since more lateral displacement will occur. The increase in lateral displacement reduces the force couple provided by the arching thrust and this causes a decrease in the transverse load capacity of the stopping. If the abutments are not rigid, then the lateral displacement will increase further, resulting in a further reduction in the transverse load capacity of the stopping.

The problem can be analyzed in terms of the stiffness of the system. The system consists of both the wall and the abutments. Since the wall and the abutments act in series with one another, the system stiffness can be expressed by equation 6.11.

$$K_{System} = \frac{K_{wall} \times K_{abutment}}{K_{wall} + K_{abutment}} \qquad \textbf{(6.11)}$$

Where K_{system} = system stiffness, lbs/in,

K_{wall} = wall stiffness, lbs/in, and

$K_{abutment}$ = abutment stiffness, lbs/in.

If the stiffness of the abutment is infinity (perfectly rigid abutment), then the wall stiffness will control the lateral displacement associated with the arching thrust through the deformation of the block as described in the previous section. However, examining equation

6.11 shows that if the abutment stiffness was equal to wall stiffness, the system stiffness would be reduced by 50 pct. Therefore, a small change in the abutment stiffness can cause significant changes in the arching capacity and transverse load capacity of a stopping.

Figure 6-10 shows that a nonlinear relationship exists between the extension into the abutment zone and the resulting lateral displacement of the wall. As the deformation of the abutment increases due to the arching thrust, the lateral displacement increases more quickly. It is also seen that the increase in lateral displacement as a function of increased deformation of the abutment is greater for taller walls than for shorter walls.

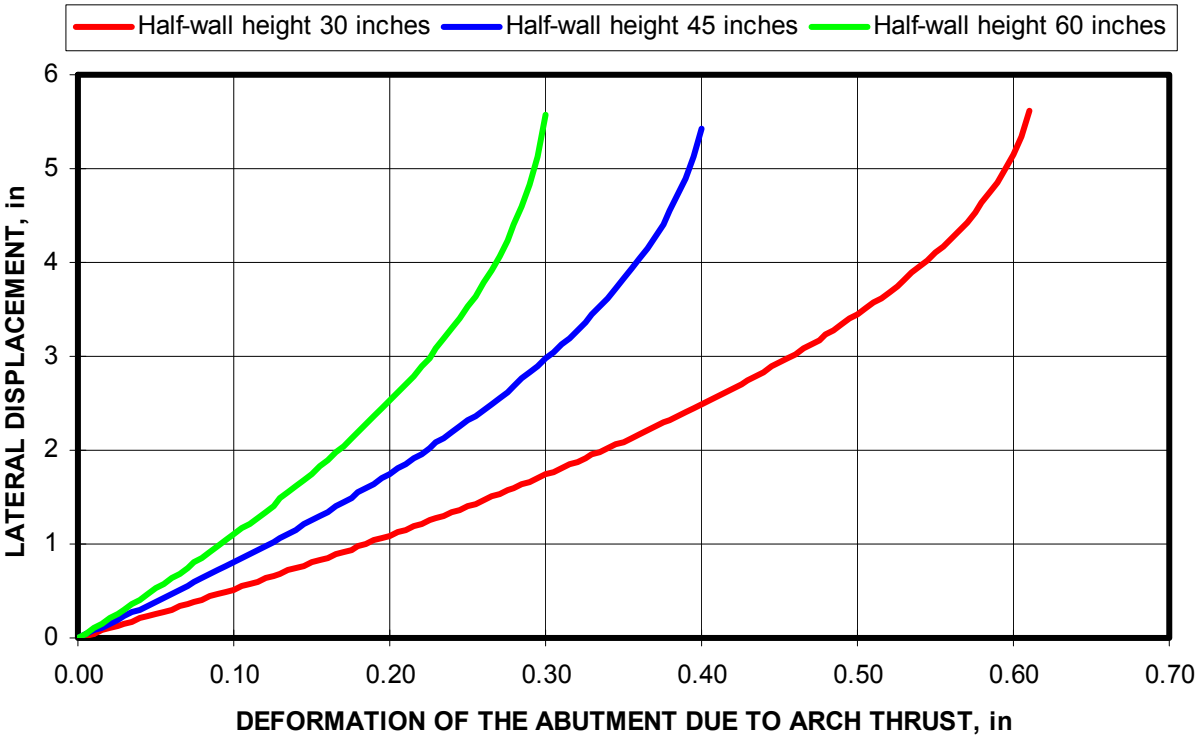

Figure 6-10. Impact of reduced abutment stiffness expressed as deformation of the abutment due to arch thrust on the lateral displacement of the stopping wall.

An experiment to show the significance of the abutment stiffness was conducted. A 45-in-high half-wall made from Portland cement block with a compressive strength of 1,727 psi was constructed for testing in the MRS, and a piece of ½-inch-thick drywall was placed on top of the wall (see figure 6-11). The impact of the drywall is shown in figure 6-12, which compares the transverse pressure from an identical wall without the drywall. As seen in figure 6-12, the transverse pressure was reduced from 888 psf to 178 psf. The lateral displacement at which the peak transverse pressure occurred increased from 1.35 inches to

1.98 inches. Therefore, a 47 pct increase in lateral displacement of 0.63 inches, caused the transverse pressure to decrease by 710 psf or 80 pct.

Figure 6-11. Test configuration using drywall to soften the abutment stiffness.

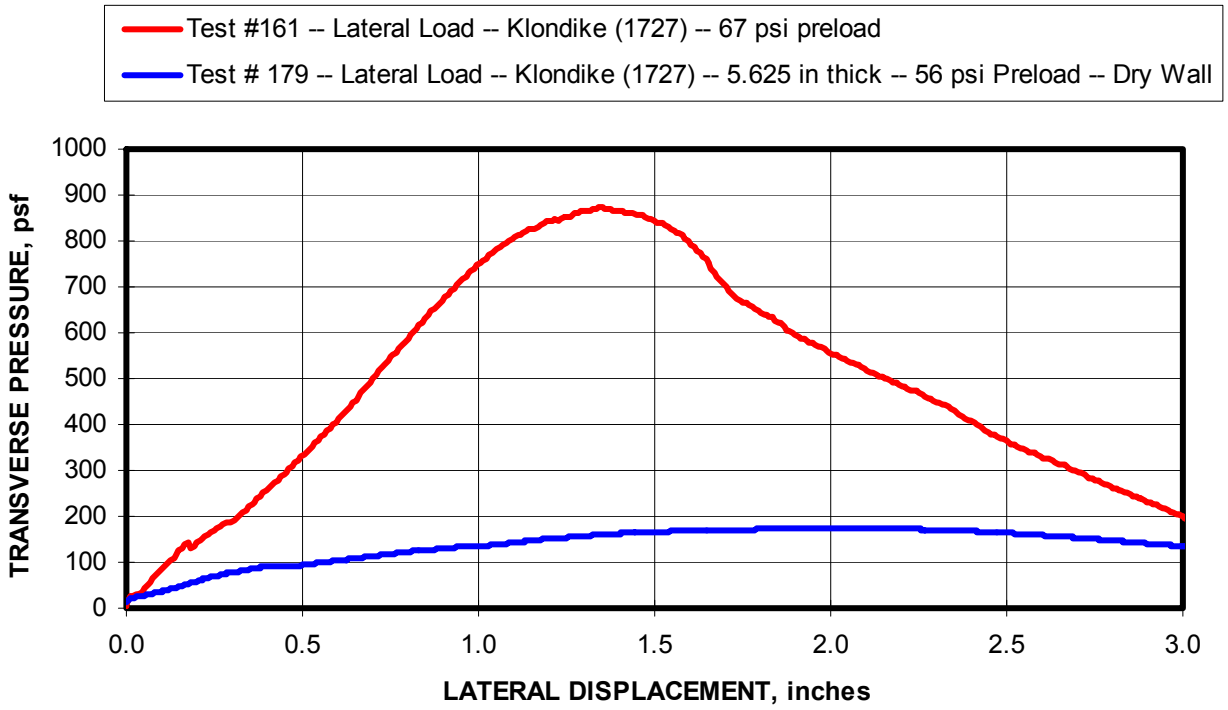

Figure 6-12. Comparison of transverse pressure determined from half-wall testing in the MRS with rigid abutment (red curve) and softened abutment from drywall roof contact.

Figure 6-13 shows a close up view of the deformation of the drywall after the completion of the test documented in figure 6-12. An indentation of approximately 1/10 of an inch occurred at the edge where the concrete block was imbedded into the drywall. Following the analysis presented in section 6.7.1, it is determined that a system modulus of 26,000 psi representing the combined effect of the block wall and drywall roof contact, would produce a reasonable approximation of the transverse pressure for this configuration as shown in figure 6-14. With a system modulus of 26,000 psi and a block modulus of 80,000 psi for this particular block, the modulus of drywall would be about 400 psi as determined from equation 6.11.

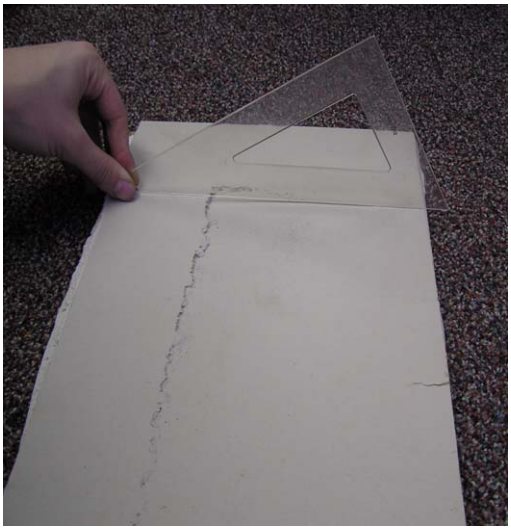

Figure 6-13. Close up view of the deformation of the drywall caused by the arching thrust force.

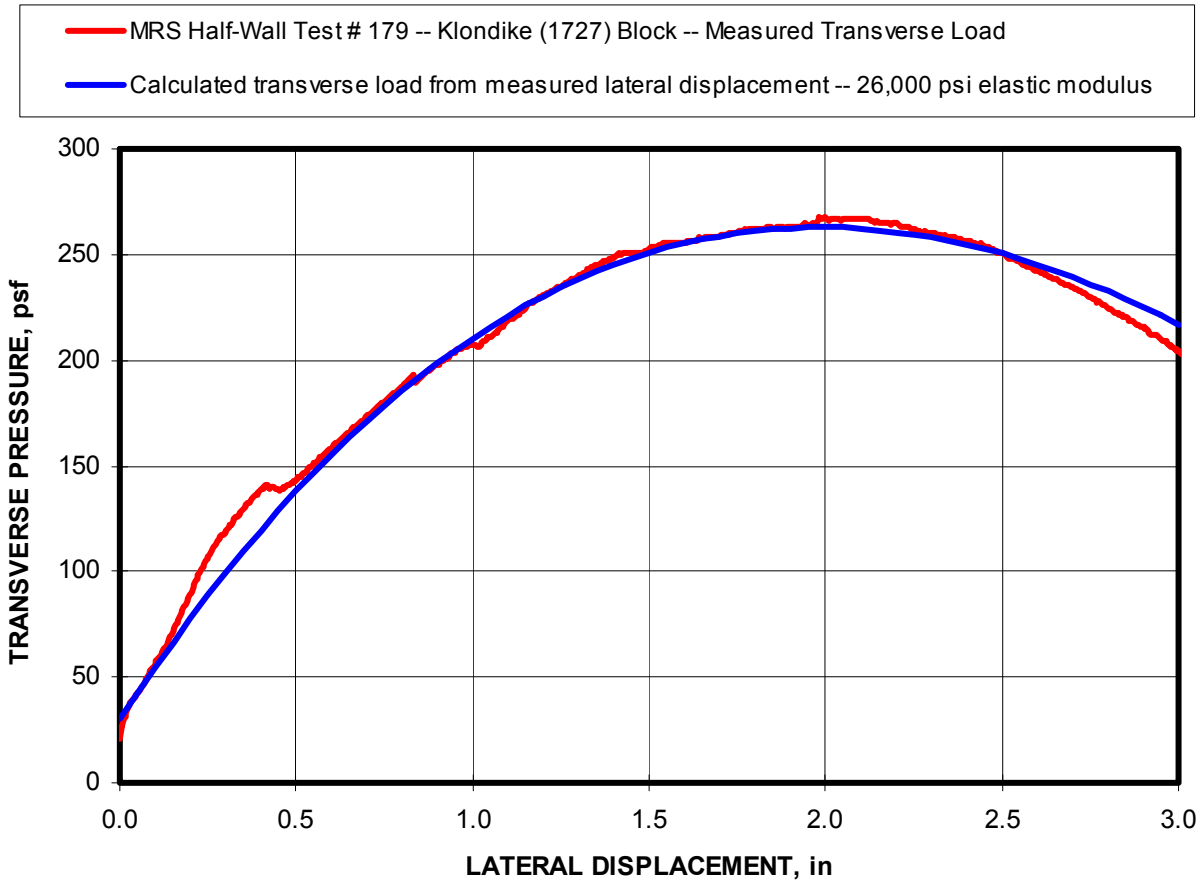

Figure 6-14. Comparison of theoretically predicted transverse pressure using the assumed 26,000-psi system modulus for the drywall abutment test and the measured transverse pressure.

In summary, the abutment stiffness can have a major impact on the transverse load capacity of a stopping. A relatively small abutment deformation of approximately 1/10 of an inch was shown to reduce the transverse pressure by 80 pct in one example. It was shown that the transverse pressure could be accurately predicted by considering the system stiffness of the block wall and the abutment if the lateral displacement is known.

6.7.2 Impact of Strain Softening of Walls to Absorb Ground Deformation

Although concrete block stoppings have considerable load resistance compared to most standing roof support systems, they often cannot fully control the ground movement, and therefore are still subject to the closure of the mine entry. Since they are very stiff structures, they can absorb relatively little deformation, less than 1 pct strain, prior to compression loading failures that destroy the integrity of the structure to function effectively

for ventilation control (Burke, 2004 and Kawenski, 1966). Figure 6-15 shows a photo of a section of a stopping wall damaged from closure of the mine opening.

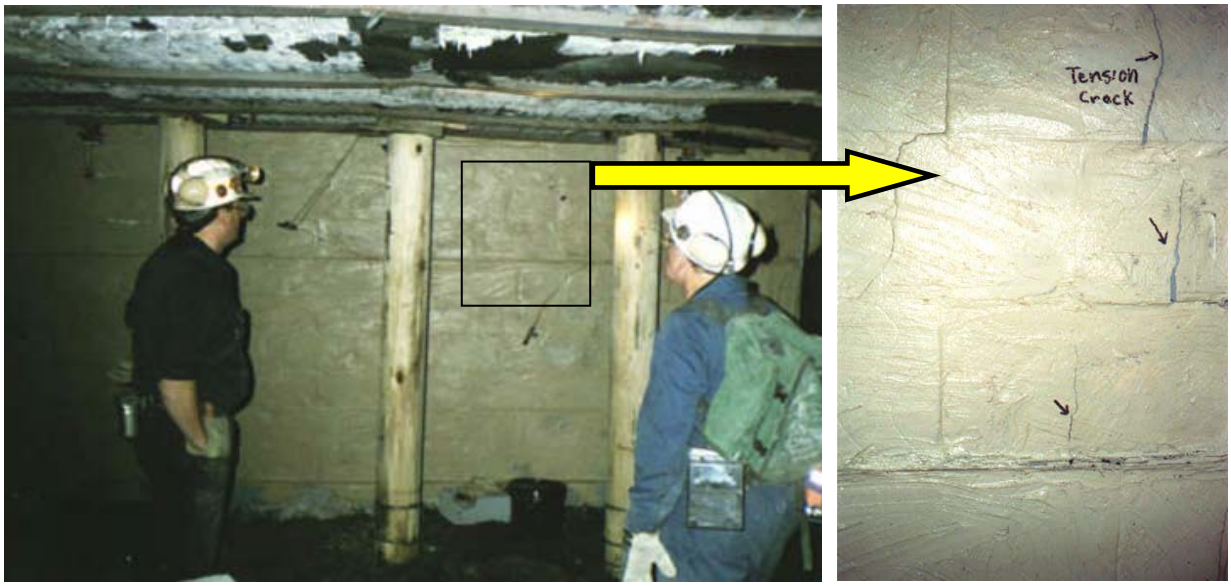

Figure 6-15. Damage of a stopping caused by roof-to-floor convergence of a mine entry.

In such conditions, some sort of strain softening material is typically incorporated into the construction to extend the life of a block stopping by allowing the wall to absorb some deformation without developing excessive compressive stresses that lead to premature failure. Currently, the most commonly used material is expanded polystyrene foam formed into squeeze blocks or planks that are sandwiched between one or more courses of a block stopping. Figure 6-16 shows a 4-ft-wide section of a stopping wall with a 2-in-thick foam plank placed between the top two courses of block, showing the wall before and after failure during a laboratory test. Figure 6-17 compares the response of the wall for vertical loading. As seen in figure 6-17, the foam increases the displacement at which failure occurs, thereby increasing the capability of the wall to yield to the simulated roof-to-floor closure of the mine entry.

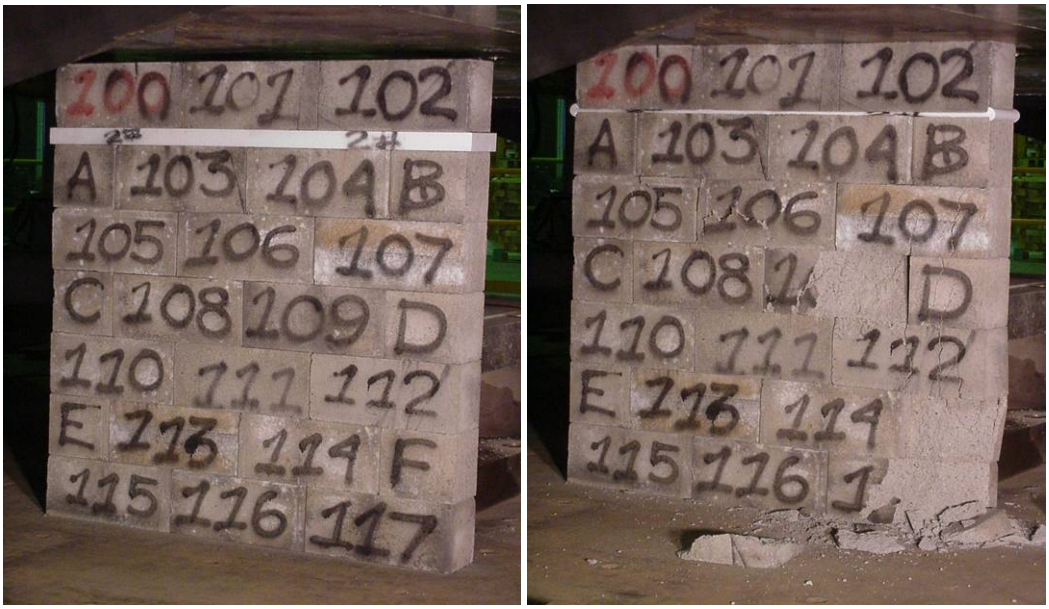

Figure 6-16. Two-inch-thick foam plank used to reduce the stiffness and extend the life of a block stopping by allowing the wall to absorb some deformation prior to failure. Only vertical loading is applied in this test.

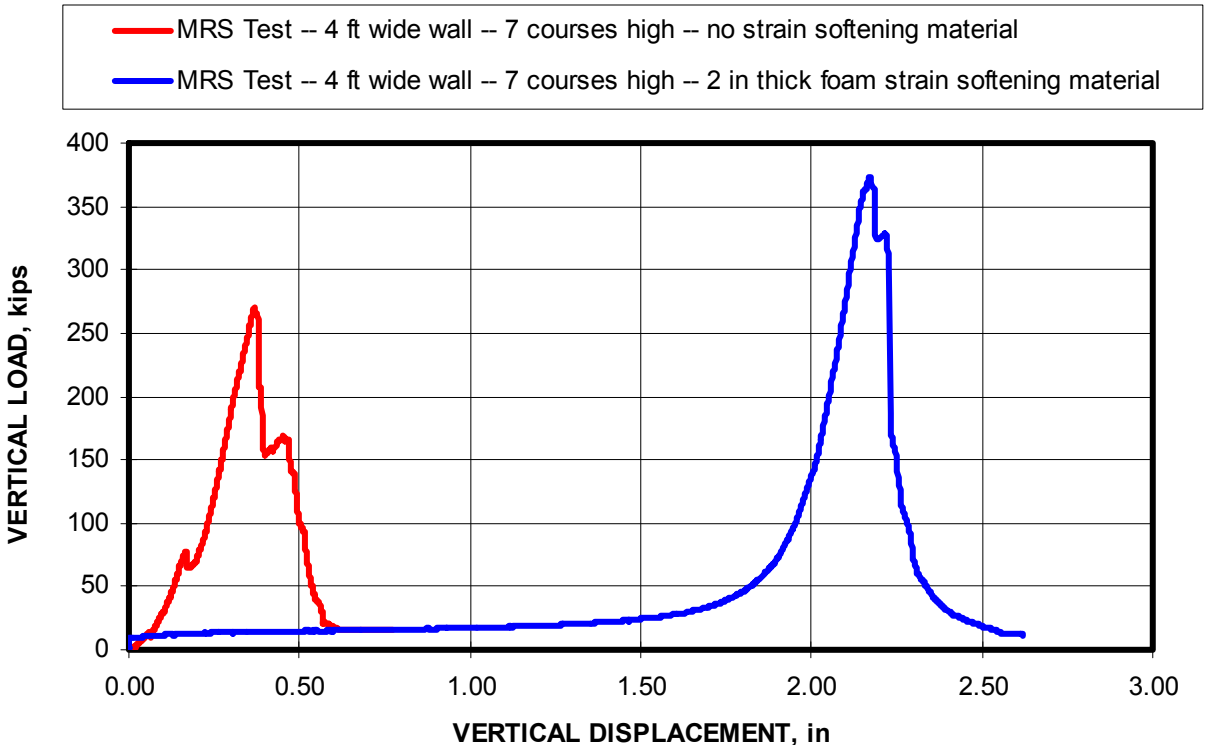

Figure 6-17. Comparison of a block stopping wall's response to vertical loading with and without a strain softening foam layer.

Although the foam is effective in enhancing the yield capability of the wall and extending the service life of the stopping in response to the closure of the mine opening, what does it do to the transverse load capacity of the stopping? As previously demonstrated, the transverse load capacity of a stopping is dramatically increased if arching can be established. As described in section 6.7.1 in the discussion of abutment stiffness, it was seen that an abutment deformation as little as 0.1 inches can degrade the transverse load capacity of a stopping by 80 pct (see figure 6-12 and 6-13). Figure 6-10 showed the theoretical relationship between the deformation of the abutment and the lateral displacement of the wall, and figure 6-6 showed the impact of increasing wall displacement on reducing the transverse load capacity of a stopping. The hypothesis developed from this assessment is that low-density foam, such as that commonly used in strain softening for mine ventilation stoppings, will not preserve the arching loading mechanism, and as such, severely degrade the transverse load capacity of the stopping.

In order to evaluate this hypothesis, a series of half-wall tests in accordance with the protocol developed in chapter 4, section 4.2, were conducted in the Mine Roof Simulator with foam as a strain softening material. The foam utilized in these tests was a 2 lb/cu ft density, polystyrene product manufactured by OPCO, Inc. in Latrobe, Pennsylvania. The product trade name is MS Blox EPS Squeeze Blocks. The foam plank was placed between the top two blocks in the half-wall as shown in figure 6-18.

Figure 6-18. Half-wall test in the MRS with 2-inch-thick foam plank placed between the top two blocks.

Figure 6-19 compares the results of two half-wall tests conducted in the MRS, one with the foam as shown in figure 6-18 and an identical block column without any foam. The peak transverse pressure without foam was 510 psf, while the peak transverse pressure with the foam-softening layer was 28 psf. The foam reduced the transverse load capacity in this test by 95 pct.

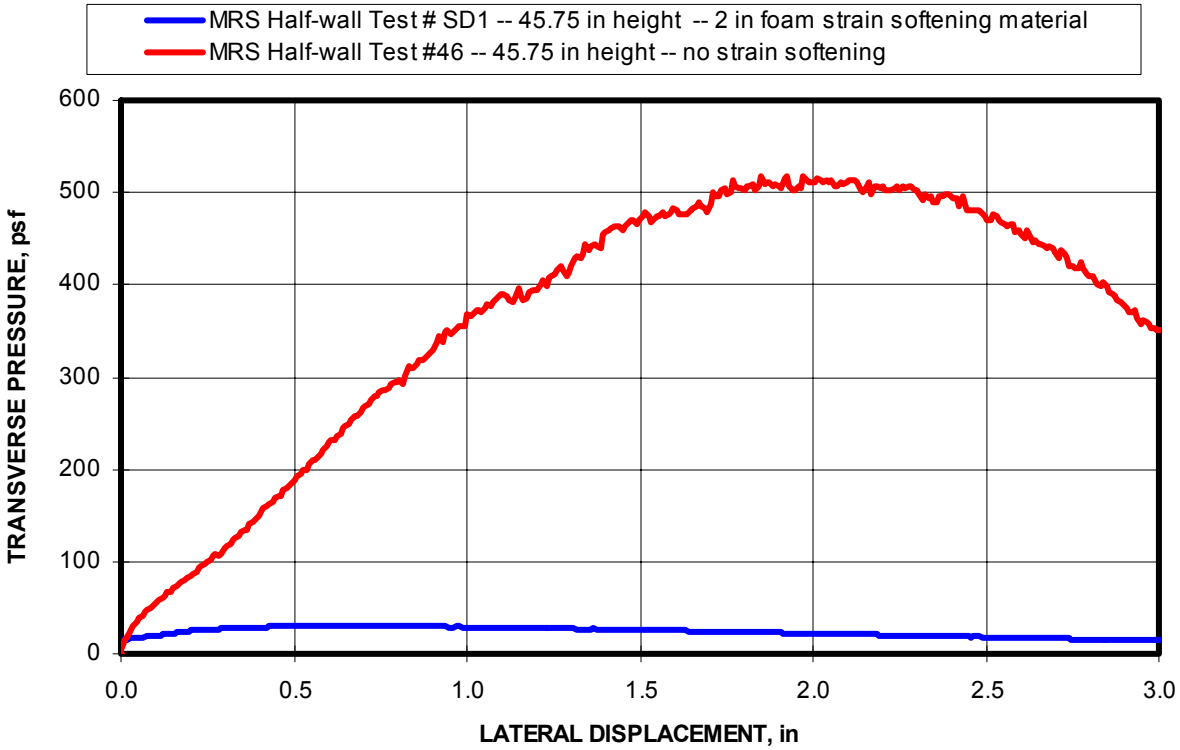

Figure 6-19. Comparison of transverse pressure development from half-wall testing in the MRS on a block wall with and without a strain-softening foam layer.

Further analysis reveals why the foam degraded the transverse pressure so severely. The low density foam has a very low modulus of elasticity. The stress-strain behavior is shown in figure 6-20 for a 12-inch long section of foam plank as tested in a MTS rock testing load frame. As seen in this figure, the modulus of elasticity is negligible through nearly 20 pct strain. This means that the foam provides very little resistance to the extension of the tension side of the wall as it rotates about the hinge points under the application of transverse pressure. The consequence of this is that little arching thrust will be developed and excessive lateral displacement will occur, the combination of which severely limits the transverse load capacity of the wall. Figure 6-21 shows the condition of the half-wall tested in the MRS

shown at 3 inches of lateral displacement and a second wall after 7 inches of lateral displacement. It is seen from figure 6-21 that the hinge is formed below the foam layer as opposed to the interface of the top block with the upper platen of the load frame. This indicates that the foam is unable to transfer any significant load between the two blocks, thus limiting the development of the arching thrust.

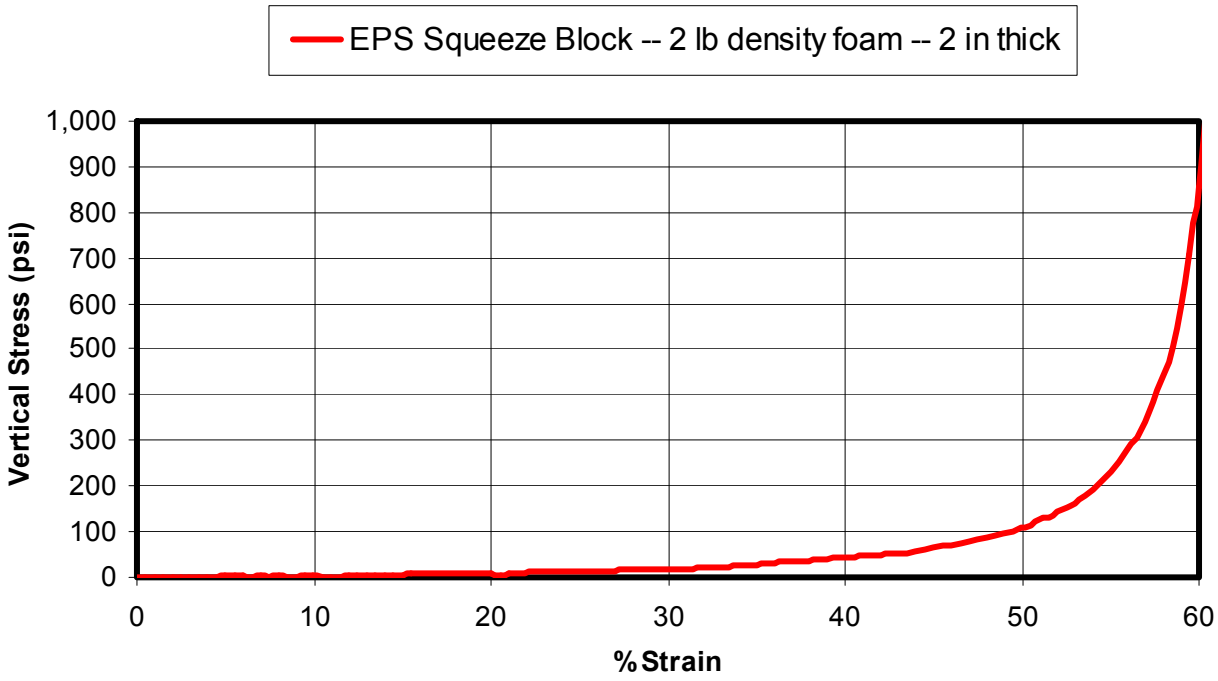

Figure 6-20. Stress-strain relationship for ESP Squeeze Block foam plank commonly used in stoppings to reduce the stiffness of the wall.

Figure 6-21. Half-walls with foam between the top two blocks shown with 3 inches of lateral displacement (left) and 7 inches of lateral displacement (right).

A closer examination of the transverse pressure that does develop with the foam reveals that the peak loading occurred at 0.57 inches of lateral displacement (see figure 6-19). At first, this seems contradictory to the theory presented thus far, which would suggest that the low modulus foam would result in a large lateral displacement at the peak transverse pressure. However, the foam is so soft that the stress distribution across the foam is more uniform and extends over the full width of the block. By examining the photo in figure 6-21, it is seen that the top block in contact with the foam does not rotate away from the upper platen of the load frame unlike the bottom block. The rotation of the wall is occurring at the block below the foam layer. It too remains fully in contact with the foam across its entire area. This implies that the resultant thrust, although very small, is acting more as a distributed load across the entire block and the resultant is closer to the middle of the block compared to conditions without the foam. In this sense, it is similar to the preloading theory explained in the next section.

6.7.3 Impact of Ground Pressures From Roof to Floor Convergence

Even without arching, a superimposed axial or vertical load acting on a stopping wall can greatly increase the transverse load capacity of the stopping. This can be analyzed using conventional beam bending analysis. In essence, vertical loading applied to a wall will act to offset the lack of tensile strength in the joints of a dry-stacking block stopping. The vertical load resists the moment induced by the application of transverse pressure. This condition can be expressed by equation 6.12 (Drysdale, 1994).

$$\rho = S \times F_v \times \frac{8}{L^2} \times 144 \qquad \textbf{(6.12)}$$

Where ρ = transverse pressure, psf,

S = section modulus, in^3/in of wall width or $t^2/6$ where t is the wall thickness,

F_v = axial load per unit area, psi, and

L = wall height, in.

As an example, consider a 5-ft-high wall constructed from conventional concrete block with a thickness of 5.625 inches. This is equivalent to the wall evaluated in test #46 previously analyzed. Using equation 6.12, if a 400-psi pressure is applied to the wall from the ground movement, the transverse load capacity (ρ) of a stopping wall would be computed as 675 psf. Without the ground pressure, this wall would have no transverse load capacity if the weight of the block were ignored as the term F_v would be zero.

$$\rho = \frac{5.625^2}{6} \times 400 \times \frac{8}{60^2} \times 144 = 675 \text{ psf} \qquad \textbf{(6.13)}$$

Next, the impact of ground pressure from the perspective of arching conditions will be examined. Arching relies on the force couple developed from the thrust force to provide the transverse load capacity in a stopping wall. When ground pressure is applied to a stopping, it can be assumed that a uniform load distribution is acting on the top and bottom contact surfaces of the wall. The resultant force under these conditions is acting along the centerline of the wall thickness. In the arching analysis conducted in chapter 5, the resultant thrust load from the arching was assumed to act a distance of one-tenth the wall thickness from the edge

of the block. When these two loading elements, arching thrust and ground pressure, are combined, the resultant force will act somewhere between the two, moving more towards the block centerline as the magnitude of the ground pressure increases (see figure 6-22).

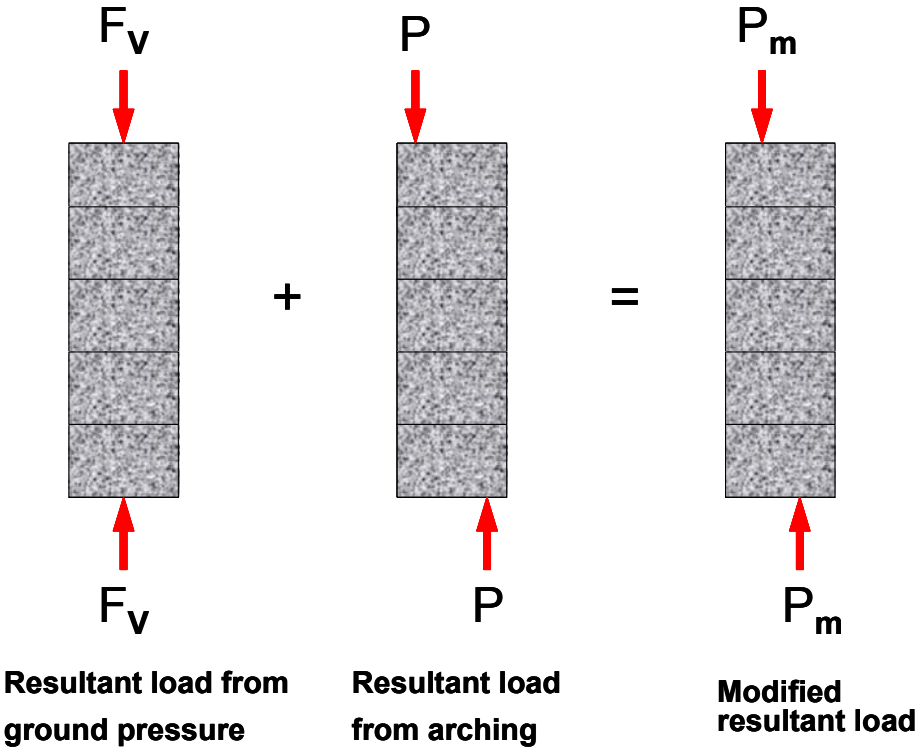

Figure 6-22. Combining arching with axial loading caused by ground pressures moves the resultant arch thrust force more towards the centerline of the wall.

Equation 5.1, which satisfies the moment equilibrium requirement for the half-wall loading, can be used to back calculate the position of the resultant thrust if the thrust force (P), lateral displacement (δ_h), and horizontal force (HF) are known. The wall thickness and height must also be known, allowing the equation to be solved for an adjusted factor to replace the "0.8" term. Hence, by substituting the variable "d" for the value 0.8, the equation can then be solved for "d" to determine the adjusted factor for the position of the resultant thrust force that will satisfy moment equilibrium for a specific axial preload.

$$P \times (0.8 \times t - \delta_h) = HF \times L/2 \quad \textbf{(6.14)}$$

Where P = arching thrust, lbs,
t = thickness of the wall, in,
δ_h = lateral displacement of wall at the mid span, in,
HF = horizontal force, lbs, and
L/2 = half-wall height, in.

$$P_m \times (d \times t - \delta_h) = HF \times L/2 \quad \textbf{(6.15)}$$

$$P_m \times d \times t - P_m \times \delta_h = HF \times L/2 \quad \textbf{(6.16)}$$

$$d = \frac{HF \times L/2 + P_m \times \delta_h}{P_m \times t} \quad \textbf{(6.17)}$$

Where d = position factor for resultant arching thrust,
P_m = modified resultant arching thrust, lbs,
t = thickness of the wall, in,
δ_h = lateral displacement of wall at the mid span, in,
HF = horizontal force, lbs, and
L/2 = half-wall height, in.

The result of the preload will be that the maximum transverse pressure will occur at a smaller lateral displacement. An example for a 30-in half-wall height with conventional Portland cement concrete block is shown in figure 6-23. In this example, the lateral displacement at which the maximum transverse pressure occurred decreased from 1.06 inches to 0.23 inches when the preload was increased from 0 to 491 psi. In essence, the axial load makes it more difficult for the half wall to rotate due to the increased compressive forces acting on the wall. Thus, the transverse pressure is generated more quickly relative to the lateral displacement of the wall.

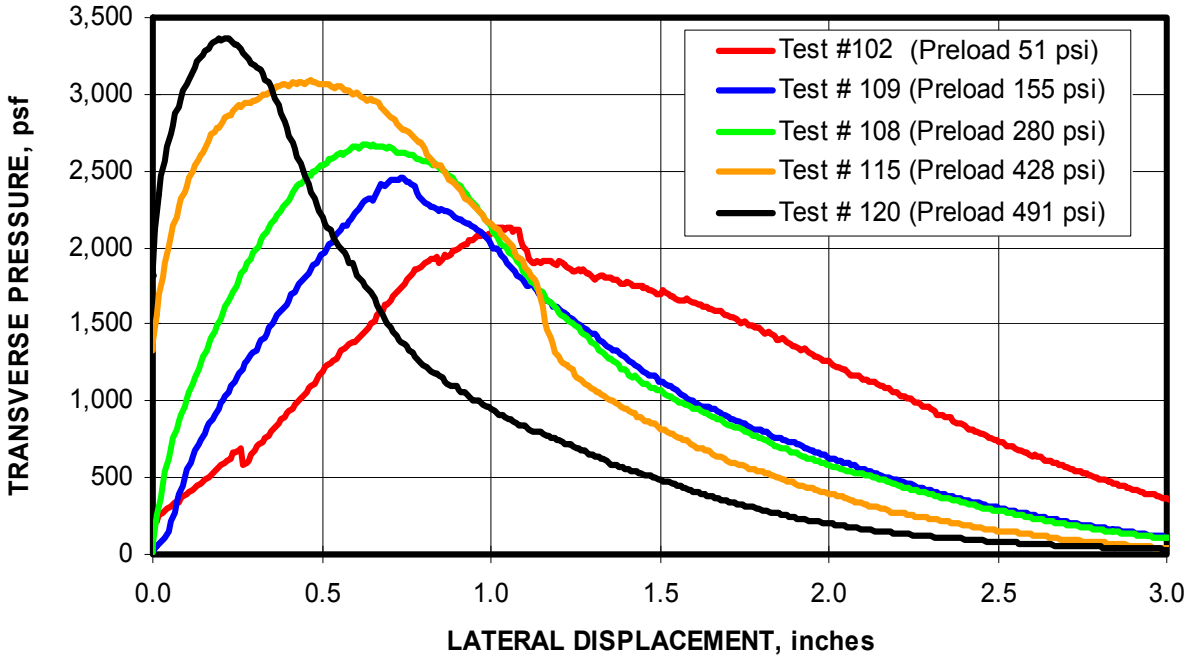

Figure 6-23. Peak transverse pressure occurs at less lateral displacement when preload is applied to the wall.

Preloading should also be examined from the perspective of the abutment stiffness and deformation. If the wall strength is sufficient to transfer the loading to the mine roof and floor, then a concern might be any damage to the immediate roof and floor may significantly degrade the arching capability of the wall. The highest strength stopping blocks have material compressive strengths of less than 3,000 psi and most have material compressive strengths of less than 1,500 psi. Since the wall structure is able to sustain stresses of only about 50 pct of the materials strength, in most cases the wall structure will be damaged long before the mine roof or floor material strength is exceeded.

Boussinesq analyses of linear elastic foundation responses also show that the stress is dissipated or attenuated quickly with depth below the contact area. At a depth of twice the width of the loaded area, the stress is less than 10 pct of the initial vertical stress and equals 90 pct of the initial stress at a depth equal to one-half the radius of the contact area. For a stopping wall that is 6-inches thick, this means that the 90 pct of the stress is relieved with the first 12 inches of ground (Perloff, 1976). Hence, the immediate roof or floor material properties are the most important when considering the abutment stiffness and its impact on

arching of a stopping wall. For layered strata that is common in coal mines, the presence of a strong layer below a weak immediate layer will focus more of the stress in the immediate layer than that indicated in figure 6-24. Even so, the relatively weak block material compared to the strength of mine roof or floor material is likely to prevent failure or punching of the block into the mine roof and floor.

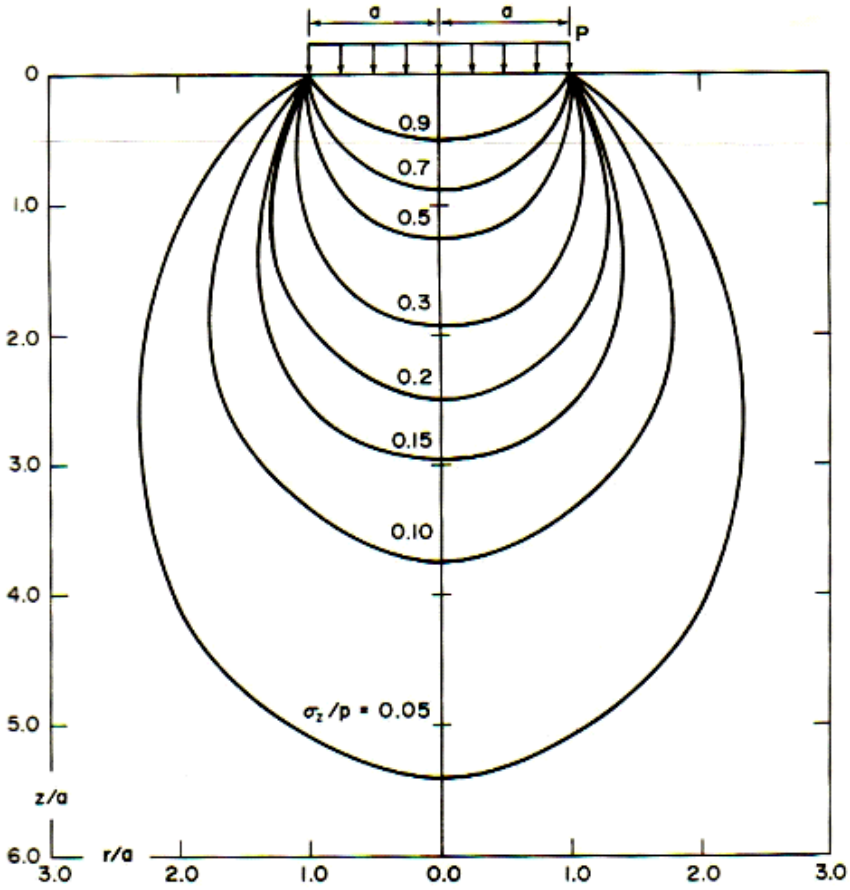

Figure 6-24. Boussinesq diagram shows that 90 pct of the stress is relieved within the first 12 inches of ground for a 6-in-thick stopping.

Although it is suggested from the previous assessment that arching is likely to occur under almost all geologic conditions in a coal mine, it is not to say that arching will not be degraded from the deformation of the immediate mine roof and floor. In fact, any deformation including the elastic response of the roof and floor abutments will reduce the transverse load capacity by causing more lateral displacement of the wall. However, a comparison of modulus between the stopping block wall and the ground also suggests that

the deformations are likely to be small. For example, the modulus of coal is generally about 300,000 psi and the modulus of overburden rock can reach as high as 3,000,000 psi. These are 1 to 2 orders of magnitude higher than the effective modulus of a block stopping wall. Assuming an axial pressure of 300 psi acting on a stopping, this equates to only 0.1 pct strain in an abutment with a modulus of 300,000 psi. If the abutment is 12 inches thick in accordance with the Boussinesq stress analysis, then this translates into only 0.012 inches of deformation. This is an order of magnitude less deformation than will occur in the wall itself at the peak transverse pressure, so the impact will be small, i.e. less than 10 pct in most cases depending on the wall geometry and wall modulus.

If the abutment response is purely elastic, the preload or pressure applied by the wall will not change the deformation response of the abutment. If however, the load-deformation characteristic of the roof or floor material is inelastic, then the preloading may help to stiffen the response of the abutments, and thereby enhance the transverse load capacity of the stopping.

6.6.4 Impact of Wedging the Wall Against the Mine Roof

A common practice when constructing a stopping wall is to use wooden wedges to tighten the wall against the mine roof. Since the wedges are installed at the hinge point, proper installation is critical to preserve the arching action of the wall during transverse loading. The wedges should ***always*** be driven in from the low pressure side of the stopping if done from one direction only, or they should be driven from both sides. This is necessary to ensure contact with the face of the wall where the arching hinge will occur. If the wedges are driven from the high pressure side of the stopping only, there will be a gap at the hinge contact face which will completely destroy the arching capability (see figure 6-25). Figure 6-26 shows this effect including wedges that are driven from the ends of the block, which would be unlikely but possible if the wall was built in step form. As seen in the figure, the transverse pressure is reduced from 500 psf to less than 20 psf when the wedges are applied from the high-pressure side. Figure 6-27 shows that if properly installed, wooden wedges will provide equal transverse pressure capability to walls that do not have any wedges but are in tight contact with the abutment. Some reduction in transverse pressure is realized when a softer pine plank board is used to interface between the top of the wall and the roof abutment.

Finally, figure 6-27 shows that the arching thrust is also preserved when the wedges are properly applied.

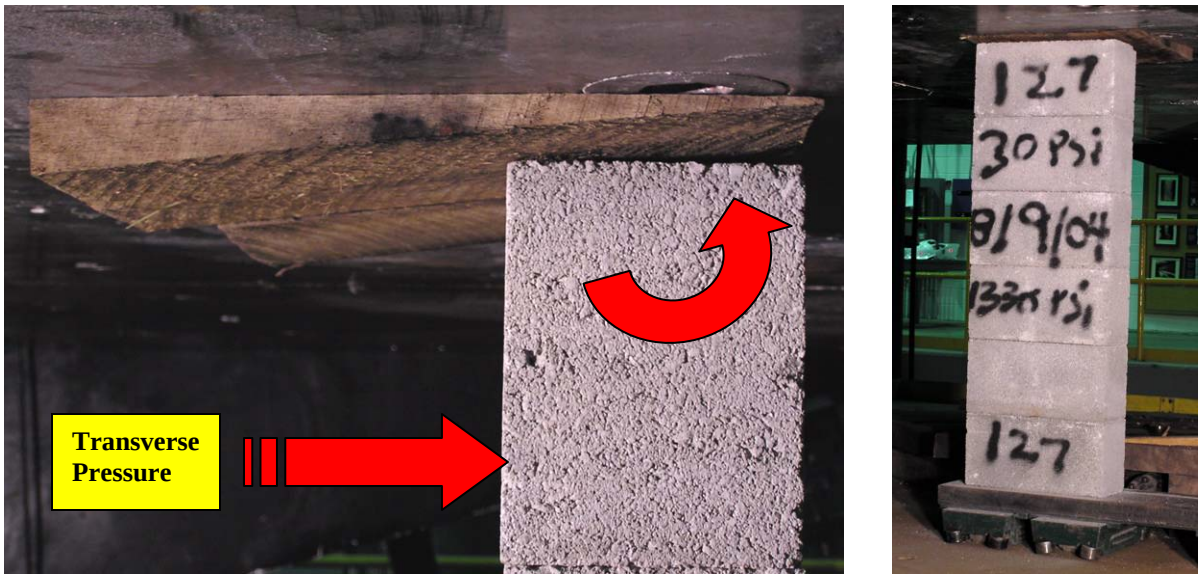

Figure 6-25. Wedges driven into stopping high pressure side allow gap to occur at tension side of stopping which completely destroys arching capability.

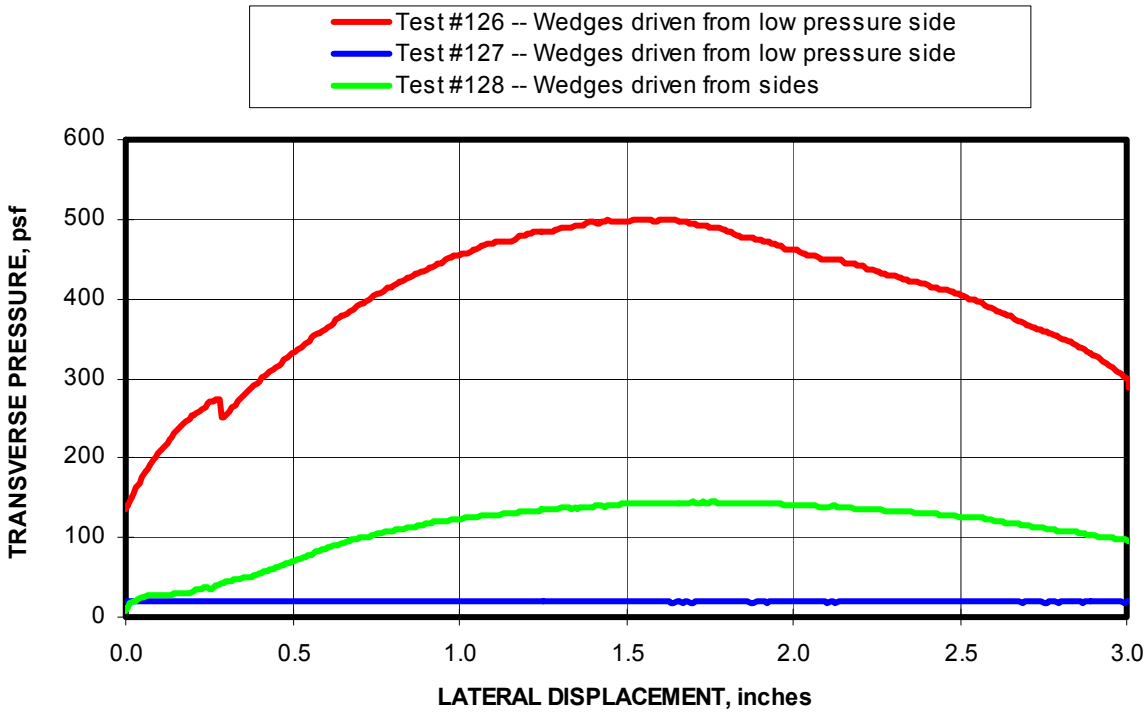

Figure 6-26. Comparison of direction of wedging on top of block stopping relative to impact on transverse load capacity.

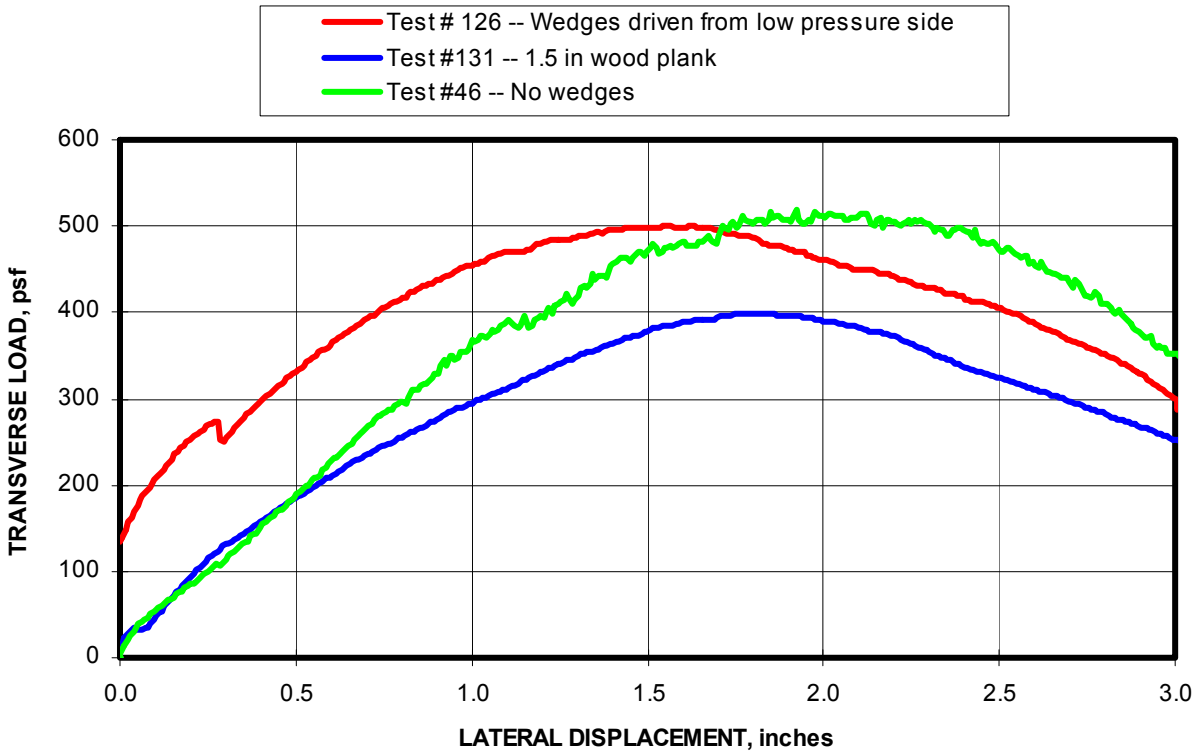

Figure 6-27. Transverse load capacity is preserved when wedges are driven from the low pressure side of the stopping.

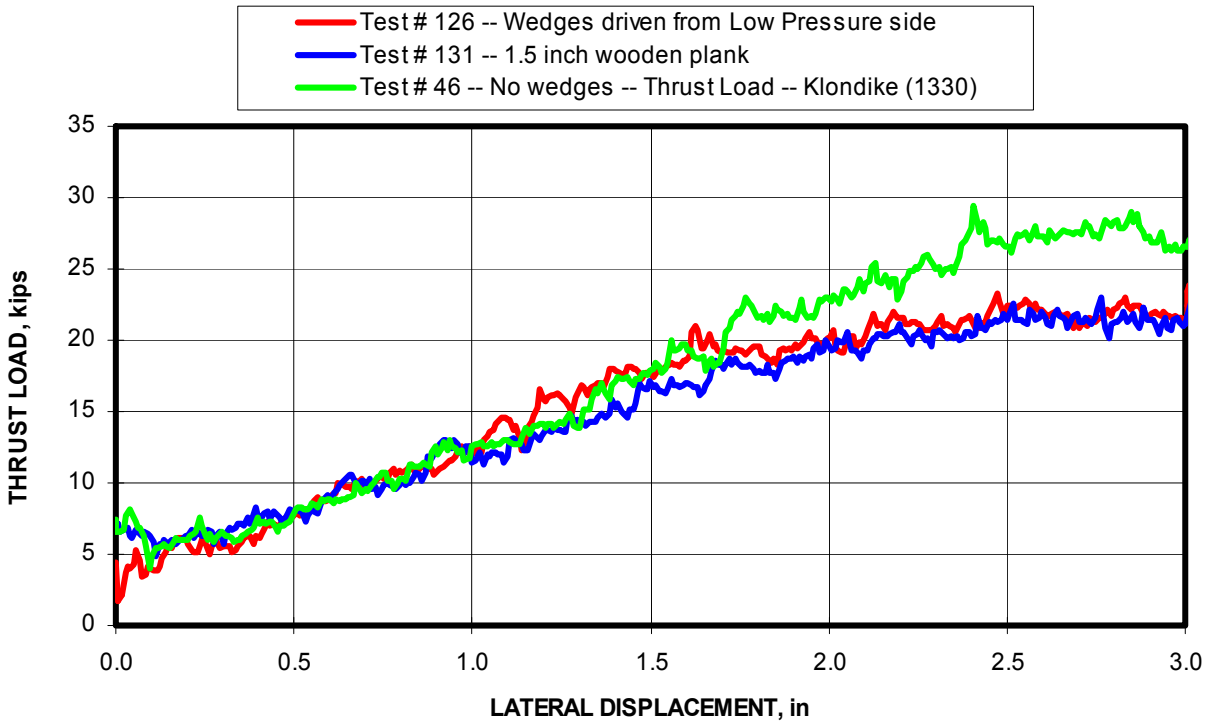

Figure 6-28. Arching thrust can also be preserved if wedging is done properly.

6.6.5 Impact of Preloading the Stopping with Grout Bags

Within the past 5 years, grout bags have been utilized to seal the perimeter around a stopping (see figure 6-29). The bags can be made in various lengths, but typically are about 4 feet long and a few inches wider than the thickness of the stopping. The bags are pressurized with a fast setting cementitious grout that expands the bag to fill the gap between the wall and surrounding coal or rock. They are pressurized by a hand pump with up to 50 psi of pressure to provide a preload to the stopping wall. Only about 50 pct of the preload is sustained with creep in the grout accounting for the loss of load with time.

Figure 6-29. Installation of seal with preloading grout bags used to seal around the perimeter of the block wall.

Figure 6-30 shows that the grout bag softens the response of the wall, and thereby can delay the failure induced by the ground convergence. In this laboratory example, a 4-ft-wide wall was tested with vertical loading, and the grout bag doubled the displacement at which failure of the block wall occurred (0.3 compared to 0.6 inches). It is also seen from the chart that the wall failed at less load when the grout bag was in place (310 kips compared to 445 kips). Since the grout bag would tend provide a uniform load distribution across the block wall and alleviate stress concentrations from block tolerances at the contact interface, the reduction in loading must be due to asymmetric loading across the thickness of the wall induced by the bag due to stretching of the grout bag.

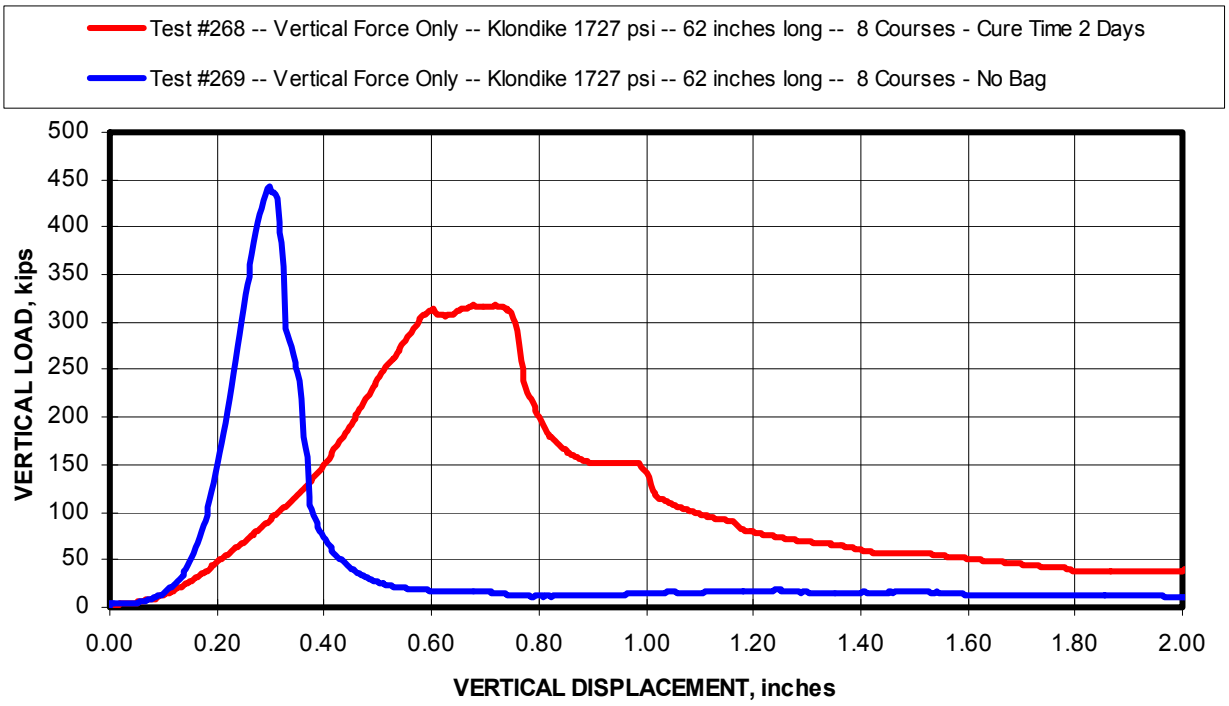

Figure 6-30. Grout bag increased the amount of displacement that can occur before the block wall fails.

Tests were also conducted in the Mine Roof Simulator on a 4-ft-wide half wall to determine the impact of the grout bag on the transverse load capacity of the stopping (see figure 6-31). Bags were placed on top of the half-walls with a 1.5 in gap between the top of the wall and the load frame platen. The bags were pressurized to about 25 psi to fill the gap. The bags were then removed and allowed to cure for 10 to 15 days prior to the transverse pressure tests. A total of 7 tests were conducted with preload pressures induced by the load frame ranging from 11 to 435 psi. The results are shown in figure 6-32 along with equivalent tests conducted without the grout bags. The bags reduced the boundary stiffness, which resulted in less transverse pressure. The transverse pressure without the bags was 2 to 3 times

Figure 6-31. Testing of a half-wall with grout bag in the Mine Roof Simulator.

greater at a given preload than measured with the grout bags. However, the grout bags would have prevented failure of the stopping by absorbing the ground deformation. The closure absorbed by the grout bag during the preloading ranged from 0.35 to 0.55 inches as shown in figure 6-33.

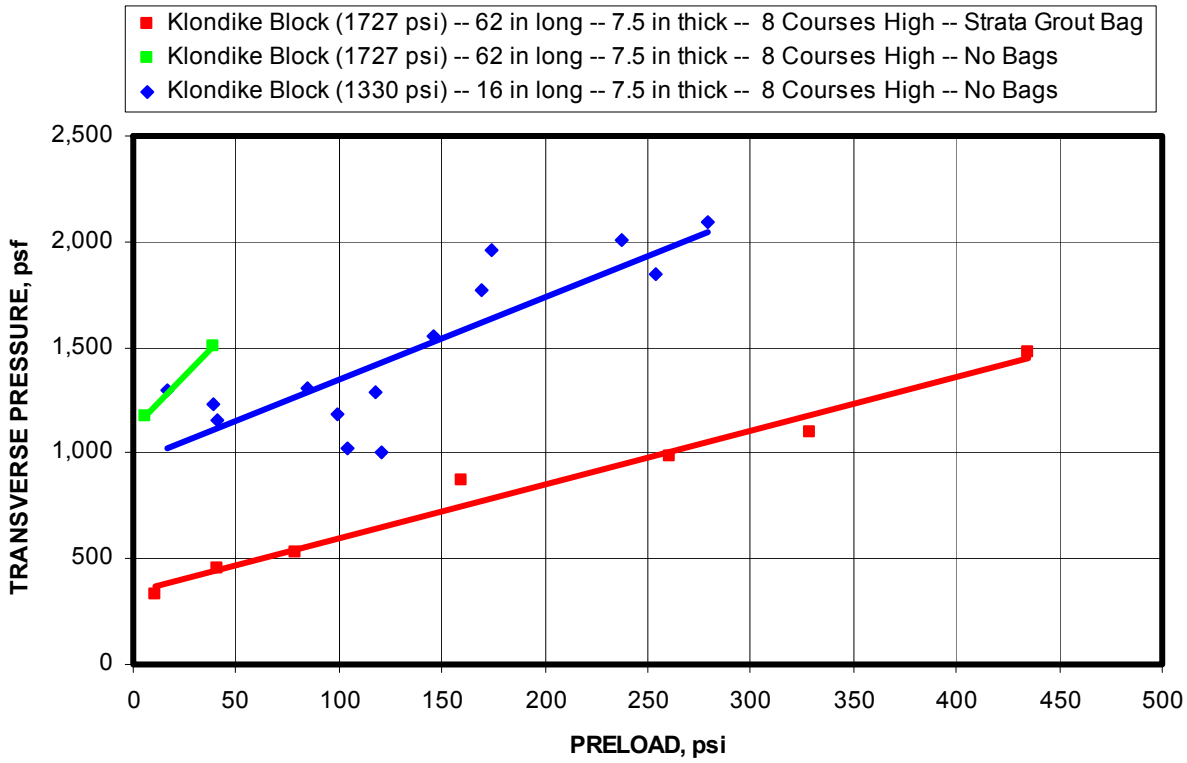

Figure 6-32. Comparison of laboratory tests with and without the grout bags.

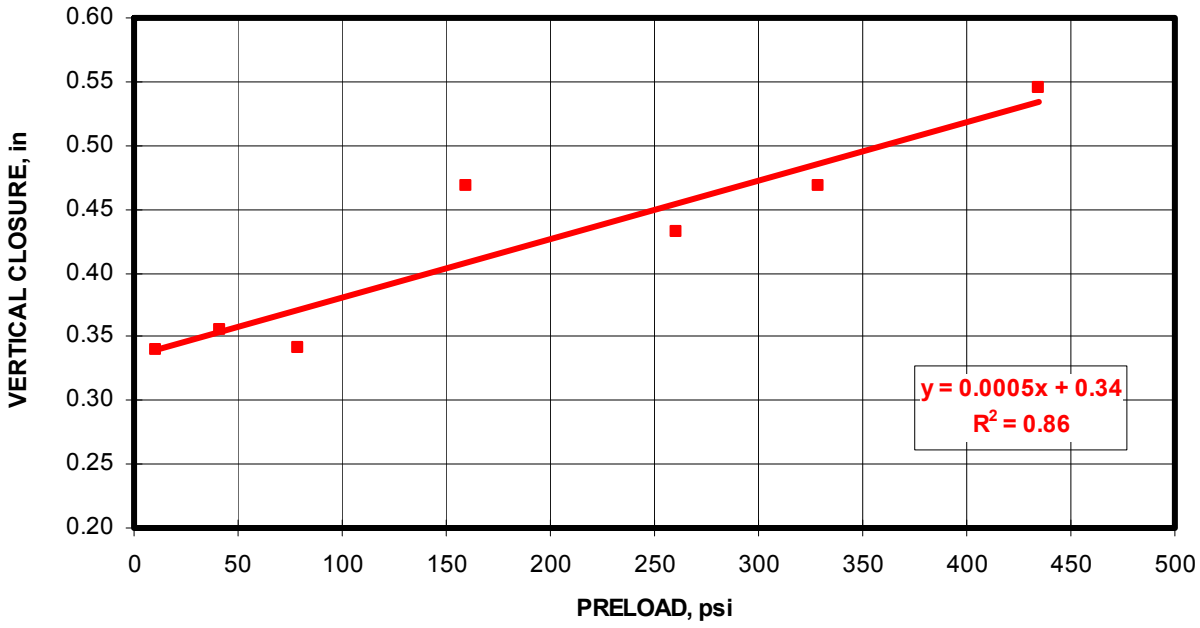

Figure 6-33. Closure absorbed by grout bag during prestressing.

CHAPTER 7: DEVELOPMENT OF PREDICTIVE TRANSVERSE PRESSSURE MODELS

The final goal is to be able to predict the transverse pressure capacity of a stopping. In order to do this, predictive models are developed based on the theoretical relationships presented in chapters 5 and 6. Two models have been developed: (1) prediction model where the lateral displacement is known, and (2) predictive model where the arching thrust force is known. A description of these two models including examples is provided.

7.1 PREDICTING THE TRANSVERSE PRESSURE FROM THE LATERAL WALL DISPLACEMENT

The first procedure assumes that the lateral displacement is known or measured. The flowchart shown in figure 7-1 describes the procedure. The first step is to calculate the deformation that occurs in the hinge areas. This is accomplished from the geometrical relationship between the lateral displacement and hinge point deformation. Next, the arching thrust can be computed from the stiffness of the wall and the mine roof and floor. From the moment equilibrium requirements, the horizontal force acting on the base of the wall can be calculated and transformed into a resultant force, which can be normalized to the transverse pressure acting on the wall.

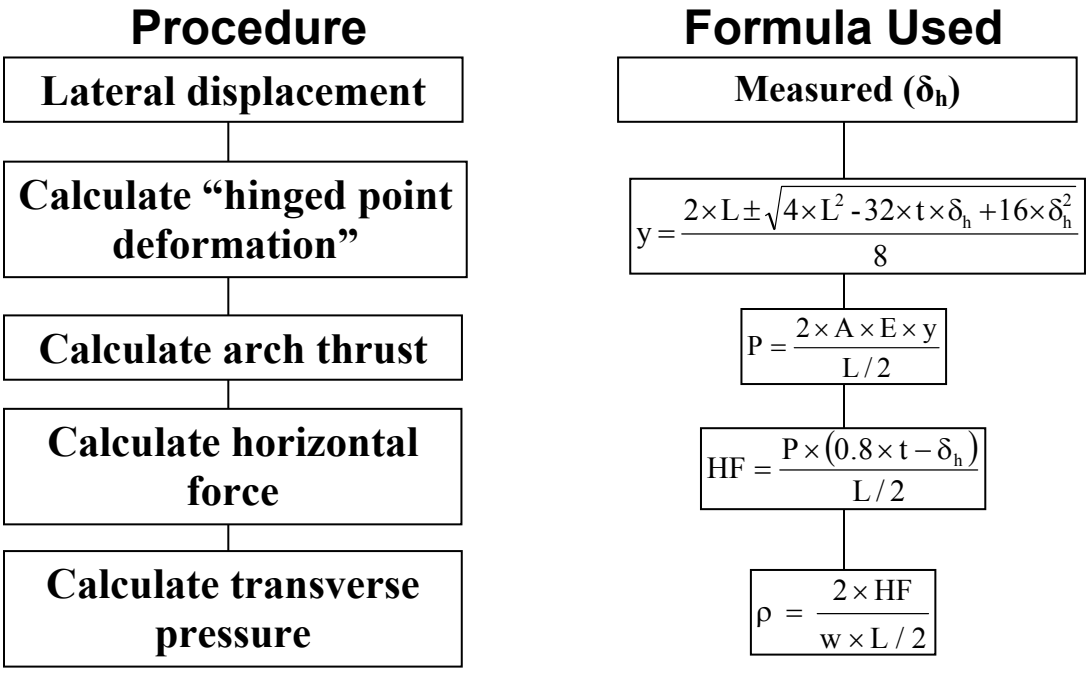

Figure 7-1. Flowchart for predicting the transverse pressure capacity of stoppings from the lateral wall displacement.

7.1.1 Example using Rigid Boundary Conditions.

The example chosen is a stopping constructed from conventional, Portland cement block, manufactured by Klondike Block and Masonry Supplies, Inc. A 6-course-high half-wall was utilized in the test providing a half-wall height of 45.75 inches, which equates to a full-wall height of 91.50 inches. The wall was 5.625 inches thick. The Klondike block has a compressive strength of 1,330 psi. The half-wall response from the biaxial test conducted in the Mine Roof Simulator is shown in figure 7-2. As seen in the figure, the peak lateral loading occurred at 1.92 inches of lateral displacement. The thrust force at the peak lateral loading was 22.8 kips as shown by the blue curve in figure 7-2.

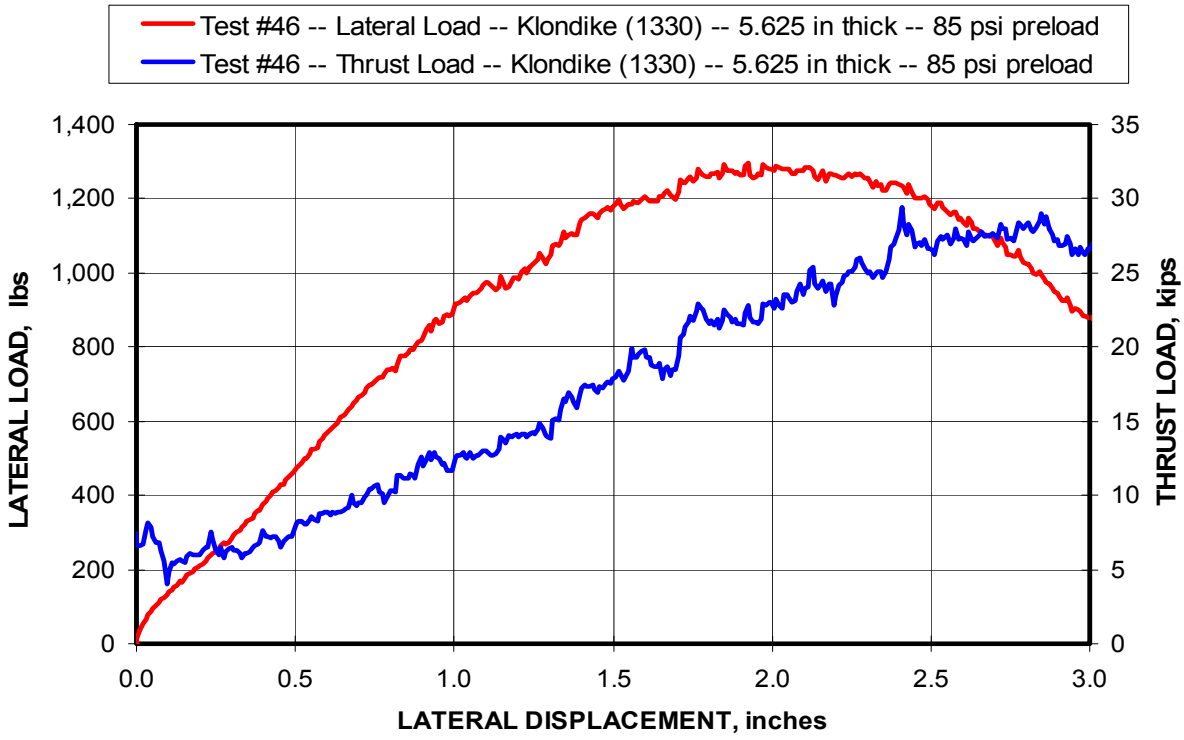

Figure 7-2 MRS test of a 6-course-high half-wall showing the measured lateral and thrust load development as a function of the applied lateral displacement.

The hinge point deformation at a lateral displacement of 1.92 inches where the peak lateral loading occurred is calculated using equation 7.1 to be 0.098 inches.

$$y = \frac{2 \times 91.5 - \sqrt{4 \times 91.5^2 - 32 \times 5.625 \times 1.92 + 16 \times 1.92^2}}{8} = 0.098 \text{ inches} \qquad \textbf{(7.1)}$$

The arching thrust can then be calculated from equation 7.2 using the hinge point deformation calculated in equation 7.1 and an elastic modulus of 60,000 psi for this particular block material. The modulus can be determined from laboratory testing or can be back calculated from the transverse pressure test results provided in this study. A unit block arching thrust of 23,134 lbs at the peak lateral loading was computed for this example.

$$P = \frac{2 \times A \times E \times y}{L/2} = \frac{2 \times (5.625 \times 16) \times 60{,}000 \times 0.098}{45.75} = 23{,}134 \text{ lbs} \qquad \textbf{(7.2)}$$

Where P = thrust load per unit block width, lbs,

A = axial loading area of the wall, in^2,

E = elastic modulus, psi,

y = deformation in each of two crush zones on half-wall section, in, and

L = full-wall height, in.

Equation 7.3 is then used to compute the horizontal force acting on the half-wall. The result is 1,305 lbs. This compares to the measured horizontal load from the half-wall test of 1,296 lbs, an error of only 0.7 pct.

$$HF = \frac{P \times (0.8 \times t - \delta_h)}{L/2} = \frac{23{,}134 \times (0.8 \times 5.625 - 1.92)}{45.75} = 1{,}305 \text{ lbs} \qquad \textbf{(7.3)}$$

The transverse pressure per unit area of the wall can then be determined using equation 7.4.

$$\rho = \frac{2 \times HF}{w \times L/2} \times 144 = \frac{2 \times 1{,}305}{16 \times 45.75} \times 144 = 514 \text{ psf} \qquad \textbf{(7.4)}$$

Figure 7-3 compares the calculated thrust force as a function of the lateral displacement to the measured thrust force for test #46. As seen in this figure, the calculated thrust force closely predicts the measured thrust force, until near the end of the test when the measured thrust force peaked and began to decline. The peak thrust force can be caused from either the mechanics of the wall behavior (i.e. moment equilibrium as described in figure 5-1) or failure of the material. The calculated thrust force is determined from the elastic response of block material and does not consider the strength of the block. The predicted thrust force simply continues to increase with increasing lateral displacement as a function of the material modulus. In this particular test, since the calculated thrust force closely matched the measured thrust force, the response of the wall was accurately predicted throughout the test (through the full range of the applied lateral displacement) as shown in figure 7-3. This also indicates that the block material strength was not controlling the transverse pressure in this particular example. The transverse pressure (see figure 7-4) was limited by the lateral displacement in this case and not the block strength. This implies that there is optimum block strength for a particular material modulus.

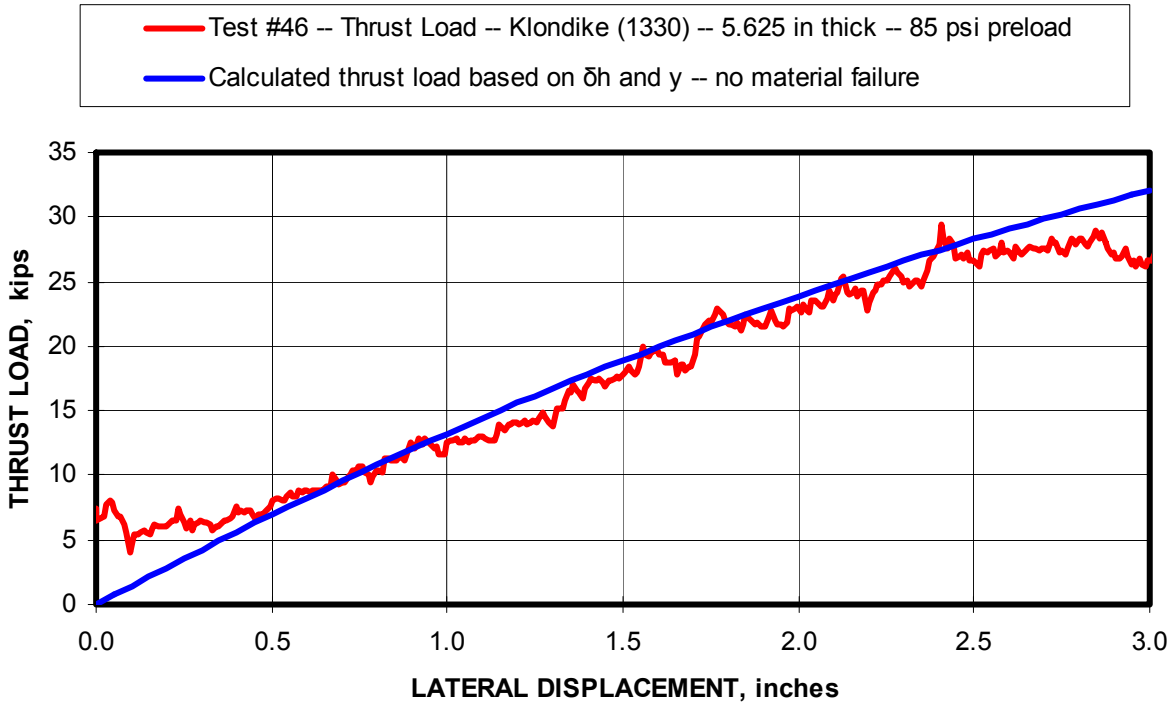

Figure 7-3. Half-wall test with theoretically calculated thrust shown by the blue line.

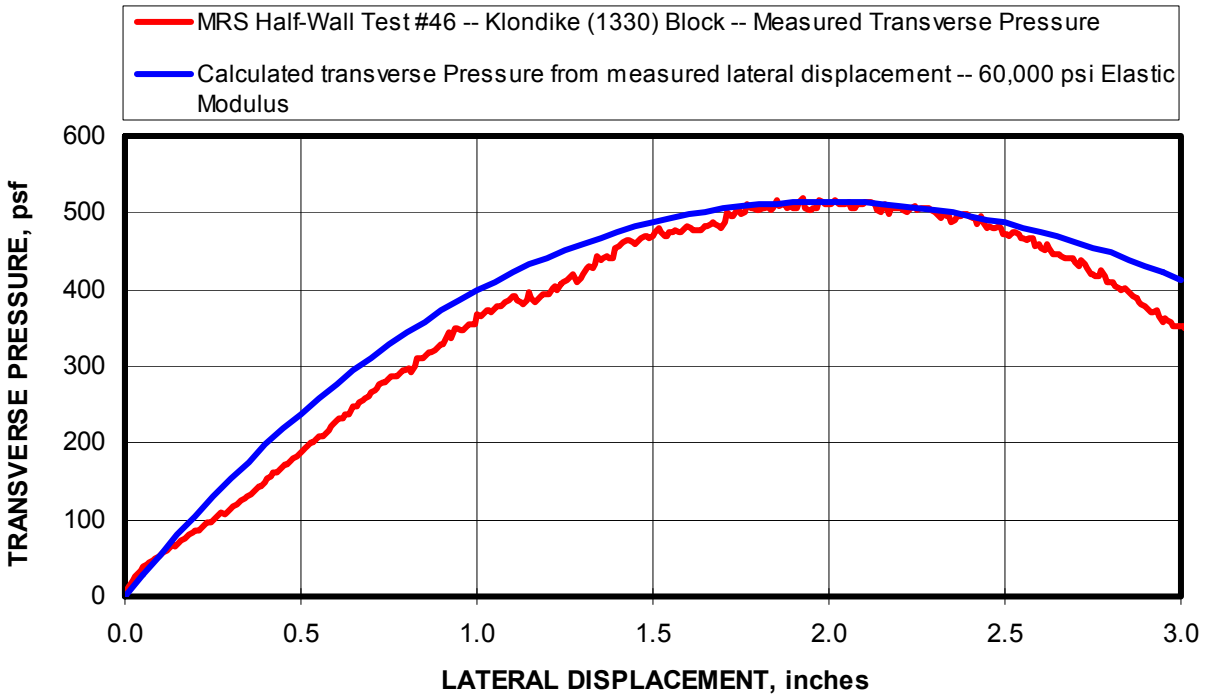

Figure 7-4. Comparison of the measured transverse pressure and the calculated transverse pressure.

Another example is depicted in figure 7-5. In this case, the predicted thrust force again closely matches the measured thrust force until the measured force peaks and begins to decline. The peak thrust force is in this case is most likely caused by failure of the material. The material has a compressive strength of 1,330 psi. The measured thrust force was approximately 37,000 lbs acting in this particular test across a single concrete block since the half-wall was only one block wide. Since the wall is rotating, forming the two hinges in the half-wall test (see figure 4-1), the contact area of the hinge zone can vary and was not measurable in the test arrangement. However, if it is assumed that the block material is failing, then the width of the contact zone can be calculated from equation 7.5. The calculated width of the hinge zone of 1.74 inches seems reasonable, and it can be speculated that the load exceeding the strength of the material caused the peak thrust force. As the lateral displacement progresses beyond the peak thrust force, moment equilibrium requirements control the thrust force response.

$$t_{cr} = \frac{P}{f_c \times w} = \frac{37{,}000}{1{,}330 \times 16} = 1.74 \text{inches} \qquad \textbf{(7.5)}$$

Where t_{cr} = hinge zone width, in,

P = thrust load, lbs,

f_c = compressive strength of the material, psi, and

w = width of the wall, in.

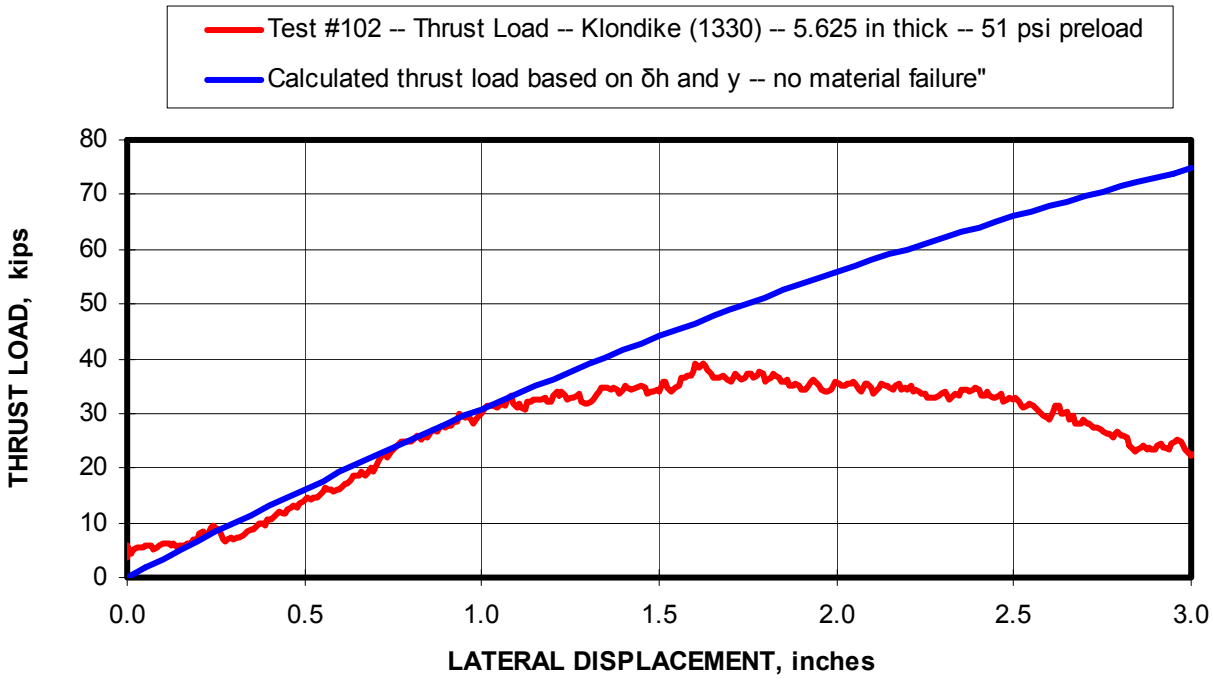

Figure 7-5. Four-course (30 in) high half-wall test result including comparison of the measured and theoretically calculated thrust load.

Figure 7-6 shows the transverse pressure as determined from the MRS half-wall test and the predicted transverse pressure using equation 5.4. Unlike test #46 where the transverse pressure was accurately predicted though the full range of applied lateral displacement, the wall response was accurately predicted up to and including the peak transverse pressure, but since there was no limit to the calculated thrust force, the post-peak response of the wall was not accurately predicted in this test. Figure 7-6 shows the predicted transverse pressure with the thrust force limited to 30,858 lbs. Interestingly, limiting the thrust force to a constant value is essentially implying an elastic-plastic material response (see figure 7-7). As seen in figure 7-8, the constant thrust force resulted in a linear decrease in the post-peak transverse pressure. This suggests that the post-peak behavior is governed primarily by the material failure.

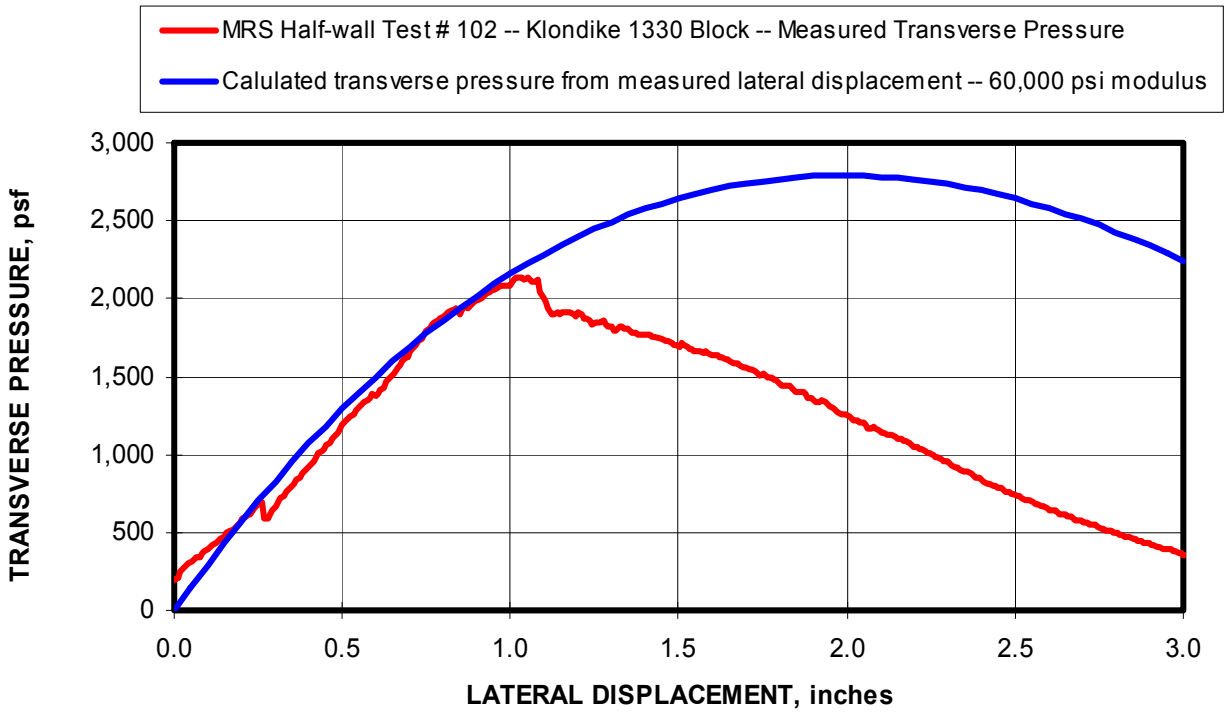

Figure 7-6. Comparison of the measured transverse pressure with that calculated theoretically from the lateral displacement.

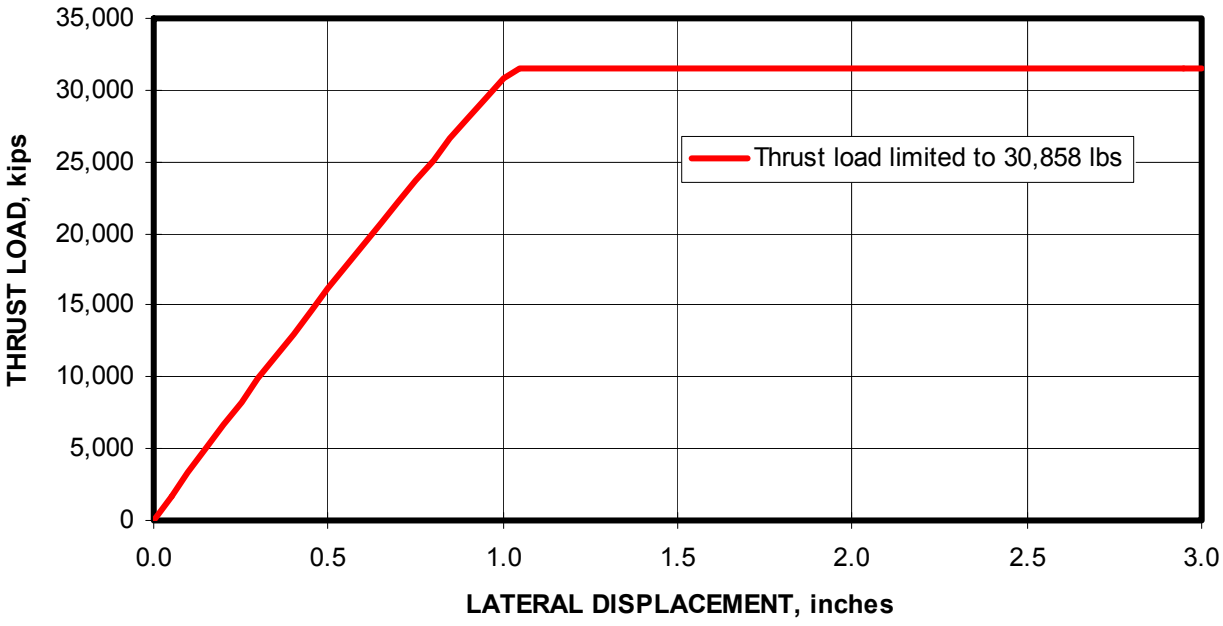

Figure 7-7. The thrust load is limited to 30,858 lbs based on the observed axial load at the measured peak transverse pressure from the MRS test.

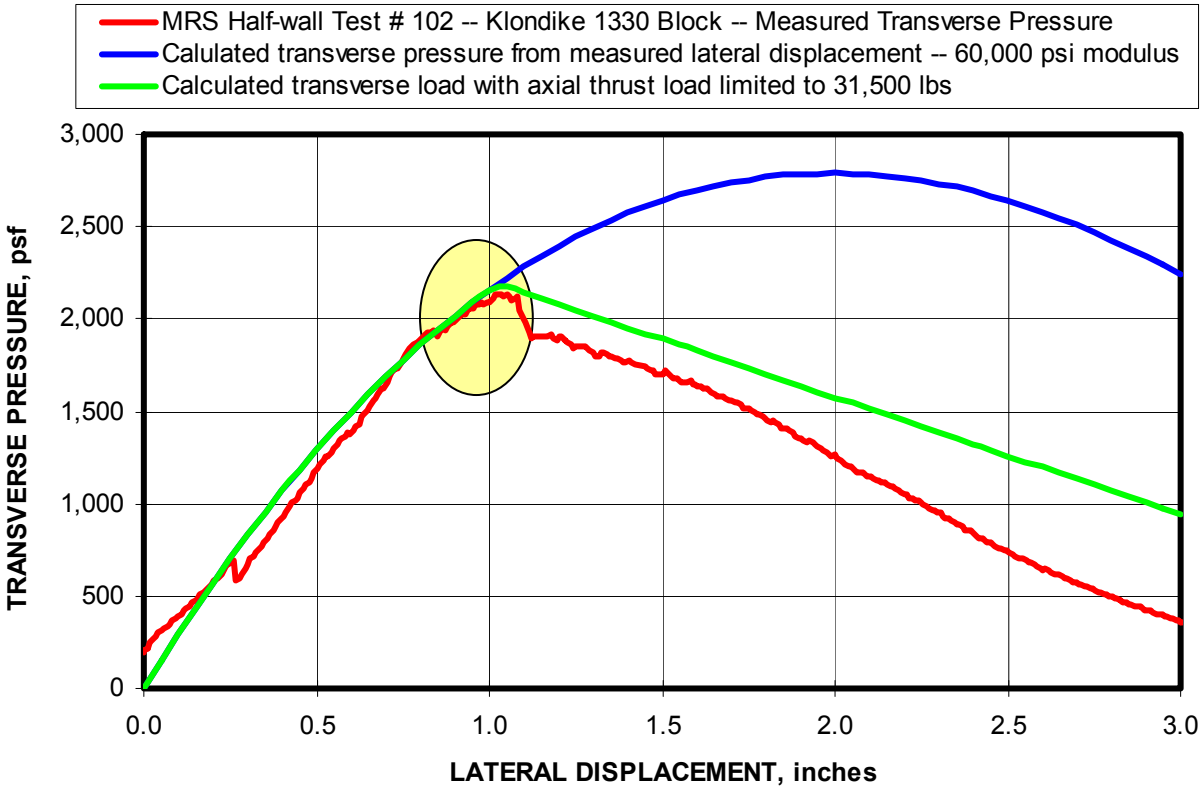

Figure 7-8. Limiting the thrust load improves the post-peak theoretical prediction of the transverse pressure in this half-wall MRS test.

7.1.2 Example using Non-Rigid Boundary Conditions.

If the boundary is not rigid, the same basic theory applies. As described in the section on theoretical factors, the system stiffness can be defined using equation 6.11 and referenced here as equation 7.6. A system modulus can also be computed using equation 7.7.

$$K_{System} = \frac{K_{wall} \times K_{abutment}}{K_{wall} + K_{abutment}} \qquad \textbf{(7.6)}$$

$$E_c = \frac{E_1 \times E_2 \times (L_1 + L_2)}{L_1 \times E_2 + L_2 \times E_1} \qquad \textbf{(7.7)}$$

Where: L_1 = thickness of the roof or floor material, in,

L_2 = height of the half-wall, in,

E_1 = Young's modulus of the wall material, psi, and

E_2 = Young's modulus of the roof or floor material, psi.

Reviewing the example provided in the Chapter 6 using the drywall as the roof contact material, the predictive model can be explained. The drywall has a relatively low modulus of 420 psi compared to the 80,000 psi for the concrete block. Using equation 7.7, the system modulus is computed as 25,995 psi. Using the system of equations documented in the flowchart in figure 7-1, the transverse pressure can be computed as a function of the lateral displacement as shown in figure 7-9.

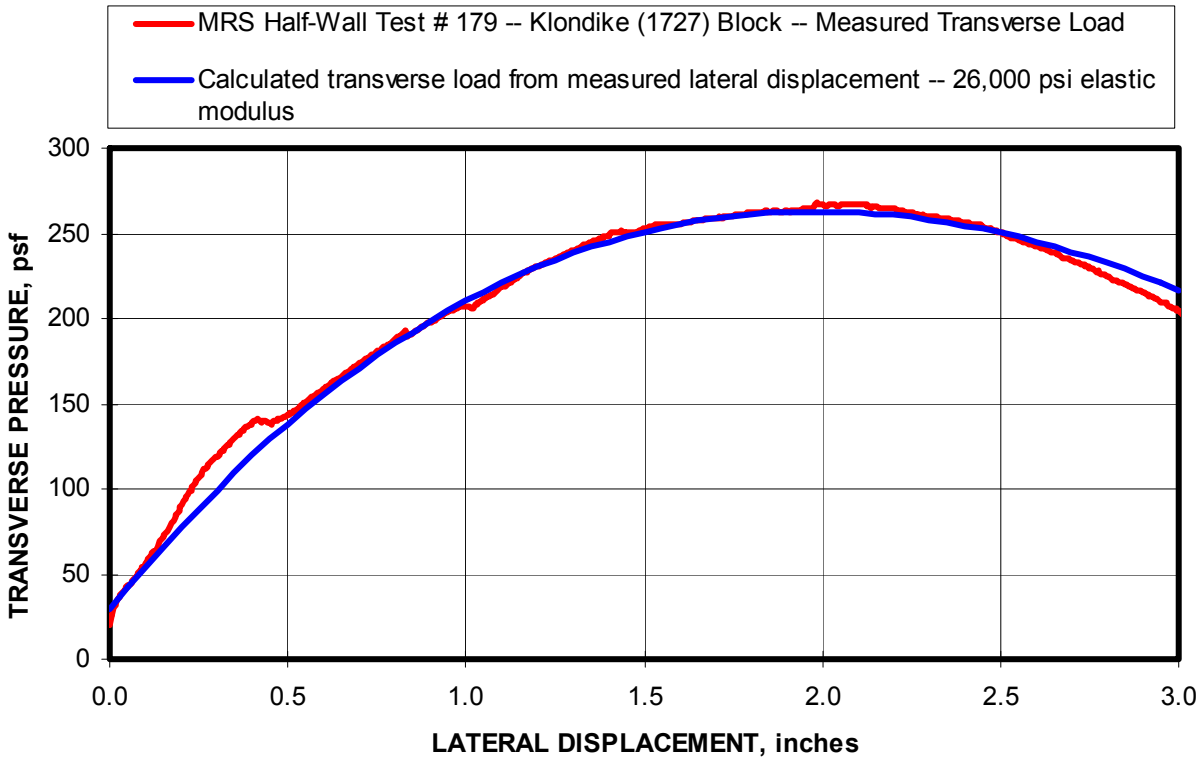

Figure 7-9. Comparison of theoretically predicted transverse pressure using the 26,000 psi system modulus for the drywall abutment test and the measured transverse pressure.

7.1.3 Example considering preloading of the wall from ground pressures.

The flowchart shown in figure 7-10 can be used to determine the transverse pressure if the wall is preloaded from convergence produced by the ground pressures. The flow chart is similar to that depicted in figure 7-1 with two additional steps added as highlighted in the yellow text boxes. The additional requirements are that the preload needs to be measured or computed and the preload needs to be added to the arching thrust developed from the wall rotation.

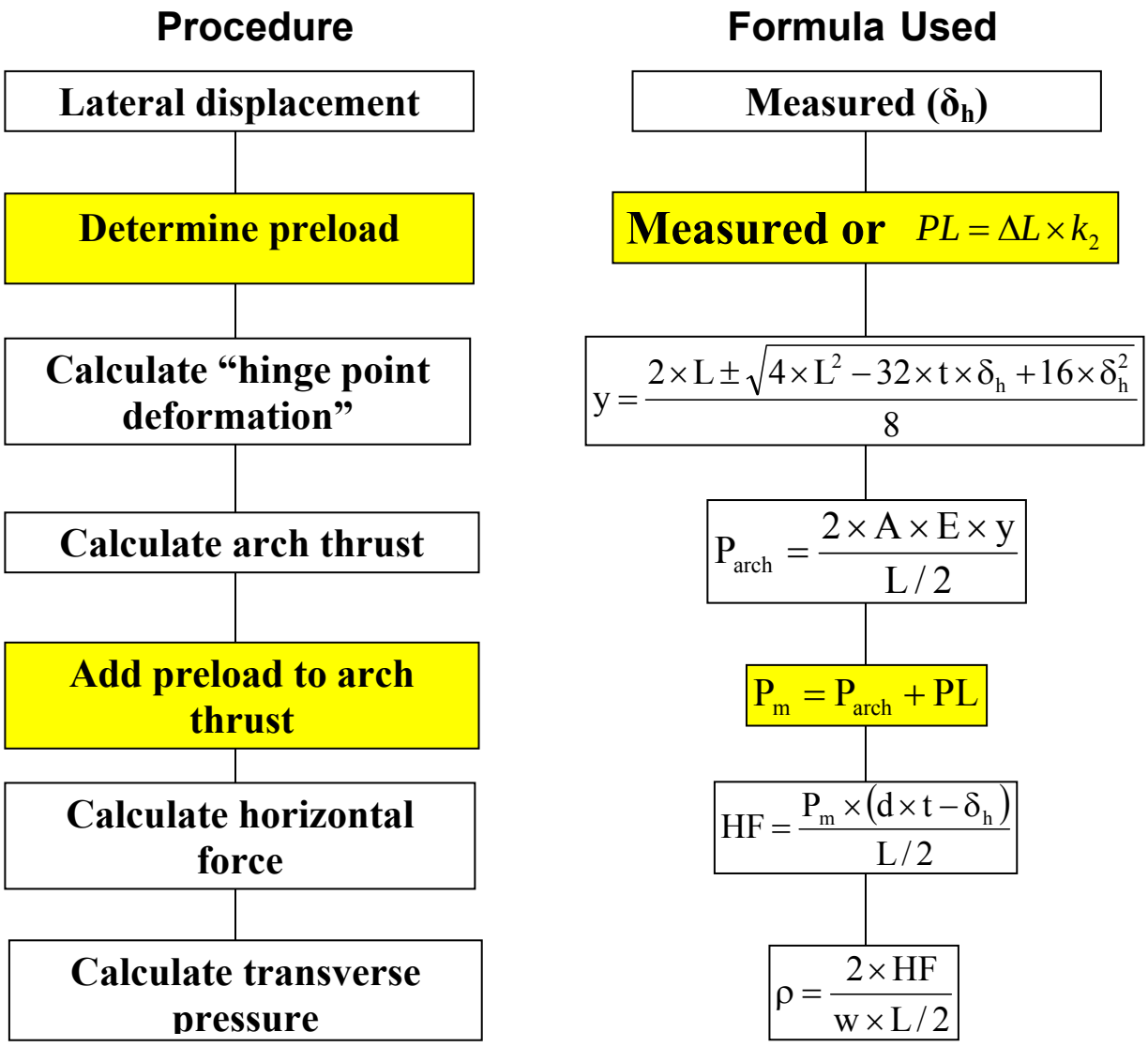

Figure 7-10. Flowchart for predicting the transverse pressure capacity of stoppings from the lateral displacement with preload applied from ground pressures.

An example considering the same wall conditions as the first example documented in section 7.1.1 will be examined for the preload condition. The half-wall height is again 45.75 inches and the wall is constructed from the same Portland cement block manufactured by Klondike Block and Brick Company. In this case, a preload of 373 psi is measured equating to a unit block preload of 33.57 kips. The laboratory test result is shown in figure 7-11.

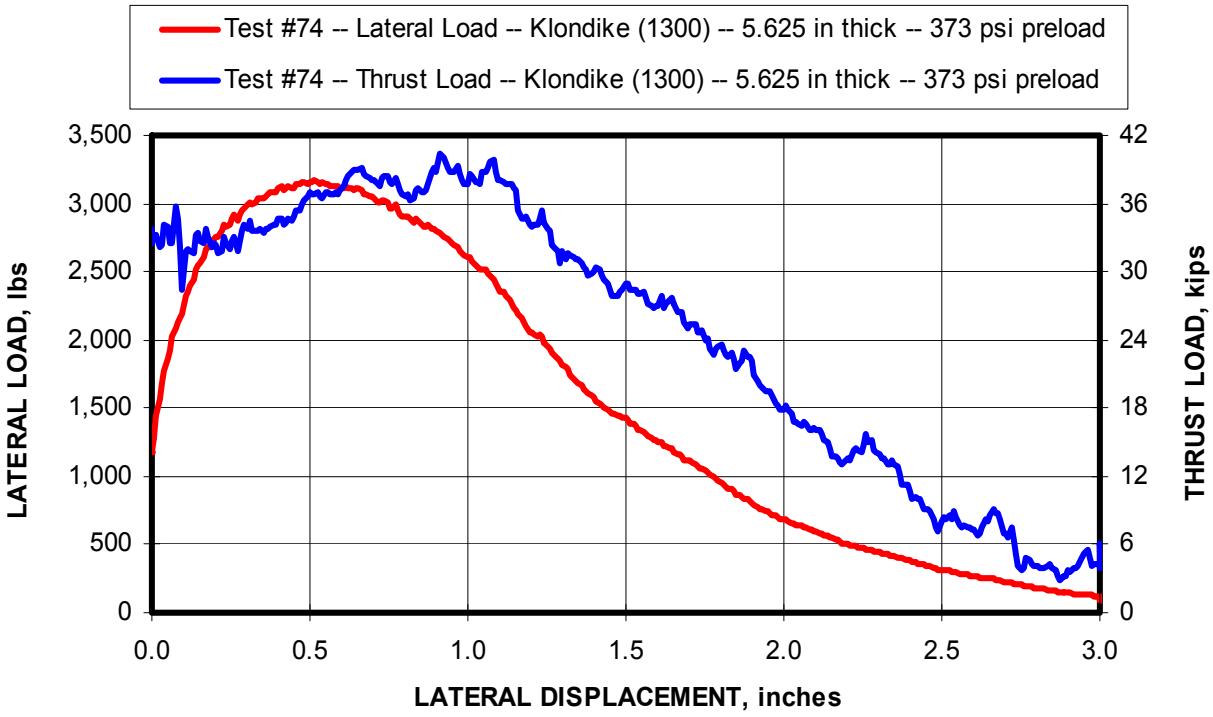

Figure 7-11. MRS test of 45.75-inch-high half-wall with 373 psi of preload.

The preload could also be determined from the crosscut convergence if the axial stiffness of the wall is known (see equation 7.8). For the wall construction considered in this example, tests in the Mine Roof Simulator have shown that the wall exhibits a biaxial stiffness (see figure 7-12). The initial response is soft and somewhat nonlinear. Once the block contact becomes uniform through the initial loading, the response is stiffer. In this case, a stiffness of 400 kips/inch is computed for a single block column half-wall constructed from conventional Portland cement block. The initial load prior to the stiff response could be added to the preload assessment to provide a more accurate prediction of preload based on convergence (see equation 7.8). If the convergence is less than 0.16 inches, the stiffness is computed from the initial response of the wall using equation 7.9.

$$PL = 5 + (\Delta L - 0.16) \times k_1 \qquad \text{If } \Delta L > 0.16 \text{ in} \qquad \textbf{(7.8)}$$

$$PL = \Delta L \times k_2 \qquad \text{If } \Delta L < 0.16 \text{ in} \qquad \textbf{(7.9)}$$

Where P = Axial preload on unit block, kips,

ΔL = Roof to floor convergence, in,

k_1 = initial stiffness of the stopping, kips/in, and

k_2 = final stiffness of the stopping, kips/in.

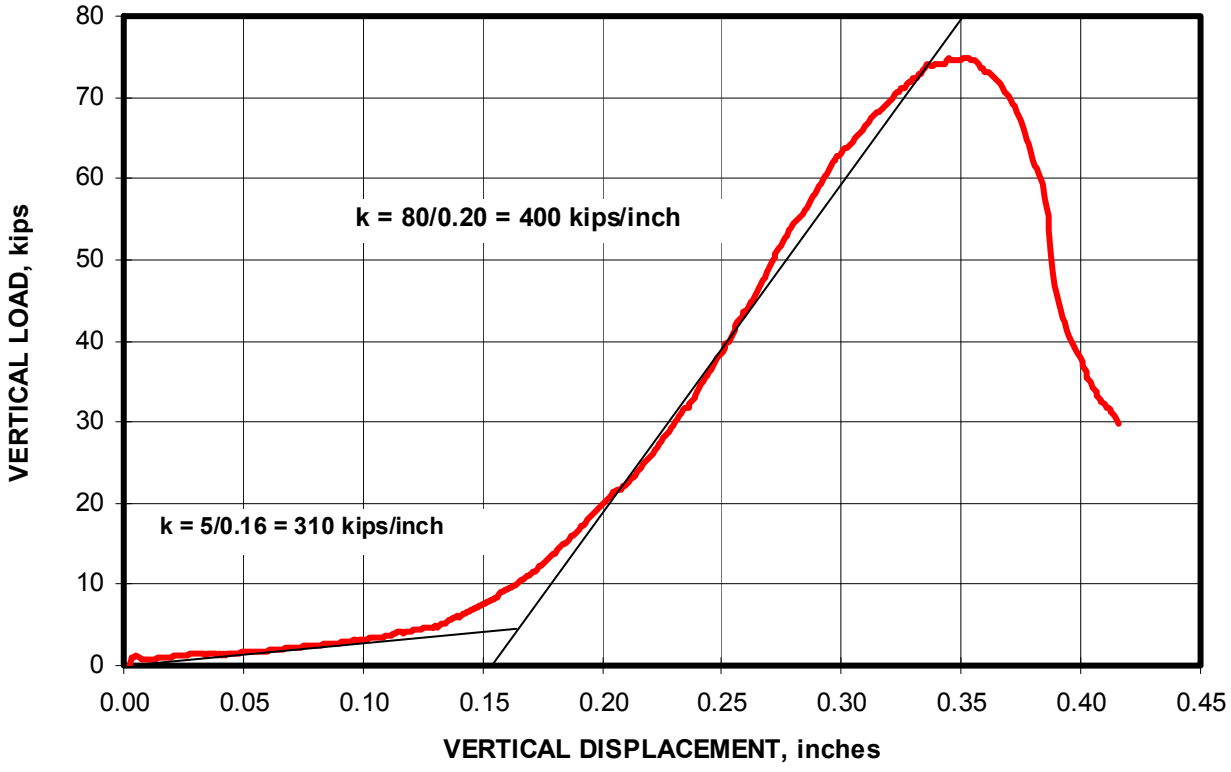

Figure 7-12. Laboratory test to determine stiffness of block column. Example shows single block column constructed from six courses of Klondike block.

The next step in the process is to compute the arch thrust force. This is computed in the same manner as the first example through the geometric relationship between the measured lateral displacement and the hinge point deformation. In this case, the hinge zone deformation is computed as 0.030 inches as shown in equation 7.10. From this, the arch thrust force can be computed as 7,150 lbs using equation 7.11.

$$y = \frac{2 \times 91.5 - \sqrt{4 \times 91.5^2 - 32 \times 5.625 \times 0.52 + 16 \times 0.52^2}}{8} = 0.030 \text{ inches} \qquad \textbf{(7.10)}$$

$$P = \frac{2 \times A \times E \times y}{L/2} = \frac{2 \times (5.625 \times 16) \times 60{,}000 \times 0.030}{45.75} = 7{,}150 \text{ lbs} \qquad \textbf{(7.11)}$$

$$P_m = P_{arch} + PL = 7.15 + 33.57 = 40.72 \text{ kips} \qquad \textbf{(7.12)}$$

The next step (see flowchart in figure 7-10) is to calculate the horizontal force acting to produce the transverse pressure of the stopping. In order to do this, the thrust adjustment factor (d) must be determined so that the modified thrust resultant force location can be incorporated into the equation. If the lateral load and thrust force were known, the thrust adjustment factor as a function of the lateral displacement could be calculated. Figure 7-13 displays the thrust adjustment factor for the test #74 examined in this example. As shown figure 7-13, the thrust adjustment factor moves outward from the center of the block toward the ends of the block thickness as the lateral displacement initially occurs. It peaks at 0.8 (the factor used when there is no preload), and then declines back below 0.8 toward 0.7 as the lateral displacement continues. Using this thrust adjustment factor, the transverse pressure curve can be duplicated (see figure 7-14) using the predictive equations for horizontal force and transverse pressure shown in the flowchart in figure 7-10.

$$d = \frac{HF \times L/2 + P_m \times \delta_h}{P_m \times t} \qquad \textbf{(7.13)}$$

Where P_m = modified resultant arching thrust, lbs,

t = thickness of the wall, in,

δ_h = lateral displacement of wall at the mid span, in,

HF = horizontal force, lbs, and

L/2 = half-wall height, in.

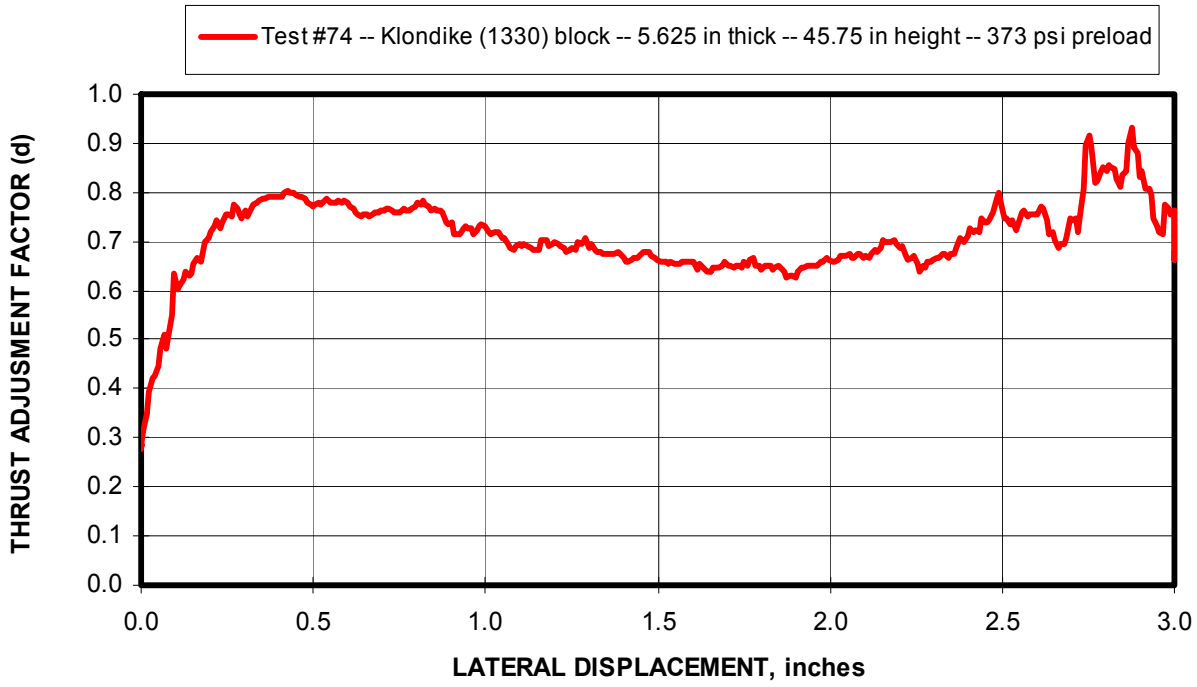

Figure 7-13. Plot of the change in the thrust adjustment factor as a function of lateral displacement of a half-wall test conducted in the MRS.

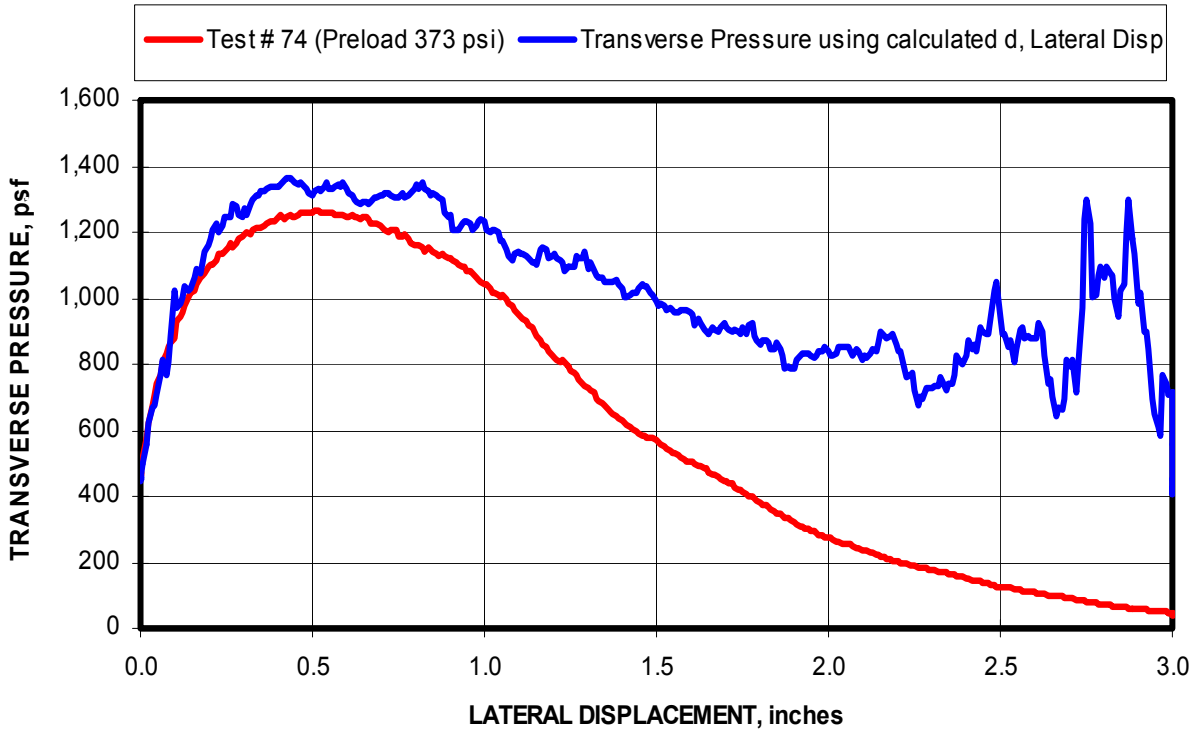

However, the horizontal force is not known, therefore, the thrust adjustment factor cannot be computed for the complete loading cycle that will allow prediction of the full transverse pressure cycle. The peak transverse pressure can still be predicted by developing a regression equation for the thrust adjustment factor at the peak loading based on laboratory test results. Table 7-1 summarizes half-wall tests conducted in the Mine Roof Simulator for 45-in-high, half-wall tests using the arching test protocol described in Chapter 4. A vertical preload was applied to the wall prior to the initiation of the lateral displacement of the base of the half wall. This preload simulates the axial loading that would be caused by ground pressures. The preload in this series of tests was increased from 0 to 763 psi. The calculated thrust adjustment factor at the maximum transverse pressure is shown in the last column of the table, and compares to the "0.8" term used in the initial analysis without preloading.

Table 7-1. MRS Half-wall tests on conventional concrete block with preload applied.

Test No.	Block Type	Wall Thickness (in)	Half-wall Height (in)	Preload (psi)	Peak Lateral Load (lb)	Lateral disp (in)	Thrust (kips)	Thrust Adjustment Factor
60	Klondike	5.625	45.75	28	1,120	2.05	20.48	0.809
59	Klondike	5.625	45.75	43	1,032	1.88	19.23	0.771
46	Klondike	5.625	45.75	85	1,296	1.92	22.79	0.804
45	Klondike	5.625	45.75	90	978	2.38	19.30	0.835
34	Klondike	5.625	45.75	109	1,246	2.10	22.11	0.832
36	Klondike	5.625	45.75	122	1,597	1.15	25.33	0.717
35	Klondike	5.625	45.75	139	1,795	1.27	28.87	0.731
37	Klondike	5.625	45.75	202	1,992	0.97	32.01	0.678
38	Klondike	5.625	45.75	247	1,579	0.98	37.92	0.513
63	Klondike	5.625	45.75	252	2,268	0.46	29.52	0.707
61	Klondike	5.625	45.75	313	2,359	0.33	34.02	0.623
74	Klondike	5.625	45.75	373	3,166	0.52	37.76	0.774
75	Klondike	5.625	45.75	390	3,617	0.41	40.59	0.798
76	Klondike	5.625	45.75	474	3,365	0.44	43.47	0.708
77	Klondike	5.625	45.75	471	3,831	0.72	52.38	0.722
78	Klondike	5.625	45.75	577	2,499	0.44	45.54	0.525
79	Klondike	5.625	45.75	534	2,779	0.56	53.48	0.620
81	Klondike	5.625	45.75	568	3,358	0.71	47.02	0.707
82	Klondike	5.625	45.75	618	3,922	0.65	59.35	0.652
83	Klondike	5.625	45.75	623	3,960	0.45	56.30	0.652
85	Klondike	5.625	45.75	763	3,776	0.45	61.08	0.583

As speculated, the adjustment factor, which is an indication of the position of resultant thrust, decreases with increasing preload pressure. A plot of the adjustment factor as a function of total axial load is shown in figure 7-15, and a trendline based on a linear regression analysis of the data is added to evaluate the correlation between the two parameters. There is considerable scatter in the data and the R^2 factor of 0.45 does not suggest a strong correlation, but the trend is towards a decreasing value for the thrust position factor as the total thrust increases.

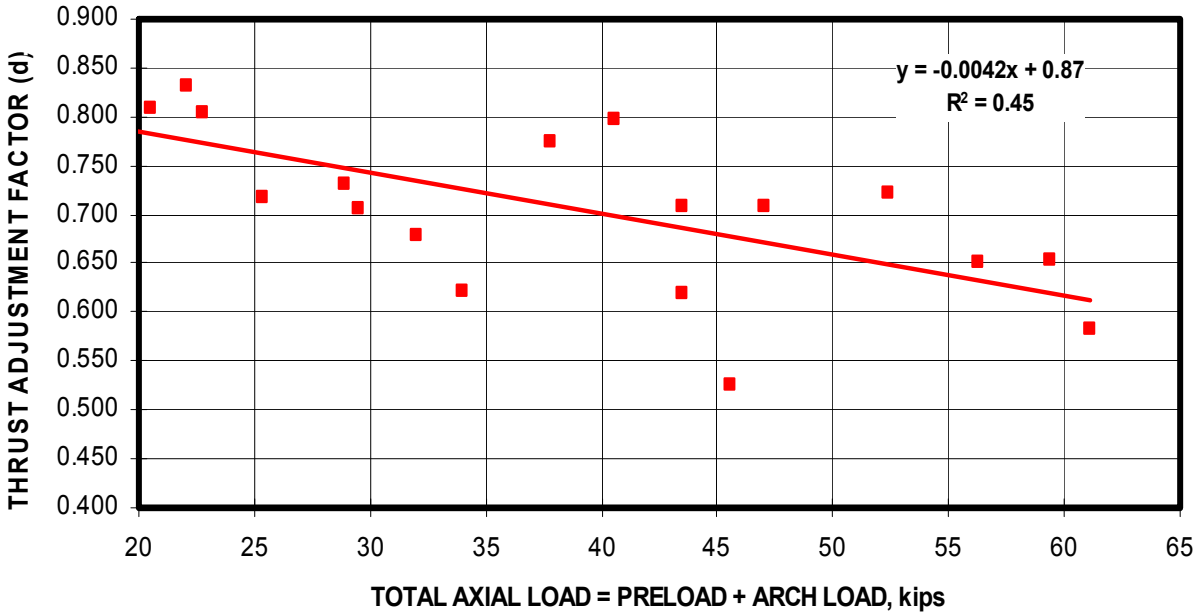

Figure 7-15. Regression trendline developed for the thrust adjustment factor for 45-in half-wall tests conducted in the MRS.

Substituting the trendline regression equation for the 0.8 term yields equation 7.14. The transverse pressure can then be calculated from the measured thrust load and lateral displacement using this equation. For the example being discussed, the peak transverse pressure is computed as 1,190 psf. This compares with the measured transverse pressure of 1,244 psf, an error of 4 pct.

$$\rho = \frac{2 \times P \times (0.8 \times t - \delta_h)}{w \times (L/2)^2} \times 144 = \frac{2 \times P_m \times [(-.0042 \times P_m + 0.8678) \times t - \delta_h]}{w \times (L/2)^2} \times 144 \qquad \textbf{(7.14)}$$

$$\rho = \frac{2 \times 40.72 \times 1000 \times ((-.0042 \times 40.72 + 0.8678) \times 5.625 - 0.52)}{16 \times 45.75^2} \times 144 = 1{,}190 \text{ psf} \qquad \textbf{(7.15)}$$

Figure 7-16 shows that the calculated transverse pressure using this prediction methodology is very well correlated to the preload. Figure 7-17 illustrates the comparison between the measured peak transverse pressure and the calculated transverse pressure for the set of tests documented in table 7-1. The graph shows that the calculated transverse pressure is consistently less than the measured transverse pressure by about 50 to 100 psf.

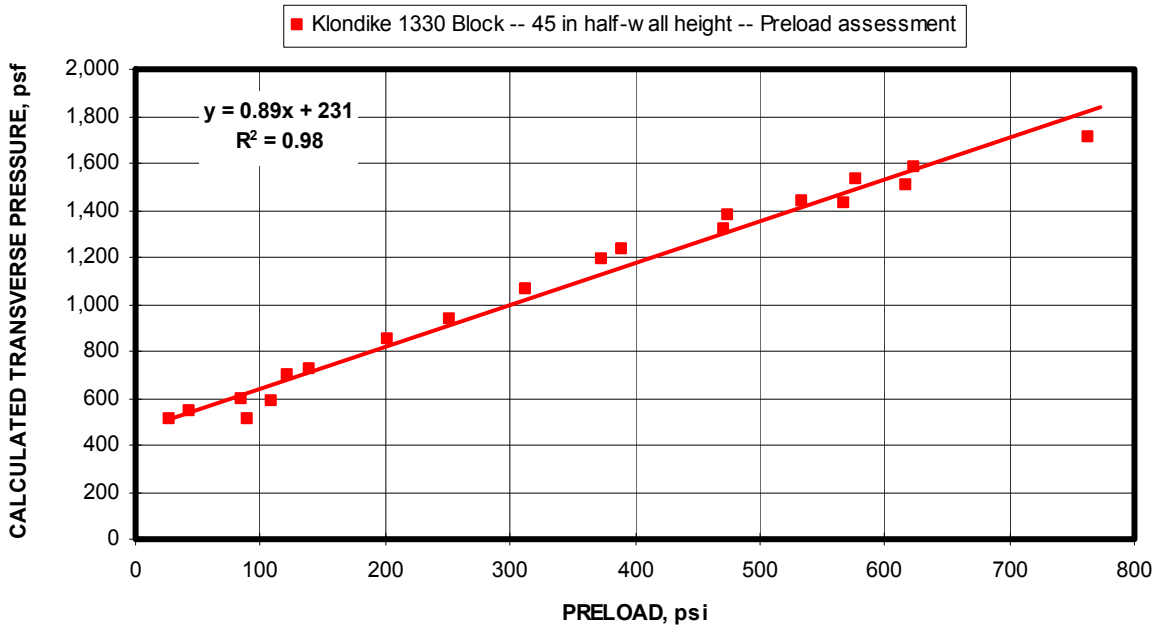

Figure 7-16. Correlation between calculated transverse pressure and the preload acting on the wall.

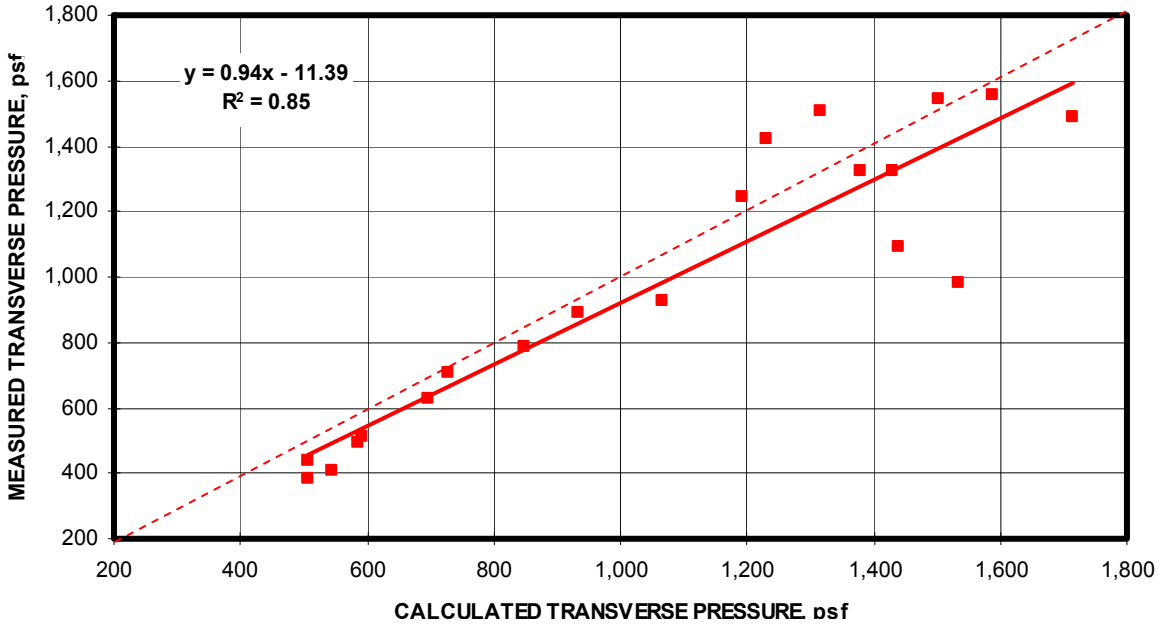

Figure 7-17. Correlation between the measured peak transverse pressure and the calculated transverse pressure from the lateral wall displacement.

7.2 PREDICTING THE TRANSVERSE PRESSURE FROM THE THRUST FORCE

In this model, the thrust force is known. The thrust force could be measured by placing a hydraulic load cell at the roof or floor interface or somewhere within the wall construction. In the laboratory, the thrust force was measured by the MRS load frame. The procedure is similar to that of the first model, except that thrust force is used to determine the deformation of the hinge points, which in turn is used to calculate the lateral displacement. The procedure is outlined in the flowchart in figure 7-18.

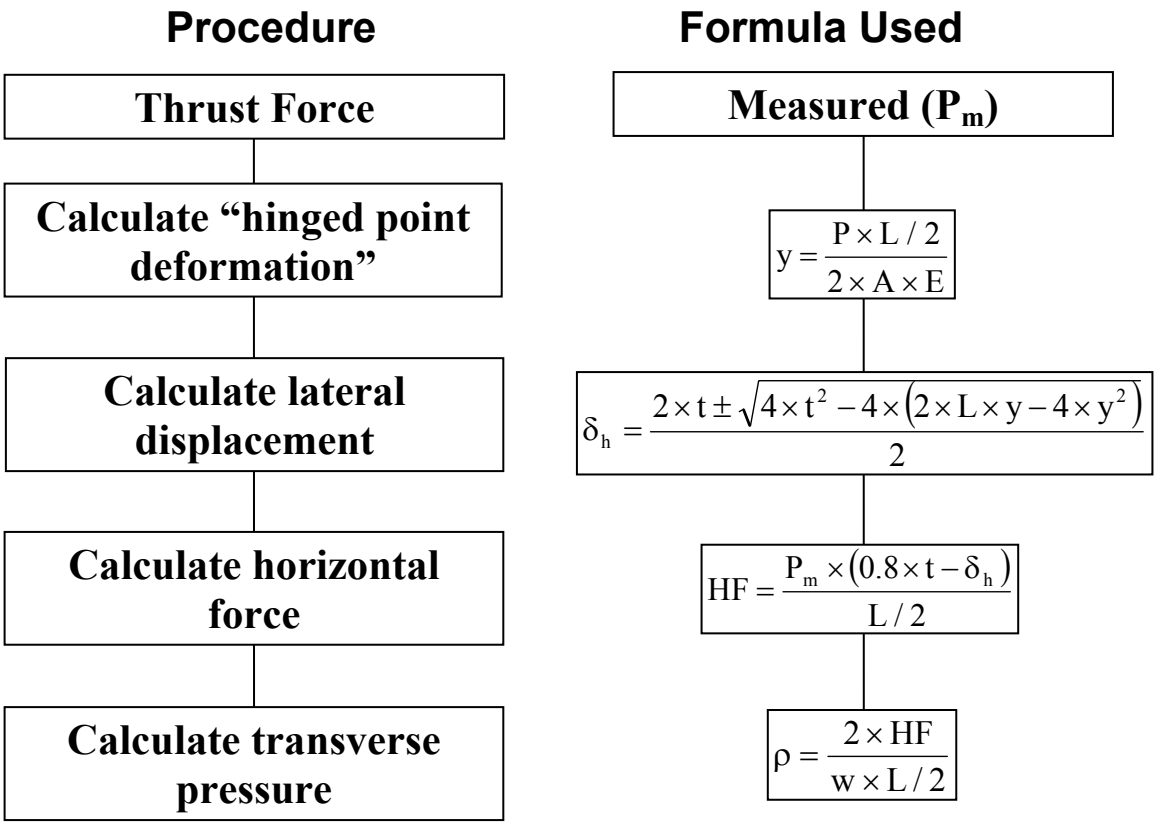

Figure 7-18. Flowchart for predicting the transverse pressure capacity of stoppings if the thrust load is known.

7.2.1 Example using Rigid Boundary Conditions.

For comparative purposes, the same test used in the previous model (section 7.1.1) will be examined here. Again, this is a 45-in-high half-wall that is nominally 6 inches thick. As shown in figure 7-2 and documented in table 7-1, the thrust force in this test was measured at 22.79 kips. Using an elastic modulus of 60,000 psi, equation 7.16 can be used to estimate the

deformation of the hinge zone occurring at each of two hinge zones on the half-wall block column evaluated in test #46.

$$y = \frac{P \times L/2}{2 \times A \times E} = \frac{22{,}800 \times 45.75}{2 \times (16 \times 5.625) \times 60{,}000} = 0.097 \text{ inches} \qquad \textbf{(7.16)}$$

Where y = deformation in each of two hinge zones on half-wall section, in,
P = thrust load = 22,800 lbs,
L/2 = half-wall height = 45.75 in,
A = axial loading area of the wall = 90 in^2, and
E = Elastic modulus = 60,000 psi.

The lateral displacement can then be determined from equation 7.17 as follows.

$$\delta_h = \frac{2 \times t - \sqrt{4 \times t^2 - 4 \times (2 \times L \times y - 4 \times y^2)}}{2} \qquad \textbf{(7.17)}$$

$$\delta_h = \frac{2 \times 5.625 - \sqrt{4 \times 5.625^2 - 4 \times (2 \times 91.5 \times 0.097 - 4 \times 0.097^2)}}{2} = 1.89 \text{ inches} \qquad \textbf{(7.18)}$$

Where δ_h = lateral displacement of wall at the mid span = 1.89 in,
t = thickness of the wall = 5.625 in,
y = deformation in each of two hinge zones on half-wall section = 0.097 in, and
L = full-wall (arching) height = 91.5, in.

The measured lateral displacement at the peak horizontal loading, which defines the maximum transverse pressure capacity of the stopping, was 1.92 inches. The predicted lateral displacement based on the measured thrust load was 1.89 inches. The error in the lateral displacement prediction is less than 2 pct, which is considered very good considering the assumptions made in this analysis.

The horizontal force can be determined using equation 7.19. In this case, the calculated horizontal force was 1,300 lbs, which compares to the measured MRS horizontal force for the laboratory test of 1,296 lbs, and error of less than 1 pct. The transverse pressure

is then computed from equation 7.20 to equal 512 psf, again an error of less than 1 pct when measured against the laboratory test.

$$HF = \frac{P \times (0.8 \times t - \delta_h)}{L/2} = \frac{22{,}790 \times (0.8 \times 5.625 - 1.89)}{45.75} = 1{,}300 \text{ lbs} \quad \textbf{(7.19)}$$

$$\rho = \frac{2 \times HF}{w \times L/2} \times 144 = \frac{2 \times 1{,}300}{16 \times 45.75} \times 144 = 512 \text{ psf} \quad \textbf{(7.20)}$$

Figure 7-19 shows the predicted transverse pressure compared to the measured transverse pressure for test #46 for the full loading cycle. This is very similar to the prediction made from the lateral displacement (see figure 7-4).

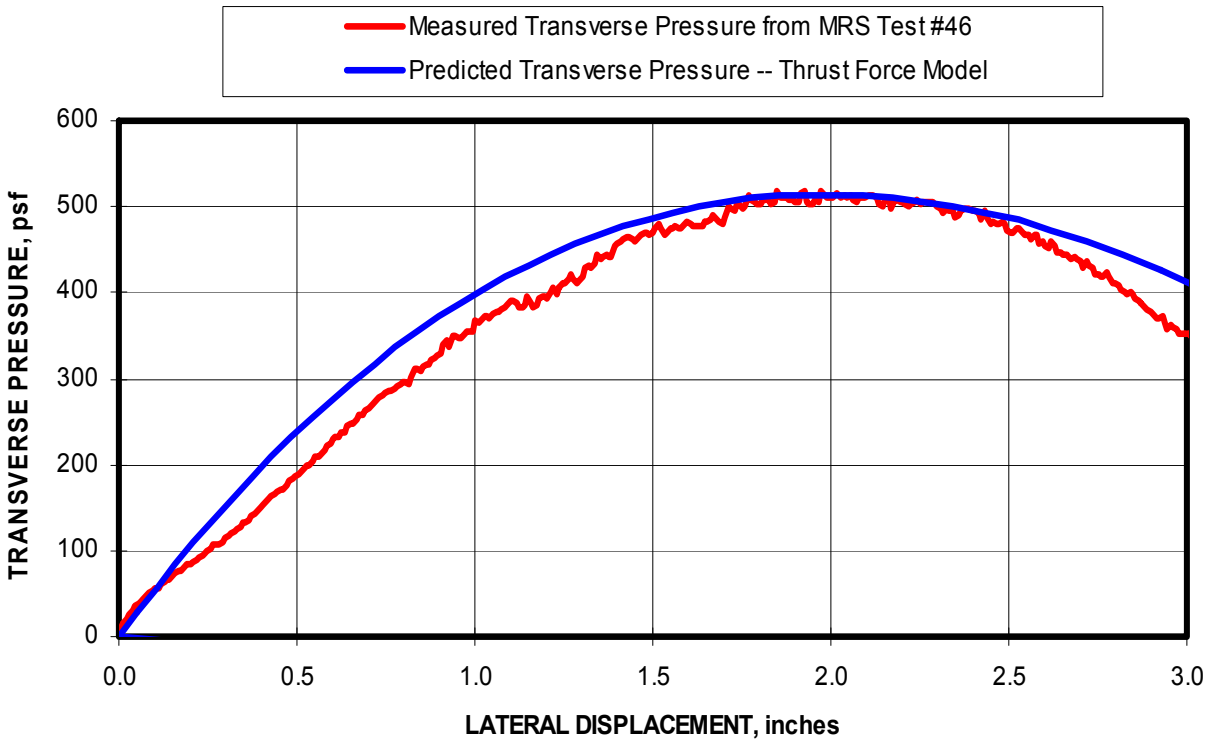

Figure 7-19. Comparison of predicted transverse pressure from the thrust force to the laboratory measured transverse pressure for a 45-inch-high half-wall test.

7.2.2 Example using Non-Rigid Boundary Conditions.

The same theory applies to the non-rigid boundary conditions for the thrust measurement model prediction as was used in the lateral displacement measurement model described in section 7.1.2. Figure 7-20 demonstrates the thrust load model using the non-rigid boundary conditions.

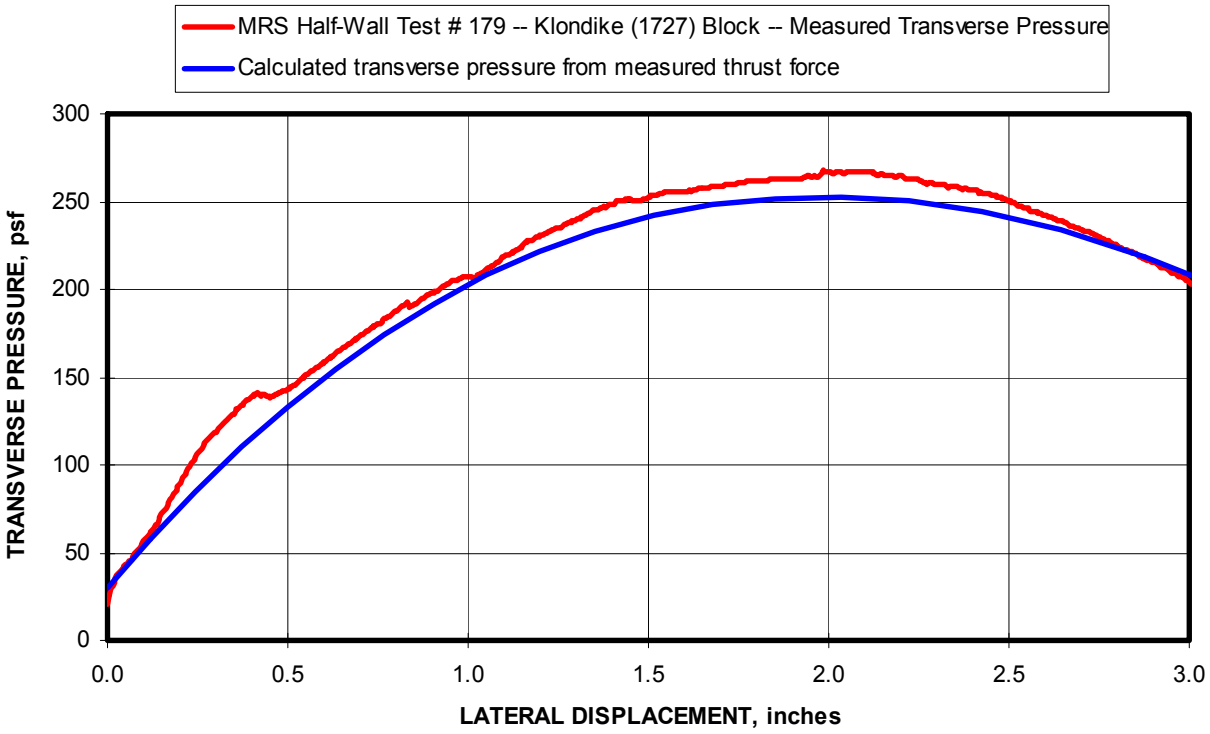

Figure 7-20. Demonstration of the thrust load model using non-rigid boundary conditions.

7.2.3 Example considering preloading of the wall from ground pressures.

A similar process to that presented in figure 7-18 can be used for predicting the transverse pressure from the thrust forces if the wall is also preloaded from the roof-to-floor convergence produced by ground pressures. The procedure is illustrated in figure 7-21.

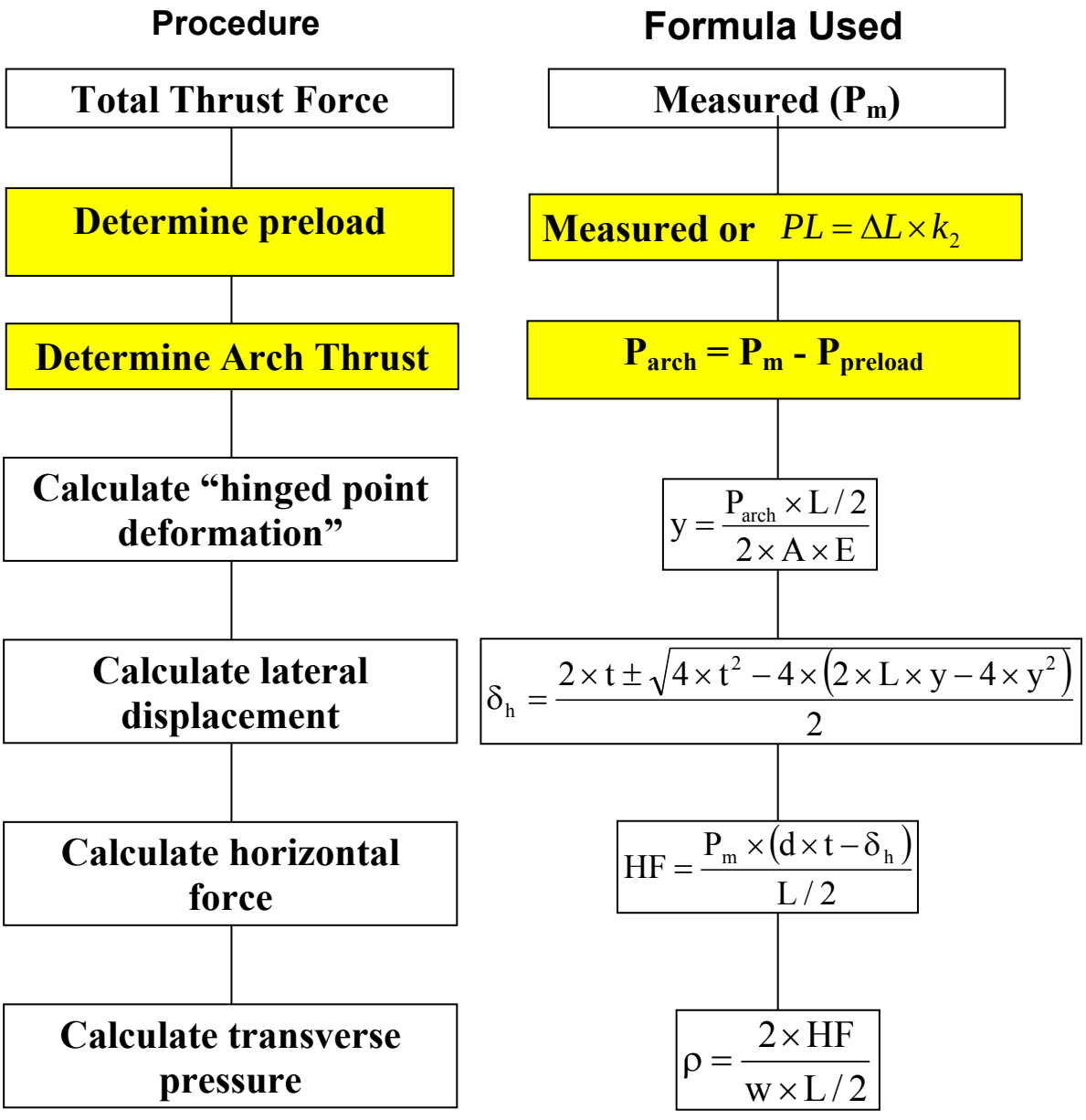

Figure 7-21. Flowchart for predicting the transverse pressure capacity of stoppings if the thrust load is known.

Test #74 will again be used as an example of the procedure. The test results were presented in figure 7-11. In this case, a preload of 373 psi equating to a unit block preload of 33.57 kips and a total thrust force of 37.76 kips at the peak transverse pressure was measured from the MRS half-wall test. Following the flowchart in figure 7-21, the thrust load produced by arching equals 4.19 kips. Equation 7.21 then computes the hinge point deformation as 0.018 inches. The lateral displacement is calculated from equation 7.22 as 0.30 inches.

$$y = \frac{P \times L/2}{2 \times A \times E} = \frac{4190 \times 45.75}{2 \times (16 \times 5.625) \times 60{,}000} = 0.018 \text{ inches} \qquad \textbf{(7.21)}$$

$$\delta_h = \frac{2 \times 5.625 - \sqrt{4 \times 5.625^2 - 4 \times \left(2 \times 91.5 \times 0.018 - 4 \times 0.018^2\right)}}{2} = 0.30 \text{ inches} \qquad \textbf{(7.22)}$$

The next step (see flowchart in figure 7-21) is to calculate the horizontal force acting to produce the transverse pressure of the stopping. As described in section 7.1.3, the thrust adjustment factor (d) must be determined so that the modified thrust resultant force location can be incorporated into the equation. Using the thrust adjustment factor as plotted in figure 7-13, the transverse pressure can be predicted for the full loading cycle as depicted in figure 7-22.

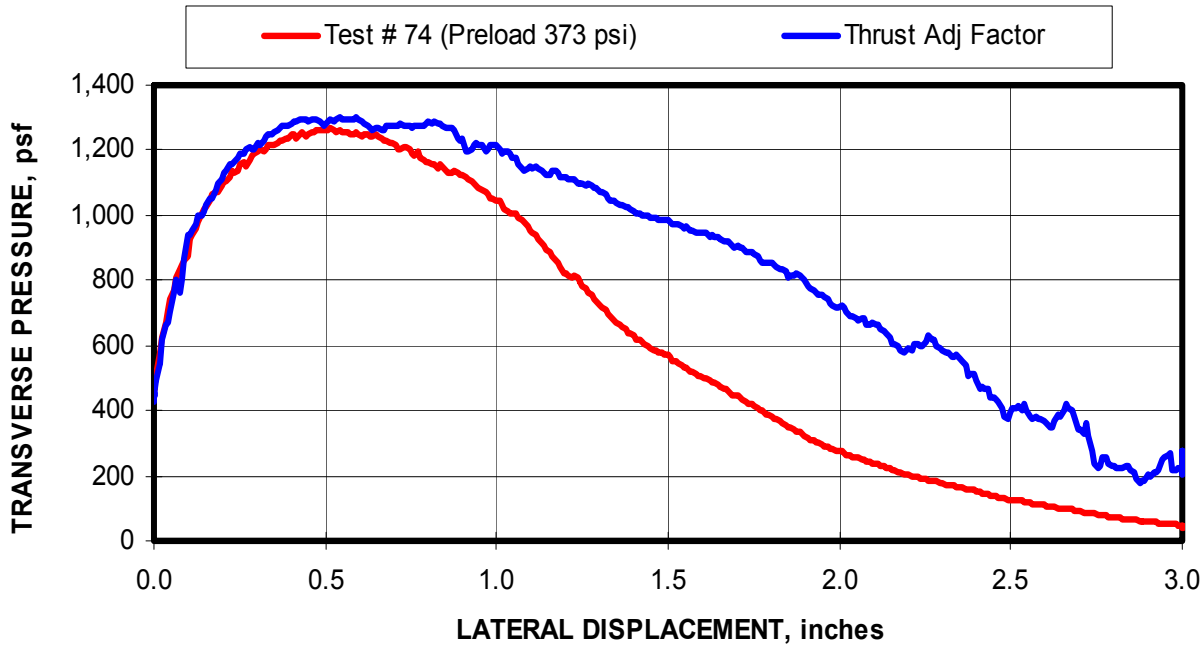

Figure 7-22. Comparison of predicted transverse pressure for full loading using the thrust prediction model compared to the measured transverse pressure from the MRS test.

As was described in the example in section 7.1.3, the peak transverse pressure can be computed using the trendline regression of the d factor computed from the empirical test data (see figure 7-15). Using this term, the maximum transverse pressure for this particular test is computed as 600 psf using equation 7.24. This compares with the measured transverse pressure of 622 psf, an error of less than 4 pct.

$$\rho = \frac{2 \times P \times (0.8 \times t - \delta_h)}{w \times (L/2)^2} \times 144 = \frac{2 \times P_m \times ((-.0042 \times P_m + 0.8678) \times t - \delta_h)}{w \times (L/2)^2} \times 144 \quad \textbf{(7.24)}$$

$$\rho = \frac{2 \times 37.76 \times 1000 \times ((-.0042 \times 37.76 + 0.8678) \times 5.625 - 0.30)}{16 \times 45.75^2} \times 144 = 1{,}200 \text{ psf} \quad \textbf{(7.25)}$$

Figure 7-23 illustrates the comparison between the measured peak transverse pressure and the calculated transverse pressure for the set of tests documented in table 7-1. The graph shows that the calculated transverse pressure is consistently less than the measured transverse pressure by about 100 to 200 psf. The prediction becomes worse at transverse pressures above 1,400 psf, which occurs at the higher preloads. One explanation for the low prediction at these high preloads is that the block may be damaged from the preload and the full arching potential is not attained in these tests. The prediction is more accurate when these high transverse pressure tests are omitted (see figure 7-24).

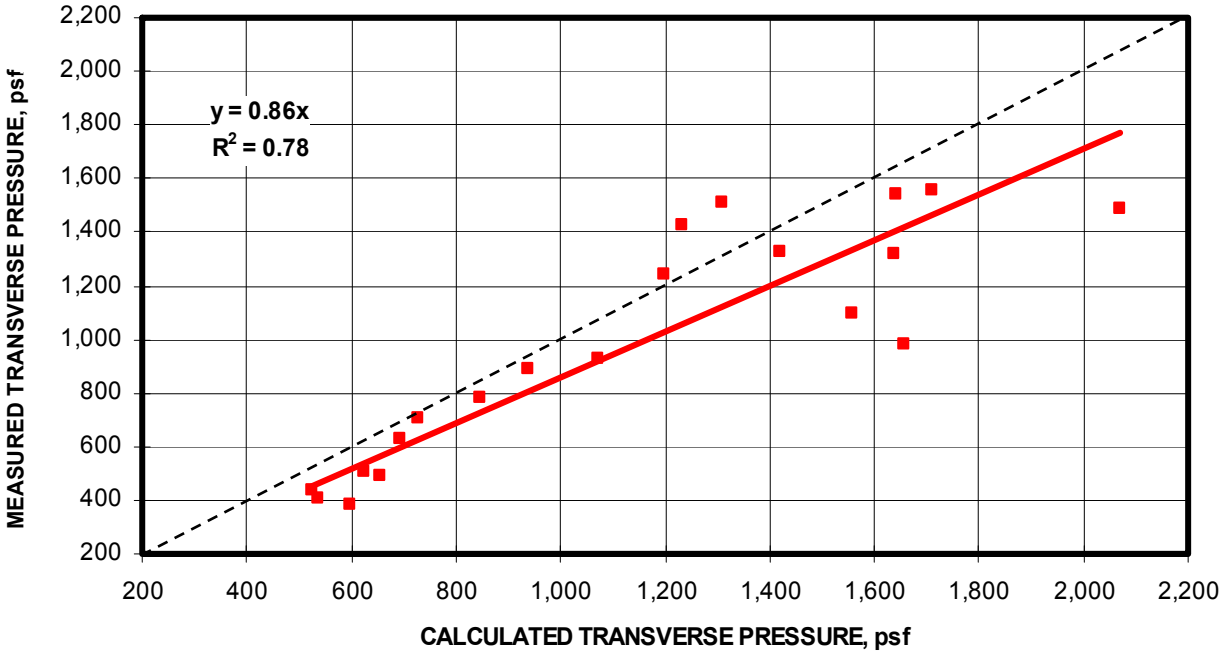

Figure 7-23. Comparison of calculated peak transverse pressure to the measured peak transverse pressure for all 45-in-high tests of this block type.

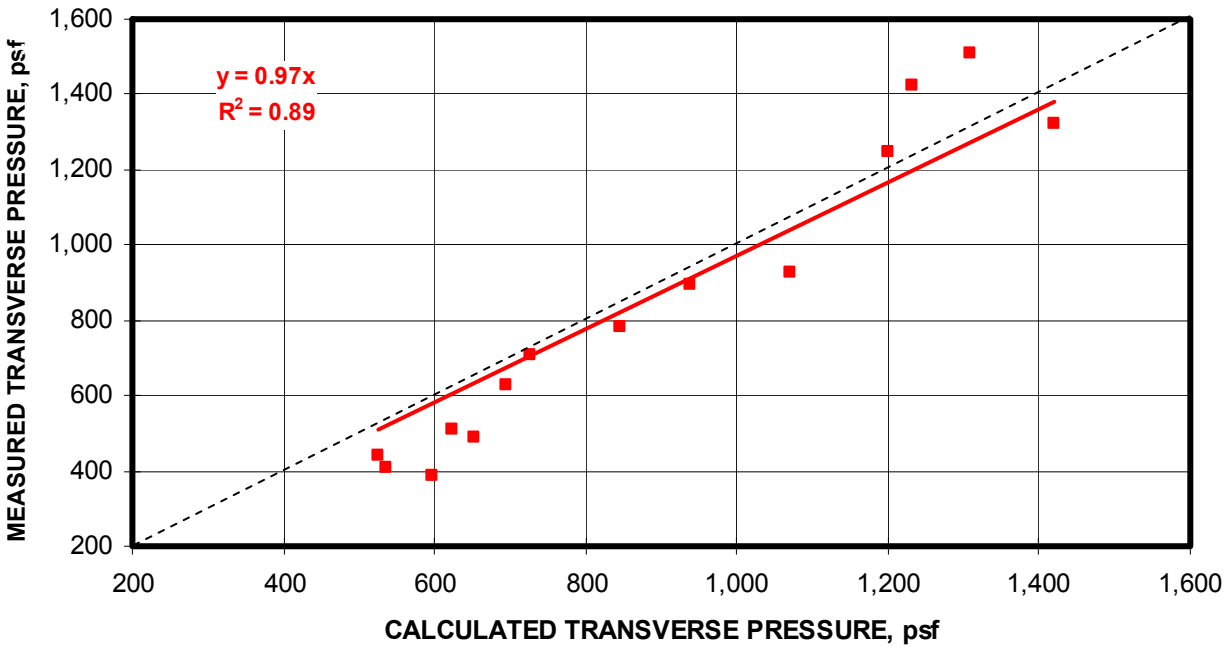

Figure 7-24. Comparison of calculated peak transverse pressure to the measured peak transverse pressure for 45-in-high tests less than 1,500 psf.

7.3 SUMMARY OF PREDICTIVE MODELS FOR COMPUTING TRANSVERSE PRESSURE CAPACITY OF MINE VENTILATION STOPPINGS

Two different models were developed to predict the transverse pressure capacity of dry-stacked mine ventilation stoppings. The same basic theory was utilized in both models; the differences were the result of the required known parameters necessary to compute the transverse pressure capacity. The two models are based on knowing: (1) the lateral displacement of the wall or (2) the thrust force acting on the wall. Since they rely on the same fundamental theory of the arching mechanics, all provide similar predictions of the transverse pressure capacity. Figure 7-25 compares an example prediction of the transverse pressure for each model with the measured transverse pressure from the MRS laboratory testing.

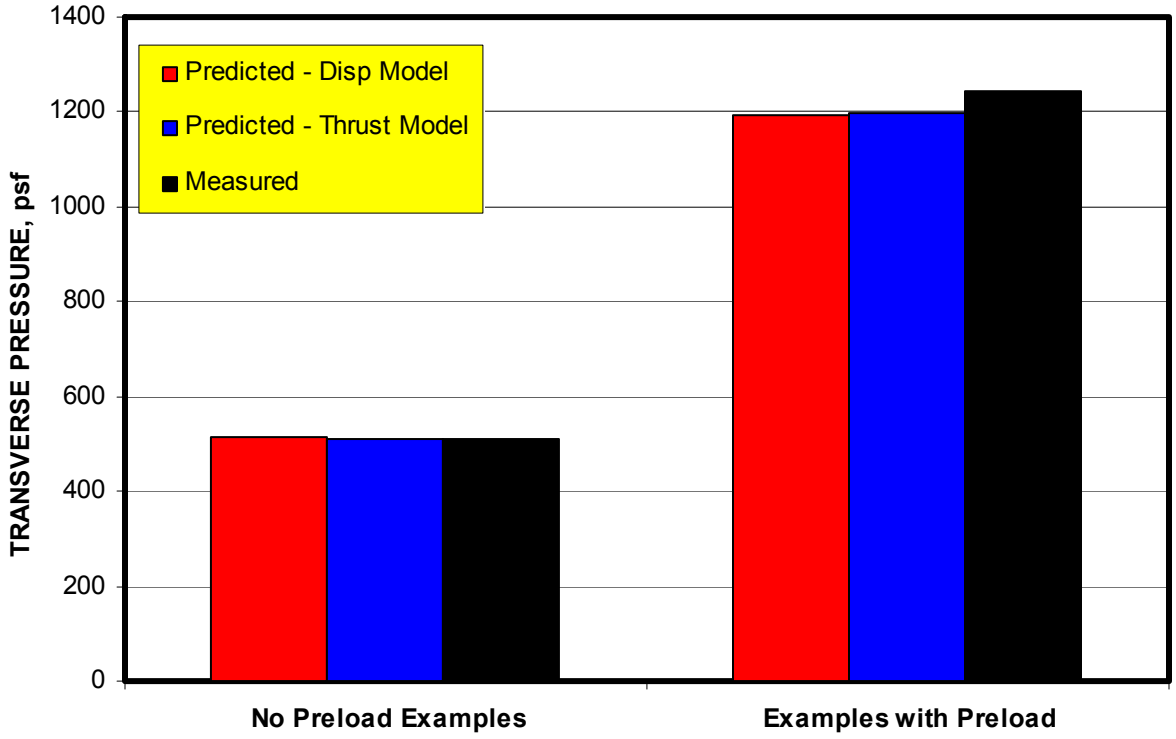

Figure 7-24. Comparison of the two predicted models and the measured transverse pressure.

CHAPTER 8: SUMMARY AND ANALYSIS OF EXPERIMENTAL TEST DATA

Several manufacturers produce blocks for the stopping construction. In addition, there are several different types of block materials. Recently, the trend has been towards lighter weight materials to reduce the construction effort and material handling injuries. Figure 8-1 depicts the strength variations of the materials used in these blocks and figure 8-2 compares the material modulus for the block materials utilized in this research. The compressive strengths range from 84 to 2,450 psi and the modulus ranges from 1,785 to 80,000 psi. The blocks can be categorized as follows: (1) conventional masonry units, (2) cellular concrete blocks, and (3) low strength or specialty type blocks. Using this classification, the average compressive strength for the conventional masonry units was 1,742 psi with an average elastic modulus of 61,000 psi. The average compressive strength for the cellular block materials was 572 psi with an average modulus of 28,000 psi. The low strength blocks had an average compressive strength of 85 psi and an elastic modulus of 5,000 psi. Also shown in figures 9-1 and 9-2 is a hollow block value of 900 psi for the compressive strength and 48,000 psi for the elastic modulus. For arch loading conditions, these differences in material properties provide a wide range of transverse pressure capacities for mine ventilation stoppings.

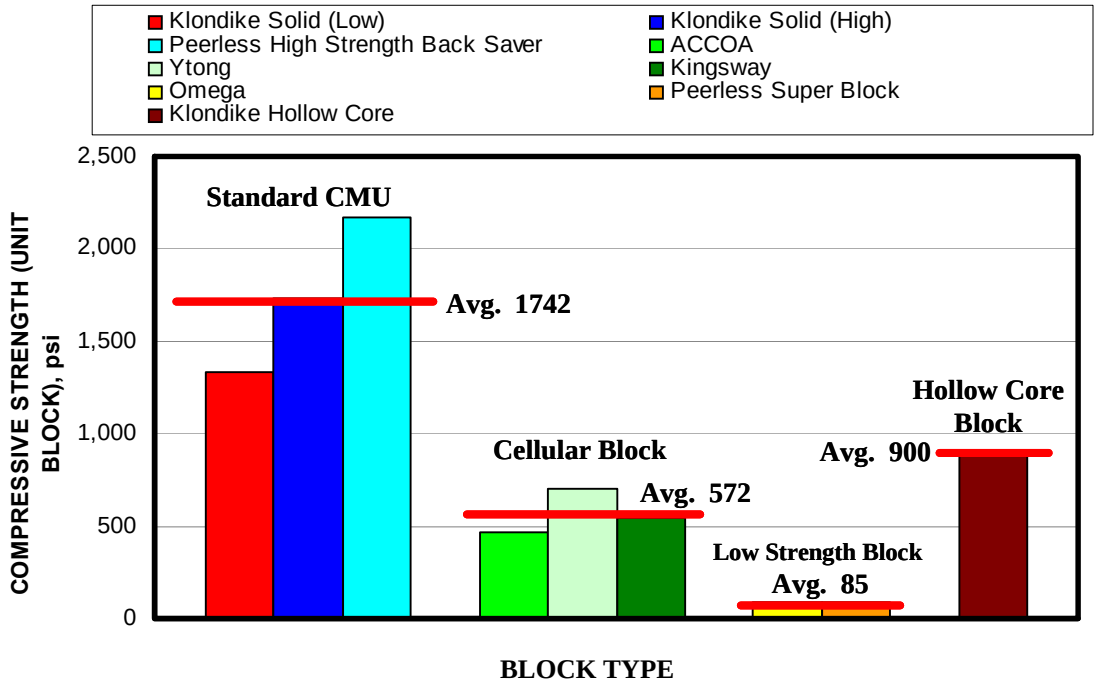

Figure 8-1. Comparison of compressive strength measured from unit block loading of various block materials examined in this research.

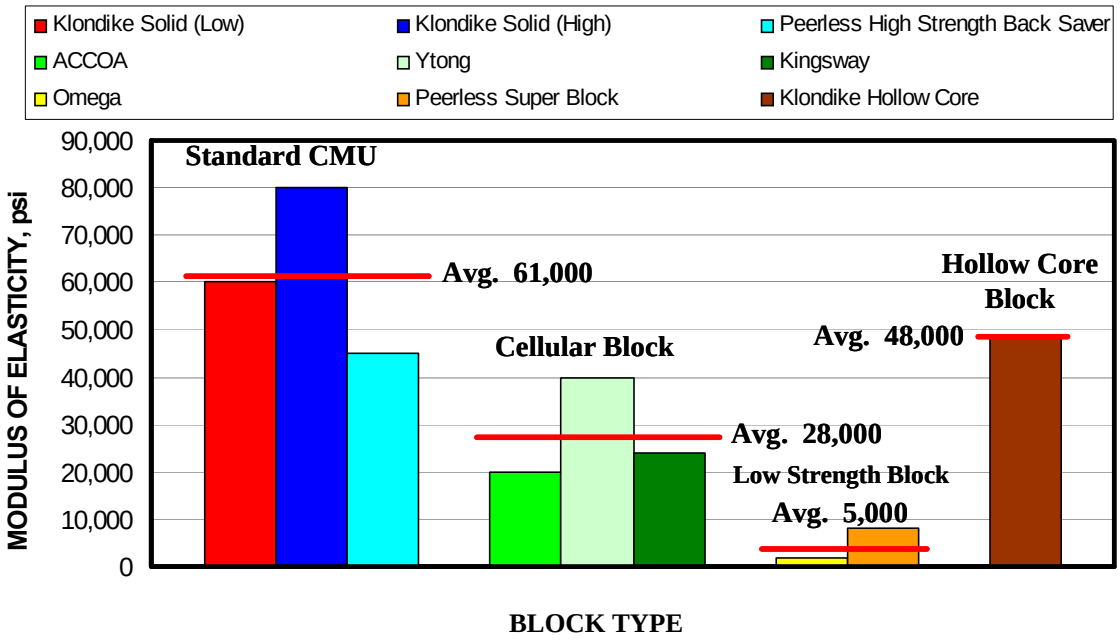

Figure 8-2. Comparison of material modulus of various block materials examined in this research for stopping construction.

A series of tests were conducted in the NIOSH Mine Roof Simulator following the protocol described in chapter 4. Tests were conducted on half-wall single or triple column block walls as documented in the protocol. The parameters varied in the test program were the wall height, wall thickness if appropriate, and the axial preload. All walls were dry-stacked block configurations, which is consistent with the practice utilized in U.S. mines. Generally, three tests were conducted of each configuration to evaluate consistency of the results. The objective of the tests was to determine the transverse loading characteristics and capacity limitations of the various block constructions under arching conditions.

8.1 KLONDIKE SOLID BLOCK

Klondike Block and Masonry Supplies Inc is located in Uniontown, PA and supplies general masonry products including concrete blocks used for mine ventilation stoppings. The block is made from conventional Portland cement and standard aggregate and is similar to conventional block using in the construction industry, just weaker in strength. These blocks are commonly used by many mines in the local area and are sometimes referred to as CMU's or concrete masonry units. Figure 8-3 shows a photo of the block.

The blocks measure 5.625 inches in thickness, 16 inches in width and 7.5 inches high as shown in the figure. This block weighs on average 47 lbs. The compressive strength varies depending on the amount of Portland cement used in the mix. Several batches of block were purchased for laboratory testing. These units had compressive strengths of 1,330, 1,727, and 1,780 psi as measured from a unit block load test.

Figure 8-3. Klondike conventional Portland cement and aggregate block.

8.1.1 Overview of the Test Program

A total of 91 tests were conducted with Klondike block. The results of the MRS half-wall tests are summarized in the tables 8-1, 8-2, and 8-3. Table 8-1 shows the results for the 1,330-psi compressive strength block with the narrow dimension used to establish the wall thickness. Table 8-2 documents the results of this same block with the wide dimension used for the wall thickness. Table 8-3 documents the results of selected tests conducted on the higher strength batches (1,727 and 1,780 psi) of the Klondike block. This batch of block produced some inconsistency in the results and it is suspected that the Portland cement content was not well controlled in this batch resulting in higher than normal variations in compressive strength and other material properties.

The standard test protocol was to evaluate three half-wall heights of 30, 45.75 and 60 inches from half-walls constructed from 4, 6, and 8 courses of block. This equates to a full stopping height ranging from 5 to 10 feet. The preload was varied in increments of 50-100 psi from 0 to 763 psi. Graphs of the measured lateral load and thrust load as a function of the lateral displacement of the wall for each test are documented in Appendix B. A tabular summary of the pertinent parameters and loading values for each test is also included Appendix C.

Table 8-1. Summary of Klondike 1330 block tests with narrow block thickness.

Block Type	Test No.	Block Width (in)	Block Height (in)	Block Length (in)	Half-wall Height (in)	Preload (psi)	Measured Transverse Pressure, (psf)
Klondike 1330	102	5.625	7.5	16	30	51	2,136
Klondike 1330	110	5.625	7.5	16	30	68	2,314
Klondike 1330	104	5.625	7.5	16	30	188	2,358
Klondike 1330	105	5.625	7.5	16	30	160	2,890
Klondike 1330	109	5.625	7.5	16	30	155	2,454
Klondike 1330	111	5.625	7.5	16	30	141	2,436
Klondike 1330	106	5.625	7.5	16	30	295	3,304
Klondike 1330	107	5.625	7.5	16	30	326	3,090
Klondike 1330	108	5.625	7.5	16	30	280	2,676
Klondike 1330	112	5.625	7.5	16	30	385	2,620
Klondike 1330	114	5.625	7.5	16	30	428	3,090
Klondike 1330	115	5.625	7.5	16	30	428	3,088
Klondike 1330	118	5.625	7.5	16	30	470	3,406
Klondike 1330	119	5.625	7.5	16	30	521	2,746
Klondike 1330	113	5.625	7.5	16	30	567	3,376
Klondike 1330	60	5.625	7.5	16	45.75	28	440
Klondike 1330	59	5.625	7.5	16	45.75	43	406
Klondike 1330	46	5.625	7.5	16	45.75	85	510
Klondike 1330	45	5.625	7.5	16	45.75	90	384
Klondike 1330	34	5.625	7.5	16	45.75	109	490
Klondike 1330	36	5.625	7.5	16	45.75	122	628
Klondike 1330	35	5.625	7.5	16	45.75	139	706
Klondike 1330	37	5.625	7.5	16	45.75	202	784
Klondike 1330	63	5.625	7.5	16	45.75	252	892
Klondike 1330	61	5.625	7.5	16	45.75	313	928
Klondike 1330	74	5.625	7.5	16	45.75	373	1,246
Klondike 1330	75	5.625	7.5	16	45.75	390	1,424
Klondike 1330	76	5.625	7.5	16	45.75	474	1,324
Klondike 1330	77	5.625	7.5	16	45.75	471	1,508
Klondike 1330	78	5.625	7.5	16	45.75	577	984
Klondike 1330	79	5.625	7.5	16	45.75	534	1,094
Klondike 1330	81	5.625	7.5	16	45.75	568	1,322
Klondike 1330	82	5.625	7.5	16	45.75	618	1,544
Klondike 1330	83	5.625	7.5	16	45.75	623	1,558
Klondike 1330	85	5.625	7.5	16	45.75	763	1,486
Klondike 1330	89	5.625	7.5	16	60	43	96
Klondike 1330	90	5.625	7.5	16	60	42	102
Klondike 1330	91	5.625	7.5	16	60	143	234
Klondike 1330	92	5.625	7.5	16	60	150	452
Klondike 1330	93	5.625	7.5	16	60	128	480
Klondike 1330	94	5.625	7.5	16	60	310	328
Klondike 1330	95	5.625	7.5	16	60	308	424
Klondike 1330	96	5.625	7.5	16	60	347	562
Klondike 1330	97	5.625	7.5	16	60	394	546
Klondike 1330	98	5.625	7.5	16	60	398	486
Klondike 1330	99	5.625	7.5	16	60	442	584
Klondike 1330	100	5.625	7.5	16	60	592	672
Klondike 1330	101	5.625	7.5	16	60	645	510

Table 8-2. Summary of Klondike 1330 block wide orientation for wall thickness.

Block Type	Test No.	Block Width (in)	Block Height (in)	Block Length (in)	Half-wall Height (in)	Preload (psi)	Measured Transverse Pressure, (psf)
Klondike 1330	65	7.5	5.75	16	45	17	1,330
Klondike 1330	66	7.5	5.75	16	45	39	1,262
Klondike 1330	64	7.5	5.75	16	45	41	1,178
Klondike 1330	73	7.5	5.75	16	45	85	1,332
Klondike 1330	39	7.5	5.75	16	45	99	1,212
Klondike 1330	72	7.5	5.75	16	45	104	1,044
Klondike 1330	40	7.5	5.75	16	45	118	1,314
Klondike 1330	41	7.5	5.75	16	45	121	898
Klondike 1330	67	7.5	5.75	16	45	146	1,586
Klondike 1330	47	7.5	5.75	16	45	169	1,814
Klondike 1330	68	7.5	5.75	16	45	174	2,000
Klondike 1330	69	7.5	5.75	16	45	237	2,056
Klondike 1330	70	7.5	5.75	16	45	254	1,444
Klondike 1330	71	7.5	5.75	16	45	279	2,138

Table 8-3. Summary of Klondike 1,727 and 1,780 block

Klondike 1780	17	5.625	7.5	16	45.75	0	300
Klondike 1780	18	5.625	7.5	16	45.75	228	1,080
Klondike 1780	23	5.625	7.5	16	45	287	1,438
Klondike 1780	24	5.625	7.5	16	45	290	1,166
Klondike 1780	25	5.625	7.5	16	45	356	940
Klondike 1780	21	7.5	5.75	16	46	23	918
Klondike 1780	20	7.5	5.75	16	46	201	3,062
Klondike 1780	19	7.5	5.75	16	46	210	3,288
Klondike 1727	151	5.625	7.5	16	30	77	1,980
Klondike 1727	152	5.625	7.5	16	30	43	2,936
Klondike 1727	153	5.625	7.5	16	30	50	1,830
Klondike 1727	154	5.625	7.5	16	30	66	2,750
Klondike 1727	155	5.625	7.5	16	30	63	2,216
Klondike 1727	156	5.625	7.5	16	30	40	2,286
Klondike 1727	157	5.625	7.5	16	30	77	2,850
Klondike 1727	200	5.625	7.5	16	37.5	41	1,102
Klondike 1727	202	5.625	7.5	16	37.5	87	1,536
Klondike 1727	158	5.625	7.5	16	45	65	842
Klondike 1727	159	5.625	7.5	16	45	69	498
Klondike 1727	161	5.625	7.5	16	45	67	888
Klondike 1727	162	5.625	7.5	16	45	59	896
Klondike 1727	199	5.625	7.5	16	52.5	89	400
Klondike 1727	203	5.625	7.5	16	52.5	107	512
Klondike 1727	198	5.625	7.5	16	60	68	248
Klondike 1727	204	5.625	7.5	16	60	73	310

8.1.2 Parametric Relationships and Trends.

Examining tables 8-1 and 8-2, it is seen that the transverse pressure capacity of the stoppings constructed from Klondike (1330-psi compressive strength) block varied from a low of 96 to a high of 3,376 psf or 0.67 to 23.44 psi. Putting this in perspective, the CFR requirement for stoppings is 39 psf (0.27 psi) and 2,880 psf (20 psi) for seals. Further examination shows that the transverse pressure is significantly affected by the wall height and then by the amount of preload and the wall thickness. Figure 8-4 displays the transverse pressure as a function of preload for 30, 46, and 60-in half-wall heights equating to full wall heights of 5.0, 7.6 and 10.0 ft. The peak transverse pressures for the 30-in-high half-walls are 6 to 8 times higher for preloads above 100 psi than that of the 60-in half-walls and 2 to 4 times higher than the 46-in-high half-walls. It is also seen from figure 8-4 that the transverse pressure is nonlinearly related to the preload and that the transverse pressure reaches an asymptotic maximum between 500-550 psi of preload. This suggests that the wall is being stressed to its maximum strength from the combination of the preload and arch compressive forces when the wall is preloaded to this level. The 1,727 and 1,780-psi block are designated separately and the inconsistency in expected results is highlighted with transparent yellow ovals. Again, it is suspected that this inconsistency in this particular block is due to quality control of the cement material mixes and the resulting block strength.

Figure 8-5 shows that the lateral displacement at the peak transverse pressure also approaches an asymptotic minimum as the preload exceeds 550 psi. This is consistent with the transverse pressure behavior expressed in figure 8-4, indicating a limitation of the transverse pressure capacity. It is seen from this figure that the lateral displacement is reduced quickly for preload pressures up to 200 psi, and then the impact diminishes for higher preloads. This indicates that it the initial addition of preload will produce a big increase in the transverse load capacity of a stopping.

The impact of the wall thickness can be seen from figure 8-6. The wall thickness was varied from the narrow block dimension (5.625 in) to the wide block dimension (7.5 in) in this graph. The wide-wall construction provides 2 to 3 times the transverse pressure capacity of the narrow thickness construction, and a similar relationship to the preload.

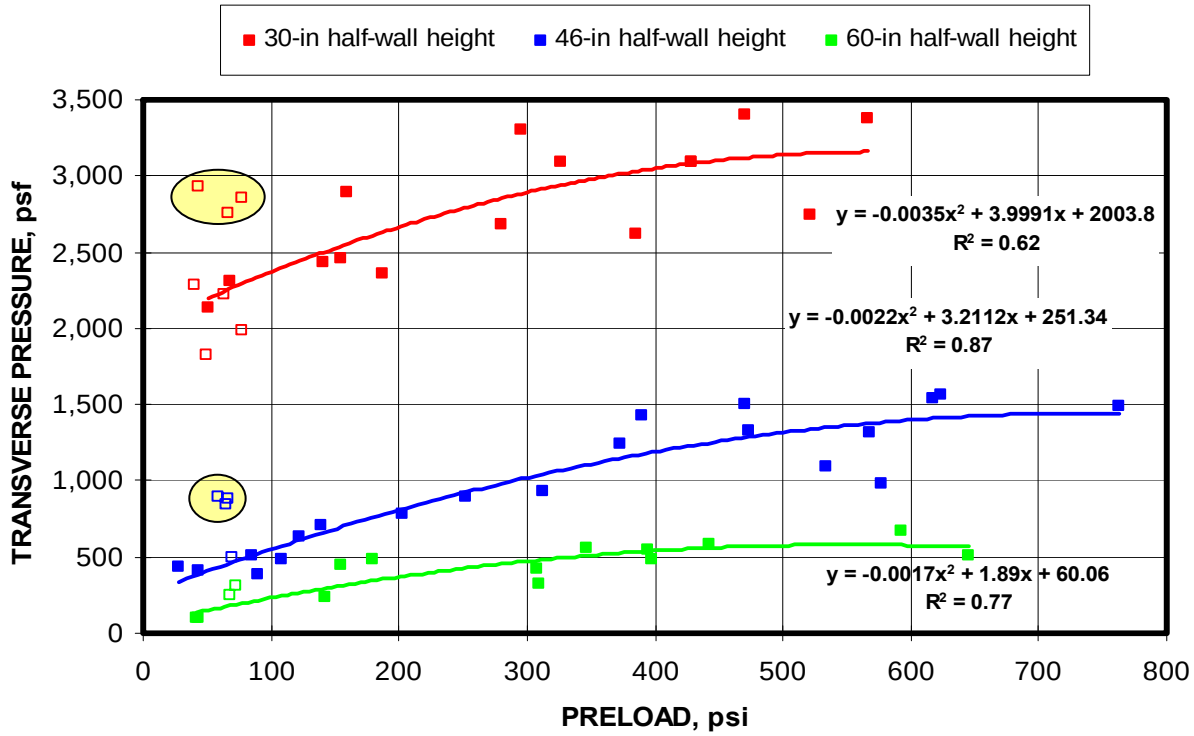

Figure 8-4. Transverse pressure as measured for MRS laboratory testing as a function of preload for three different half-wall heights.

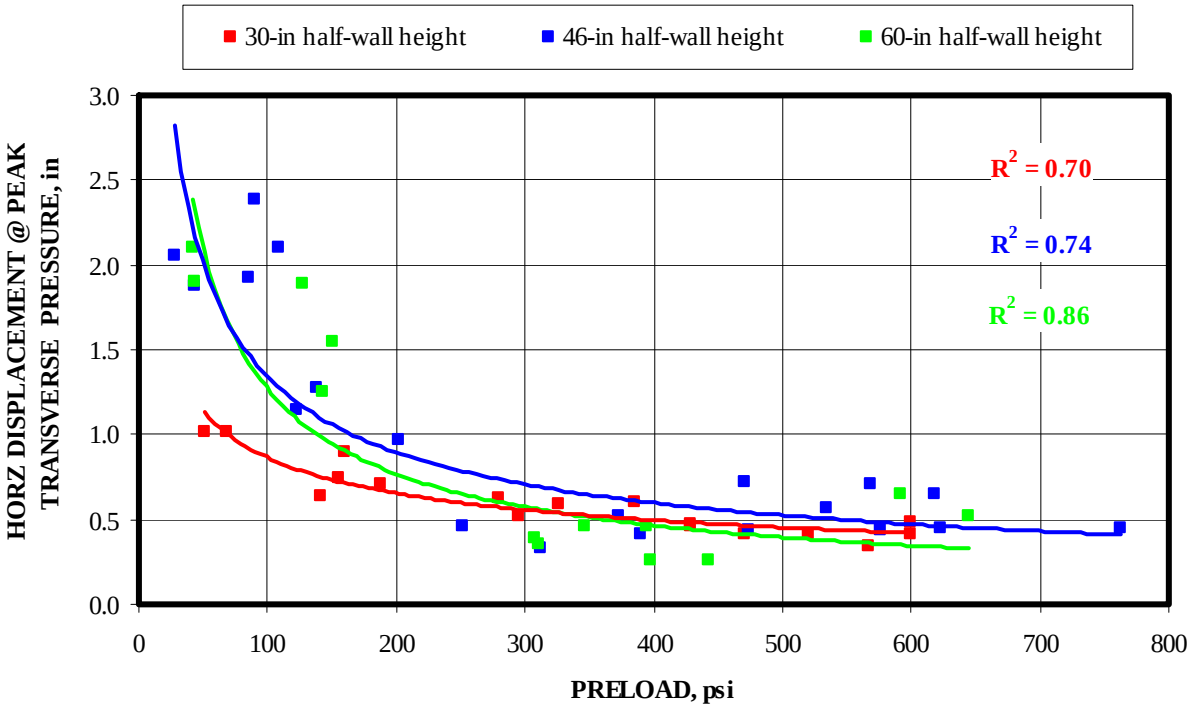

Figure 8-5. Lateral displacement at which peak transverse pressure occurs also reaches an asymptotic minimum as the preload exceeds 600 psi.

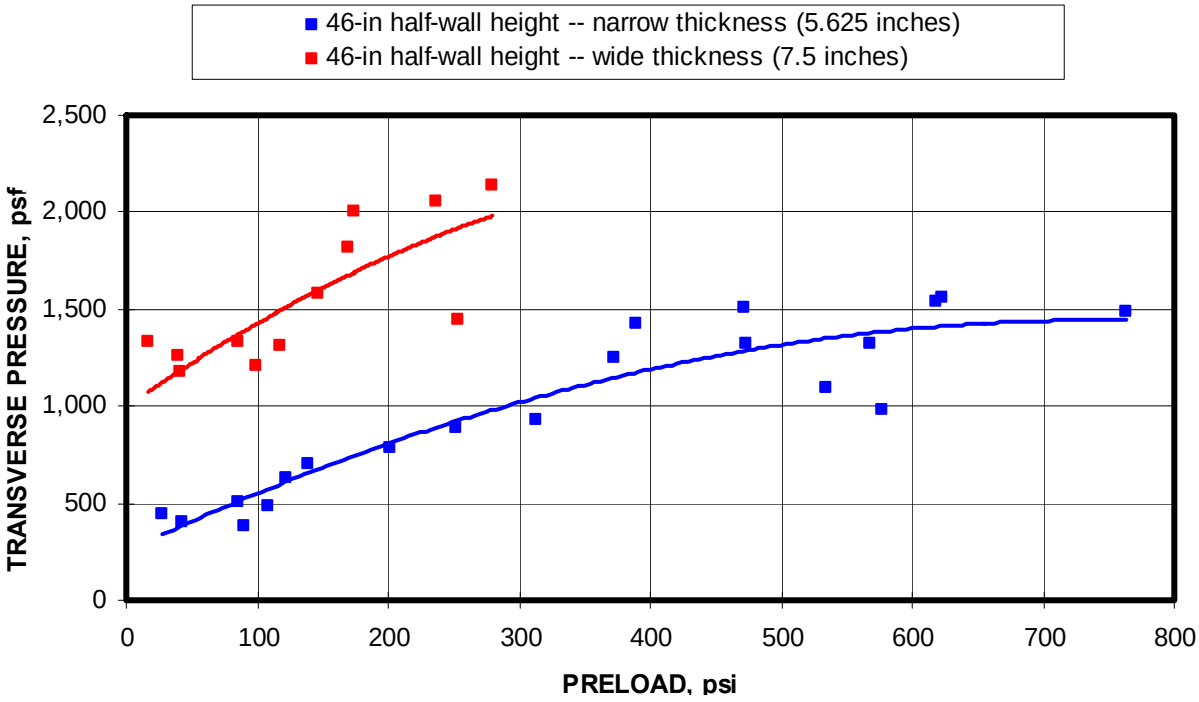

Figure 8-6. Comparison of narrow and wide wall thickness for Klondike block as a function of preload.

Further examination of the parametric relationships confirms the arching theory as presented in chapters 5 and 6. Figure 8-7 shows that the transverse pressure is directly related to the lateral force acting on the half-wall during the laboratory tests. Figure 8-8 shows that the lateral force is also directly related to the thrust force. This is also consistent with the arching theory. Finally, figure 8-9 shows the relationship between the transverse pressure and the arch thrust. This graph resembles the plot of transverse pressure versus preload shown in figure 8-4. The preload also limits the thrust load for the 46 and 60-in half-wall tests. The 30-in half-wall test appears to be linear, suggesting that the thrust load is not yet reaching its limit for this configuration and could possible sustain higher preloads.

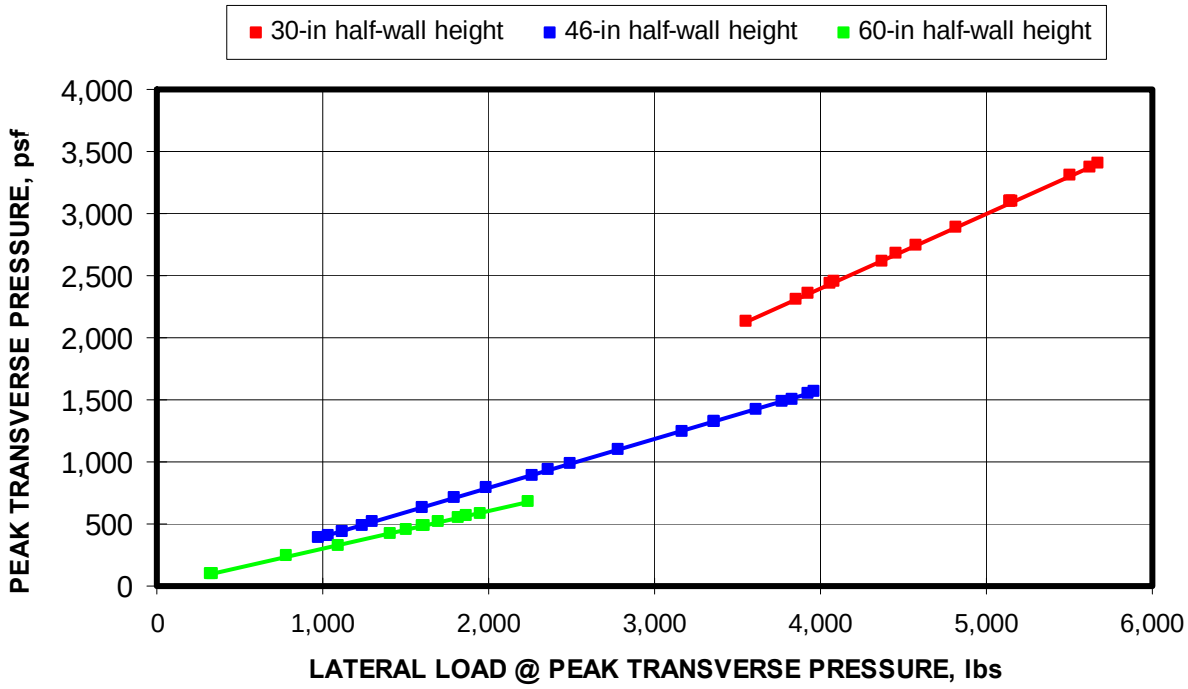

Figure 8-7. Transverse pressure is directly related to the lateral load acting on the half-wall in the MRS laboratory test.

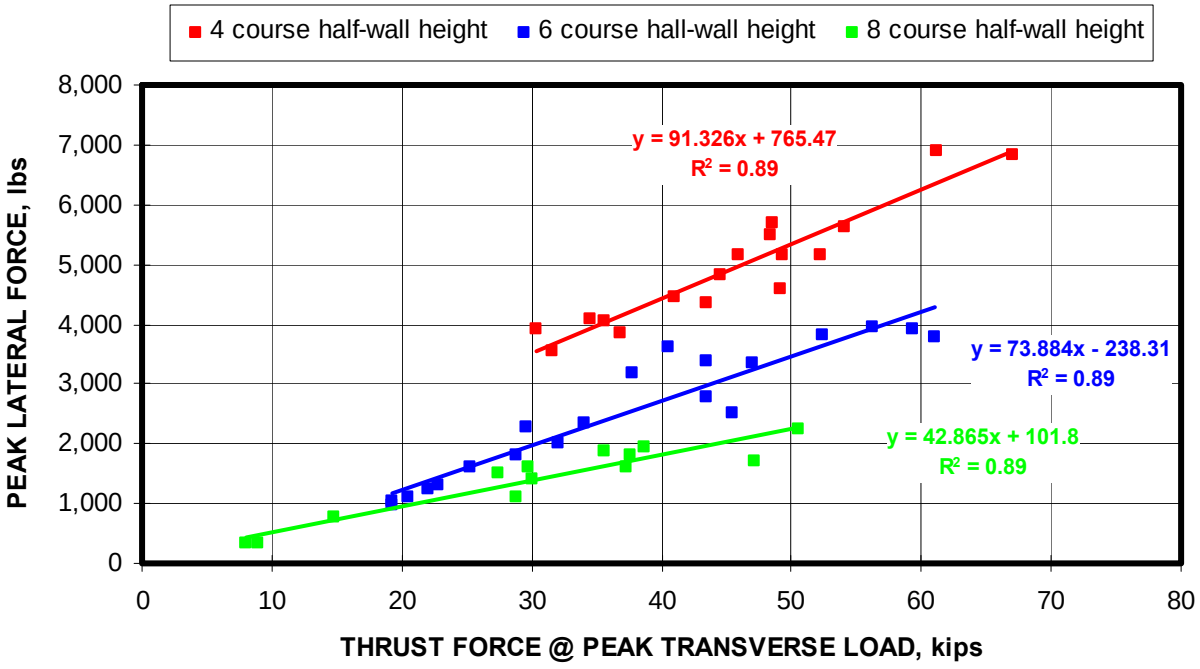

Figure 8-8. Lateral force is also directly related to the thrust force.

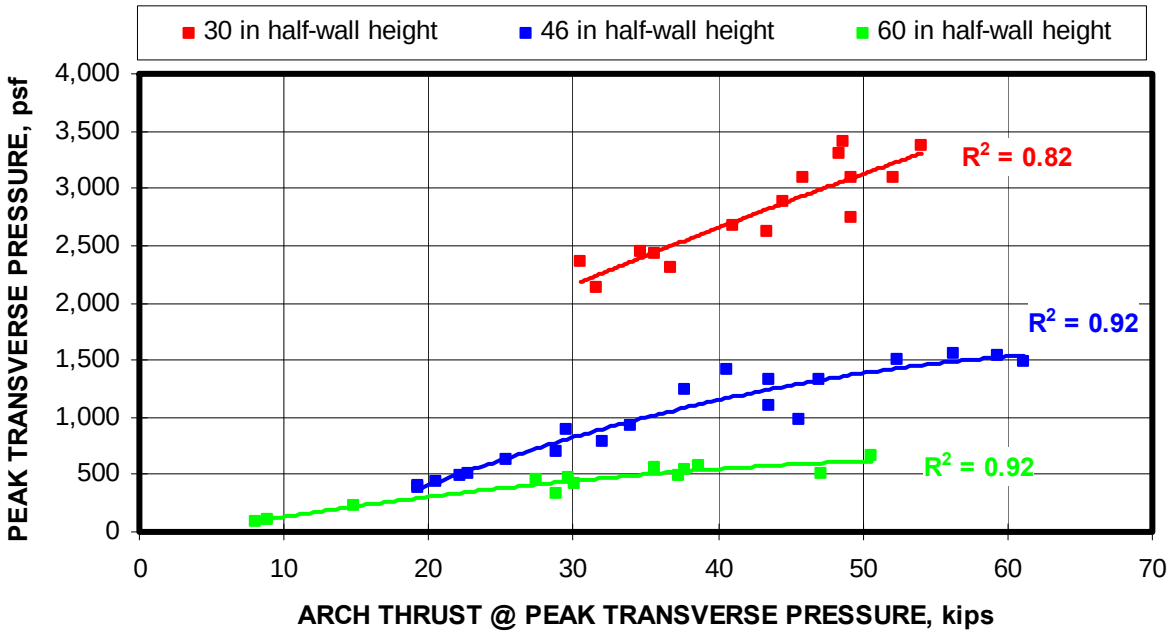

Figure 8-9. Relationship between the transverse pressure and the arch thrust for MRS laboratory tests conducted at three different half-wall heights.

Figure 8-10 depicts the relationship for tests with less than 100 psi preload between the transverse pressure and the calculated material modulus (E), the wall thickness (t), and the wall height (L) expressed as by the term E x $(t/L)^2$. Included in this data set are the 1,727 and 1,780 psi compressive strength block results documented in table 8-3 and a few miscellaneous, high strength (2,450 psi) Portland cement block tests of uncertain manufacturer. The chart shows that 90 pct of the transverse pressure of a stopping is determined by this relationship. The material modulus is a significant parameter since it determines the amount of thrust force developed and ultimately the amount of lateral displacement of the wall, both of which control the arching mechanics of the wall. If the modulus is related to the compressive strength of the block material, the modulus factor could be replaced by the compressive strength as previous research suggests (Barczak, 2004).

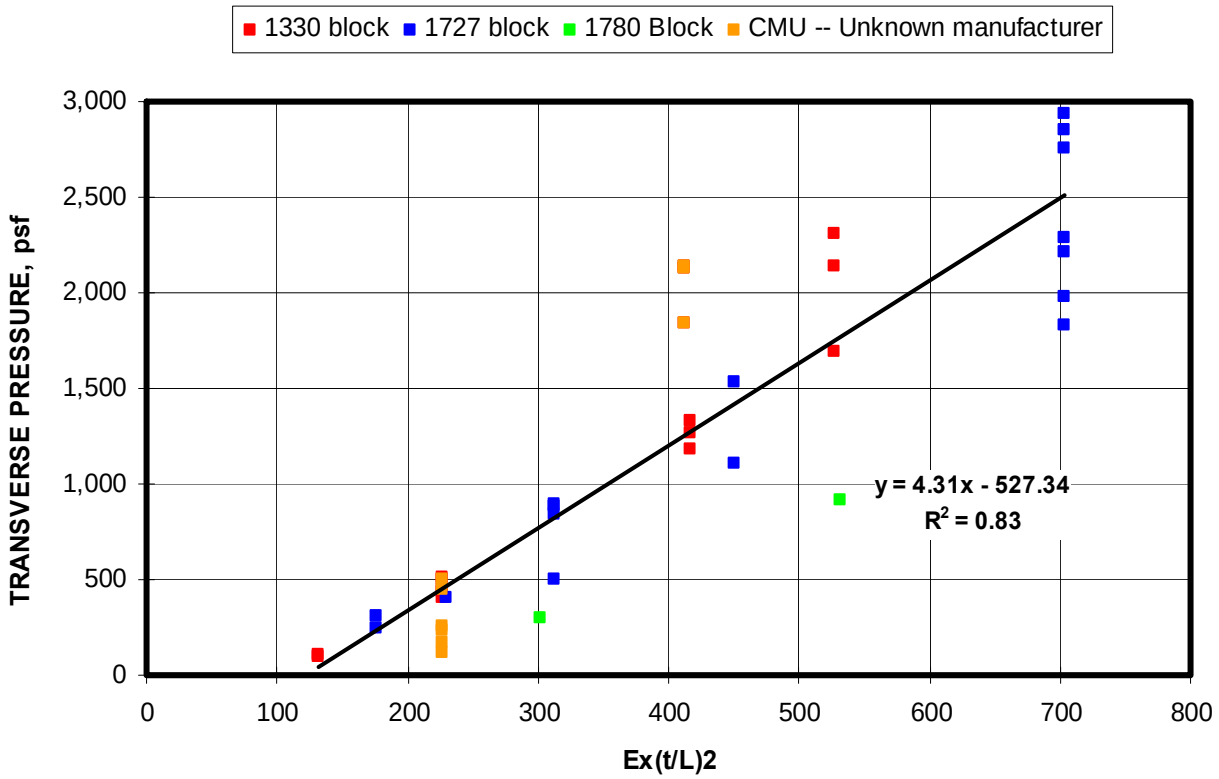

Figure 8-10. Correlation of factors involving the material modulus (E), wall thickness (t), and wall height (L) to the transverse pressure capacity of a stopping.

8.1.3 Evaluation of the Predictive Models

The next goal is to evaluate the capability to predict the transverse pressure. If the thrust force and its resultant location and lateral force are known, the transverse pressure capacity of a stopping can be predicted with nearly 100 pct accuracy. If the thrust force location is instead calculated from the empirical relationship described in chapter 6 and shown in figure 8-11 for three half-wall heights considered in this analysis, the transverse pressure can still be predicted with a 98 pct accuracy as depicted by the open red square data points shown in figure 8-12. Each data point in figure 8-12 represents an individual laboratory test. As seen in the figure, the accuracy of the prediction is fairly consistent throughout the full range of transverse pressure conducted in the laboratory testing for three different wall heights, and includes preloading of wall from 0 to 763 psi.

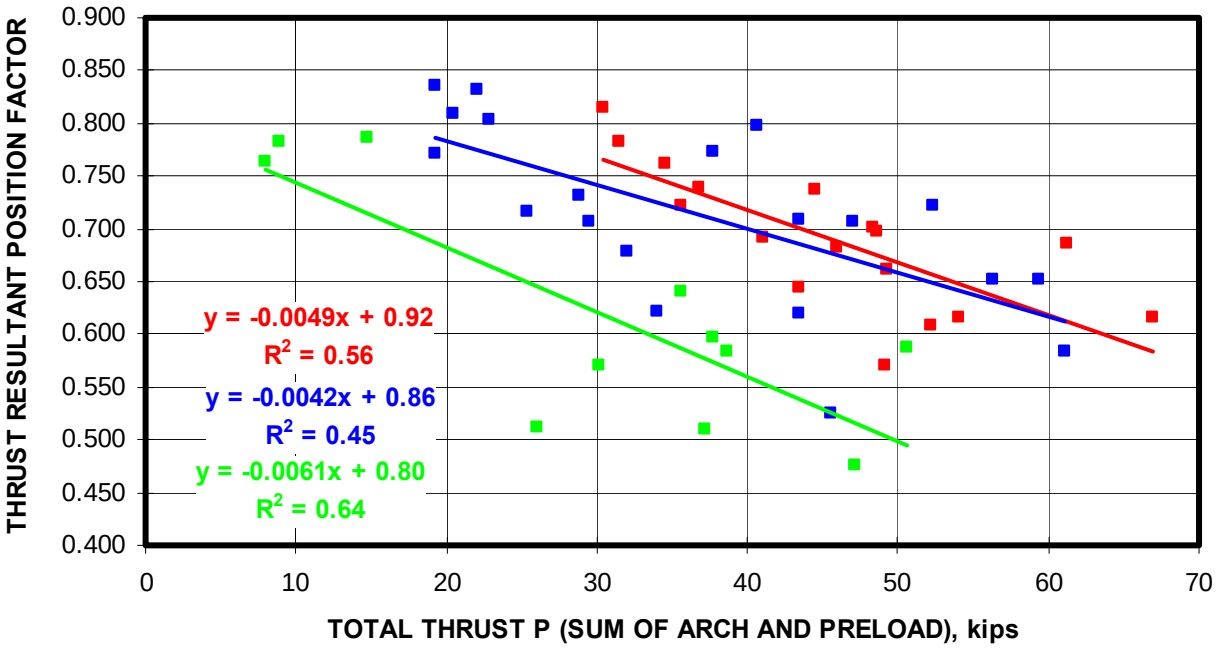

Figure 8-11. Resultant thrust force location for three wall heights as a function of the total arch thrust (Klondike solid block).

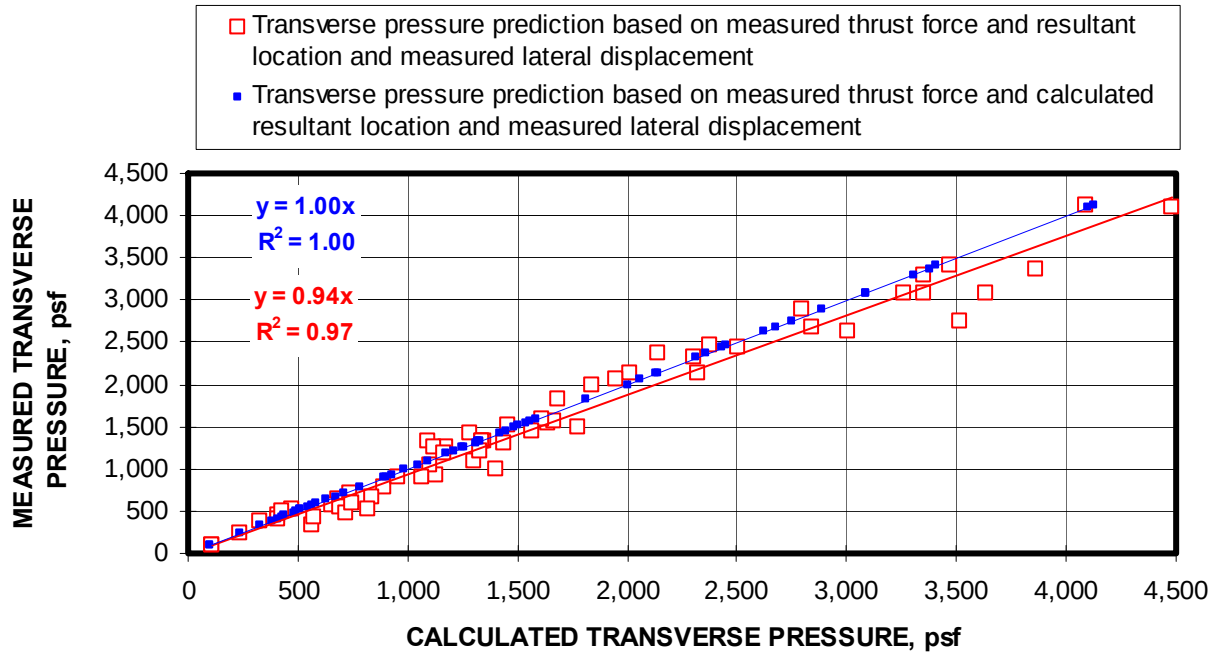

Figure 8-12. Prediction of transverse pressure when both the lateral load and arch thrust are known. Blue curves predicts transverse pressure when resultant thrust force location is also known and red squares show predicted transverse pressure when resultant thrust force location is calculated from empirical data.

If either the thrust force or the lateral displacement is known, then the transverse pressure can still be calculated. It is recalled from chapter 7 that two methods were developed. Method 1 predicts the transverse pressure from the measured lateral displacement. Method 2 predicts the transverse pressure from the measured thrust force. Figure 8-13 illustrates the predictive capability of these models showing the measured transverse pressure vs. the predicted transverse pressure for each half-wall laboratory test. Both methods predict the transverse pressure with reasonably good accuracy with regression coefficients for the slope of the line comparing the predicted to the measured transverse pressure equaling 0.91 and 0.95, respectively. The trend line can be thought of as an average measure of the model's capability. For example, the slope of the trend line for the lateral displacement model indicates that the model over predicts the measured transverse pressure by 5 pct, while the thrust model over predicts the measured response by 4 pct.

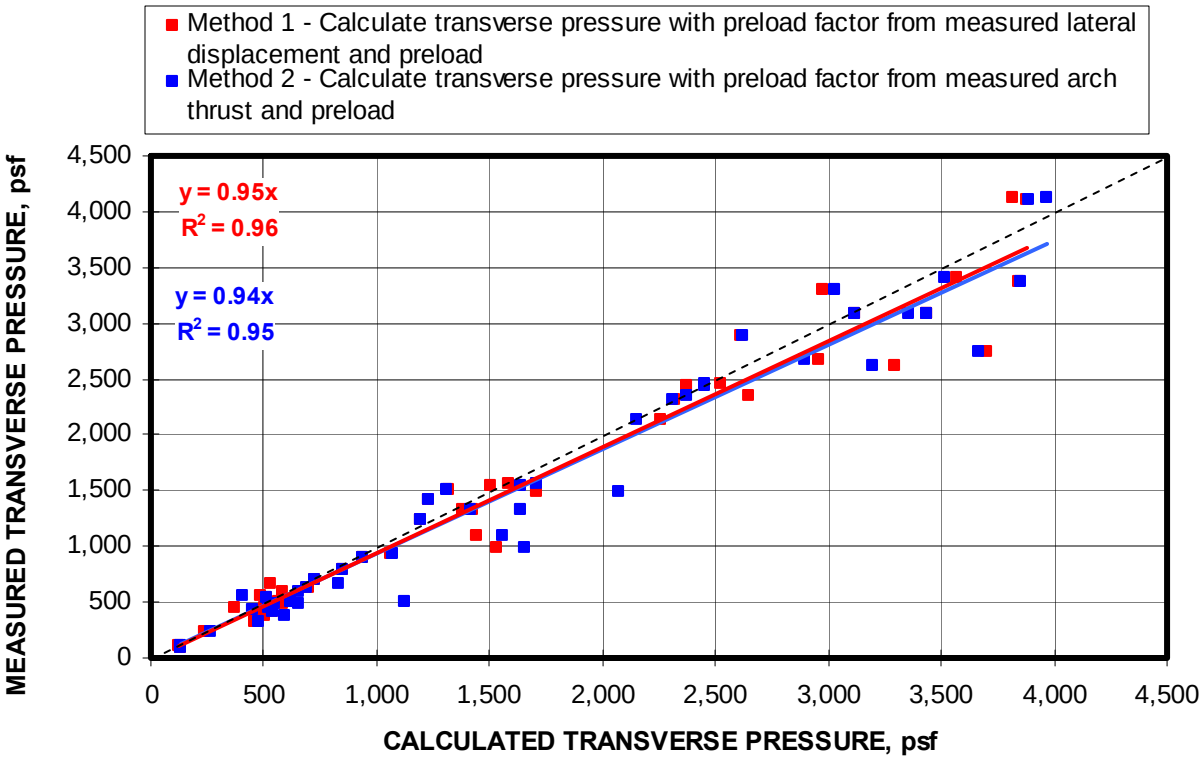

Figure 8-13. Prediction of transverse pressure from known thrust and lateral loads.

8.1.4 Theoretical Impact of Boundary Stiffness

A theoretical assessment of the impact of the boundary stiffness is conducted by varying the system modulus of elasticity (see equation 6.11 and 7.7). Recalling the

theoretical assessment of arching mechanics described in chapters 5 and 6, the modulus of elasticity determines the deformations of the wall and the boundary, i.e. the mine roof and floor. The system modulus reflects the series stiffness equivalent of the wall and roof and floor structure. The theoretical assessment is made by reducing the system modulus to 75, 50, and 25 pct of the rigid boundary condition, and computing the transverse pressure using the lateral displacement model developed in chapter 7. For comparative purposes, if the boundary stiffness were equal to the wall stiffness, the system stiffness would be reduced by 50 pct. Likewise, if the boundary stiffness were 3 times that of the wall, the system stiffness would be 75 pct of the rigid boundary condition, and if the boundary stiffness were one third of the wall stiffness, the system stiffness would be 25 pct of the rigid boundary condition.

Figure 8-14 shows the impact of the reduction in system modulus to 25, 50, and 75 pct of the rigid boundary condition at 3 different wall heights as a function of preload. First, it can be concluded from figure 8-14 that as the boundary modulus is reduced, the transverse pressure capacity of the stopping will also be reduced. It is seen from this figure that the impact of reductions in boundary modulus will have a greater impact in terms of absolute reductions in transverse pressure for shorter walls than it will for taller walls. For the example shown in figure 8-14, the transverse pressure for test number 102 for the 30-in half-wall height, the transverse pressure was reduced from 2,256 psf for the rigid boundary condition to 940 psf when the boundary modulus is one third of the wall modulus, thereby reducing the system modulus to 25 pct of the rigid boundary condition. This represents a 58 pct decrease in the transverse pressure capacity of the stopping. The percent reduction in transverse pressure remains the same for all wall heights.

Figures 8-15 through 8-17 show the impact of reductions in system modulus for half-wall heights of 30, 46, and 60 inches. In these figures, the transverse pressure is plotted as a function of preload, which varies from zero to 600 psi. These figures indicate the reductions in transverse pressure because of reduction in boundary stiffness (lower system modulus) are reduced as the preload increases. Using the 30-in-high half-wall as an example, the 58 pct decrease in transverse pressure which occurred by reducing the system modulus to 25 pct of the rigid boundary condition, drops to a 7 pct reduction at a preload of 567 psi.

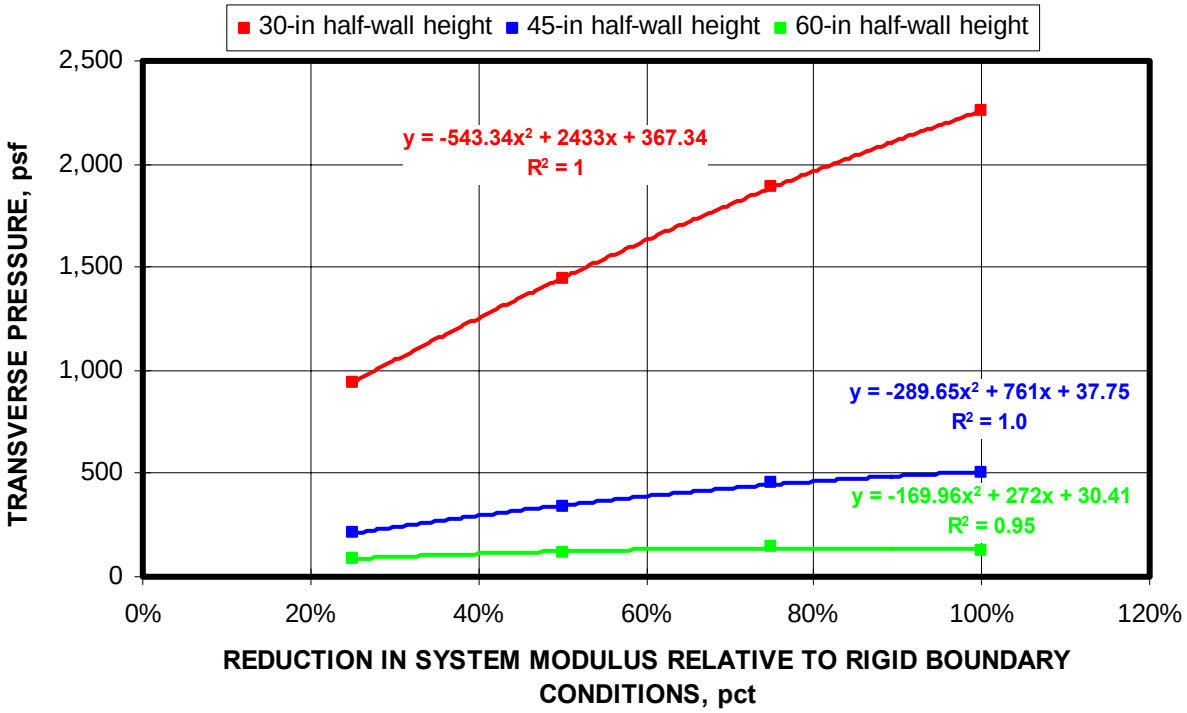

Figure 8-14. Impact of reducing the boundary stiffness on transverse pressure capacity of stopping. Data shows individual test at different wall heights with no preload.

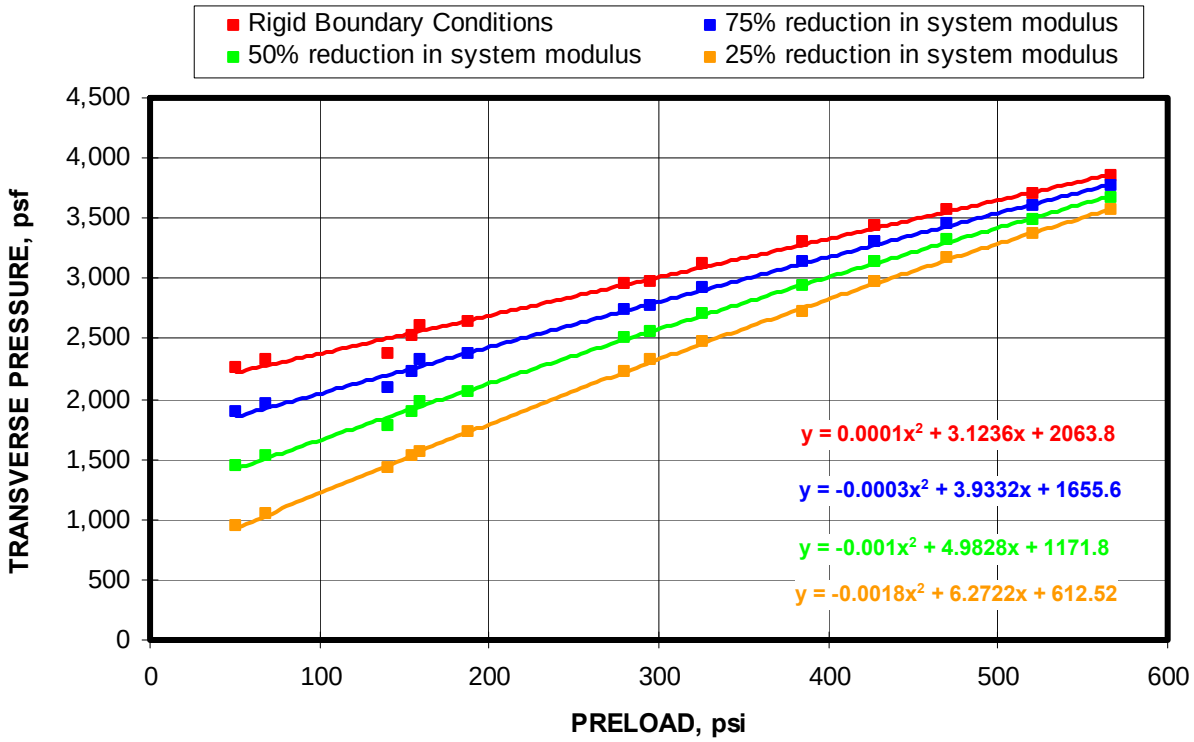

Figure 8-15. Impact of boundary stiffness reductions compared to rigid arching conditions as a function of preload for 30-in-high half-walls.

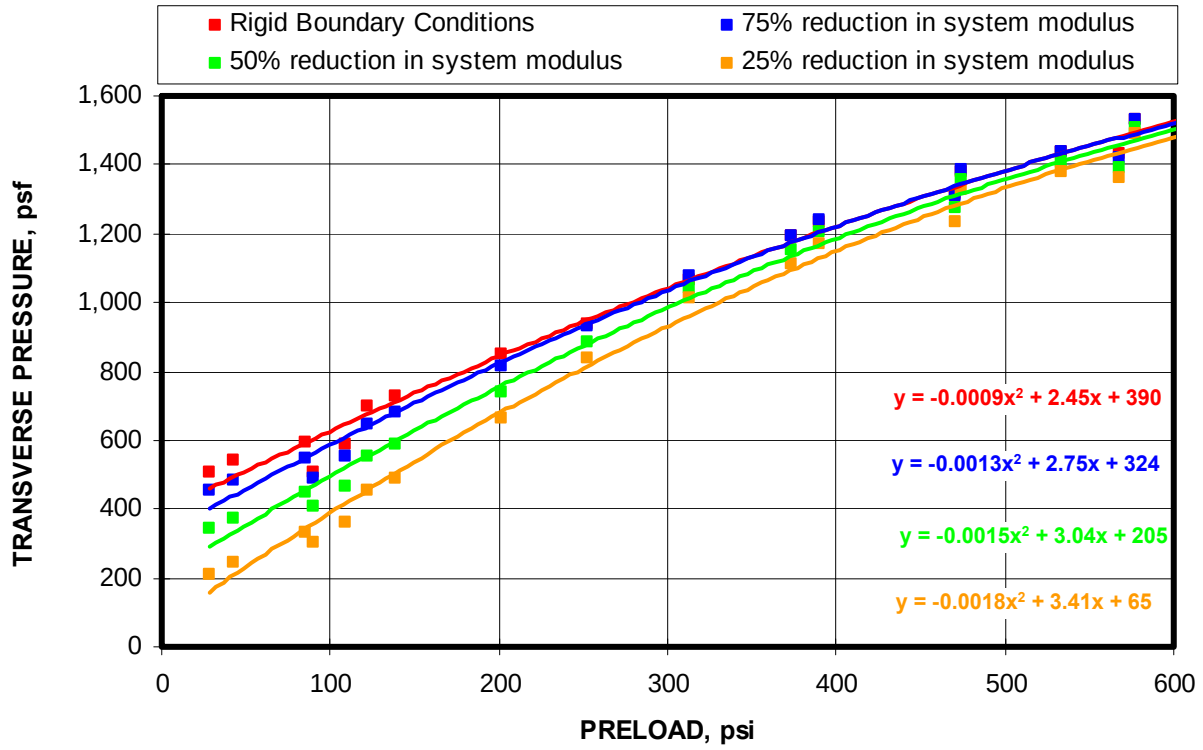

Figure 8-16. Impact of boundary stiffness reductions compared to rigid arching conditions as a function of preload for 46-inch-high half-wall constructions.

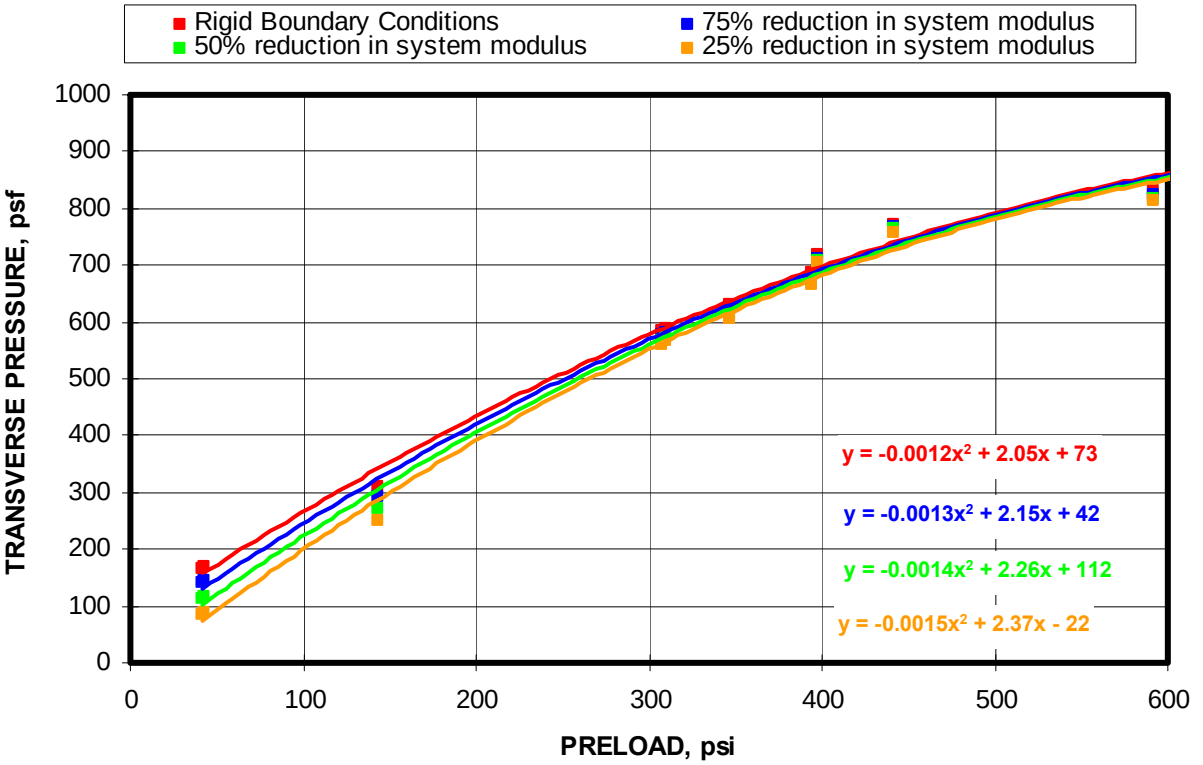

Figure 8-17. Impact of boundary stiffness reductions compared to rigid arching conditions as a function of preload for 60-inch-high half-wall constructions.

8.2 PEERLESS BACKSAVER

Peerless Block & Masonry Company is located in St. Albans, WV and has been supplying masonry products to the mining industry for over 50 years. The block is made from lightweight aggregate, cement, and bottom ash. The blocks are manufactured in 6x8x16-in and 8x8x16--in sizes. The 6x8x16-in units were purchased for the laboratory tests. A 6x8x16-in block weighs approximately 39 lbs. Figure 8-18 shows a photo of the block. Two batches of this block were purchased. The first blocks were cured for over 2 years before being tested. At the time of the laboratory testing, these block exhibited a unit block compressive strength of 2,169 psi. Additional block were purchased later and were cured only 2 weeks prior to testing. These blocks exhibited a unit block compressive strength of 1,070 psi. Tests of a six-course column of block provided compressive strengths of about 75 pct of the unit block tests. It is believed the reduction in apparent strength is due to the stress concentrations at the block joints caused by differences in dimensional tolerances.

Figure 8-18. Peerless Backsaver block.

8.2.1 Overview of the Test Program

A total of 33 tests were conducted with Peerless Backsaver block. The results of the MRS half-wall tests are summarized in the tables 8-4, and 8-5. Table 8-4 shows the results for the fully cured, 2,169-psi compressive strength block with the narrow dimension used to establish the wall thickness. Table 8-5 documents the results of the same style block that was only cured for two weeks resulting in a reduced compressive strength. The standard test protocol was to evaluate three half-wall heights of 30, 45 and 60 inches from half-walls constructed from 4, 6, and 8 courses of block. This equates to a full stopping height ranging from 5 to 10 feet. Limited block quantities forced a reduced scope of testing relative to preloading. The preload was varied from 3 to 165 psi for the 30-in-high half-walls, from 12

to 362 psi for the 45-in-high half-walls, and from 22 to 447 for the 60-in-high half-walls. Nominal preloads of 50-75 psi were applied to the partially cured block tests shown in table 8-5. Graphs of the measured lateral load and thrust load as a function of the lateral displacement of the wall for each test are documented in Appendix B. A tabular summary of the pertinent parameters and loading values for each test is also included Appendix C.

Table 8-4. Summary of normal strength Peerless Backsaver block tests.

Block Type	Test No.	Block Width (in)	Block Height (in)	Block Length (in)	Half-wall Height (in)	Preload (psi)	Measured Transverse Pressure (psf)
Peerless Backsavers	297	5.875	7.5	16	30	3	2,072
Peerless Backsavers	298	5.875	7.5	16	30	10	1,928
Peerless Backsavers	295	5.875	7.5	16	30	16	2,174
Peerless Backsavers	296	5.875	7.5	16	30	19	2,766
Peerless Backsavers	292	5.875	7.5	16	30	21	2,492
Peerless Backsavers	293	5.875	7.5	16	30	50	2,130
Peerless Backsavers	301	5.875	7.5	16	30	100	2,732
Peerless Backsavers	294	5.875	7.5	16	30	104	2,132
Peerless Backsavers	299	5.875	7.5	16	30	80	2,508
Peerless Backsavers	300	5.875	7.5	16	30	165	3,136
Peerless Backsavers	261	5.875	7.5	15.5	45	12	268
Peerless Backsavers	260	5.875	7.5	15.5	45	25	438
Peerless Backsavers	262	5.875	7.5	15.5	45	78	614
Peerless Backsavers	266	5.875	7.5	15.5	45	94	706
Peerless Backsavers	289	5.875	7.5	15.5	45	121	1,032
Peerless Backsavers	291	5.875	7.5	15.5	45	143	1,122
Peerless Backsavers	264	5.875	7.5	15.5	45	178	1,302
Peerless Backsavers	265	5.875	7.5	15.5	45	182	756
Peerless Backsavers	290	5.875	7.5	15.5	45	210	884
Peerless Backsavers	267	5.875	7.5	15.5	45	265	752
Peerless Backsavers	288	5.875	7.5	15.5	45	362	828
Peerless Backsavers	282	5.875	7.5	15.5	60	22	126
Peerless Backsavers	283	5.875	7.5	15.5	60	57	202
Peerless Backsavers	284	5.875	7.5	15.5	60	132	220
Peerless Backsavers	285	5.875	7.5	15.5	60	183	374
Peerless Backsavers	286	5.875	7.5	15.5	60	239	680
Peerless Backsavers	287	5.875	7.5	15.5	60	447	400

Table 8-5. Summary of low strength Peerless Backsaver block tests.

Block Type	Test No.	Block Width (in)	Block Height (in)	Block Length (in)	Half-wall Height (in)	Preload (psi)	Measured Transverse Pressure (psf)
Peerless Backsavers	355	5.625	7.5	15.5	30	72	1,900
Peerless Backsavers	356	5.625	7.5	15.5	30	60	1,652
Peerless Backsavers	357	5.625	7.5	15.5	45	45	428
Peerless Backsavers	358	5.625	7.5	15.5	45	54	500
Peerless Backsavers	359	5.625	7.5	15.5	60	66	84
Peerless Backsavers	360	5.625	7.5	15.5	60	52	156

8.1.2 Parametric Relationships and Trends.

Examining tables 8-4 and 8-5, it is seen that the transverse pressure capacity of the stoppings constructed from fully cured Peerless Backsaver block varied from a low of 84 to a high of 3,136 psf or 0.058 to 21.78 psi. As with the Klondike block discussed in the previous section, the transverse pressure is most significantly affected by the wall height and the amount of preload. Figure 8-19 displays the transverse pressure as a function of preload for 30, 45, and 60-in half-wall heights. The transverse pressures for the 30-in-high half-walls are 6 to 8 times higher than that of the 60-in-high half-walls and 3 to 5 times higher than the 45-in-high half-walls for preloads above 50 psi. It is also seen from figure 8-19 that the transverse pressure is nonlinearly related to the preload for the 30-in-high and 45-in-high half-walls and reaches an asymptotic maximum between 250-300 psi of preload for these wall heights. Preloads above 175 psi were not applied to the 30-in-high half-walls. As a result, the asymptotic maximum for these wall constructions was not reached. The partially cured block walls are shown in figure 8-19 designated with open square data point labels. As seen in the figure, the 60-in-high and 45-in-high partially cured block walls match the fully cured wall responses reasonably well with only slightly lower transverse pressure capacities. However, the transverse pressure responses for the partially cured, 30-in-high half-walls were considerably less than the fully cured walls. Upon closer examination of the wall response, it is seen from the test data in figure 8-20 that the partially cured wall begins with the same transverse pressure response, but at approximately 2,500 lbs of lateral loading, it slows in its load development, most likely due to partial failure of the material.

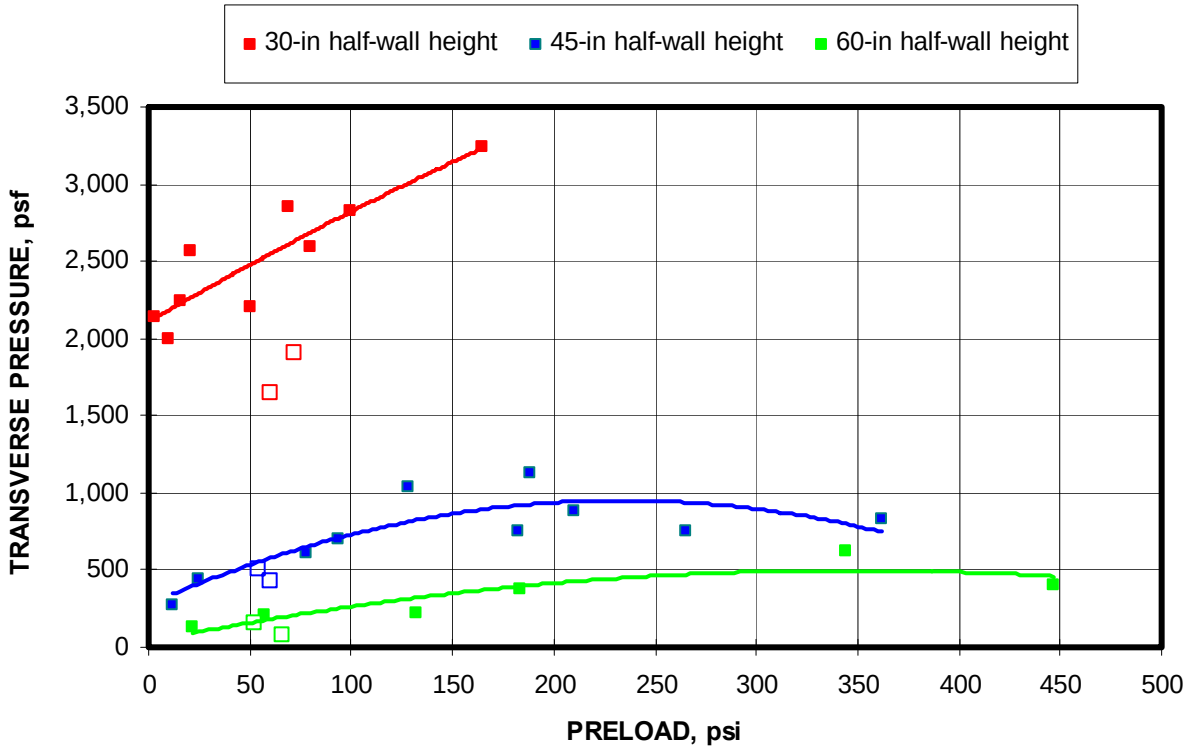

Figure 8-19. Transverse pressure as measured from MRS laboratory testing as a function of preload for three different half wall heights (Peerless Backsaver block).

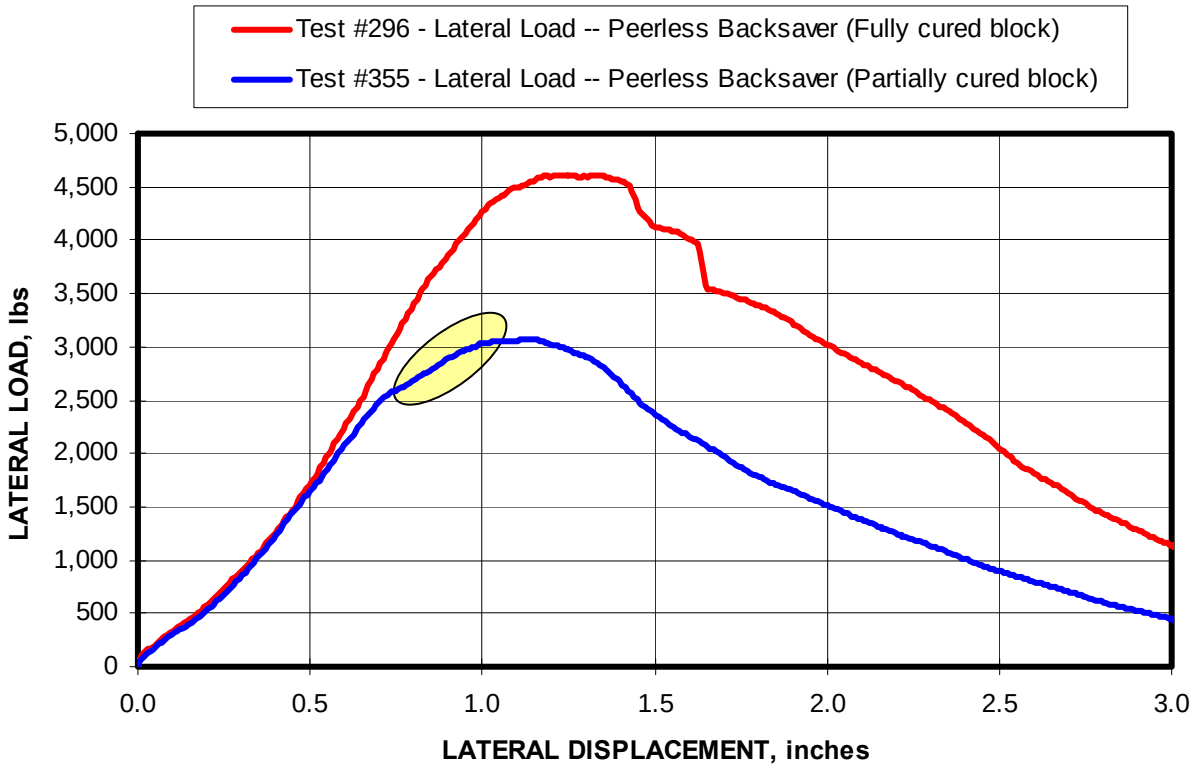

Figure 8-20. Decrease in lateral load development with partially cured Peerless Backsaver block.

Figure 8-21 shows that the lateral displacement at the peak transverse pressure also approaches an asymptotic minimum as the preload exceeds 250 psi. This is consistent with the transverse pressure behavior expressed in figure 8-19, indicating a limitation of the transverse loading capacity.

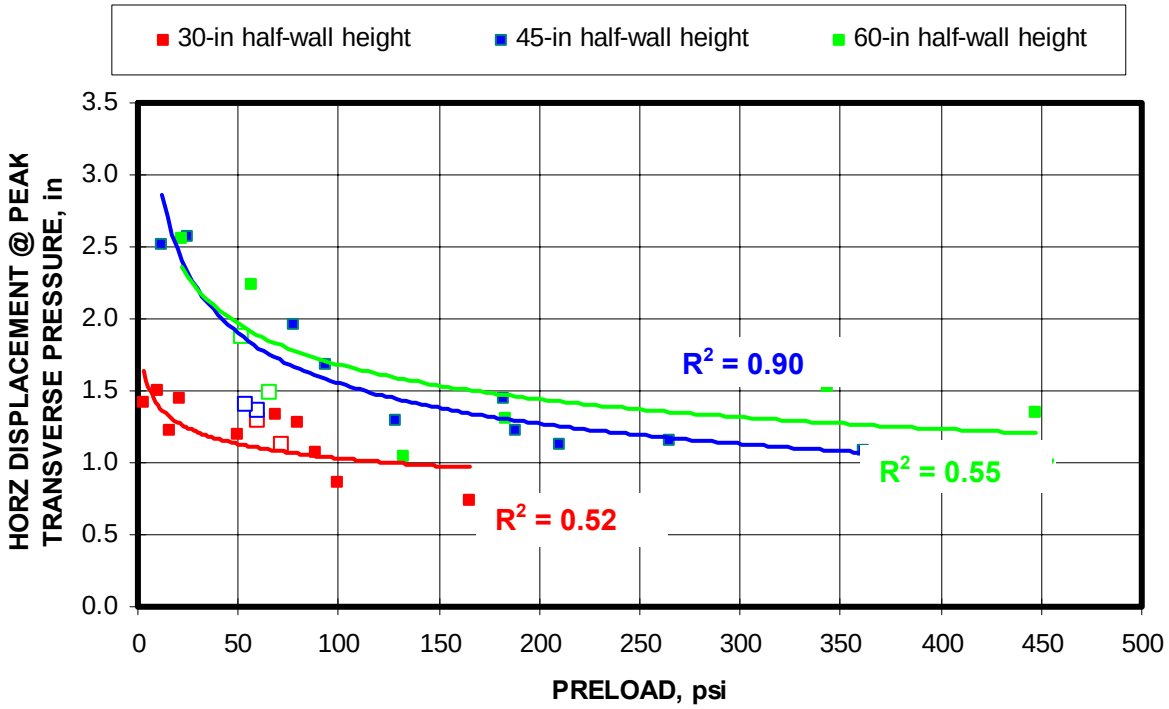

Figure 8-21. Lateral displacement at which peak transverse pressure occurs also reaches an asymptotic minimum as the preload exceeds 250 psi.

Further examination of the parametric relationships confirms the arching theory as presented in chapters 5 and 6. Figure 8-22 shows that the transverse pressure is directly related to the lateral force acting on the half-wall during the laboratory tests. Figure 8-23 shows that the lateral force is also directly related to the thrust force. This is also consistent with the arching theory. Finally, figure 8-24 shows the relationship between the transverse pressure and the arch thrust. This graph resembles the plot of transverse pressure versus preload shown in figure 8-19. The preload also limits the thrust load for the 45-in-high half-wall tests. The transverse pressure for 30-in half-wall test increases throughout the loading range, suggesting that the thrust load has not yet reached its limit for this configuration and could possible sustain higher preloads. The 60-in-high half-wall test also does not reach a clear asymptote.

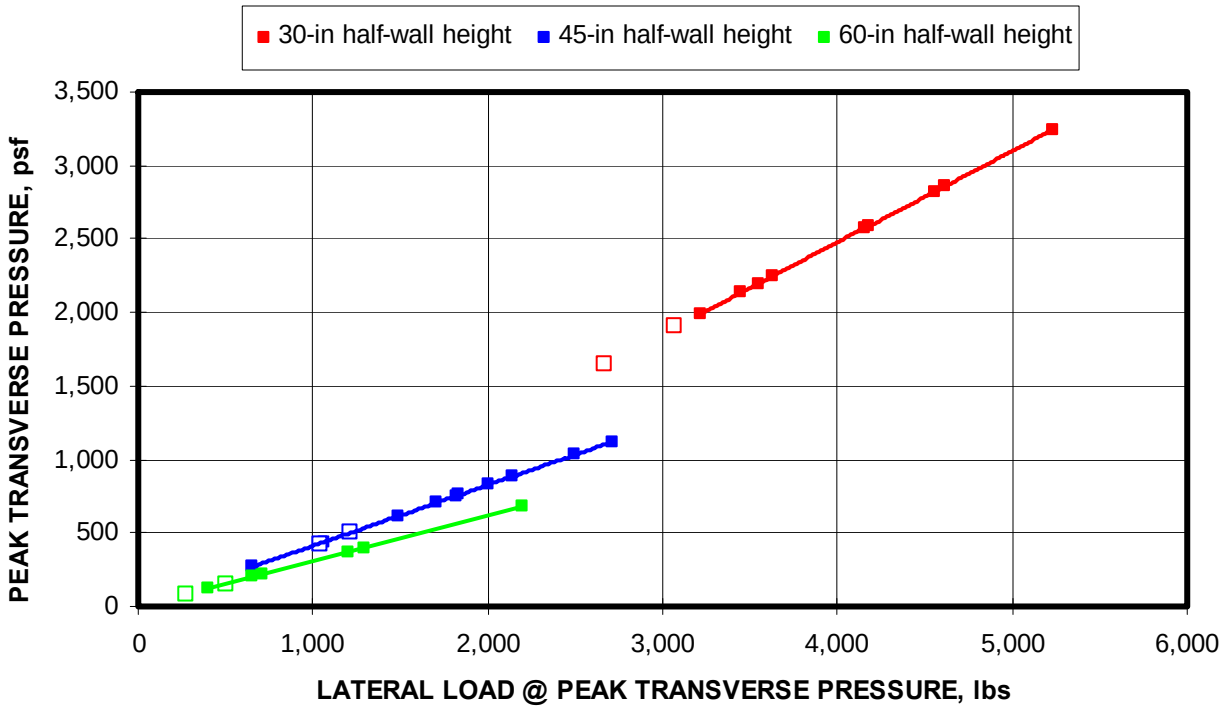

Figure 8-22. Transverse pressure is directly related to the lateral load acting on the half wall in the MRS laboratory test (Peerless Backsaver block).

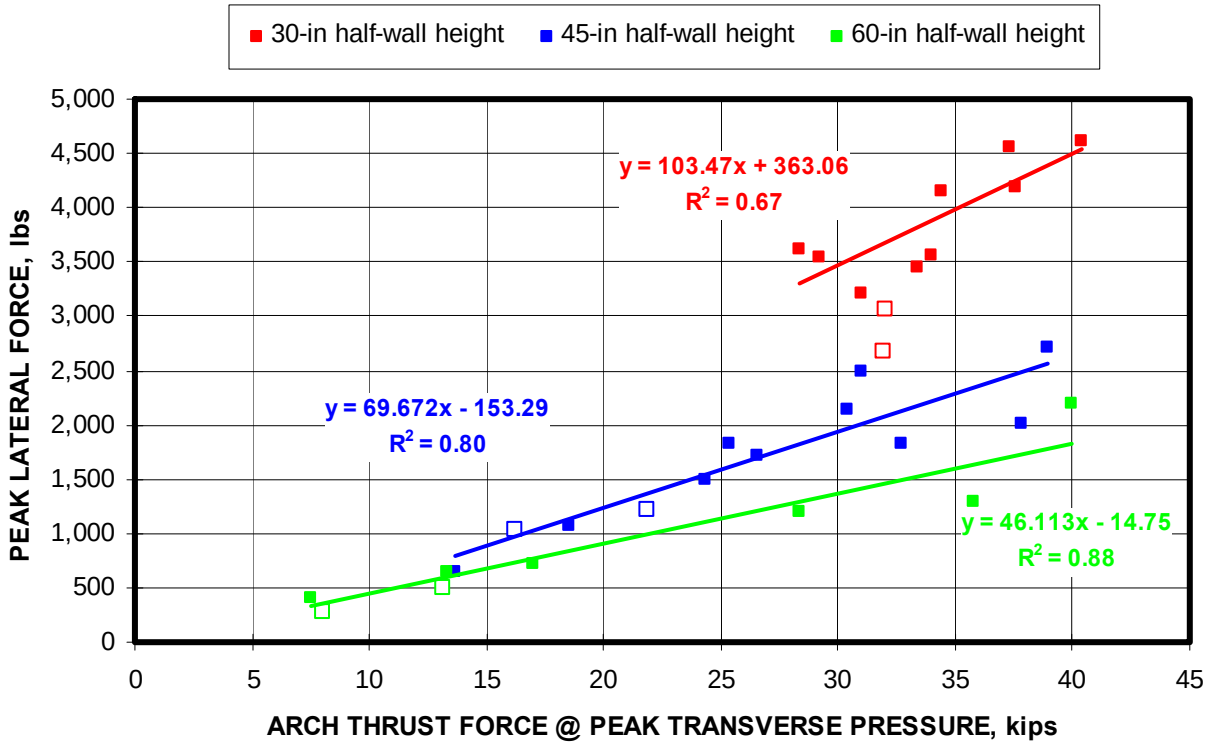

Figure 8-23. Lateral force is also directly related to the thrust force (Peerless Backsaver block).

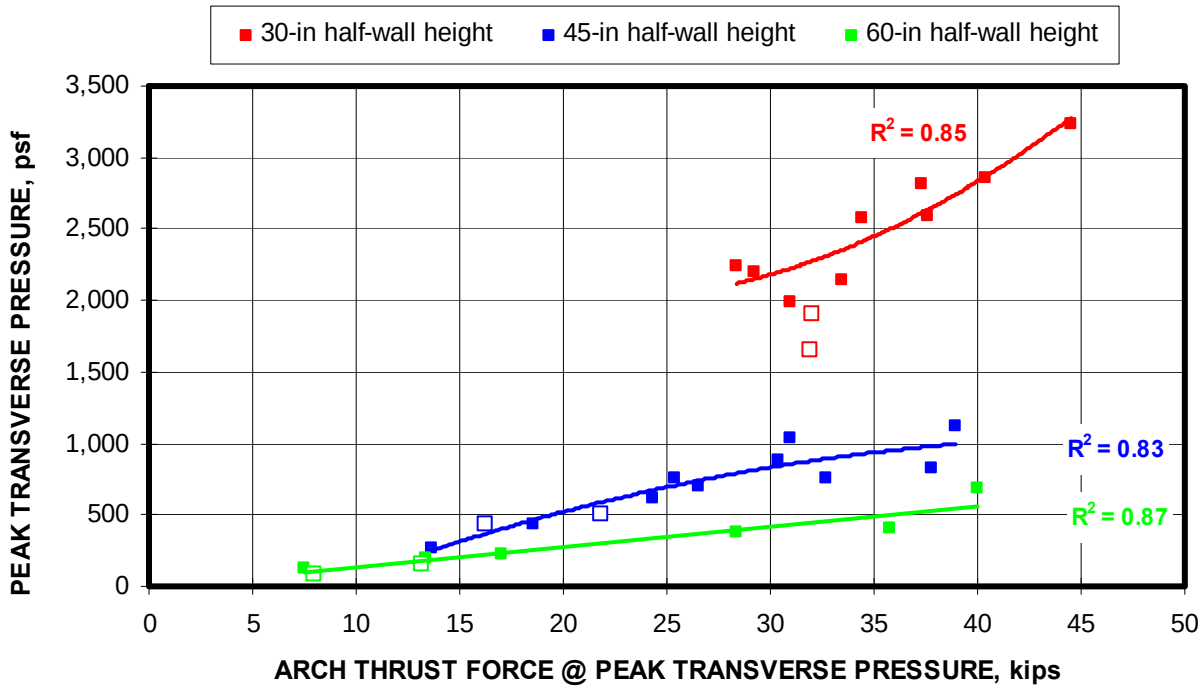

Figure 8-24. Relationship between the transverse pressure and the arch thrust for MRS laboratory tests conducted at three different half-wall heights (Peerless Backsaver block).

Figure 8-25 depicts the relationship for tests with less than 75 psi preload between the transverse pressure and the material modulus (E), the wall thickness (t), and the wall height (L) expressed as by the term E x $(t/L)^2$. Both the fully cured and partially cured blocks are included in this analysis. The chart shows that 96 pct of the transverse pressure of a stopping is determined by this relationship. The material modulus is a significant parameter since it determines the amount of thrust force developed and ultimately the amount of lateral displacement of the wall, both of which control the arching mechanics of the wall. If the modulus is related to the compressive strength of the block material, the modulus factor could be replaced by the compressive strength as previous research suggests (Barczak, 2004).

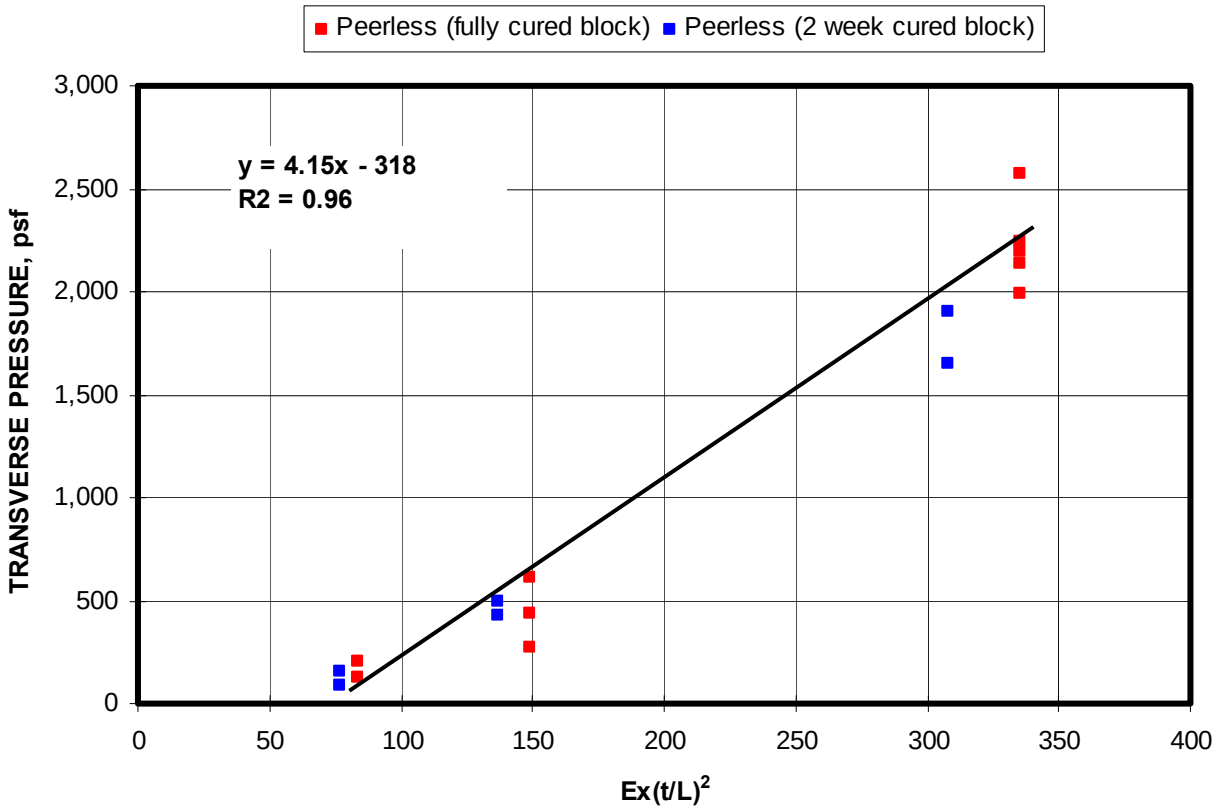

Figure 8-25. Correlation of factors involving the material modulus (E), wall thickness (t), and wall height (L) to the transverse load capacity of a stopping (Peerless Backsaver block).

8.2.3 Evaluation of Predictive Models

If the thrust force and its resultant location and lateral load are known, the transverse pressure capacity of a stopping can be predicted with nearly 100 pct accuracy. If the thrust force location is instead calculated from the empirical model described in chapter 6 and shown in figure 8-26 for three half-wall heights considered in this analysis, the transverse pressure can still be predicted to within 1 pct of the measured transverse pressure from the laboratory tests. Each data point in figure 8-27 represents an individual laboratory test. As seen in the figure, the accuracy of the prediction is consistent throughout the full range of transverse pressure conducted in the laboratory testing for three different wall heights, and includes preloading of wall from zero to 447 psi.

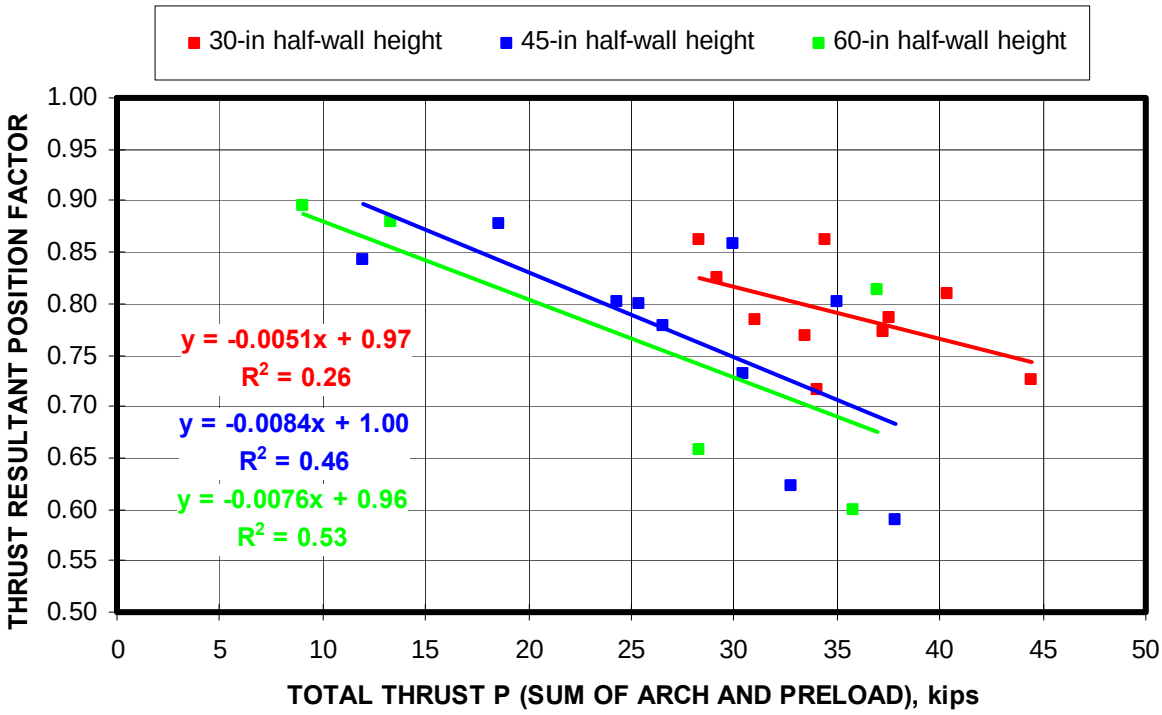

Figure 8-26. Resultant thrust force location for three wall heights as a function of the total arch thrust (Peerless Backsaver block).

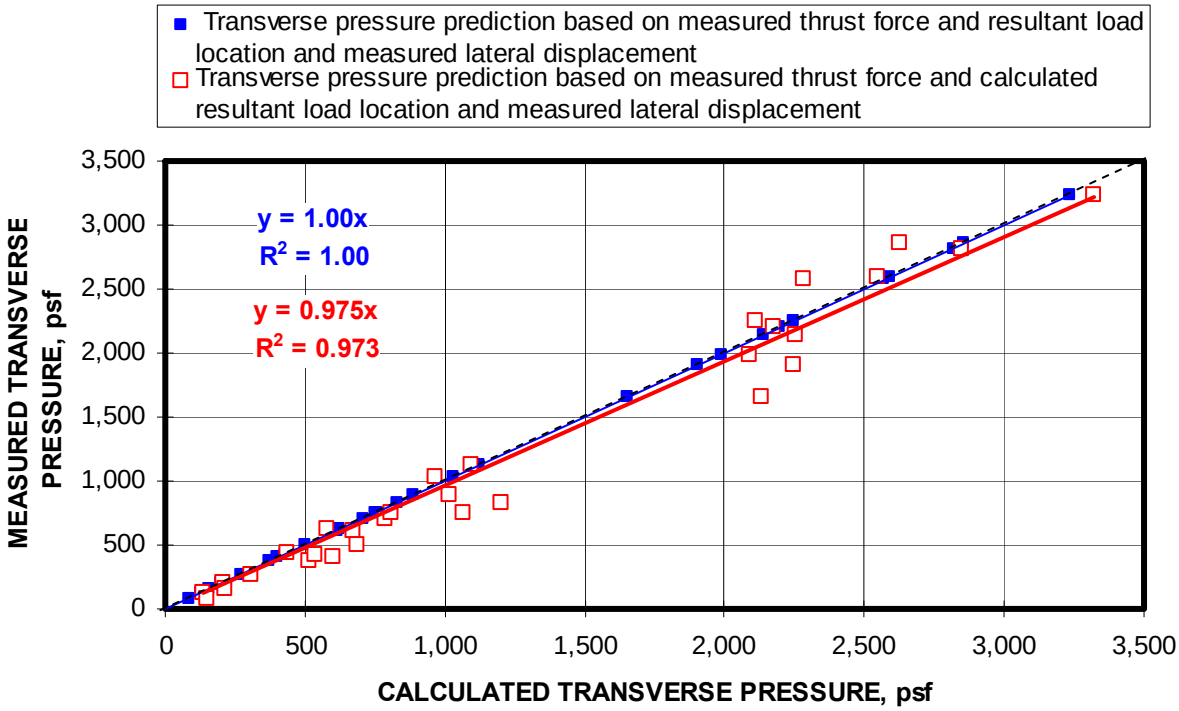

Figure 8-27. Prediction of transverse pressure when both the lateral load and arch thrust are known. Blue curves predicts transverse pressure when resultant thrust force location is also known and red squares show predicted transverse pressure when resultant thrust force location is calculated from empirical data.

If either the lateral displacement or the arch thrust is known, then the transverse pressure can still be calculated. Again, it is recalled from chapter 7 that two methods were developed. Method 1 predicts the transverse pressure from the measured lateral displacement. Method 2 predicts the transverse pressure from the measured thrust force. Figure 8-28 illustrates the predictive capability of these models showing the measured transverse pressure vs. the predicted transverse pressure for each half-wall laboratory test. Based on the calculated trend lines, both models very accurately predicted the measured transverse pressure.

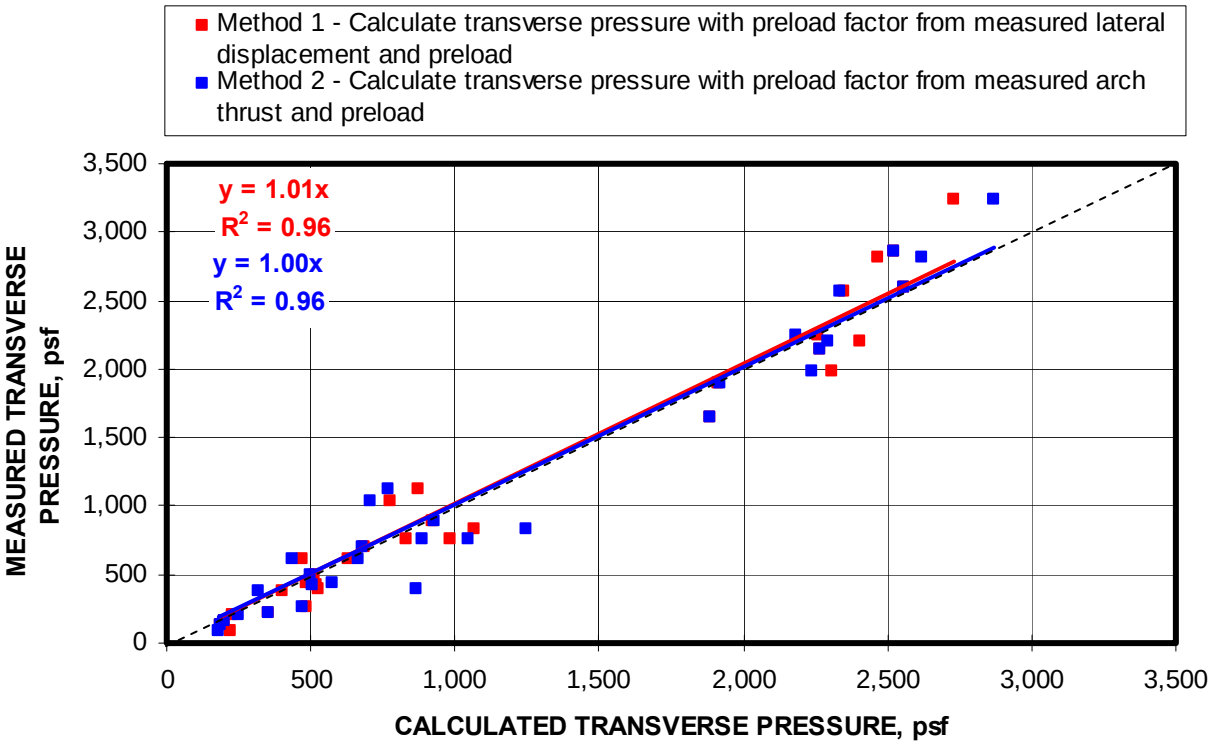

Figure 8-28. Prediction of transverse pressure from two methods (Peerless Backsaver block).

8.2.4 Theoretical Impact of Boundary Stiffness

A theoretical assessment of the impact of the boundary stiffness is conducted by varying the system modulus of elasticity (see equation 6.11 an 7.7). Recalling the theoretical assessment of arching mechanics described in chapters 5 and 6, the modulus of elasticity determines the deformations of the wall and the boundary, i.e. the mine roof and floor. The system modulus reflects the series stiffness equivalent of the wall and roof and floor

structure. The theoretical assessment is made by reducing the system modulus to 75, 50, and 25 pct of the rigid boundary condition, and computing the transverse pressure using the lateral displacement model developed in chapter 7. For comparative purposes, if the boundary stiffness were equal to the wall stiffness, the system stiffness would be reduced by 50 pct. Likewise, if the boundary stiffness were three times that of the wall, the system stiffness would be 75 pct of the rigid boundary condition, and if the boundary stiffness were one third of the wall stiffness, the system stiffness would be 25 pct of the rigid boundary condition.

Figure 8-29 shows the impact of the reduction in system modulus to 25, 50, and 75 pct of the rigid boundary condition at 3 different wall heights as a function of preload. First, it can be concluded from figure 8-29 that as the boundary modulus is reduced, the transverse pressure capacity of the stopping will also be reduced. It is seen from this figure that the impact of reductions in boundary modulus will have a greater impact in terms of absolute reductions in transverse pressure for shorter walls than it will for taller walls. For the example shown in figure 8-29, the transverse pressure for test number 297 for the 30-in half-wall height, the transverse pressure was reduced from 2,268 psf for the rigid boundary condition to 580 psf when the boundary modulus is one third of the wall modulus, thereby reducing the system modulus to 25 pct of the rigid boundary condition. This represents a 74 pct decrease in the transverse pressure capacity of the stopping. The percent reduction in transverse pressure remains the same for all three wall heights.

Figures 8-30 through 8-31 show the impact of reductions in system modulus for half-wall heights of 30, 46, and 60 inches. In these figures, the transverse pressure is plotted as a function of preload, which varies from 0 to 450 psi. These figures indicate the reductions in transverse pressure because of reduction in boundary stiffness (lower system modulus) are reduced as the preload increases. Using the 30-in-high half-wall as an example, the 74 pct decrease in transverse pressure which occurred by reducing the system modulus to 25 pct of the rigid boundary condition, drops to a 41 pct reduction at a preload of 165 psi.

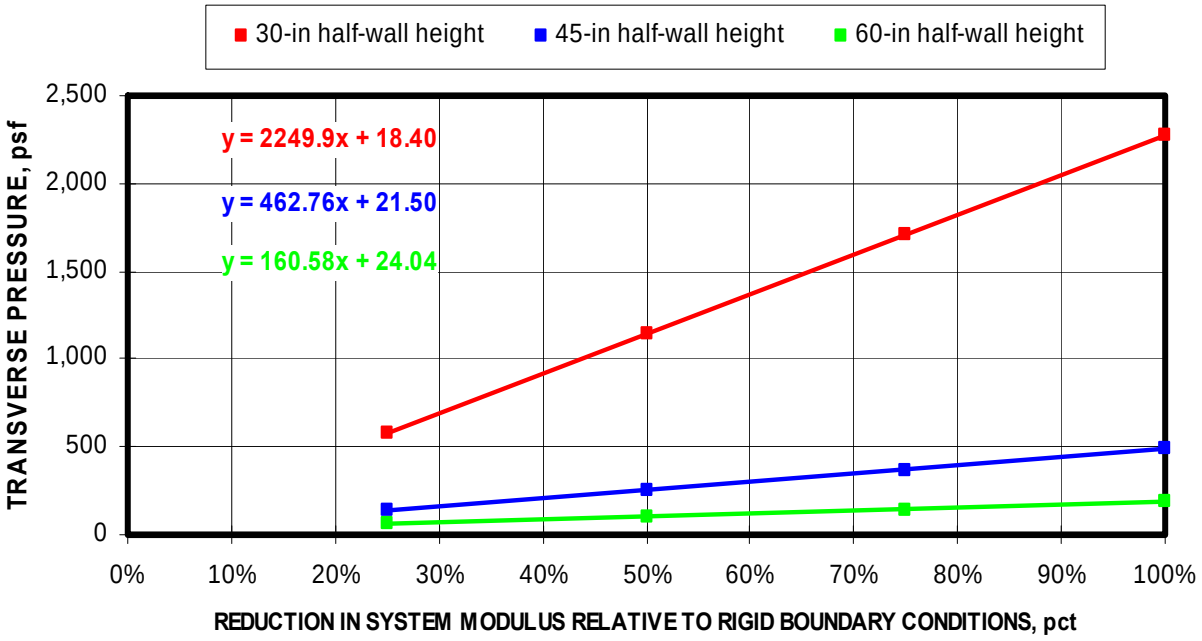

Figure 8-29. Impact of reducing the boundary stiffness on transverse pressure capacity of stopping (Peerless Backsaver block).

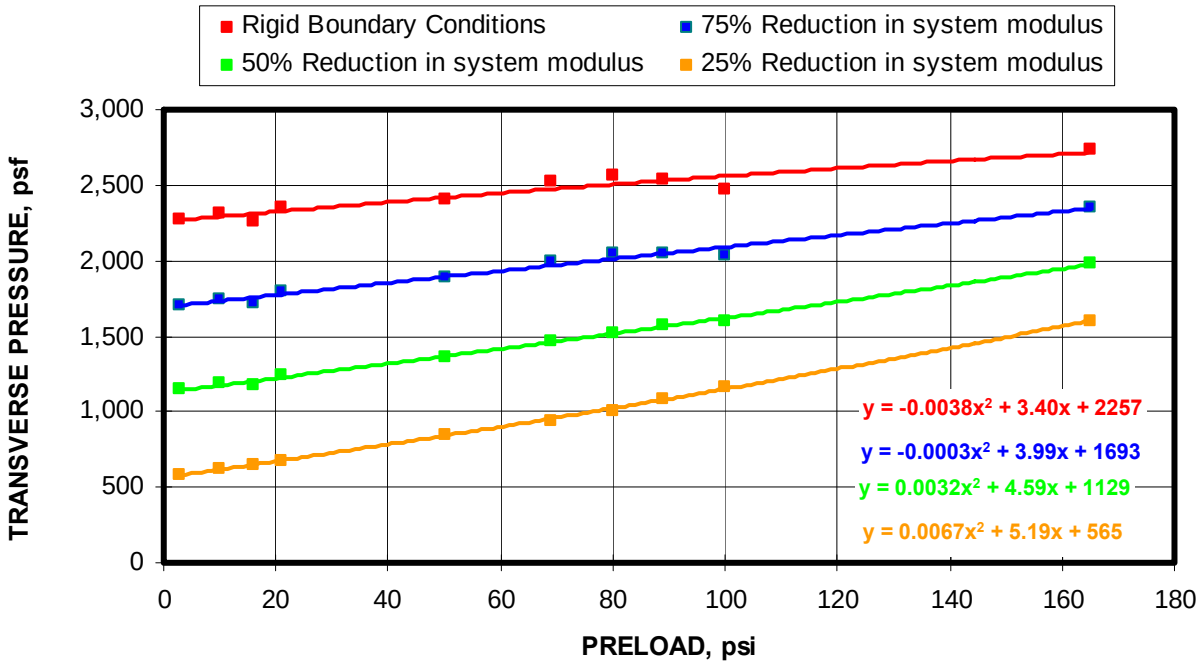

Figure 8-30. Impact of boundary stiffness reductions compared to rigid arching conditions as a function of preload for 30-inch-high half-wall constructions (Peerless Backsaver block).

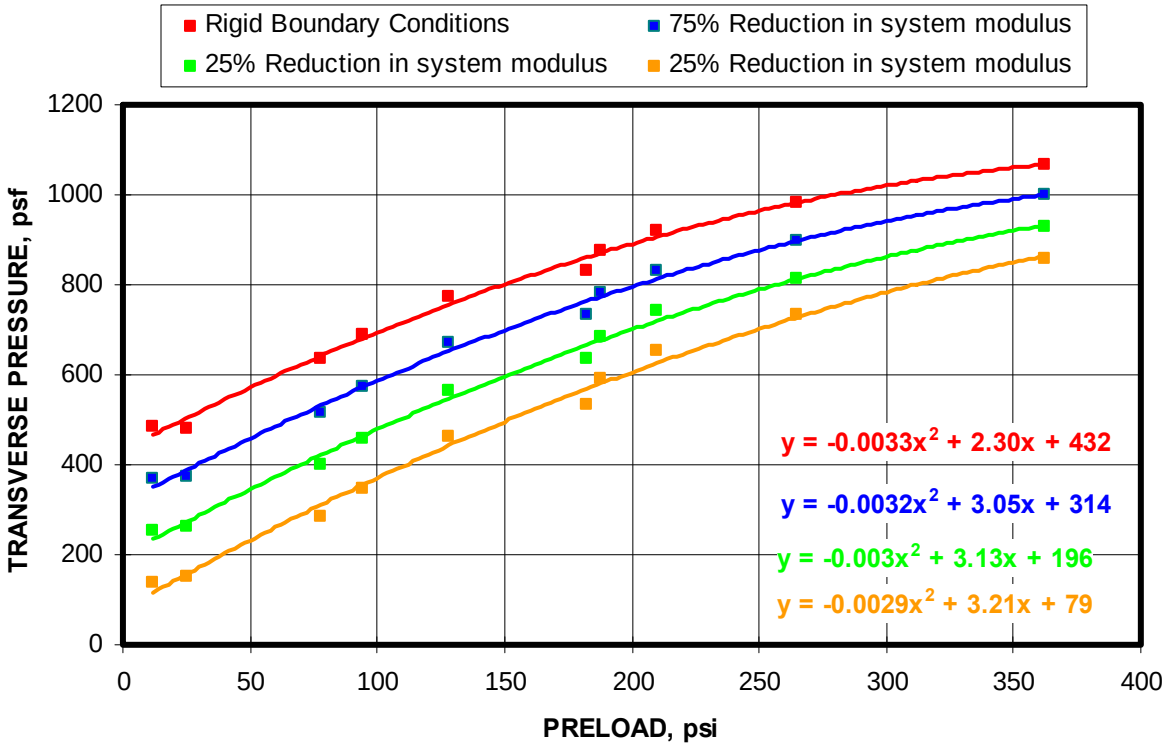

Figure 8-31. Impact of boundary stiffness reductions compared to rigid arching conditions as a function of preload for 46-inch-high half-wall constructions (Peerless Backsaver block).

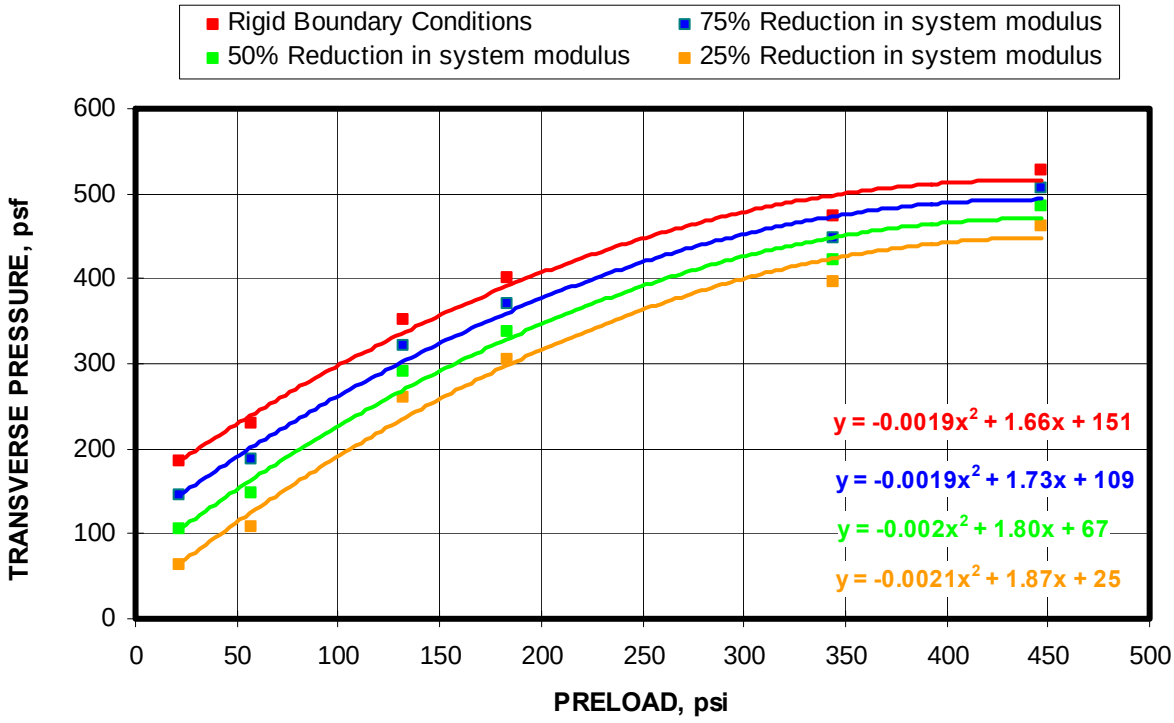

Figure 8-32. Impact of boundary stiffness reductions compared to rigid arching conditions as a function of preload for 60-inch-high half-wall constructions (Peerless Backsaver block).

8.3 KLONDIKE HOLLOW CORE BLOCK

Klondike Block & Masonry Supplies Inc is located in Uniontown, PA and supplies general masonry products including concrete blocks used for mine ventilation stoppings. The block is made from conventional Portland cement and standard aggregate with the same basic formulation that is used to make the solid blocks. Figure 8-33 shows a photo of the block. The blocks measure 5.625 inches in thickness, 15.5 inches in width and 7.5 inches high. The core holes measure 3.5 x 3.5 inches leaving an edge thickness of approximately one inch. This block weighs on average 32 lbs. The unit block compressive strength was measured at 907 psi compared to the 1,330 psi strength of the solid block (see figure 8-34). The thin webs and facing obviously contribute to the lower strength.

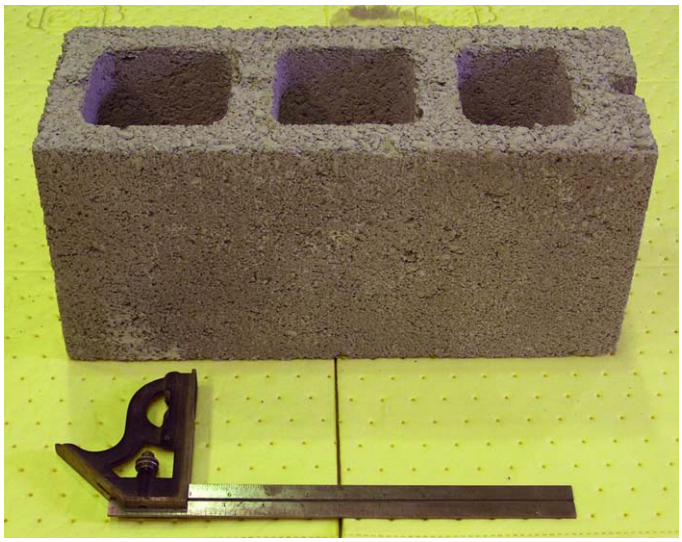

Figure 8-33. Hollow core concrete block (manufactured by Klondike).

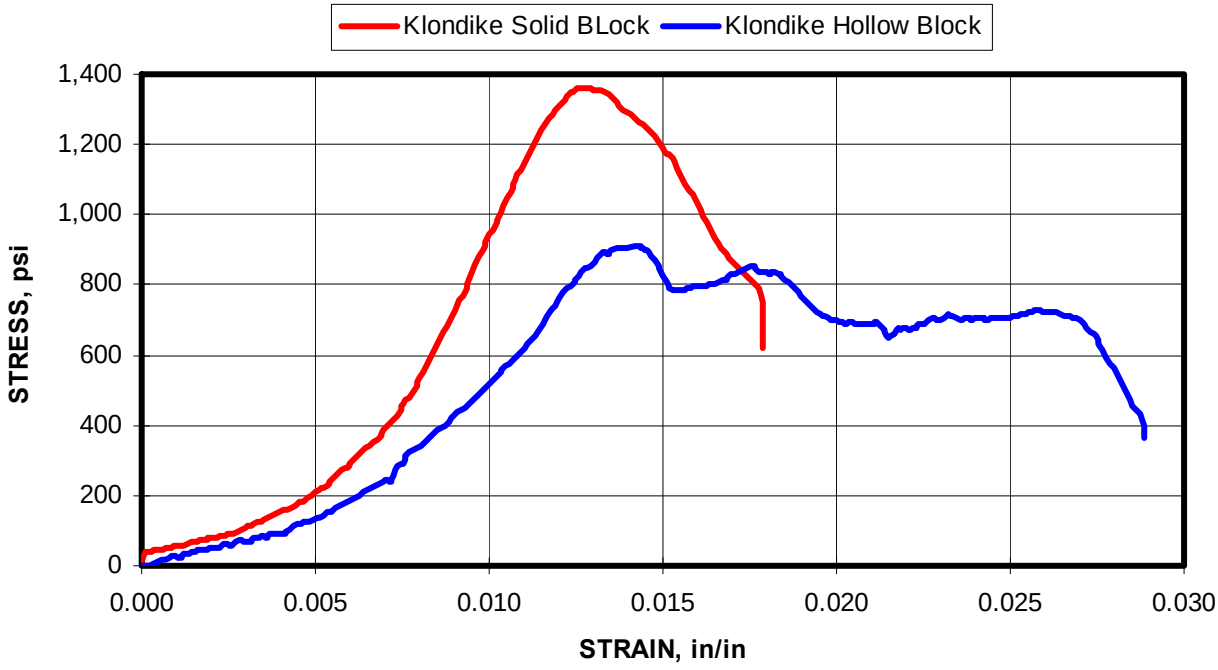

Figure 8-34. Comparison of the compressive strength of solid and hollow core block.

8.3.1 Overview of the Test Program

A total of 23 tests were conducted with hollow core Klondike block. The results of the MRS half-wall tests are summarized in the table 8-6. The standard test protocol was to evaluate three half-wall heights of 30, 45.75 and 60 inches from half-walls constructed from 4, 6, and 8 courses of block. This equates to a full stopping height of 5 to 10 feet. The preload was varied in increments of approximately 50 psi from 0 to 212 psi. Graphs of the measured lateral load and thrust load as a function of the lateral displacement of the wall for each test are documented in Appendix B. A tabular summary of the pertinent parameters and loading values for each test is also included Appendix C.

Table 8-6. Summary of Klondike, hollow-core block, half-wall tests in the MRS.

Block Type	Test No.	Block Width (in)	Block Height (in)	Block Length (in)	Half-wall Height (in)	Adjusted Preload (psi)	Measured Transverse Pressure, (psf)
Klondike Hollow Block	330	5.625	7.5	15.5	30	29	1,338
Klondike Hollow Block	331	5.625	7.5	15.5	30	55	1,062
Klondike Hollow Block	340	5.625	7.5	15.5	30	57	1,384
Klondike Hollow Block	334	5.625	7.5	15.5	30	80	1,586
Klondike Hollow Block	338	5.625	7.5	15.5	30	91	1,600
Klondike Hollow Block	332	5.625	7.5	15.5	30	116	1,168
Klondike Hollow Block	339	5.625	7.5	15.5	30	117	1,544
Klondike Hollow Block	337	5.625	7.5	15.5	30	140	966
Klondike Hollow Block	336	5.625	7.5	15.5	30	155	938
Klondike Hollow Block	335	5.625	7.5	15.5	30	172	1,282
Klondike Hollow Block	333	5.625	7.5	15.5	30	212	1,424
Klondike Hollow Block	321	5.625	7.5	15.5	45	22	150
Klondike Hollow Block	314	5.625	7.5	15.5	45	28	130
Klondike Hollow Block	315	5.625	7.5	15.5	45	99	472
Klondike Hollow Block	323	5.625	7.5	15.5	45	87	456
Klondike Hollow Block	320	5.625	7.5	15.5	45	120	634
Klondike Hollow Block	322	5.625	7.5	15.5	45	129	708
Klondike Hollow Block	318	5.625	7.5	15.5	45	131	746
Klondike Hollow Block	317	5.625	7.5	15.5	45	188	540
Klondike Hollow Block	319	5.625	7.5	15.5	45	184	768
Klondike Hollow Block	324	5.625	7.5	15.5	45	207	828
Klondike Hollow Block	325	5.625	7.5	15.5	60	78	134
Klondike Hollow Block	327	5.625	7.5	15.5	60	80	168
Klondike Hollow Block	328	5.625	7.5	15.5	60	129	158
Klondike Hollow Block	329	5.625	7.5	15.5	60	212	222

8.3.2 Parametric Relationships and Trends.

Examining table 8-6, it is seen that the transverse pressure capacity of the stoppings constructed from Klondike hollow core block varied from a low of 130 to a high of 1,600 psf or 0.90 to 11.11 psi for the test configurations documented in the table. In general, the hollow core block transverse pressure performance was less consistent than the solid core block. Figure 8-35 displays the transverse pressure as a function of preload for 30, 45, and 60-in half-wall heights. The transverse pressures for the 30-in-high half-walls were 6 to 8 times higher for preloads above 25 psi than that of the 60-in-high half-walls and 2 to 4 times higher than the 45-in-high half-walls. The 45-in half-wall height displays the nonlinear behavior between the transverse pressure and the preload as was observed in the solid core block walls, reaching an asymptotic level at about 175 psi of preload. Compared to the solid core block, which reached as asymptotic load at about 550 psi, it appears that the hollow core block is not able to sustain preload stresses as well as the solid core block. The 30 and 60-inch high half-wall tests did not provide the same trend. For these wall configurations, it appears that the preload made relatively little difference in the transverse pressure capacity of the stopping. The 30-in-high half-wall trend line even suggests that the transverse pressure capacity decreases slightly with increasing preload. The most likely cause of this behavior was the walls were damaged from even minimal preload.

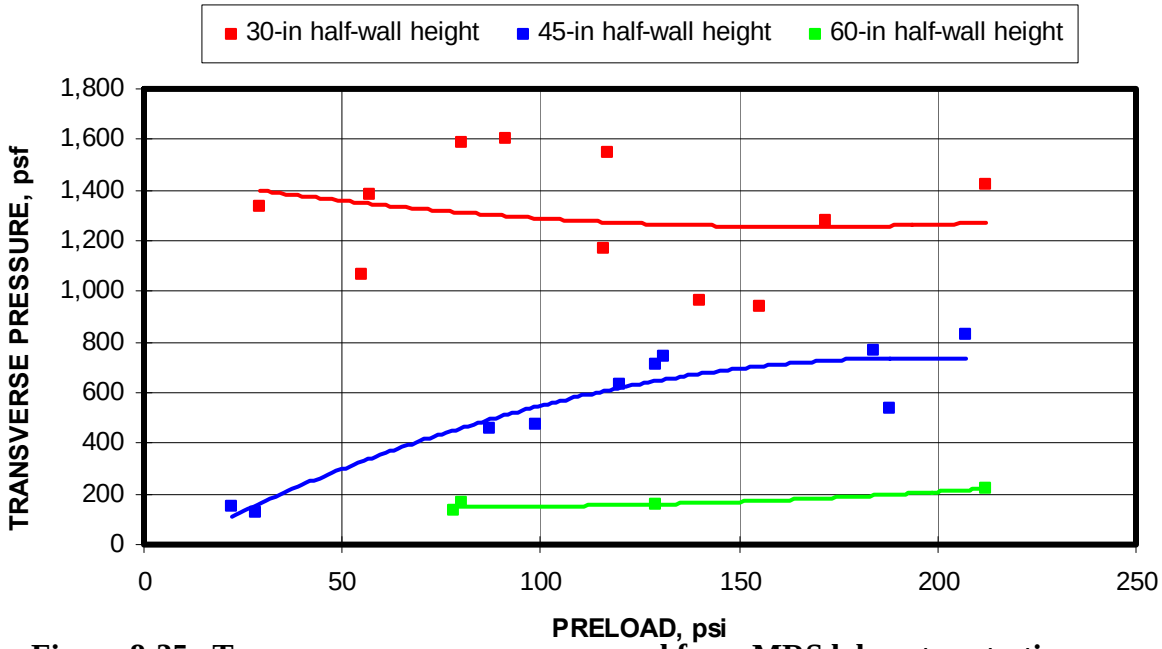

Figure 8-35. Transverse pressure as measured from MRS laboratory testing as a function of preload for three different half-wall heights (Klondike hollow core block).

A review of the test results shows that localized failures of the block at the hinge points were occurring as the transverse pressure was developing for the 30-inch-high half-wall configurations. Figure 8-36 shows one example. In this example, the wall was preloaded with 172 psi. The lateral load began to build as expected with the onset of the induced lateral displacement, but at approximately 0.3 inches of lateral displacement, the lateral load decreased as the wall was not able to sustain the arch thrust force (i.e. decrease in thrust load shown by blue curve in figure 8-36). Following this load-shedding event, the lateral load recovered and increased until another load-shedding event occurred at 1.1 inches of lateral displacement. The lateral load again recovered reaching a maximum of 2,070 lbs at 1.6 inches of lateral displacement. Figure 8-37 gives another example at only 90 psi of preload pressure. Figure 8-38 shows that the lateral displacement at the peak transverse pressure also approaches an asymptotic minimum as the preload exceeds 200 psi. This is consistent with the transverse pressure behavior expressed in figure 8-35, indicating a limitation of the transverse pressure capacity.

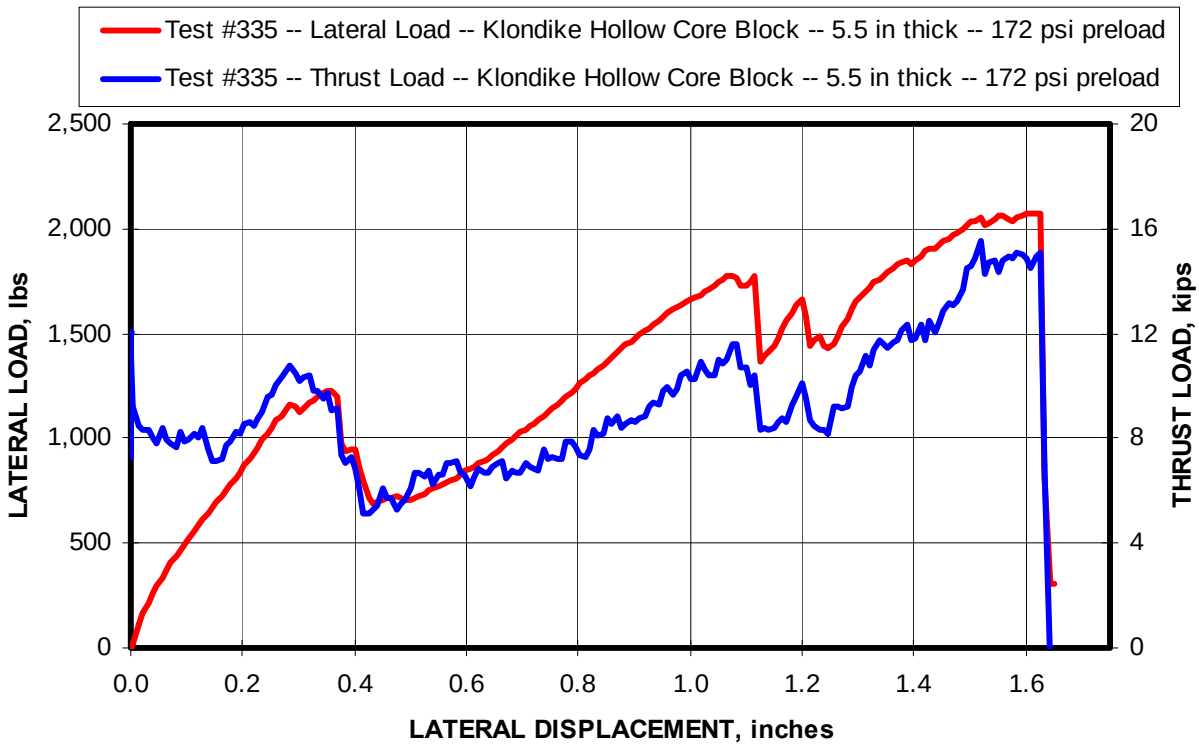

Figure 8-36. Example of 30-in-high half wall test where the wall was not able to sustain the arch thrust load during localized failure of the block during transverse pressure resulting in lateral load shedding twice during the loading cycle.

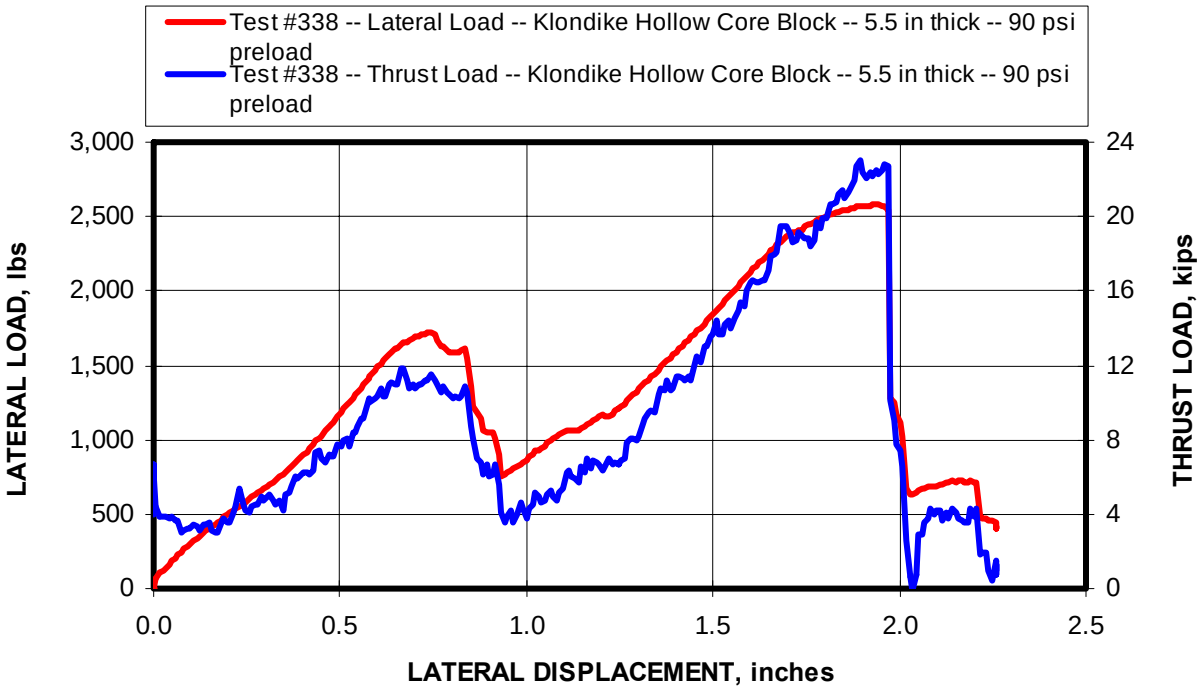

Figure 8-37. Another example where the arch thrust force was not sustained during the full loading cycle.

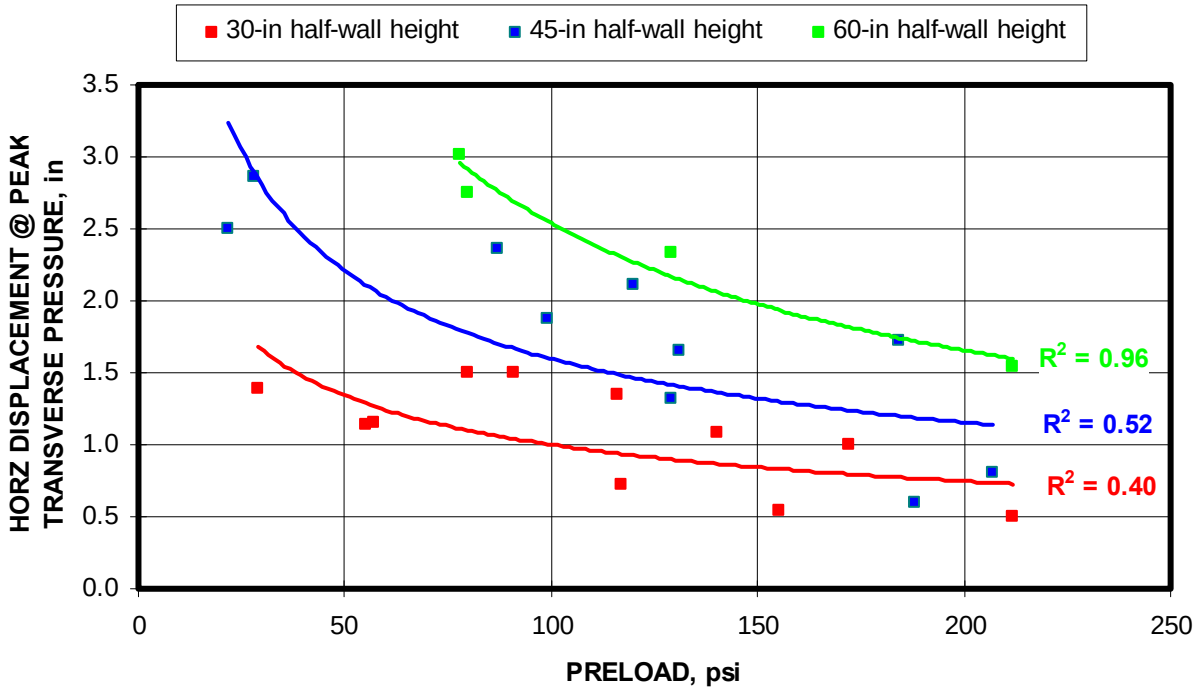

Figure 8-38. Lateral displacement at which peak transverse pressure occurs approaches asymptotic minimum as preload exceeds 200 psi (Klondike hollow core block).

Further examination of the parametric relationships confirms the arching theory as presented in chapter 6. Figure 8-39 shows that the transverse pressure is directly related to the lateral force acting on the half-wall during the laboratory tests, despite the inconsistency in the transverse pressure performance. Figure 8-40 shows that the lateral force is also directly related to the thrust force. This is also consistent with the arching theory. Finally, figure 8-41 shows the relationship between the transverse pressure and the arch thrust. The preload also limits the thrust force for the half-wall tests. The maximum lateral force and arch thrust force attained at the highest preloads in the 60-in-high half-wall test was significantly less than that of the other two wall heights.

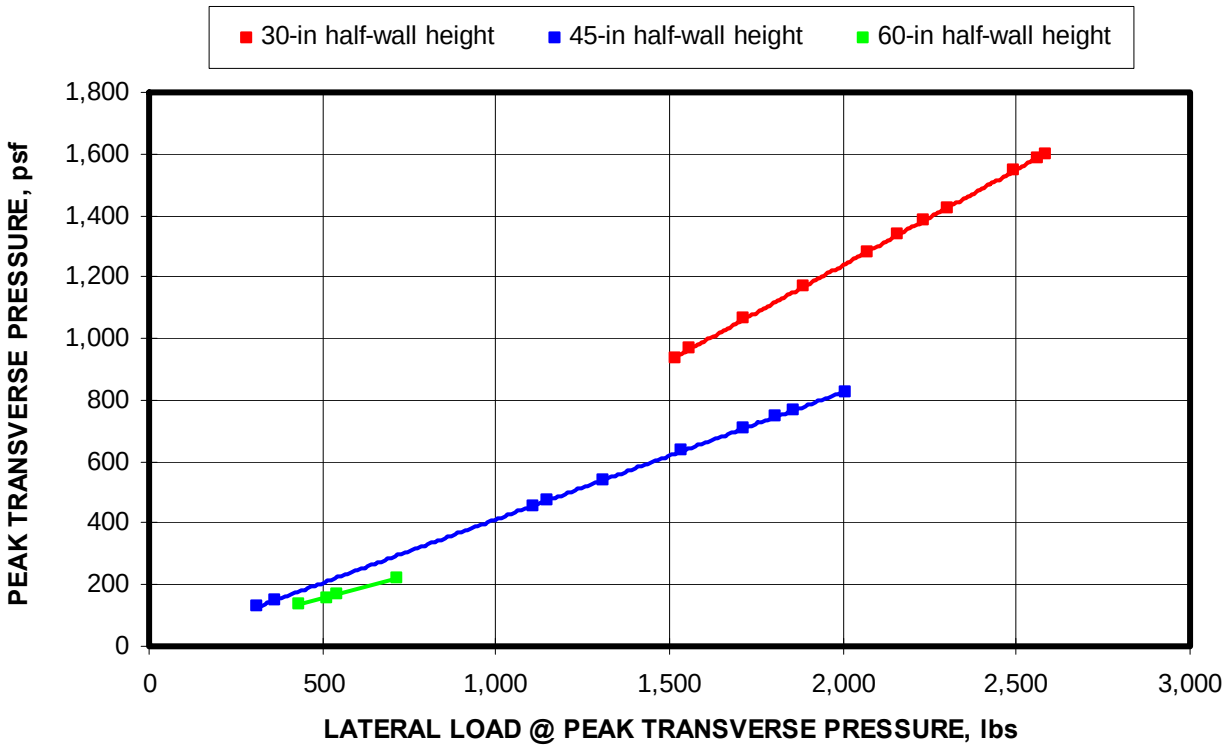

Figure 8-39. Transverse pressure is directly related to the lateral load acting on the half wall in the MRS laboratory test (Klondike hollow core block).

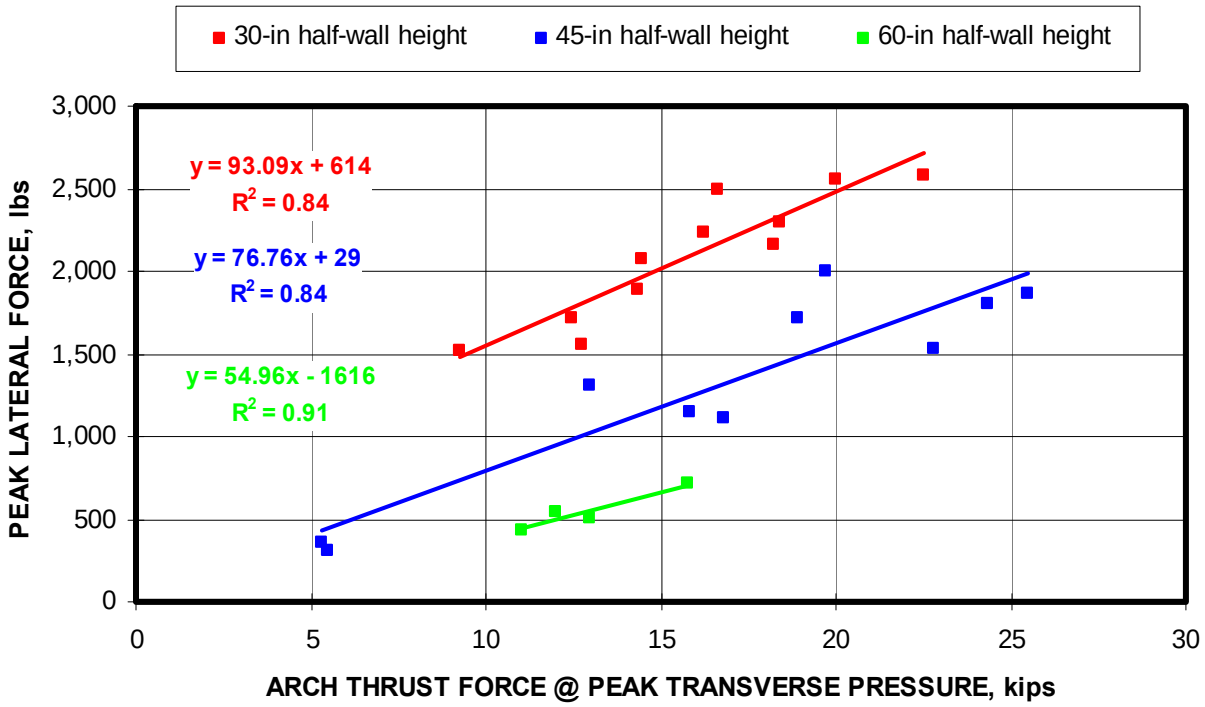

Figure 8-40. Lateral force is also directly related to the thrust force (Klondike hollow core block).

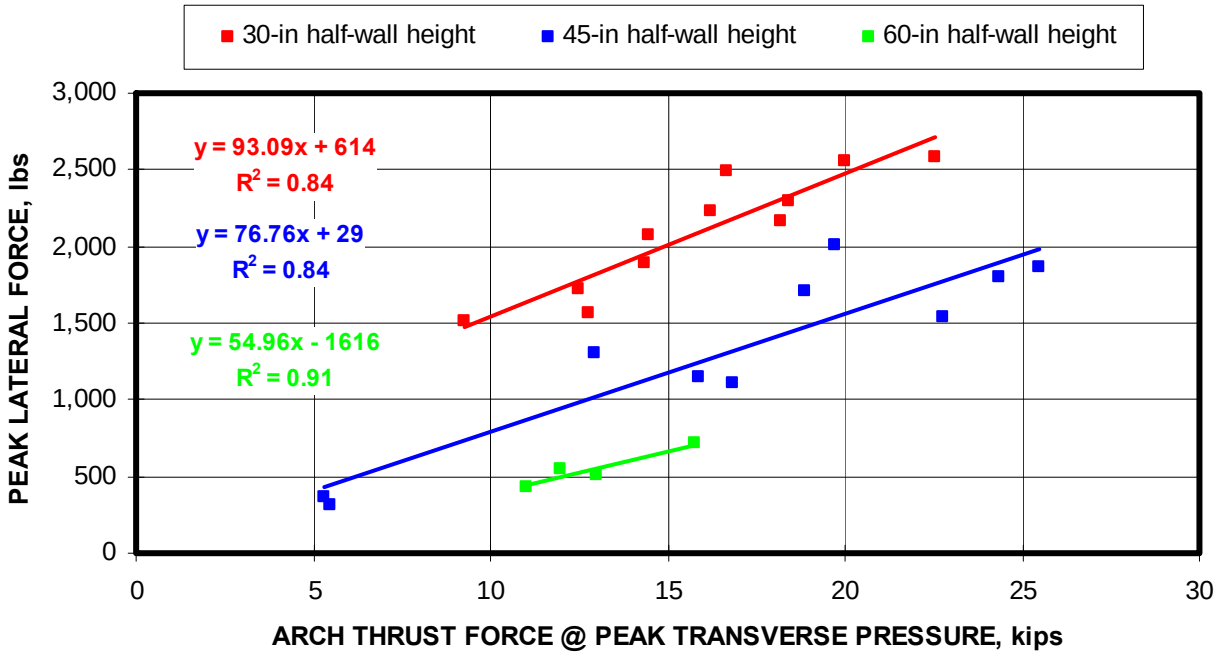

Figure 8-41. Relationship between the transverse pressure and the arch thrust for MRS laboratory tests conducted at three different half-wall heights (Klondike hollow core block).

Figure 8-42 depicts the relationship for tests with less than 100 psi preload between the transverse pressure and the material modulus (E), the wall thickness (t), and the wall height (L) expressed as by the term E x $(t/L)^2$. The chart shows that 91 pct of the transverse pressure of a stopping is determined by this relationship. The material modulus is a significant parameter since it determines the amount of thrust force developed and ultimately the amount of lateral displacement of the wall, both of which control the arching mechanics of the wall. If the modulus is related to the compressive strength of the block material, the modulus factor could be replaced by the compressive strength as previous research suggests (Barczak, 2004).

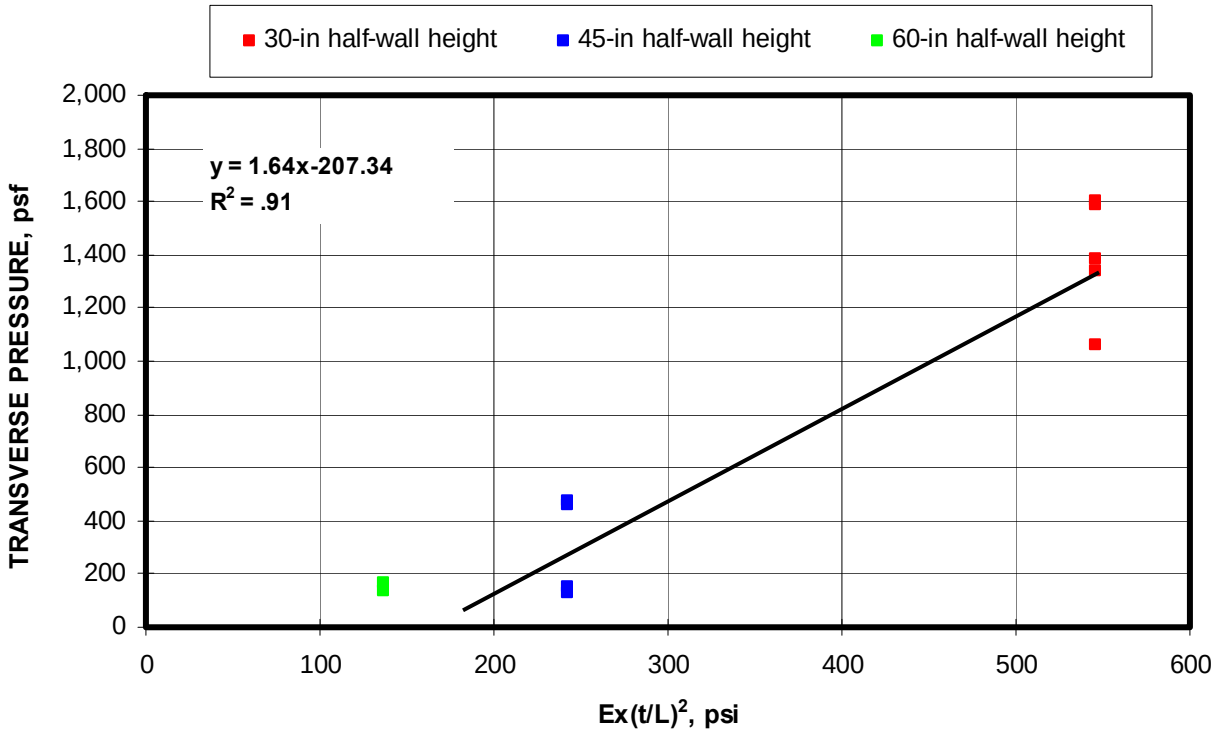

Figure 8-42. Correlation of factors involving the material modulus (E), wall thickness (t), and wall height (L) to the transverse pressure capacity of a stopping (Klondike hollow core block).

8.3.3 Evaluation of the Predictive Models

The next goal is to evaluate the capability to predict the transverse pressure. If the thrust force and its resultant location and lateral force are known, the transverse pressure capacity of a stopping can be predicted with less than 1 pct error. Figure 8-43 shows the calculated resultant thrust force location factor for each of the three half-wall heights. A few comments are made relative to this factor for the hollow core block. First, the factor for the 30 and 45-in-high half-wall constructions is larger than it was for the solid core block. For these wall heights, there is less reduction in the factor when the thrust force increases than was seen for the solid block. It is believed that these differences are attributed to the damage and localized failure of the block during the transverse pressure development as described in section 8.3.2 and illustrated in figures 8-36 and 8-37. The 60-in half-wall height constructions showed a large change in the resultant thrust location factor with increasing arch thrust. This change appears abnormally large primarily due to the high initial values at the lower thrust forces.

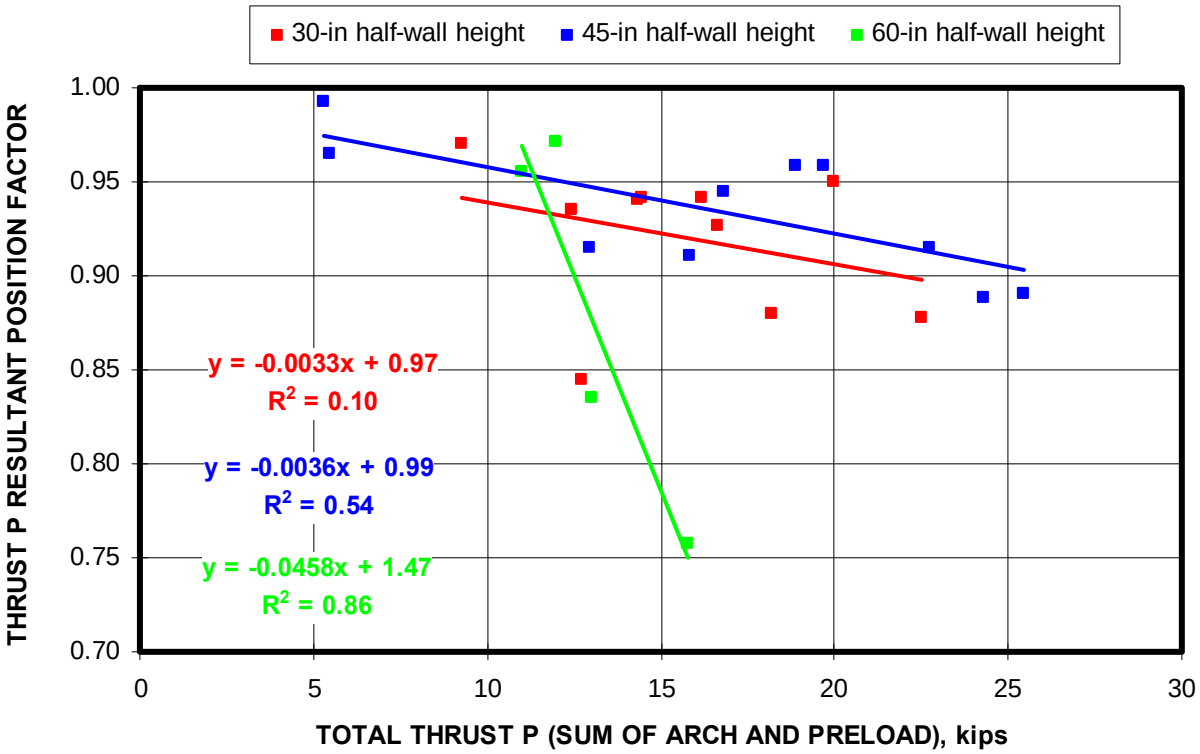

Figure 8-43. Resultant thrust force location for three wall heights as a function of the total arch thrust (Klondike hollow core block).

If the thrust force location is instead calculated from the empirical model described in chapter 6 and shown in figure 8-43 for three half-wall heights considered in this analysis, the transverse pressure can still be predicted with a 94 pct accuracy as depicted by the open red square data points shown in figure 8-44. Each data point in figure 8-44 represents an individual laboratory test. As seen in the figure, the accuracy of the prediction is fairly consistent throughout the full range of transverse pressure conducted in the laboratory testing with one exception at the highest calculated transverse pressure (high preload condition) where the predicted transverse pressure was nearly 400 psf lower than the measured transverse pressure for this one test.

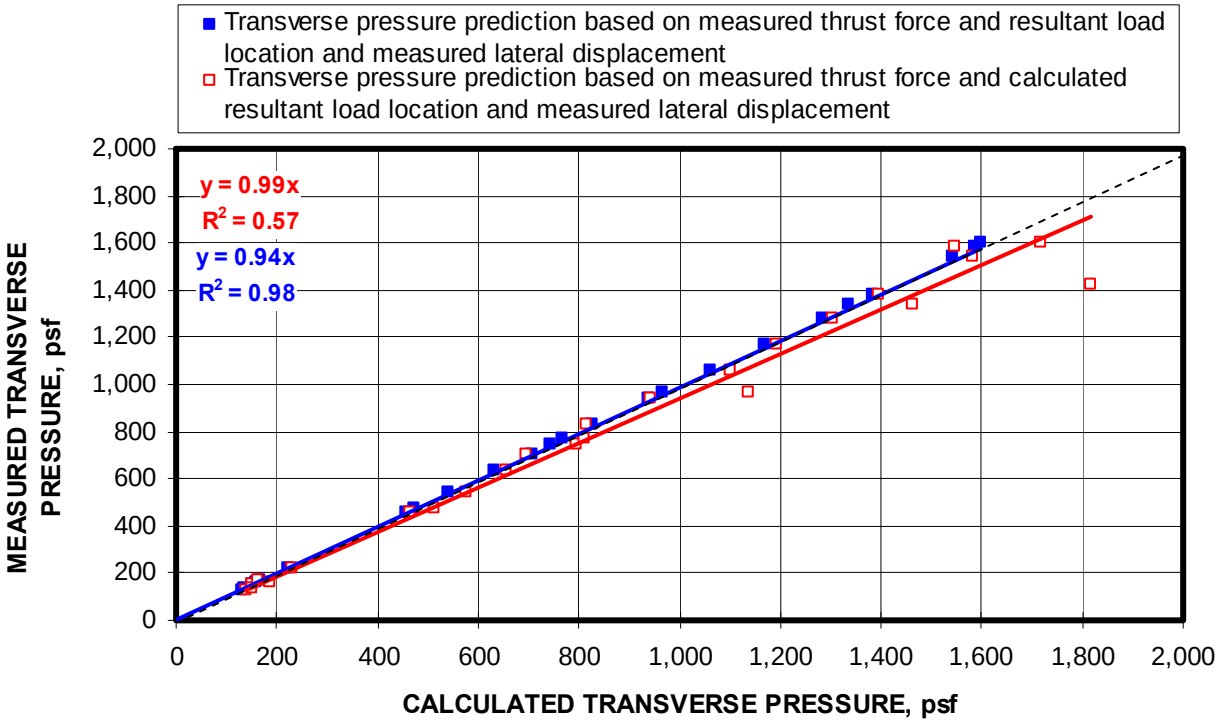

Figure 8-44. Prediction of transverse pressure when both the lateral load and arch thrust are known. Blue curves predicts transverse pressure when resultant thrust force location is also known and red squares show predicted transverse pressure when resultant thrust force location is calculated from empirical data.

If either the arch thrust or lateral displacement is known, then the transverse pressure can still be calculated. It is recalled from chapter 7 that two methods were developed. Method 1 predicts the transverse pressure from the measured lateral displacement. Method 2 predicts the transverse pressure from the measured thrust force. Figure 8-45 illustrates the predictive capability of these two methods showing the measured transverse pressure vs. the predicted transverse pressure for each half-wall laboratory test. It is seen from figure 8-45 that both methods significantly over predict the measured transverse pressure when the regression trend lines are employed. Method 2, where the thrust force is known, is the more accurate of the two models and does a reasonable job (less than 15 pct error) of predicting the transverse pressure. Upon closer examination, it is seen that the transverse pressure predictions for both methods are much more accurate for transverse pressures below 1,000 psf. Only the 30-in-high half-walls provide transverse pressure capacities greater than 1,000 psf. Again, it is believed that these walls are being damaged prematurely from the preload resulting in the lower than expected transverse pressure.

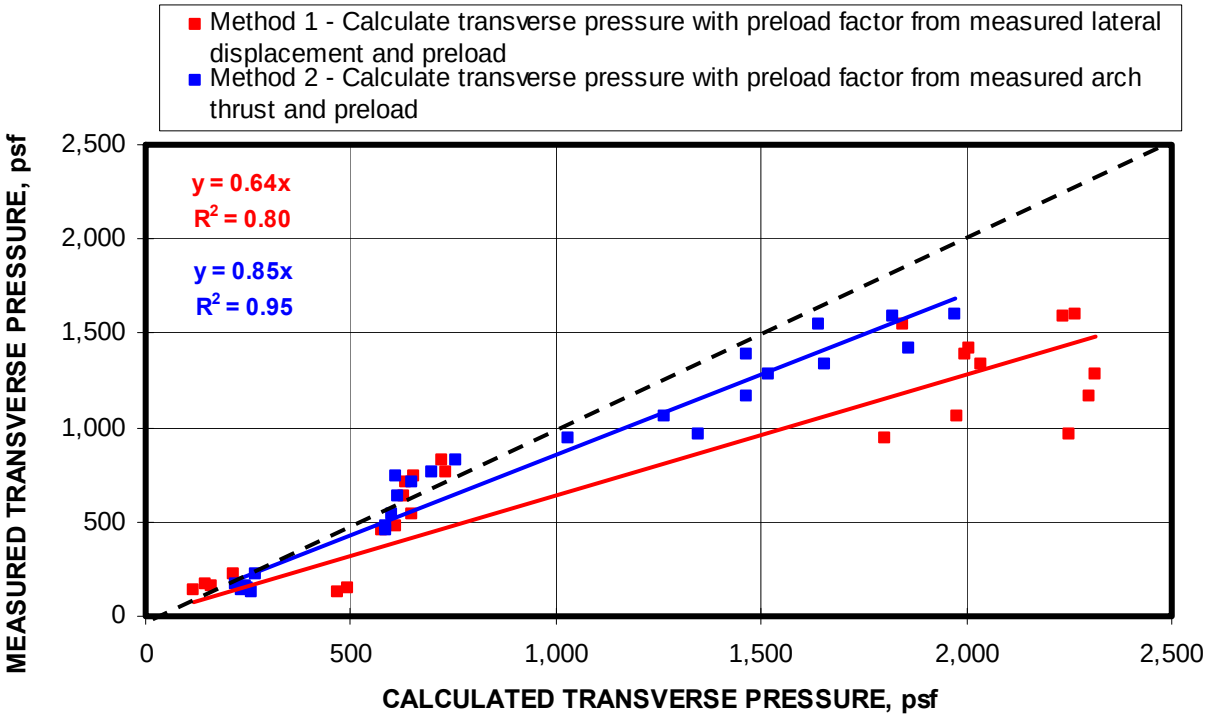

Figure 8-45. Prediction of transverse pressure from known thrust and lateral loads with a constant material modulus for all tests.

Figure 8-46 shows the prediction of the two models when the material modulus for the 30-in-high half-walls is reduced by 50 pct from 65,000 psi to 32,500 psi. This modification significantly improves the prediction of all three models, in particular for the 30-in-high half-wall constructions. The justification for doing this again lies in the premature failures of the block during the transverse pressure development for the short wall constructions. Essentially, these failures increase the lateral displacement of the wall, which can be accounted for by a reduced material modulus (see chapter 6).

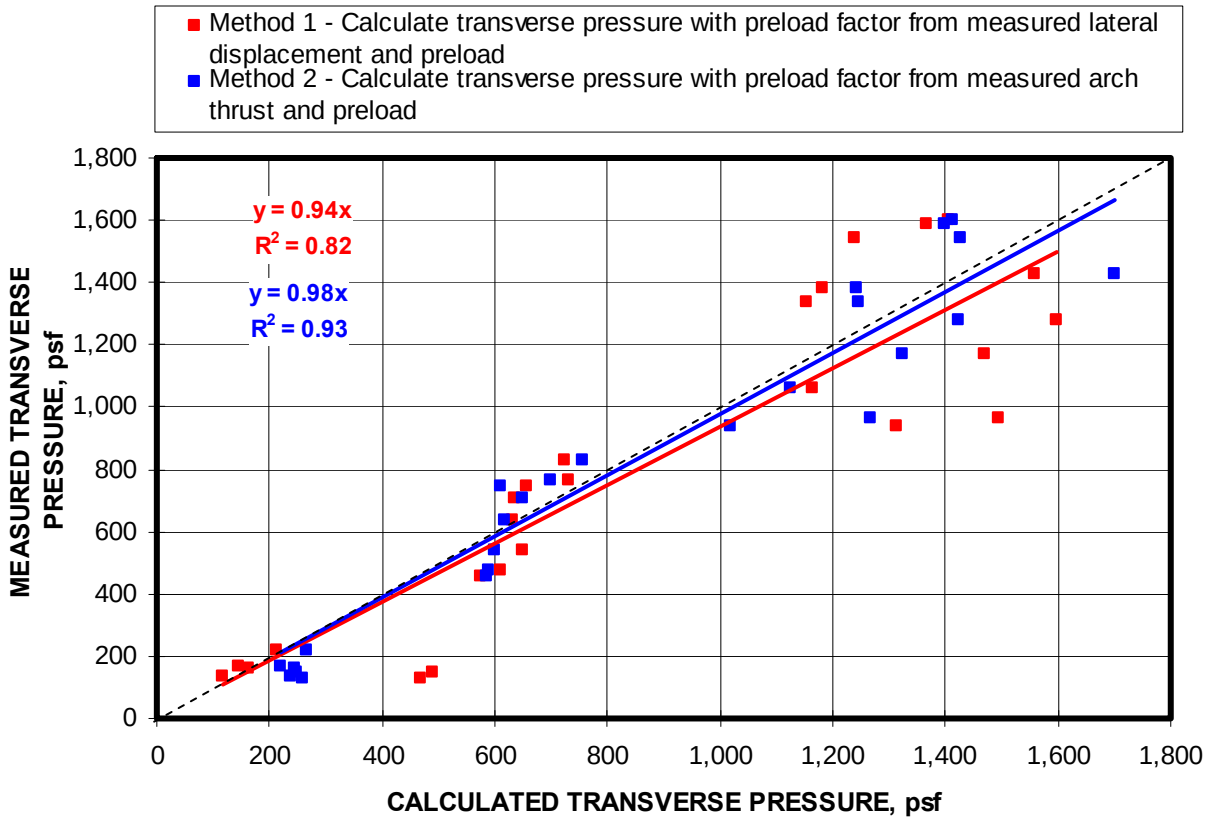

Figure 8-46. Prediction of transverse pressure from known thrust and lateral loads where the material modulus for the 30-in-high half-walls was reduced by 50 pct.

8.3.4. Theoretical Impact of Boundary Stiffness

Figure 8-47 shows the impact of the reduction in system modulus to 25, 50, and 75 pct of the rigid boundary condition at three different wall heights. It is seen from this figure that the impact of reductions in boundary modulus will have a greater impact in terms of absolute reductions in transverse pressure for shorter walls than it will for taller walls. For the example shown in figure 8-47, the transverse pressure for test number 330 for the 30-in half-wall height, the transverse pressure was reduced from 1,152 psf for the rigid boundary condition to 398 psf when the boundary modulus is one third of the wall modulus thereby reducing the system modulus to 25 pct of the rigid boundary condition. This represents a 65 pct decrease in the transverse pressure capacity of the stopping. The percent reduction in transverse pressure remains the same for all three wall heights.

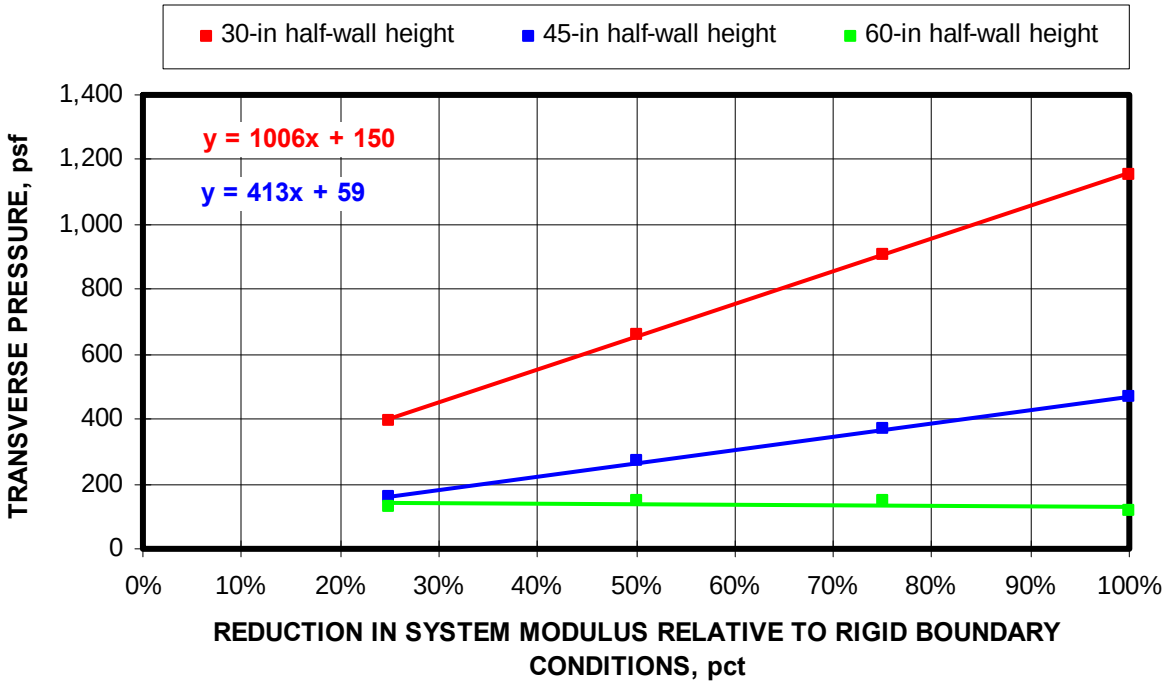

Figure 8-47. Impact of reducing the boundary stiffness on transverse pressure capacity of stopping. Data shows individual test at different wall heights with no preload.

Figures 8-48 through 8-50 show the impact of reductions in system modulus for half-wall heights of 30, 45, and 60 inches. In these figures, the transverse pressure is plotted as a function of preload, which varies from 0 to 212 psi. These figures indicate the reductions in transverse pressure as a result of reduction in boundary stiffness (lower system modulus) are reduced as the preload increases. Using the 30-in-high half-wall as an example, the 65 pct decrease in transverse pressure which occurred by reducing the system modulus to 25 pct of the rigid boundary condition drops to a 48 pct reduction at a preload of 212 psi.

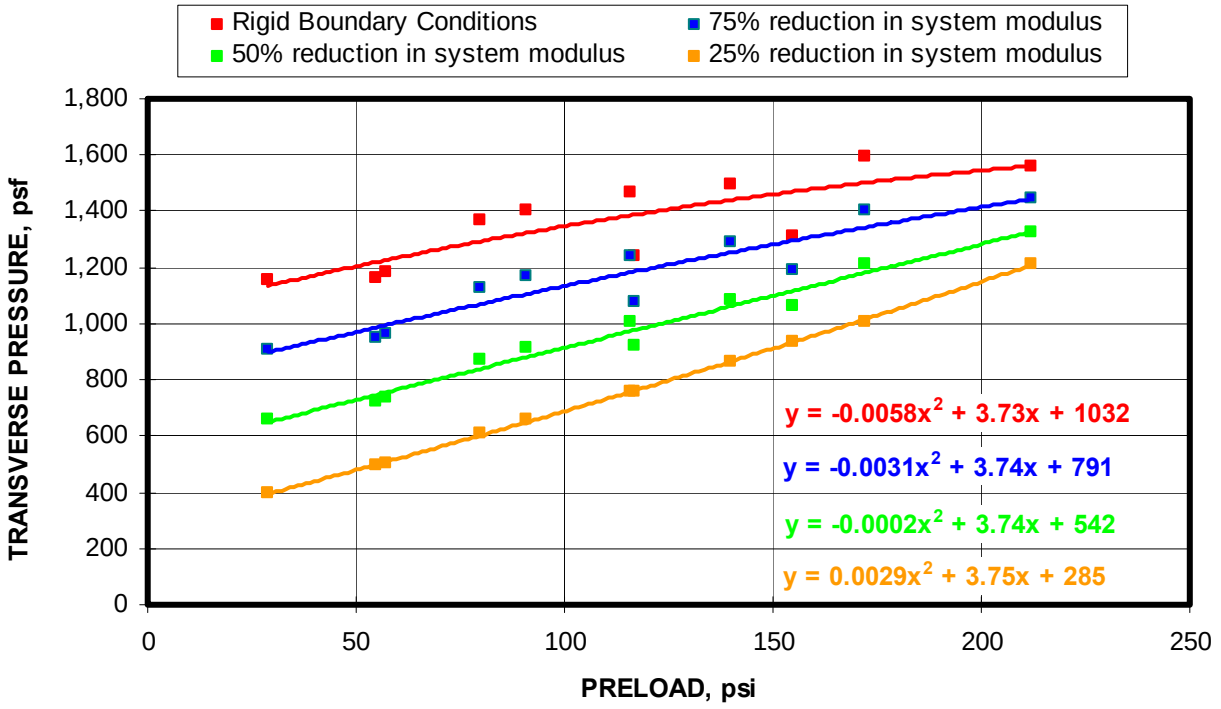

Figure 8-48. Impact of boundary stiffness reductions compared to rigid arching conditions as a function of preload for 30-inch-high half-wall constructions (Klondike hollow core block).

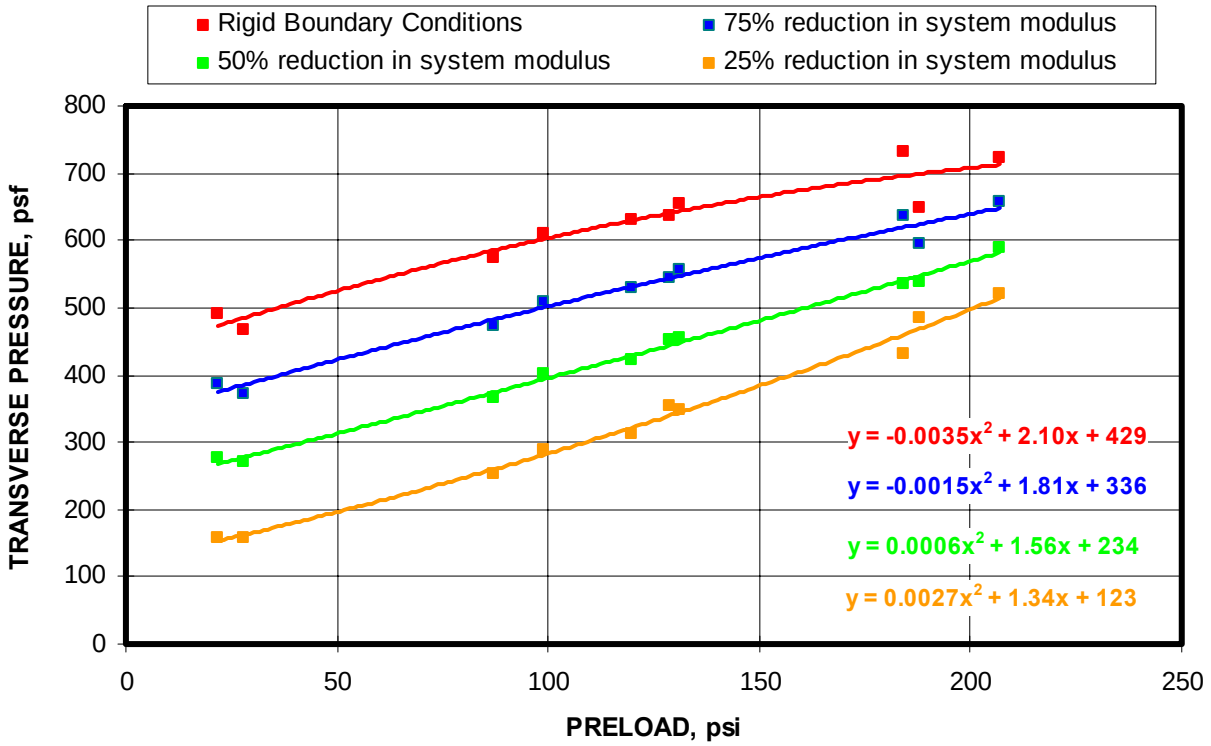

Figure 8-49. Impact of boundary stiffness reductions compared to rigid arching conditions as a function of preload for 45-inch-high half-wall constructions (Klondike hollow core block).

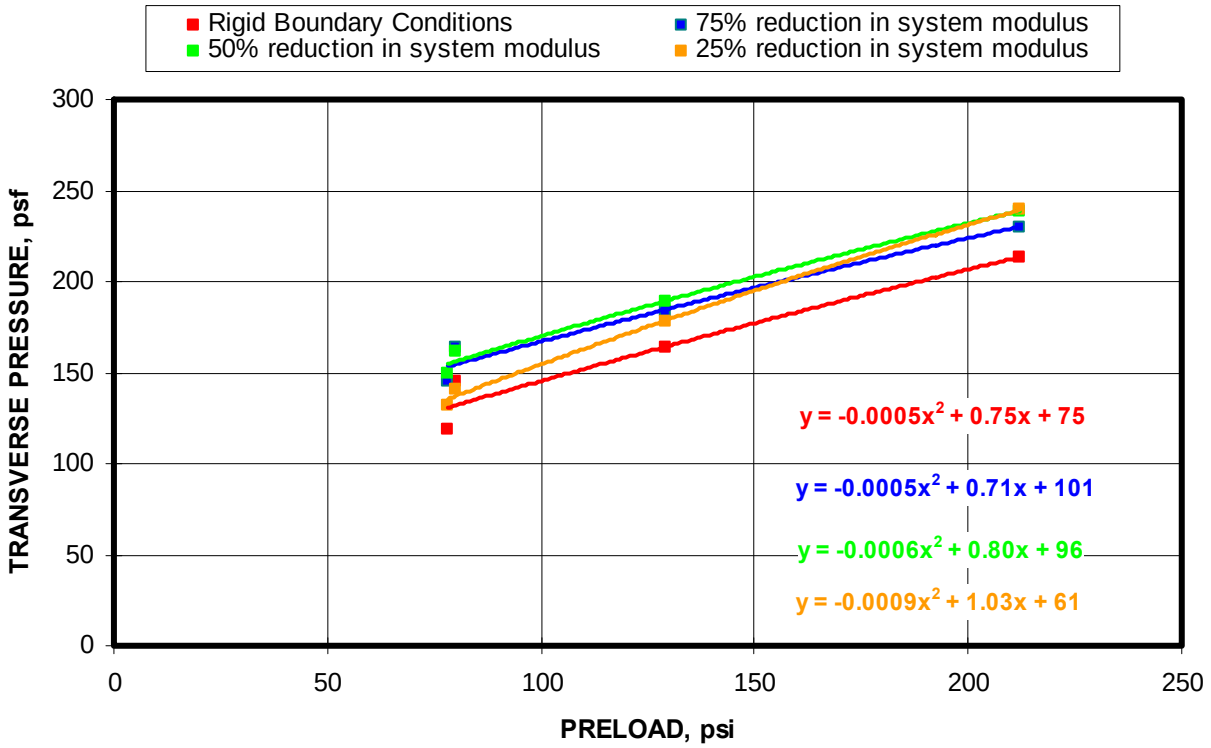

Figure 8-50. Impact of boundary stiffness reductions compared to rigid arching conditions as a function of preload for 60-inch-high half-wall constructions (Klondike hollow core block).

8.4 ACCOA AUTOCLAVED AERATED CONCRETE BLOCK

Aerated Concrete Corporation of America (ACCOA) located just north of Orlando, Florida is the largest manufacturer of autoclaved aerated concrete (AAC) in the United States. Its primary use is the construction industry where the block is used for both load bearing and non-load bearing applications. Autoclaved aerated concrete is a process where material with entrained air is cured in an autoclaved oven to formulate air pockets within the concrete structure. This provides a very low-density material that is light weight, durable, and easy to cut, making it attractive for mine ventilation stopping (see figure 8-51). Silica is the largest dry raw material. Copper mine tailings are often used for the silica source. Other materials include sand and flyash fillers. The silica reacts with the aluminum to form a chemical reaction, which creates millions of tiny air cells that give AAC its unique properties. Only about 20 pct of the material is cement. The material is more air than anything else. Interestingly, AAC was invented in Sweden in 1923 as an alternative to their rapidly depleting timber supplies. Unlike normal concrete, AAC block are very resistant to thermal change. Figure 8-52 shows a house in California constructed from AAC block that survived a devastating fire that destroyed 336 homes and 17,000 acres.

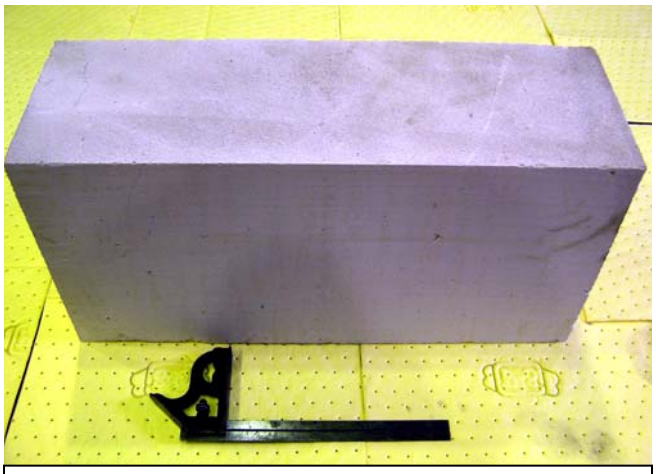

Figure 8-51. AAC block manufactured by Aerated Concrete Corporation of America.

Figure 8-52. Fire resistance capability of aerated concrete block is shown by this house which survived devastating fire in California.

They were approved for mine use by MSHA in 2003. This product is currently distributed to the mining industry through Lee Supply in Charleroi, Pennsylvania. The block is manufactured in thicknesses of 6 and 8 inches with heights of 12 inches and a width of 24 inches. Figure 8-51 shows a photo of a 6-in-thick block. This block weighs on average 16 lbs. The unit block compressive strength was measured from laboratory testing at 421 psi.

8.4.1 Overview of the Test Program

A total of 18 tests were conducted with ACC block. DSA Sales Inc of Pittsburgh, PA. donated a limited supply of the block. Due to the limited supply, only the 48-in half-wall height was evaluated in the research program. Efforts to obtain additional block for testing were unsuccessful due to limited funding. The results of the MRS half-wall tests are summarized in the table 8-7. The preload was varied in increments of 50 psi from zero to 300 psi. Graphs of the measured lateral load and thrust load as a function of the lateral displacement of the wall for each test are documented in Appendix B. A tabular summary of the pertinent parameters and loading values for each test is also included Appendix C.

Table 8-7. Summary of ACC block tests.

Block Type	Test No.	Block Width (in)	Block Height (in)	Block Length (in)	Half-wall Height (in)	Preload (psi)	Measured Transverse Pressure, (psf)
ACC 6	26	6	12	24	48	3	166
ACC 6	27	6	12	24	48	3	186
ACC 6	48	6	12	24	48	30	184
ACC 6	49	6	12	24	48	60	228
ACC 6	50	6	12	24	48	75	264
ACC 6	28	6	12	24	48	120	358
ACC 6	32	6	12	24	48	132	340
ACC 6	29	6	12	24	48	136	276
ACC 6	33	6	12	24	48	136	326
ACC 6	31	6	12	24	48	293	338
ACC 6	30	6	12	24	48	300	320
ACC 8	56	8	12	24	48	18	498
ACC 8	55	8	12	24	48	20	552
ACC 8	54	8	12	24	48	38	434
ACC 8	53	8	12	24	48	40	528
ACC 8	62	8	12	24	48	97	794
ACC 8	51	8	12	24	48	111	682
ACC 8	58	8	12	24	48	238	678

8.4.2 Parametric Relationships and Trends.

Examining table 8-7, it is seen that the transverse pressure capacity of the stoppings constructed from Florida block varied from a low of 166 to a high of 678 psf or 1.15 to 4.71 psi. Figure 8-53 displays the transverse pressure as a function of preload for the 6-in and 8-in thick block walls. The transverse pressures for the 8-in-thick half-walls are 2 to 3 times higher than the 6-in-thick half-walls. It is also seen from figure 8-52 that the transverse pressure is nonlinearly related to the preload and that the transverse pressure approaches an asymptotic maximum at approximately 200 psi for the 6-in-thick walls and 150 psi for the 8-in-thick walls. This suggests that the wall is being stressed to its maximum strength from the combination of the preload and arch compressive forces when the wall is preloaded to this level.

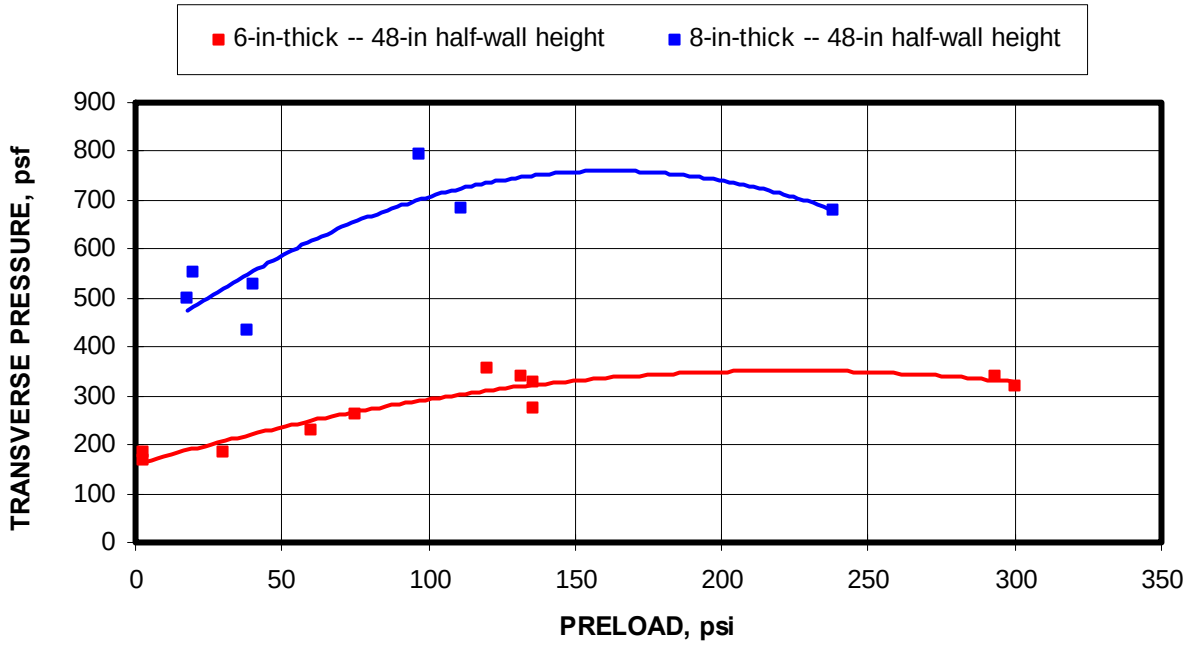

Figure 8-53. Transverse pressure as measured from MRS laboratory testing as a function of preload for 48-inch-high half-walls (AAC Block from Florida).

Figure 8-54 shows that the lateral displacement at the peak transverse pressure also approaches an asymptotic minimum as the preload exceeds 150-200 psi. This is consistent with the transverse pressure behavior expressed in figure 8-53, indicating a limitation of the transverse pressure capacity.

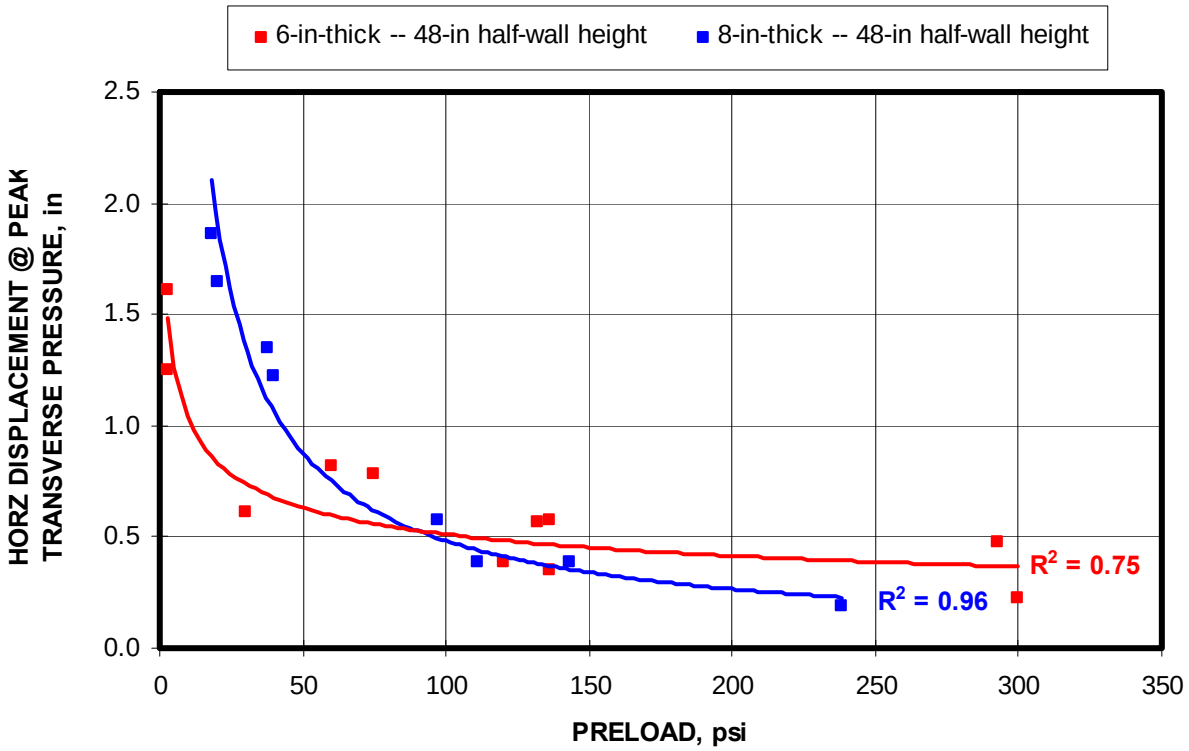

Figure 8-54. Lateral displacement at which peak transverse pressure occurs also reaches an asymptotic minimum as the preload approaches 150 psi (AAC Block from Florida).

Further examination of the parametric relationships confirms the arching theory as presented in chapters 5 and 6. Figure 8-55 shows that the transverse pressure is directly related to the lateral load acting on the half-wall during the laboratory tests. Figure 8-56 shows that the lateral load is also directly related to the thrust force. This is also consistent with the arching theory. Finally, figure 8-57 shows the relationship between the transverse pressure and the arch thrust. This graph resembles the plot of transverse pressure versus preload shown in figure 8-53, showing that the arch thrust also reaches an asymptotic value.

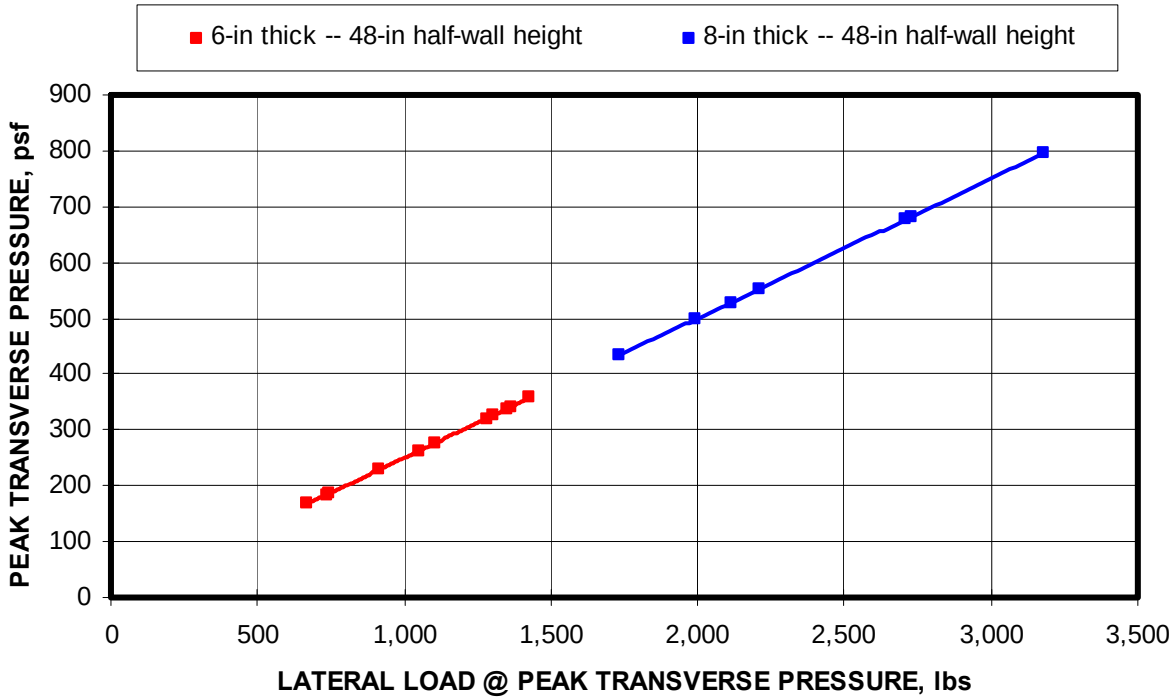

Figure 8-55. Transverse pressure is directly related to the lateral load acting in the 48-inch-high half-wall MRS laboratory tests (AAC Block from Florida).

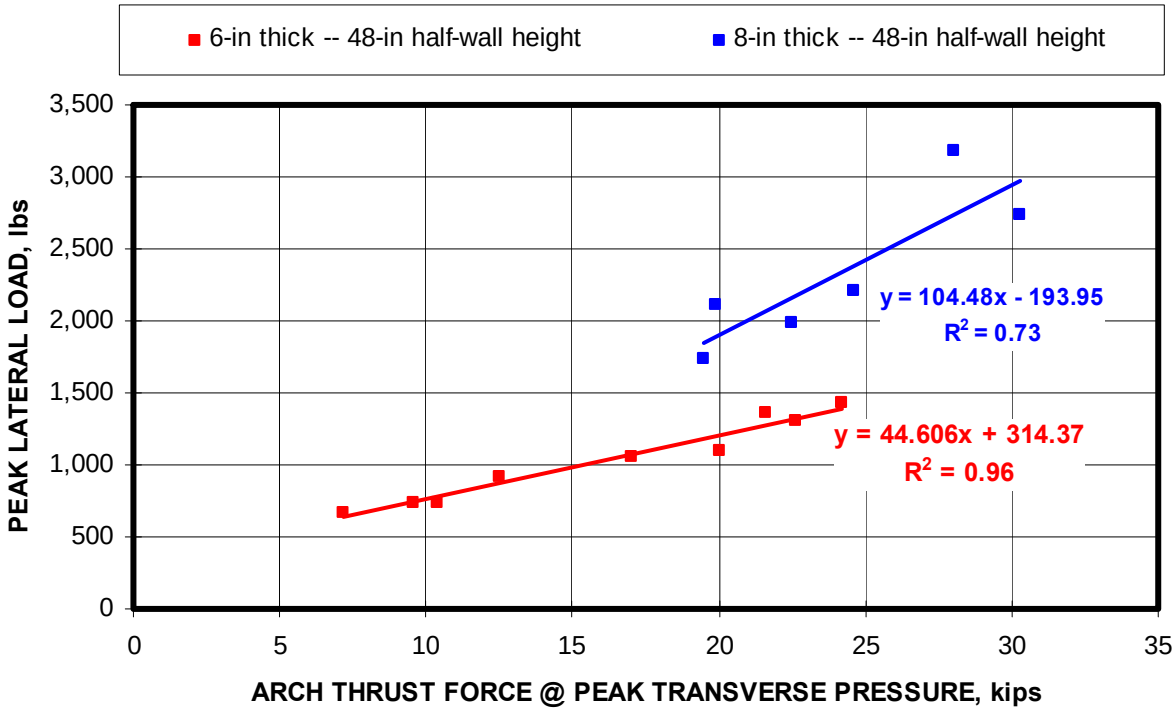

Figure 8-56. Relationship between the lateral load and the arch thrust for MRS laboratory tests for the 48-inch half-wall height (AAC Block from Florida).

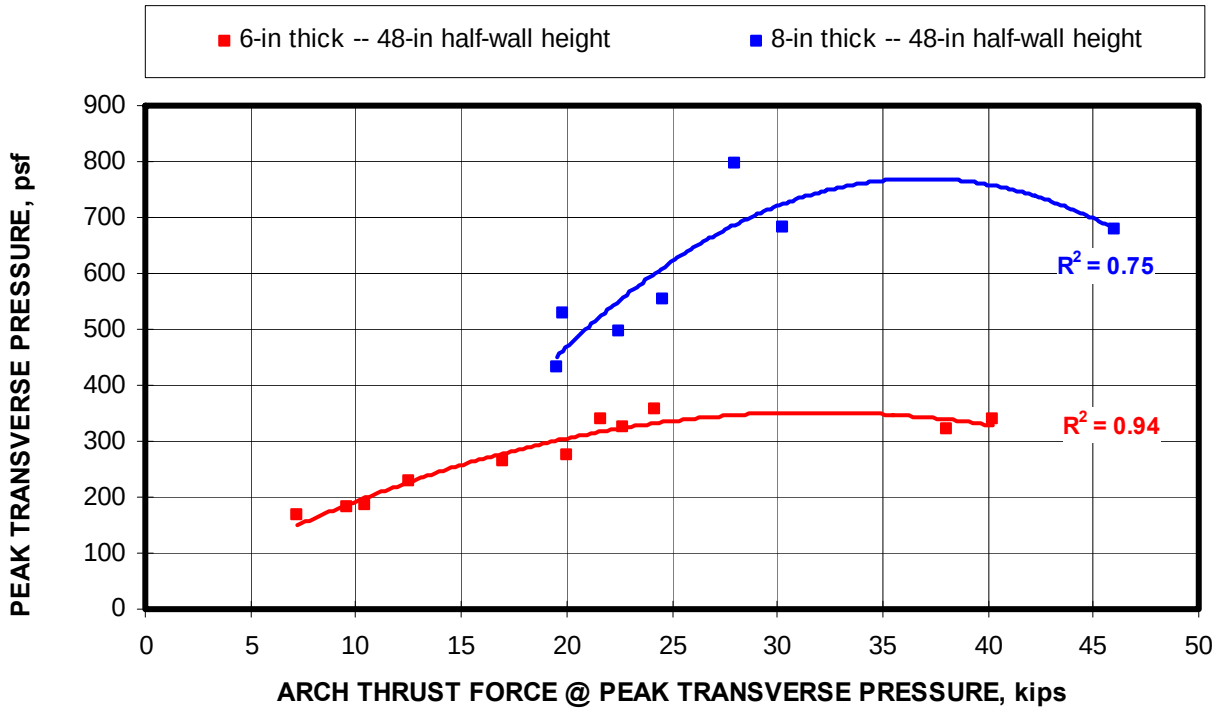

Figure 8-57. Relationship between the transverse pressure and the arch thrust for MRS laboratory tests conducted at 48-inch half-wall height (AAC Block from Florida).

Figure 8-58 depicts the relationship for tests with less than 100 psi preload between the transverse pressure and the material modulus (E), the wall thickness (t), and the wall height (L) expressed as by the term $Ex(t/L)^2$. The chart shows that 93 pct of the transverse pressure of a stopping is determined by this relationship. The material modulus is a significant parameter since it determines the amount of thrust force developed and ultimately the amount of lateral displacement of the wall, both of which control the arching mechanics of the wall. If the modulus is related to the compressive strength of the block material, the modulus factor could be replaced by the compressive strength as previous research suggests (Barczak, 2004).

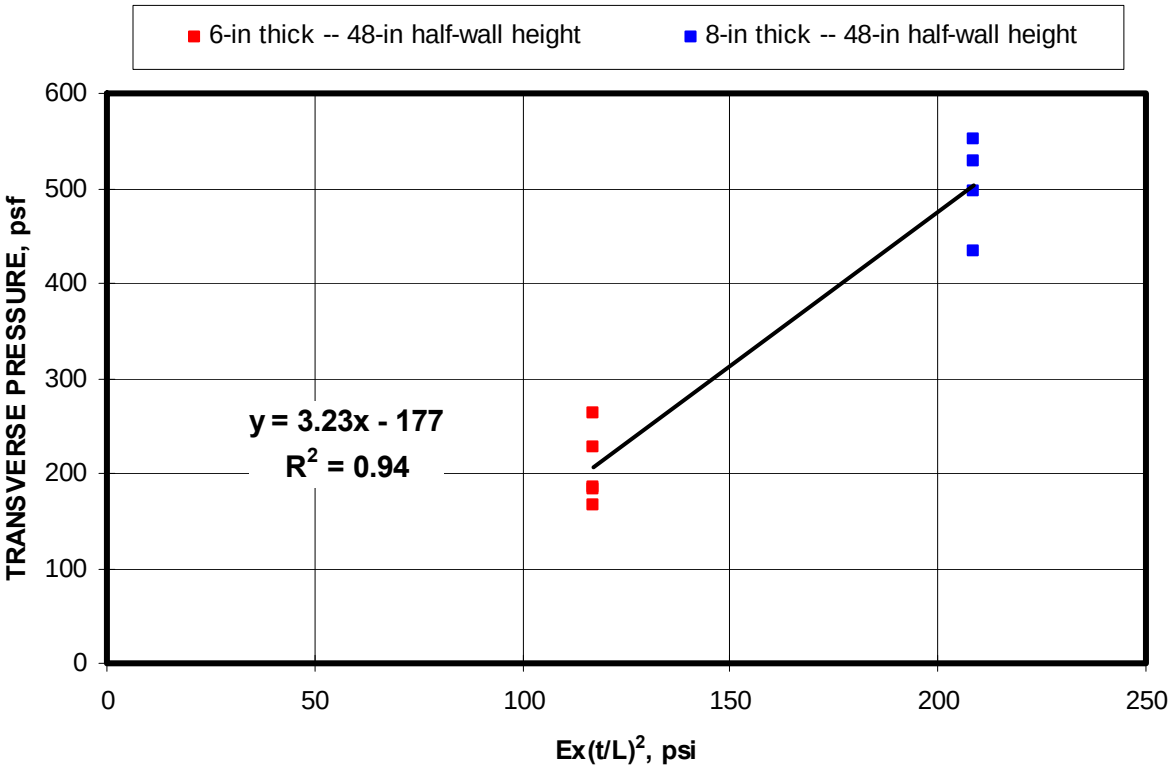

Figure 8-58. Correlation of factors involving the material modulus (E), wall thickness (t), and wall height (L) to the transverse pressure capacity of a stopping (AAC Block from Florida).

Evaluation of Predictive Models

The next goal is to evaluate the capability to predict the transverse pressure. If the thrust force and its resultant location and lateral load are known, the transverse pressure capacity of a stopping can be predicted with nearly 100 pct accuracy. If the thrust force location is instead calculated from the empirical model described in chapter 6 and shown in figure 8-59 for the two block thicknesses considered in this analysis, the transverse pressure can still be predicted with 99 pct accuracy as depicted by the open red square data points shown in figure 8-60. Each data point in figure 8-60 represents an individual laboratory test. As seen in the figure, the accuracy of the prediction is consistent throughout the full range of transverse pressure conducted in the laboratory testing, and includes preloading of wall from zero to 300 psi and three different wall heights.

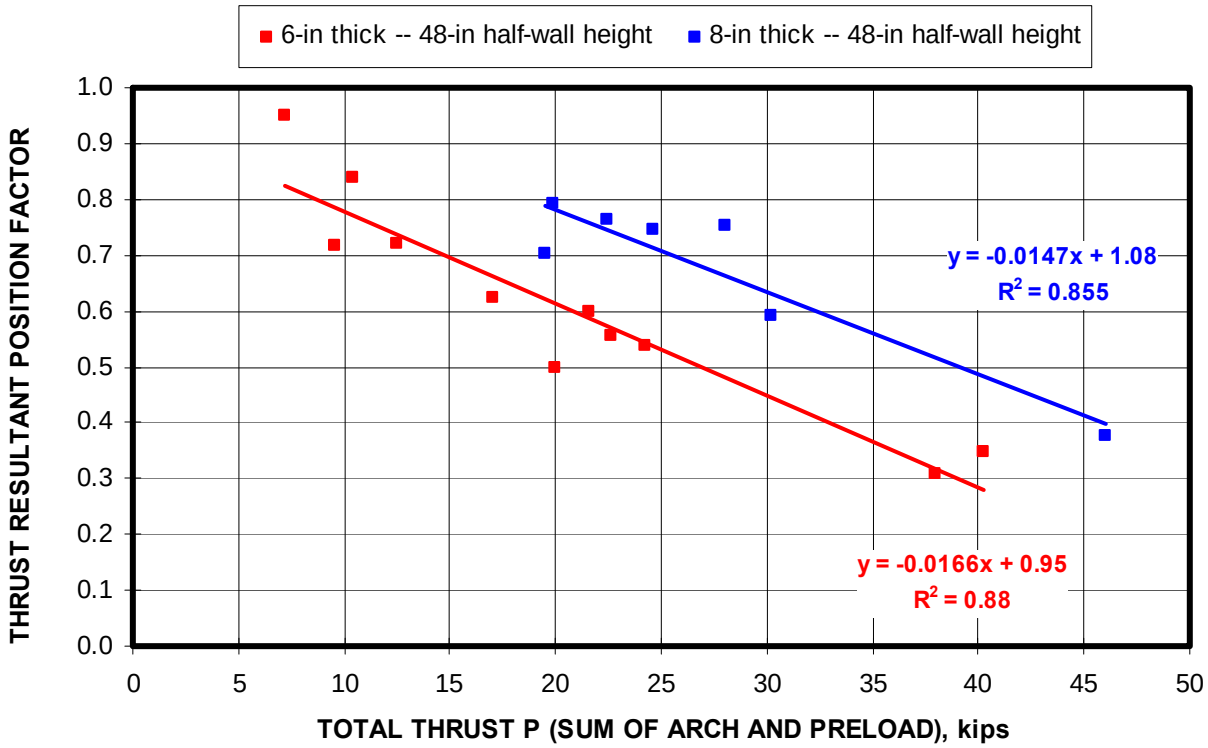

Figure 8-59. Resultant thrust force location for two block thicknesses as a function of the total arch thrust (AAC block from Florida).

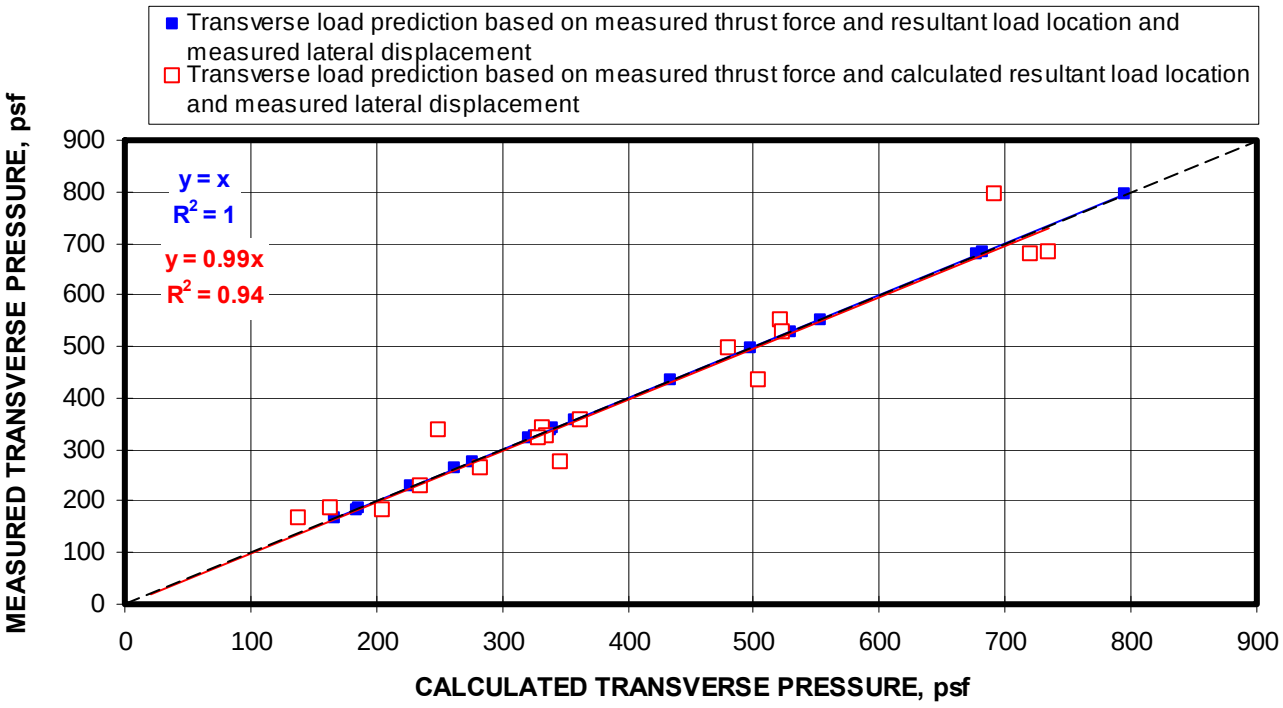

Figure 8-60. Prediction of transverse pressure when both the lateral load and arch thrust are known. Blue curves predicts transverse pressure when resultant thrust force location is also known and red squares show predicted transverse pressure when resultant thrust force location is calculated from empirical data (AAC block from Florida).

If either the arch thrust or the lateral displacement is known, then the transverse pressure can still be calculated. It is recalled from chapter 7 that two methods were developed. Method 1 predicts the transverse pressure from the measured lateral displacement. Method 2 predicts the transverse pressure from the measured thrust force. Figures 8-61 illustrates the predictive capability of these models showing the measured transverse pressure vs. the predicted transverse pressure for each half-wall laboratory test. The overall accuracy of the predictive models is reasonably good (error less than 10 pct). However, as highlighted in this graph with yellow colored ovals, some laboratory tests are not accurately predicted. Further examination of these tests indicates that failure was occurring during the preloading of the half-wall prior to the application of transverse pressure. Figure 8-62 shows an example where the thrust force decreased immediately after the preload was applied and continued to decrease throughout the loading cycle. Figure 8-63 shows that the predictive models are improved when these premature failures are eliminated from the data set.

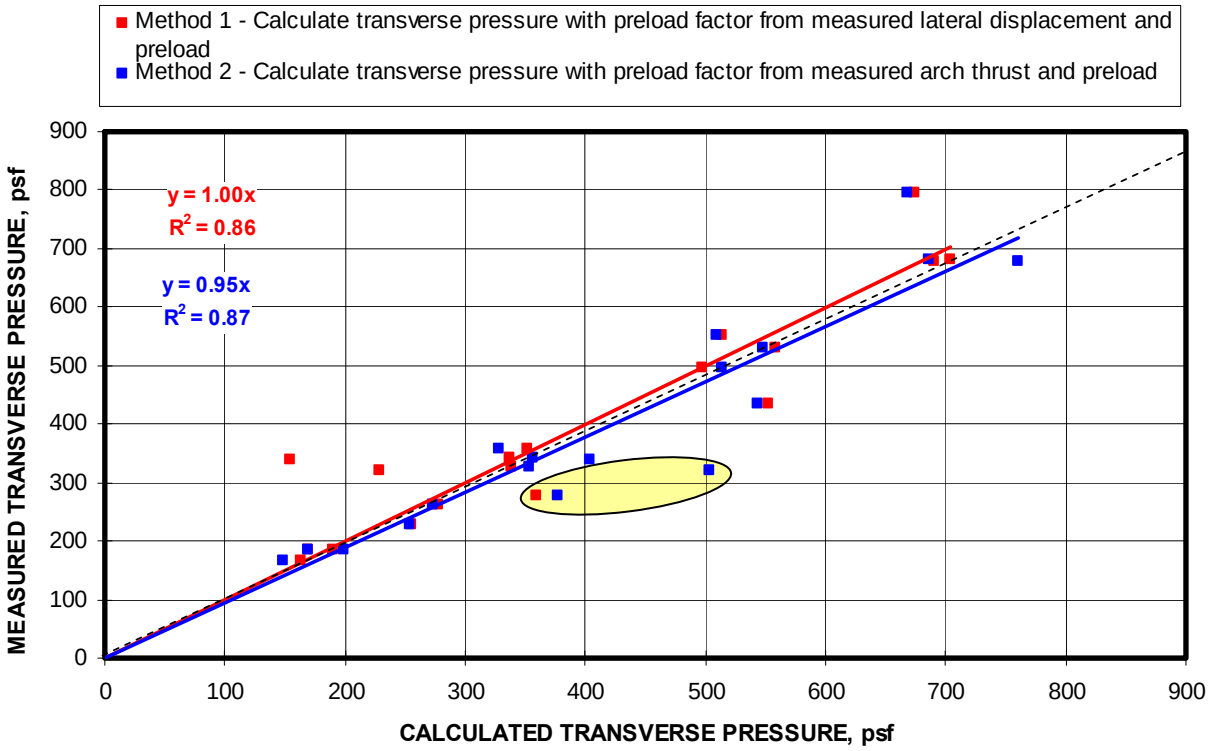

Figure 8-61. Prediction of transverse pressure from known thrust and lateral loads (AAC block from Florida).

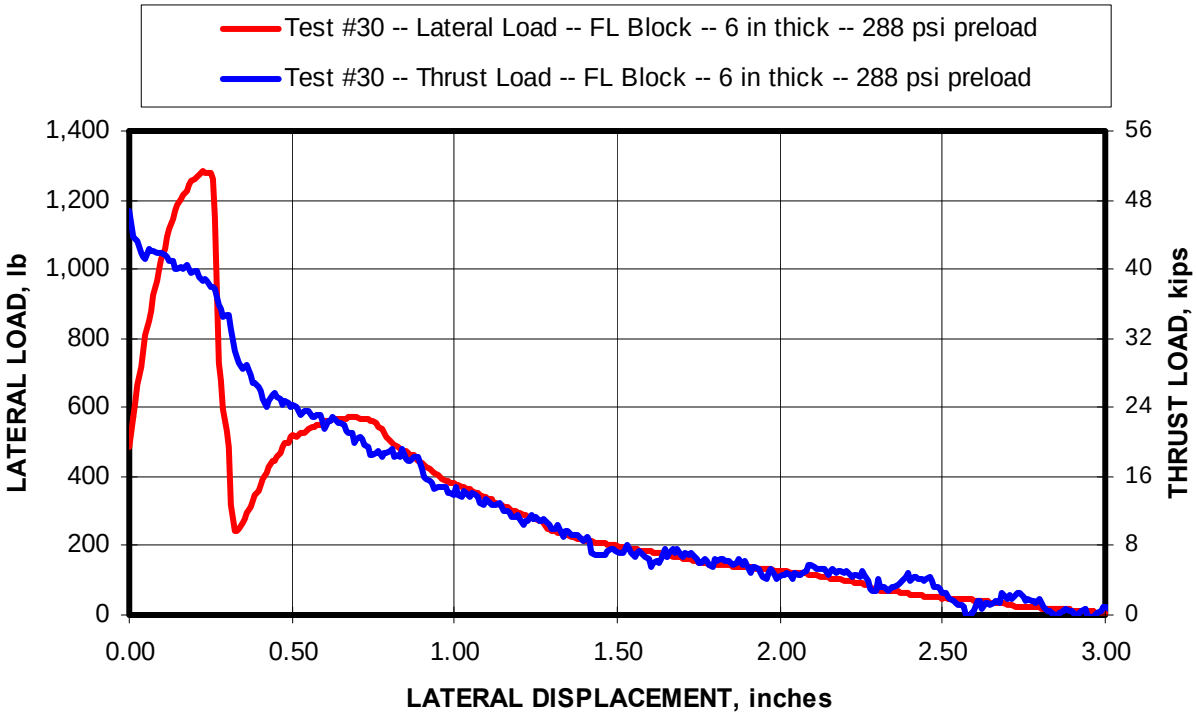

Figure 8-62. Example of test with high preload showing how the thrust force decreases immediately after the preload is applied and continues to decrease through the full loading cycle.

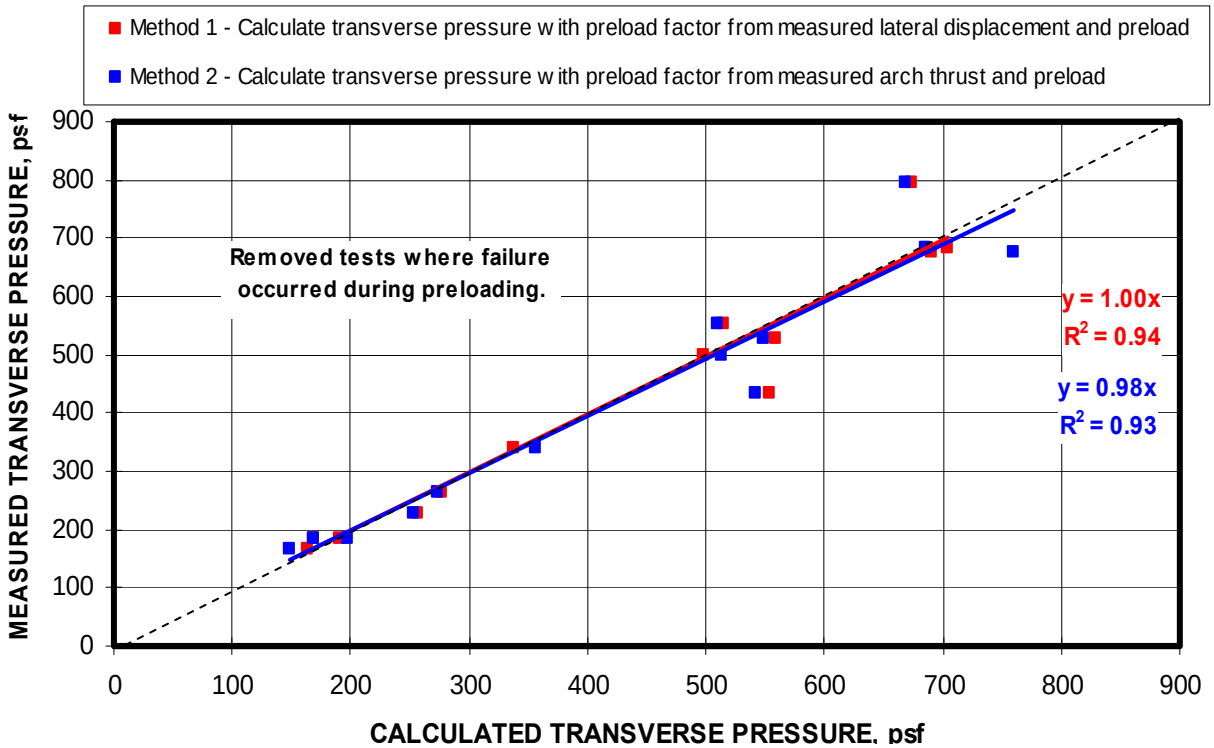

Figure 8-63. Prediction of transverse pressure from known thrust and lateral loads with premature failures removed (AAC block from Florida).

8.4.4 Theoretical Impact of Boundary Stiffness

A theoretical assessment of the impact of the boundary stiffness is conducted by varying the system modulus of elasticity (see equation 6.11 and 7.7). The modulus of elasticity determines the deformations of the wall and the boundary, i.e. the mine roof and floor. The system modulus reflects the series stiffness equivalent of the wall and roof and floor structure. The theoretical assessment is made by reducing the system modulus to 75, 50, and 25 pct of the rigid boundary condition, and using the lateral displacement model to calculate the transverse pressure. For comparative purposes, if the boundary stiffness were equal to the wall stiffness, the system stiffness would be reduced by 50 pct. Likewise, if the boundary stiffness were three times that of the wall, the system stiffness would be 75 pct of the rigid boundary condition, and if the boundary stiffness were one third of the wall stiffness, the system stiffness would be 25 pct of the rigid boundary condition.

Figure 8-64 shows the impact of the reduction in system modulus to 25, 50, and 75 pct of the rigid boundary condition for both the 6-in and 8-in thickness configurations. First, it can be concluded from figure 8-64 that as the boundary modulus is reduced, the transverse pressure capacity of the stopping will also be reduced. It is seen from this figure that the impact of reductions in boundary modulus will have a greater impact in terms of absolute reductions in transverse pressure for thicker walls than it will for thinner walls. For the example shown in figure 8-64, the transverse pressure for test number 56 for the 8-in-thick half-wall, was reduced from 498 psf for the rigid boundary condition to 156 psf when the boundary modulus is one third of the wall modulus, thereby reducing the system modulus to 25 pct of the rigid boundary condition. This represents a 69 pct decrease in the transverse pressure capacity of the stopping. Figures 8-65 and 8-66 show the impact of reductions in system modulus for both the 6-in-thick and 8-in-thick walls including the walls with preload. The transverse pressure is plotted as a function of preload, which is scaled from 0 to 160 psi in these plots to eliminate the cases where premature failures were occurring from the higher preloads. These figures indicate the reductions in transverse pressure because of reduction in boundary stiffness (lower system modulus) are reduced as the preload increases through this range. Using the 8-in-thick half-wall as an example, the 69 pct decrease in transverse pressure which occurred by reducing the system modulus to 25 pct of the rigid boundary condition drops to a 19 pct reduction at a preload of 143 psi.

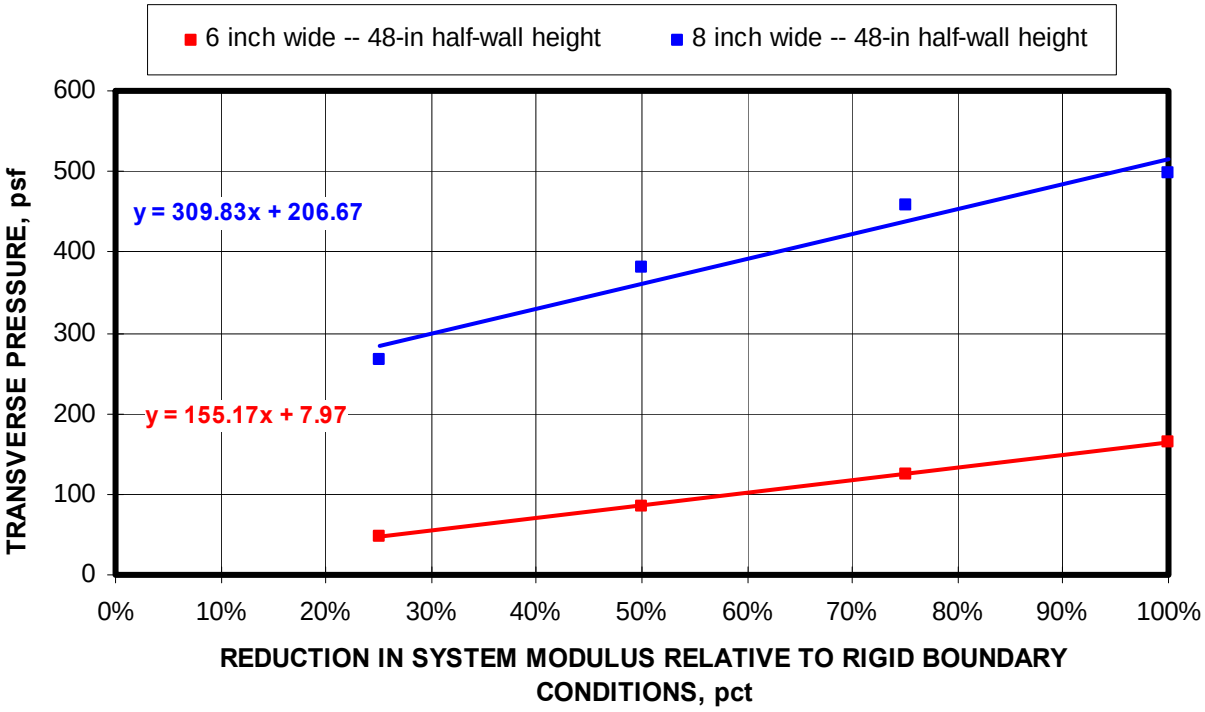

Figure 8-64. Impact of reducing the boundary stiffness on transverse pressure capacity of stopping. Data shows individual test at different wall heights with no preload (AAC block from Florida).

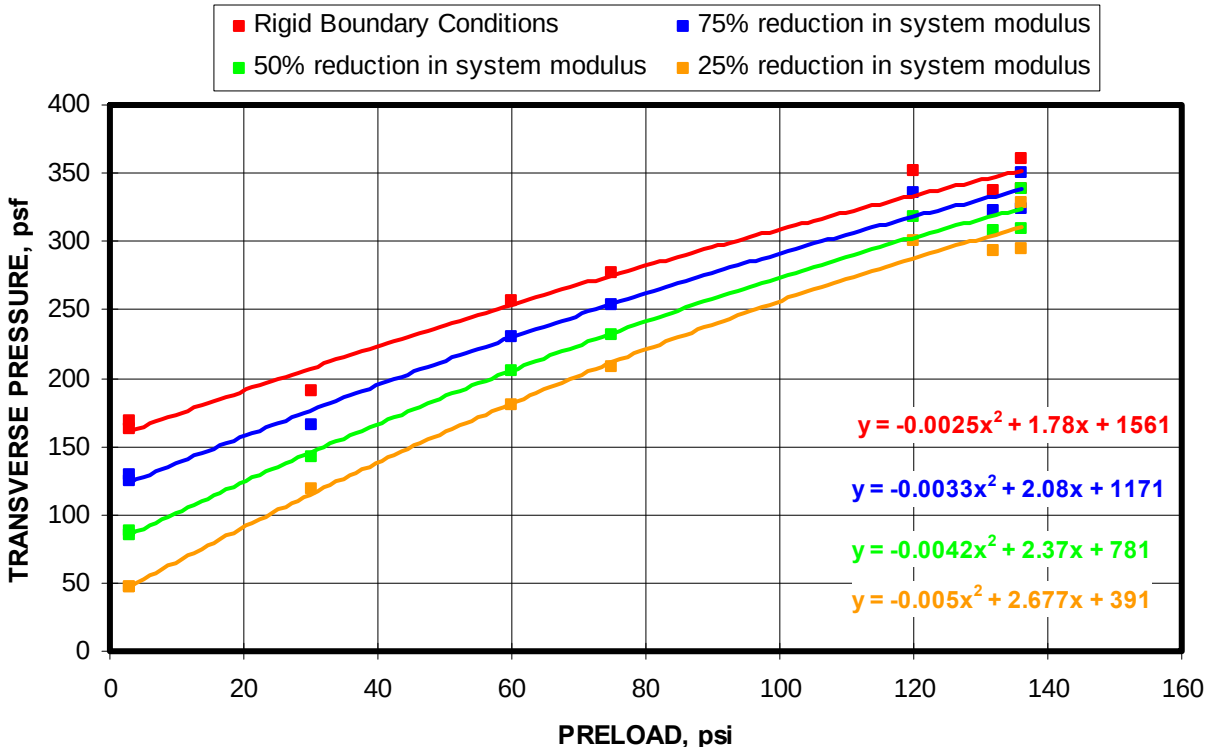

Figure 8-65. Impact of boundary stiffness reductions compared to rigid arching conditions as a function of preload for 6-inch-thick half-wall constructions (AAC block from Florida).

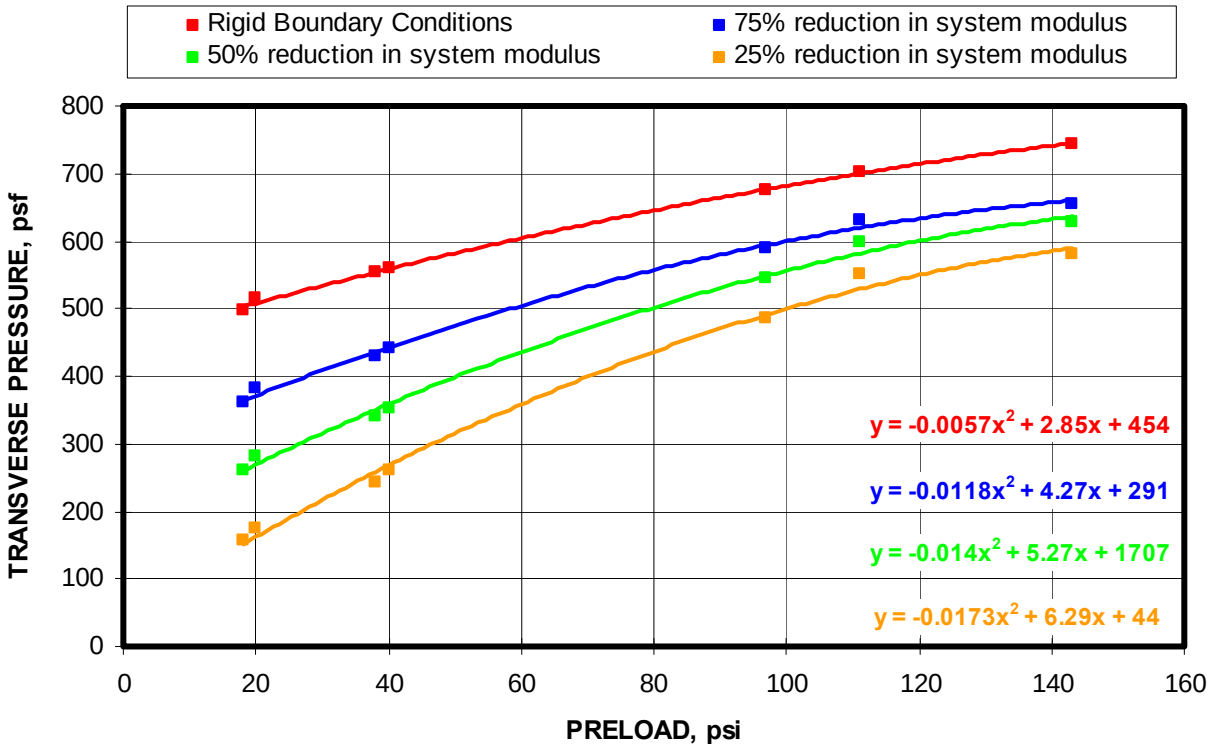

Figure 8-66. Impact of boundary stiffness reductions compared to rigid arching conditions as a function of preload for 8-inch-thick half-wall constructions (AAC block from Florida).

8.4 YTONG BLOCK

Ytong is also an autoclaved aerated concrete (AAC) block, similar in material properties to that of the block described in the previous section. This block is now manufactured by Safecrete in Ringgold, Georgia, although the block that was tested was believed to be from a Florida plant. As previously described, the air pores within the formed structure characterize the material. The Ytong block had a unit block compressive strength of 705 psi, a 67 pct increase compared to the previously

Figure 8-67. Ytong autoclaved aerated concrete block.

discussed ACCOA block. The block that was tested measured nominally 8 inches thick and 8 inches high by 24 inches wide. Figure 8-67 shows a photo of a 7.875-inch-thick block. This block weighs on average 29 lbs.

8.5.1 Overview of the Test Program

A total of 16 tests were conducted with Ytong block. The scope of testing included three half-wall heights of 31.50, 47.25, and 63.00 inches. The preload was varied in increments of 50 psi from 0 to 145 psi. The results of the MRS half-wall tests are summarized in the table 8-8. Graphs of the measured lateral load and thrust load as a function of the lateral displacement of the wall for each test are documented in Appendix B. A tabular summary of the pertinent parameters and loading values for each test is also included Appendix C.

Table 8-8. Summary of Ytong block tests.

Block Type	Test No.	Block Width (in)	Block Height (in)	Block Length (in)	Half-wall Height (in)	Preload (psi)	Measured Transverse Pressure, (psf)
Ytong	239	7.875	7.875	24	31.5	3	2,150
Ytong	249	7.875	7.875	24	31.5	7	1,822
Ytong	243	7.875	7.875	24	31.5	51	2,016
Ytong	250	7.875	7.875	24	31.5	58	2,272
Ytong	251	7.875	7.875	24	31.5	94	2,186
Ytong	241	7.875	7.875	24	31.5	107	2,160
Ytong	242	7.875	7.875	24	31.5	145	2,590
Ytong	234	7.875	7.875	24	47.25	15	562
Ytong	235	7.875	7.875	24	47.25	53	772
Ytong	237	7.875	7.875	24	47.25	109	1,034
Ytong	238	7.875	7.875	24	47.25	132	1,060
Ytong	245	7.875	7.875	24	63	10	262
Ytong	246	7.875	7.875	24	63	38	386
Ytong	252	7.875	7.875	24	63	69	360
Ytong	247	7.875	7.875	24	63	99	384
Ytong	248	7.875	7.875	24	63	142	448

8.5.2 Parametric Relationships and Trends.

Examining table 8-8, it is seen that the transverse pressure capacity of the stoppings constructed from Ytong block varied from a low of 262 to a high of 2,590 psf or 1.82 to 17.99 psi. The transverse pressure is most significantly affected by the wall height as with previous block tests. Figure 8-68 displays the transverse pressure as a function of preload for the three different wall heights and preload varying from 0 to 150 psi. The transverse pressures for the 31.5-in-high half-walls are 5-6 times that of the 63-in-high half-walls and two to 4 times higher than the 47.25-in-high half-walls. The impact of the preload was less than was observed with the conventional Portland cement block (section 8.1), which is consistent with the results observed for the Florida AACOA block as well. The 47.25-in-high half-wall showed the familiar trend of nonlinear response with preload, but here too the impact was rather small, with a decrease of 47 pct in transverse pressure when the preload was decreased from 132 psi to 15 psi. In terms of percent, the least impact was observed with the shortest wall height (31.5 inches). It is also seen from figure 8-68 that the transverse pressure approaches an asymptotic maximum at approximately 125 psi, suggesting the block strength is being exceeded at this loading.

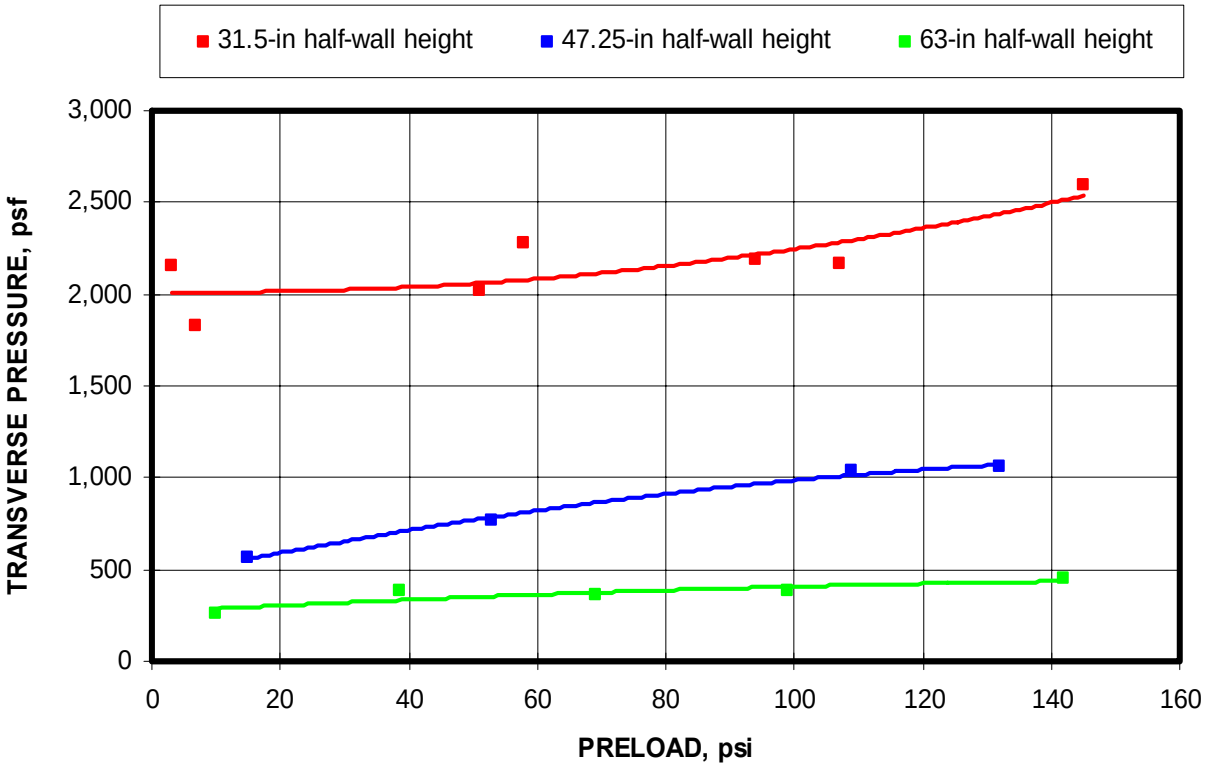

Figure 8-68. Transverse pressure as measured from MRS laboratory testing as a function of preload for three different half-wall heights (Ytong AAC block).

Figure 8-69 shows that the lateral displacement at the peak transverse pressure also approaches an asymptotic minimum as the preload approaches 125 psi. This is consistent with the transverse pressure behavior expressed in figure 8-68, indicating a limitation of the transverse pressure capacity.

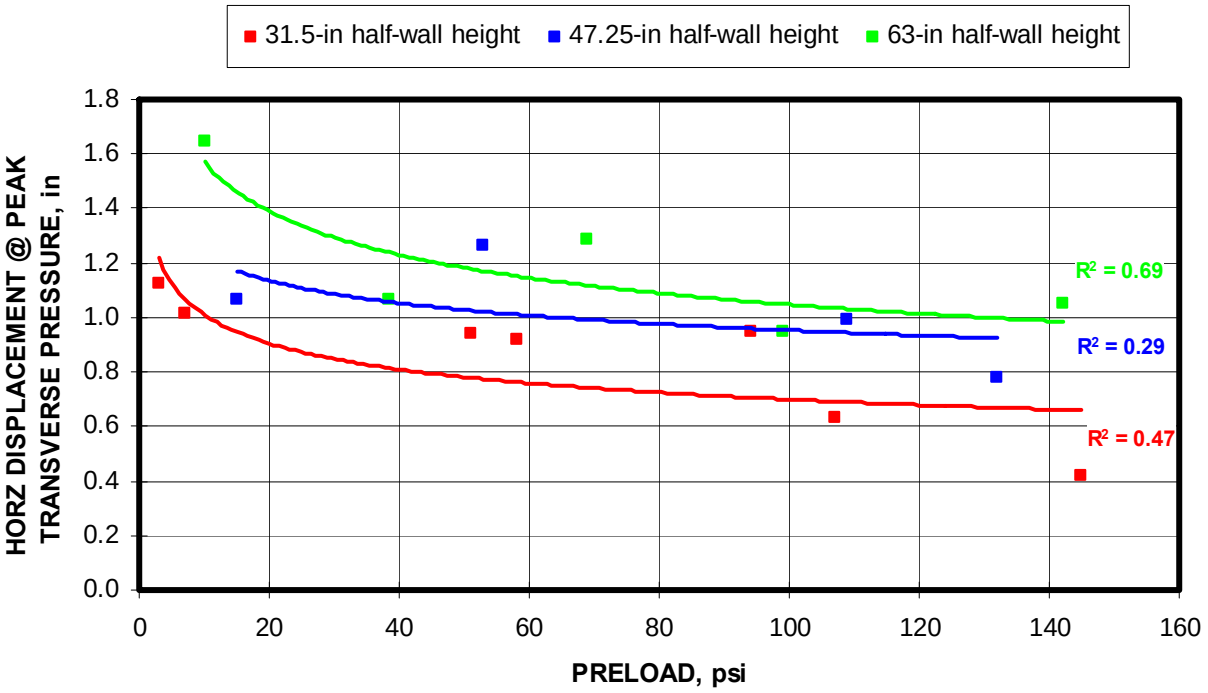

Figure 8-69. Lateral displacement at which peak transverse pressure occurs also reaches an asymptotic minimum as the preload approaches 130 psi (Ytong AAC block).

Further examination of the parametric relationships confirms the arching theory as presented in chapters 5 and 6. Figure 8-70 shows that the transverse pressure is directly related to the lateral load acting on the half-wall during the laboratory tests. Figure 8-71 shows that the lateral load is also directly related to the thrust force. This is also consistent with the arching theory. Finally, figure 8-72 shows the relationship between the transverse pressure and the arch thrust. This graph is somewhat inconsistent with the previous analysis in that the transverse pressure does not reach an asymptotic level with the increasing arch thrust, suggesting that the material strength has not been reached at the preloads considered in this analysis.

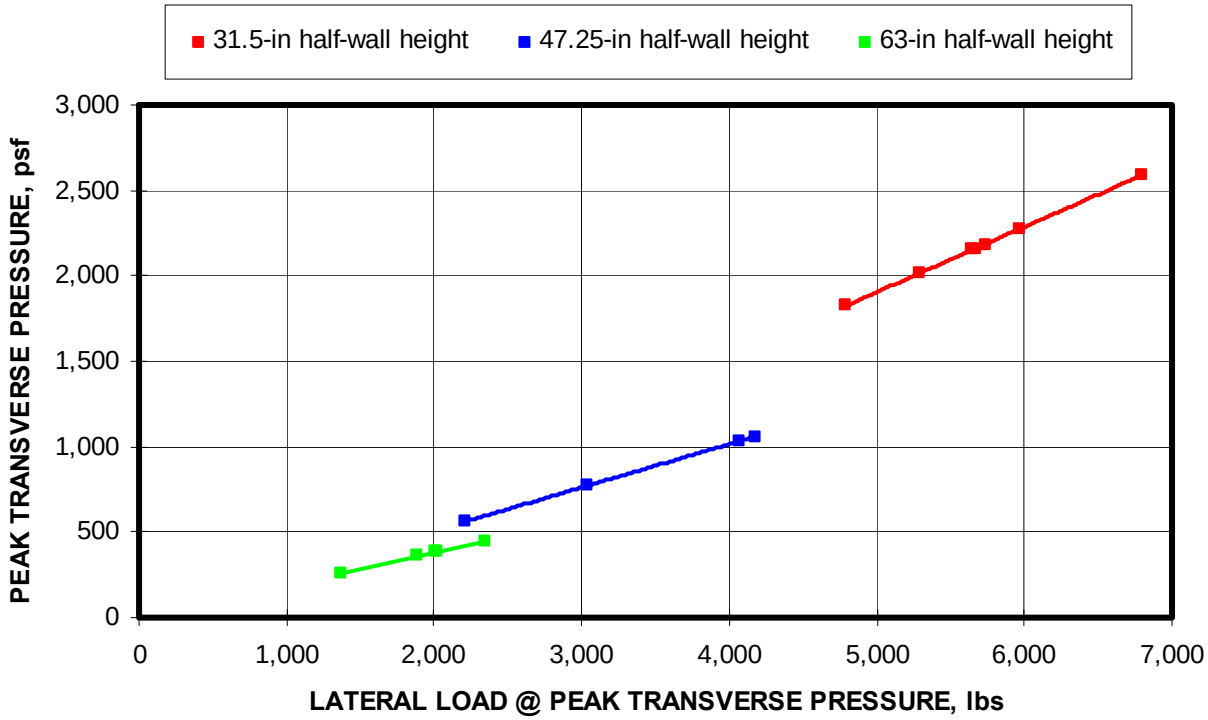

Figure 8-70. Transverse pressure is directly related to the lateral load acting on the half-wall in the MRS laboratory tests (Ytong AAC block).

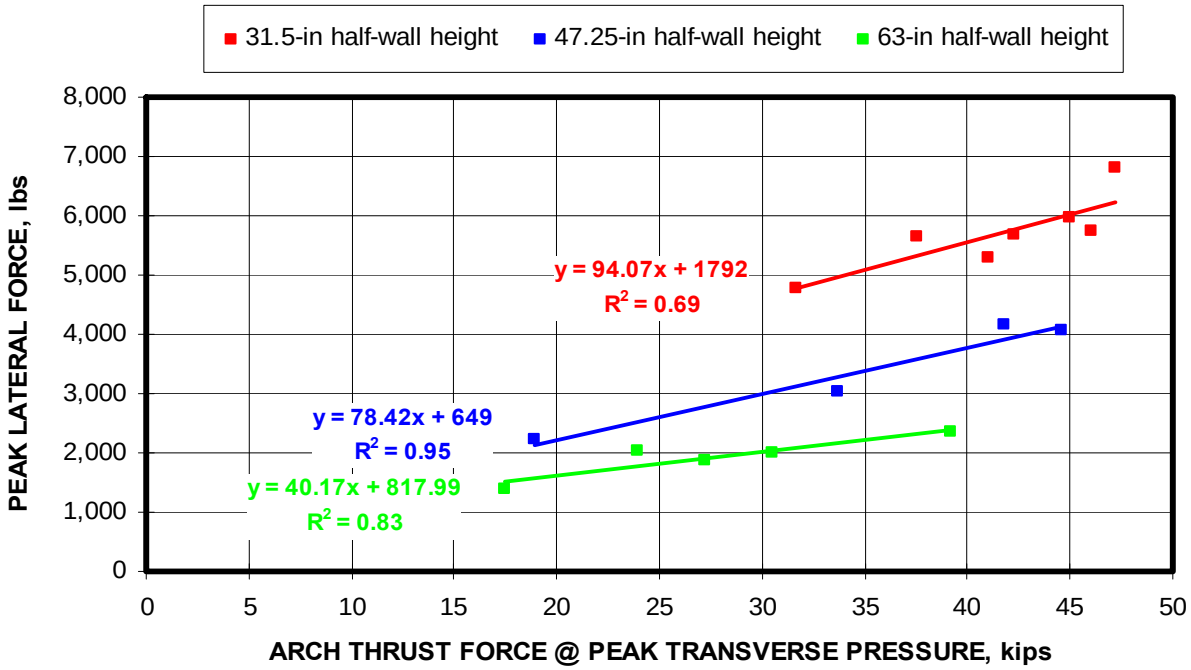

Figure 8-71. Relationship between the lateral load and the arch thrust for MRS laboratory tests for three different wall heights (Ytong AAC block).

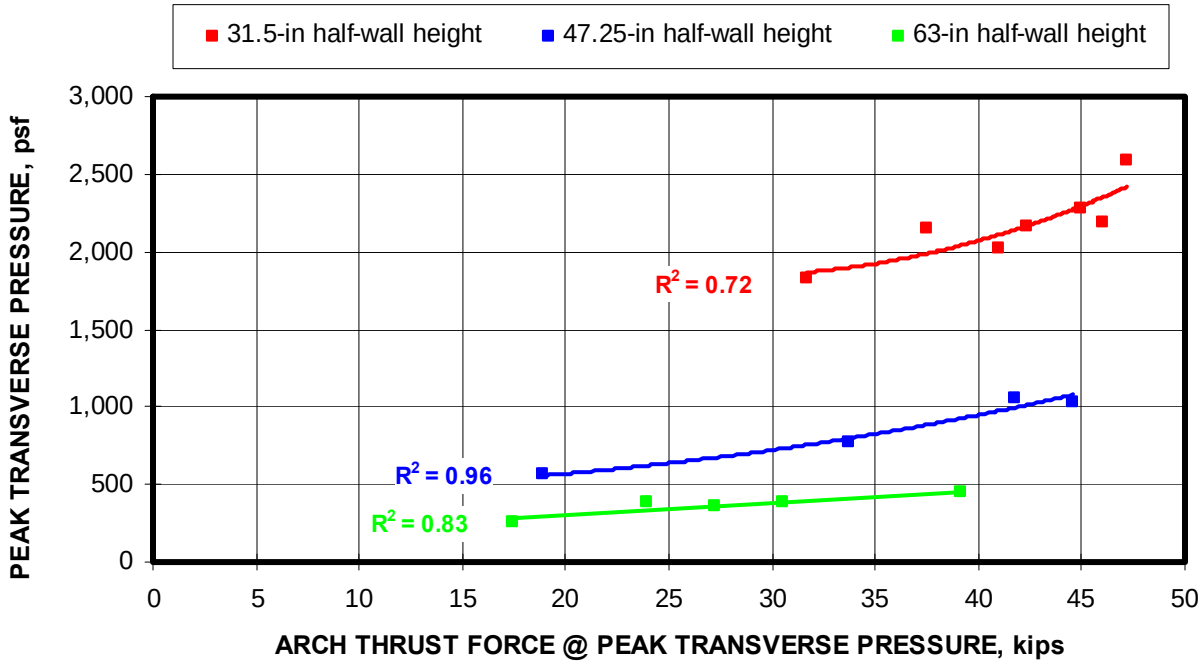

Figure 8-72. Relationship between the transverse pressure and the arch thrust for MRS laboratory tests conducted at three different wall heights (Ytong AAC block).

Figure 8-73 depicts the relationship for tests with less than 100 psi preload between the transverse pressure and the material modulus (E), the wall thickness (t), and the wall height (L) expressed as by the term $Ex(t/L)^2$. The chart shows that 98 pct of the transverse pressure of a stopping is determined by this relationship. The material modulus is a significant parameter since it determines the amount of thrust force developed and ultimately the amount of lateral displacement of the wall, both of which control the arching mechanics of the wall. If the modulus is related to the compressive strength of the block material, the modulus factor could be replaced by the compressive strength as previous research suggests (Barczak, 2004).

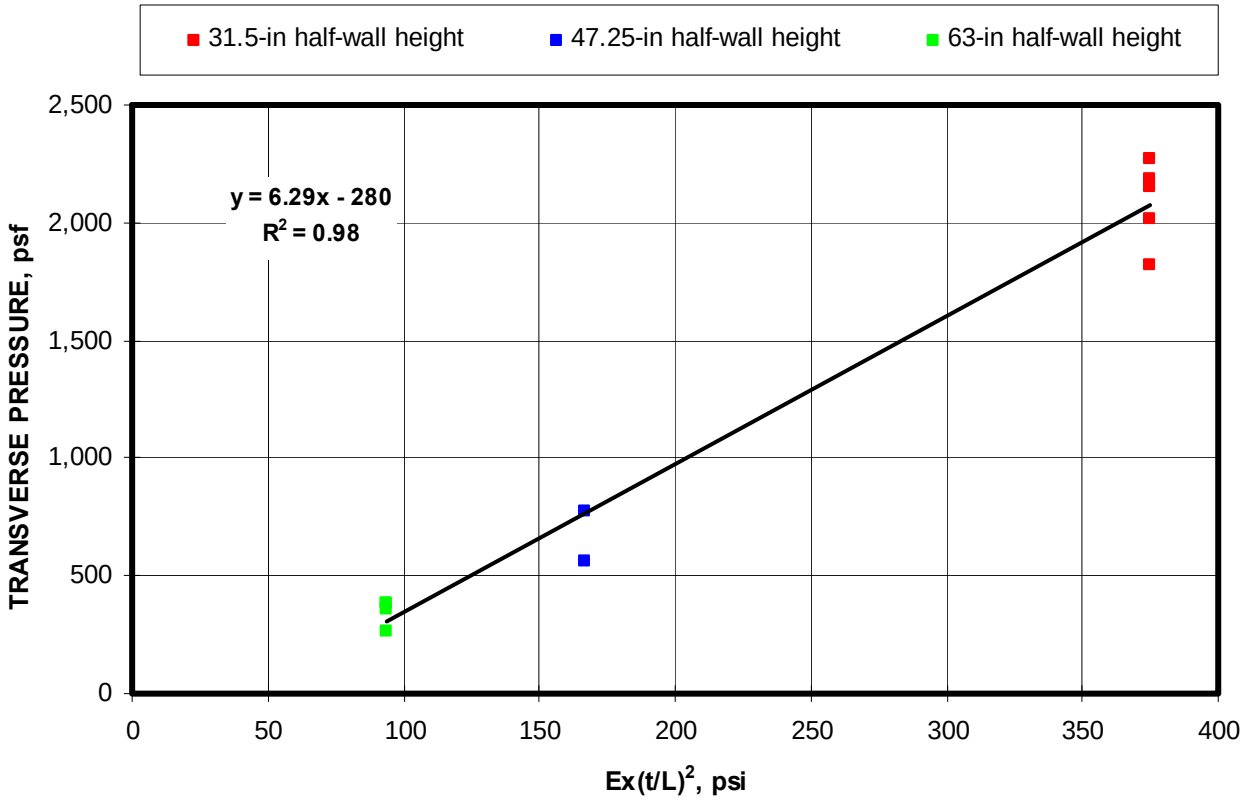

Figure 8-73. Correlation of factors involving the material modulus (E), wall thickness (t), and wall height (L) to the transverse pressure capacity of a stopping (AAC Block from Florida).

8.5.3 Evaluation of Predictive Models

The next goal is to evaluate the capability to predict the transverse pressure. If the thrust force and its resultant location and lateral load are known, the transverse pressure capacity of a stopping can be predicted with nearly 100 pct accuracy. If the thrust force location is instead calculated from the empirical model described in chapter 6 and shown in figure 8-74 for three half-wall heights considered in this analysis, the transverse pressure can still be predicted with a 99 pct accuracy as depicted by the open red square data points shown in figure 8-75. Each data point in figure 8-75 represents an individual laboratory test. As seen in the figure, the accuracy of the prediction is consistent throughout the full range of transverse pressure conducted in the laboratory testing, and includes preloading of wall from 0 to 160 psi and three different wall heights.

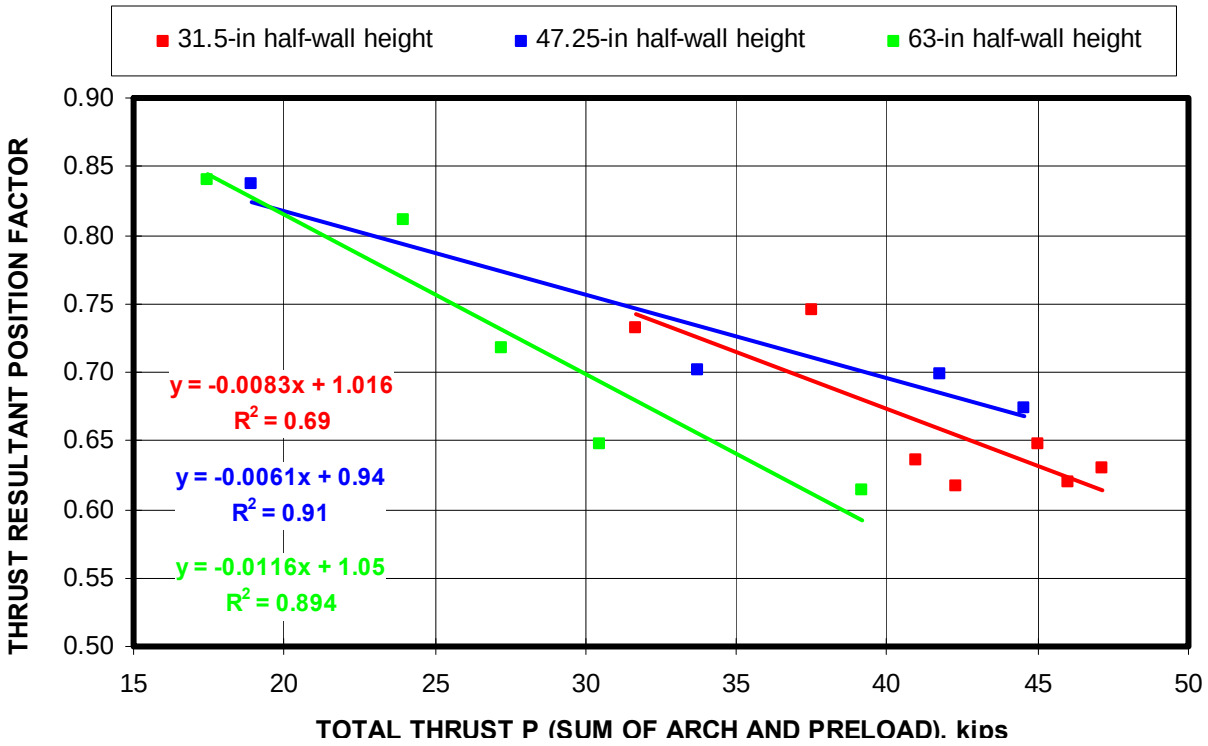

Figure 8-74. Resultant thrust force location for three wall heights as a function of the total arch thrust (AAC block from Florida).

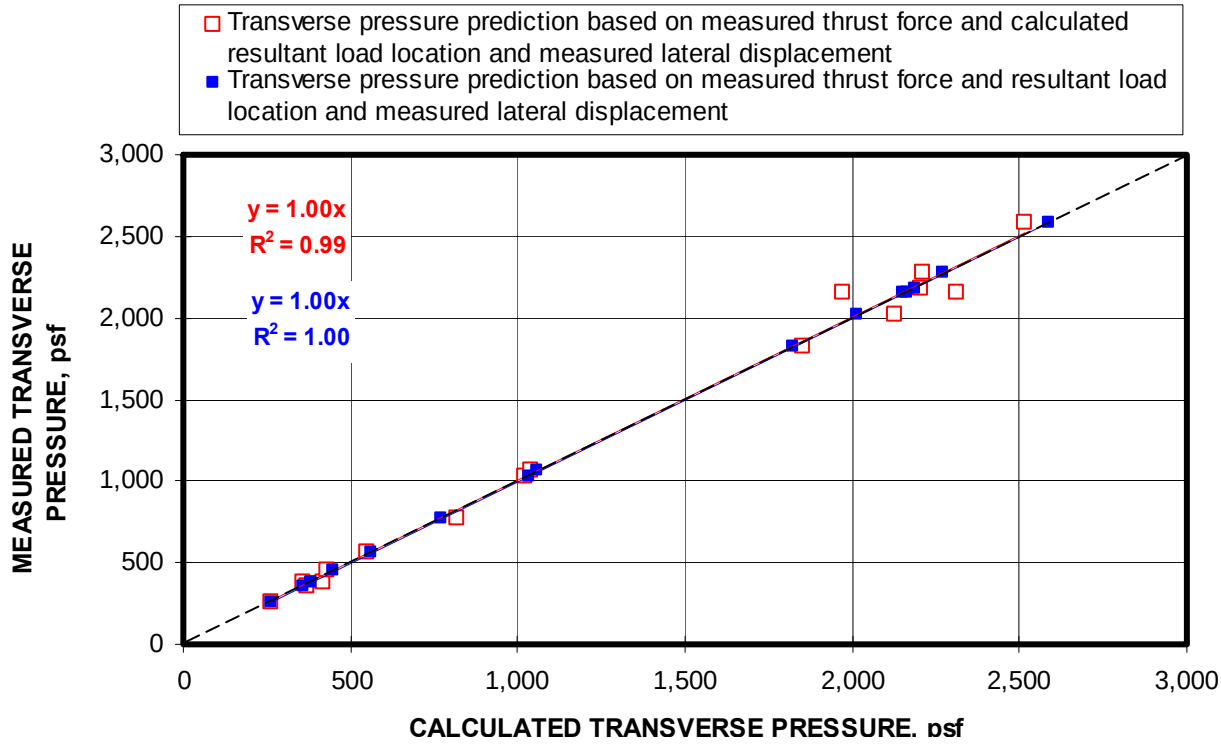

Figure 8-75. Prediction of transverse pressure when both the lateral load and arch thrust are known. Blue curves predicts transverse pressure when resultant thrust force location is also known and red squares show predicted transverse pressure when resultant thrust force location is calculated from empirical data (Ytong AAC block).

If either the arch thrust or the lateral displacement is known, then the transverse pressure can still be calculated. It is recalled from chapter 7 that two methods were developed. Method 1 predicts the transverse pressure from the measured lateral displacement. Method 2 predicts the transverse pressure from the measured thrust force. Figure 8-76 illustrates the predictive capability of these two methods showing the measured transverse pressure vs. the predicted transverse pressure for each half-wall laboratory test. Methods 1 and 2, which either utilize the measured lateral displacement or measured thrust load, on average provide very accurate predictions (1 pct error based on trend line).

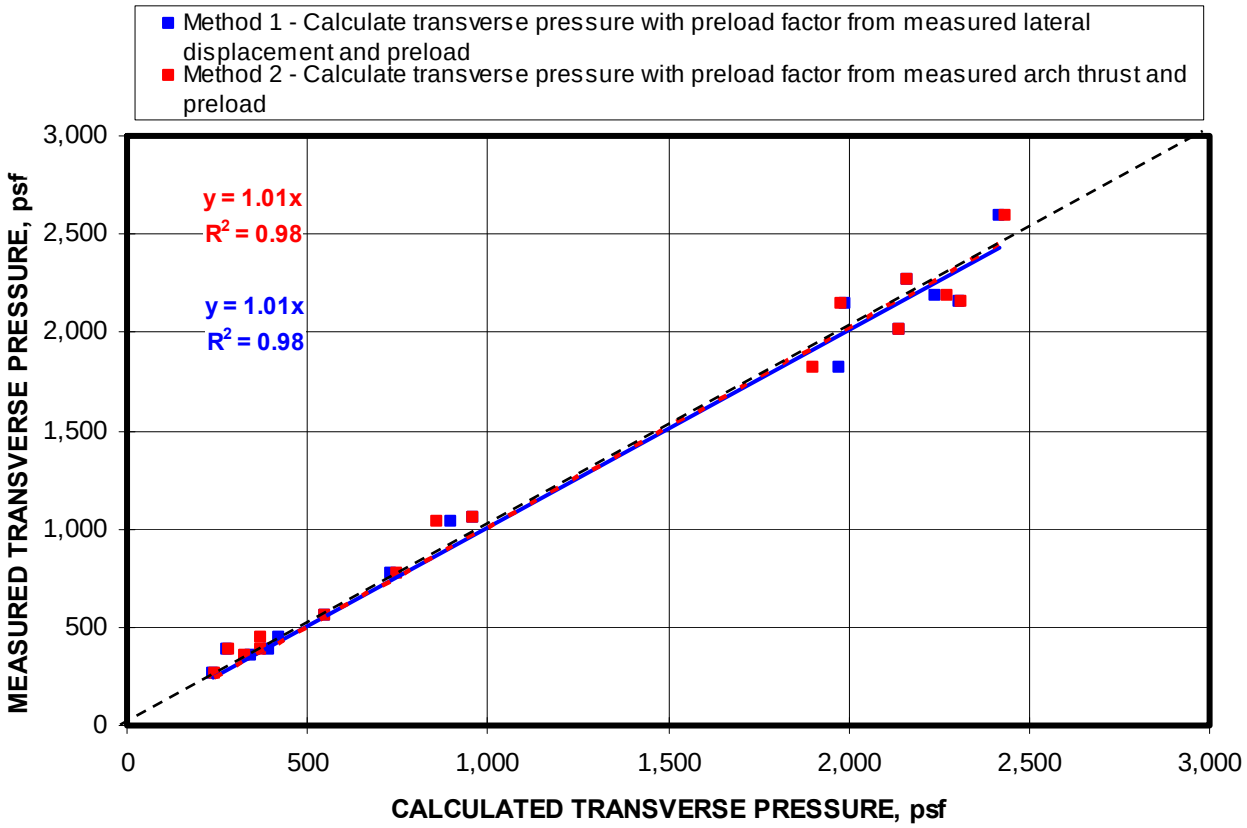

Figure 8-76. Prediction of transverse load from known thrust and lateral loads with premature failures removed (Ytong AAC block).

8.5.4 Theoretical Impact of Boundary Stiffness

A theoretical assessment of the impact of the boundary stiffness is conducted by varying the system modulus of elasticity (see equation 6.11 and 7.7). The modulus of elasticity determines the deformations of the wall and the boundary, i.e. the mine roof and

floor. The system modulus reflects the series stiffness equivalent of the wall and roof and floor structure. The theoretical assessment is made by reducing the system modulus to 75, 50, and 25 pct of the rigid boundary condition, and the transverse pressure is calculated using the lateral displacement model developed in chapter 7. For comparative purposes, if the boundary stiffness were equal to the wall stiffness, the system stiffness would be reduced by 50 pct. Likewise, if the boundary stiffness were three times that of the wall, the system stiffness would be 75 pct of the rigid boundary condition, and if the boundary stiffness were one third of the wall stiffness, the system stiffness would be 25 pct of the rigid boundary condition.

Figure 8-77 shows the impact of the reduction in system modulus to 25, 50, and 75 pct of the rigid boundary condition at three different wall heights as a function of preload. First, it can be concluded from figure 8-77 that as the boundary modulus is reduced, the transverse pressure capacity of the stopping will also be reduced. It is seen from this figure that the impact of reductions in boundary modulus will have a greater impact in terms of absolute reductions in transverse pressure for thicker walls than it will for thinner walls. For the example shown in figure 8-77, the transverse pressure for test number 239 for the 31.5-in-high half-wall, the transverse pressure was reduced from 1,988 psf for the rigid boundary condition to 744 psf when the boundary modulus is one third of the wall modulus, thereby reducing the system modulus to 25 pct of the rigid boundary condition. This represents a 63 pct decrease in the transverse pressure capacity of the stopping.

Figures 8-78 through 8-80 show the impact of reductions in system modulus for half-wall heights of 31.5, 47.25, and 63 inches. In these figures, the transverse pressure is plotted as a function of preload, which is scaled from 0 to 160 psi in these plots. These figures indicate the reductions in transverse pressure as a result of reduction in boundary stiffness (lower system modulus) are reduced as the preload increases through this range. Using the 31.5-in-high half-wall as an example, the 63 pct decrease in transverse pressure which occurred by reducing the system modulus to 25 pct of the rigid boundary condition, drops to a 15 pct reduction at a preload of 145 psi.

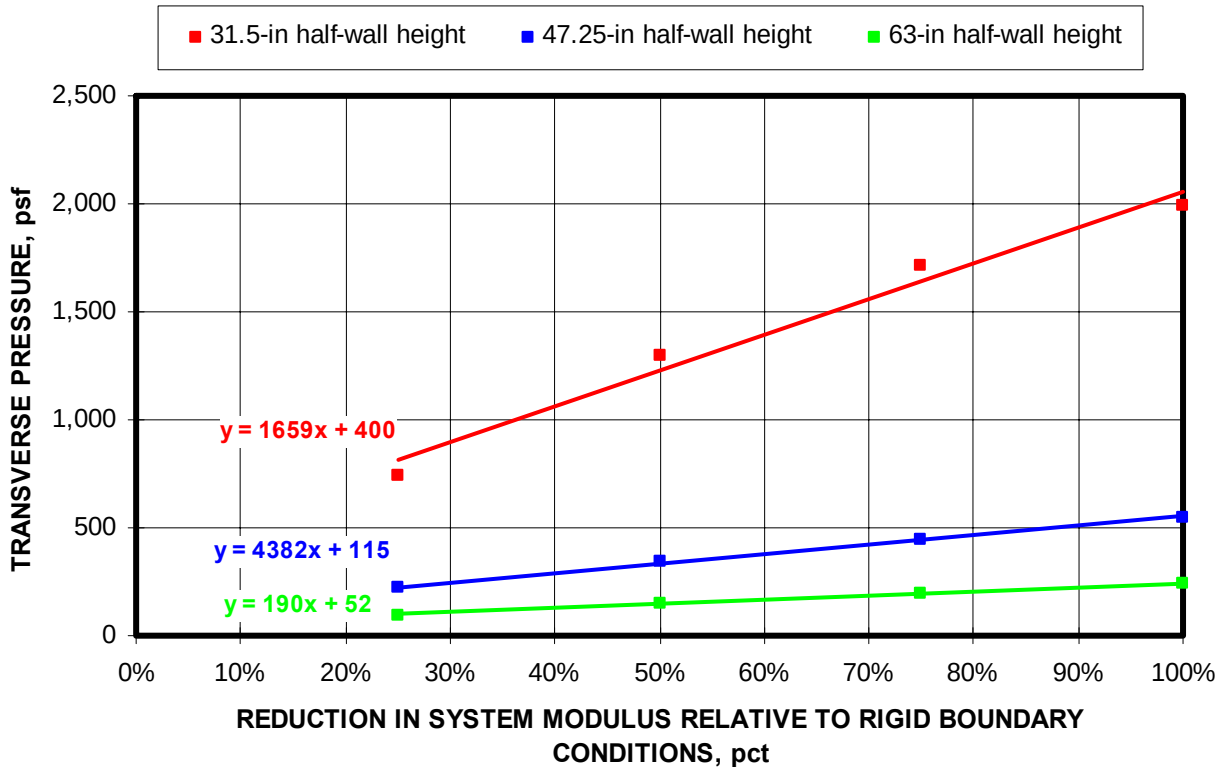

Figure 8-77. Impact of reducing the boundary stiffness on transverse pressure capacity of stopping. Data shows individual test at different wall heights with no preload (Ytong AAC block).

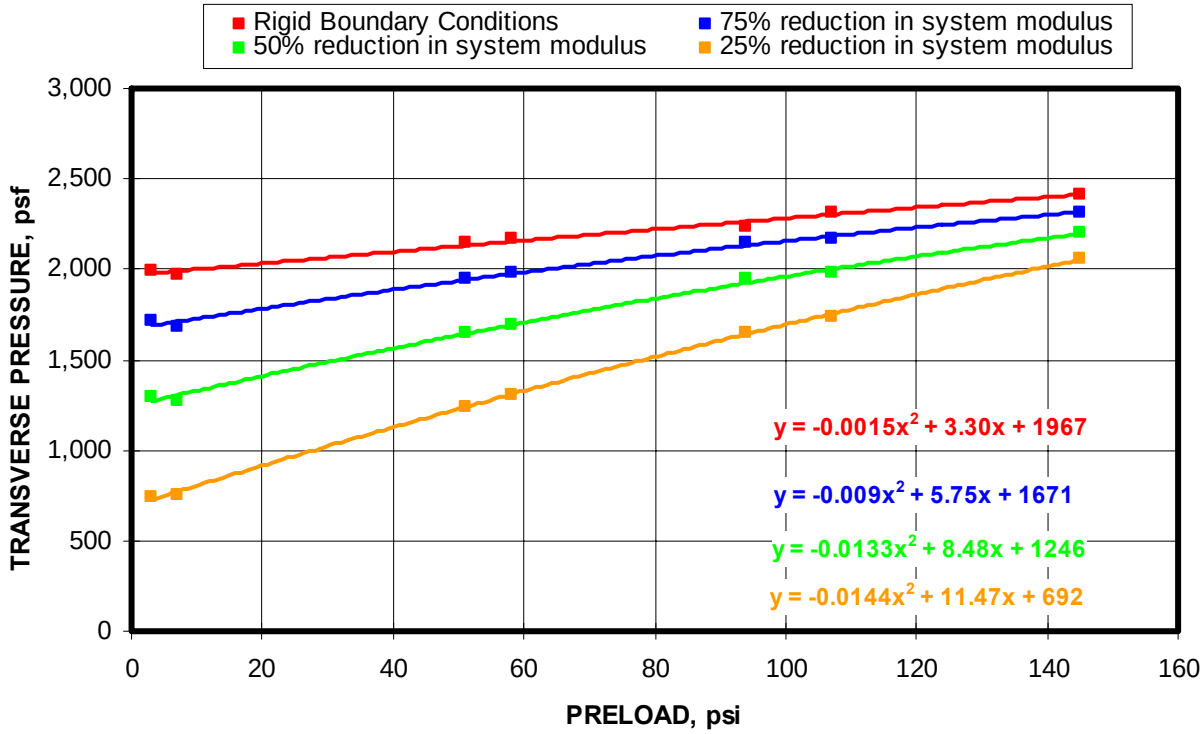

Figure 8-78. Impact of boundary stiffness reductions compared to rigid arching conditions as a function of preload for 31.5-in-high half-wall constructions (Ytong AAC block).

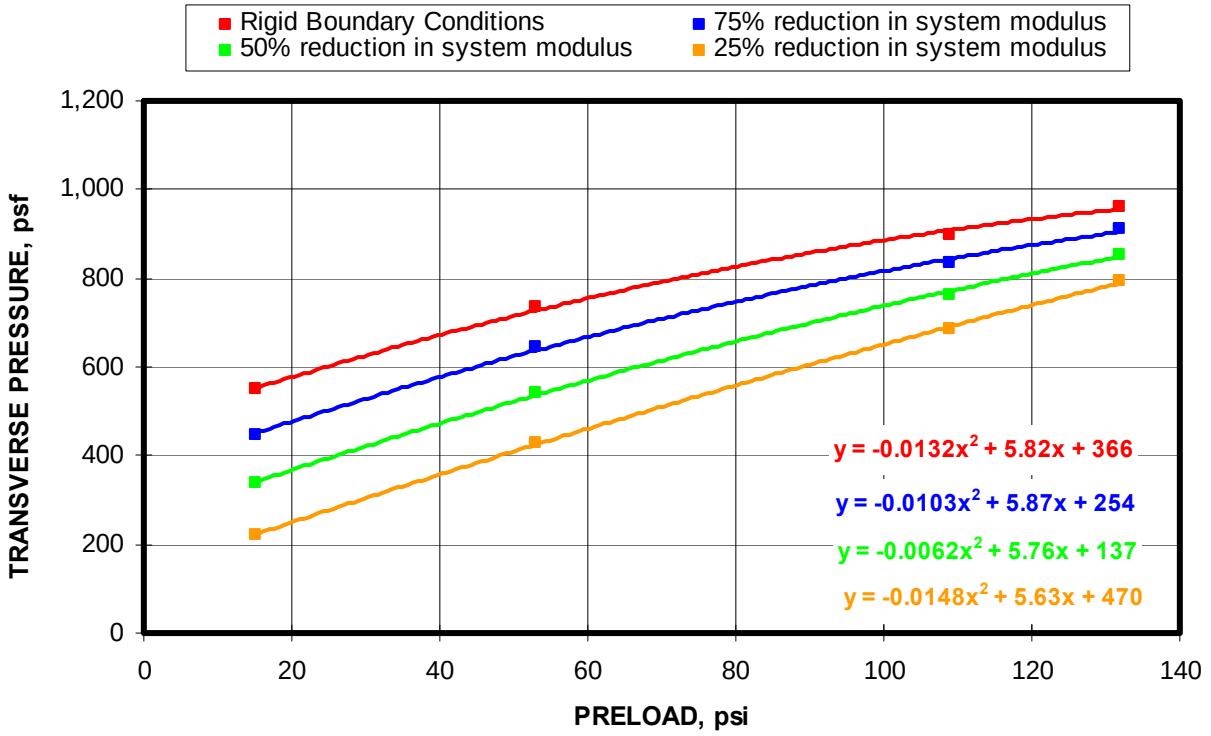

Figure 8-79. Impact of boundary stiffness reductions compared to rigid arching conditions as a function of preload for 47.25-in-high half-wall constructions (Ytong AAC block).

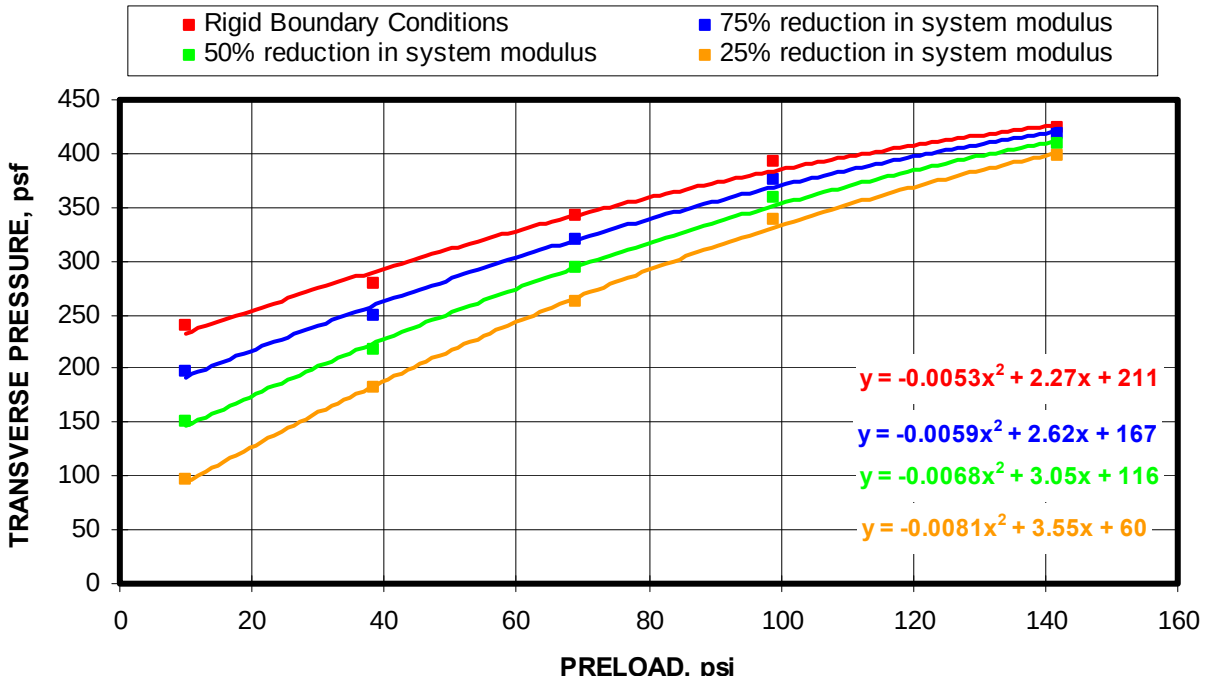

Figure 8-80. Impact of boundary stiffness reductions compared to rigid arching conditions as a function of preload for 63-in-high half-wall constructions (Ytong AAC block).

8.6 KINGSWAY BLOCK

Kingsway is another autoclaved aerated concrete (AAC) block, similar in material properties to that of the block described in the previous two sections. This block was manufactured by KTL Technologies in England, and was the block that was utilzied as part of the underground verification of the arching mechanism and laboratory testing protocol. As previously described, the air pores within the formed structure characterize the material. The Kingsway block had a unit block compressive strength of 546 psi. A photo of the block is shown in figure 8-81, including a close-up of the block showing the air pockets within the concrete structure. The block that was tested measured nominally 5-7/8 inches thick and 8-3/8 inches high by 15-1/4 inches wide. This block weighs on average 21 lbs.

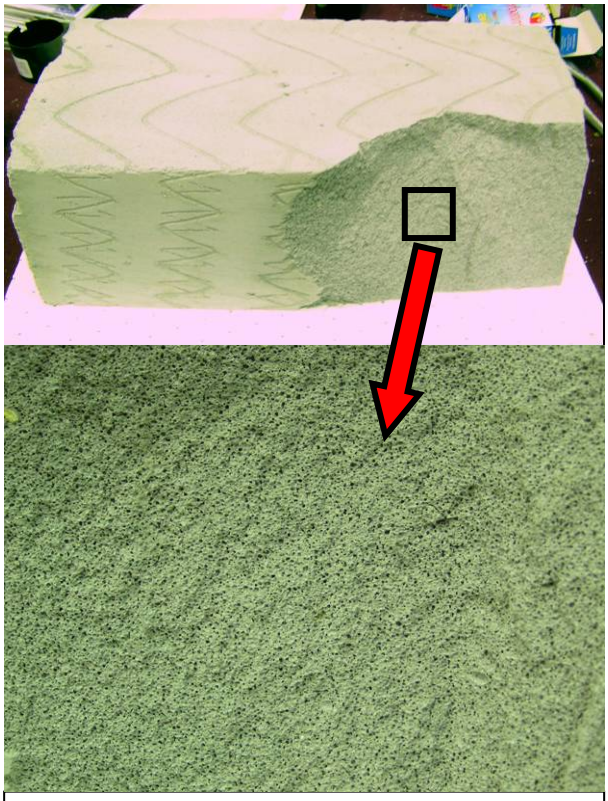

Figure 8-81. Kingsway AAC block including close-up of highlighted section showing air pockets within concrete structure..

8.6.1 Overview of the Test Program

A total of 9 tests were conducted with Kingsway block. The scope of testing included four half-wall heights of 33.5, 41.875, 50.25, and 58.625 inches. Due to the limited number of block available, there was no attempt to vary the preload as part of the test program. A nominal preload of 50-100 psi was applied for all tests. The results of the MRS half-wall tests are summarized in the table 8-9. Graphs of the measured lateral load and thrust load as a function of the lateral displacement of the wall for each test are documented in Appendix B. A tabular summary of the pertinent parameters and loading values for each test is also included Appendix C.

Table 8-9. Summary of test configurations and results for the Kingsway block.

Block Type	Test #	Block Width (in)	Block Height (in)	Block Length (in)	Half-wall Height (in)	Preload (psi)	Measured Transverse Pressure, (psf)
Kingsway	147	5.875	8.375	17.25	33.5	65	758
Kingsway	148	5.875	8.375	17.25	33.5	54	834
Kingsway	SD2	5.875	8.375	17.25	41.875	50	462
Kingsway	SD1	5.875	8.375	17.25	41.875	50	388
Kingsway	137	5.875	8.375	17.25	41.875	80	448
Kingsway	138	5.875	8.375	17.25	41.875	66	406
Kingsway	139	5.875	8.375	17.25	50.25	89	226
Kingsway	135	5.875	8.375	17.25	58.625	45	174
Kingsway	136	5.875	8.375	17.25	58.625	64	138

8.6.2 Parametric Relationships and Trends.

Examining table 8-9, it is seen that the transverse pressure capacity of the stoppings constructed from Kingsway block varied from a low of 138 to a high of 834 psf or 0.95 to 5.79 psi. The transverse pressure is most significantly affected by the wall height as with previous block tests. Figure 8-82 shows that the transverse pressure is directly related to the lateral load acting on the half-wall during the laboratory tests. In this graph, the data are grouped by wall height. The 50.25 and 58.625 half-wall height, which amounts to one course of block height difference, are grouped together for the regression analysis since there is only one test at the 58.625-in height. This degrades the analysis slightly. This data grouping is also included in figures 8-83 and 8-84. Figure 8-83 shows that the lateral load is also directly related to the thrust force. This is also consistent with the arching theory. Finally, figure 8-84 shows the relationship between the transverse pressure and the arch thrust. Unlike previous analyses, there is insufficient change in preload in this data set to cause the transverse pressure to reach an asymptotic level with the increasing arch thrust. Due to the small changes in preload, the arch thrust for a specific height also changes relatively little (less than 5 kips) for each of the height evaluations.

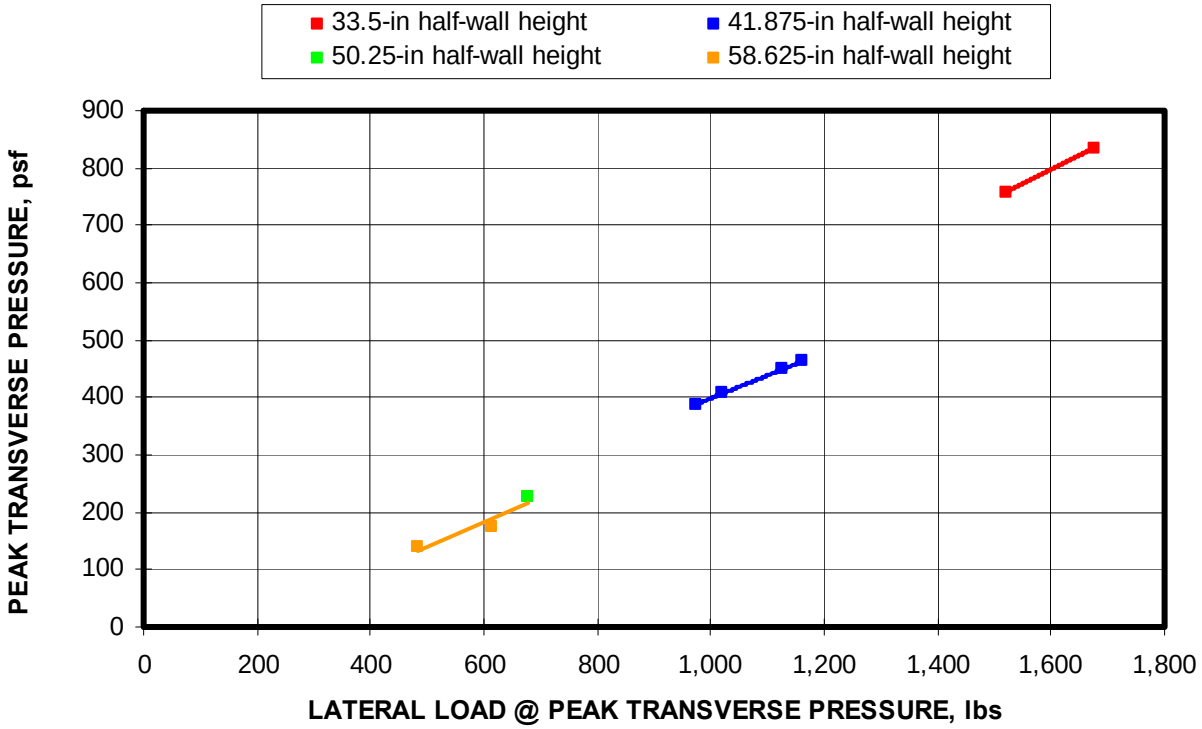

Figure 8-82. Transverse pressure is directly related to the lateral load acting on the half-wall in the MRS laboratory tests (Kingsway AAC block).

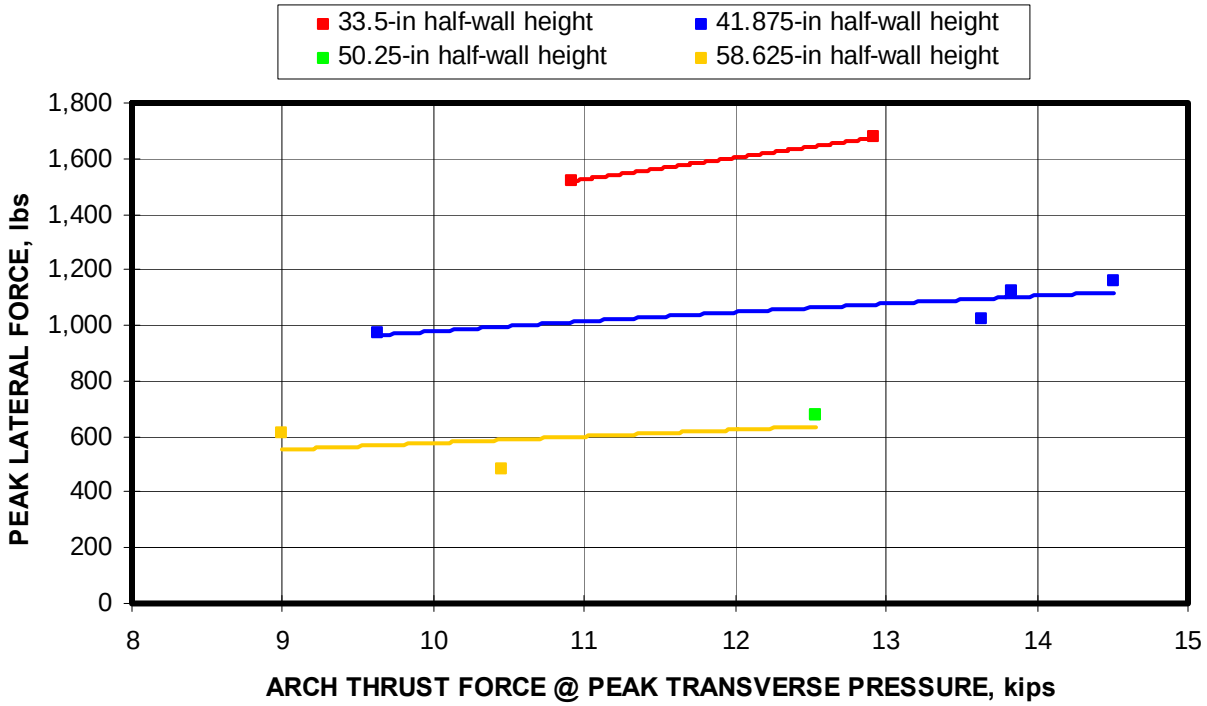

Figure 8-83. Relationship between the lateral load and the arch thrust for MRS laboratory tests for different wall heights (Kingsway AAC block).

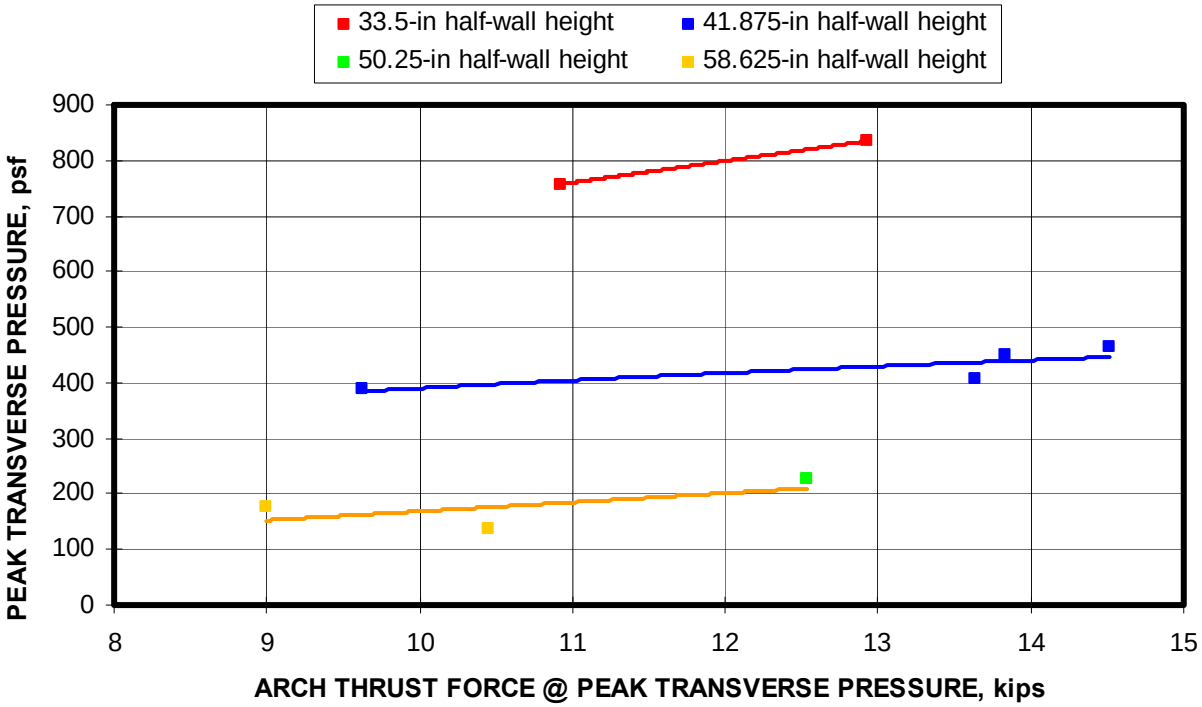

Figure 8-84. Relationship between the transverse pressure and the arch thrust for MRS laboratory tests conducted at different wall heights (Kingsway AAC block).

Figure 8-85 depicts the relationship for tests with less than 100 psi preload between the transverse pressure and the material modulus (E), the wall thickness (t), and the wall height (L) expressed as by the term E x $(t/L)^2$. The chart shows that 98 pct of the transverse pressure of a stopping is determined by this relationship. The material modulus is a significant parameter since it determines the amount of thrust force developed and ultimately the amount of lateral displacement of the wall, both of which control the arching mechanics of the wall. If the modulus is related to the compressive strength of the block material, the modulus factor could be replaced by the compressive strength as previous research suggests (Barczak, 2004).

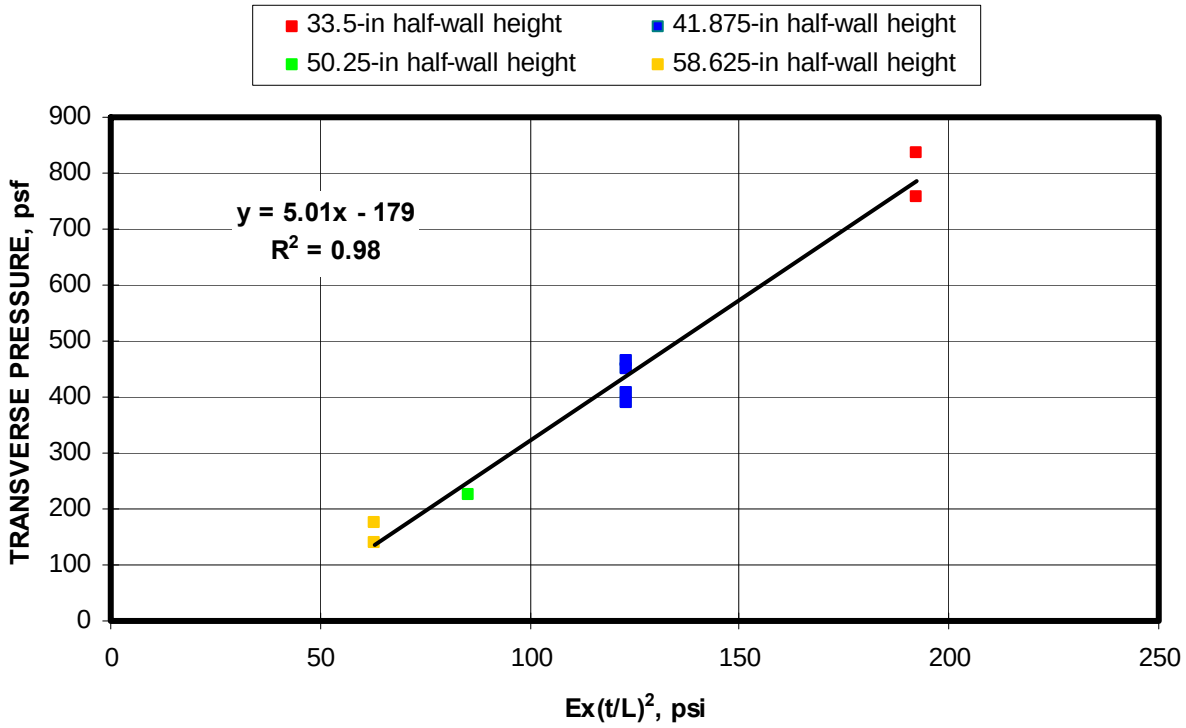

Figure 8-85. Correlation of factors involving the material modulus (E), wall thickness (t), and wall height (L) to the transverse pressure capacity of a stopping (Kingsway AAC Block).

8.6.3 Evaluation of Predictive Models

The next goal is to evaluate the capability to predict the transverse pressure. If the thrust force and its resultant location and lateral load are known, the transverse pressure capacity of a stopping can be predicted with nearly 100 pct accuracy. If the thrust force location is instead calculated from the empirical model described in chapter 6 and shown in figure 8-86 for three half-wall heights considered in this analysis, the transverse pressure can still be predicted with a 92 pct accuracy as depicted by the open red square data points shown in figure 8-87. Each data point in figure 8-87 represents an individual laboratory test. As seen in the figure, the accuracy of the prediction is consistent throughout the full range of transverse pressure conducted in the laboratory testing.

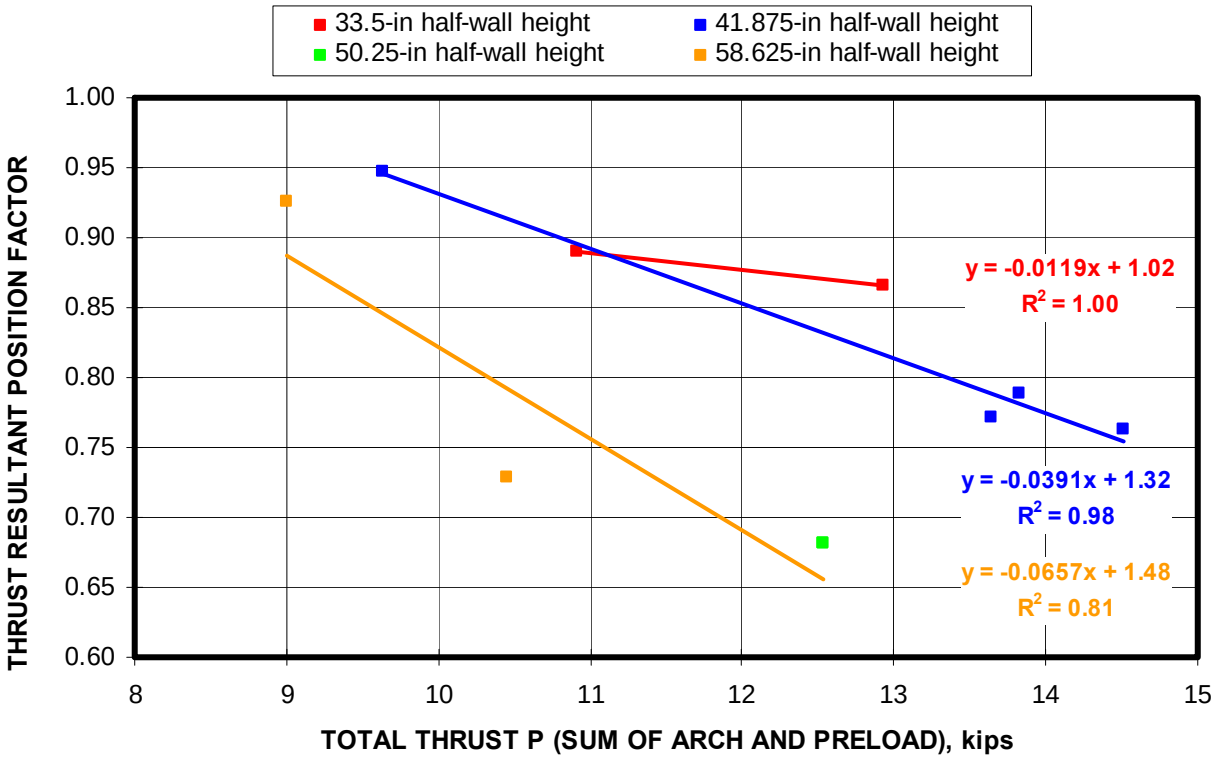

Figure 8-86. Resultant thrust force location for three wall heights as a function of the total arch thrust (Kingsway AAC block).

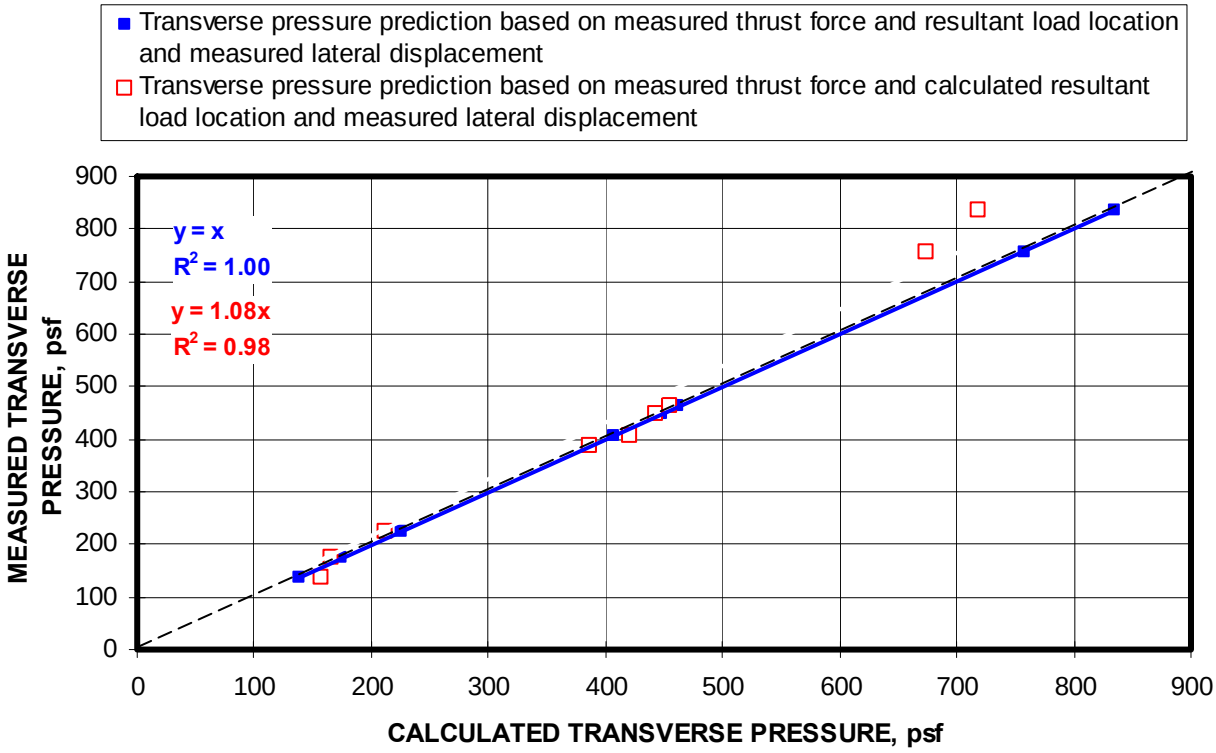

Figure 8-87. Prediction of transverse pressure when both the lateral load and arch thrust are known. Blue curves predicts transverse pressure when resultant thrust force location is also known and red squares show predicted transverse pressure when resultant thrust force location is calculated from empirical data (Kingsway AAC block).

If either the thrust force or lateral displacement is known, then the transverse pressure can still be predicted. It is recalled from chapter 7 that two methods were developed. Method 1 predicts the transverse pressure from the measured lateral displacement. Method 2 predicts the transverse pressure from the measured thrust force. Figure 8-88 illustrates the predictive capability of these two methods showing the measured transverse pressure vs. the predicted transverse pressure for each half-wall laboratory test. Method 1 slightly under predicts the transverse pressure by about 3 pct, while method 2 slightly over predicts the transverse pressure by about 1 pct.

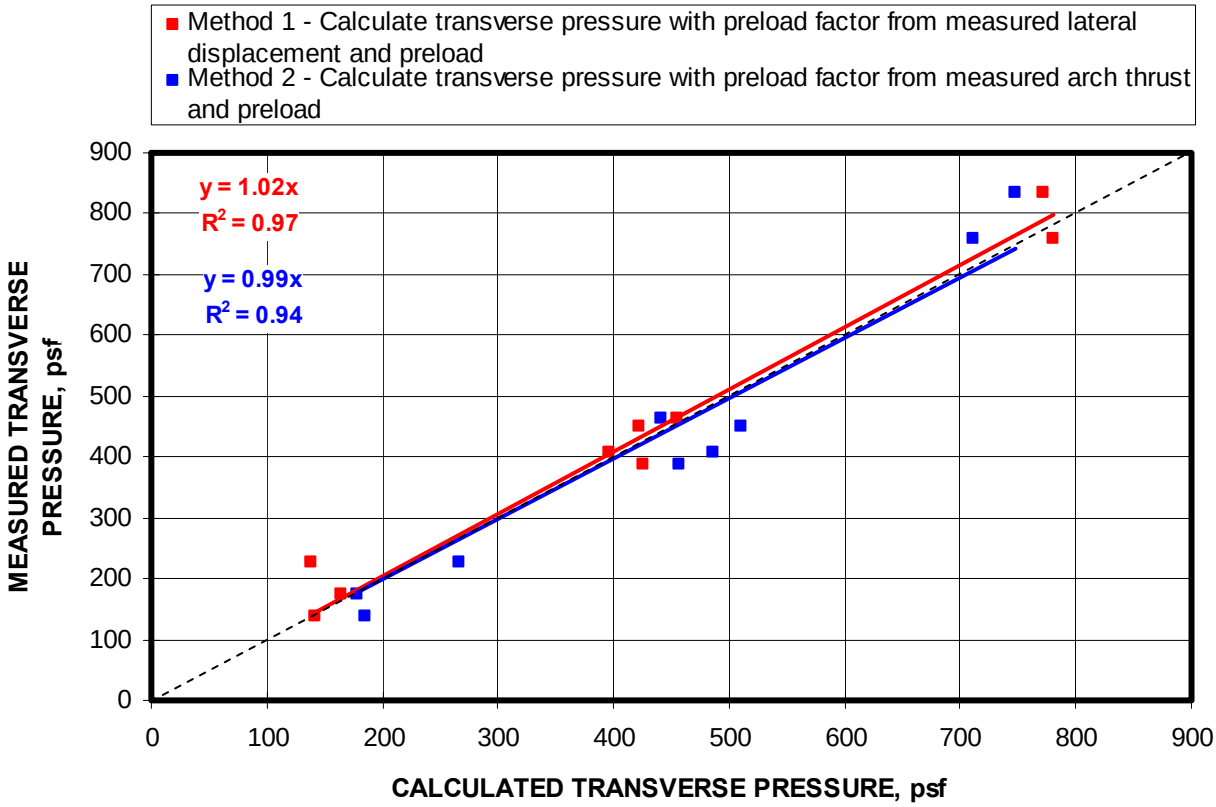

Figure 8-88. Prediction of transverse pressure from known thrust and lateral loads with premature failures removed (Kingsway AAC block).

8.6.4 Theoretical Impact of Boundary Stiffness

A theoretical assessment of the impact of the boundary stiffness is conducted by varying the system modulus of elasticity (see equation 6.11 or 7.7). The modulus of elasticity determines the deformations of the wall and the boundary, i.e. the mine roof and floor. The system modulus reflects the series stiffness equivalent of the wall and roof and floor structure. The theoretical assessment is made by reducing the system modulus to 75, 50, and

25 pct of the rigid boundary condition. For comparative purposes, if the boundary stiffness were equal to the wall stiffness, the system stiffness would be reduced by 50 pct. Likewise, if the boundary stiffness were three times that of the wall, the system stiffness would be 75 pct of the rigid boundary condition, and if the boundary stiffness were one third of the wall stiffness, the system stiffness would be 25 pct of the rigid boundary condition.

Figure 8-89 shows the impact of the reduction in system modulus to 25, 50, and 75 pct of the rigid boundary condition at 3 different wall heights as a function of preload. For the example, the transverse pressure for test number 239 for the 33.5-in-high half-wall, the transverse pressure was reduced from 780 psf for the rigid boundary condition to 540 psf when the boundary modulus is one third of the wall modulus, thereby reducing the system modulus to 25 pct of the rigid boundary condition. This represents a 31 pct decrease in the transverse pressure capacity of the stopping.

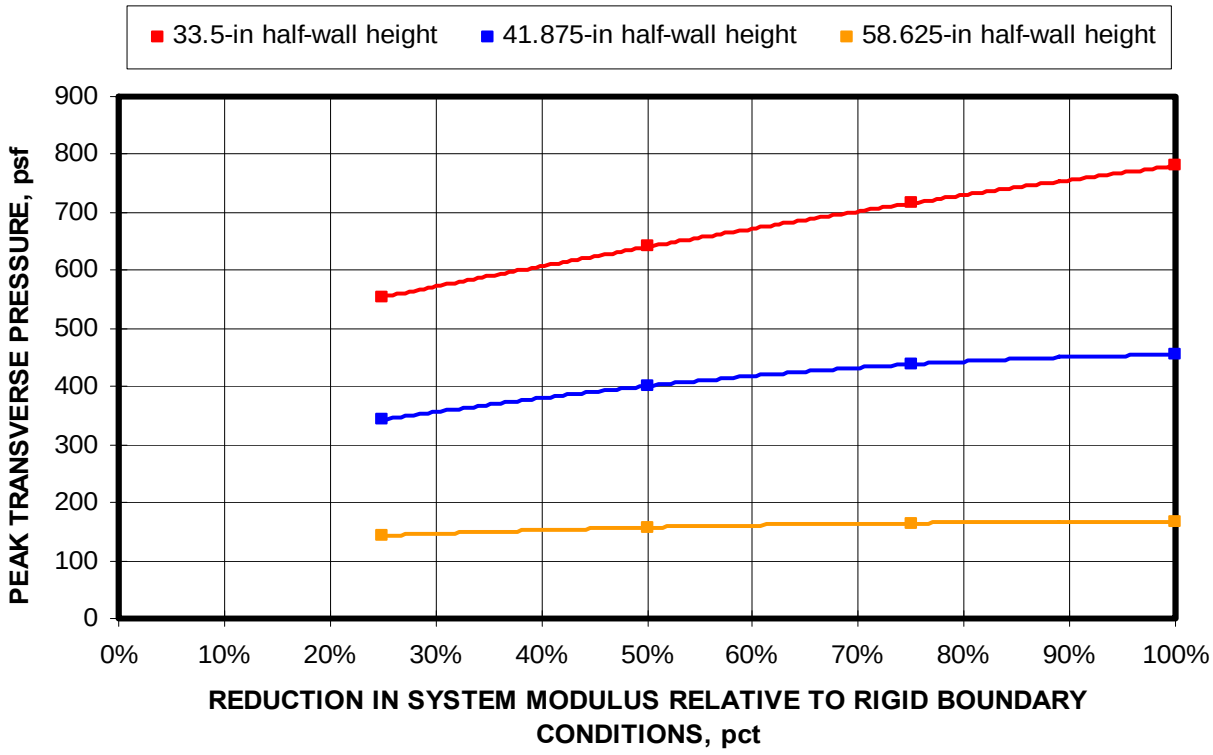

Figure 8-89. Impact of reducing the boundary stiffness on transverse pressure capacity of stopping. Data shows individual test at different wall heights with no preload (Kingsway AAC block).

8.7 OMEGA BLOCK

Omega block are manufactured by Burrell Mining Products Inc. located in New Kensington, Pennsylvania near Pittsburgh. The block is composed of Portland cement and flyash and also contains air pores within the concrete structure to create a very low density material (22 lbs per cubic foot). The block can easily be cut with a handsaw. The block as shown in figure 8-90 measures nominally 8 in thick, 24 in wide, and 16 in in height and weighs just less than 40 lbs, yet it covers the same area as three regular concrete blocks that weigh as much as 50 lbs each. The compressive strength is only 84 psi, making it the weakest block evaluated in this research effort thusfar. The block is brittle and susceptible to damage from handling. Small fiberglass fibers are imbedded in the mix to help hold the material together and improve its post failure loading characteristics.

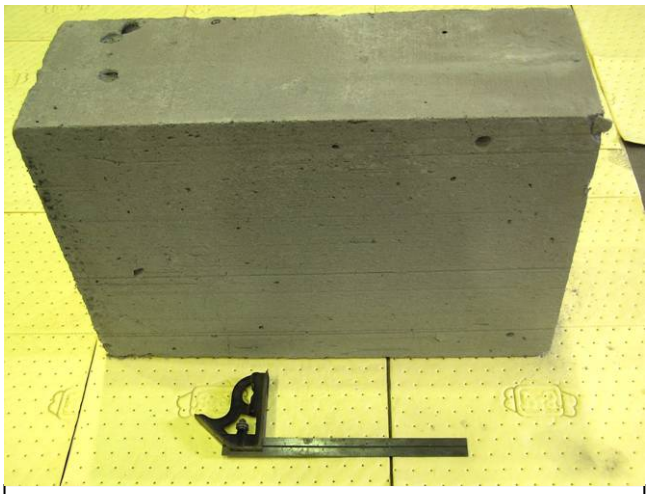

Figure 8-90. Omega block manufactured by Burrell Mining Products Inc.

8.7.1 Overview of the Test Program

A total of 22 tests were conducted with Omega block. Half-wall configurations at heights of 32, 48, and 64 inches from 2, 3, and 4 courses of block were evaluated in the test program. The results of the MRS half-wall tests are summarized in the table 8-10. The low compressive strength of the block did not allow much variation of preload. A nominal preload was applied and measured once the test began, although the magnitude could not be precisely controlled, with the result that the preload varied from 1 to 27 psi. The low strength of the block resulted in thrust loading that was near the measurable limits of the load frame. This contributed to some of the inconsistency in the test results. Graphs of the measured lateral load and thrust load as a function of the lateral displacement of the wall for each test are documented in Appendix B. A tabular summary of the pertinent parameters and loading values for each test is also included Appendix C.

Table 8-10. Summary of Omega block tests.

Block Type	Test No.	Block Width (in)	Block Height (in)	Block Length (in)	Half-wall Height (in)	Preload (psi)	Measured Transverse Pressure, (psf)
Omega Block	221	8	16	24	32	2	176
Omega Block	220	8	16	24	32	5	184
Omega Block	174	8	16	24	32	8	254
Omega Block	169	8	16	24	32	8	210
Omega Block	143	8	16	24	32	9	188
Omega Block	170	8	16	24	32	15	282
Omega Block	175	8	16	24	32	27	288
Omega Block	144	8	16	24	32	28	230
Omega Block	172	8	16	24	48	1	42
Omega Block	222	8	16	24	48	6	40
Omega Block	173	8	16	24	48	8	110
Omega Block	168	8	16	24	48	14	70
Omega Block	167	8	16	24	48	20	128
Omega Block	141	8	16	24	48	23	130
Omega Block	142	8	16	24	48	27	100
Omega Block	223	8	16	24	64	8	16
Omega Block	165	8	16	24	64	12	16
Omega Block	176	8	16	24	64	14	14
Omega Block	177	8	16	24	64	15	18
Omega Block	145	8	16	24	64	20	24
Omega Block	166	8	16	24	64	21	30
Omega Block	146	8	16	24	64	27	50

8.7.2 Parametric Relationships and Trends.

Examining table 8-10, it is seen that the transverse pressure capacity of the stoppings constructed from Omega block varied from a low of 14 to a high of 288 psf or 0.03 to 2.00 psi. Figure 8-91 displays the transverse pressure as a function of preload for the three half-wall heights. The transverse pressures for the 32-in-high half-walls are an order of magnitude higher than the 64-in-high half-walls. It is also seen from figure 8-91 that the transverse pressure is nonlinearly related to the preload and that the transverse pressure approaches an asymptotic maximum at approximately 20 psi for the 32 and 48 in-high walls. The upward slope 64-in high wall curve suggests the peak loading has not been reached, but the data at the low preloads is inconsistent and it is likely that the 64-in-high walls are also approaching a transverse pressure limit. Figure 8-92 plots the lateral displacement at which the peak transverse pressure is achieved as a function of preload using the complete data set.

Although the correlation is very weak, the trend is that the lateral displacement also approaches an asymptotic level at about 20 psi.

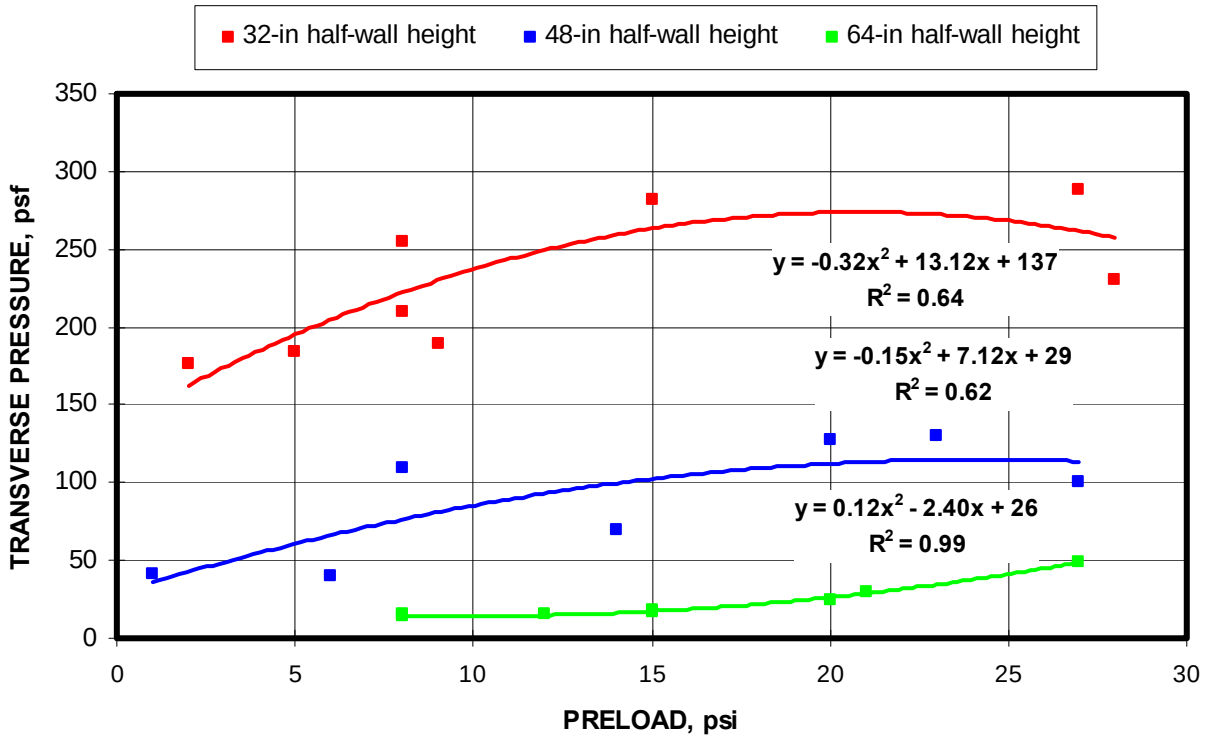

Figure 8-91. Transverse pressure as measured from MRS laboratory testing as a function of preload for three half-wall heights (Omega Block).

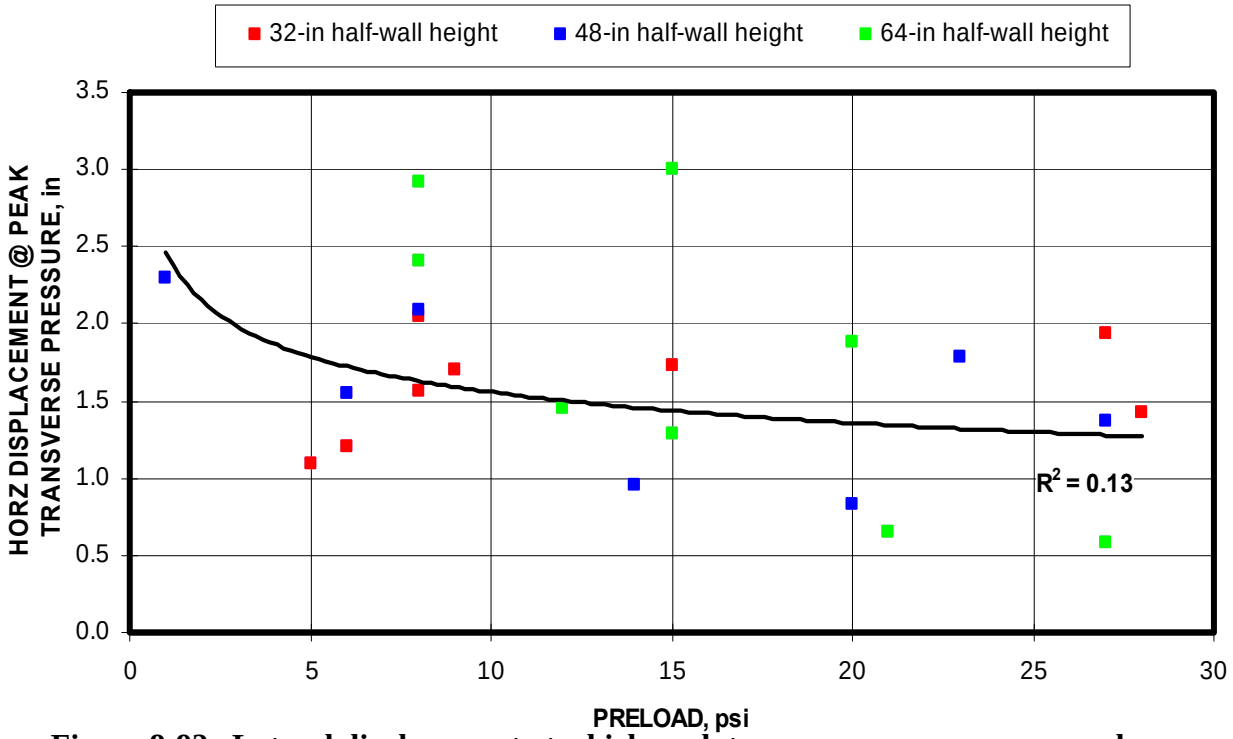

Figure 8-92. Lateral displacement at which peak transverse pressure occurs also reaches an asymptotic minimum as the preload approaches 150 psi (Omega Block).

Further examination of the parametric relationships confirms the arching theory as presented in chapter 6. Figure 8-93 shows that the transverse pressure is directly related to the lateral force acting on the half-wall during the laboratory tests. Figure 8-94 shows that the lateral force is also directly related to the thrust force. This is also consistent with the arching theory. Finally, figure 8-95 shows the relationship between the transverse pressure and the arch thrust. This graph resembles the plot of transverse pressure versus preload shown in figure 8-91, showing that the arch thrust also reaches an asymptotic value.

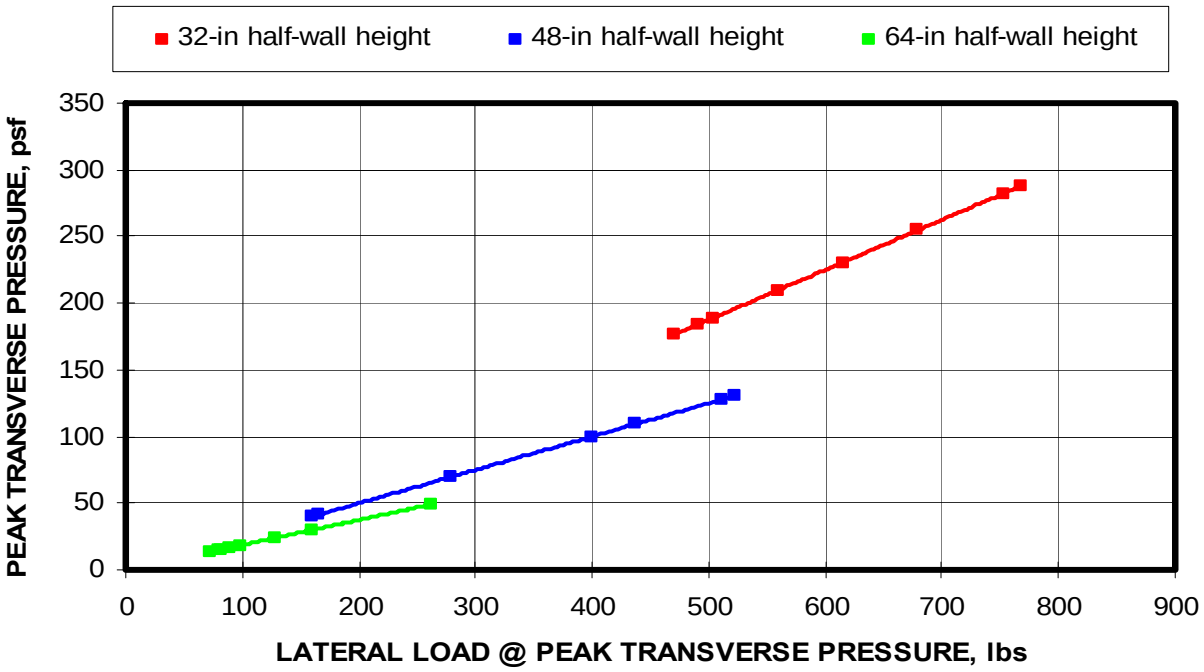

Figure 8-93. Relationship between the lateral load and the arch thrust for MRS laboratory tests for three half-wall heights (Omega Block).

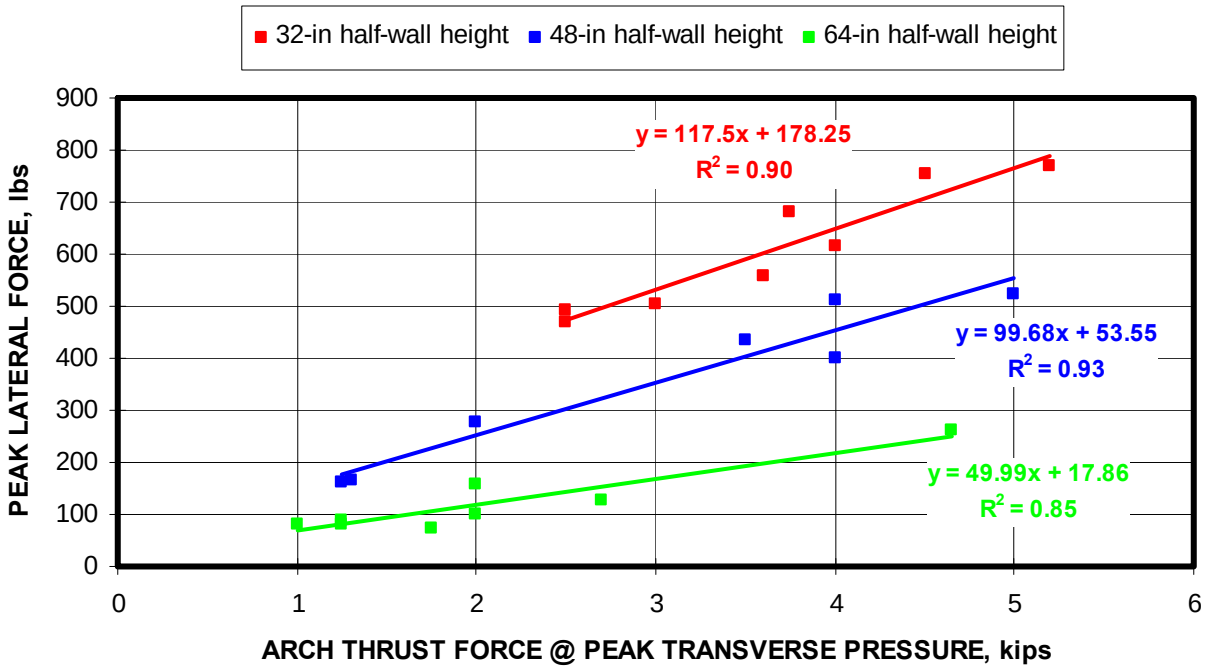

Figure 8-94. Relationship between the lateral load and the arch thrust for MRS laboratory tests for three half-wall heights (Omega Block).

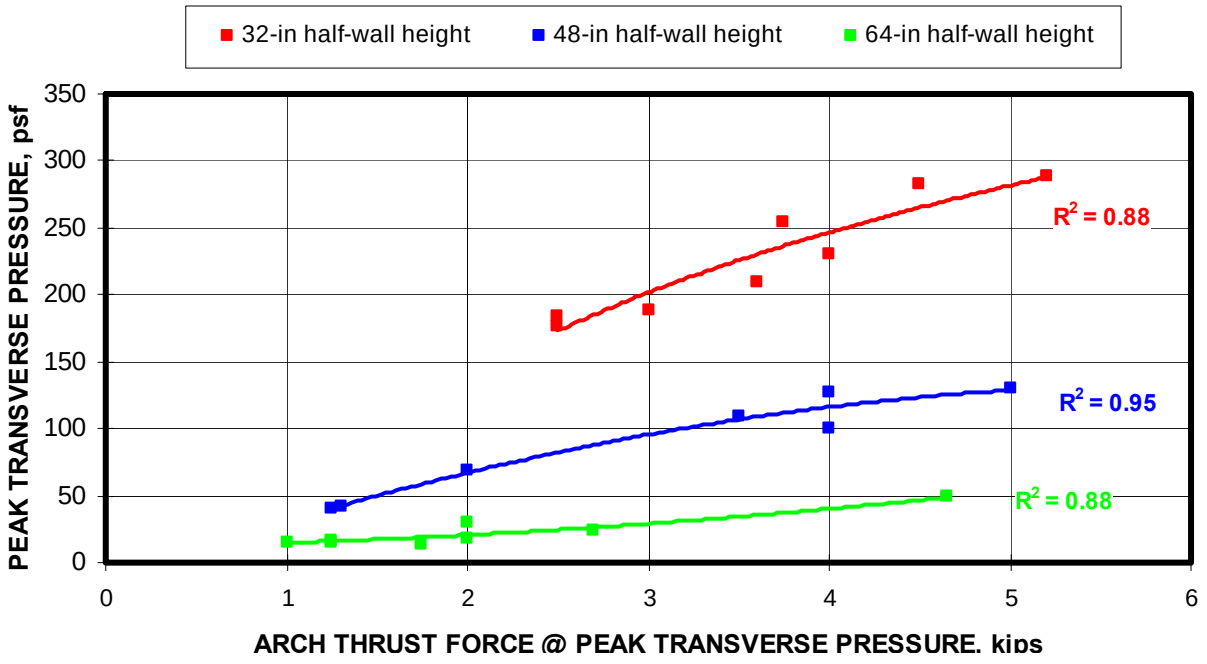

Figure 8-95. Relationship between the transverse pressure and the arch thrust for MRS laboratory tests conducted at three half-wall heights (Omega Block).

Figure 8-96 depicts the relationship between the transverse pressure and the material modulus (E), the wall thickness (t), and the wall height (L) expressed as by the term E x $(t/L)^2$. The general trend of increasing transverse pressure with increasing E x $(t/L)^2$ is typical of other block types. However, as seen in the chart, the data for the Omega block is scattered resulting in a poor correlation compared to other block types. The chart shows that 24 pct of the transverse pressure of a stopping is determined by this relationship. This material is very weak and prone to damage even from handling. Small amounts of preload can substantially damage the block. This accounts for the scatter and poor correlation. The material modulus is a significant parameter since it determines the amount of thrust force developed and ultimately the amount of lateral displacement of the wall, both of which control the arching mechanics of the wall. However, the air pores and weak concrete matrix and localized damage to the block from the test preparation or transverse pressure development cause the material modulus to vary from block to block.

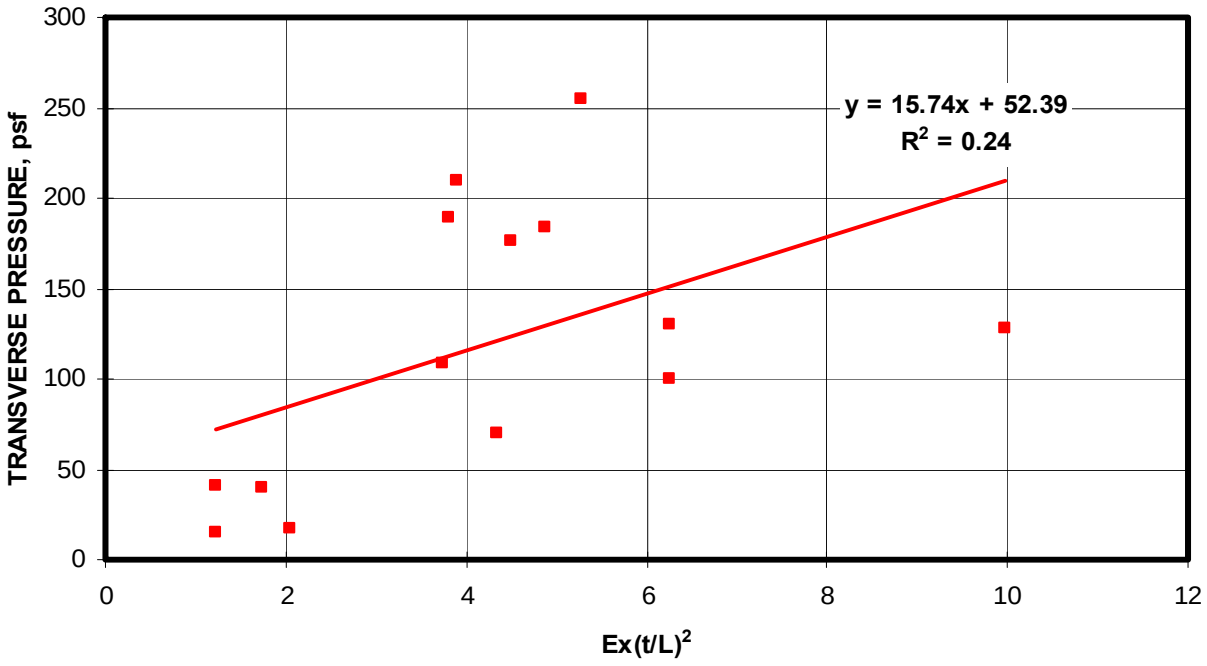

Figure 8-96. Correlation of factors involving the material modulus (E), wall thickness (t), and wall height (L) to the transverse pressure capacity of a stopping (Omega Block).

8.7.3 Evaluation of Predictive Models

The next goal is to evaluate the capability to predict the transverse pressure. If the thrust force and its resultant location and lateral load are known, the transverse pressure capacity of a stopping can be predicted with nearly 100 pct accuracy. If the thrust force location is instead calculated from the empirical model described in chapter 6 and shown in figure 8-97 for three half-wall heights considered in this analysis, the transverse pressure can still be predicted to better than 99 pct accuracy as depicted by the open red square data points shown in figure 8-98. Each data point in figure 8-98 represents an individual laboratory test. As seen in the figure, the accuracy of the prediction is consistent throughout the full range of transverse pressure conducted in the laboratory testing, and includes preloading of wall from 0 to 27 psi and three different wall heights. Hence, while the wall performances may not be very consistent, if the thrust and lateral displacement are known, the arching mechanics still dictate a good measure of the transverse pressure capacity.

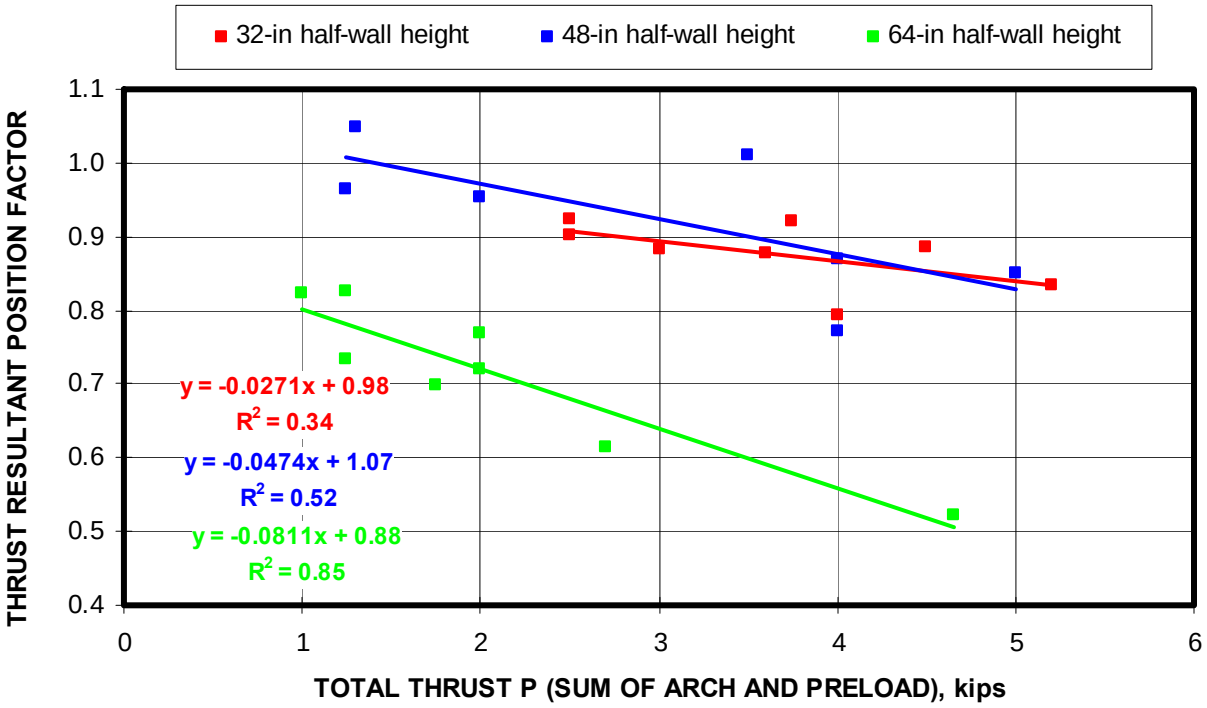

Figure 8-97. Resultant thrust force location for three wall heights as a function of the total arch thrust (Omega block).

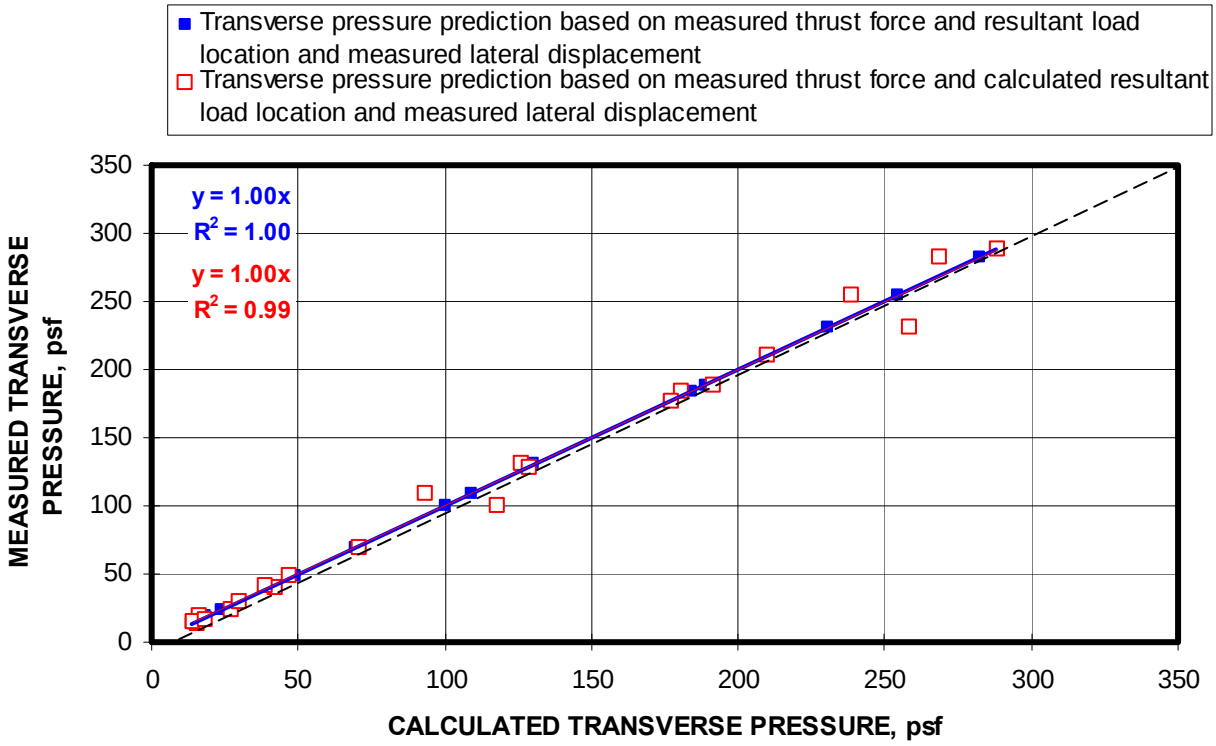

Figure 8-98. Prediction of transverse pressure when both the lateral load and arch thrust are known. Blue curves predicts transverse pressure when resultant thrust force location is also known and red squares show predicted transverse pressure when resultant thrust force location is calculated from empirical data (Omega block).

If either the thrust force or the lateral displacement is known, then the transverse pressure can still be calculated. It is recalled from chapter 7 that two methods were developed. Method 1 predicts the transverse pressure from the measured lateral displacement. Method 2 predicts the transverse pressure from the measured thrust force. Figures 8-99 illustrates the predictive capability of these models showing the measured transverse pressure vs. the predicted transverse pressure for each half-wall laboratory test. The accuracy of the predictive models is less than that developed for previous blocks, due in large part to the inconsistency of the block material properties and low thrust loads. Overall, the accuracy of the models is within 15 pct of the measured transverse pressure based on the trend line, although individual test predictions can be considerably less accurate. Models 1 and 2, which are based on measured lateral displacements (method 1) or measured thrust forces (method 2) tend to over predict the transverse pressure.

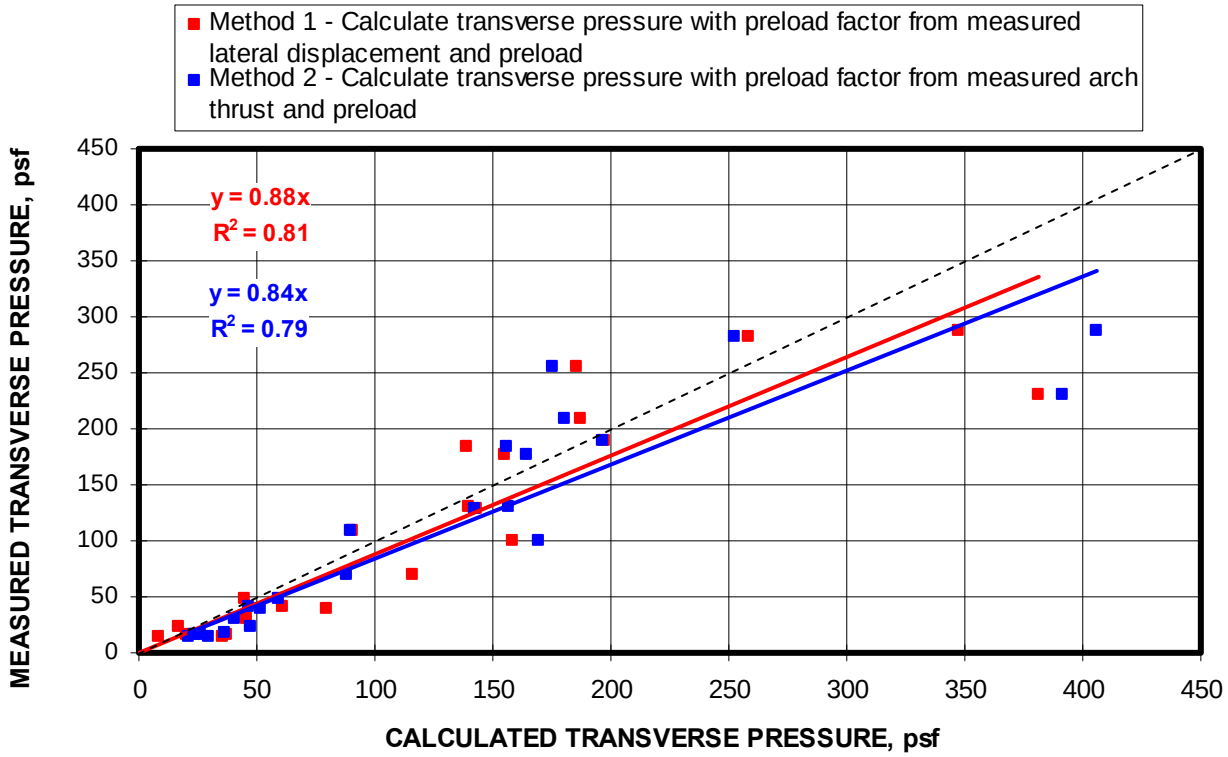

Figure 8-99. Prediction of transverse pressure from known thrust and lateral loads (Omega block).

8.7.4 Theoretical Impact of Boundary Stiffness

A theoretical assessment of the impact of the boundary stiffness is conducted by varying the system modulus of elasticity (see equation 6.11 and 7.7). The modulus of elasticity determines the deformations of the wall and the boundary, i.e. the mine roof and floor. The system modulus reflects the series stiffness equivalent of the wall and roof and floor structure. The theoretical assessment is made by reducing the system modulus to 75, 50, and 25 pct of the rigid boundary condition, and using the lateral displacement model developed in chapter 7 to calculate the transverse pressure. For comparative purposes, if the boundary stiffness were equal to the wall stiffness, the system stiffness would be reduced by 50 pct. Likewise, if the boundary stiffness were three times that of the wall, the system stiffness would be 75 pct of the rigid boundary condition, and if the boundary stiffness were one third of the wall stiffness, the system stiffness would be 25 pct of the rigid boundary condition.

Figure 8-100 shows the impact of the reduction in system modulus to 25, 50, and 75 pct of the rigid boundary condition at each of the three half-wall heights. Unlike other walls where the block material modulus was considerably higher, reductions in boundary stiffness have less impact on the Omega block especially at the higher wall heights. For the example shown in figure 8-100, the transverse pressure is reduced by 30 pct for the shortest wall construction (32-in-high half-wall) when the system modulus is reduced to 25 pct of the rigid boundary condition, 12 pct for the 48-in-high half-wall construction, and is essentially unchanged for the 64-in-high half-wall construction.

Figures 8-101 and 8-103 show the impact of reductions in system modulus for the three half-wall construction heights as a function of the preload. Since the preload range was very limited (only 28 psi maximum preload applied), these figures show that there was not much impact by the preload, although in general, the reductions in transverse pressure as a result of reduction in boundary stiffness (lower system modulus) are reduced as the preload increases through this range.

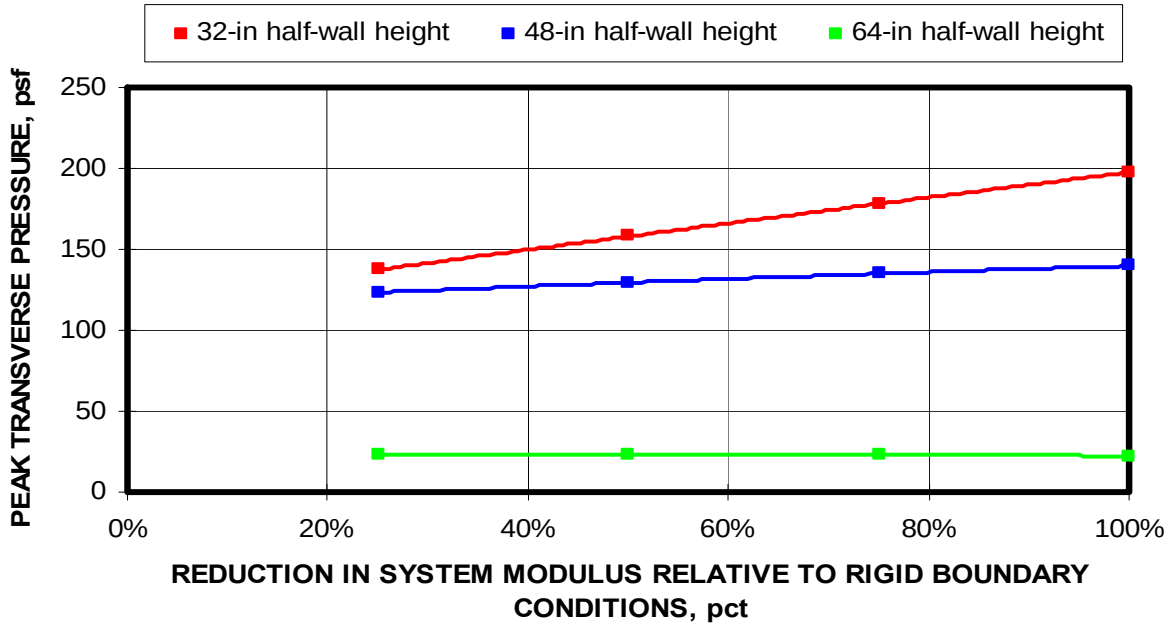

Figure 8-100. Impact of reducing the boundary stiffness on transverse pressure capacity of stopping. Data shows individual test at different wall heights with no preload (Omega block).

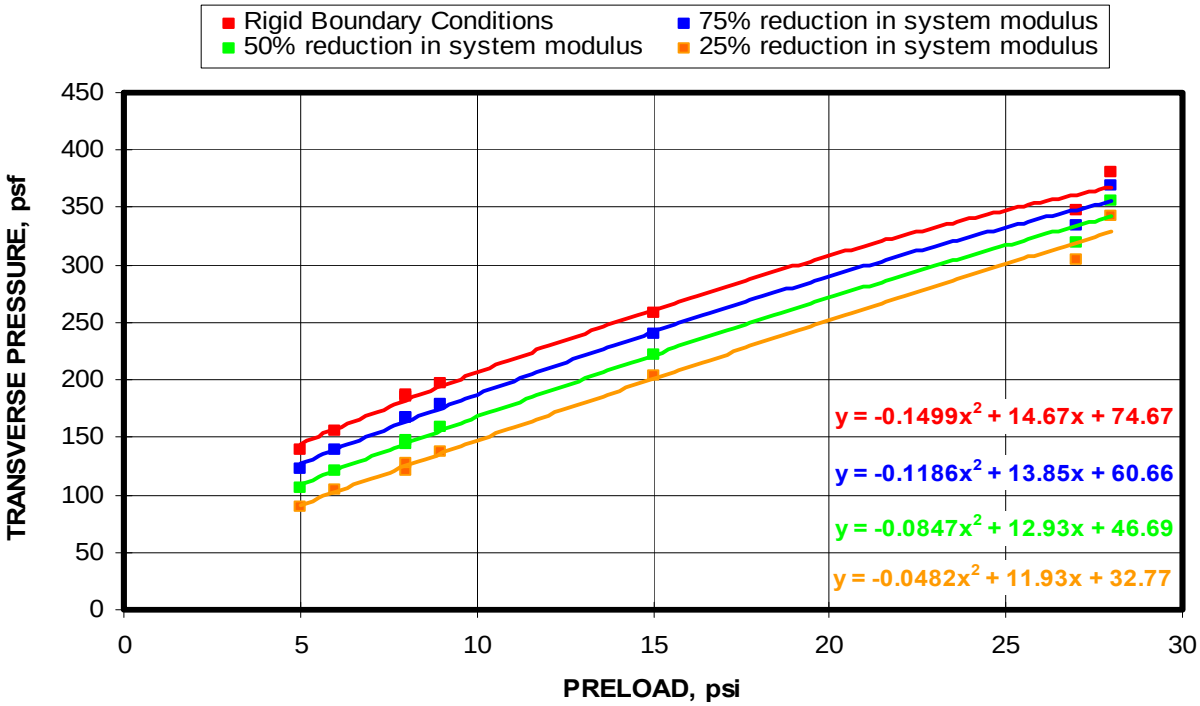

Figure 8-101. Impact of boundary stiffness reductions compared to rigid arching conditions as a function of preload for 32-inch-high half-wall constructions (Omega block).

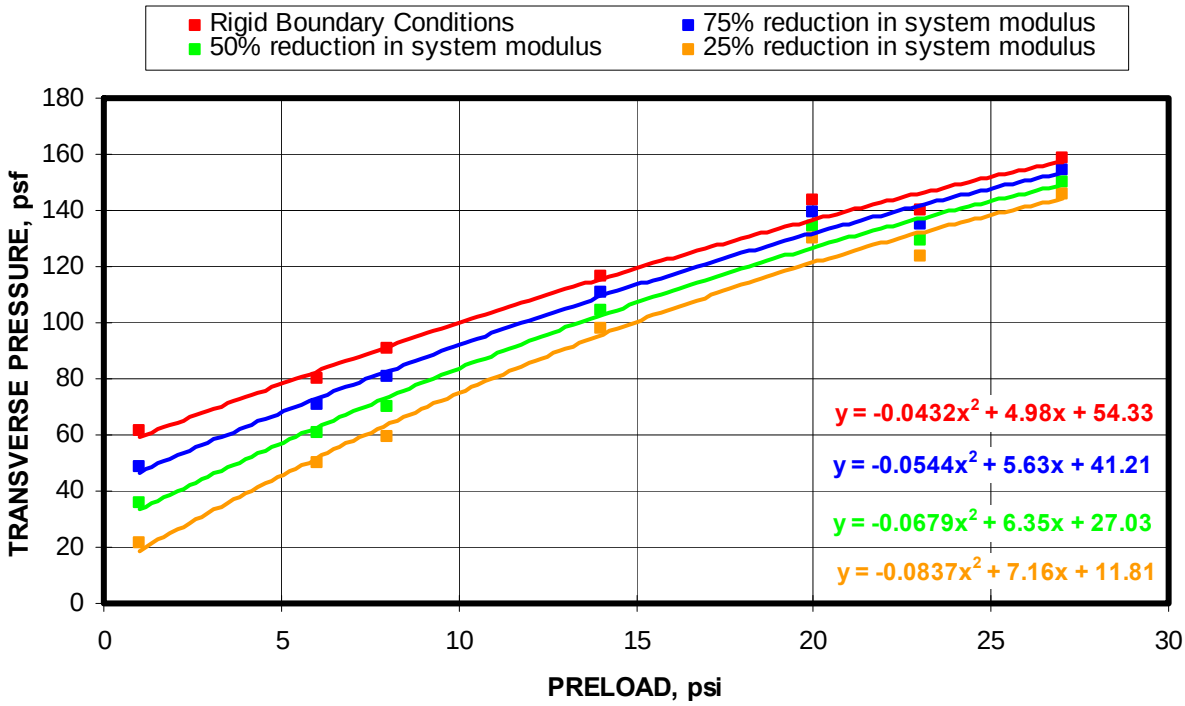

Figure 8-102. Impact of boundary stiffness reductions compared to rigid arching conditions as a function of preload for 48-inch-high half-wall constructions (Omega block).

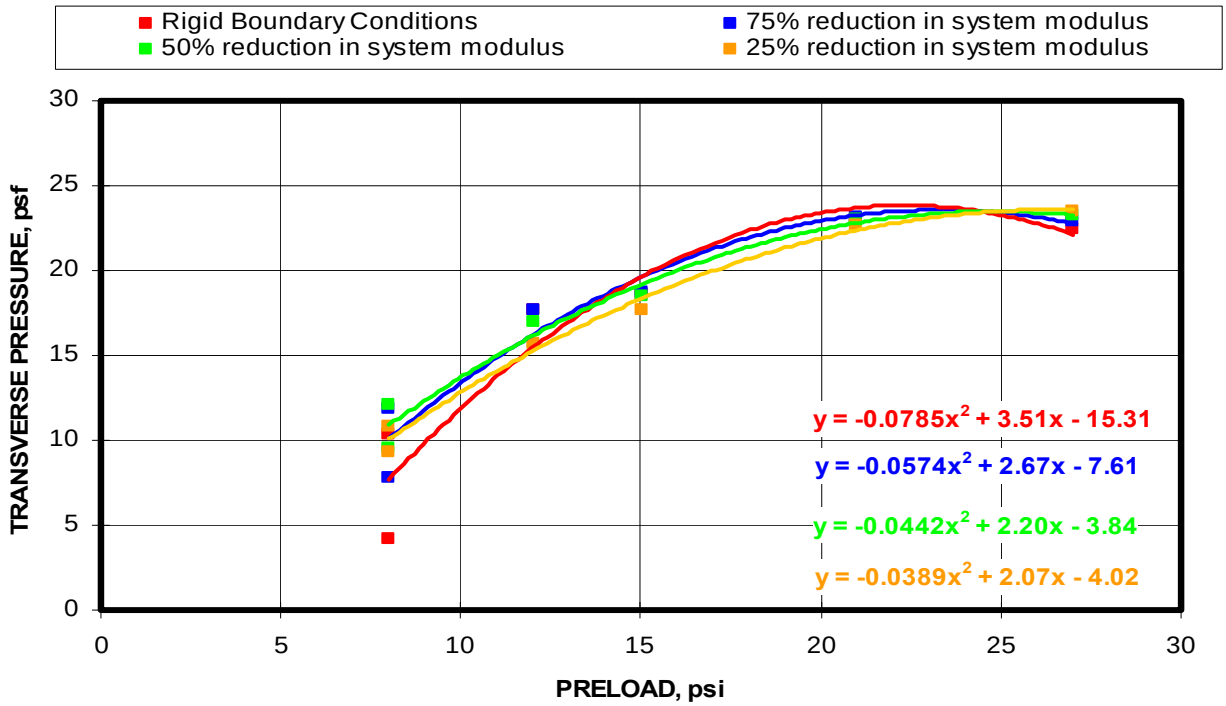

Figure 8-103. Impact of boundary stiffness reductions compared to rigid arching conditions as a function of preload for 64-inch-high half-wall constructions (Omega block).

8.8 PEERLESS SUPER BLOCK

Peerless Block & Masonry Company from St. Albans, West Virginia also makes an ultra light weight block called the Super Block (figure 8-104). This block is characterized by styrofoam pellets that are imbedded in the concrete mix to provide a low density material. Included in the mix is polypropelene fibers to help hold the weak material together during failure. With a density of only 38 lbs per cubic foot, this allows an oversized block to be produced that maintains a reasonable lifting weight of less than 50 lbs for a 6x16x24-in block. The block is also manufactured in a conventional 6x8x16-in block that weighs about 16 lbs. The unit block compressive strength is 86 psi, comparable to the Omega block described in the previous section.

Figure 8-104. Peerless Super Block test set up (showing two blocks stacked on top of one another).

8.8.1 Overview of the Test Program

A total of 31 tests were conducted with Peerless Super Block, 25 with the 6x16x24-in size block and 6 with the 6x8x16-in size block with half-wall configurations at heights of 32, 46, 48, and 64 inches. A single column of block was used for the large size Super Block while 3 blocks were used to form the width of the half-wall for the small Super Block tests. The small block tests were conducted at the 46-in half-wall height only. The results of the MRS half-wall tests are summarized in the table 8-11. The low compressive strength of the block did not allow much variation of preload. These blocks also have a low compressive strength, which limited the amount of preload that could be applied. For the single block column tests with the large block, the preload varied from 7 to 60 psi and from 5 to 89 psi for the three-column wide small block tests. The low strength of the block resulted in thrust loading that was near the measurable limits of the load frame. This contributed to some of the inconsistency in the test results. Graphs of the measured lateral load and thrust load as a function of the lateral displacement of the wall for each test are documented in Appendix B.

A tabular summary of the pertinent parameters and loading values for each test is also included Appendix C.

Table 8-11. Summary of Peerless Super Block Testing.

Block Type	Test No.	Block Width (in)	Block Height (in)	Half-wall Length (in)	Half-wall Height (in)	Preload (psi)	Measured Transverse Pressure, (psf)
Peerless Super Block	216	5.8	16	24	32	7	114
Peerless Super Block	218	5.8	16	24	32	16	104
Peerless Super Block	217	5.8	16	24	32	17	130
Peerless Super Block	219	5.8	16	24	32	21	86
Peerless Super Block	208	5.8	16	24	32	54	96
Peerless Super Block	209	5.8	16	24	32	56	104
Peerless Super Block	214	5.8	16	24	48	12	30
Peerless Super Block	195	5.8	16	24	48	29	48
Peerless Super Block	190	5.8	24	24	48	37	38
Peerless Super Block	191	5.8	16	24	48	38	42
Peerless Super Block	211	5.8	16	24	48	41	68
Peerless Super Block	197	5.8	16	24	48	42	54
Peerless Super Block	193	5.8	16	24	48	42	48
Peerless Super Block	192	5.8	16	24	48	45	46
Peerless Super Block	210	5.8	16	24	48	56	50
Peerless Super Block	196	5.8	16	24	48	60	58
Peerless Super Block	194	5.8	16	24	48	63	62
Peerless Super Block	231	5.8	16	24	64	4	6
Peerless Super Block	225	5.8	16	24	64	14	10
Peerless Super Block	230	5.8	16	24	64	22	6
Peerless Super Block	205	5.8	16	24	64	33	16
Peerless Super Block	229	5.8	16	24	64	34	20
Peerless Super Block	232	5.8	16	24	64	54	18
Peerless Super Block	233	5.8	16	24	64	53	24
Peerless Super Block	206	5.8	16	24	64	56	10
Peerless Super Block (small)	302	5.75	7.625	46.5	45.75	5	12
Peerless Super Block (small)	303	5.75	7.625	46.5	45.75	20	24
Peerless Super Block (small)	304	5.75	7.625	46.5	45.75	30	42
Peerless Super Block (small)	305	5.75	7.625	46.5	45.75	57	66
Peerless Super Block (small)	307	5.75	7.625	46.5	45.75	80	70
Peerless Super Block (small)	308	5.75	7.625	46.5	45.75	89	84

8.8.2 Parametric Relationships and Trends.

Examining table 8-11, it is seen that the transverse pressure capacity of the stoppings constructed from Peerless Super Block varied from a low of 14 to a high of 126 psf or .01 to 0.88 psi. Figure 8-106 displays the transverse pressure as a function of preload for the three half-wall heights. The transverse pressures for the 32-in-high half-walls are 5 to 7 times higher than the 64-in-high half-walls. It is also seen from figure 8-106 that the transverse pressure is nonlinearly related to the preload and that the transverse pressure approaches an asymptotic maximum at approximately 35-40 psi for the 64-in-high half-walls. The upward slope of the 48-in-high half-wall curve suggests the peak loading has not been reached, and it appears that for this data the 32-in-high half-walls was damaged when the preload was applied. Figure 8-106 plots the lateral displacement at which the peak transverse pressure is achieved as a function of preload for the 32-in-high and 48-in-high half-walls. The 64-in-half-wall response was inconsistent and did not follow a clear trend. Although the correlation is very weak, the trend is that the lateral displacement also approaches an asymptotic level.

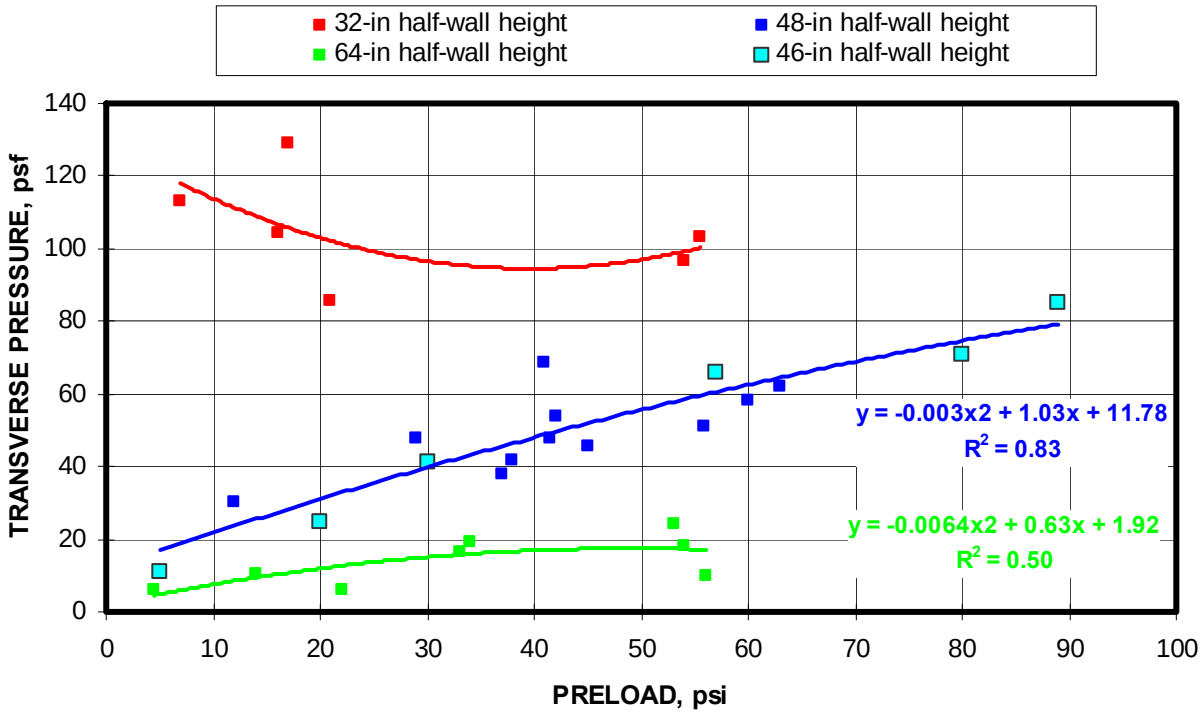

Figure 8-105. Transverse pressure as measured from MRS laboratory testing as a function of preload for three half-wall heights (Peerless Super Block).

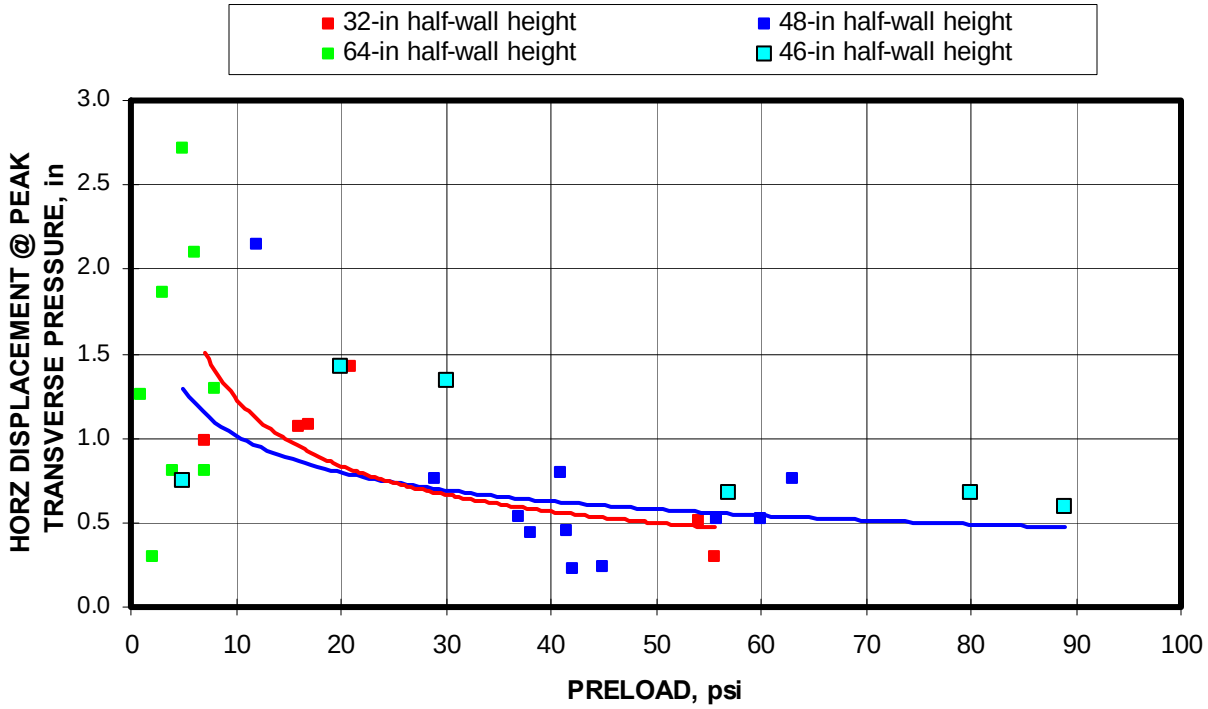

Figure 8-106. Lateral displacement at which peak transverse pressure occurs also reaches an asymptotic minimum as the preload approaches 70-80 psi (Peerless Super Block).

Further examination of the parametric relationships confirms the arching theory as presented in chapter 6. Figure 8-107 shows that the transverse pressure is directly related to the lateral force acting on the half-wall during the laboratory tests. Figure 8-108 shows that the lateral force is also directly related to the thrust force. In this case, the short wall correlation is not good. The thrust forces are relatively low and are at the limit of the load frame can accurately measure, but the block performance was also inconsistent at the short heights with failure and damage to the block occurring during the loading cycle to a greater extent than in the other test configurations. Finally, figure 8-109 shows the relationship between the transverse pressure and the arch thrust. This graph resembles the plot of transverse pressure versus preload shown in figure 8-105, showing that the arch thrust also reaches an asymptotic value. Here again, the correlation is not good for the short wall tests.

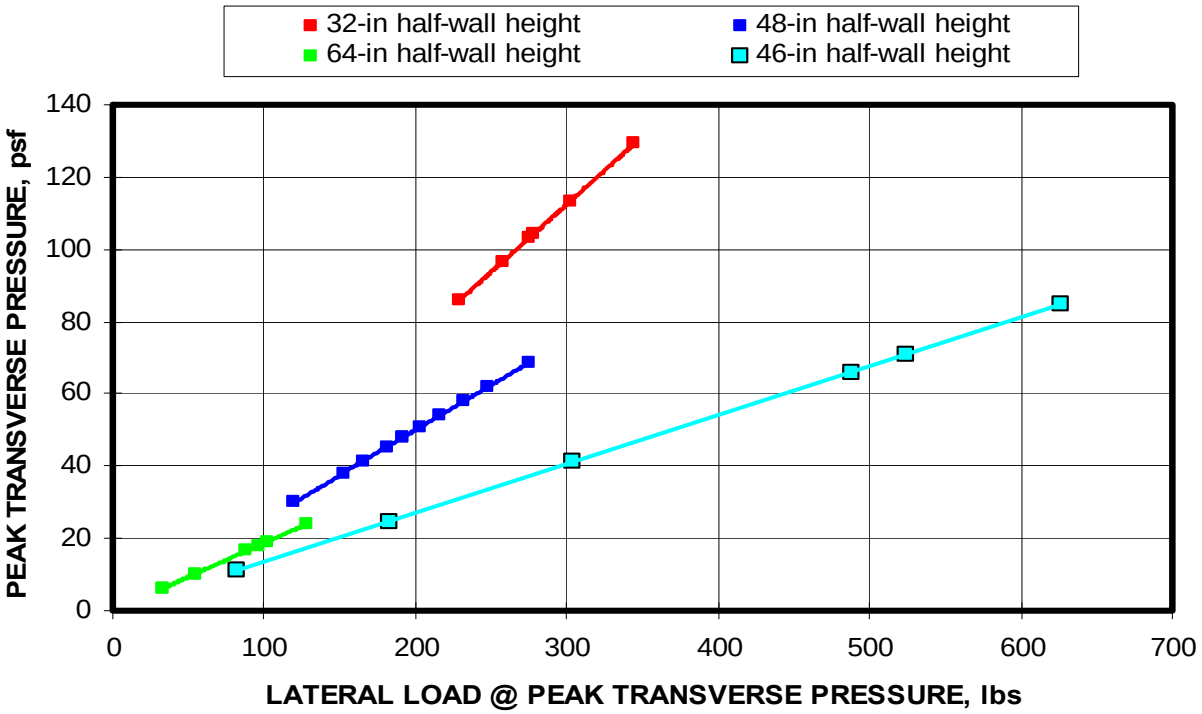

Figure 8-107. Relationship between the lateral load and the arch thrust for MRS laboratory tests for three half-wall heights (Peerless Super Block).

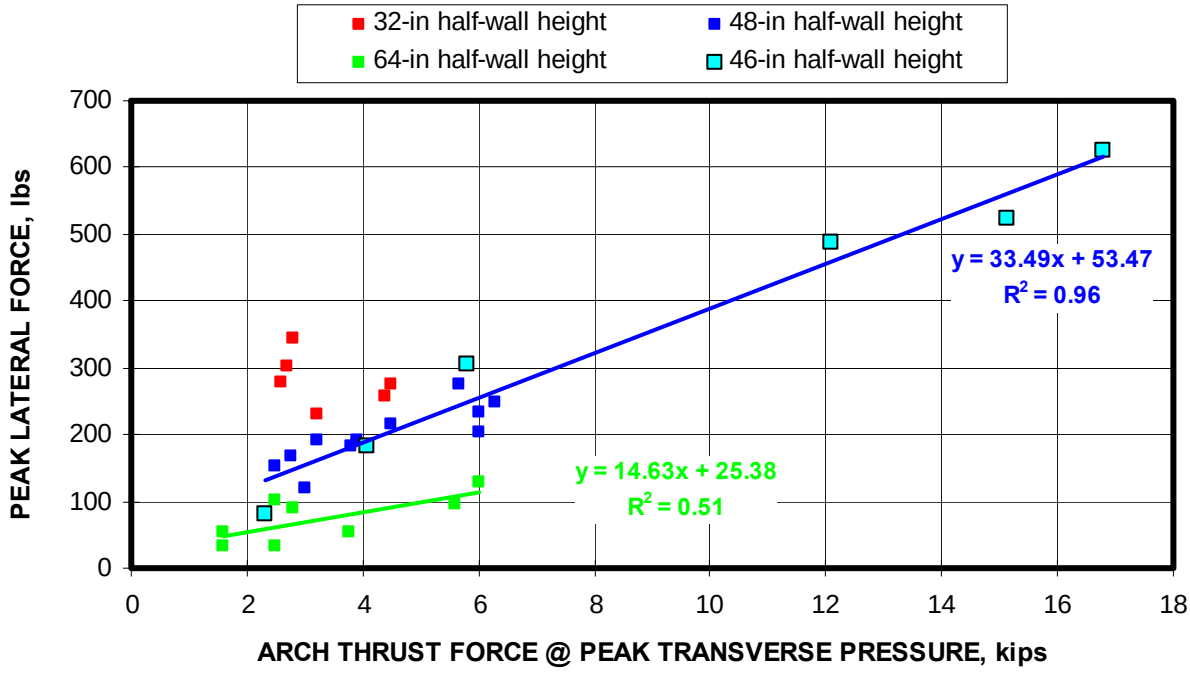

Figure 8-108. Relationship between the lateral load and the arch thrust for MRS laboratory tests for three half-wall heights (Peerless Super Block).

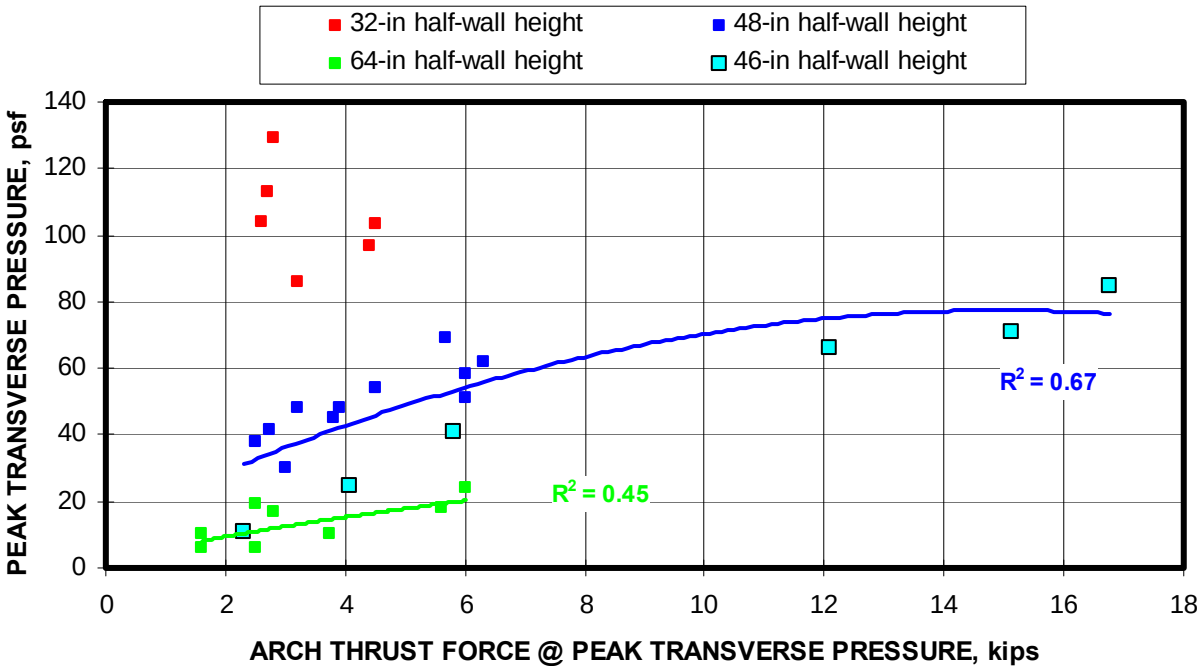

Figure 8-109. Relationship between the transverse pressure and the arch thrust for MRS laboratory tests conducted at three half-wall heights (Peerless Super Block).

Figure 8-110 depicts the relationship between the transverse pressure and the material modulus (E), the wall thickness (t), and the wall height (L) expressed as by the term E x $(t/L)^2$. The general trend of increasing transverse pressure with increasing E x $(t/L)^2$ is typical of other block types. The chart shows that 63 pct of the transverse pressure of a stopping is determined by this relationship. It is noted that the shortest half-wall (32-in) were eliminated from this data set. As shown in the previous analyses of the arching parameters, the 32-in-high half-walls did not correlated well to the observed trends in the 48 and 64-in-high half-wall tests. This material is very weak and prone to damage even from the initial preloading. Figure 8-111 compares two 32-in-high half-wall tests where the thrust load development is nearly identical in each test with the exception of a slight difference in the initial preload. However, as seen in the graph, the lateral load responses are significantly different. This type of behavior accounts for the scatter and poor correlation of the data. The material modulus is a significant parameter since it determines the amount of thrust force developed and ultimately the amount of lateral displacement of the wall, both of which control the arching mechanics of the wall, and the distribution of the Styrofoam pellets is not consistent and cause localized changes in the block material properties (see figure 8-112).

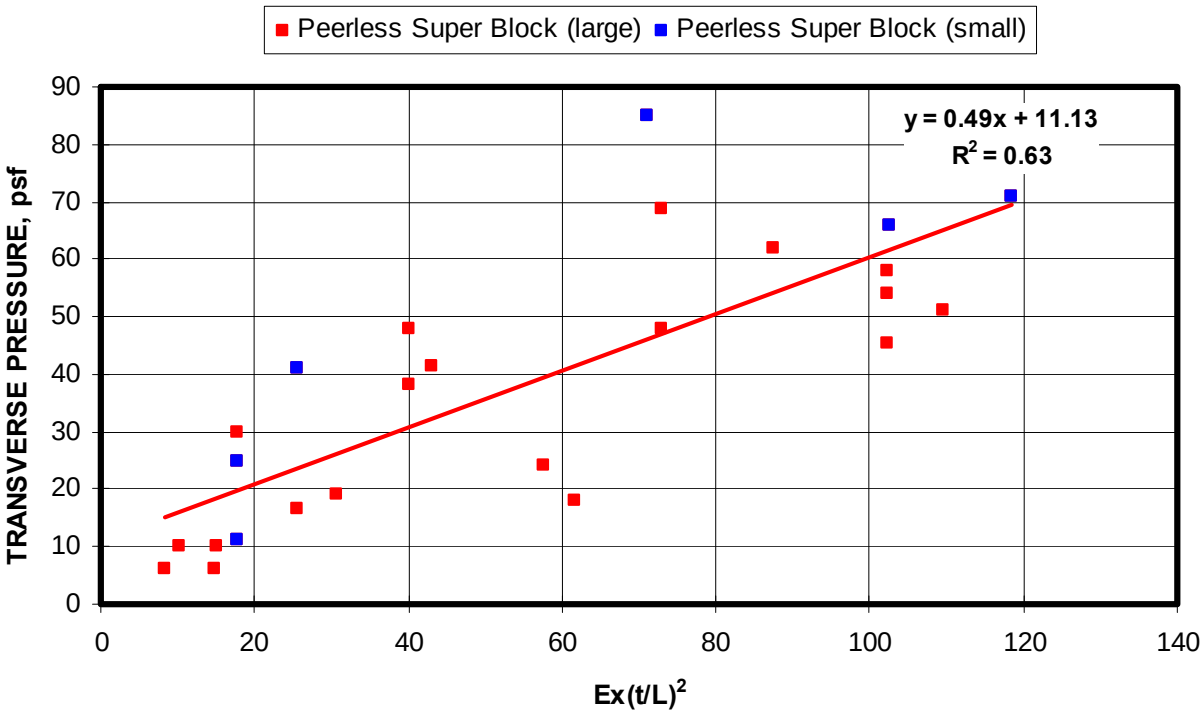

Figure 8-110. Separation of weak block from thrust empirical prediction equation provides more accurate model predictive capability for Peerless Super Block.

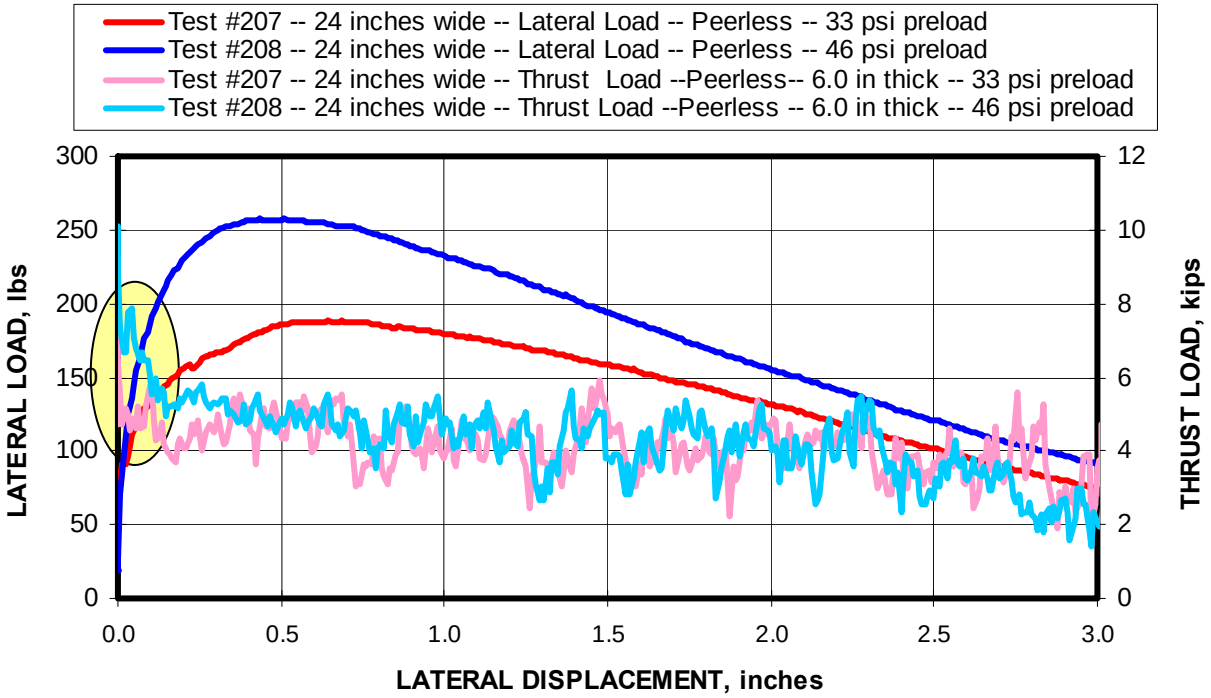

Figure 8-111. Two tests on 32-in-high half-walls show very similar thrust load development except at the initial preloading and significantly different transverse pressure (Peerless Super Block).

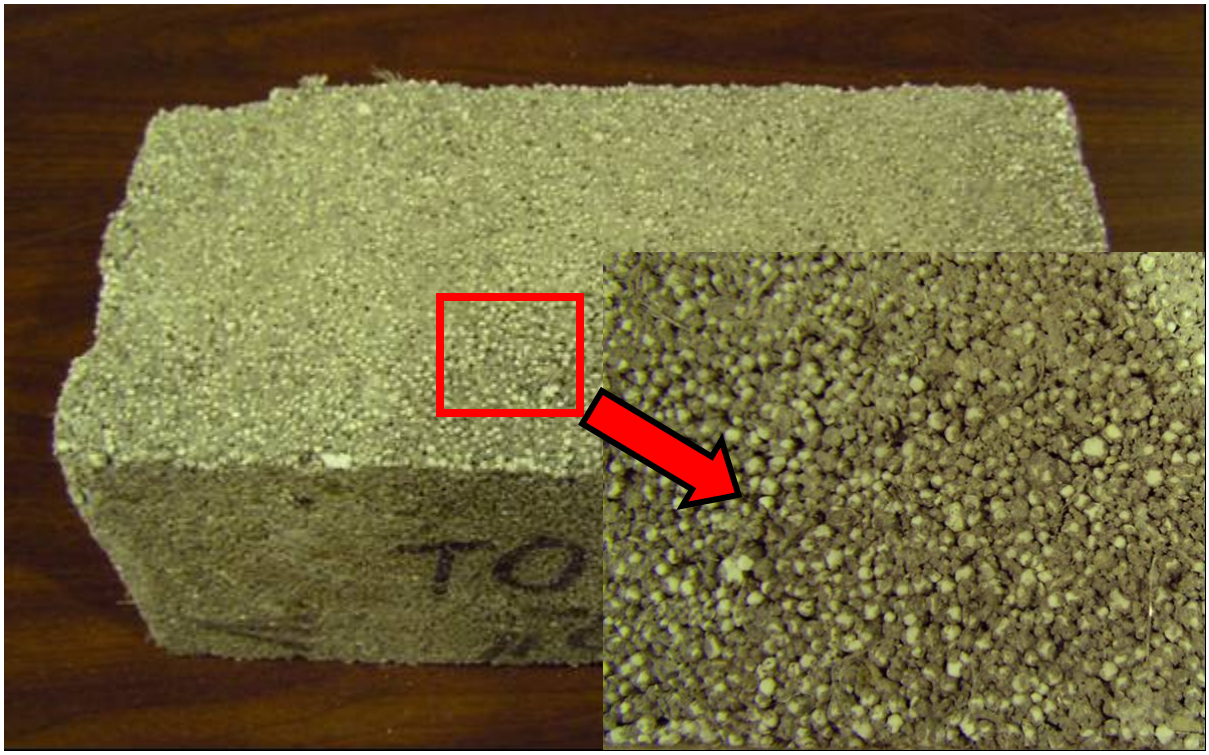

Figure 8-112. Photo of Peerless Super Block with close-up showing Styrofoam pellets (small white objects in photo) imbedded in concrete mix.

8.8.3 Evaluation of Predictive Models

The next goal is to evaluate the capability to predict the transverse pressure. If the thrust force and its resultant location and lateral load are known, the transverse pressure capacity of a stopping can be predicted with nearly 100 pct accuracy. If the thrust force location is instead calculated from the empirical model described in chapter 6 and shown in figure 8-113 for three half-wall heights considered in this analysis, the transverse pressure can still be predicted to better than 98 pct accuracy as depicted by the open red square data points shown in figure 8-114. Each data point in figure 8-114 represents an individual laboratory test. As seen in the figure, the accuracy of the prediction is consistent throughout the full range of transverse pressure conducted in the laboratory testing, and includes preloading of wall from zero to 89 psi and three different wall heights. Hence, while the wall performances may not be very consistent, if the thrust and lateral displacement are known, the arching mechanics still dictate a good measure of the transverse pressure capacity.

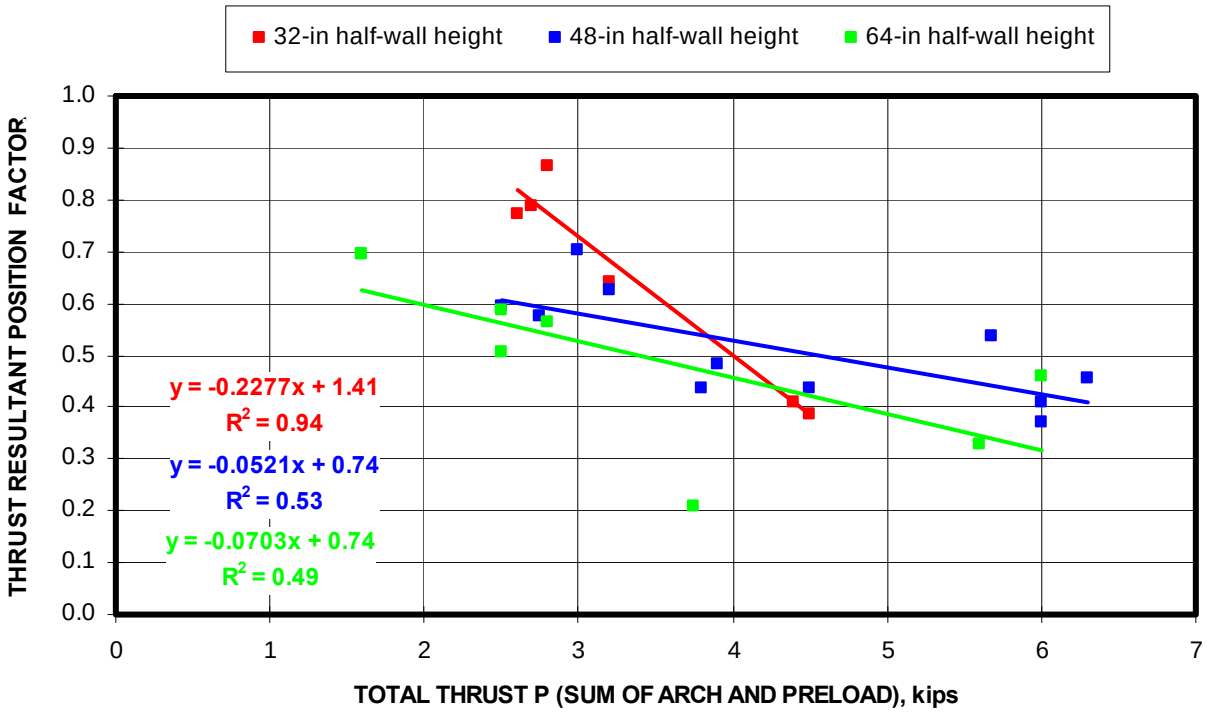

Figure 8-113. Resultant thrust force location for three wall heights as a function of the total arch thrust (Peerless Super Block).

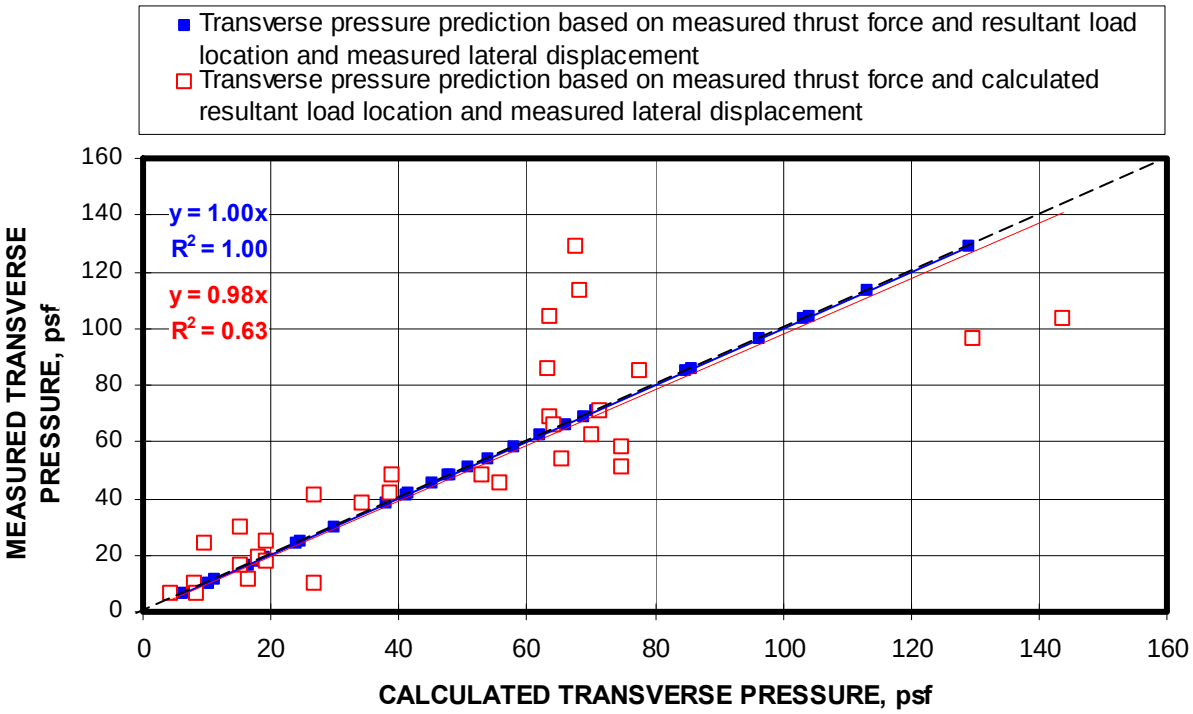

Figure 8-114. Prediction of transverse pressure when both the lateral load and arch thrust are known. (Peerless Super Block).

If either the thrust force or the lateral displacement is known, than the transverse pressure can still be calculated. Method 1 predicts the transverse pressure from the measured lateral displacement. Method 2 predicts the transverse pressure from the measured thrust force. Figures 8-115 illustrates the predictive capability of these two models showing the measured transverse pressure vs. the predicted transverse pressure for each half-wall laboratory test. The accuracy of the predictive models is not very good, due in large part to the inconsistency of the block material properties and low thrust loads. Method 2, which is based on the measured thrust forces over predicts the transverse pressure by a considerable amount. This is due in large part to the fact that the thrust load never increases during the transverse pressure development. Figure 8-111 was one example of this behavior. About 80 pct of the tests as highlighted in bold print in table 8-8 were this way. The block just deforms as the transverse pressure is developed, resulting in poor correlations in the model predictions.

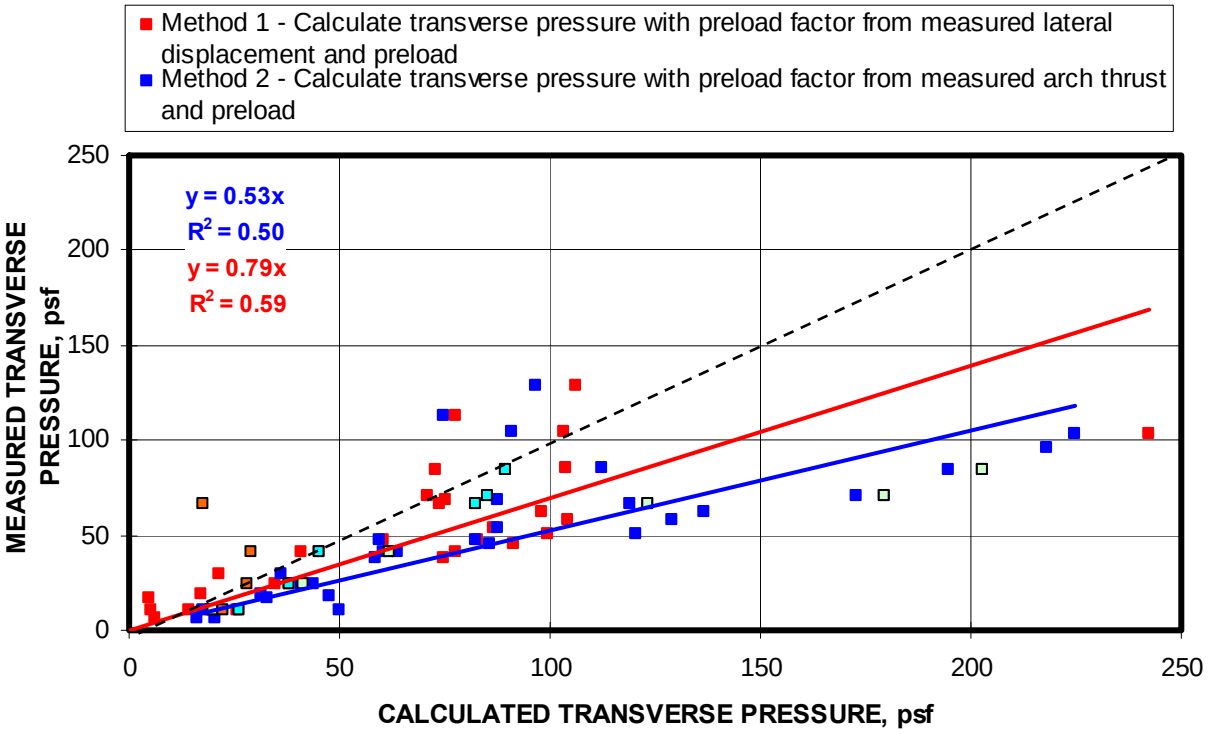

Figure 8-115. Prediction of transverse pressure from known thrust and lateral loads (Peerless Super Block).

8.8.4 Theoretical Impact of Boundary Stiffness

The inconsistency in the test results due to the very low material modulus for the Super Block make the theoretical assessment of the impact of boundary stiffness somewhat unreliable. Figure 8-116 shows the impact at 46-in half-wall height, which provided the most consistent test results. In this figure, the trend is consistent with other weak block materials, showing that the preload does reduce the transverse pressure for rigid boundary conditions, but has relatively little impact at very low boundary stiff nesses.

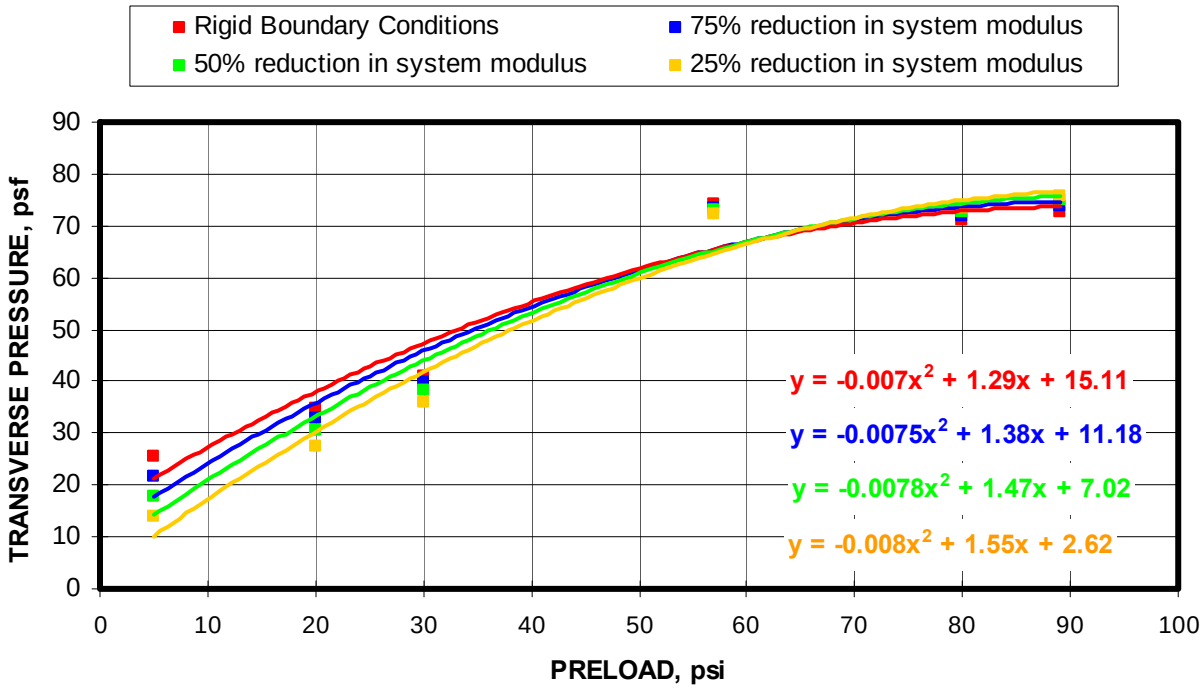

Figure 8-116. Impact of boundary stiffness reductions compared to rigid arching conditions as a function of preload for 46-in-high half-wall constructions (Peerless Super Block).

CHAPTER 9: UNIVERSAL DESIGN EQUATIONS FOR STOPPING BLOCK WALLS

Chapter 8 showed that if either the arching thrust or the lateral displacement is known, then the maximum transverse load of the stopping could be predicted with reasonable accuracy using the two predictive models developed in chapter 7. While these measurements could be made on stoppings in a mine and these models used to provide valuable information of the transverse loading of the stopping, a more generic model that does not require in service performance measurements is needed to develop design equations for stoppings. To fulfill this objective, models are developed based on the wall geometry (thickness and height) and the elastic modulus of the material, which utilize empirical data from the laboratory testing to provide for transverse load determinations of various stopping constructions.

The wall thickness and height are known parameters for any stopping construction. The elastic modulus can be determined from material property testing. Tests were conducted on a column of full size stopping blocks, whereby vertical load was applied to the block column of equivalent height to the half-wall MRS tests. The wall is tilted slightly to a configuration that is consistent with the orientation of the wall during the applied transverse loading. The result is shown in figure 9-1 for a Portland cement block that has been utilized in several examples in this dissertation, where it is shown that the block has a modulus of 50,000 psi. The modulus is computed at the early loading stage where the strains are consistent with the wall deformation during arching as measured in the MRS laboratory tests. Although this modulus is an order of magnitude less than what the elastic modulus is reported for concrete materials, the value should be considered an “apparent modulus” rather than a true elastic modulus since the block is being loaded in an unconventional manner compared to ASTM laboratory test requirements for modulus determinations. The important point is that this value is consistent with the theoretical analysis of arching where back calculation of the modulus computed a value of 60,000 psi for this particular block.

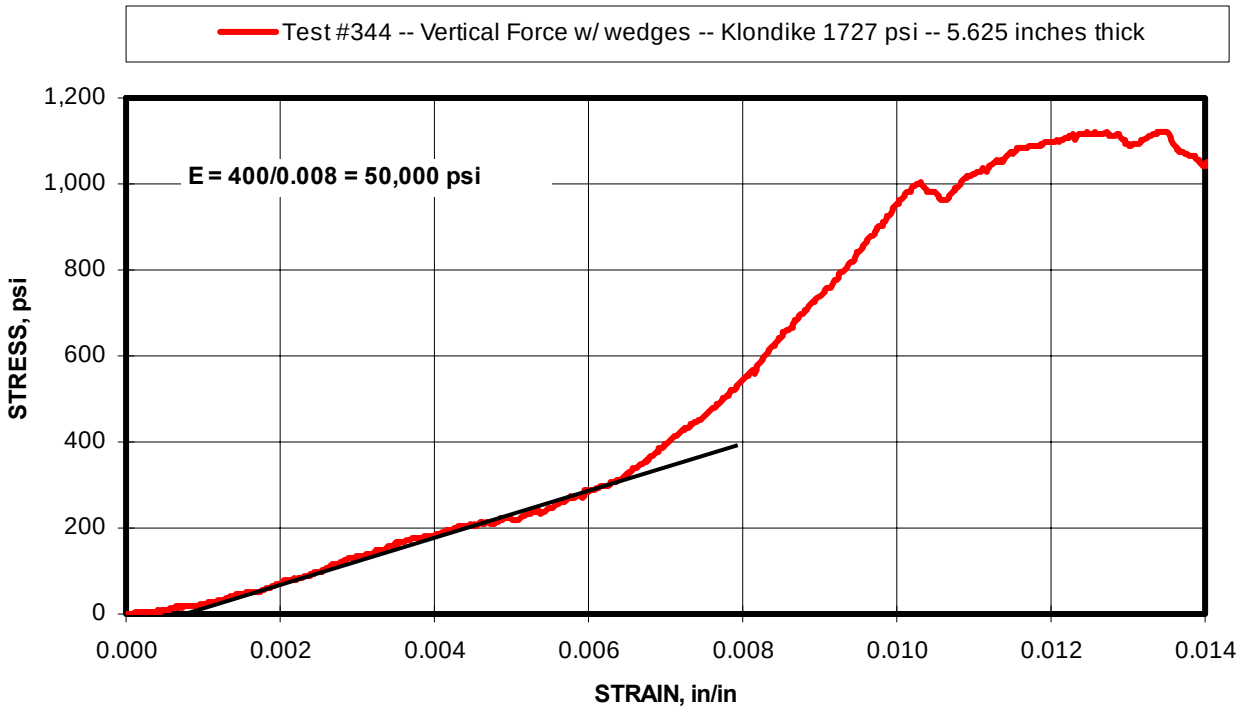

Figure 9-1. Test conducted in MRS on 6-course-high half wall to determine apparent elastic modulus for the block material.

It was shown in chapter 8 that when the modulus is back calculated for a specific test then a strong correlation exists between the transverse load and the term $Ex(t/L)^2$ where E is the modulus, t is the wall thickness, and L is wall height. The goal of this generalized design is to develop a design equation, which uses a constant modulus for a specific block type. Since preloading of the wall from ground pressures is also possible in any underground mine, incorporating preload pressure into this generalized design equation was also considered a necessary requirement.

Modulus values for each block type were back-calculated from the half-walls tests conducted in the MRS. From this, a modulus representing each block was determined as part of a profile characterization for that block. These values were shown in the chart in figure 8-2 and are summarized here in tabular form (table 9-1). With these values, and known parameters for wall thickness and height, the $Ex(t/L)^2$ term was computed and correlated to the measured transverse pressure. The next step was to incorporate preload into the process. A full empirical model is developed by performing a multivariable regression analysis, that in addition to the $Ex(t/L)^2$, includes the preload pressure. A hybrid theoretical model is also developed whereby the normalized total thrust force is determined from a multivariable

regression of the $Ex(t/L)^2$ term and preload. As part of this process, a multivariable regression analysis is also made to determine the thrust resultant position factor as a function of the wall height and thrust. Then using the flowchart shown in figure 9-2, the hinge point deformation and lateral displacement are computed from the arching theory presented in chapter 5. This model is an empirical equivalent to Model 2 (Thrust Model) presented in Chapter 8. A second hybrid theoretical model is developed which utilizes a multivariable regression analysis to compute the lateral displacement as a function of the $Ex(t/L)^2$ term and preload. This model would be an empirical equivalent to Model 1 (Lateral Displacement Model) presented in Chapter 8 and is expressed by the flowchart in figure 9-3. A third model combines the two by using empirical multivariable regression analysis to compute both the normalized thrust and the lateral displacement as illustrated in the flowchart in figure 9-4. The inclusion of the lateral displacement into the design equation through this process improves the prediction accuracy. The hybrid theoretical models also provide more information that can be beneficial to a design engineer or researcher. Also included in the block profile listing in table 9-1 is a preload limit. This represents the maximum preload that the block wall can sustain relative to the transverse loading. If the preload exceeds these amounts, localized failures will limit and sometimes reduce the transverse load capacity of the stopping.

The design equations using these two approaches are presented for each specific block manufacturer as well as a more general category of block type, namely (1) standard concrete masonry block made from Portland cement and aggregate fillers, (2) cellular concrete block materials, and (3) low strength or specialty type block categories which at present include Omega Block and the Peerless Super Block composed of Styrofoam-imbedded concrete (see table 9-1). The standard concrete block or CMU as they are sometimes called is represented by the Klondike and Peerless Backsaver block in this data set. The cellular concrete block is represented by the Ytong, Aerated Concrete Corporation, and Kingsway block. As with any empirical model, these models will improve as additional test data become available. However, with the data set provided from the MRS half-wall testing, these design equations are shown to provide good approximations of the transverse load capacity of the various mine ventilation stopping constructions currently being utilized throughout the U.S.

Table 9-1. Profile characteristics for various block materials examined in this study.

Specific Block	Block Category	Modulus (psi)	Compressive Strength (psi)[1]	Preload limit (psi)
Klondike Solid Block (standard)	Standard Solid CMU	60,000	832	500
Klondike Solid Block (High strength)	Standard Solid CMU	80,000	1,564	500
Peerless Back Saver	Standard Solid CMU	40,000	1637	250
Klondike Hollow Core	Standard Hollow-Core CMU	65,000	882	200
Ytong	Cellular Concrete	40,000	705	150
Aerated Concrete Corp	Cellular Concrete	20,000	446	250
Kingsway	Cellular Concrete	24,000	546	150
Omega	Specialty Block	4,500	70	25
Peerless Super Block	Specialty Block	5,000	32	40

[1] Unit block compressive strength.

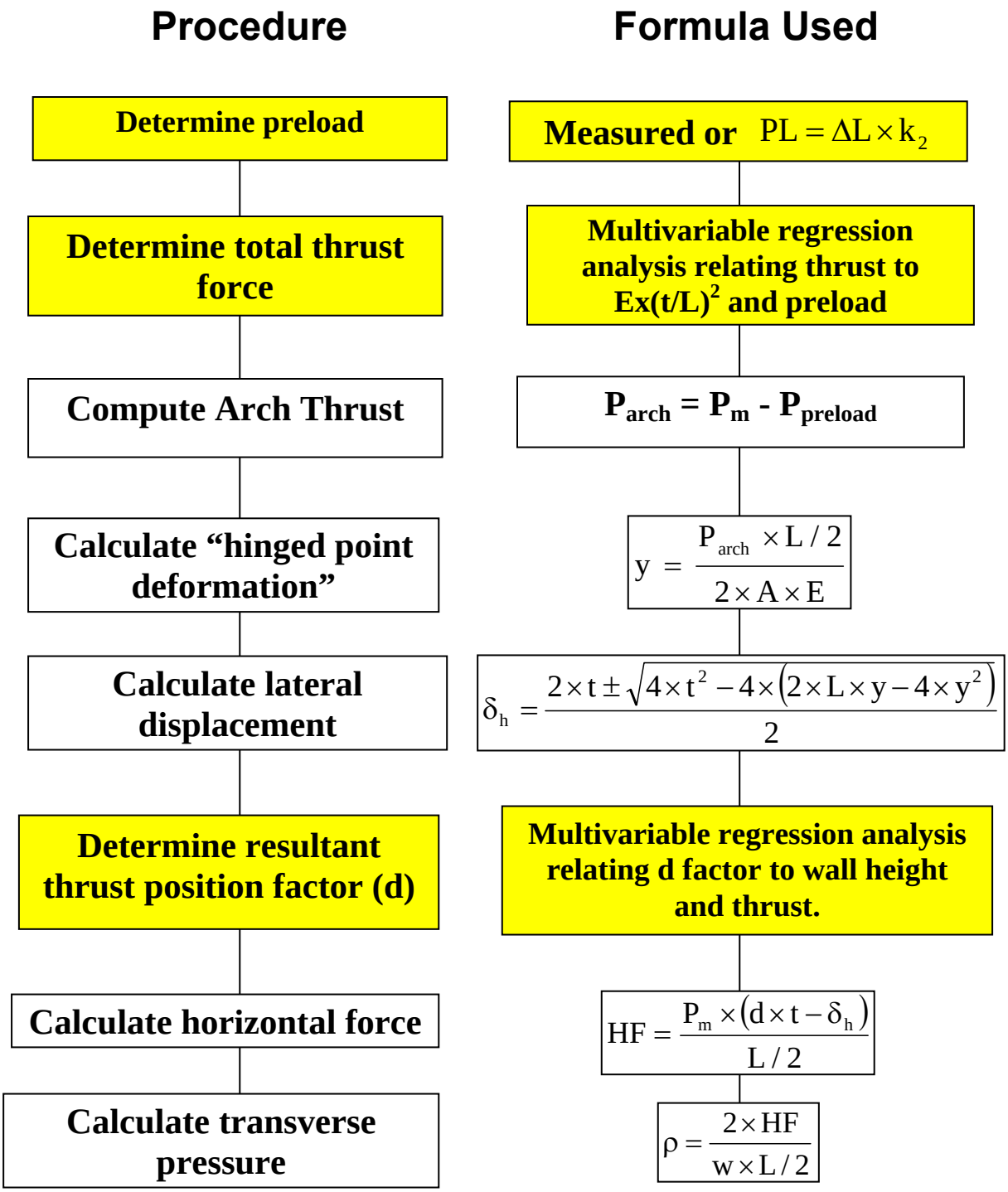

Figure 9-2. Flowchart for predicting the transverse load capacity of stoppings (Hybrid Theoretical Thrust Model).

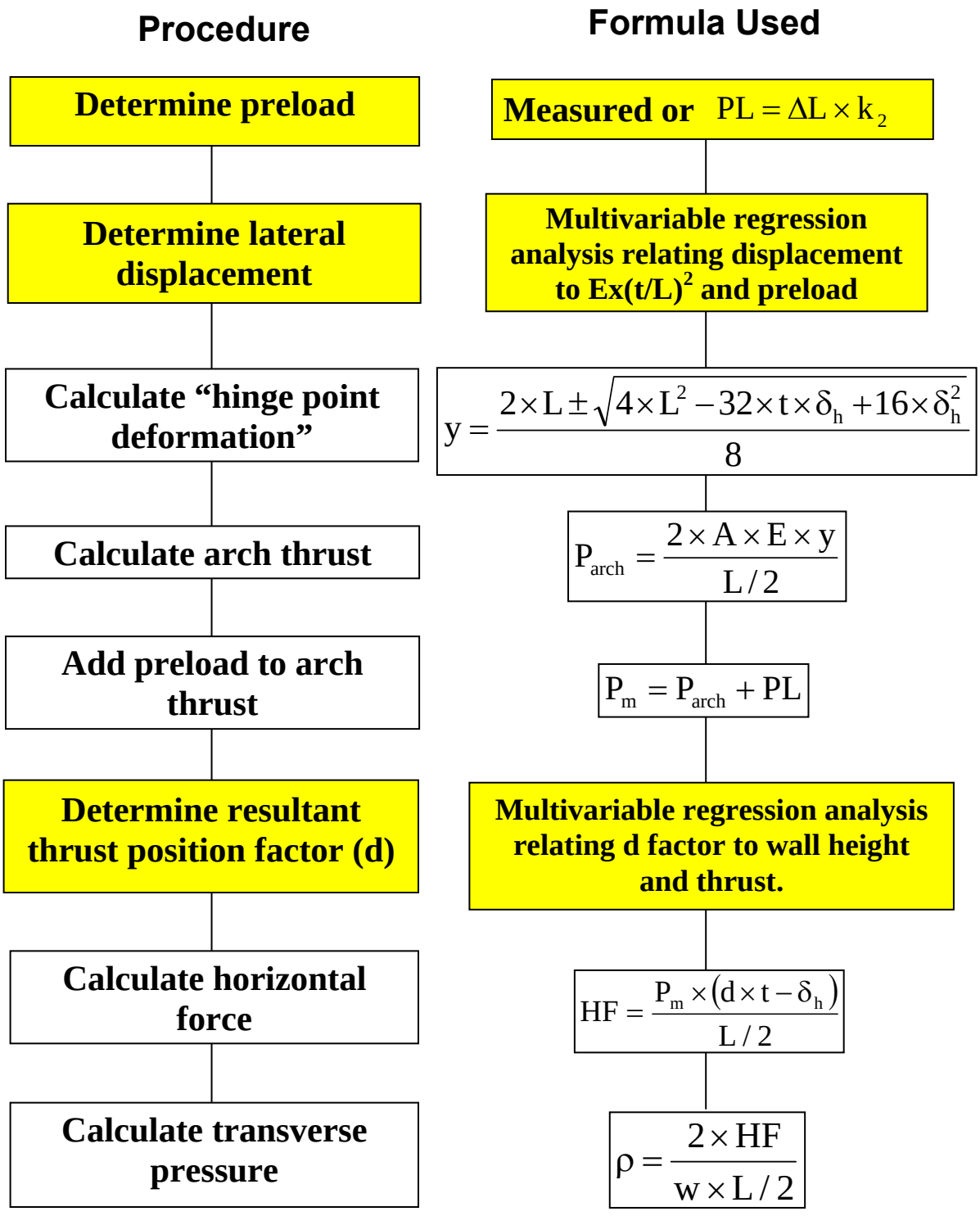

Figure 9-3. Flowchart for predicting the transverse load capacity of stoppings (Hybrid Theoretical Lateral Displacement Model).

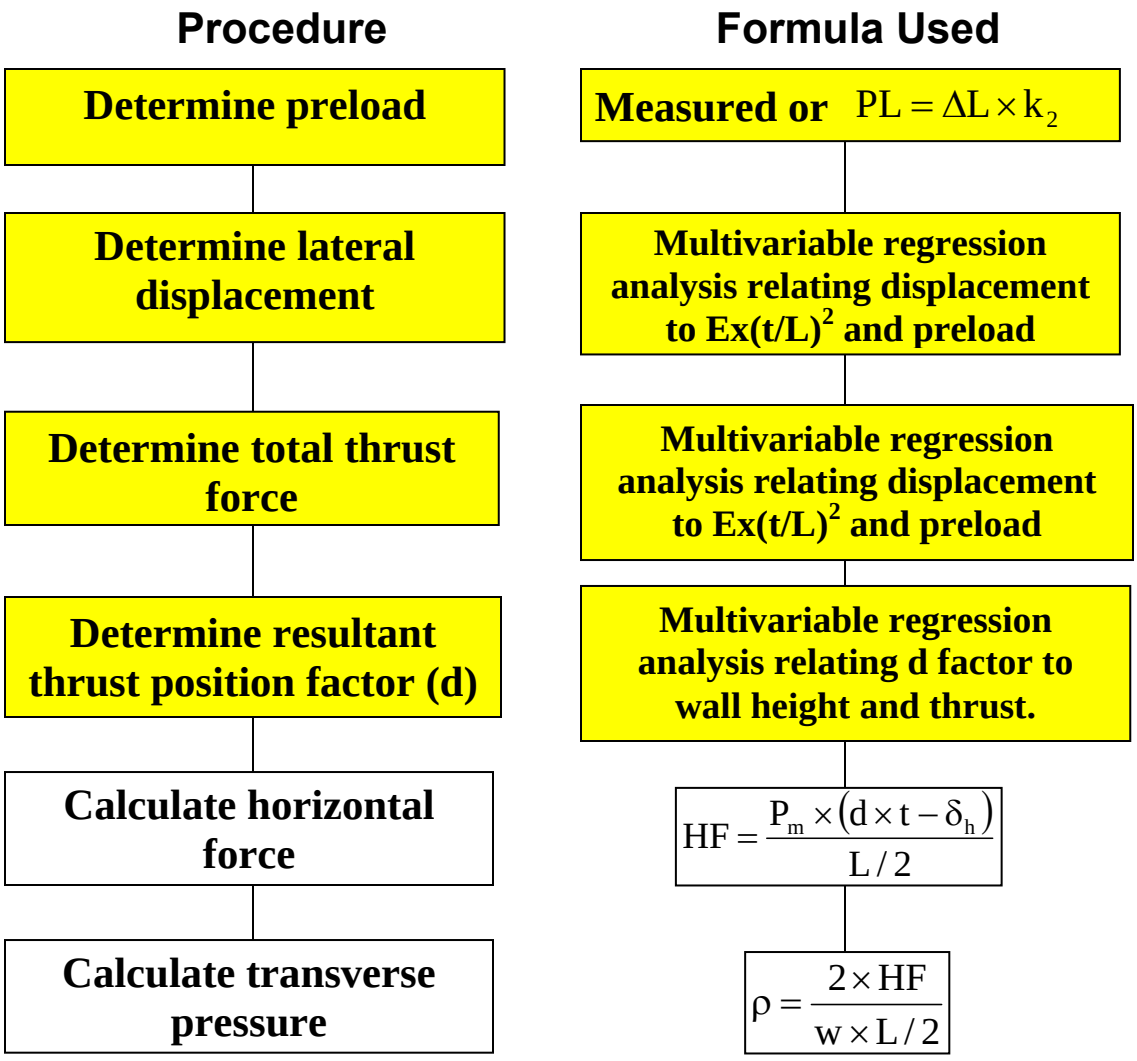

Figure 9-4. Flowchart for predicting the transverse load capacity of stoppings (Combined Hybrid Theoretical Thrust and Lateral Displacement Model).

9.1 SPECIFIC BLOCK DESIGN

Design equations are developed for each block of a specific manufacturer. The first design formulation will be based on the full empirical model where the transverse load is determined from a multivariable regression analysis of the half-wall tests conducted for that particular block. Following this, hybrid theoretical design formulations based part on empirical evaluations and part theoretical calculations will be presented.

9.1.1 Klondike Solid Block

As described in Chapter 8, these are standard CMU block made from Portland cement and aggregate. Most of the testing was done with these blocks, since historically they have been the most commonly used style of block. The block measures nominally 6x8x16 inches and weighs about 50 lbs each.

9.1.1.1 Full Empirical Model

Table 9-2 shows the results of the multivariable regression analysis correlating the transverse load to the $Ex(t/L)^2$ term and preload. From this regression analysis, the design equation for Klondike solid core block is shown in equation 9.1

$$\text{Transverse Load} = 5.3208 \times Ex(t/L)^2 + 2.3123 \times \text{Preload} - 994 \qquad \textbf{(9.1)}$$

Where E = material modulus = 60,000 psi for Klondike block,

t = wall thickness, in,

L = full wall height, in, and

Preload = ground pressure preload, psi.

Table 9-2. Regression analysis for determining transverse load from modulus and wall geometry parameters.

Regression Statistics	
Multiple R	0.9173
R Square	0.8415
Adjusted R Square	0.8379
Standard Error	403.7352
Observations	91

ANOVA

	df	SS	MS	F	Significance F
Regression	2	76138801	38069401	233.5516	0.0000
Residual	88	14344187	163002		
Total	90	90482988			

	Coefficients	Standard Error	t Stat	P-value	Lower 95%	Upper 95%	Lower 95.0%	Upper 95.0%
Intercept	-993.8975	123.4804	-8.0490	0.0000	-1239.2890	-748.5060	-1239.2890	-748.5060
E x (t/L)^2	5.3208	0.2555	20.8222	0.0000	4.8130	5.8286	4.8130	5.8286
Preload	2.3123	0.2202	10.5018	0.0000	1.8747	2.7499	1.8747	2.7499

Figure 9-5 displays the accuracy of the model for the three wall heights that were evaluated in the laboratory test program. Plotted on this graph are the measured transverse pressure from the laboratory tests and the transverse pressure for that condition that was calculated using equation 9-1 for a particular wall construction and preload pressure. As seen in the figure, the model predictions are most accurate for the 45-in half-wall height and least accurate for the 30-in half-wall height. The transverse capacity is under predicted throughout the preload range for the 30-in half-wall height. Since the performance in the laboratory testing were least consistent at the low heights, and this is an empirical model, then it makes sense that the model is least accurate for the low height as well. The 45-in-high performance is accurately predicted by the empirical formula. The transverse pressure is also under predicted for preloads less than 300 psi for the 60-in-high configurations. Figure 9-6 shows transverse pressure predictions using this empirical design model for 6-in-thick walls constructed from Klondike block ranging in height from 5 to 10 feet in one foot increments with preloads ranging from 0 to 600 psi. The negative y-intercept on this chart for the 9 and 10-ft-high walls indicates the inaccuracies of this model for the high heights at lower preloads.

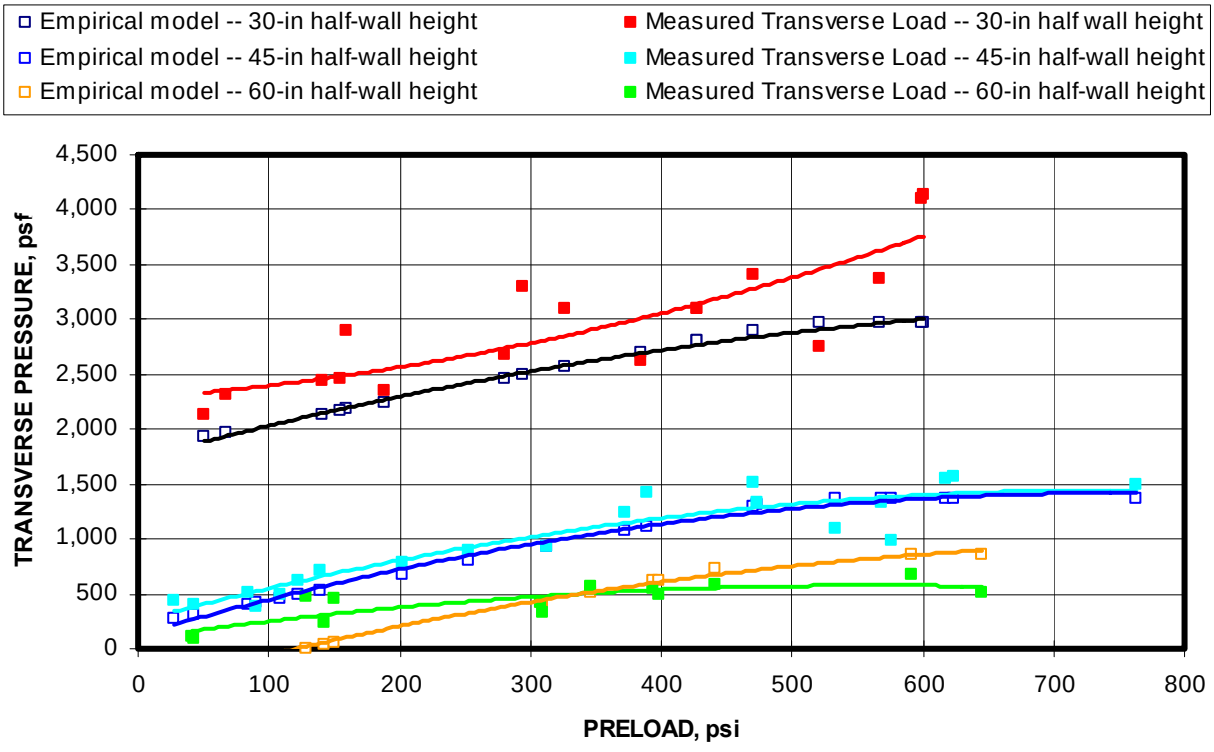

Figure 9-5. Comparison of design equation predictions with measured transverse load from laboratory testing (Full Empirical Model – Klondike block).

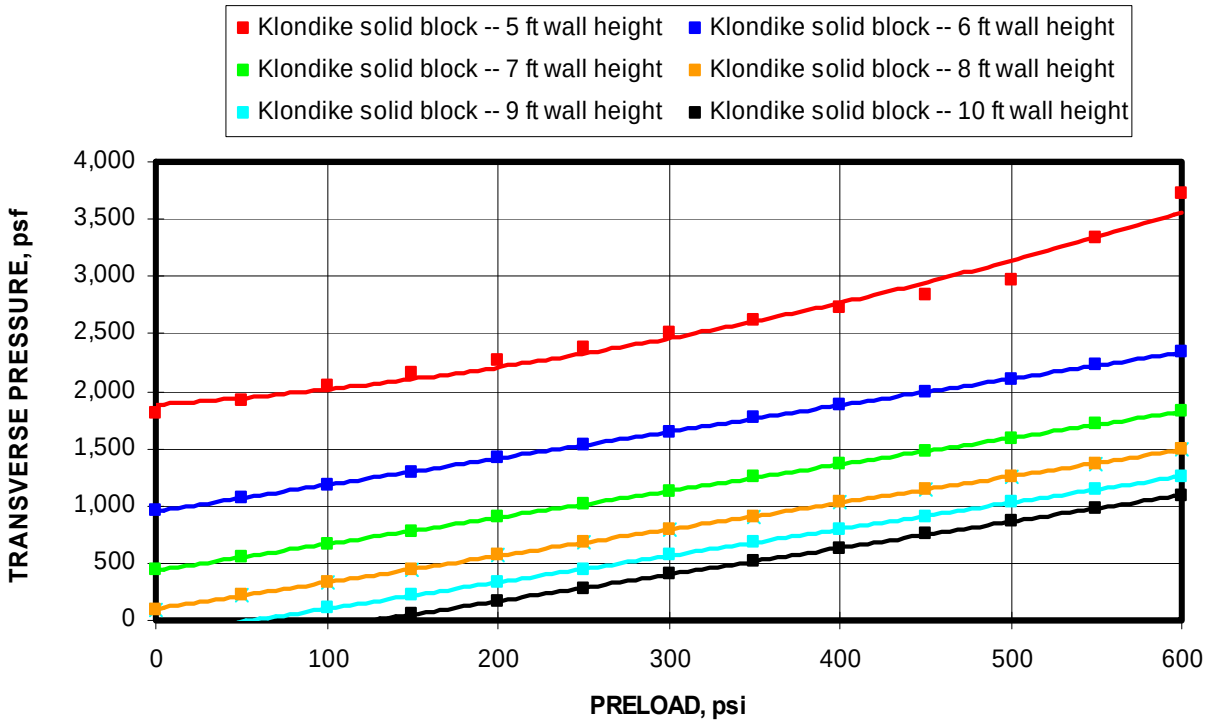

Figure 9-6. Transverse load capacity predictions for 6-in-thick walls constructed from Klondike solid block for walls heights ranging from 5 to 10 ft (Full Empirical Model).

9.1.1.2 Hybrid Theoretical Models

Transverse load capacity forecasts will be made using the three hybrid theoretical models: (1) Hybrid Thrust Model, (2) Hybrid Lateral Displacement Model, and (3) Hybrid Combination Thrust and Lateral Displacement Model.

9.1.1.2.1 Hybrid Thrust Model

As seen in the flowchart in figure 9-2, the Hybrid Thrust Model determines the normalized thrust force from a multivariable relationship between the thrust force and the $Ex(t/L)^2$ term and preload, both of which are considered to be known parameters. The multivariable linear regression analysis based on 91 laboratory tests of various wall constructions is summarized in table 9-3. Equation 9.2 is used to compute the normalized thrust force per unit width of wall. Table 9-4 documents the multivariable regression analysis results used to determine the resultant thrust position factor (d).

Table 9-3. Multivariable regression analysis for determining arching thrust.

Regression Statistics	
Multiple R	0.8126
R Square	0.6603
Adjusted R Square	0.6525
Standard Error	0.5130
Observations	91.0000

ANOVA

	df	SS	MS	F	Significance F
Regression	2.0000	45.0061	22.5031	85.5116	0.0000
Residual	88.0000	23.1579	0.2632		
Total	90.0000	68.1640			

	Coefficients	Standard Error	t Stat	P-value	Lower 95%	Upper 95%	Lower 95.0%	Upper 95.0%
Intercept	0.6100	0.1569	3.8878	0.0002	0.2982	0.9218	0.2982	0.9218
$E * (t/L)^2$	0.0025	0.0003	7.8052	0.0000	0.0019	0.0032	0.0019	0.0032
Preload	0.0034	0.0003	12.0278	0.0000	0.0028	0.0039	0.0028	0.0039

$$P/BL = 0.0025 \times Ex(t/L)^2 + 0.0034 \times Preload + 0.6100 \quad \textbf{(9.2)}$$

Where P/BL = Normalized thrust per unit width of block, kips/in,

E = Elastic modulus = 60,000 psi for Klondike solid block,

t = wall thickness, in,

L = height of wall, in, and

Preload = preload pressure, psi.

Table 9-4. Multivariable regression analysis for determining resultant thrust position factor.

Regression Statistics	
Multiple R	0.4564
R Square	0.2083
Adjusted R Square	0.1903
Standard Error	0.0946
Observations	91.0000

ANOVA

	df	SS	MS	F	Significance F
Regression	2	0.2073	0.1036	11.5767	0.0000
Residual	88	0.7878	0.0090		
Total	90	0.9951			

	Coefficients	Standard Error	t Stat	P-value	Lower 95%	Upper 95%	Lower 95.0%	Upper 95.0%
Intercept	0.9547	0.0629	15.1796	0.0000	0.8297	1.0797	0.8297	1.0797
Half-wall Height	-0.0021	0.0011	-2.0121	0.0473	-0.0043	0.0000	-0.0043	0.0000
Thrust	-0.0036	0.0008	-4.7918	0.0000	-0.0052	-0.0021	-0.0052	-0.0021

Resultant Thrust Position Factor (d) = -.0021 x Half-wall height - .0036 x Thrust + .9547 **(9.3)**

Figure 9-7 compares the results of the predicted transverse load capacities from the hybrid theoretical thrust model with the measured laboratory test results for half-wall heights of 30, 45, and 60 inches with varying preloads. As seen from the graph, the predictions overall are improved compared to the full empirical model presented in figure 9-5, especially for the 60-in half-wall height. Figure 9-8 shows transverse load predictions using this Hybrid Thrust Model for 6-in-thick walls constructed from Klondike block ranging in height from 5 to 10 feet in one foot increments with preloads ranging from 0 to 600 psi.

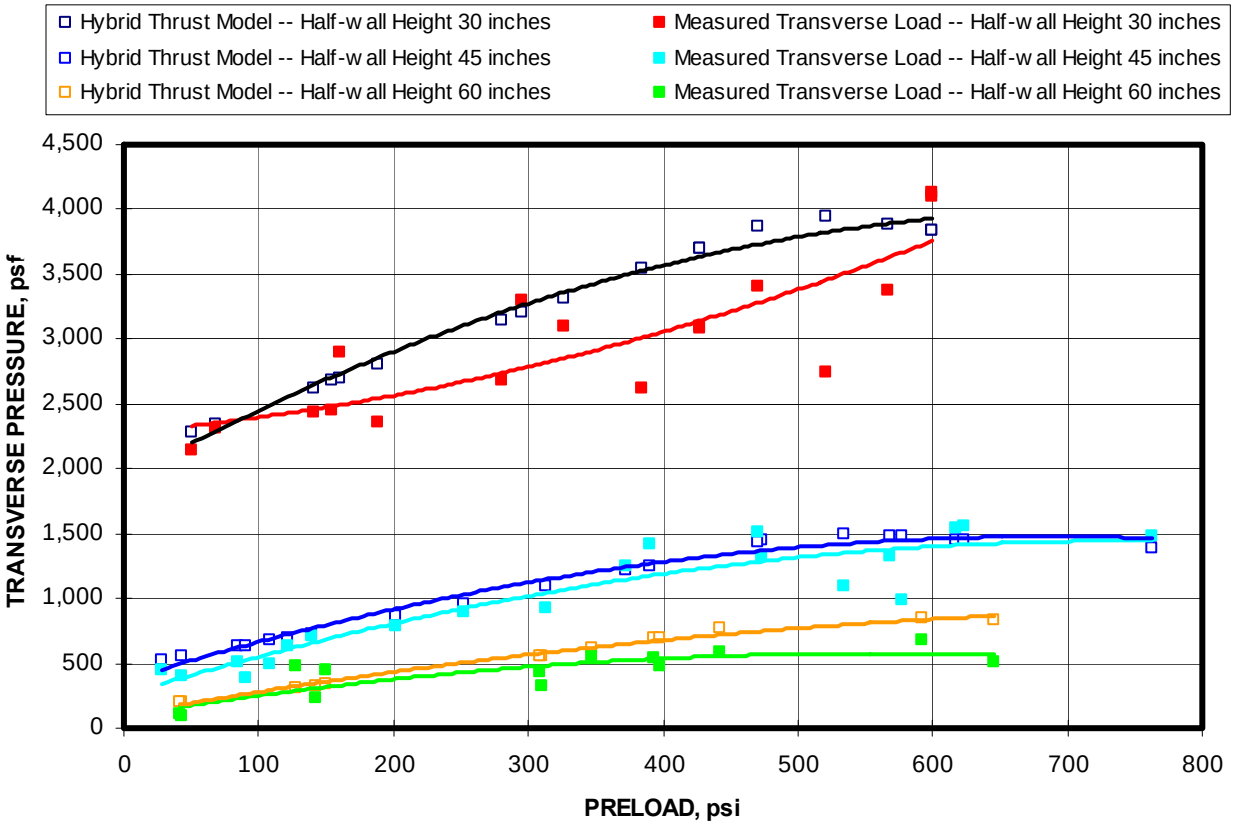

Figure 9-7. Comparison of transverse load capacities from design equations to the measured transverse load from laboratory tests (Hybrid Theoretical Thrust Model).

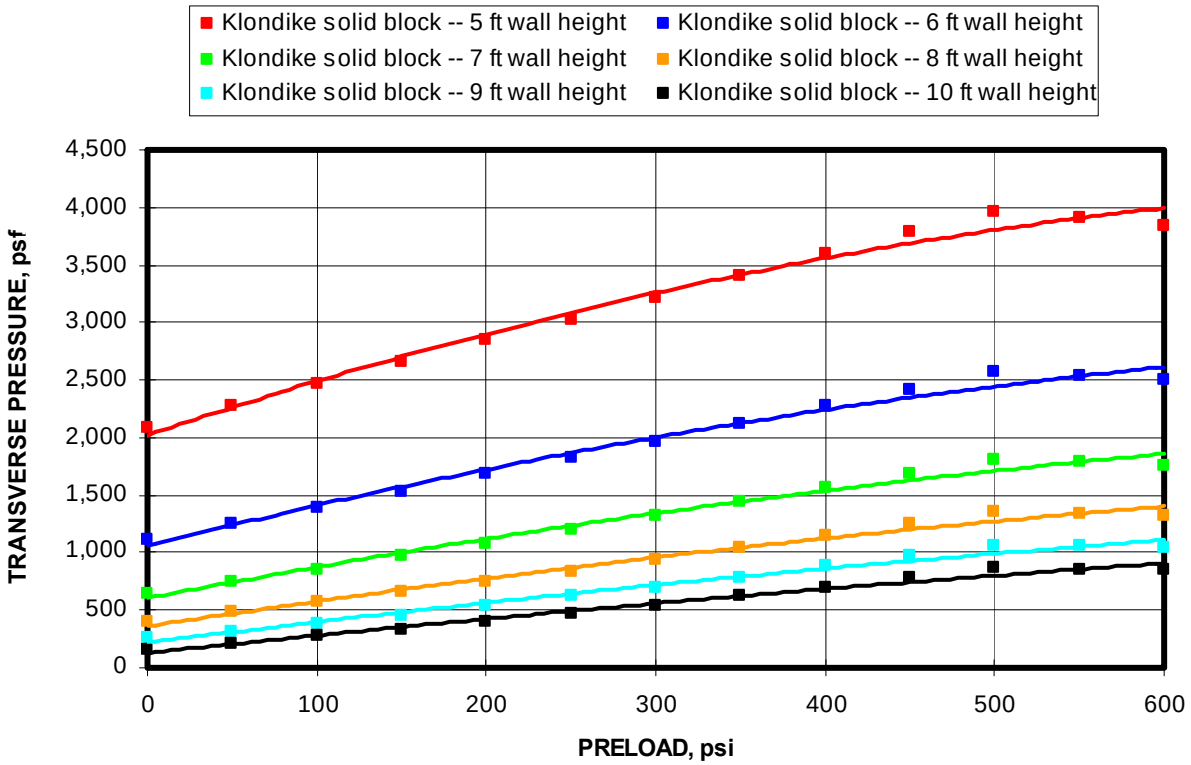

Figure 9-8. Transverse load capacity predictions for 6-in-thick walls constructed from Klondike solid block for walls heights ranging from 5 to 10 ft (Hybrid Theoretical Thrust Model).

9.1.1.2.2 Hybrid Lateral Displacement Model

As seen in the flowchart in figure 9-3, the Hybrid Lateral Displacement Model determines the lateral displacement force from a multivariable relationship from the $Ex(t/L)^2$ term and preload, both of which are considered to be known parameters. The multivariable linear regression analysis based on 91 laboratory tests of various wall constructions is summarized in table 9-5. Equation 9.4 is used to compute lateral displacement of the wall. Table 9-4 documented the multivariable regression analysis results used to determine the resultant thrust position factor (d) for the Hybrid Thrust Model. This equation is also used for computing the resultant thrust adjustment factor for this model, except the calculated thrust forces are used instead of the measured thrust forces.

$$\text{Lateral Displacement} = -0.0009 \times Ex(t/L)^2 - 0.0023 \times \text{Preload} + 1.8776 \quad \textbf{(9.4)}$$

Regression Statistics	
Multiple R	0.7499
R Square	0.5623
Adjusted R Square	0.5524
Standard Error	0.3978
Observations	91

Table 9-5. Multivariable regression analysis for determining lateral displacement.

ANOVA

	df	SS	MS	F	Significance F
Regression	2	17.8906	8.9453	56.5349	0.0000
Residual	88	13.9239	0.1582		
Total	90	31.8146			

	Coefficients	Standard Error	t Stat	P-value	Lower 95%	Upper 95%	Lower 95.0%	Upper 95.0%
Intercept	1.877627	0.121658	15.433636	0.000000	1.635857	2.119397	1.635857	2.119397
$E * (t/L)^2$	-0.000862	0.000252	-3.422179	0.000945	-0.001362	-0.000361	-0.001362	-0.000361
Preload	-0.002297	0.000217	-10.588914	0.000000	-0.002728	-0.001866	-0.002728	-0.001866

Figure 9-9 compares the results of the predicted transverse load capacities from the hybrid theoretical lateral displacement model with the measured laboratory test results for half-wall heights of 30, 45, and 60 inches with varying preloads. As seen from the graph, the predictions overall are similar to the hybrid theoretical thrust model presented in figure 9-7, slightly more accurate for the highest wall and slightly less accurate for the shortest wall. Figure 9-10 shows transverse load predictions using the hybrid theoretical lateral displacement for 6-in-thick walls constructed from Klondike block ranging in height from 5 to 10 feet in one foot increments with preloads ranging from 0 to 600 psi.

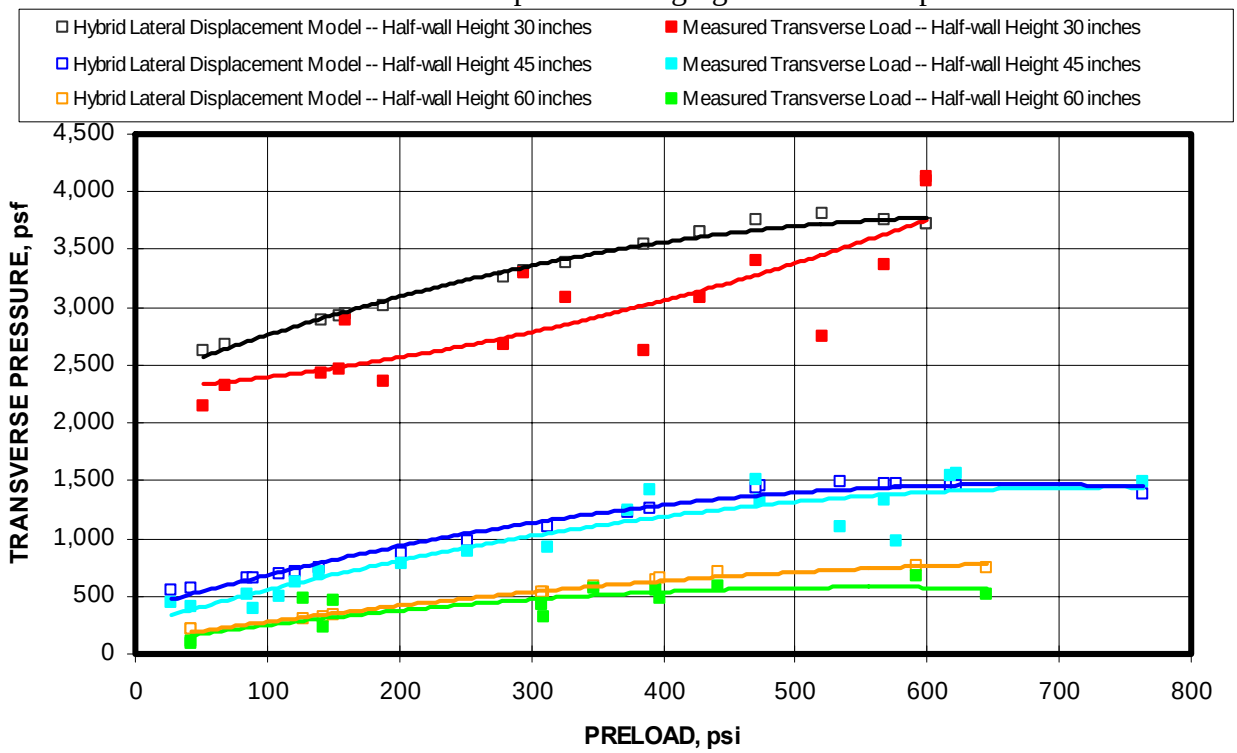

Figure 9-9. Comparison of transverse load capacities from design equations to the measured transverse load from laboratory tests (Hybrid Theoretical Lateral Displacement Model).

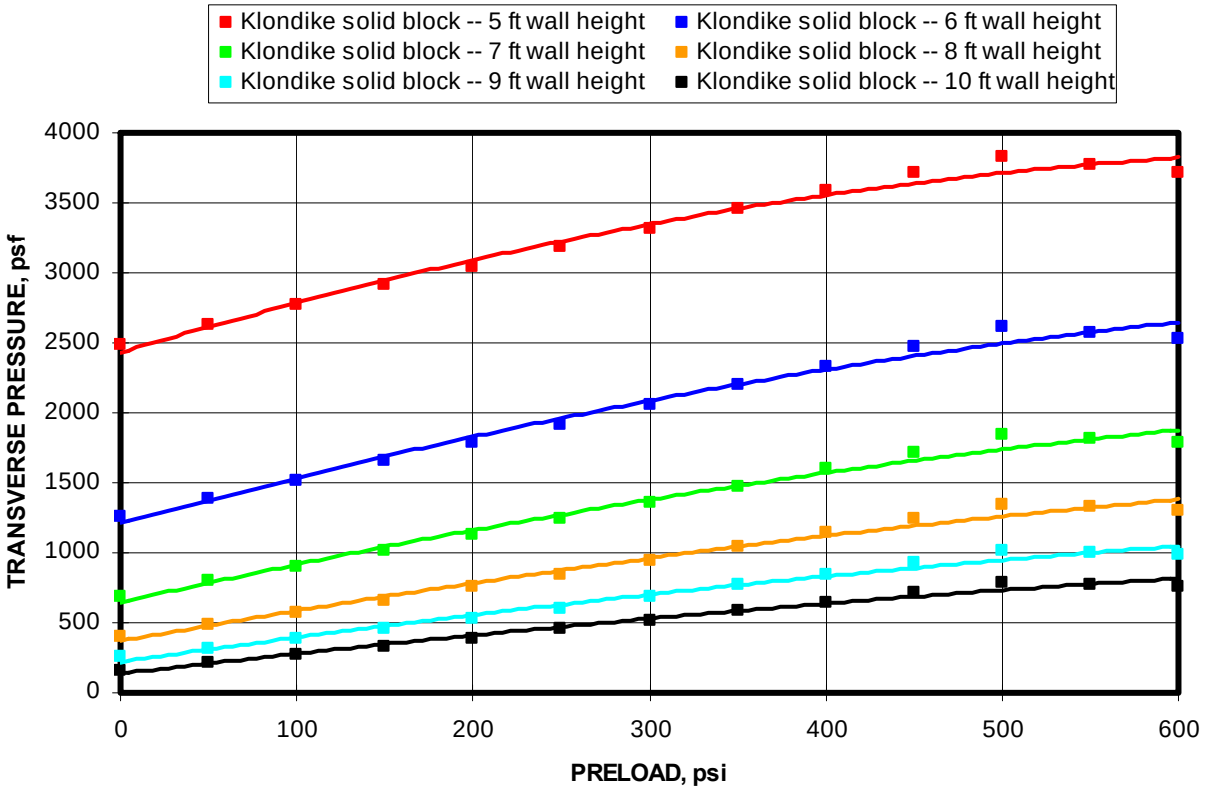

Figure 9-10. Transverse load capacity predictions for 6-in-thick walls constructed from Klondike solid block for walls heights ranging from 5 to 10 ft (Hybrid Theoretical Lateral Displacement Model).

9.1.1.2.3 Hybrid Combination Model

The Hybrid Combination Model combines the previous two models by empirically determining both the thrust and lateral displacement. Figure 9-11 compares this model's predictions of transverse load capacity to the measured transverse load capacities from the laboratory testing. The results are similar to the other two models, but overall are slightly more accurate, especially for the higher walls. For completeness, figure 9-12 is included which displays the transverse load predictions using the hybrid theoretical combination model for 6-in-thick walls constructed from Klondike block ranging in height from 5 to 10 feet in one foot increments with preloads ranging from 0 to 600 psi.

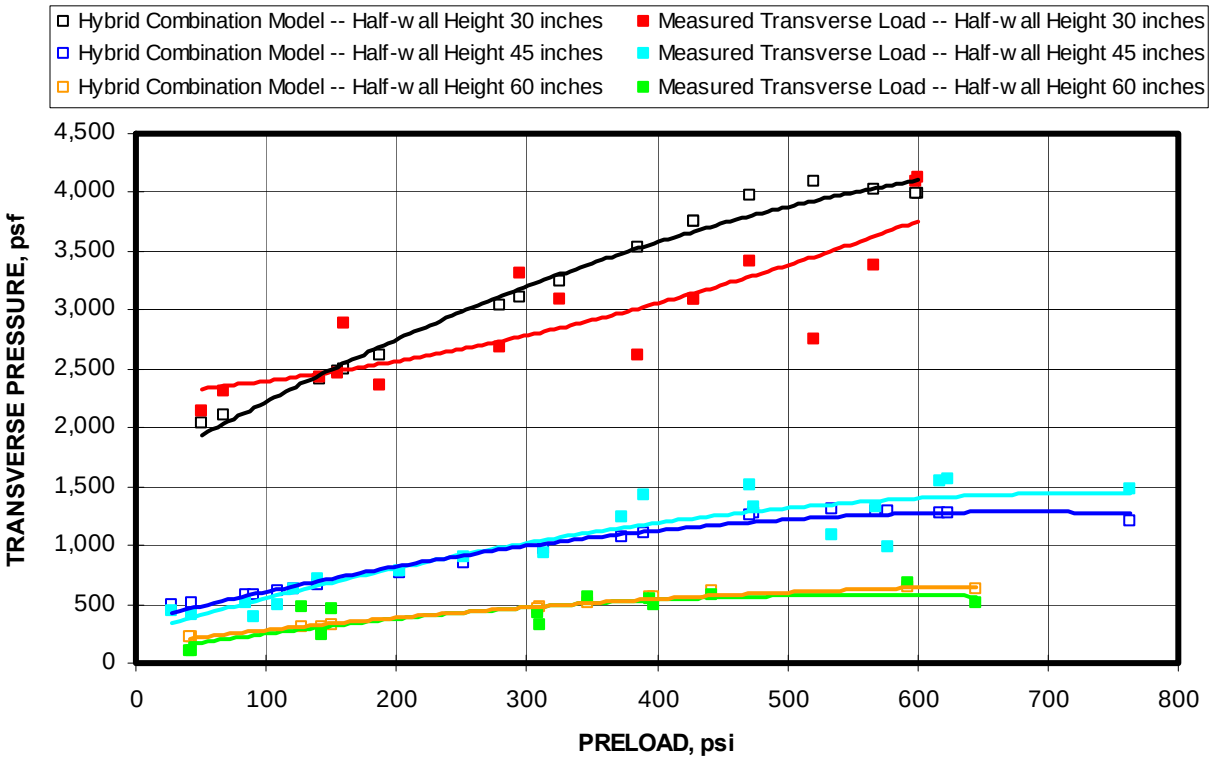

Figure 9-11. Comparison of transverse load capacities from design equations to the measured transverse load from laboratory tests (Hybrid Theoretical Combination Model).

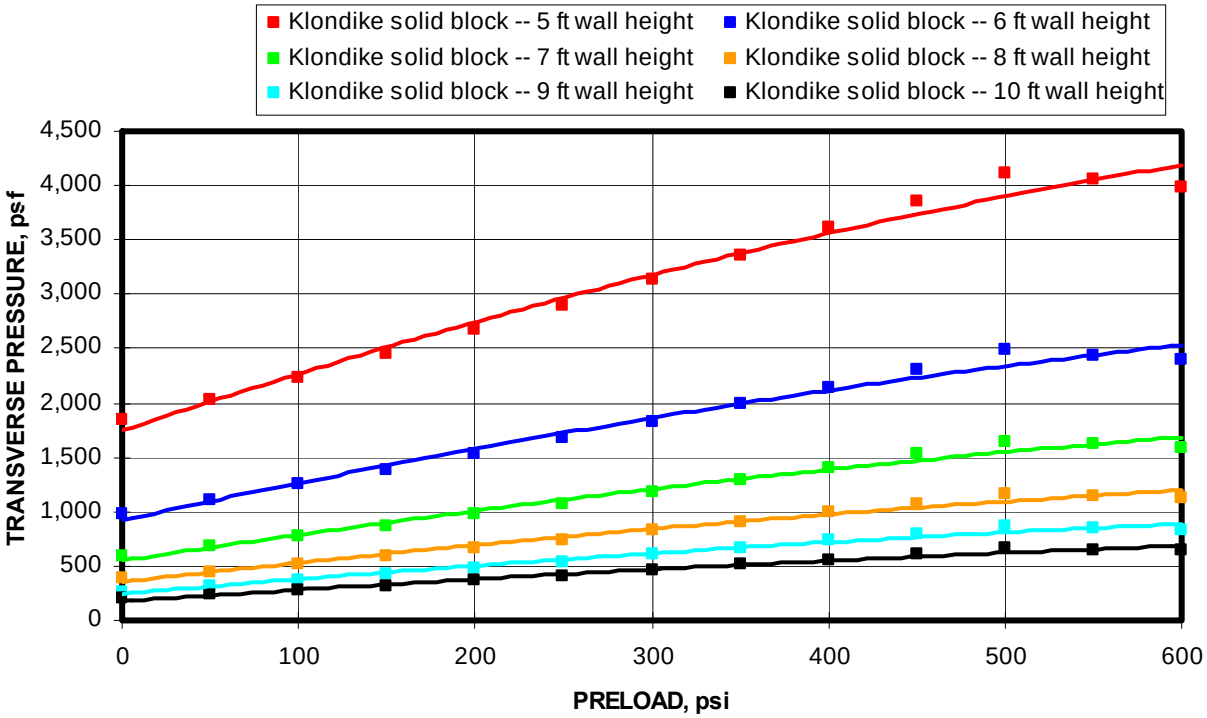

Figure 9-12. Transverse load capacity predictions for 6-in-thick walls constructed from Klondike solid block for walls heights ranging from 5 to 10 ft (Hybrid Theoretical Combination Model).

9.1.1.3 Summary of Design Equations for Klondike Block

In summary, a full empirical design model and three hybrid theoretical design models were developed for the Klondike block stopping constructions. Figure 9-13 displays the calculated transverse load capacities from the full empirical model compared to the measured capacities from the MRS tests. The dashed line represents a perfect correlation between the calculated and measured capacities. The red trend line represents the linear regression between the measured and calculated capacities. The regression line shows that on average the model tends to under predict the transverse pressure by 3 pct. The shaded blue area is a +/- 400 psf variation from the perfect correlation. Examining the chart, it is seen that 85% of the data falls within this variation. Figure 9-14 displays this same information for the three hybrid theoretical design models. Based on the regression trend line correlating the calculated transverse pressures to the measured transverse pressures, the combination model, which computes both the thrust and lateral displacement from laboratory test data, is the most accurate of the three, with a 3 pct difference between the calculated and measured pressures. The least accurate is the lateral displacement model with a 12 pct difference. Examining the +/-400 psf variation (blue shading), the thrust model and the combination model have 90% of the data within this variation, while the lateral displacement model has only 81 pct of the data within this tolerance.

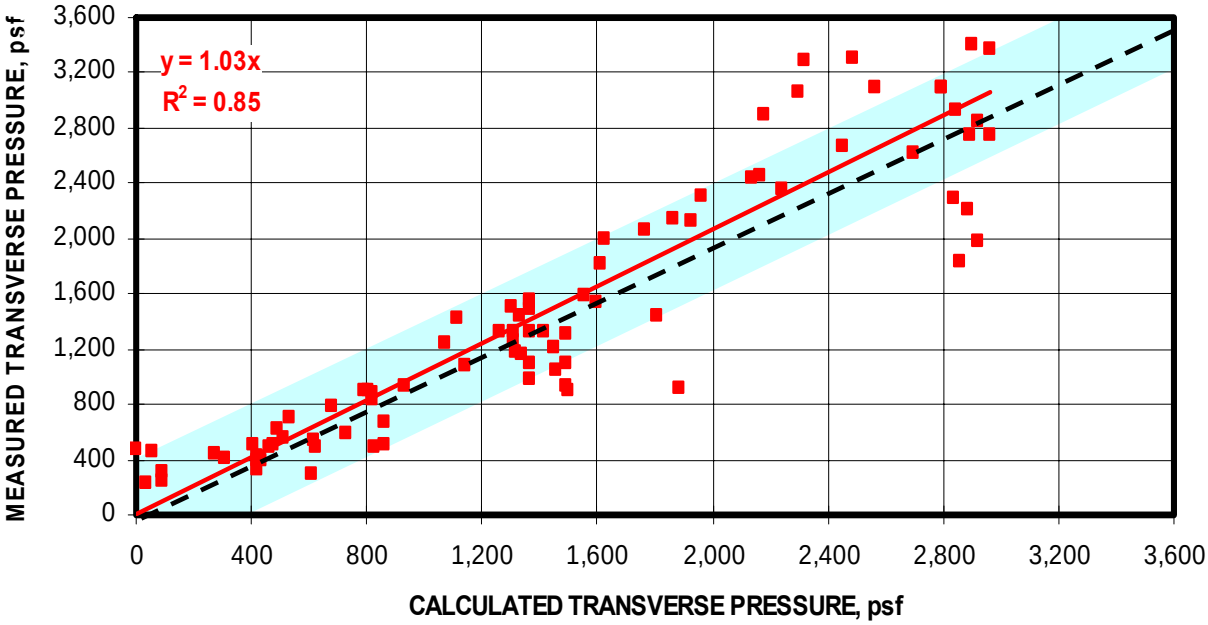

Figure 9-13. Comparison of predicted transverse load capacities compared to the measured capacities for the MRS laboratory tests (Full Empirical Model).

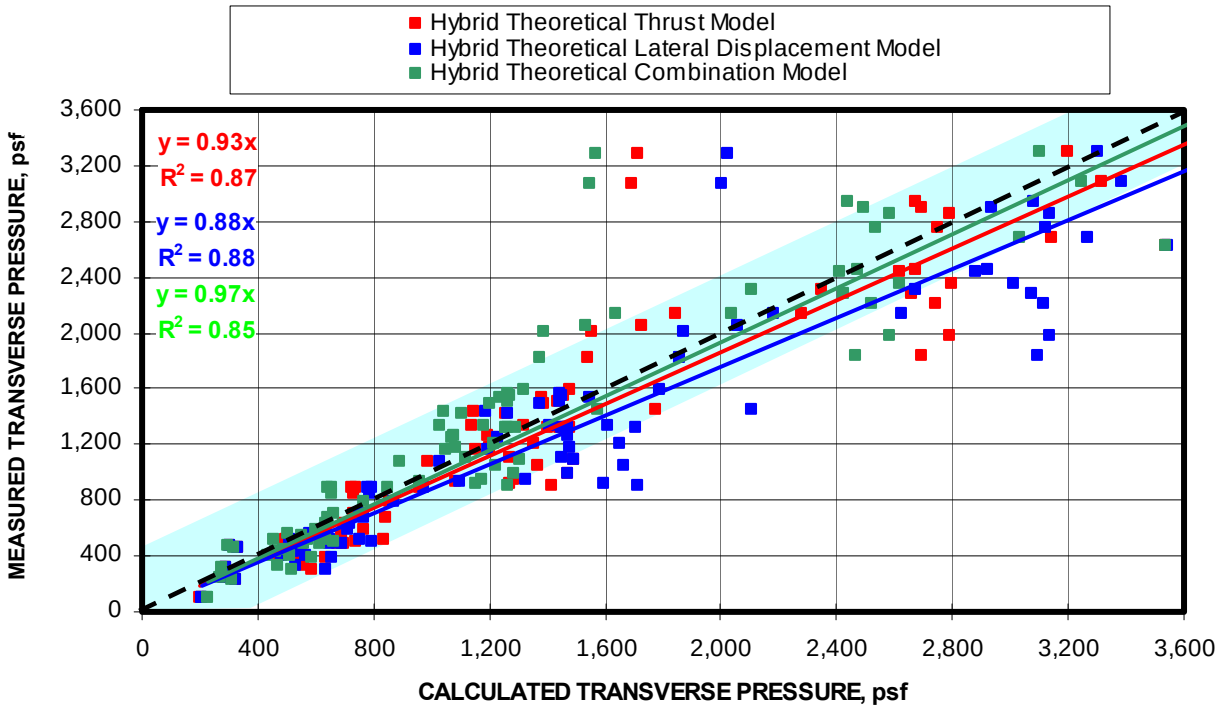

Figure 9-14. Comparison of predicted transverse load capacities compared to the measured capacities for the MRS laboratory tests (Hybrid Theoretical Models).

9.1.4 Peerless Backsaver Block

The Peerless Backsaver block is also a conventional Portland cement block with lighter weight aggregate to reduce the block weight. The block measures nominally 6x8x16-in and weighs about 40 lbs compared to the 50 lb weight of the Klondike block.

9.1.2.1 Full Empirical Model

Table 9-6 shows the results of the multivariable regression analysis correlating the transverse pressure to the $Ex(t/L)^2$ and preload. From this regression analysis, the design equation for Peerless Backsaver block is shown in equation 9.5.

$$\text{Transverse Load} = 7.2992 \times Ex(t/L)^2 + 1.4732 \times \text{Preload} - 823.0570 \quad \textbf{(9.5)}$$

Where E = material modulus = 45,000 psi for Peerless Backsaver block,

t = wall thickness, in,

L = full wall height, in, and

Preload = ground pressure preload, psi.

Table 9-6. Multivariable regression analysis for determining transverse load from modulus and wall geometric parameters.

Regression Statistics	
Multiple R	0.9646
R Square	0.9305
Adjusted R Square	0.9255
Standard Error	266.6961
Observations	31

ANOVA

	df	SS	MS	F	Significance F
Regression	2	26644022.68	13322011	187.2994	0.0000
Residual	28	1991550.617	71126.81		
Total	30	28635573.3			

	Coefficients	Standard Error	t Stat	P-value	Lower 95%	Upper 95%	Lower 95.0%	Upper 95.0%
Intercept	-823.0570	137.3686	-5.9916	0.0000	-1104.4442	-541.6698	-1104.4442	-541.6698
E x $(t/L)^2$	7.2992	0.3856	18.9316	0.0000	6.5094	8.0889	6.5094	8.0889
Preload	1.4732	0.4763	3.0932	0.0045	0.4976	2.4488	0.4976	2.4488

Figure 9-15 displays the accuracy of the model for the three wall heights that were evaluated in the laboratory test program. Plotted on this graph are the measured transverse pressure from the laboratory tests and the calculated transverse pressure using equation 9-5 for that particular construction. As seen in the figure, the model predictions are most accurate for the 45-in half-wall height and least accurate for the 30-in half-wall height. The transverse capacity is under predicted at high preloads for the 30-in half-wall height. Since the laboratory tests results were least consistent at the low heights, and this is an empirical model, then it makes sense that the model is least accurate for this height as well. The 45-in high performance is accurately predicted by the empirical formula. The transverse pressure is consistently under predicted by about 150 psf for the 60-in-high tests. Figure 9-16 shows transverse load predictions using this empirical design model for 6-in-thick walls constructed from Peerless Backsaver block ranging in height from 5 to 10 feet in one foot increments with preloads ranging from 0 to 500 psi.

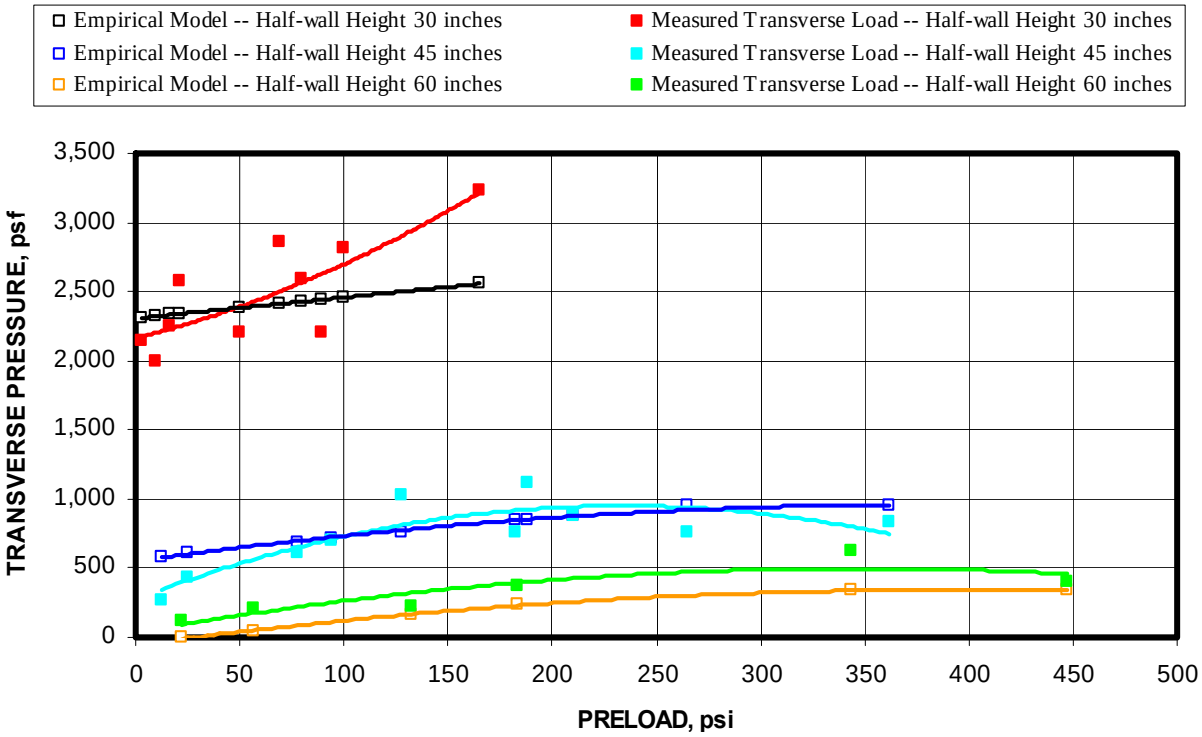

Figure 9-15. Comparison of design equation predictions with measured transverse load from laboratory testing (Full Empirical Model – Peerless Backsaver block).

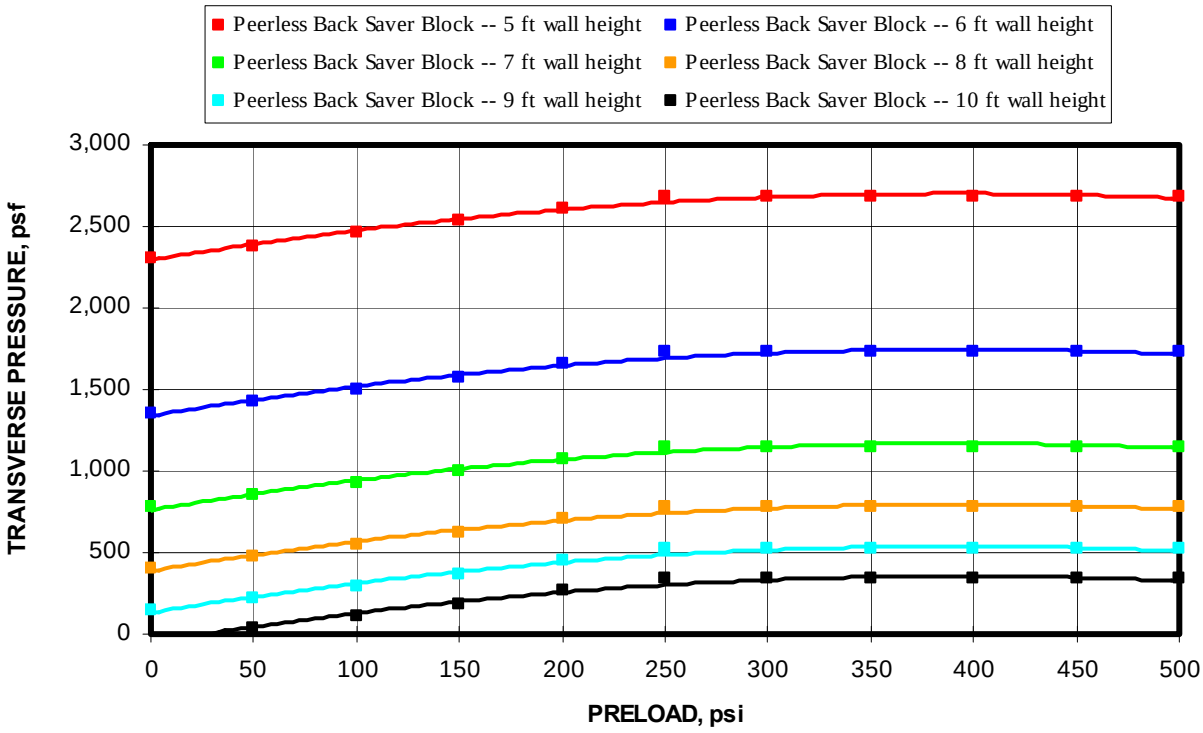

Figure 9-16. Transverse load capacity predictions for 6-in-thick walls constructed from Peerless Backsaver block for walls heights ranging from 5 to 10 ft (Full Empirical Model).

9.1.2.2 Hybrid Theoretical Models

Transverse load capacity forecasts will be made using the three hybrid theoretical models: (1) Hybrid Thrust Model, (2) Hybrid Lateral Displacement Model, and (3) Hybrid Combination Thrust and Lateral Displacement Model.

9.1.2.2.1 Hybrid Thrust Model

As seen in the flowchart in figure 9-2, the Hybrid Thrust Model determines the normalized thrust force from a multivariable relationship between the thrust force and the $Ex(t/L)^2$ term and preload, both of which are considered to be known parameters. The multivariable linear regression analysis based on 31 laboratory tests of various wall constructions is summarized in table 9-7. Equation 9.6 is used to compute the normalized thrust force per unit width of wall. Table 9-8 documents the multivariable regression analysis results used to determine the resultant thrust position factor (d).

Table 9-7. Multivariable regression analysis for determining arching thrust.

Regression Statistics	
Multiple R	0.9347
R Square	0.8736
Adjusted R Square	0.8646
Standard Error	0.2333
Observations	31

ANOVA

	df	SS	MS	F	Significance F
Regression	2	10.5350	5.2675	96.7916	0.0000
Residual	28	1.5238	0.0544		
Total	30	12.0588			

	Coefficients	Standard Error	t Stat	P-value	Lower 95%	Upper 95%	Lower 95.0%	Upper 95.0%
Intercept	0.2142	0.1202	1.7828	0.0855	-0.0319	0.4604	-0.0319	0.4604
E*(t/L)^2	0.0041	0.0003	12.1584	0.0000	0.0034	0.0048	0.0034	0.0048
Preload	0.0045	0.0004	10.7029	0.0000	0.0036	0.0053	0.0036	0.0053

$$P/BL = 0.0041 \times Ex(t/L)^2 + 0.0045 \times Preload + 0.2142 \quad \textbf{(9.6)}$$

Where P/BL = Normalized thrust per unit width of block, kips/in,

E = Elastic modulus = 45,000 psi for Peerless Backsaver block,

t = wall thickness, in,

L = height of wall, in, and

Preload = preload pressure, psi.

Regression Statistics	
Multiple R	0.4035961
R Square	0.1628898
Adjusted R Square	0.1030963
Standard Error	0.0856843
Observations	31

Table 9.8. Multivariable regression analysis for determining resultant thrust position.

ANOVA

	df	SS	MS	F	Significance F
Regression	2	0.0400	0.0200	2.7242	0.0830
Residual	28	0.2056	0.0073		
Total	30	0.2456			

	Coefficients	Standard Error	t Stat	P-value	Lower 95%	Upper 95%	Lower 95.0%	Upper 95.0%
Intercept	0.9222	0.0764	12.0676	0.0000	0.7657	1.0787	0.7657	1.0787
Half-wall Height	-0.0016	0.0013	-1.2474	0.2226	-0.0044	0.0011	-0.0044	0.0011
Thurst	-0.0026	0.0013	-2.0064	0.0546	-0.0052	0.0001	-0.0052	0.0001

Resultant Thrust Adjustment Factor (d) = -.0016 x half-wall height - .0026 x Thrust + .9222 **(9.7)**

Figure 9-17 compares the results of the predicted transverse load capacities from the hybrid theoretical thrust model with the measured laboratory test results for half-wall heights of 30, 45, and 60 inches with varying preloads. As seen from the graph, the predictions overall are improved compared to the full empirical model presented in figure 9-15 for all three wall heights. Figure 9-18 shows transverse pressure predictions using this empirical design model for 6-in-thick walls constructed from Peerless Backsaver ranging in height from 5 to 10 feet in one foot increments with preloads ranging from 0 to 500 psi.

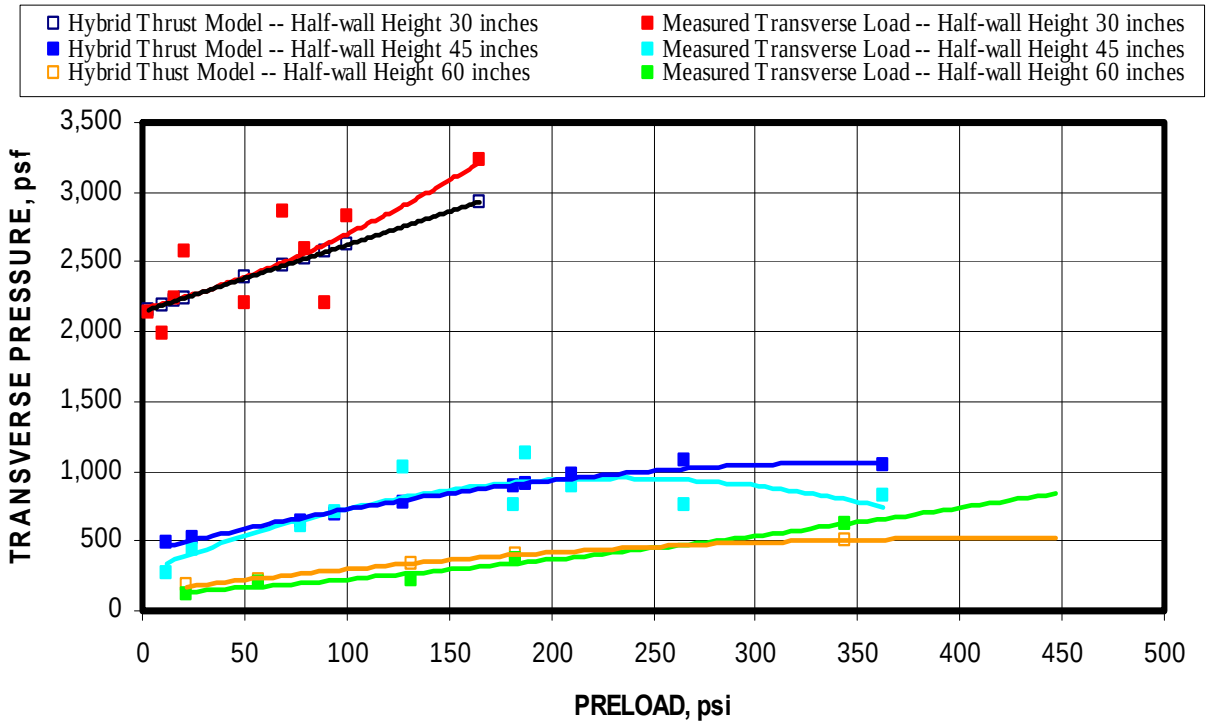

Figure 9-17. Comparison of transverse load capacities from design equations to the measured transverse load from laboratory tests (Hybrid Theoretical Thrust Model).

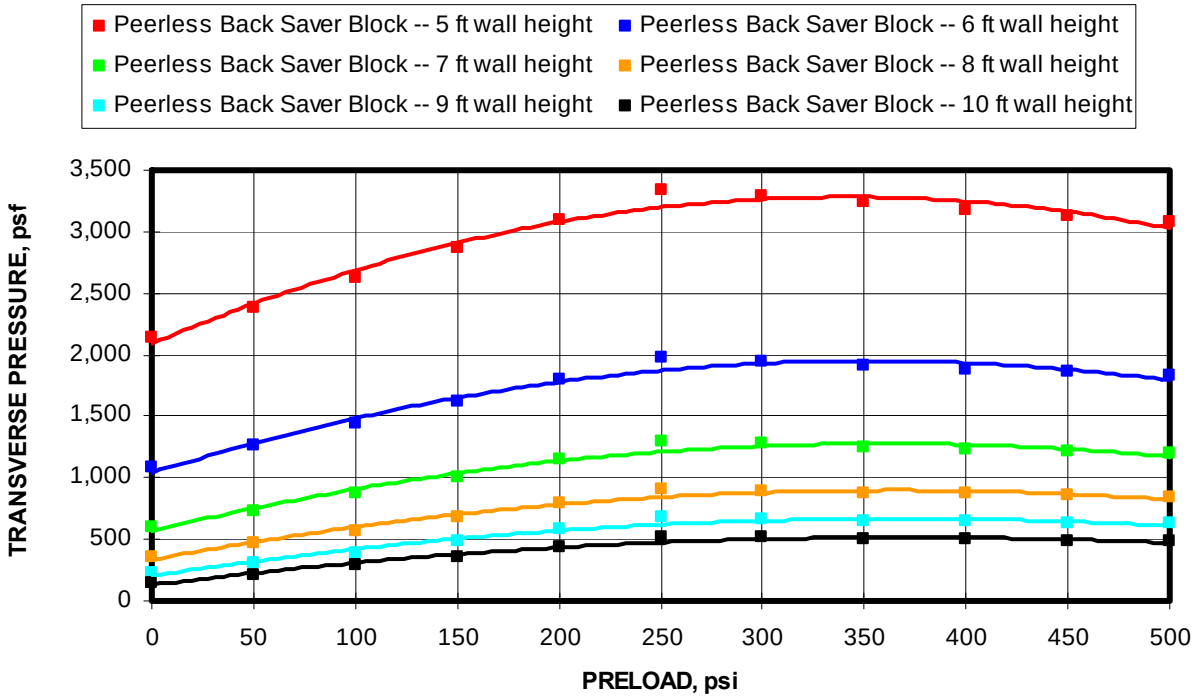

Figure 9-18. Transverse load capacity predictions for 6-in-thick walls constructed from Peerless Backsaver block for walls heights ranging from 5 to 10 ft (Hybrid Theoretical Thrust Model).

9.1.2.2.2 Hybrid Lateral Displacement Model

As seen in the flowchart in figure 9-3, the Hybrid Lateral Displacement Model determines the lateral displacement from a multivariable relationship from the $Ex(t/L)^2$ term and preload, both of which are considered to be known parameters. The multivariable linear regression analysis based on 31 laboratory tests of various wall constructions is summarized in table 9-9. Equation 9.8 is used to compute the lateral wall displacement. Table 9-8 documented the multivariable regression analysis results used to determine the resultant thrust position factor (d) for the Hybrid Thrust Model. This equation is also used for computing the resultant thrust adjustment factor for this model, except the calculated thrust forces are used instead of the measured thrust forces.

$$\text{Lateral Displacement} = -0.0023 \times Ex(t/L)^2 - 0.0026 \times \text{Preload} + 2.3454 \quad \textbf{(9.8)}$$

Regression Statistics	
Multiple R	0.7190
R Square	0.5169
Adjusted R Square	0.4824
Standard Error	0.3377
Observations	31

Table 9-9. Multivariable regression for determining lateral displacement.

ANOVA

	df	SS	MS	F	Significance F
Regression	2	3.4179	1.7090	14.9814	0.0000
Residual	28	3.1940	0.1141		
Total	30	6.6120			

	Coefficients	Standard Error	t Stat	P-value	Lower 95%	Upper 95%	Lower 95.0%	Upper 95.0%
Intercept	2.3454	0.1740	13.4823	0.0000	1.9891	2.7018	1.9891	2.7018
E*(t/L)^2	-0.0023	0.0005	-4.6992	0.0001	-0.0033	-0.0013	-0.0033	-0.0013
Preload	-0.0026	0.0006	-4.3164	0.0002	-0.0038	-0.0014	-0.0038	-0.0014

Figure 9-19 compares the results of the predicted transverse load capacities from the hybrid theoretical lateral displacement model with the measured laboratory test results for half-wall heights of 30, 45, and 60 inches with varying preloads. As seen from the graph, the predictions overall are slightly worse than those provided by the hybrid thrust model. Figure 9-20 shows transverse load predictions using the hybrid theoretical lateral displacement for 6-in-thick walls constructed from Peerless Backsaver block ranging in height from 5 to 10 feet in one foot increments with preloads ranging from 0 to 500 psi.

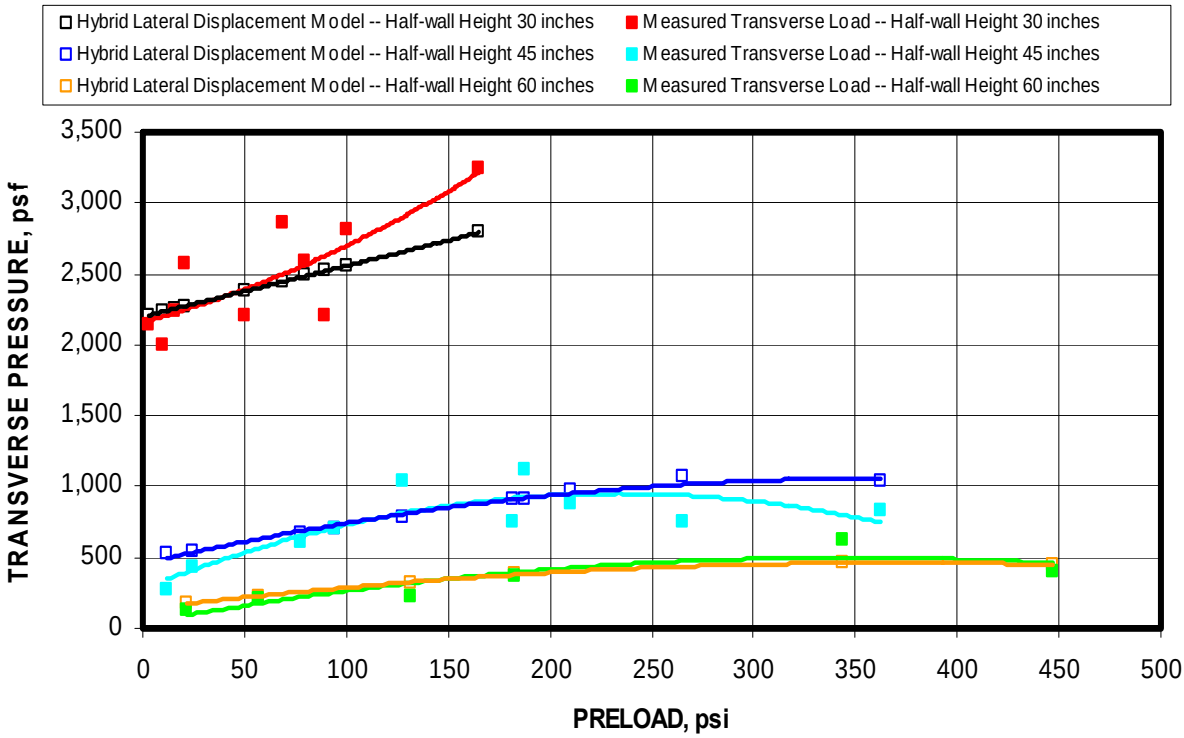

Figure 9-19. Comparison of transverse load capacities from design equations to the measured transverse load from laboratory tests (Hybrid Theoretical Lateral Displacement Model).

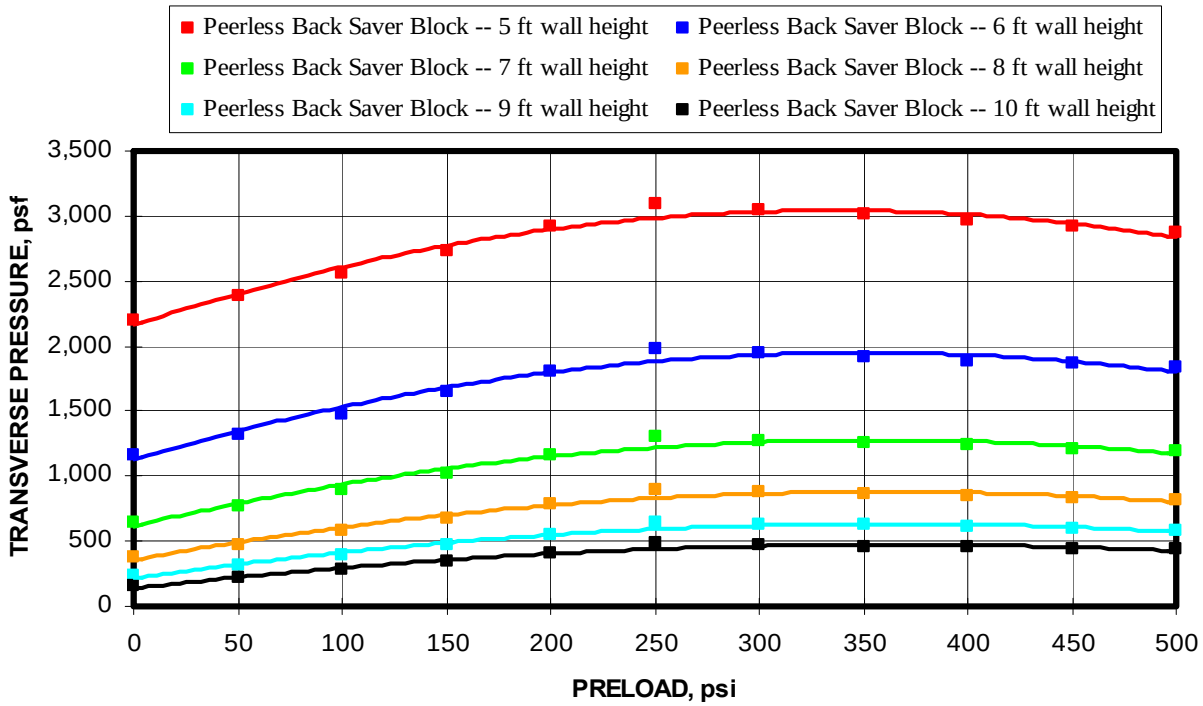

Figure 9-20. Transverse load capacity predictions for 6-in-thick walls constructed from Peerless Backsaver block for walls heights ranging from 5 to 10 ft (Hybrid Theoretical Lateral Displacement Model).

9.1.2.2.3 Hybrid Combination Model

The Hybrid Combination Model combines the previous two models by empirically determining both the thrust and lateral displacement. Figure 9-21 compares this model's predictions of transverse load capacity to the measured transverse load capacities from the laboratory testing. The results are similar to the other two models, but overall are slightly more accurate, especially for the shorter walls. For completeness, figure 9-21 is included which displays the transverse load predictions using the hybrid theoretical combination model for 6-in-thick walls constructed from Peerless Backsaver block ranging in height from 5 to 10 feet in one foot increments with preloads ranging from 0 to 500 psi.

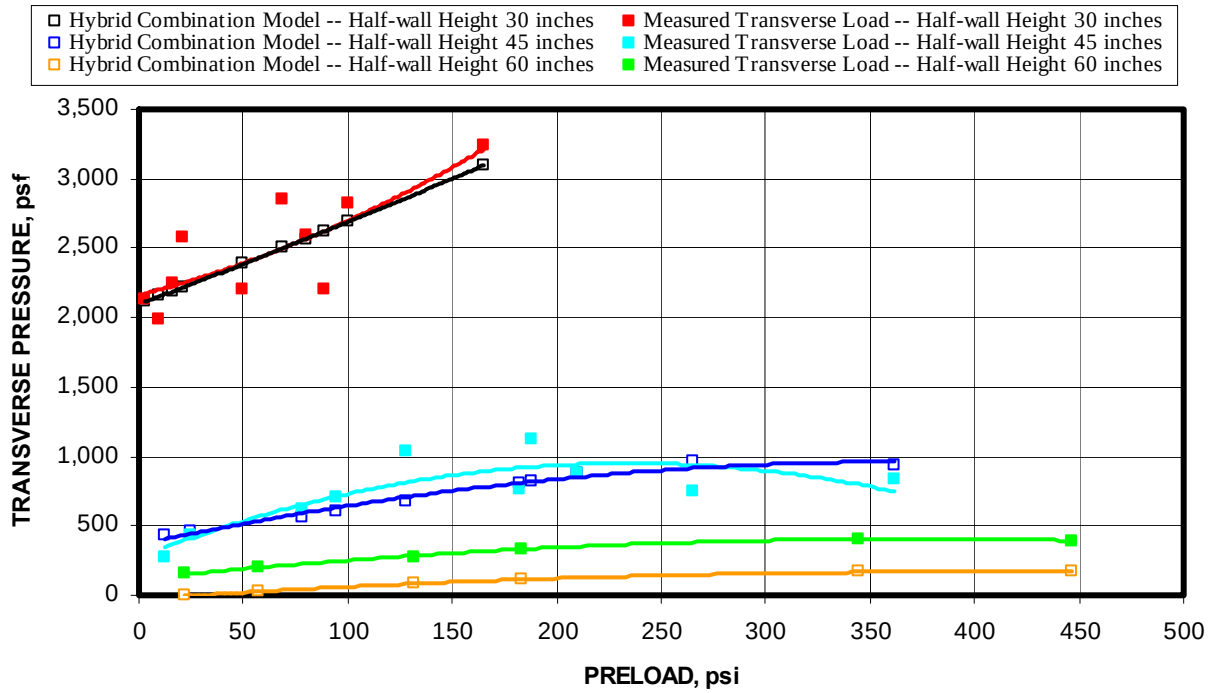

Figure 9-21. Comparison of transverse load capacities from design equations to the measured transverse load from laboratory tests (Hybrid Theoretical Combination Model).

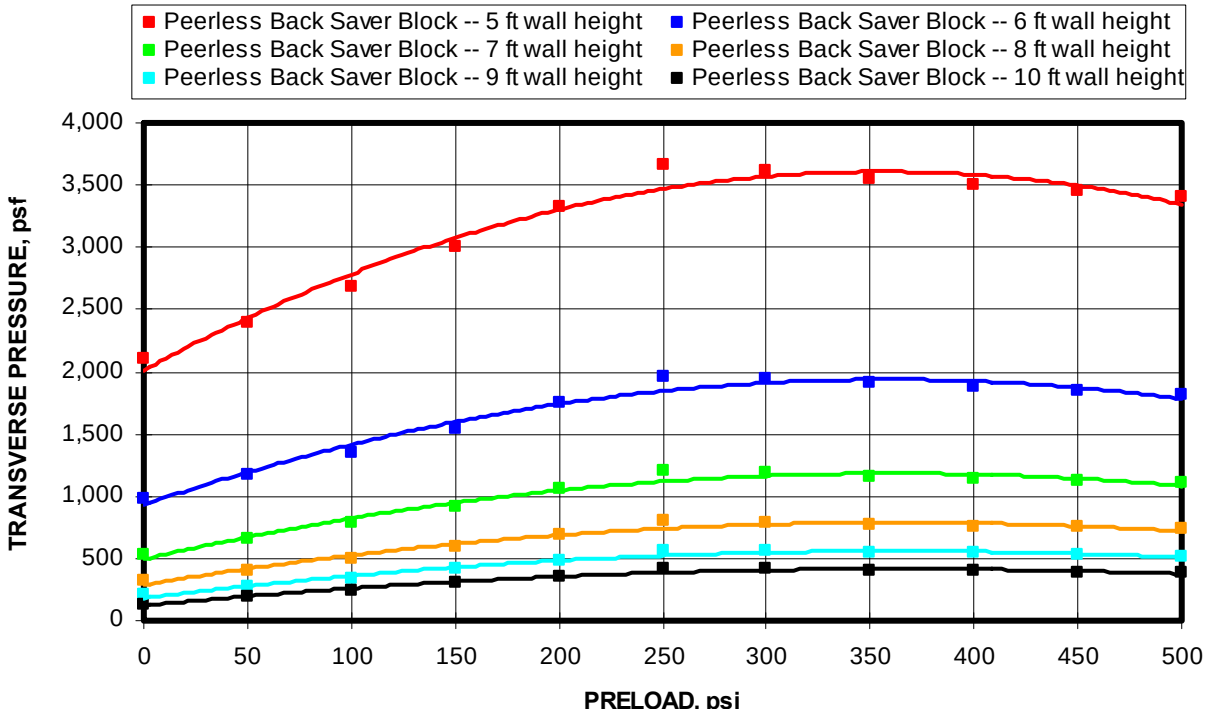

Figure 9-22. Transverse load capacity predictions for 6-in-thick walls constructed from Peerless Backsaver block for walls heights ranging from 5 to 10 ft (Hybrid Theoretical Combination Model).

9.1.2.3 Summary of Design Equations for Peerless Backsaver Block

In summary, a full empirical design model and three hybrid theoretical design models were developed for the Peerless Backsaver block stopping constructions. Figure 9-23 displays the calculated transverse load capacities from full empirical model compared to the measured capacities from the MRS tests. The dashed line represents a perfect correlation between the calculated and measured capacities. The red trend line represents the linear regression between the measured and calculated capacities. The regression line shows less than 1 pct difference between the measured and calculated transverse pressure for the empirical model. The shaded blue area is a +/- 400 psf variation from the perfect correlation. Examining the chart, it is seen that 93% of the data falls within this variation. Figure 9-24 displays this same information for the three hybrid theoretical design models. All three models produced very accurate results based on the regression trend line correlating the calculated transverse loads to the measured transverse loads with less than 1 pct differences between measured and calculated transverse load. Examining the +/-400 psf variation (blue shading), all three models have 96% of the data within this variation.

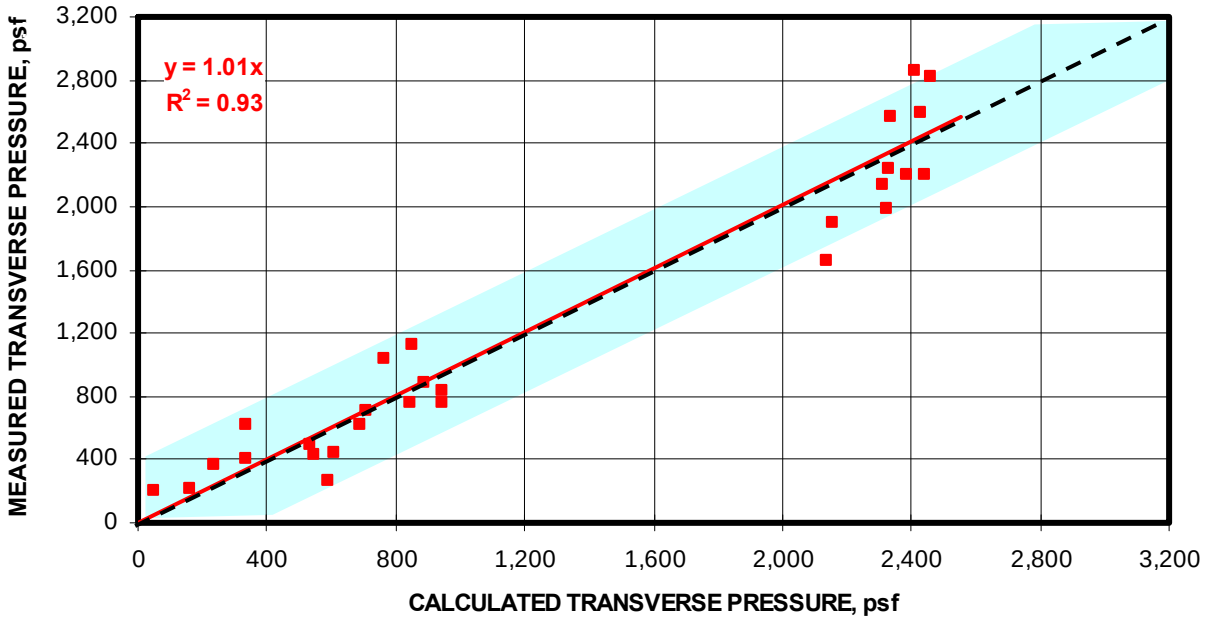

Figure 9-23. Comparison of predicted transverse load capacities compared to the measured capacities for the MRS laboratory tests (Full Empirical Model).

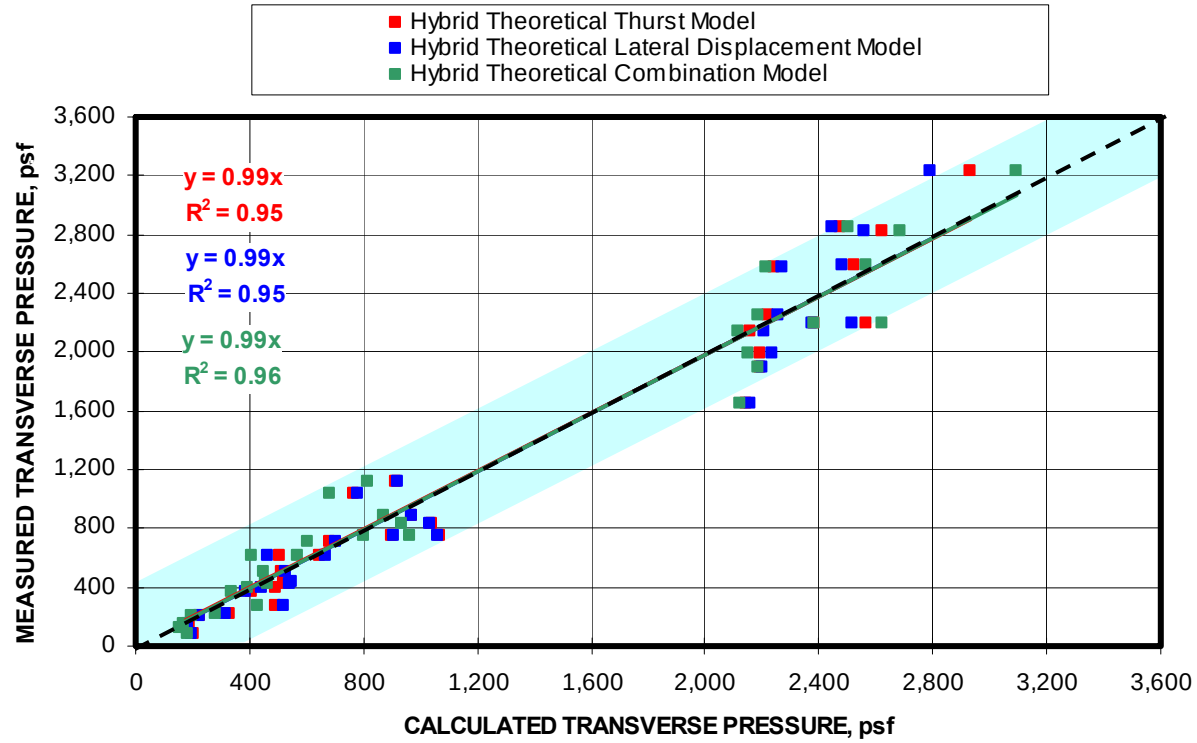

Figure 9-24. Comparison of predicted transverse load capacities compared to the measured capacities for the MRS laboratory tests (Hybrid Theoretical Models).

9.1.3 ACCOA Autoclaved Aerated Concrete Block

The ACCOA Autoclaved Aerated Concrete Block is an aerated concrete block that is a different class of block than the conventional CMU. The low density allows for a larger block size. The block measures nominally 6x12x24 inches or 8x12x24 inches. The 6-in-thick block weighs 16 lbs, comparable to that the smaller-sized CMU blocks.

9.1.2.1 Full Empirical Model

Table 9-10 shows the results of the multivariable regression analysis correlating the transverse load to the $Ex(t/L)^2$ and preload. From this regression analysis, the design equation for ACCOA block is shown in equation 9.9.

$$\text{Transverse Load} = 5.7270 \times Ex(t/L)^2 + 0.6562 \times \text{Preload} - 252.8541 \quad \textbf{(9.9)}$$

Where E = material modulus = 20,000 psi for ACCOA block,

t = wall thickness, in,

L = full wall height, in, and

Preload = ground pressure preload, psi.

Table 9-10. Multivariable regression analysis for determining transverse load from modulus and wall geometric parameters.

Regression Statistics	
Multiple R	0.9254
R Square	0.8564
Adjusted R Square	0.8373
Standard Error	75.4559
Observations	18

ANOVA

	df	SS	MS	F	Significance F
Regression	2	509362	254681	44.7311	0.0000
Residual	15	85404	5694		
Total	17	594766			

	Coefficients	Standard Error	t Stat	P-value	Lower 95%	Upper 95%	Lower 95.0%	Upper 95.0%
Intercept	-252.8541	71.6948	-3.5268	0.0031	-405.6681	-100.0402	-405.6681	-100.0402
E x $(t/L)^2$	5.7270	0.6126	9.3486	0.0000	4.4213	7.0328	4.4213	7.0328
Preload	0.6562	0.2009	3.2659	0.0052	0.2280	1.0845	0.2280	1.0845

Figure 9-25 displays the accuracy of the model. Only one height was evaluated in the test program. Two block widths, 6 and 8 inches, were evaluated. Plotted on this graph are

the measured transverse pressure from the laboratory tests and the calculated transverse pressure using equation 9-9. As seen in the figure, the model predictions are most accurate for the 6-in-thick half-walls. In general, thicker wall constructions for all block types behave more erratic. A limited number of tests, particularly with the 8-inch-thick walls due to limited block availability, are also contributing to the variability in the model predictions. Figure 9-26 shows transverse pressure predictions using this empirical design model for 6-in-thick walls constructed from ACCOA block ranging in height from 5 to 10 feet in one foot increments with preloads ranging from 0 to 300 psi.

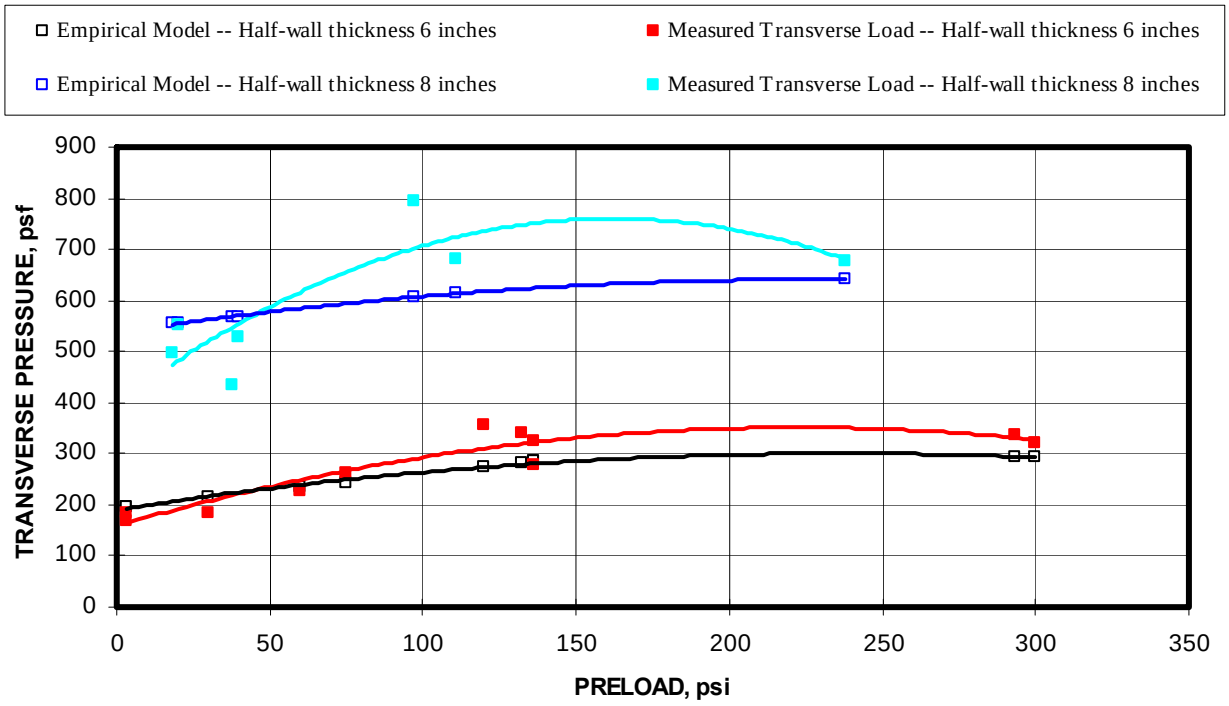

Figure 9-25. Comparison of design equation predictions with measured transverse load from laboratory testing (Full Empirical Model – ACCOA block).

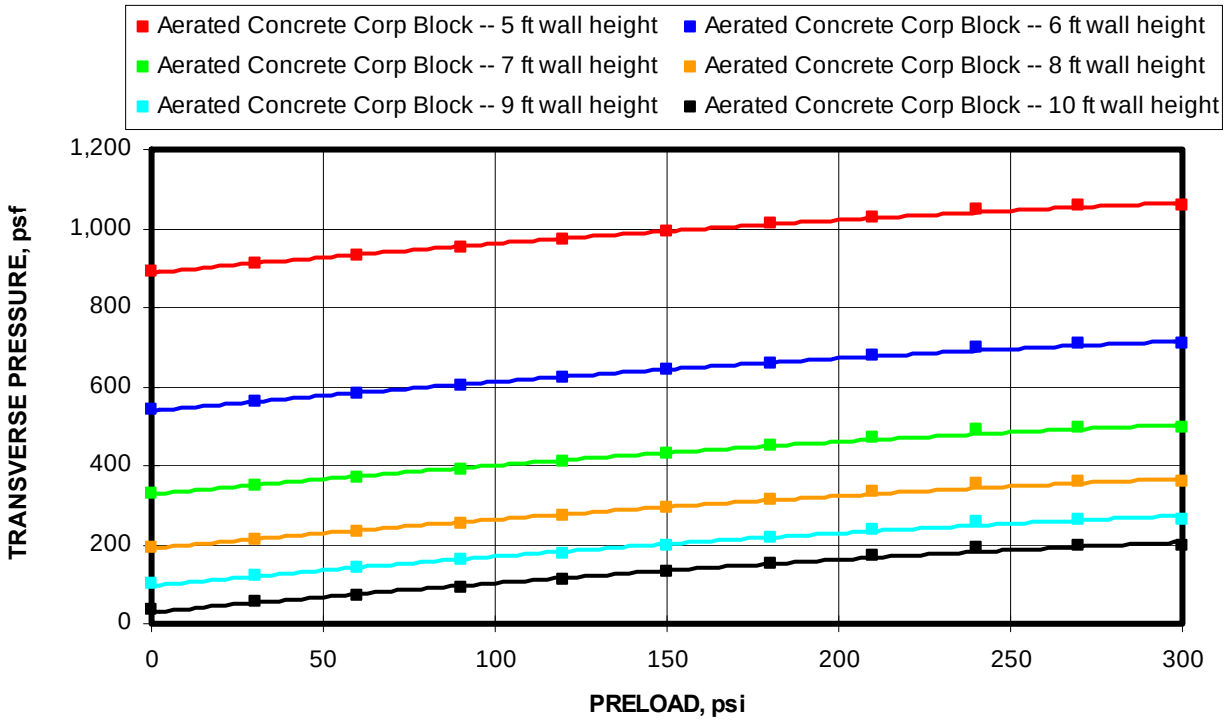

Figure 9-26. Transverse load capacity predictions for 6-in-thick walls constructed from ACCOA block for walls heights ranging from 5 to 10 ft (Full Empirical Model).

9.1.3.2 Hybrid Theoretical Models

Since testing was conducted at only one height, the hybrid theoretical models, which require empirical assessment of the thrust force, became erratic at heights other than the test height. As a result, no further development of the hybrid theoretical models was pursued.

9.1.3.3 Summary of Design Equation for ACCOA block

Figure 9-27 displays the calculated transverse load capacities from the full empirical model compared to the measured capacities from the MRS tests. The dashed line represents a perfect correlation between the calculated and measured capacities. The red trend line represents the linear regression between the measured and calculated capacities. The regression trend line shows less than 1 pct difference between the measured and calculated transverse pressure. The shaded blue area is a +/- 100 psf variation from the perfect correlation. Examining the chart, it is seen that 89% of the data falls within this variation.

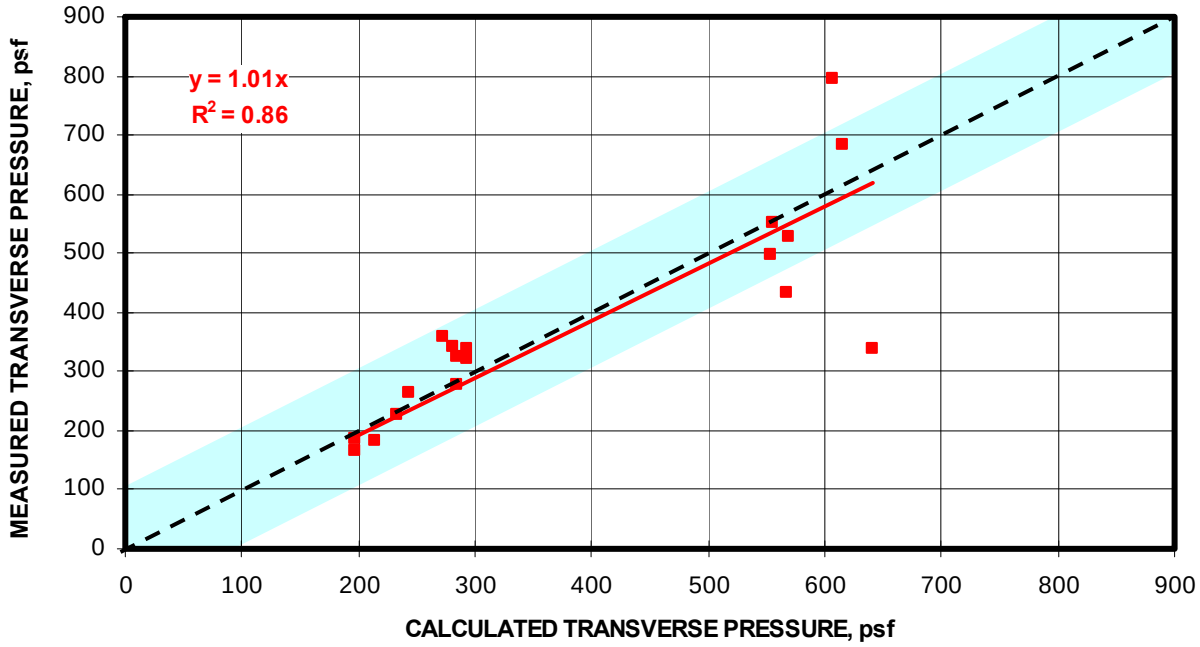

Figure 9-27. Comparison of predicted transverse load capacities compared to the measured capacities for the MRS laboratory tests (Full Empirical Model).

9.1.4 Ytong Block

The Ytong Block is also a cellular concrete block designed to provide a low density material that allows a large block size with a reasonable block weight. The block measures nominally 8x8x24 inches and weighs about 29 lbs.

9.1.4.1 Full Empirical Model

Table 9-11 shows the results of the multivariable regression analysis correlating the transverse load to the $Ex(t/L)^2$ and preload. From this regression analysis, the design equation for Ytong block is shown in equation 9.10.

$$\text{Transverse Load} = Ex(t/L)^2 \times 3.8807 + 2.9706 \times \text{Preload} - 452 \quad \textbf{(9.10)}$$

Where E = material modulus = 40,000 psi for Ytong block,

t = wall thickness, in,

L = full wall height, in, and

Preload = ground pressure preload, psi.

Regression Statistics	
Multiple R	0.9907
R Square	0.9815
Adjusted R Square	0.9787
Standard Error	124.8443
Observations	16

Table 9-11. Multivariable regression analysis for determining transverse load from modulus and wall geometric parameters.

ANOVA

	df	SS	MS	F	Significance F
Regression	2	10753022	5376511	344.9557	0.0000
Residual	13	202619	15586		
Total	15	10955642			

	Coefficients	Standard Error	t Stat	P-value	Lower 95%	Upper 95%	Lower 95.0%	Upper 95.0%
Intercept	-451.5333	83.2427	-5.4243	0.0001	-631.3683	-271.6984	-631.3683	-271.6984
E x (t/L)^2	3.8807	0.1485	26.1297	0.0000	3.5598	4.2015	3.5598	4.2015
Preload	2.9706	0.6612	4.4924	0.0006	1.5420	4.3991	1.5420	4.3991

Figure 9-28 compares the results of the predicted transverse load capacities from the hybrid theoretical thrust model with the measured laboratory test results for half-wall heights of 31.5, 47.25, and 63 inches with varying preloads. As seen from the graph, the predictions from the full empirical model are good for all three half-wall heights. Figure 9-29 shows transverse load predictions using this empirical design model for walls constructed from Ytong block ranging in height from 5 to 10 feet in one foot increments with preloads ranging from 0 to 200 psi.

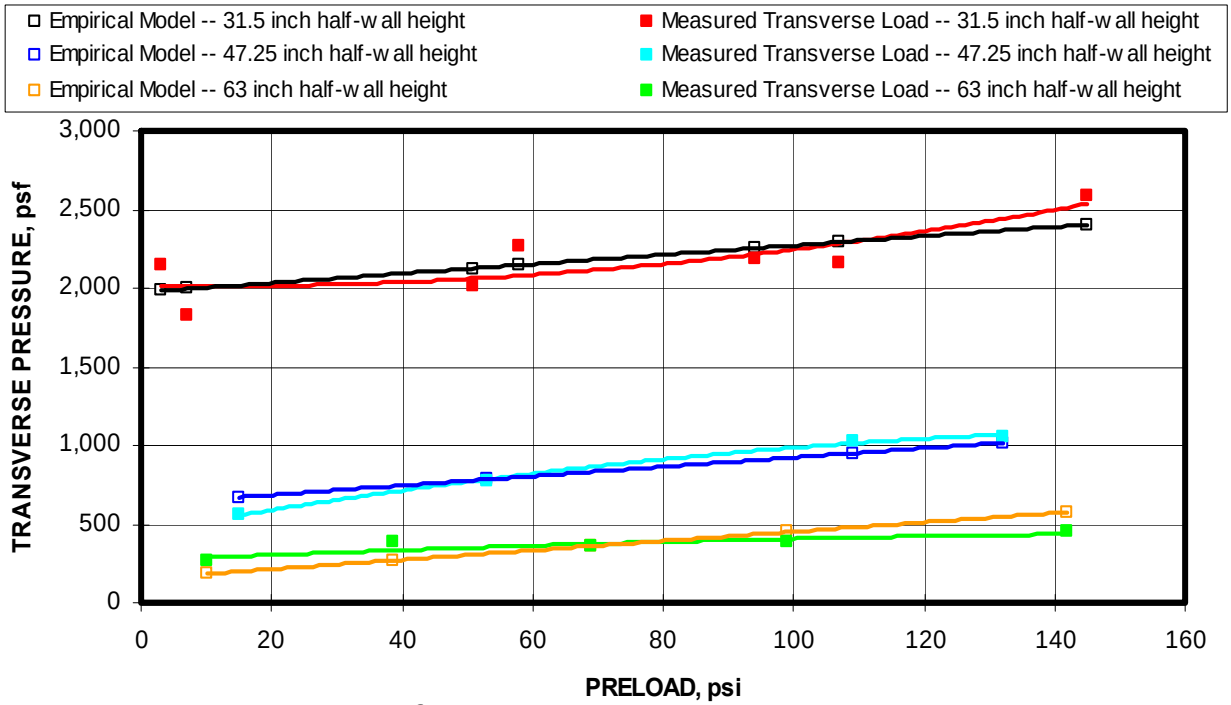

Figure 9-28. Comparison of design equation predictions with measured transverse load from laboratory testing (Full Empirical Model – Ytong block).

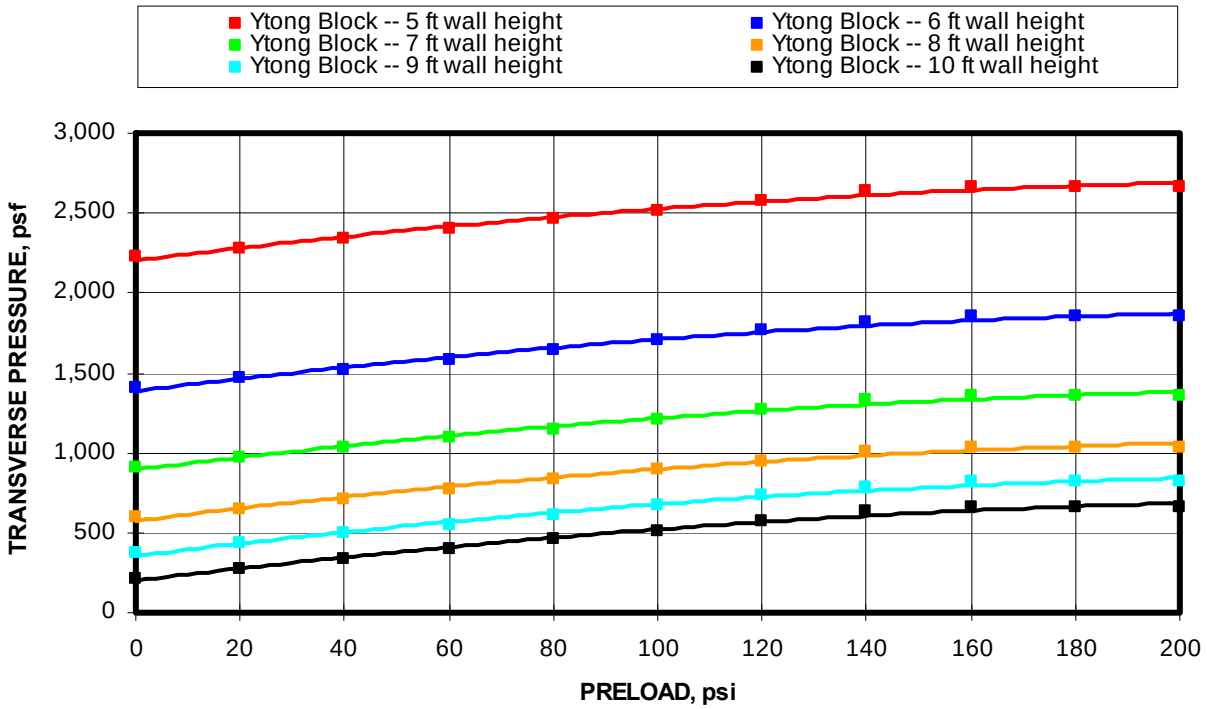

Figure 9-29. Transverse load capacity predictions for 6-in-thick walls constructed from Ytong block for walls heights ranging from 5 to 10 ft (Full Empirical Model).

9.1.4.2 Hybrid Theoretical Models

Transverse load capacity forecasts will be made using the three hybrid theoretical models: (1) Hybrid Thrust Model, (2) Hybrid Lateral Displacement Model, and (3) Hybrid Combination Thrust and Lateral Displacement Model.

9.1.4.2.1 Hybrid Thrust Model

As seen in the flowchart in figure 9-2, the Hybrid Thrust Model determines the normalized thrust force from a multivariable relationship between the thrust force and the $Ex(t/L)^2$ term and preload, both of which are considered to be known parameters. The multivariable linear regression analysis based on 15 laboratory tests of various wall constructions is summarized in table 9-12. Equation 9.11 is used to compute the normalized thrust force per unit width of wall. Table 9-13 documents the multivariable regression analysis results used to determine the resultant thrust position factor (d).

Table 9-12. Multivariable regression analysis for determining arching thrust.

Regression Statistics	
Multiple R	0.9304
R Square	0.8657
Adjusted R Square	0.8433
Standard Error	0.1645
Observations	15

ANOVA

	df	SS	MS	F	Significance F
Regression	2	2.0940	1.0470	38.6840	0.0000
Residual	12	0.3248	0.0271		
Total	14	2.4188			

	Coefficients	Standard Error	t Stat	P-value	Lower 95%	Upper 95%	Lower 95.0%	Upper 95.0%
Intercept	0.5809	0.1106	5.2544	0.0002	0.3400	0.8218	0.3400	0.8218
E*(t/L)^2	0.0012	0.0002	5.6695	0.0001	0.0007	0.0016	0.0007	0.0016
Preload	0.0061	0.0009	6.4907	0.0000	0.0040	0.0081	0.0040	0.0081

$$P/BL = Ex(t/L)^2 \times .0012 + 0.0061 \times \text{Preload} + 0.5809 \quad \textbf{(9.11)}$$

Where P/BL = Normalized thrust per unit width of block, kips/in,

E = Elastic modulus = 40,000 psi for Ytong block,

t = wall thickness, in,

L = height of wall, in, and

Preload = preload pressure, psi.

Table 9-13. Multivariable regression analysis for determining resultant thrust position factor.

Regression Statistics	
Multiple R	0.8945
R Square	0.8001
Adjusted R Square	0.7668
Standard Error	0.0383
Observations	15

ANOVA

	df	*SS*	*MS*	*F*	*Significance F*
Regression	2	0.0703	0.0352	24.0127	0.0001
Residual	12	0.0176	0.0015		
Total	14	0.0879			

	Coefficients	*Standard Error*	*t Stat*	*P-value*	*Lower 95%*	*Upper 95%*	*Lower 95.0%*	*Upper 95.0%*
Intercept	1.0308	0.0839	12.2918	0.0000	0.8481	1.2135	0.8481	1.2135
Half-wall Height	-0.0011	0.0010	-1.1802	0.2608	-0.0032	0.0010	-0.0032	0.0010
Thrust	-0.0080	0.0013	-5.9816	0.0001	-0.0109	-0.0051	-0.0109	-0.0051

$$d = -0.0011 \times \text{Half-wall Height} - 0.0080 \times \text{Thrust} + 1.0308 \quad \textbf{(9.12)}$$

Figure 9-30 compares the results of the predicted transverse load capacities from the hybrid theoretical thrust model with the measured laboratory test results for half-wall heights of 31.5, 47.25, and 63 inches with varying preloads. As seen from the graph, the predictions overall are less accurate than the full empirical model presented in figure 9-28, especially for the 31.5-in half-wall height. Figure 9-31 shows transverse load predictions using this hybrid thrust model for walls constructed from Ytong block ranging in height from 5 to 10 feet in one foot increments with preloads ranging from 0 to 200 psi.

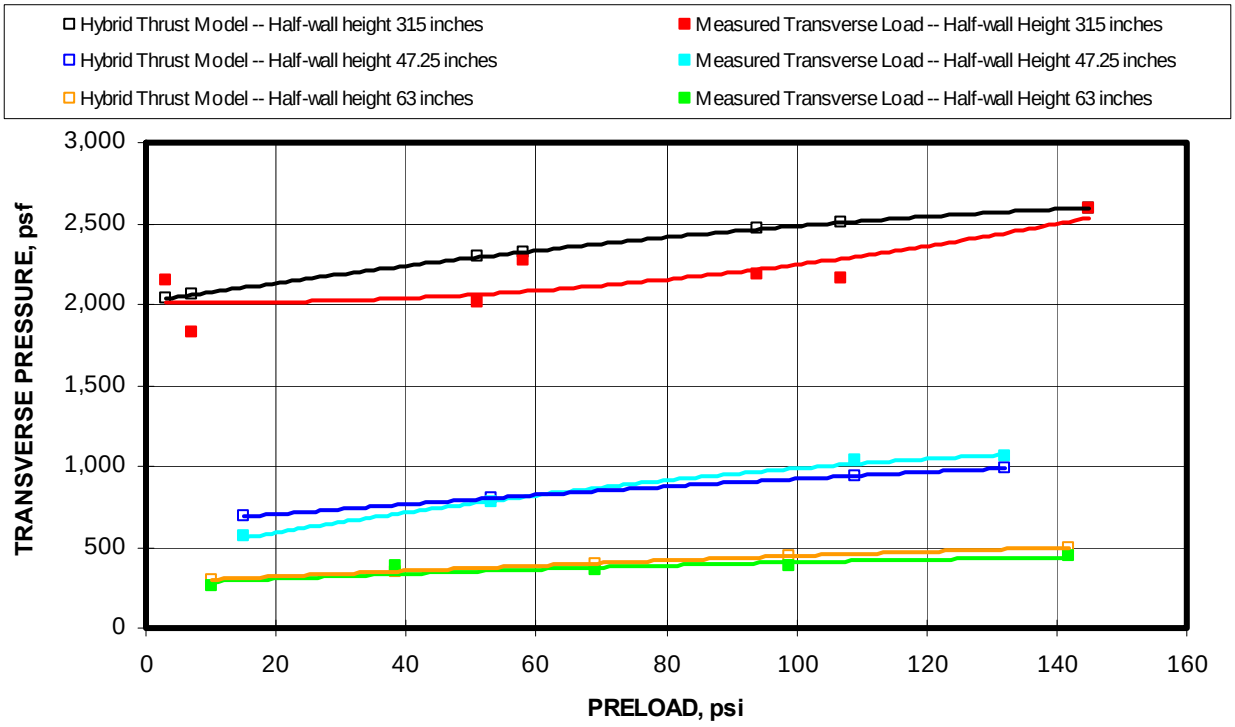

Figure 9-30. Comparison of transverse load capacities from design equations to the measured transverse load from laboratory tests (Hybrid Theoretical Thrust Model).

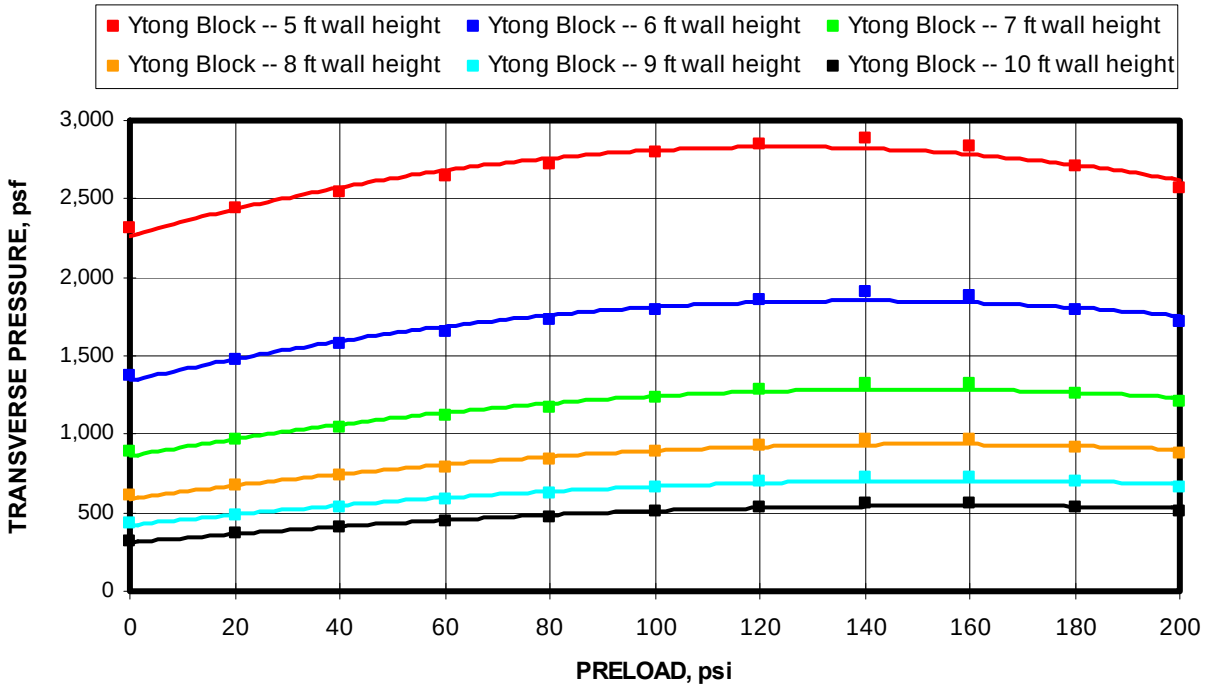

Figure 9-31. Transverse load capacity predictions for 6-in-thick walls constructed from Ytong block for walls heights ranging from 5 to 10 ft (Hybrid Theoretical Thrust Model).

9.1.4.2.2 Hybrid Lateral Displacement Model

As seen in the flowchart in figure 9-3, the Hybrid Lateral Displacement Model determines the lateral displacement force from a multivariable relationship from the $Ex(t/L)^2$ term and preload, both of which are considered to be known parameters. The multivariable linear regression analysis based on 15 laboratory tests of various wall constructions is summarized in table 9-14. Equation 9.13 is used to compute lateral wall displacement. Table 9-13 documented the multivariable regression analysis results used to determine the resultant thrust position factor (d) for the Hybrid Thrust Model. This equation is also used for computing the resultant thrust adjustment factor for this model, except the calculated thrust forces are used instead of the measured thrust forces.

$$\text{Lateral Displacement} = -0.0007 \times Ex(t/L)^2 - 0.0037 \times \text{Preload} + 1.55778 \quad \textbf{(9.13)}$$

Table 9-14. Multivariable regression for determining lateral displacement.

Regression Statistics	
Multiple R	0.8545
R Square	0.7301
Adjusted R Square	0.6852
Standard Error	0.1587
Observations	15

ANOVA

	df	SS	MS	F	Significance F
Regression	2	0.8177	0.4089	16.2343	0.0004
Residual	12	0.3022	0.0252		
Total	14	1.1200			

	Coefficients	Standard Error	t Stat	P-value	Lower 95%	Upper 95%	Lower 95.0%	Upper 95.0%
Intercept	1.5578	0.1066	14.6072	0.0000	1.3254	1.7901	1.3254	1.7901
E*(t/L)^2	-0.0007	0.0002	-3.7989	0.0025	-0.0012	-0.0003	-0.0012	-0.0003
Preload	-0.0037	0.0009	-4.0903	0.0015	-0.0057	-0.0017	-0.0057	-0.0017

Figure 9-32 compares the results of the predicted transverse load capacities from the hybrid theoretical lateral displacement model with the measured laboratory test results for half-wall heights of 31.5, 47.25, and 63 inches with varying preloads. As seen from the graph, the predictions overall are similar to the hybrid theoretical thrust model presented in figure 9-29 and slightly less accurate than the empirical model. Figure 9-33 shows transverse load predictions using the hybrid theoretical lateral displacement for walls constructed from Ytong block ranging in height from 5 to 10 feet in one foot increments with preloads ranging from 0 to 200 psi.

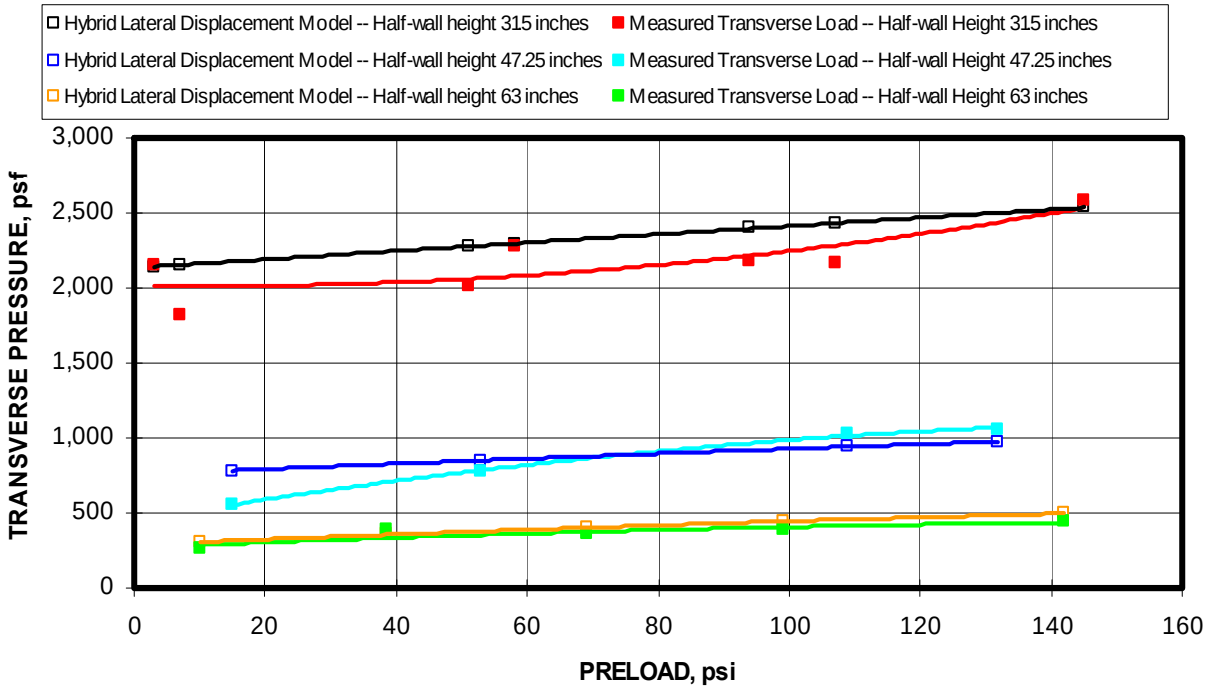

Figure 9-32. Comparison of transverse load capacities from design equations to the measured transverse load from laboratory tests (Hybrid Theoretical Lateral Displacement Model).

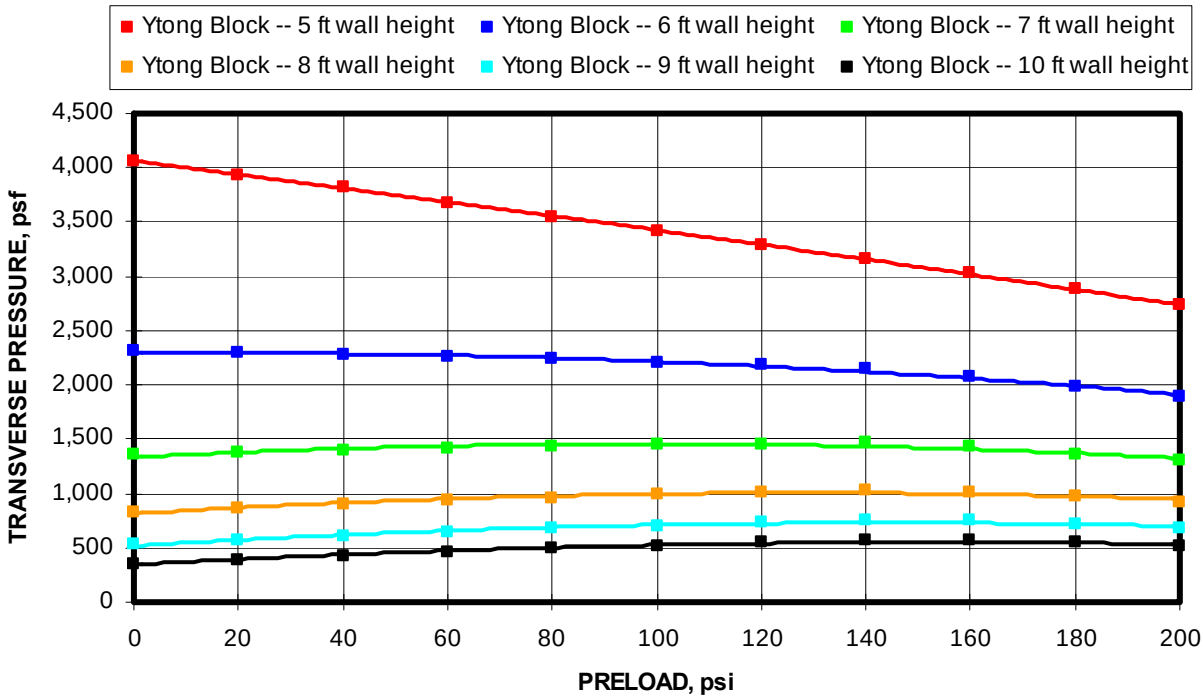

Figure 9-33. Transverse load capacity predictions for 6-in-thick walls constructed from Ytong block for walls heights ranging from 5 to 10 ft (Hybrid Theoretical Lateral Displacement Model).

9.1.4.2.3 Hybrid Combination Model

The Hybrid Combination Model combines the previous two models by empirically determining both the thrust and lateral displacement. Figure 9-34 compares this model's predictions of transverse load capacity to the measured transverse load capacities from the laboratory testing. The combination model is considerably more accurate than the thrust or lateral displacement model. For completeness, figure 9-35 is included which displays the transverse load predictions using the hybrid theoretical combination model for 6-in-thick walls constructed from Ytong block ranging in height from 5 to 10 feet in one foot increments with preloads ranging from 0 to 200 psi.

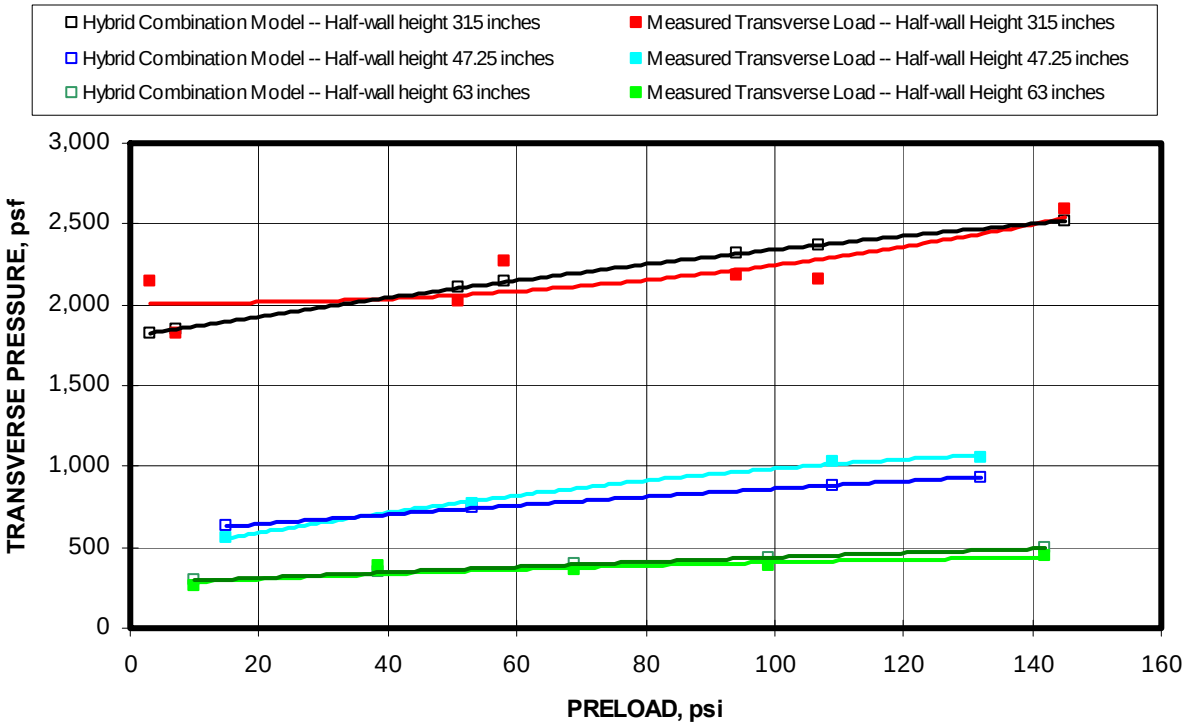

Figure 9-34. Comparison of transverse load capacities from design equations to the measured transverse load from laboratory tests (Hybrid Theoretical Combination Model).

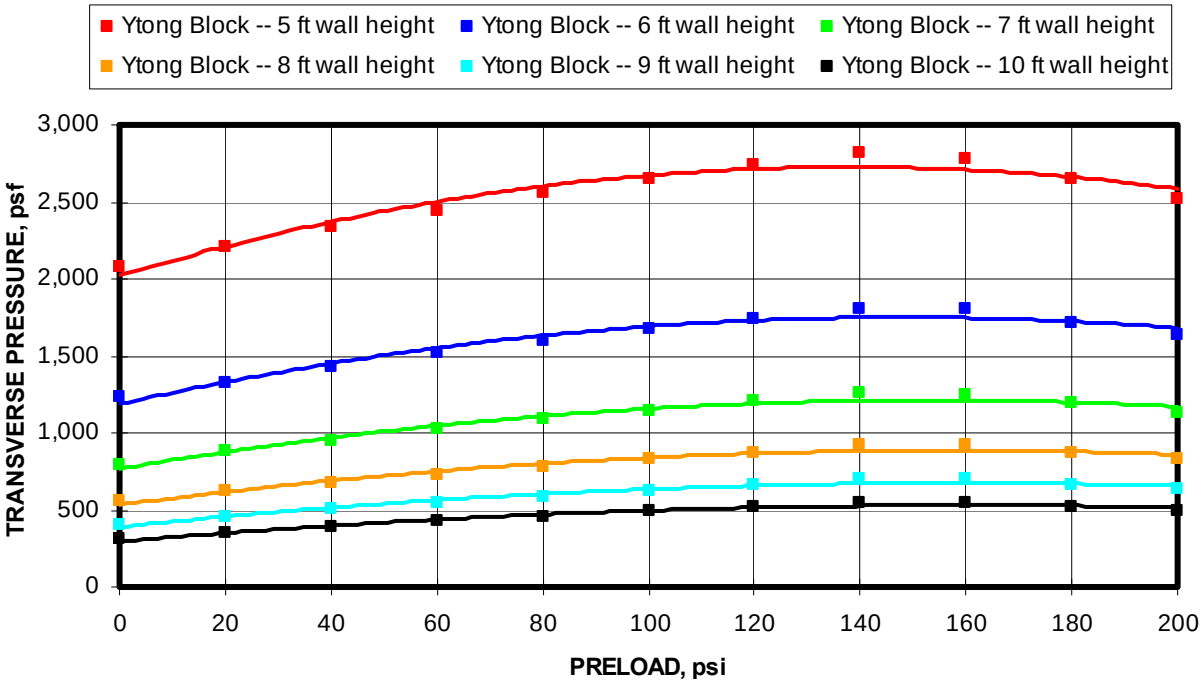

Figure 9-35. Transverse load capacity predictions for 6-in-thick walls constructed from Ytong block for walls heights ranging from 5 to 10 ft (Hybrid Theoretical Combination Model).

9.1.4.3 Summary of Design Equations for Ytong Block

In summary, a full empirical design model and three hybrid theoretical design models were developed for the Ytong block stopping constructions. Figure 9-36 displays the calculated transverse load capacities from full empirical model compared to the measured capacities from the MRS tests. The dashed line represents a perfect correlation between the calculated and measured capacities. The red trend line represents the linear regression and shows that on average the model predicts the transverse pressure to within a 1 pct error. The shaded blue area is a +/- 400 psf variation from the perfect correlation. Examining the chart, it is seen that 100% of the data falls within this variation. Figure 9-37 displays this same information for the three hybrid theoretical design models. The hybrid combination model which empirically determines both the arching thrust and lateral displacement provides the most accurate predictions of the transverse pressure. The difference between the measured and calculated transverse pressure with this model is less than 1 pct. The hybrid thrust and hybrid lateral displacement model both over predict the transverse pressure with an error of 6 pct. Examining the +/-400 psf variation (blue shading), all three models have 100% of the data within this variation.

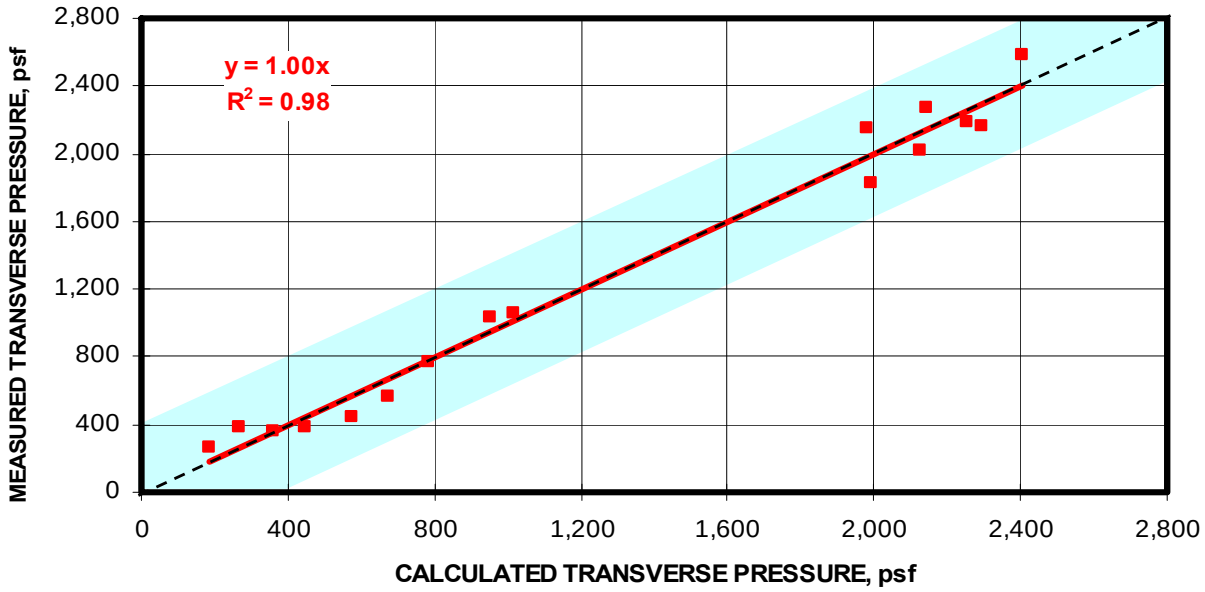

Figure 9-36. Comparison of predicted transverse load capacities compared to the measured capacities for the MRS laboratory tests (Full Empirical Model).

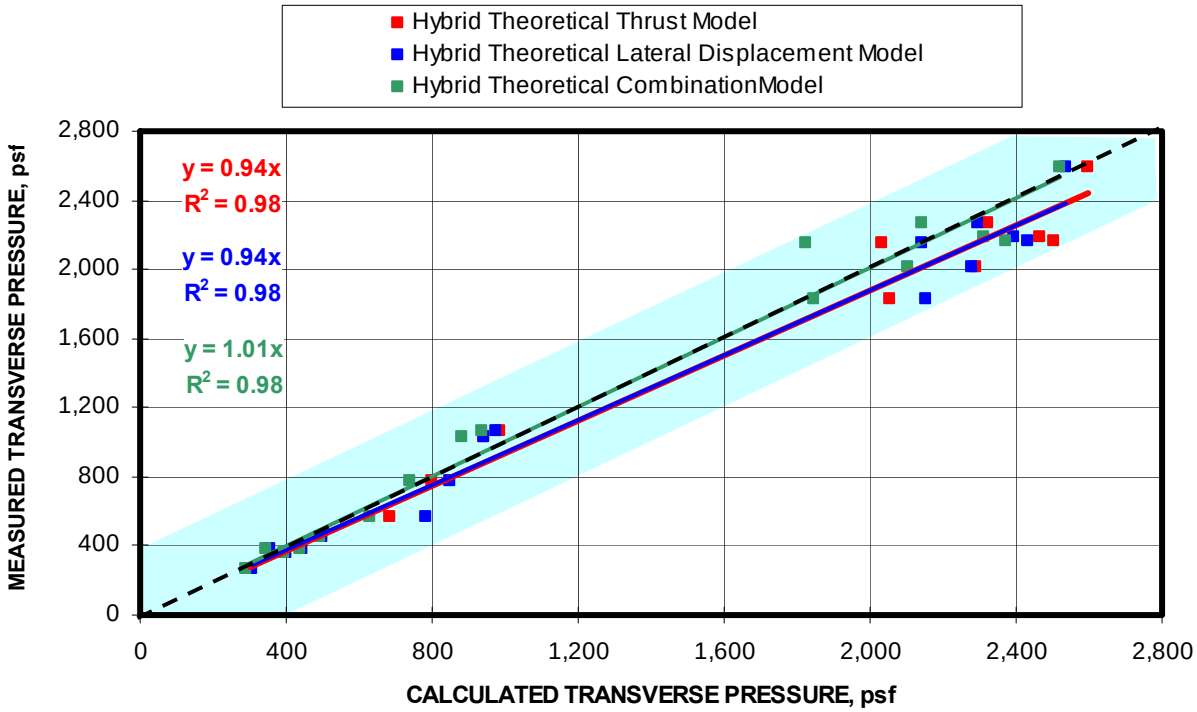

Figure 9-37. Comparison of predicted transverse load capacities compared to the measured capacities for the MRS laboratory tests (Hybrid Theoretical Models).

9.1.5 Kingsway Block

Kingsway is another cellular concrete block used for stopping construction. This block measures nominally 6x8x17 inches and weighs on average 21 lbs. It has a moderate compressive strength of 546 psi. Only 8 tests were conducted with the Kingsway block. Although more test results would produce a better block model, it is believed that there were sufficient test variables to construct a useful model.

9.1.5.1 Full Empirical Model

Table 9-15 shows the results of the multivariable regression analysis correlating the transverse load to the $Ex(t/L)^2$ and preload. From this regression analysis, the design equation for Kingsway block is shown in equation 9.14.

$$\text{Transverse Load} = 5.3608 \times E(t/L)^2 - 0.2822 \times \text{Preload} - 172 \quad \textbf{(9.14)}$$

Where E = material modulus = 24,000 psi for Kingsway block,

t = wall thickness, in,

L = full wall height, in, and

Preload = ground pressure preload, psi.

Table 9-15. Multivariable regression analysis for determining transverse load from modulus and wall geometric parameters.

Regression Statistics	
Multiple R	0.9879
R Square	0.9759
Adjusted R Square	0.9663
Standard Error	40.6704
Observations	8

ANOVA

	df	SS	MS	F	Significance F
Regression	2	335241	167620	101.3372	0.0001
Residual	5	8270	1654		
Total	7	343511			

	Coefficients	Standard Error	t Stat	P-value	Lower 95%	Upper 95%	Lower 95.0%	Upper 95.0%
Intercept	-172.6684	104.0557	-1.6594	0.1579	-440.1517	94.8149	-440.1517	94.8149
E x (t/L)^2	5.3608	0.4124	12.9984	0.0000	4.3006	6.4210	4.3006	6.4210
Preload	-0.2822	1.1932	-0.2365	0.8224	-3.3495	2.7851	-3.3495	2.7851

Figure 9-38 compares the predicted transverse load capacities from the empirical model with the measured laboratory results for the three half-wall heights with varying preloads. Due to limited availability of the block, the preload was not varied much in this

series of tests. As seen in the figure, the model predictions are reasonably accurate for the 42-in and 50-in half-wall heights. Only two tests were conducted at the 33-in half-wall height, and the model prediction is a reasonable approximation of the average of these two tests. Figure 9-39 shows transverse load predictions using this empirical design model for walls constructed from Kingsway block ranging in height from 5 to 10 feet in one foot increments with preloads ranging from 0 to 100 psi. The model shows little variation with preload. This is due to the lack of variation of preload in the test data.

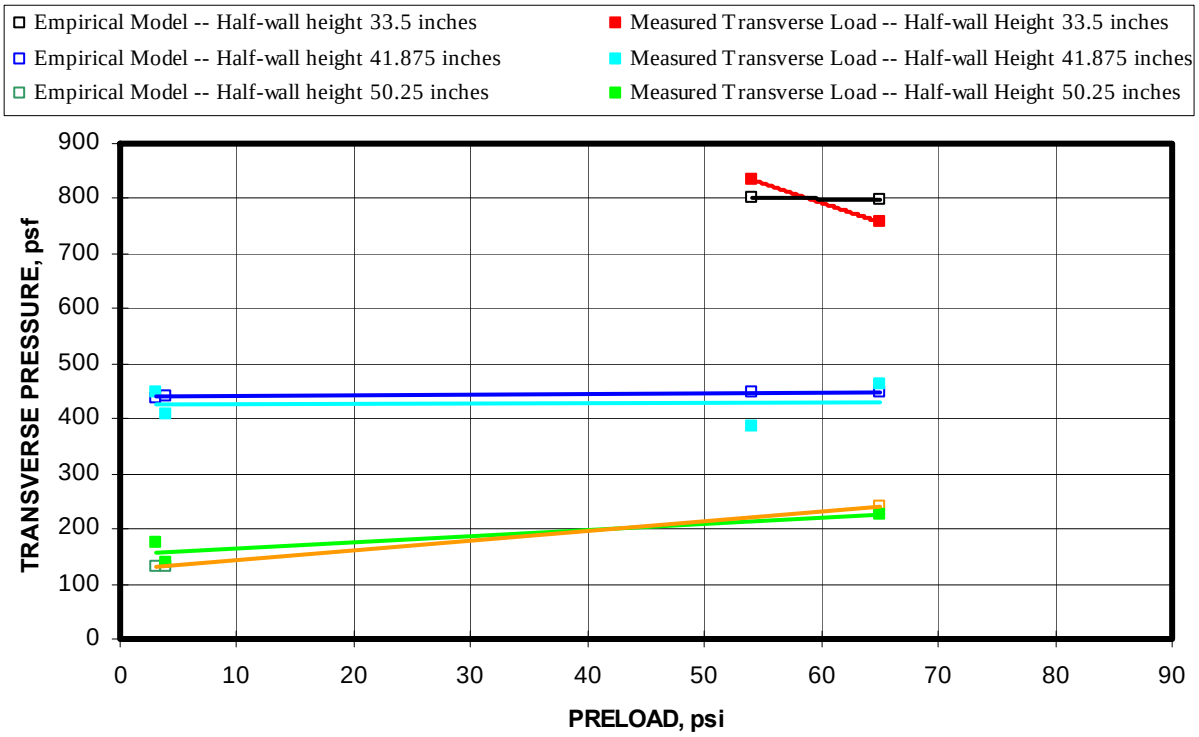

Figure 9-38. Comparison of design equation predictions with measured transverse load from laboratory testing (Full Empirical Model – Kingsway block).

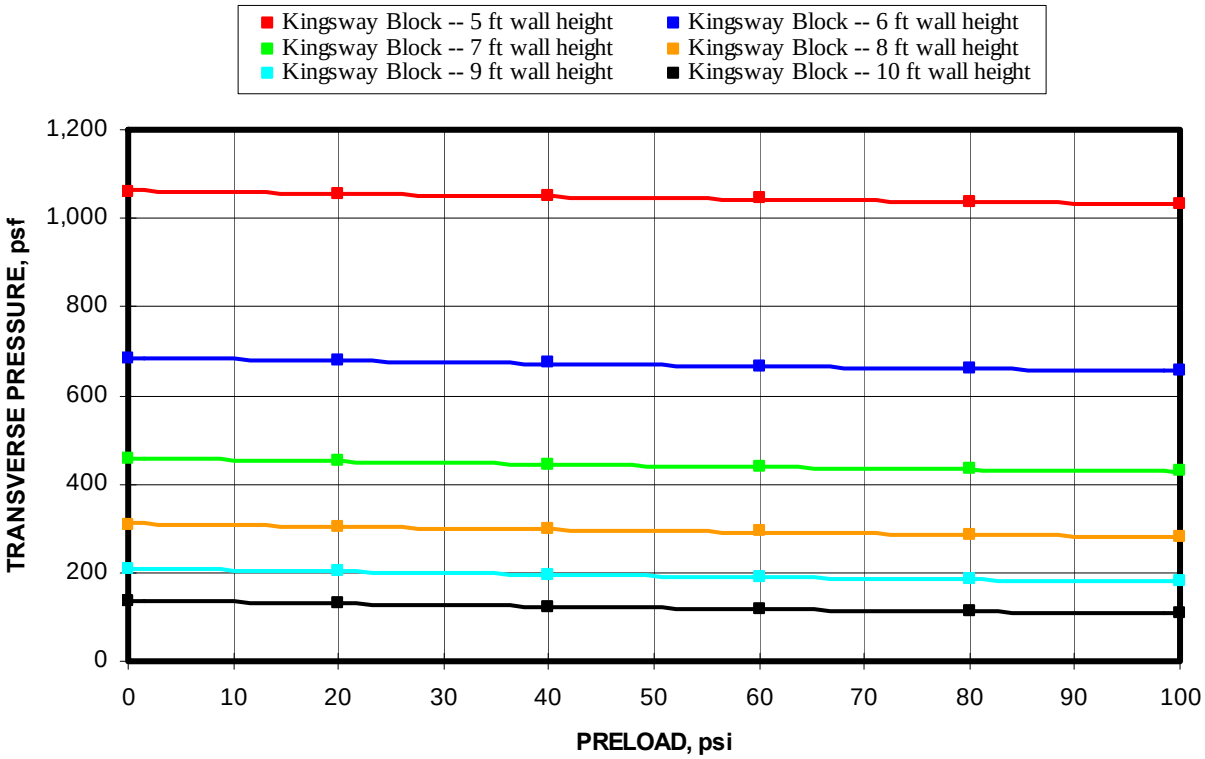

Figure 9-39. Transverse load capacity predictions for walls constructed from Kingsway solid block for walls heights ranging from 5 to 10 ft (Full Empirical Model).

9.1.5.2 Hybrid Theoretical Models

Transverse load capacity forecasts will be made using the three hybrid theoretical models: (1) Hybrid Thrust Model, (2) Hybrid Lateral Displacement Model, and (3) Hybrid Combination Thrust and Lateral Displacement Model.

9.1.5.2.1 Hybrid Thrust Model

As seen in the flowchart in figure 9-2, the Hybrid Thrust Model determines the normalized thrust force from a multivariable relationship between the thrust force and the $Ex(t/L)^2$ term and preload, both of which are considered to be known parameters. The multivariable linear regression analysis based on 8 laboratory tests of various wall constructions is summarized in table 9-16. Equation 9.15 is used to compute the normalized thrust force per unit width of wall. Table 9-17 documents the multivariable regression analysis results used to determine the resultant thrust position factor (d).

Table 9-16. Multivariable regression analysis for determining arching thrust.

Regression Statistics	
Multiple R	0.6356
R Square	0.4040
Adjusted R Square	0.1656
Standard Error	0.1024
Observations	8

ANOVA

	df	SS	MS	F	Significance F
Regression	2	0.0356	0.0178	1.6944	0.2743
Residual	5	0.0525	0.0105		
Total	7	0.0880			

	Coefficients	Standard Error	t Stat	P-value	Lower 95%	Upper 95%	Lower 95.0%	Upper 95.0%
Intercept	0.2850	0.2621	1.0873	0.3265	-0.3888	0.9588	-0.3888	0.9588
E*(t/L)^2	0.0018	0.0010	1.7771	0.1357	-0.0008	0.0045	-0.0008	0.0045
Preload	0.0034	0.0030	1.1396	0.3061	-0.0043	0.0112	-0.0043	0.0112

$$P/BL = .0018 \times Ex(t/L)^2 + 0.0034 \times Preload + 0.2850 \quad \textbf{(9.15)}$$

Where P/BL = Normalized thrust per unit width of block, kips/in,

E = Elastic modulus = 24,000 psi for Kingsway block,

t = wall thickness, in,

L = height of wall, in, and

Preload = preload pressure, psi.

Table 9-17. Multivariable regression analysis for determining resultant thrust position factor.

Regression Statistics	
Multiple R	0.8682
R Square	0.7538
Adjusted R Square	0.6553
Standard Error	0.0509
Observations	8

ANOVA

	df	SS	MS	F	Significance F
Regression	2	0.0396	0.0198	7.6528	0.0301
Residual	5	0.0129	0.0026		
Total	7	0.0525			

	Coefficients	Standard Error	t Stat	P-value	Lower 95%	Upper 95%	Lower 95.0%	Upper 95.0%
Intercept	1.7532	0.2443	7.1759	0.0008	1.1251	2.3812	1.1251	2.3812
Half-wall Height	-0.0087	0.0027	-3.2620	0.0224	-0.0155	-0.0018	-0.0155	-0.0018
Thrust	-0.0453	0.0123	-3.6724	0.0144	-0.0770	-0.0136	-0.0770	-0.0136

$$d = -0.0087 \times \text{Half-wall Height} - 0.0453 \times \text{Thrust} + 1.7532 \quad \textbf{(9.16)}$$

Figure 9-40 compares the results of the predicted transverse load capacities from the hybrid theoretical thrust model with the measured laboratory test results for half-wall heights

of 33, 42, and 50 inches with varying preloads. As seen from the graph, this theoretical model over predicts the transverse load for all three heights. As a result, this model does not provide an improvement over the full empirical model presented in figure 9-38. Figure 9-41 shows transverse load predictions using this empirical design model for walls constructed from Kingsway block ranging in height from 5 to 10 feet in one foot increments with preloads ranging from 0 to 140 psi.

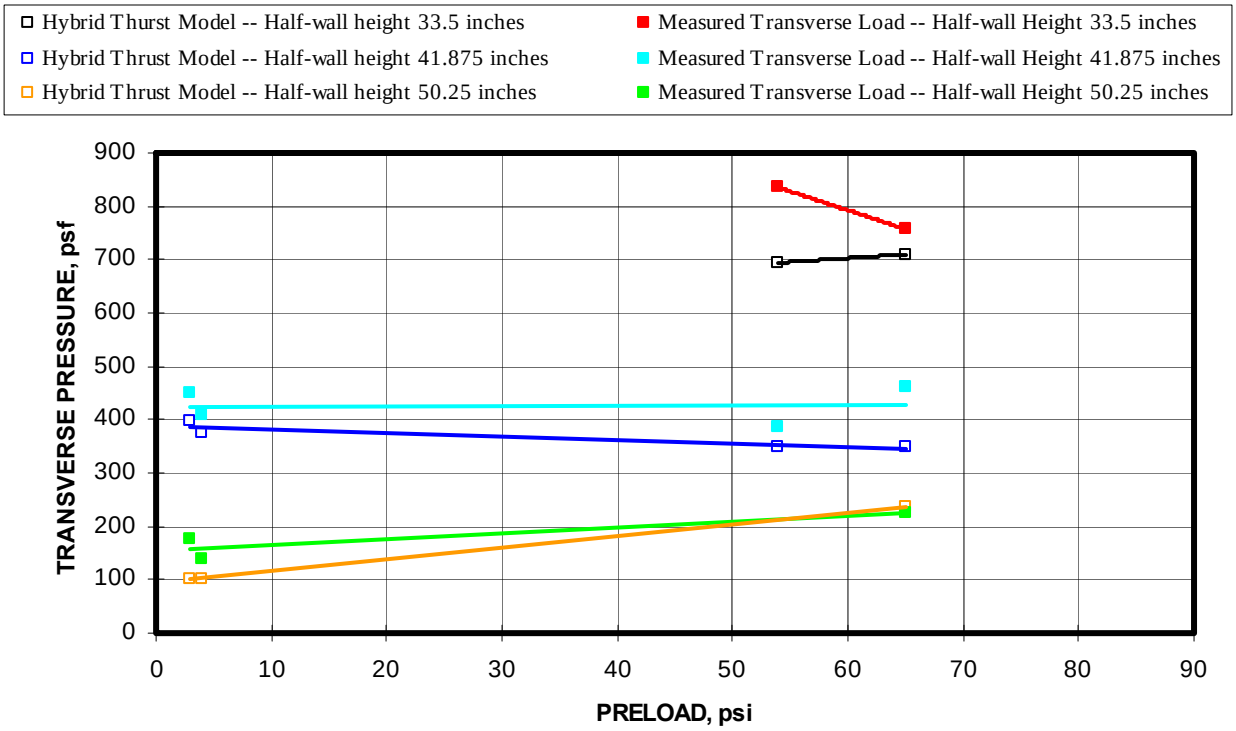

Figure 9-40. Comparison of transverse load capacities from design equations to the measured transverse load from laboratory tests (Hybrid Theoretical Thrust Model).

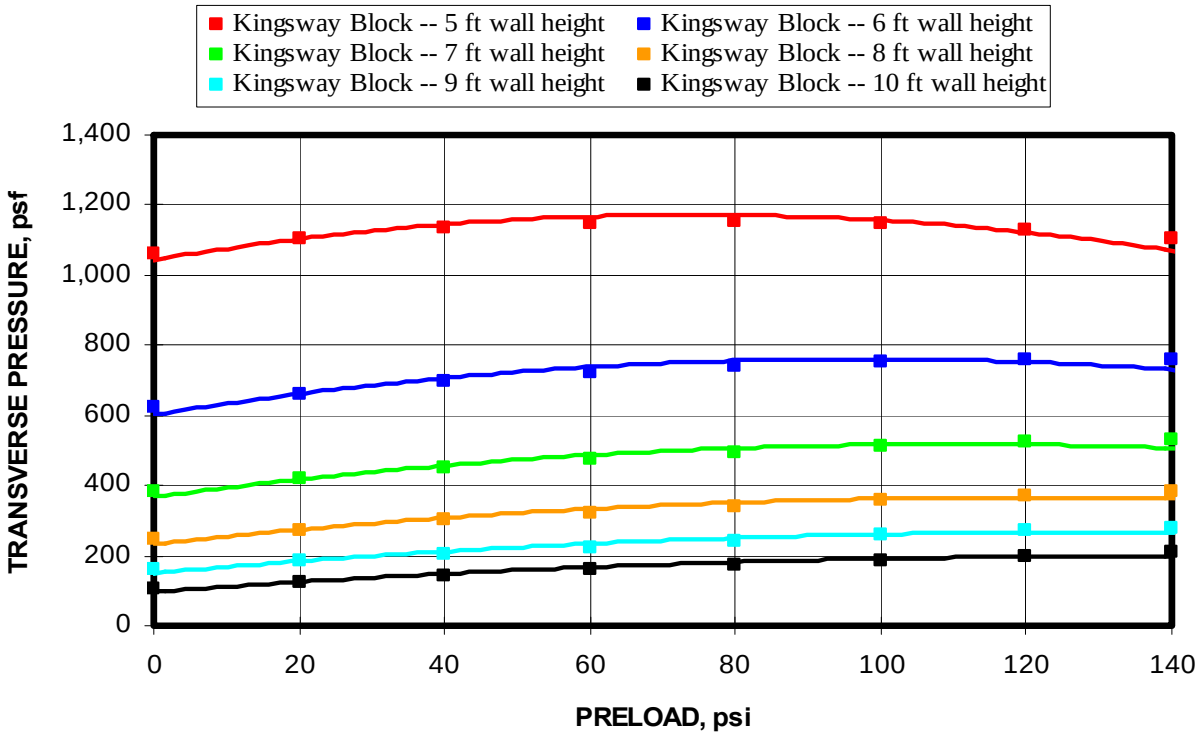

Figure 9-41. Transverse load capacity predictions for 6-in-thick walls constructed from Kingsway solid block for walls heights ranging from 5 to 10 ft (Hybrid Theoretical Thrust Model).

9.1.5.2.2 Hybrid Lateral Displacement Model

As seen in the flowchart in figure 9-3, the Hybrid Lateral Displacement Model determines the lateral displacement force from a multivariable relationship from the $Ex(t/L)^2$ term and preload, both of which are considered to be known parameters. The multivariable linear regression analysis based on 8 laboratory tests of various wall constructions is summarized in table 9-18. Equation 9.17 is used to compute the lateral wall displacement. Table 9-17 documented the multivariable regression analysis results used to determine the resultant thrust position factor (d) for the Hybrid Thrust Model. This equation is also used for computing the resultant thrust adjustment factor for this model, except the calculated thrust forces are used instead of the measured thrust forces.

$$\text{Lateral Displacement} = -0.0057 \times Ex(t/L)^2 - 0.0020 \times \text{Preload} + 2.0018 \qquad \textbf{(9.17)}$$

Table 9-18. Multivariable regression analysis for determining lateral displacement.

Regression Statistics	
Multiple R	0.8920
R Square	0.7956
Adjusted R Square	0.7138
Standard Error	0.1327
Observations	8

ANOVA

	df	SS	MS	F	Significance F
Regression	2	0.3425	0.1713	9.7297	0.0189
Residual	5	0.0880	0.0176		
Total	7	0.4306			

	Coefficients	Standard Error	t Stat	P-value	Lower 95%	Upper 95%	Lower 95.0%	Upper 95.0%
Intercept	2.0018	0.3395	5.8971	0.0020	1.1292	2.8743	1.1292	2.8743
E*(t/L)^2	-0.0057	0.0013	-4.2282	0.0083	-0.0091	-0.0022	-0.0091	-0.0022
Preload	-0.0020	0.0039	-0.5033	0.6361	-0.0120	0.0080	-0.0120	0.0080

Figure 9-42 compares the results of the predicted transverse load capacities from the hybrid theoretical lateral displacement model with the measured laboratory test results for half-wall heights of 33, 42, and 50 inches with varying preloads. As seen from the graph, the

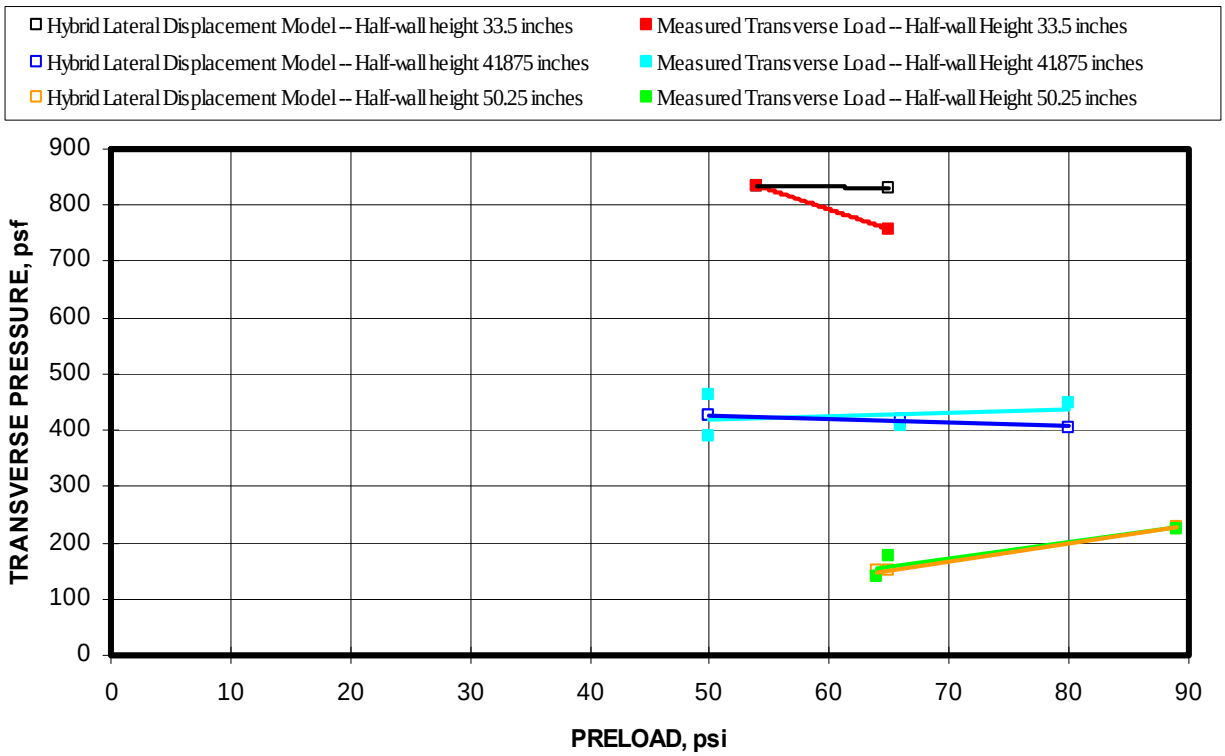

Figure 9-42. Comparison of transverse load capacities from design equations to the measured transverse load from laboratory tests (Hybrid Theoretical Lateral Displacement Model).

predictions are significantly better than the hybrid theoretical thrust model presented in figure 9-40. Figure 9-43 shows transverse load predictions using the hybrid theoretical lateral displacement for walls constructed from Kingsway block ranging in height from 5 to 10 feet in one foot increments with preloads ranging from 0 to 140 psi.

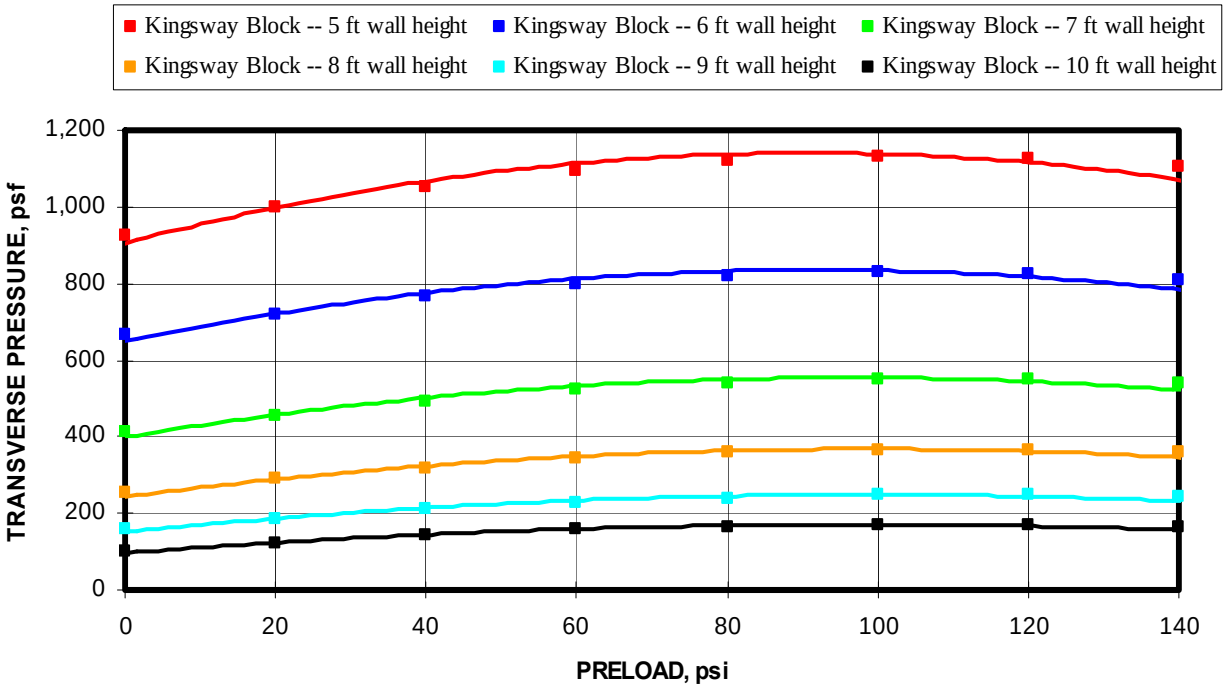

Figure 9-43. Transverse load capacity predictions for walls constructed from Kingsway block for heights ranging from 5 to 10 ft (Hybrid Theoretical Lateral Displacement Model).

9.1.5.2.3 Hybrid Combination Model

The Hybrid Combination Model combines the previous two models by empirically determining both the thrust and lateral displacement. Figure 9-44 compares this model's predictions of transverse load capacity to the measured transverse load capacities from the laboratory testing. This model provides a more accurate prediction of the transverse pressure than the thrust model, but since it utilizes the thrust model information, it is not quite as accurate as the lateral displacement model. Figure 9-45 displays the transverse load predictions using the hybrid theoretical combination model for walls constructed from Kingsway block ranging in height from 5 to 10 feet in one foot increments with preloads ranging from 0 to 140 psi.

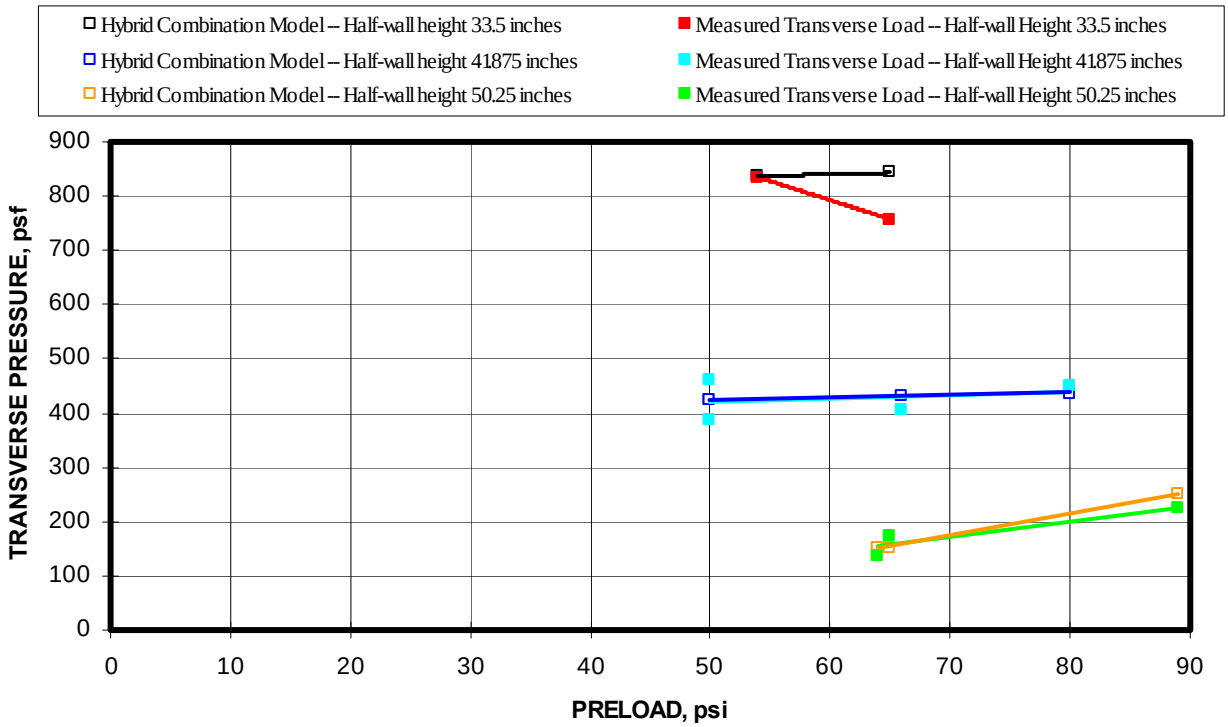

Figure 9-44. Comparison of transverse load capacities from design equations to the measured transverse load from laboratory tests (Hybrid Theoretical Combination Model).

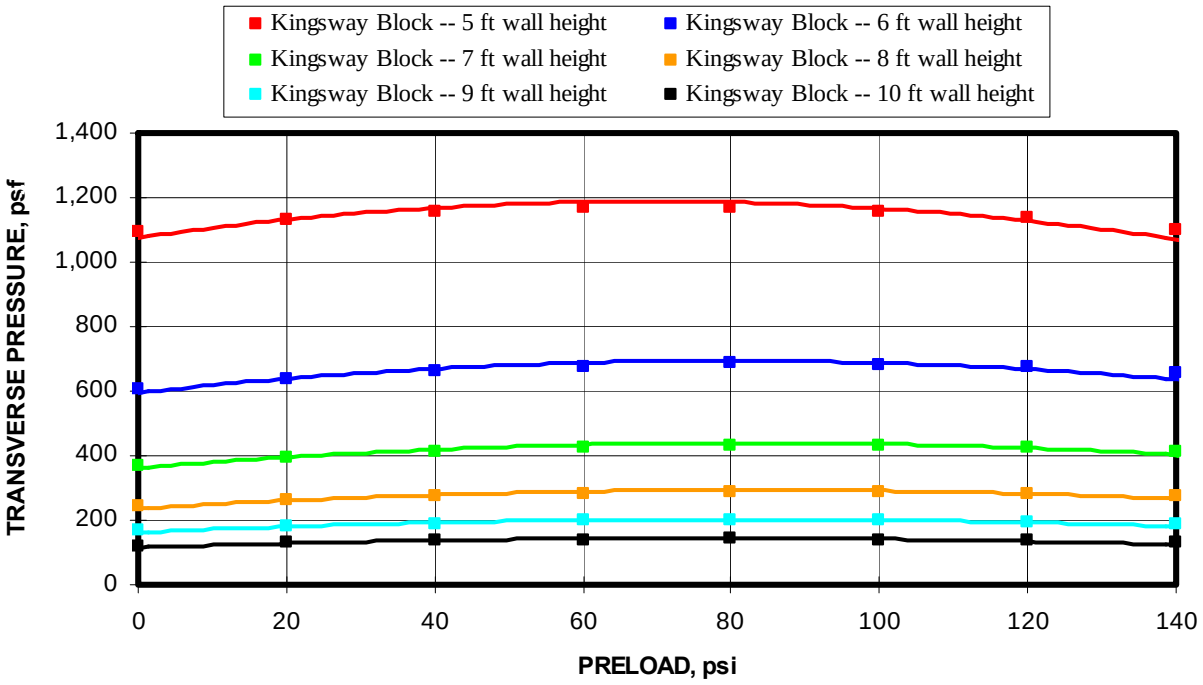

Figure 9-45. Transverse load capacity predictions for walls constructed from Kingsway block for walls heights ranging from 5 to 10 ft (Hybrid Theoretical Combination Model).

9.1.5.3 Summary of Design Equations for Kingsway Block

In summary, a full empirical design model and three hybrid theoretical design models were developed for the Kingsway block stopping constructions. Figure 9-46 displays the calculated transverse load capacities from full empirical model compared to the measured capacities from the MRS tests. The dashed line represents a perfect correlation between the calculated and measured capacities. The red trend line represents the linear regression between the measured and calculated capacities. The regression lines shows that on average the model tends to over predict the transverse load by a slight amount. The regression trend line shows a 2 pct difference between the measured and calculated transverse load. The shaded blue area is a +/- 100 psf variation from the perfect correlation. Examining the chart, it is seen that 100% of the data falls within this variation. Figure 9-47 displays this same information for the three hybrid theoretical design models. Based on the regression trend line correlating the calculated transverse loads to the measured transverse loads, the lateral displacement model is the most accurate, slightly better than the combination model. Both models predict the load to within 2 pct of the measure transverse load. The least accurate is the thrust model with a 10 pct difference. Examining the +/-100 psf variation (blue shading), all models have 100% of the data within this variation.

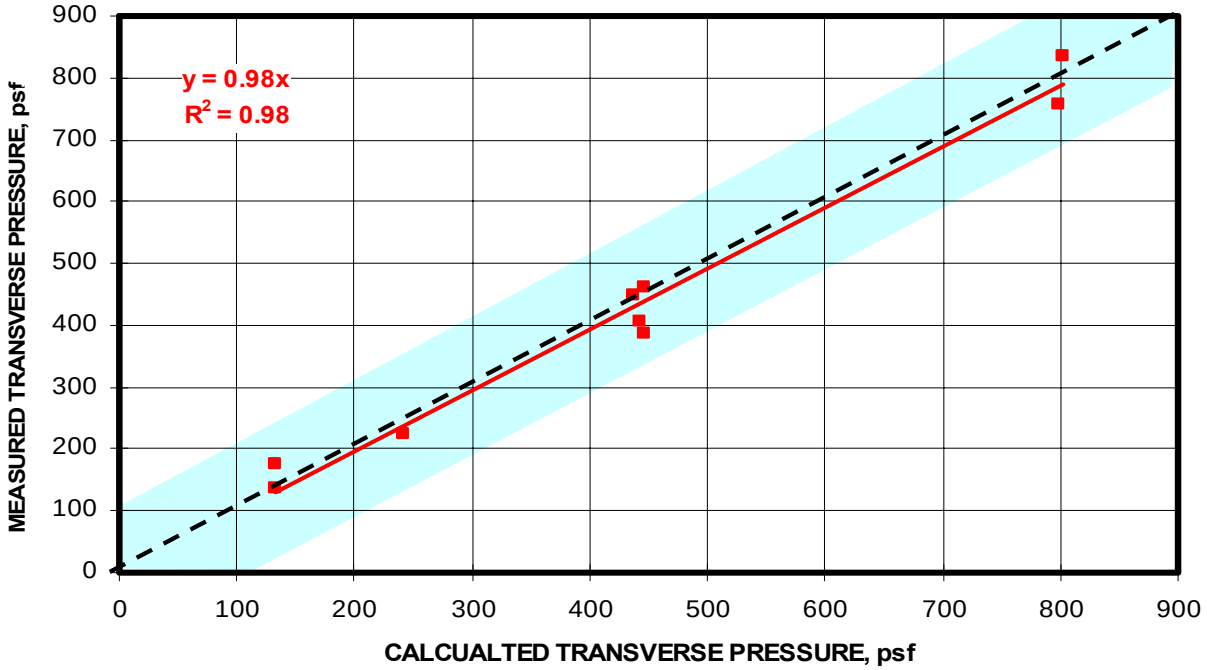

Figure 9-46. Comparison of predicted transverse load capacities compared to the measured capacities for the MRS laboratory tests (Full Empirical Model).

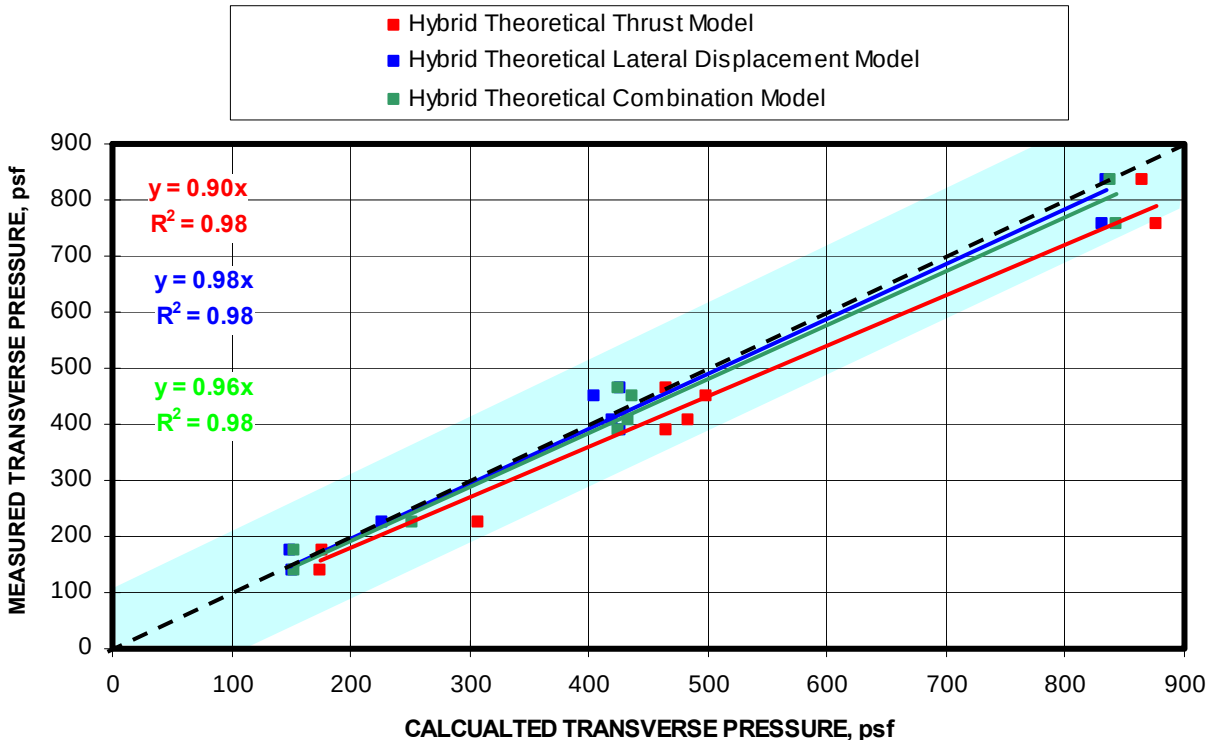

Figure 9-47. Comparison of predicted transverse load capacities compared to the measured capacities for the MRS laboratory tests (Hybrid Theoretical Models).

9.1.6 Omega Block

Omega is another cellular concrete block used for stopping construction. This block measures nominally 8x16x24 inches and weighs on average 47 lbs. The material is very weak with a compressive strength of only 80 psi. It is also a brittle material that is often damaged in places simply from handling of the stopping block. These characteristics lead to inconsistencies in performance and difficulty in constructing accurate predictive models. A total of 22 tests were conducted with the Omega block, sufficient to produce a valid set of theoretical and empirical prediction models.

9.1.5.1 Full Empirical Model

In order to improve the accuracy of the model predictions, the modulus was varied as a function of half-wall height according to equation 9.18. In reality, the modulus is not changing, but the deformation zone associated with the wall rotation produces a differing behavior. Changing the modulus is one way to adjust for this issue and incorporate the response into the existing prediction models. Table 9-19 shows the results of the multivariable regression analysis correlating the transverse load to the $Ex(t/L)^2$ and preload. From this regression analysis, the design equation for Omega block is shown in equation 9.19.

$$\text{Modulus (E)} = 0.0271 \times \text{Half-wall height}^{2.8681} \quad \textbf{(9.18)}$$

Table 9-19. Multivariable regression analysis for determining transverse load from modulus and wall geometric parameters.

Regression Statistics	
Multiple R	0.8074
R Square	0.6520
Adjusted R Square	0.6153
Standard Error	59.0914
Observations	22

ANOVA

	df	SS	MS	F	Significance F
Regression	2	124275	62137	17.7953	0.0000
Residual	19	66344	3492		
Total	21	190619			

	Coefficients	Standard Error	t Stat	P-value	Lower 95%	Upper 95%	Lower 95.0%	Upper 95.0%
Intercept	325.9738	48.3696	6.7392	0.0000	224.7351	427.2126	224.7351	427.2126
E x (t/L)^2	-19.9940	3.4063	-5.8697	0.0000	-27.1234	-12.8646	-27.1234	-12.8646
Preload	2.5990	1.5544	1.6720	0.1109	-0.6544	5.8523	-0.6544	5.8523

$$\text{Transverse Load} = -19.9940 \times Ex(t/L)^2 + 2.5990 \times \text{Preload} + 325.9738 \quad \textbf{(9.19)}$$

Where E = material modulus = 600 to 4,500 psi for Omega block,

t = wall thickness, in,

L = full wall height, in, and

Preload = ground pressure preload, psi.

Figure 9-48 compares the predicted transverse load capacities from the empirical model with the measured laboratory results for the half wall heights with varying preloads. Due to the relative weakness of the block, the preload was not varied much. As seen in the figure, the model over predicts the transverse load for the 48-in and 64-in half-wall heights and under predicts the load for the 32-in half-wall height. In part, this is reflection of the difference in the hinge point deformation at the different wall heights. Figure 9-49 shows transverse load predictions using this empirical design model for walls constructed from Omega block ranging in height from 5 to 10 feet in one foot increments with preloads ranging from 0 to 30 psi, which is the limiting preload to prevent premature failure of the stopping wall. Again, the inconsistencies in the transverse loading are largely due to localized failures of this weak block material.

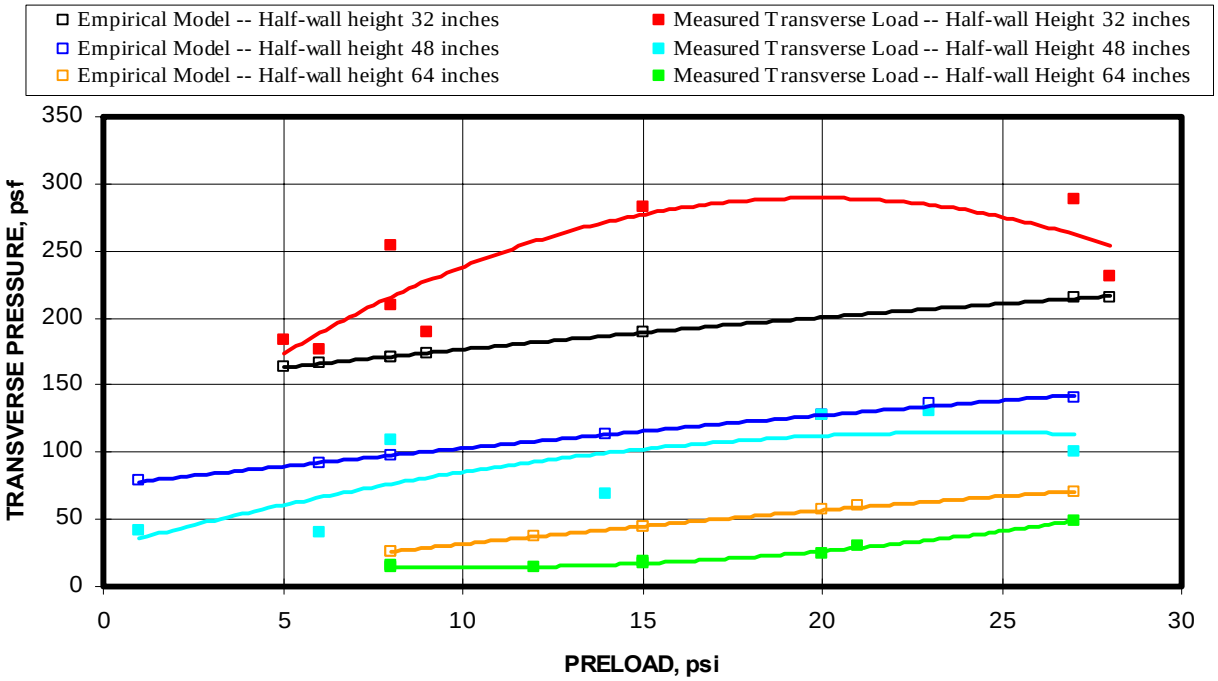

Figure 9-48. Comparison of design equation predictions with measured transverse load from laboratory testing (Full Empirical Model – Omega block).

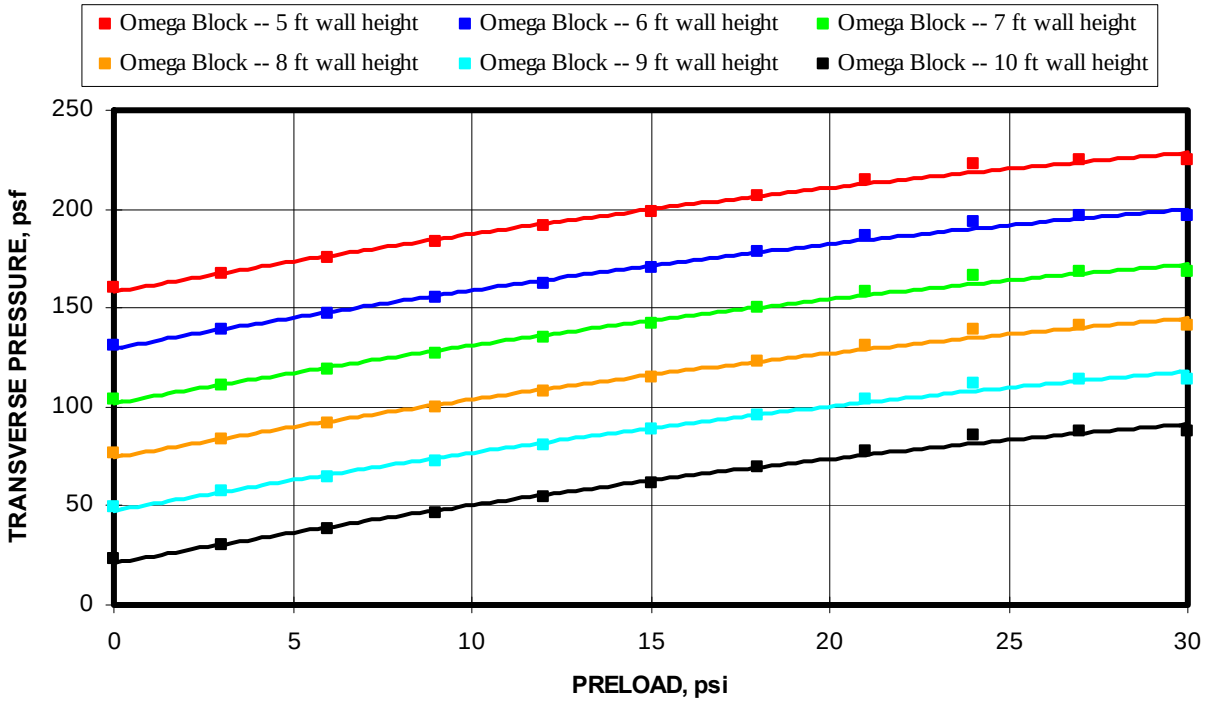

Figure 9-49. Transverse load capacity predictions for 8-in-thick walls constructed from Omega block for walls heights ranging from 5 to 10 ft (Full Empirical Model).

9.1.6.2 Hybrid Theoretical Models

Transverse load capacity forecasts will be made using the three hybrid theoretical models: (1) Hybrid Thrust Model, (2) Hybrid Lateral Displacement Model, and (3) Hybrid Combination Thrust and Lateral Displacement Model.

9.1.6.2.1 Hybrid Thrust Model

As seen in the flowchart in figure 9-2, the Hybrid Thrust Model determines the normalized thrust force from a multivariable relationship between the thrust force and the $Ex(t/L)^2$ term and preload, both of which are considered to be known parameters. The multivariable linear regression analysis based on 22 laboratory tests of various wall constructions is summarized in table 9-20. Equation 9.20 is used to compute the normalized thrust force per unit width of wall. Table 9-21 documents the multivariable regression analysis results used to determine the resultant thrust position factor (d).

Table 9-20. Multivariable regression analysis for determining arching thrust.

Regression Statistics	
Multiple R	0.8319
R Square	0.6920
Adjusted R Square	0.6596
Standard Error	0.0331
Observations	22

ANOVA

	df	SS	MS	F	Significance F
Regression	2	0.0468	0.0234	21.3487	0.0000
Residual	19	0.0208	0.0011		
Total	21	0.0677			

	Coefficients	Standard Error	t Stat	P-value	Lower 95%	Upper 95%	Lower 95.0%	Upper 95.0%
Intercept	0.1586	0.0271	5.8515	0.0000	0.1019	0.2154	0.1019	0.2154
E*(t/L)^2	-0.0083	0.0019	-4.3563	0.0003	-0.0123	-0.0043	-0.0123	-0.0043
Preload	0.0046	0.0009	5.2978	0.0000	0.0028	0.0064	0.0028	0.0064

$$P/BL = - 0.0083 \times Ex(t/L)^2 + 0.0046 * Preload + 0.1586 \quad \textbf{(9.20)}$$

Where P/BL = Normalized thrust per unit width of block, kips/in,

E = Elastic modulus = 600 to 4,500 psi for Omega block,

t = wall thickness, in,

L = height of wall, in, and

Preload = preload pressure, psi.

Table 9-21. Multivariable regression analysis for determining resultant thrust position factor.

Regression Statistics	
Multiple R	0.7478
R Square	0.5592
Adjusted R Square	0.5128
Standard Error	0.0876
Observations	22

ANOVA

	df	SS	MS	F	Significance F
Regression	2	0.1852	0.0926	12.0531	0.0004
Residual	19	0.1460	0.0077		
Total	21	0.3311			

	Coefficients	Standard Error	t Stat	P-value	Lower 95%	Upper 95%	Lower 95.0%	Upper 95.0%
Intercept	1.3723	0.1137	12.0712	0.0000	1.1343	1.6102	1.1343	1.6102
Half-wall Height	-0.0080	0.0016	-4.8343	0.0001	-0.0114	-0.0045	-0.0114	-0.0045
Thrust	-0.0524	0.0163	-3.2092	0.0046	-0.0866	-0.0182	-0.0866	-0.0182

$$d = -0.0080 \times \text{Half-wall Height} - 0.0524 \times \text{Thrust} + 1.3723 \quad \textbf{(9.21)}$$

Figure 9-50 compares the results of the predicted transverse load capacities from the hybrid theoretical thrust model with the measured laboratory test results for half-wall heights of 32, 48, and 64 inches with varying preloads. As seen from the graph, the predictions

overall are improved compared to the full empirical model presented in figure 9-48, especially for the 32 and 48-in half-wall height. The transverse load for the 32-in half-wall height is now over predicted, while is was under predicted for the empirical model. Overall, the accuracy for the 32-in half-wall response remains about the same with this model. Figure 9-51 shows transverse load predictions using this empirical design model for 8-in-thick walls constructed from Omega block ranging in height from 5 to 10 feet in one foot increments with preloads ranging from 0 to 30 psi.

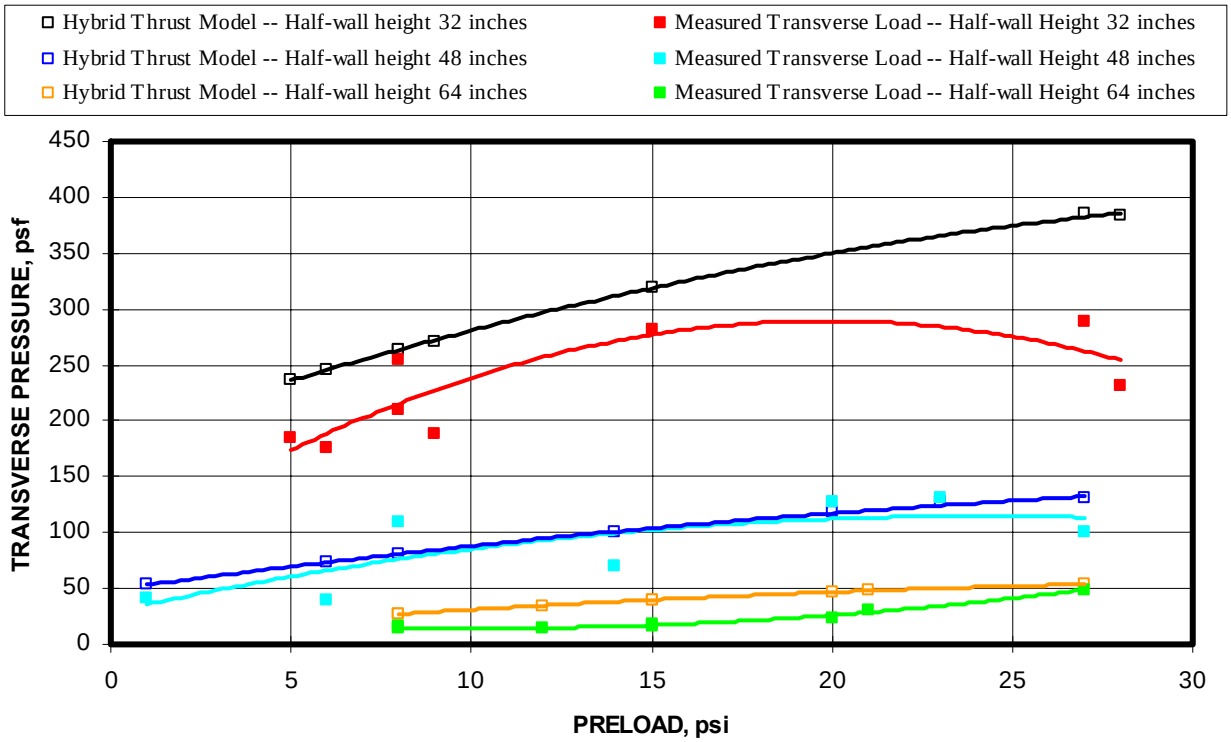

Figure 9-50. Comparison of transverse load capacities from design equations to the measured transverse load from laboratory tests (Hybrid Theoretical Thrust Model).

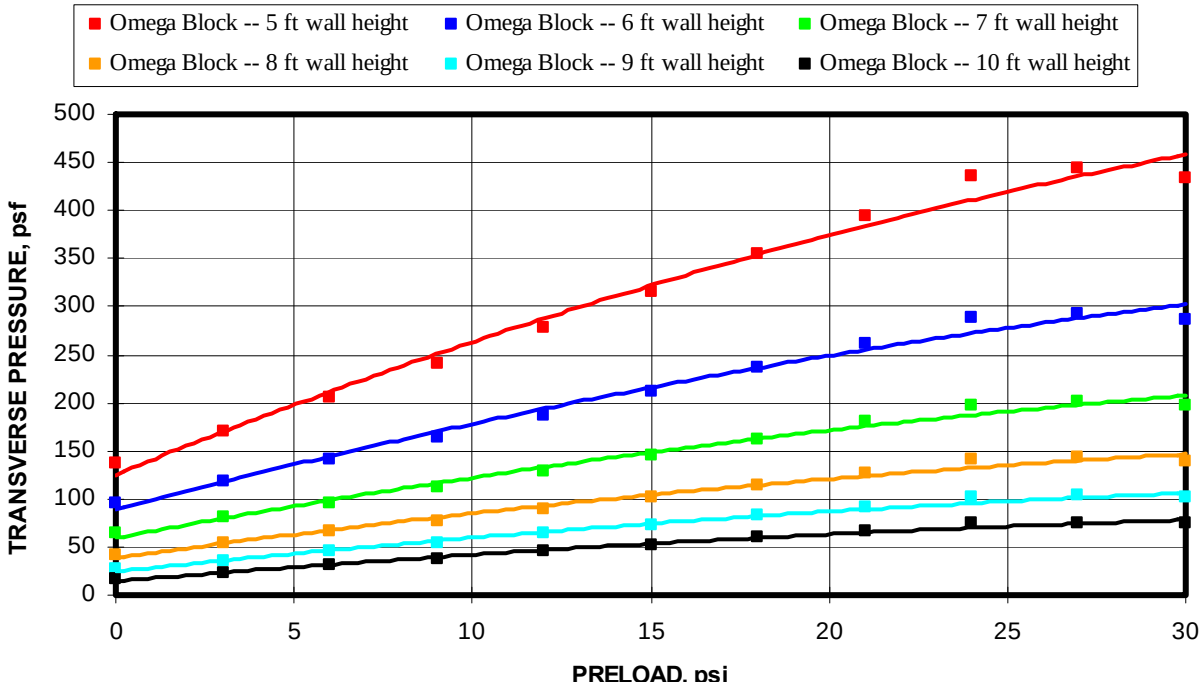

Figure 9-51. Transverse load capacity predictions for 8-in-thick walls constructed from Omega block for walls heights ranging from 5 to 10 ft (Hybrid Theoretical Thrust Model).

9.1.6.2.2 Hybrid Lateral Displacement Model

As seen in the flowchart in figure 9-3, the Hybrid Lateral Displacement Model determines the lateral displacement force from a multivariable relationship from the $Ex(t/L)^2$ term and preload, both of which are considered to be known parameters. The multivariable linear regression analysis based on 22 laboratory tests of various wall constructions is summarized in table 9-22. Equation 9.22 is used to compute the lateral displacement. Table 9-21 documents the multivariable regression analysis results. Equation 9.21 is also used for computing the resultant thrust adjustment factor for this model, except the calculated thrust forces are used instead of the measured thrust forces.

$$\text{Lateral Displacement} = 0.0333 \times Ex(t/L)^2 - 0.0293 \times \text{Preload} + 1.6449 \qquad \textbf{(9.22)}$$

Table 9-22. Multivariable regression analysis for determining lateral displacement.

Regression Statistics	
Multiple R	0.4002
R Square	0.1602
Adjusted R Square	0.0717
Standard Error	0.6337
Observations	22

ANOVA

	df	SS	MS	F	Significance F
Regression	2	1.4549	0.7275	1.8116	0.1905
Residual	19	7.6297	0.4016		
Total	21	9.0846			

	Coefficients	Standard Error	t Stat	P-value	Lower 95%	Upper 95%	Lower 95.0%	Upper 95.0%
Intercept	1.6449	0.5187	3.1710	0.0050	0.5592	2.7305	0.5592	2.7305
E*(t/L)^2	0.0332	0.0365	0.9102	0.3741	-0.0432	0.1097	-0.0432	0.1097
Preload	-0.0293	0.0167	-1.7575	0.0949	-0.0642	0.0056	-0.0642	0.0056

Figure 9-52 compares the results of the predicted transverse load capacities from the hybrid theoretical lateral displacement model with the measured laboratory test results for half-wall heights of 32, 48, and 64 inches with varying preloads. As seen from the graph, the prediction for the 32-in high half-wall is significantly improved compared to the thrust model. Prediction at the other two wall heights is about the same as that of the thrust model. Figure 9-53 shows transverse load predictions using the hybrid theoretical lateral displacement for walls constructed from Omega block ranging in height from 5 to 10 feet in one foot increments with preloads ranging from 0 to 30 psi.

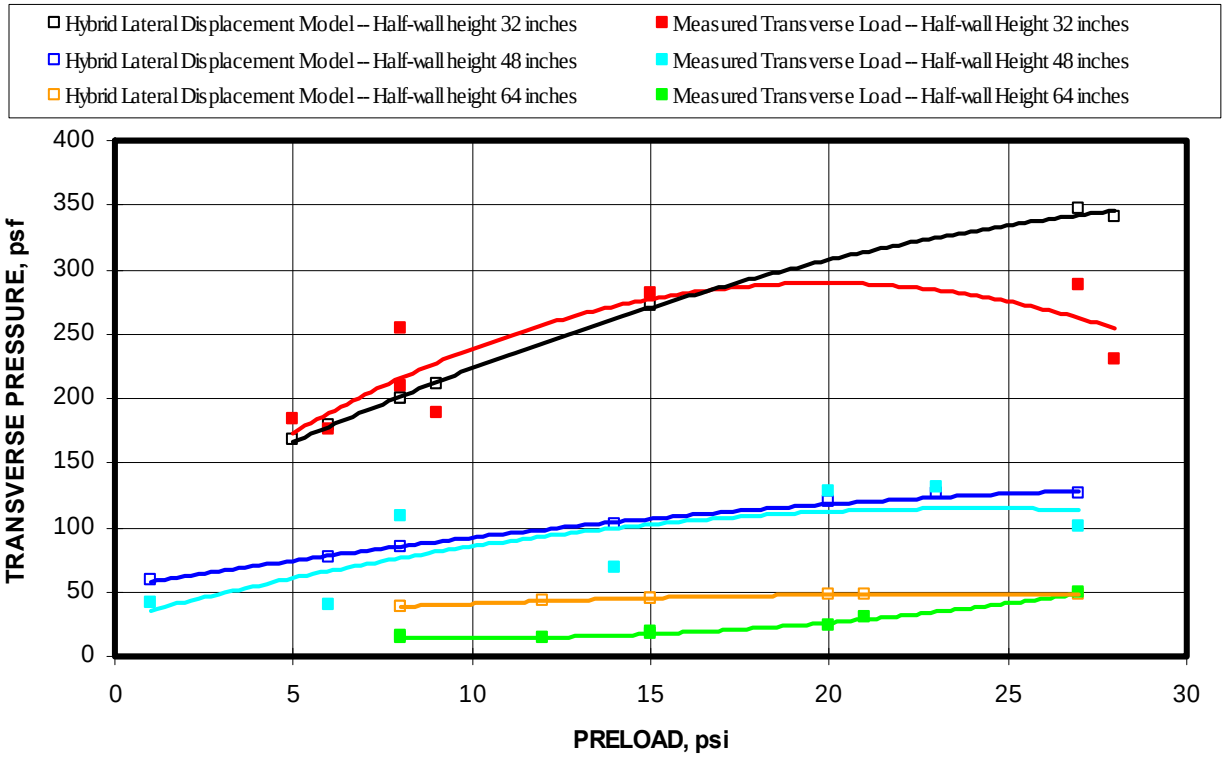

Figure 9-52. Comparison of transverse load capacities from design equations to the measured transverse load from laboratory tests (Hybrid Theoretical Lateral Displacement Model).

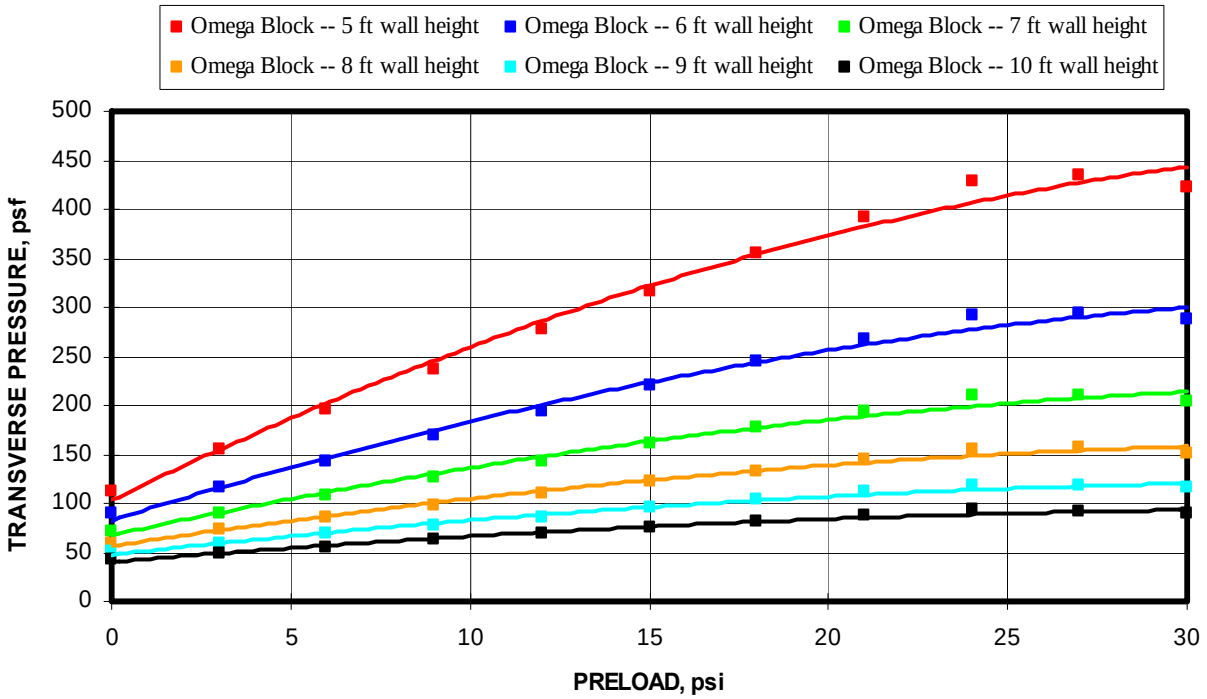

Figure 9-53. Transverse load capacity predictions for 8-in-thick walls constructed from Omega block for walls heights ranging from 5 to 10 ft (Hybrid Theoretical Lateral Displacement Model).

9.1.6.2.3 Hybrid Combination Model

The Hybrid Combination Model combines the previous two models by empirically determining both the thrust and lateral displacement. Figure 9-54 compares this model's predictions of transverse load capacity to the measured transverse load capacities from the laboratory testing. Overall, the results with the combination thrust and lateral displacement model are improved over the individual models. The transverse load predictions for the low (32-in-high half-wall) and high (64-in-high half-wall) wall heights are significantly improved. The prediction at the 48-in half-wall height is slightly worse. For completeness, figure 9-55 is included which displays the transverse load predictions using the hybrid theoretical combination model for 8-in-thick walls constructed from Omega block ranging in height from 5 to 10 feet in one foot increments with preloads ranging from 0 to 30 psi.

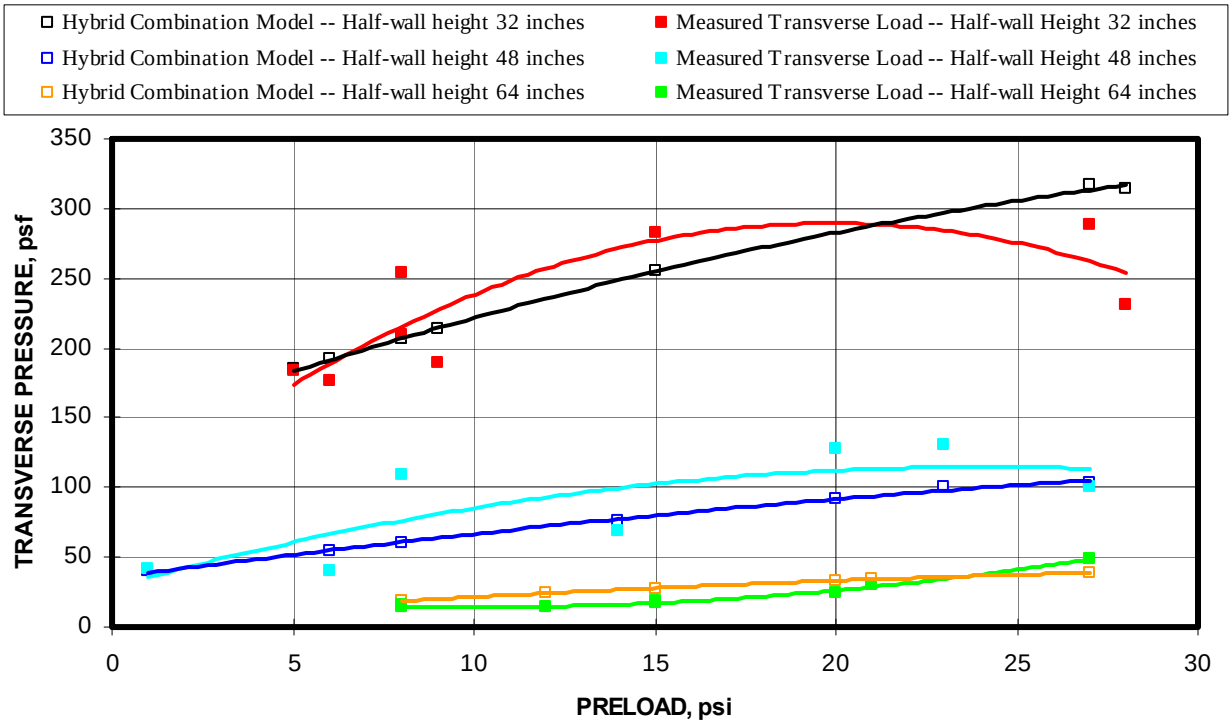

Figure 9-54. Comparison of transverse load capacities from design equations to the measured transverse load from laboratory tests (Hybrid Theoretical Combination Model).

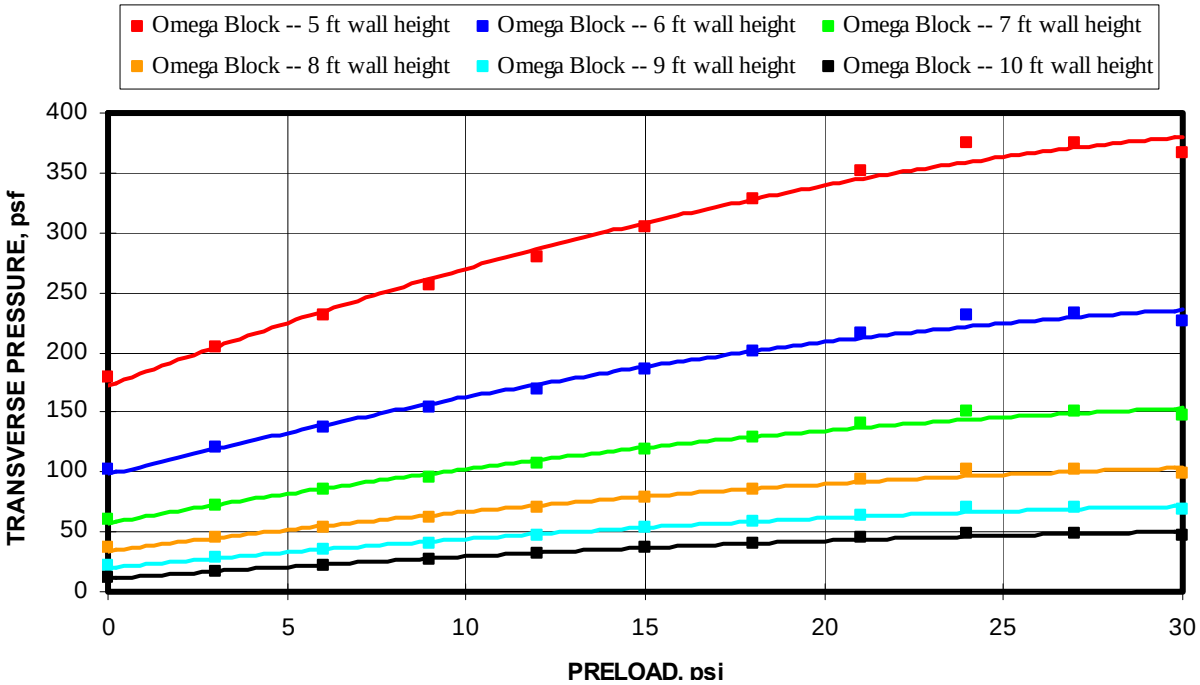

Figure 9-55. Transverse load capacity predictions for 8-in-thick walls constructed from Omega block for walls heights ranging from 5 to 10 ft (Hybrid Theoretical Combination Model).

9.1.6.3 Summary of Design Equations for Omega Block

In summary, a full empirical design model and three hybrid theoretical design models were developed for the Omega block stopping constructions. Figure 9-56 displays the calculated transverse load capacities from full empirical model compared to the measured capacities from the MRS tests. The model over predicts the short and medium height walls and under predicts the high wall height performance. The dashed line represents a perfect correlation between the calculated and measured capacities. The red trend line represents the linear regression between the measured and calculated capacities. The regression lines shows that on average the model tends to under predict the transverse load. The regression trend line shows a 10 pct difference between the measured and calculated transverse load. The shaded blue area is a +/- 40 psf variation from the perfect correlation. Examining the chart, it is seen that 73% of the data falls within this variation. Figure 9-57 displays this same information for the three hybrid theoretical design models. Based on the regression trend line correlating the calculated transverse loads to the measured transverse loads, the combination model, which computes both the thrust and lateral displacement from laboratory test data, is the most accurate of the three, with a 4 pct difference in calculated and measured loads. The least accurate is the thrust model with 23 pct difference, largely due to the over prediction of high wall performance. Examining the +/-50 psf variation (blue shading), the combination model has 100% of the data within this variation. The lateral displacement model has 86 pct of the data within this variation, while the thrust model has only 68 pct of the data within the +/-50 psf variation.

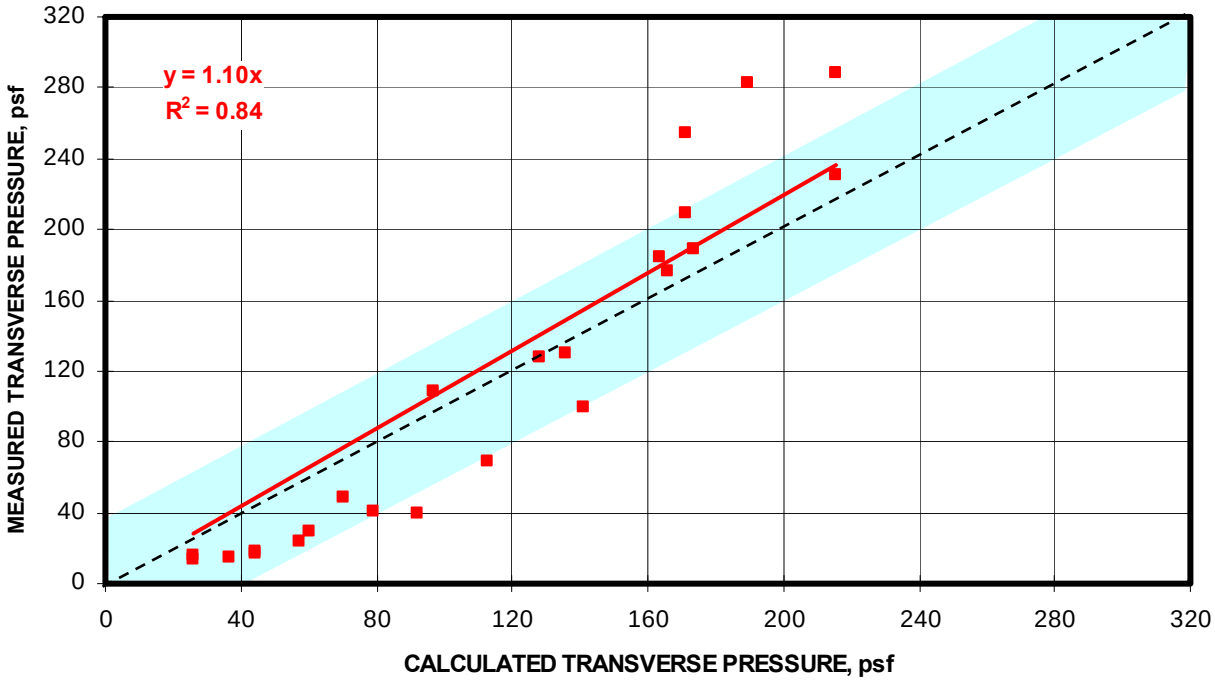

Figure 9-56. Comparison of predicted transverse load capacities compared to the measured capacities for the MRS laboratory tests (Full Empirical Model).

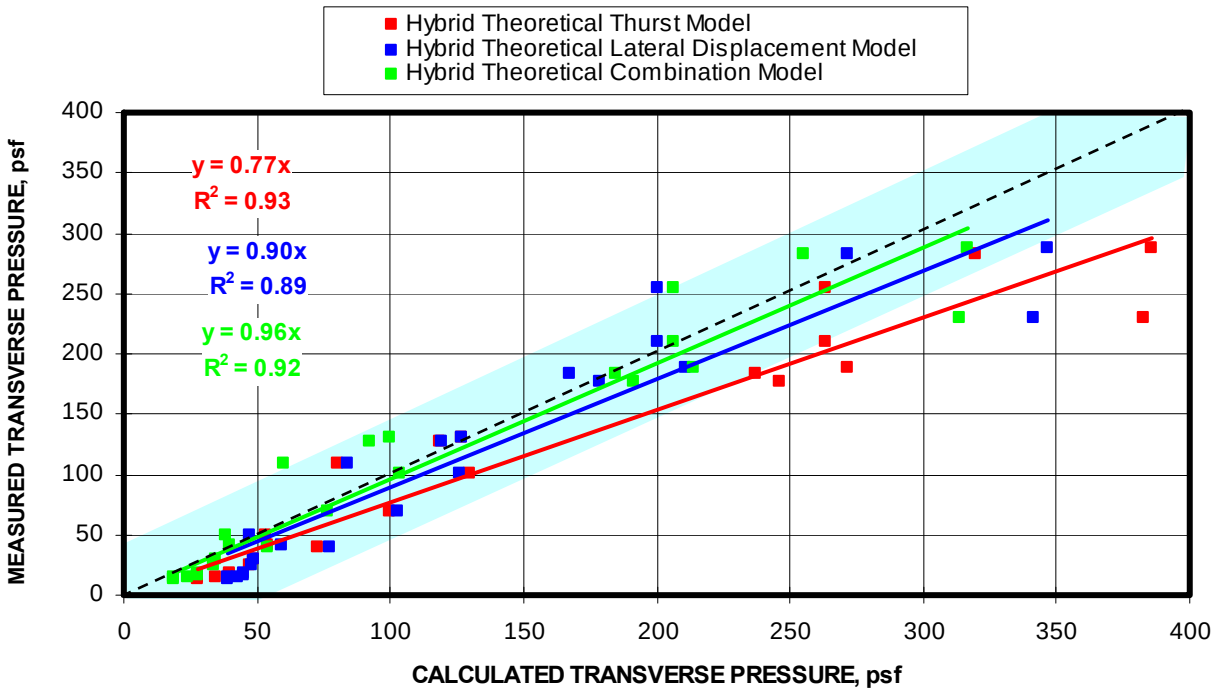

Figure 9-57. Comparison of predicted transverse load capacities compared to the measured capacities for the MRS laboratory tests (Hybrid Theoretical Models).

9.1.7 Peerless Super Block

Peerless Super Block is unique block construction with imbedded Styrofoam pellets in a very weak concrete mix. It has a compressive strength of only 86 psi, comparable to the Omega block. This block measures nominally 6x16x24 inches and weighs approximately 16 lbs. Thirty tests were conducted with the Peerless Super block, providing a good data set to construct the prediction models; however, the non-uniform distribution of the foam pellets and very weak concrete material led to inconsistent performance of the stopping walls.

9.1.7.1 Full Empirical Model

In order to improve the accuracy of the model predictions, the modulus was varied as a function of half-wall height according to equation 9.23. In reality, the modulus is not changing, but the deformation zone associated with the wall rotation produces a differing behavior. Changing the modulus is one way to adjust for this issue and incorporate the response into the existing prediction models. Table 9-23 shows the results of the multivariable regression analysis correlating the transverse load to the $Ex(t/L)^2$ and preload. From this regression analysis, the design equation for Peerless Super Block is shown in equation 9.24.

$$\text{Modulus (E)} = 5.5098 \times \text{Half-wall height}^{1.7793} \quad \textbf{(9.23)}$$

Table 9-23. Multivariable regression analysis for determining transverse load from modulus and wall geometric parameters.

Regression Statistics	
Multiple R	0.6405
R Square	0.4102
Adjusted R Square	0.3665
Standard Error	26.2746
Observations	30

ANOVA

	df	SS	MS	F	Significance F
Regression	2	12965	6482	9.3898	0.0008
Residual	27	18640	690		
Total	29	31604			

	Coefficients	Standard Error	t Stat	P-value	Lower 95%	Upper 95%	Lower 95.0%	Upper 95.0%
Intercept	-142.1965	46.0870	-3.0854	0.0047	-236.7591	-47.6340	-236.7591	-47.6340
E x $(t/L)^2$	8.3052	2.1515	3.8602	0.0006	3.8907	12.7198	3.8907	12.7198
Preload	0.6435	0.2355	2.7320	0.0110	0.1602	1.1268	0.1602	1.1268

Transverse Load = 8.3052 x E x $(t/L)^2$ + .6435 x Preload – 142.1965 **(9.24)**

Where E = material modulus = 3,000 to 10,000 psi for Peerless Super Block,

t = wall thickness, in,

L = full wall height, in, and

Preload = ground pressure preload, psi.

Figure 9-58 compares the predicted transverse load capacities from the empirical model with the measured laboratory results for the half wall heights with varying preloads. As seen in the figure, the model predictions are reasonably accurate only for the 48-in half-wall height. The transverse load is considerably over predicted for the 64-in half-wall height and under predicted for the 32-in half-wall height. This discrepancy is a tradeoff in the modulus adjustment values, which were adjusted to give the best-fit overall for all the models. Figure 9-59 shows transverse load predictions using this empirical design model for walls constructed from Peerless Super Block ranging in height from 5 to 10 feet in one foot increments with preloads ranging from 0 to 100 psi.

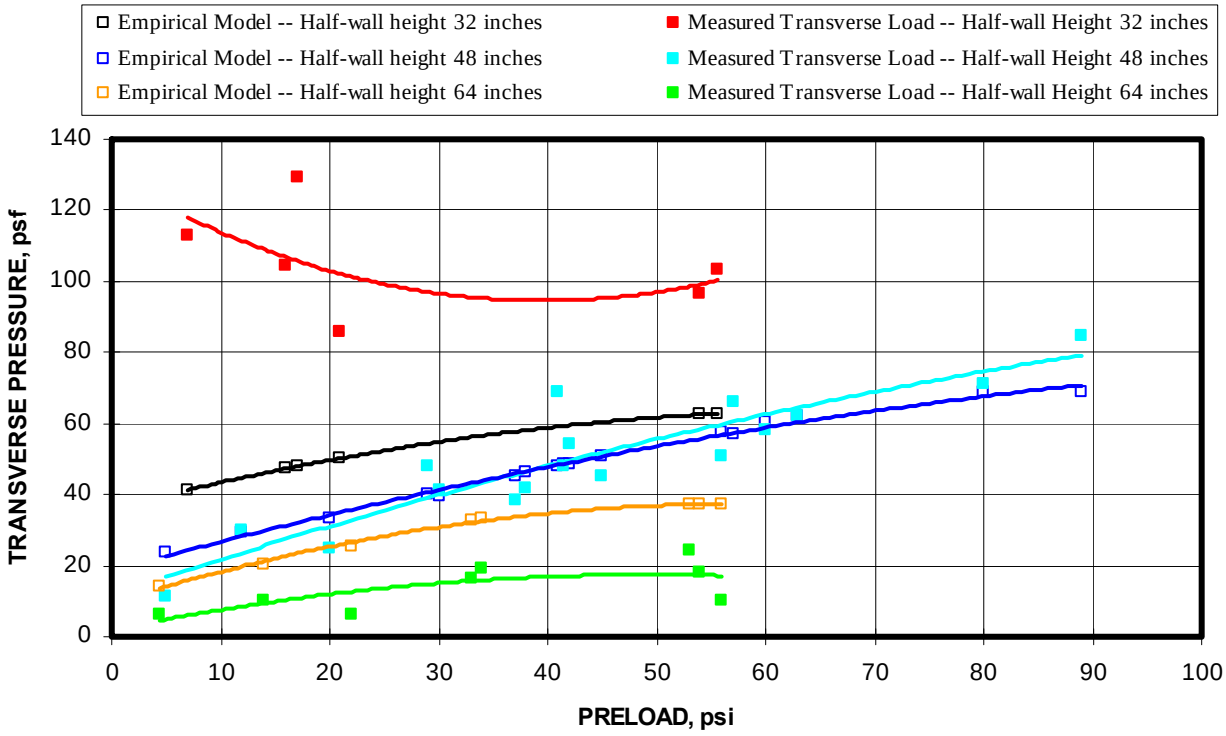

Figure 9-58. Comparison of design equation predictions with measured transverse load from laboratory testing (Full Empirical Model – Peerless Super Block).

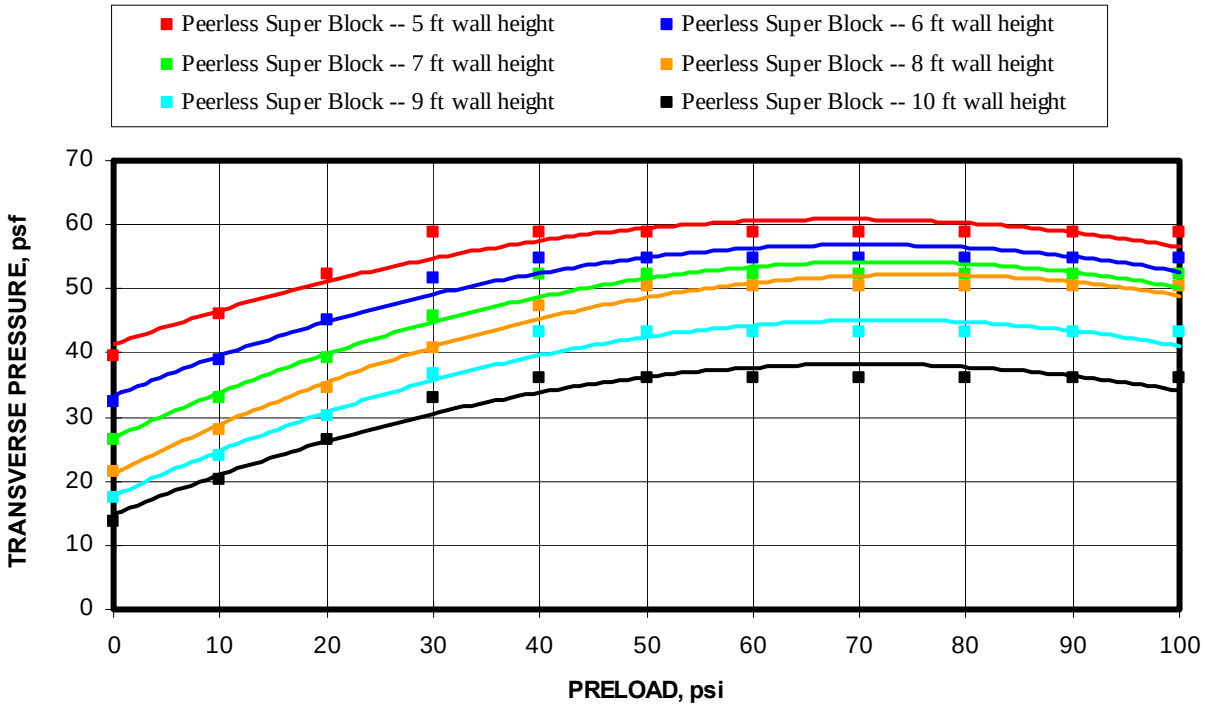

Figure 9-59. Transverse load capacity predictions for 6-in-thick walls constructed from Peerless Super Block for walls heights ranging from 5 to 10 ft (Full Empirical Model).

9.1.7.2 Hybrid Theoretical Models

Transverse load capacity forecasts will be made using the three hybrid theoretical models: (1) Hybrid Thrust Model, (2) Hybrid Lateral Displacement Model, and (3) Hybrid Combination Thrust and Lateral Displacement Model.

9.1.7.2.1 Hybrid Thrust Model

As seen in the flowchart in figure 9-2, the Hybrid Thrust Model determines the normalized thrust force from a multivariable relationship between the thrust force and the $Ex(t/L)^2$ term and preload, both of which are considered to be known parameters. The multivariable linear regression analysis based on 30 laboratory tests of various wall constructions is summarized in table 9-25. Equation 9.26 is used to compute the normalized thrust force per unit width of wall. Table 9-26 documents the multivariable regression analysis results used to determine the resultant thrust position factor (d).

Table 9-25. Multivariable regression analysis for determining arching thrust.

Regression Statistics	
Multiple R	0.8994
R Square	0.8089
Adjusted R Square	0.7948
Standard Error	0.0358
Observations	30

ANOVA

	df	SS	MS	F	Significance F
Regression	2	0.1461	0.0731	57.1581	0.0000
Residual	27	0.0345	0.0013		
Total	29	0.1807			

	Coefficients	Standard Error	t Stat	P-value	Lower 95%	Upper 95%	Lower 95.0%	Upper 95.0%
Intercept	0.0603	0.0627	0.9612	0.3450	-0.0684	0.1890	-0.0684	0.1890
E*(t/L)^2	-0.0012	0.0029	-0.4027	0.6903	-0.0072	0.0048	-0.0072	0.0048
Preload	0.0033	0.0003	10.3648	0.0000	0.0027	0.0040	0.0027	0.0040

$$P/BL = - 0.0012 \times Ex(t/L)^2 + .0033 \times Preload + .0603 \quad \textbf{(9.26)}$$

Where P/BL = Normalized thrust per unit width of block, kips/in,

E = Elastic modulus = 3,000 to 10,000 psi for Peerless Super Block,

t = wall thickness, in,

L = height of wall, in, and

Preload = preload pressure, psi.

Table 9-26. Multivariable regression analysis for determining resultant thrust position factor.

Regression Statistics	
Multiple R	0.6405
R Square	0.4102
Adjusted R Square	0.3665
Standard Error	13.1373
Observations	30

ANOVA

	df	SS	MS	F	Significance F
Regression	2	3241.1529	1620.5764	9.3898	0.0008
Residual	27	4659.9095	172.5892		
Total	29	7901.0624			

	Coefficients	Standard Error	t Stat	P-value	Lower 95%	Upper 95%	Lower 95.0%	Upper 95.0%
Intercept	-71.0983	23.0435	-3.0854	0.0047	-118.3796	-23.8170	-118.3796	-23.8170
E*(t/L)^2	4.1526	1.0758	3.8602	0.0006	1.9453	6.3599	1.9453	6.3599
Preload	0.3218	0.1178	2.7320	0.0110	0.0801	0.5634	0.0801	0.5634

$$d = -0.0034 \times \text{Half-wall Height} - 0.0188 \times \text{Thrust} + 0.7892 \quad \textbf{(9.27)}$$

Figure 9-60 compares the results of the predicted transverse load capacities from the hybrid theoretical thrust model with the measured laboratory test results for half-wall heights

of 32, 48, and 64 inches with varying preloads. As seen from the graph, the model over predicts the transverse load with the exception of the 32-in half-wall height at the lower preloads. This is caused primarily by discrepancies in the lateral displacement, which is theoretically determined from the thrust load. In several tests, the block would fail causing temporary transverse load shedding during the transverse load development. This would produce a large lateral displacement at times that would not be accurately predicted by the model. The thrust model is also hampered by inconsistent thrust development. At times, the thrust would decrease from the initial preload, instead of building thrust as the arching develops. This is due to weak material and inconsistent presence of the foam pellets in the hinge area. Figure 9-61 shows transverse load predictions using this empirical design model for 6-in-thick walls constructed from Peerless Super Block ranging in height from 5 to 10 feet in one foot increments with preloads ranging from 0 to 100 psi.

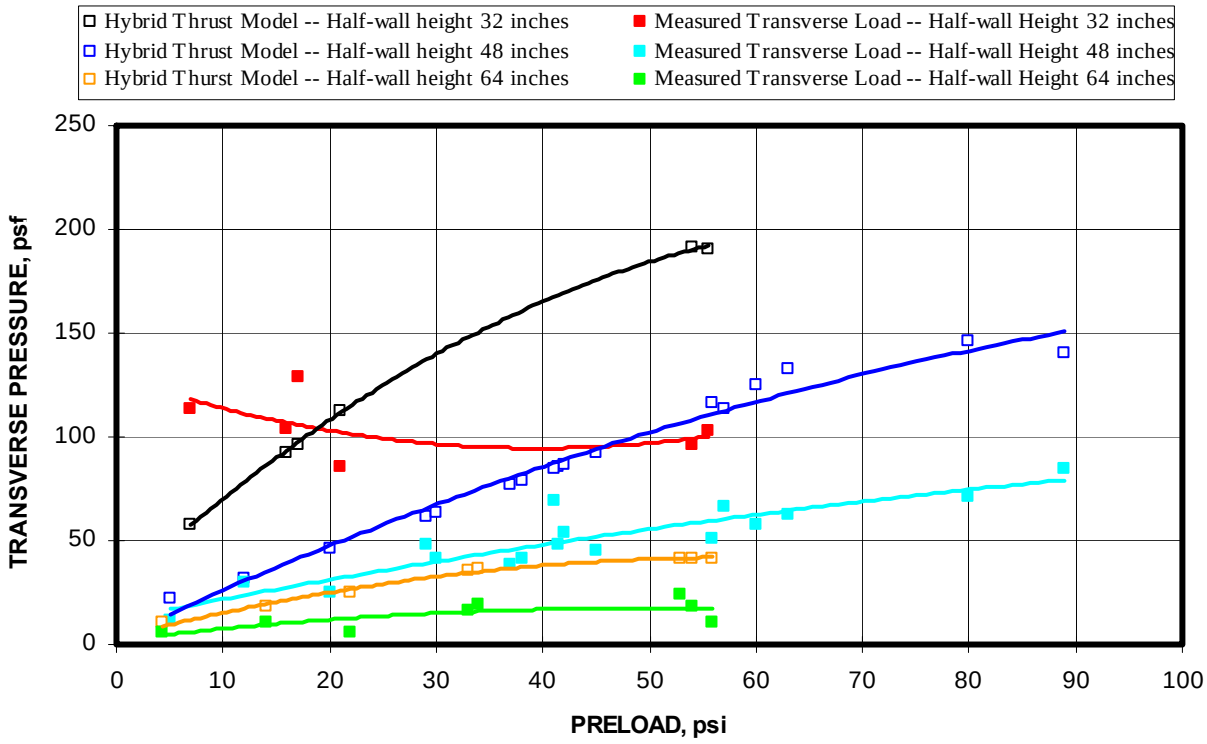

Figure 9-60. Comparison of transverse load capacities from design equations to the measured transverse load from laboratory tests (Hybrid Theoretical Thrust Model).

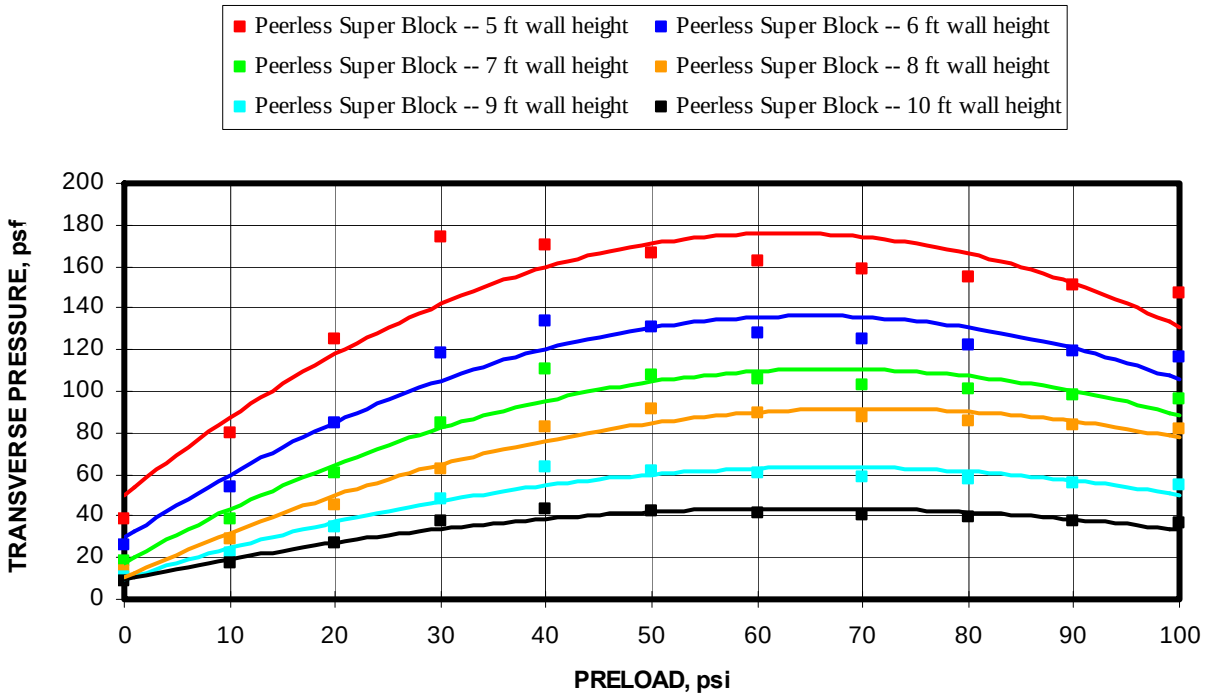

Figure 9-61. Transverse load capacity predictions for 6-in-thick walls constructed from Peerless Super Block for walls heights ranging from 5 to 10 ft (Hybrid Theoretical Thrust Model).

9.1.7.2.2 Hybrid Lateral Displacement Model

As seen in the flowchart in figure 9-3, the Hybrid Lateral Displacement Model determines the lateral displacement force from a multivariable relationship from the $Ex(t/L)^2$ term and preload, both of which are considered to be known parameters. The multivariable linear regression analysis based on 30 laboratory tests of various wall constructions is summarized in table 9-27. Equation 9.28 is used to compute the lateral wall displacement. Table 9-26 documented the multivariable regression analysis results used to determine the resultant thrust position factor (d) for the Hybrid Thrust Model. This equation is also used for computing the resultant thrust adjustment factor for this model, except the calculated thrust forces are used instead of the measured thrust forces.

$$\text{Lateral Displacement} = 0.0038 \times Ex(t/L)^2 - 0.0177 \times \text{Preload} + 1.5636 \quad \textbf{(9.28)}$$

Regression Statistics	
Multiple R	0.6082
R Square	0.3699
Adjusted R Square	0.3233
Standard Error	0.5098
Observations	30

Table 9-27. Multivariable regression analysis for determining lateral displacement.

ANOVA

	df	SS	MS	F	Significance F
Regression	2	4.1200	2.0600	7.9263	0.0020
Residual	27	7.0170	0.2599		
Total	29	11.1370			

	Coefficients	Standard Error	t Stat	P-value	Lower 95%	Upper 95%	Lower 95.0%	Upper 95.0%
Intercept	1.5636	0.8942	1.7485	0.0917	-0.2712	3.3983	-0.2712	3.3983
E*(t/L)^2	0.0038	0.0417	0.0918	0.9276	-0.0818	0.0895	-0.0818	0.0895
Preload	-0.0177	0.0046	-3.8736	0.0006	-0.0271	-0.0083	-0.0271	-0.0083

Figure 9-62 compares the results of the predicted transverse load capacities from the hybrid theoretical lateral displacement model with the measured laboratory test results for half-wall heights of 32, 48, and 64 inches with varying preloads. As seen from the graph, the predictions overall are similar to the hybrid theoretical thrust model presented in figure 9-60. Figure 9-63 shows transverse load predictions using the hybrid theoretical lateral displacement for walls constructed from Peerless Super Block ranging in height from 5 to 10 feet in one foot increments with preloads ranging from 0 to 100 psi.

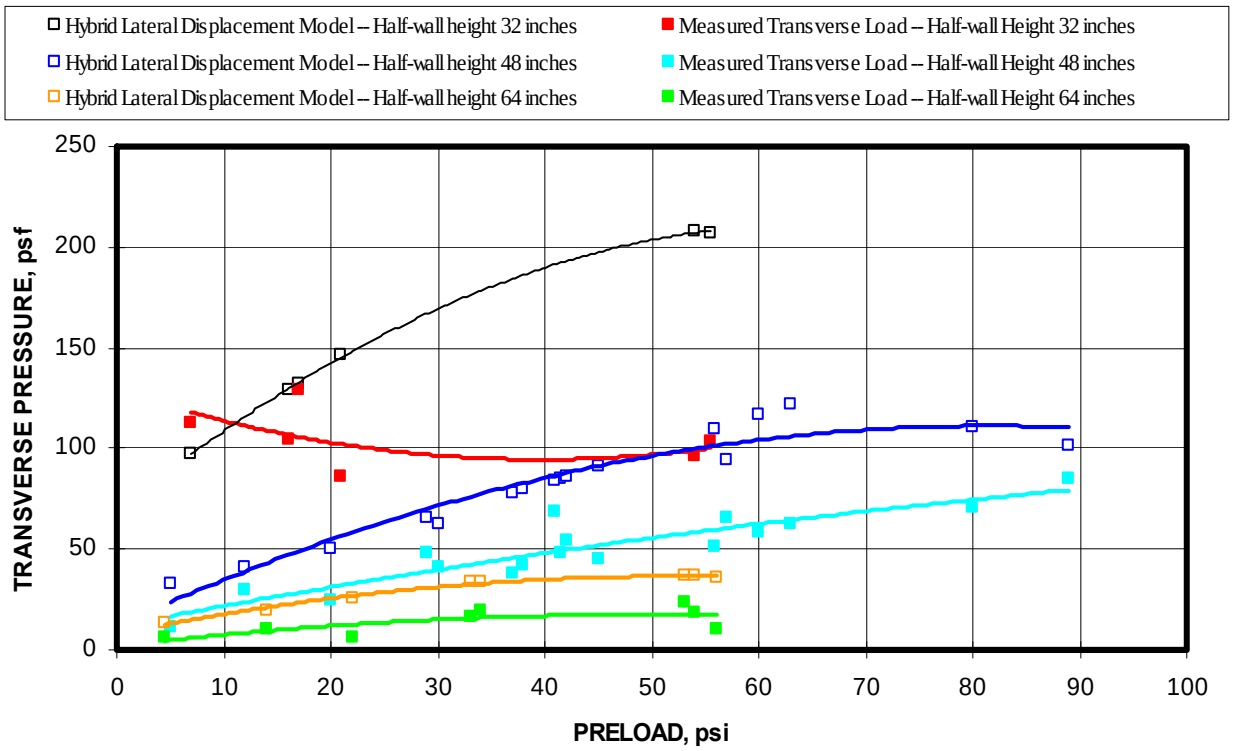

Figure 9-62. Comparison of transverse load capacities from design equations to the measured transverse load from laboratory tests (Hybrid Theoretical Lateral Displacement Model).

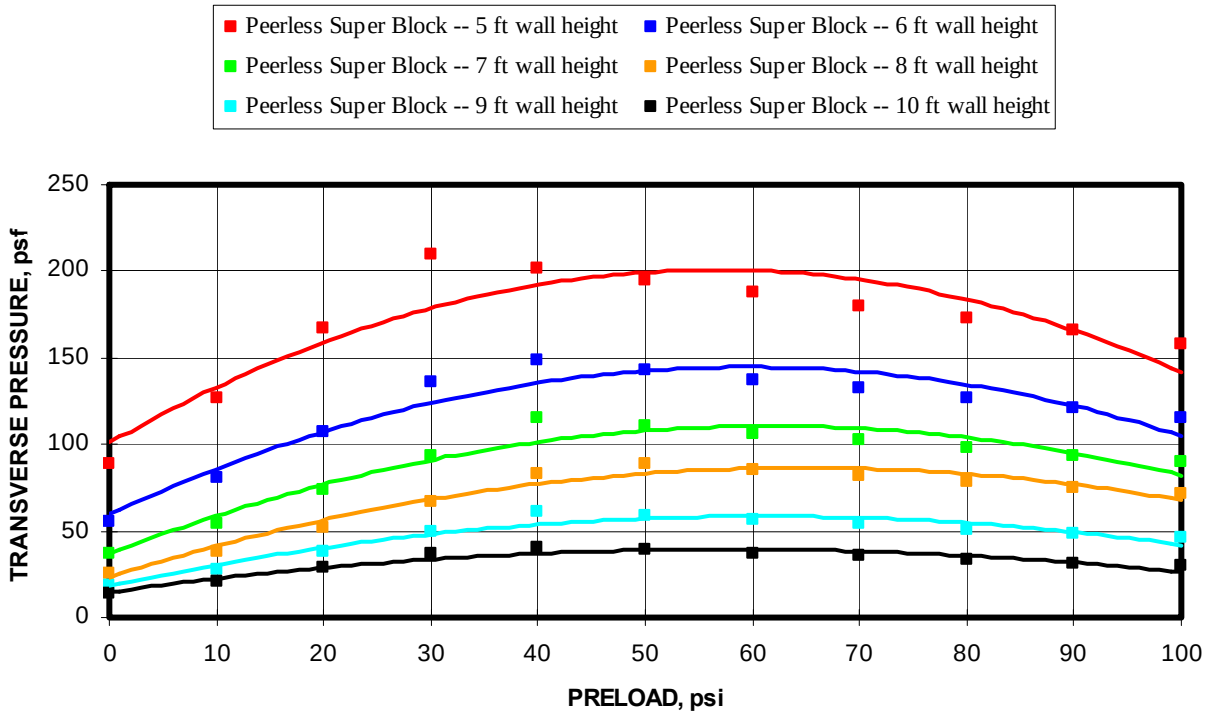

Figure 9-63. Comparison of transverse load capacities from design equations to the measured transverse load from laboratory tests (Hybrid Theoretical Lateral Displacement Model).

9.1.7.2.3 Hybrid Combination Model

The Hybrid Combination Model combines the previous two models by empirically determining both the thrust and lateral displacement. Figure 9-64 compares this model's predictions of transverse load capacity to the measured transverse load capacities from the laboratory testing. The results are much improved over the other two models, especially for 32 and 48-in half-wall heights. This improved prediction capability is due to use of empirical data for both the thrust and lateral displacement parameters. For completeness, figure 9-65 is included which displays the transverse load predictions using the hybrid theoretical combination model for 6-in-thick walls constructed from Peerless Super Block ranging in height from 5 to 10 feet in one foot increments with preloads ranging from 0 to 100 psi.

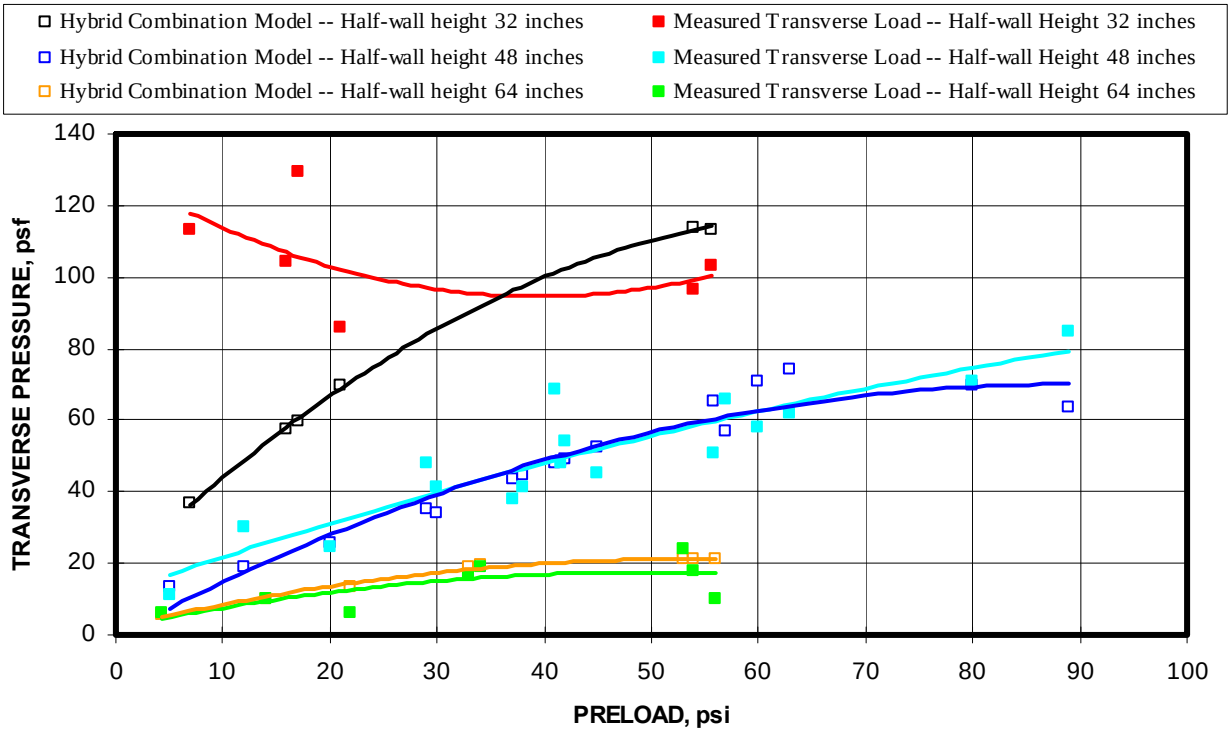

Figure 9-64. Comparison of transverse load capacities from design equations to the measured transverse load from laboratory tests (Hybrid Theoretical Combination Model).

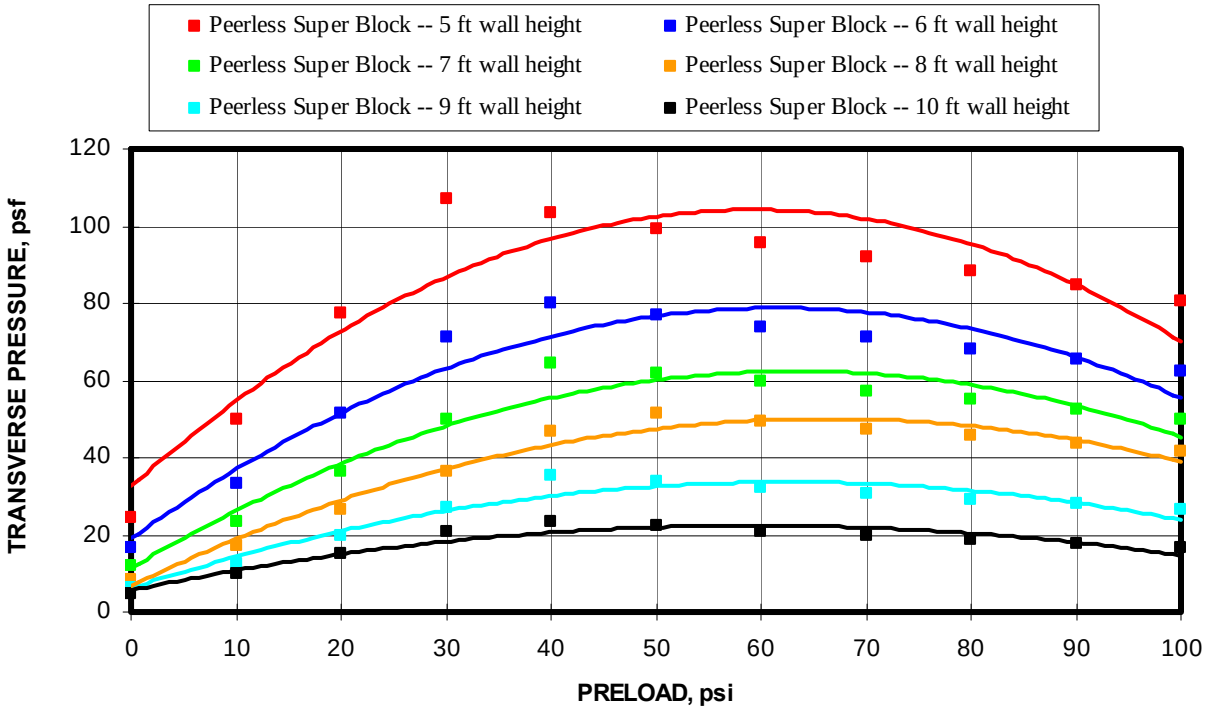

Figure 9-65. Transverse load capacity predictions for 6-in-thick walls constructed from Peerless Super Block for walls heights ranging from 5 to 10 ft (Hybrid Theoretical Combination Model).

9.1.7.3 Summary of Design Equations for Peerless Super Block

In summary, a full empirical design model and three hybrid theoretical design models were developed for the Peerless Super Block stopping constructions. Figure 9-66 displays the calculated transverse load capacities from full empirical model compared to the measured capacities from the MRS tests. The dashed line represents a perfect correlation between the calculated and measured capacities. The red trend line represents the linear regression between the measured and calculated capacities. The regression line shows that on average the model under predicts the transverse load, although this is largely due to the poor prediction of the shortest wall height. The regression trend line shows a 20 pct difference between the measured and calculated transverse load. The shaded blue area is a +/- 20 psf variation from the perfect correlation. Examining the chart, it is seen that 73% of the data falls within this variation. Figure 9-67 displays this same information for the three hybrid theoretical design models. Based on the regression trend line correlating the calculated transverse loads to the measured transverse loads, the combination model, which computes both the thrust and lateral displacement from laboratory test data, is clearly the most accurate of the three, with a 3 pct difference in calculated and measured loads. The thrust and lateral displacement model produce similar results with an error of 39 pct. Examining the +/-20 psf variation (blue shading), the hybrid combination model has 73 pct of the data within this variation, while the thrust model and the lateral displacement models only 27 and 43 pct respectively of their data within this variation.

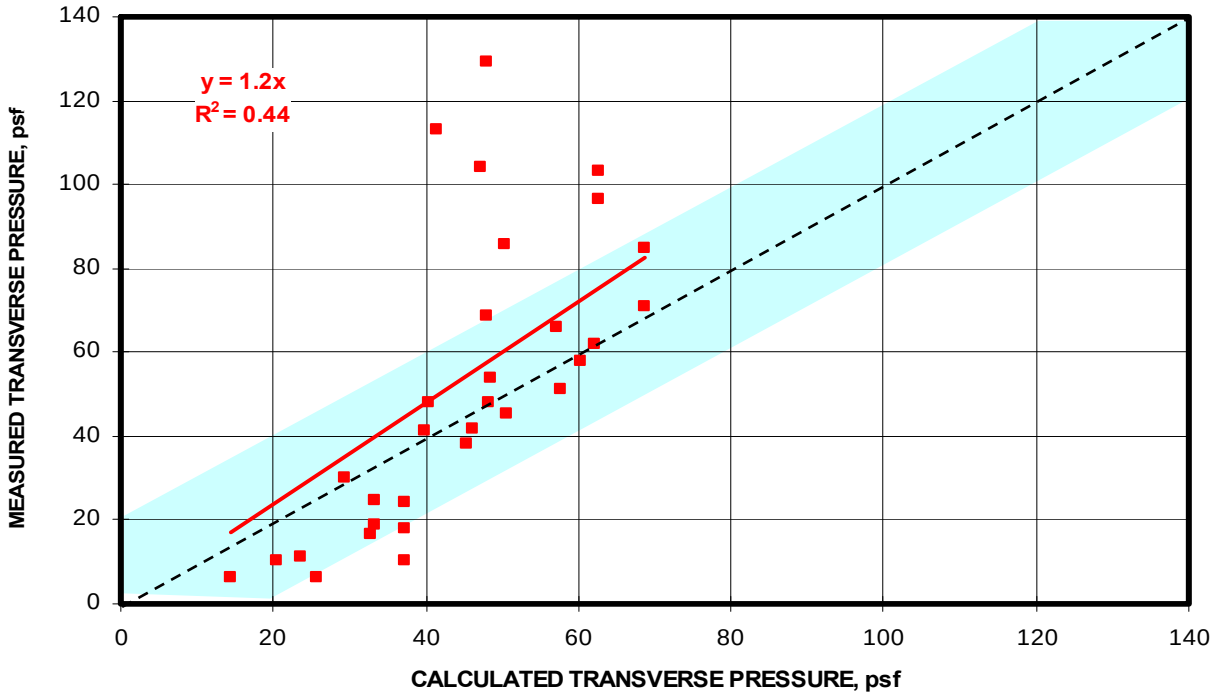

Figure 9-66. Comparison of predicted transverse load capacities compared to the measured capacities for the MRS laboratory tests (Full Empirical Model).

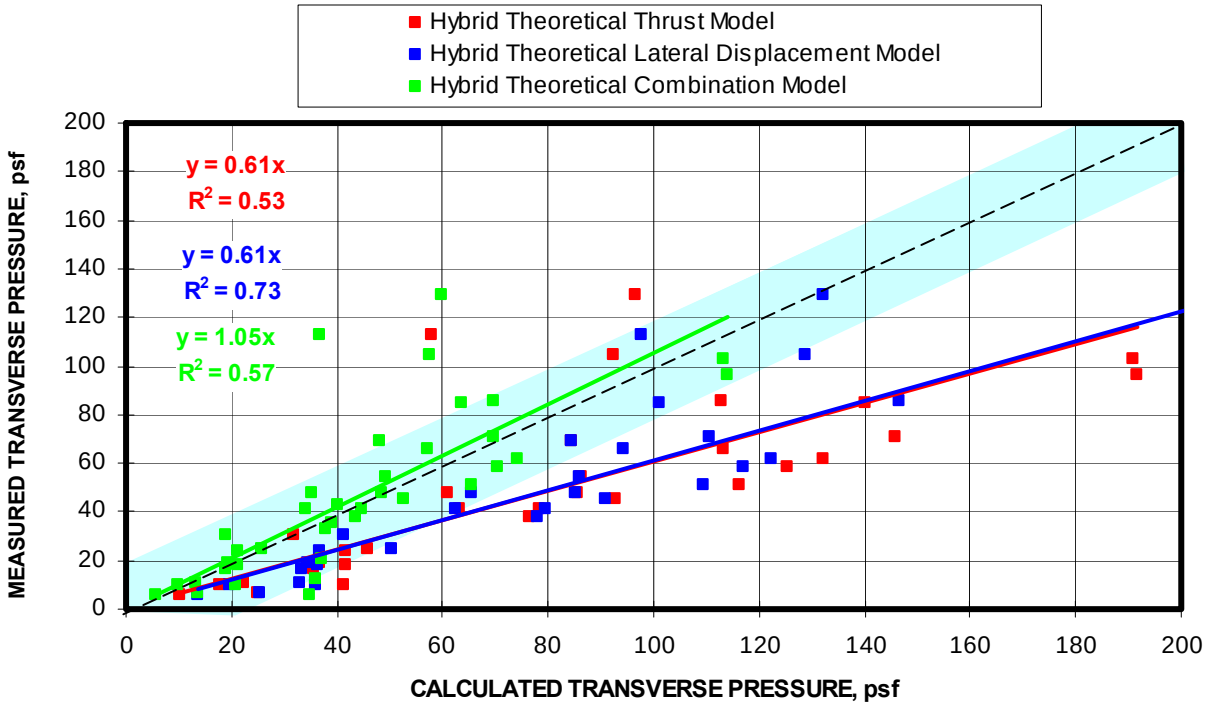

Figure 9-67. Comparison of predicted transverse load capacities compared to the measured capacities for the MRS laboratory tests (Hybrid Theoretical Models).

9.1.8 Klondike Hollow Core Block

Klondike Hollow Core Block is a standard Portland cement block with three hollow core areas to reduce the material volume and weight of the block. This block measures nominally 6x8x16 inches, but weighs only 32 lbs compared to the 47 lbs weight of the standard solid block. Its compressive strength is 907 psi compared to 1,330 psi for the solid block. A total of 23 tests were conducted with the Klondike Hollow Core Block, sufficient to produce good block models for transverse load prediction.

9.1.8.1 Full Empirical Model

In order to improve the accuracy of the model predictions, the modulus was varied as a function of half-wall height according to equation 9.29. In reality, the modulus is not changing, but the deformation zone associated with the wall rotation produces a differing behavior. Changing the modulus is one way to adjust for this issue and incorporate the response into the existing prediction models. Table 9-28 shows the results of the multivariable regression analysis correlating the transverse load to the $Ex(t/L)^2$ and preload. From this regression analysis, the design equation for Klondike Hollow Core Block is shown in equation 9.30.

$$\text{Modulus (E)} = 1491.2 \times \text{Half-wall height} - 5263.2 \quad \textbf{(9.29)}$$

Table 9-28. Multivariable regression analysis for determining transverse load from modulus and wall geometric parameters.

Regression Statistics	
Multiple R	0.7523
R Square	0.5660
Adjusted R Square	0.5226
Standard Error	342.4931
Observations	23

ANOVA

	df	SS	MS	F	Significance F
Regression	2	3059879	1529939	13.0428	0.0002
Residual	20	2346031	117302		
Total	22	5405910			

	Coefficients	Standard Error	t Stat	P-value	Lower 95%	Upper 95%	Lower 95.0%	Upper 95.0%
Intercept	-1186.8305	409.3905	-2.8990	0.0089	-2040.8038	-332.8572	-2040.8038	-332.8572
E x $(t/L)^2$	7.3129	1.4371	5.0888	0.0001	4.3152	10.3106	4.3152	10.3106
Preload	1.2685	1.3743	0.9231	0.3670	-1.5982	4.1352	-1.5982	4.1352

Transverse Load = 7.3129 x Ex$(t/L)^2$ + 1.2685 x Preload – 1187 **(9.30)**

Where E = material modulus = 32,500 to 85,000 psi for Klondike Hollow Core Block,

t = wall thickness, in,

L = full wall height, in, and

Preload = ground pressure preload, psi.

Figure 9-68 compares the predicted transverse load capacities from the empirical model with the measured laboratory results for the half wall heights with varying preloads. As seen in the figure, the transverse load predictions do not change much with preload, which is uncharacteristic of most other block materials. The empirical predictions of transverse pressure are reasonably accurate for the 60-in half-wall height and the 48-in half-wall height at higher preloads, but the transverse pressure prediction for the 30-in half-wall height is considerably lower than the measured results. Figure 9-69 shows transverse load predictions using this empirical design model for walls constructed from Klondike Hollow Core Block ranging in height from 5 to 10 feet in one foot increments with preloads ranging from 0 to 300 psi.

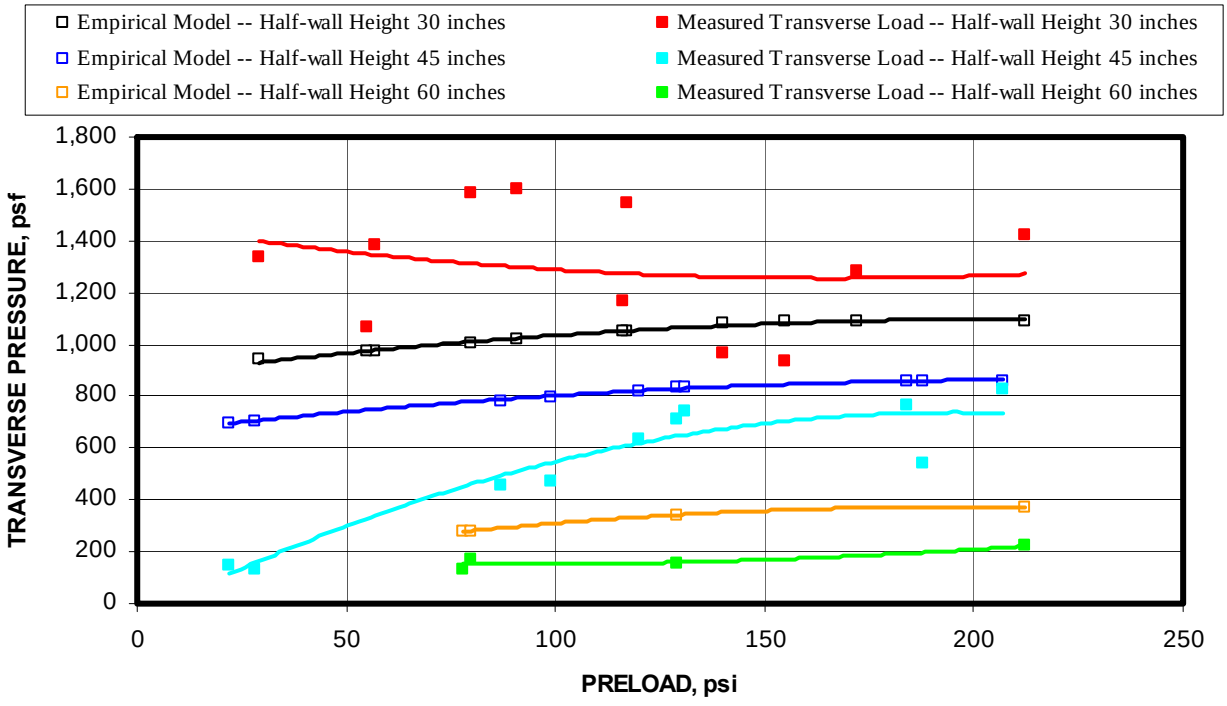

Figure 9-68. Comparison of design equation predictions with measured transverse load from laboratory testing (Full Empirical Model – Klondike Hollow Core Block).

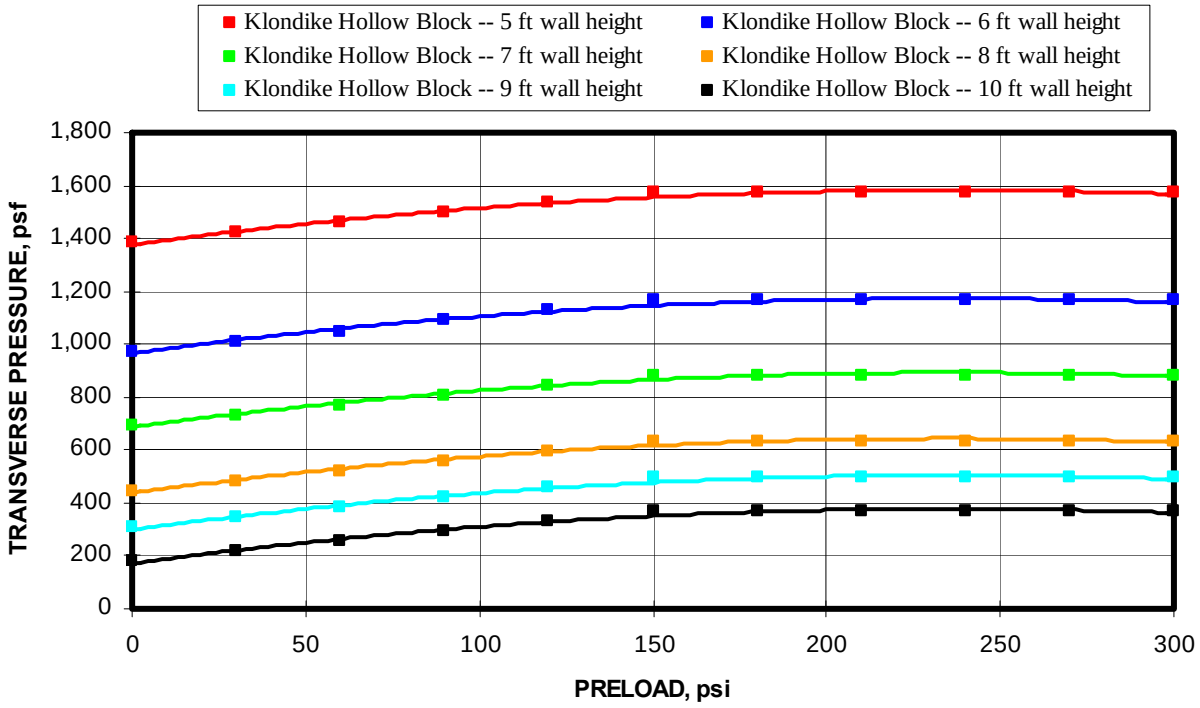

Figure 9-69. Transverse load capacity predictions for 6-in-thick walls constructed from Klondike Hollow Core Block for walls heights ranging from 5 to 10 ft (Full Empirical Model).

9.1.8.2 Hybrid Theoretical Models

Transverse load capacity forecasts will be made using the three hybrid theoretical models: (1) Hybrid Thrust Model, (2) Hybrid Lateral Displacement Model, and (3) Hybrid Combination Thrust and Lateral Displacement Model.

9.1.8.2.1 Hybrid Thrust Model

As seen in the flowchart in figure 9-2, the Hybrid Thrust Model determines the normalized thrust force from a multivariable relationship between the thrust force and the $Ex(t/L)^2$ term and preload, both of which are considered to be known parameters. The multivariable linear regression analysis based on 23 laboratory tests of various wall constructions is summarized in table 9-29. Equation 9.31 is used to compute the normalized thrust force per unit width of wall. Table 9-30 documents the multivariable regression analysis results used to determine the resultant thrust position factor (d).

Table 9-29. Multivariable regression analysis for determining arching thrust.

Regression Statistics	
Multiple R	0.4695
R Square	0.2204
Adjusted R Square	0.1425
Standard Error	0.3223
Observations	23

ANOVA

	df	SS	MS	F	Significance F
Regression	2	0.5875	0.2937	2.8278	0.0829
Residual	20	2.0775	0.1039		
Total	22	2.6650			

	Coefficients	Standard Error	t Stat	P-value	Lower 95%	Upper 95%	Lower 95.0%	Upper 95.0%
Intercept	0.2936	0.3853	0.7622	0.4548	-0.5100	1.0973	-0.5100	1.0973
E*(t/L)^ 2	0.0015	0.0014	1.1424	0.2668	-0.0013	0.0044	-0.0013	0.0044
Preload	0.0028	0.0013	2.1860	0.0409	0.0001	0.0055	0.0001	0.0055

$$P/BL = 0.0015 \times Ex(t/L)^2 + 0.0028 \times Preload + 0.2936 \quad \textbf{(9.31)}$$

Where P/BL = Normalized thrust per unit width of block, kips/in,

E = Elastic modulus = 32,500 to 85,000 psi for Klondike Hollow Core Block,

t = wall thickness, in,

L = height of wall, in, and

Preload = preload pressure, psi.

Table 9-30. Multivariable regression analysis for determining resultant thrust position factor.

Regression Statistics	
Multiple R	0.4086
R Square	0.1670
Adjusted R Square	0.0837
Standard Error	0.0511
Observations	23

ANOVA

	df	SS	MS	F	Significance F
Regression	2.0000	0.0105	0.0052	2.0044	0.1609
Residual	20.0000	0.0522	0.0026		
Total	22.0000	0.0627			

	Coefficients	Standard Error	t Stat	P-value	Lower 95%	Upper 95%	Lower 95.0%	Upper 95.0%
Intercept	1.0272	0.0557	18.4469	0.0000	0.9110	1.1433	0.9110	1.1433
Half-wall Height	-0.0013	0.0010	-1.3059	0.2064	-0.0034	0.0008	-0.0034	0.0008
Thrust	-0.0033	0.0020	-1.6450	0.1156	-0.0076	0.0009	-0.0076	0.0009

$$d\ factor = -0.0013 \times Half\text{-}wall\ Height - 0.0033 \times Thrust + 1.0272 \quad \textbf{(9.32)}$$

Figure 9-70 compares the results of the predicted transverse load capacities from the hybrid theoretical thrust model with the measured laboratory test results for half-wall heights

of 30, 45, and 60 inches with varying preloads. As seen from the graph, the predictions for the 30-in half-wall height are improved over that of the empirical model. Conversely, the 60-in half-wall height predictions are less accurate for this model. Figure 9-71 shows transverse pressure predictions using this empirical design model for 6-in-thick walls constructed from Klondike Hollow Core Block ranging in height from 5 to 10 feet in one foot increments with preloads ranging from 0 to 300 psi.

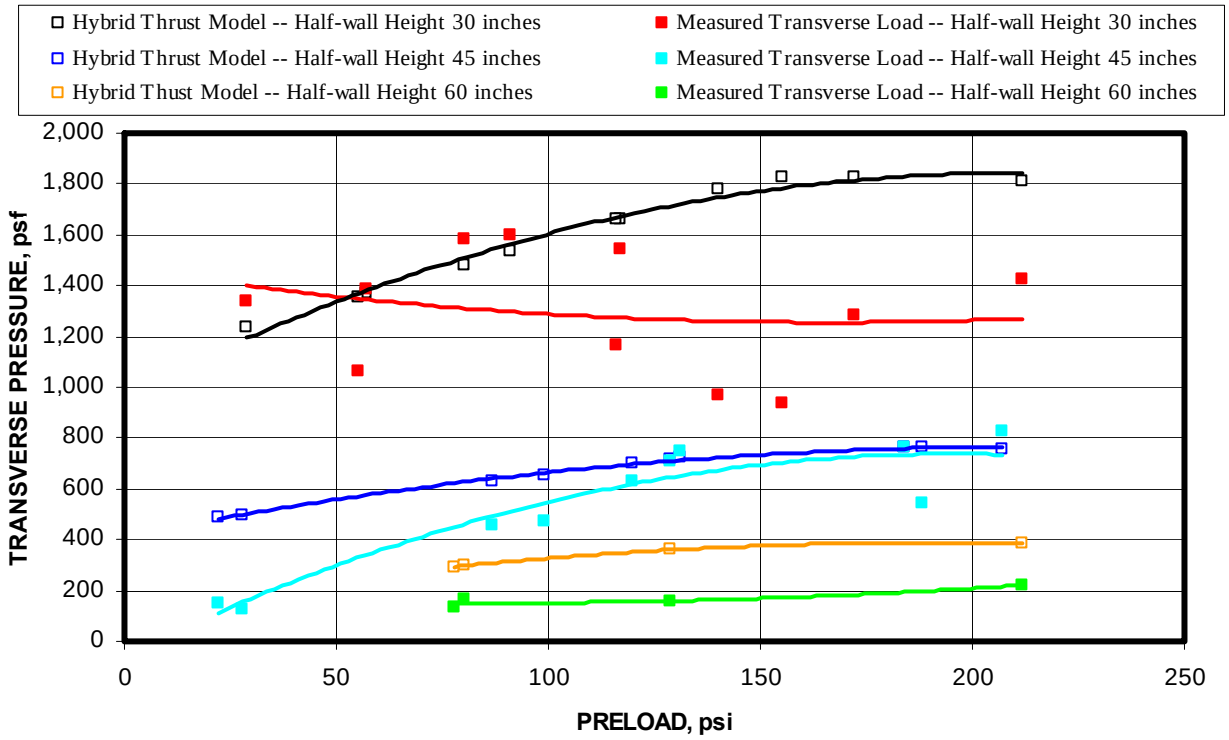

Figure 9-70. Comparison of transverse load capacities from design equations to the measured transverse load from laboratory tests (Hybrid Theoretical Thrust Model).

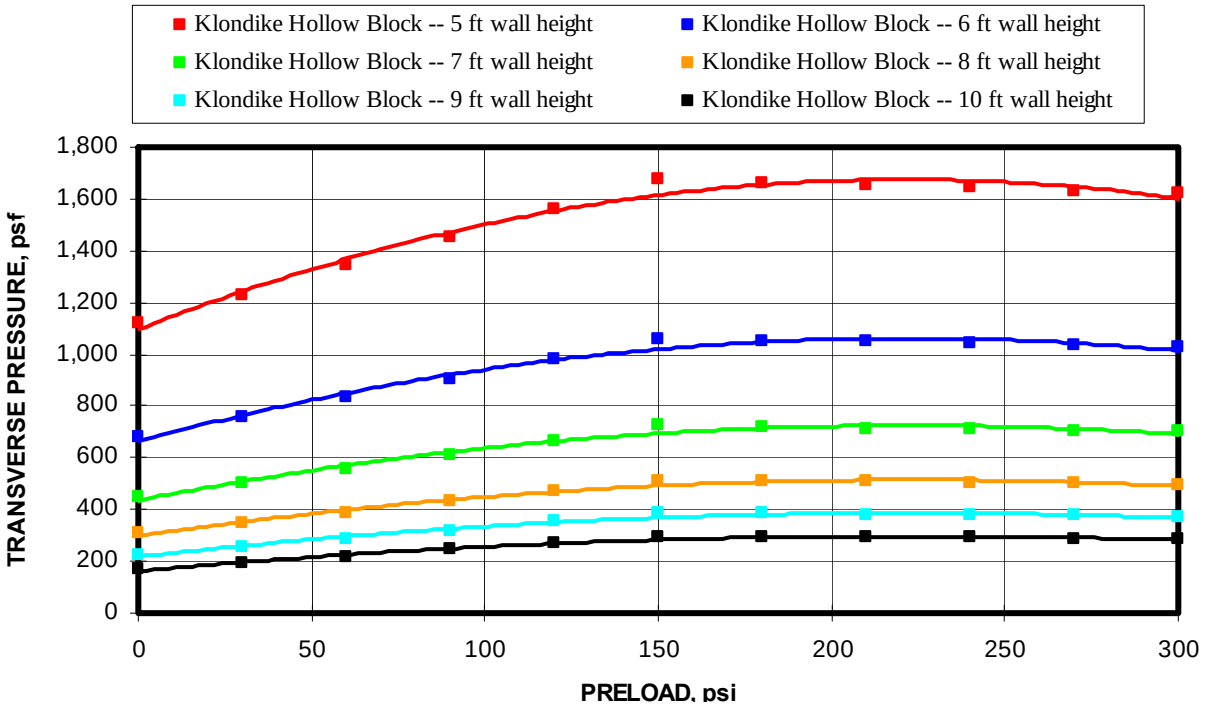

Figure 9-70. Transverse load capacity predictions for 6-in-thick walls constructed from Klondike Hollow Core Block for walls heights ranging from 5 to 10 ft (Hybrid Theoretical Thrust Model).

9.1.8.2.2 Hybrid Lateral Displacement Model

As seen in the flowchart in figure 9-3, the Hybrid Lateral Displacement Model determines the lateral displacement force from a multivariable relationship from the $Ex(t/L)^2$ term and preload, both of which are considered to be known parameters. The multivariable linear regression analysis based on 23 laboratory tests of various wall constructions is summarized in table 9-31. Equation 9.33 is used to compute the lateral displacement. Table 9-32 documented the multivariable regression analysis results used to determine the resultant thrust position factor (d) for the Hybrid Thrust Model. This equation is also used for computing the resultant thrust adjustment factor for this model, except the calculated thrust forces are used instead of the measured thrust forces.

$$\text{Lateral Displacement} = -0.0095 \times Ex(t/L)^2 - 0.0085 \times \text{Preload} + 4.9588 \quad \textbf{(9.33)}$$

Regression Statistics	
Multiple R	0.8575
R Square	0.7353
Adjusted R Square	0.7089
Standard Error	0.3966
Observations	23

Table 9-31. Multivariable regression analysis for determining lateral displacement.

ANOVA

	df	SS	MS	F	Significance F
Regression	2	8.7406	4.3703	27.7826	0.0000
Residual	20	3.1461	0.1573		
Total	22	11.8867			

	Coefficients	Standard Error	t Stat	P-value	Lower 95%	Upper 95%	Lower 95.0%	Upper 95.0%
Intercept	4.9588	0.4741	10.4597	0.0000	3.9699	5.9477	3.9699	5.9477
E*(t/L)^ 2	-0.0095	0.0017	-5.7071	0.0000	-0.0130	-0.0060	-0.0130	-0.0060
Preload	-0.0085	0.0016	-5.3216	0.0000	-0.0118	-0.0051	-0.0118	-0.0051

Figure 9-72 compares the results of the predicted transverse load capacities from the hybrid theoretical lateral displacement model with the measured laboratory test results for half-wall heights of 30, 45, and 60 inches. As seen from the graph, the predictions less accurate than those determined from the hybrid theoretical thrust model presented in figure 9-70. Figure 9-73 shows transverse load predictions using the hybrid theoretical lateral displacement for walls constructed from Klondike Hollow Core Block ranging in height from 5 to 10 feet in one foot increments with preloads ranging from 0 to 300 psi.

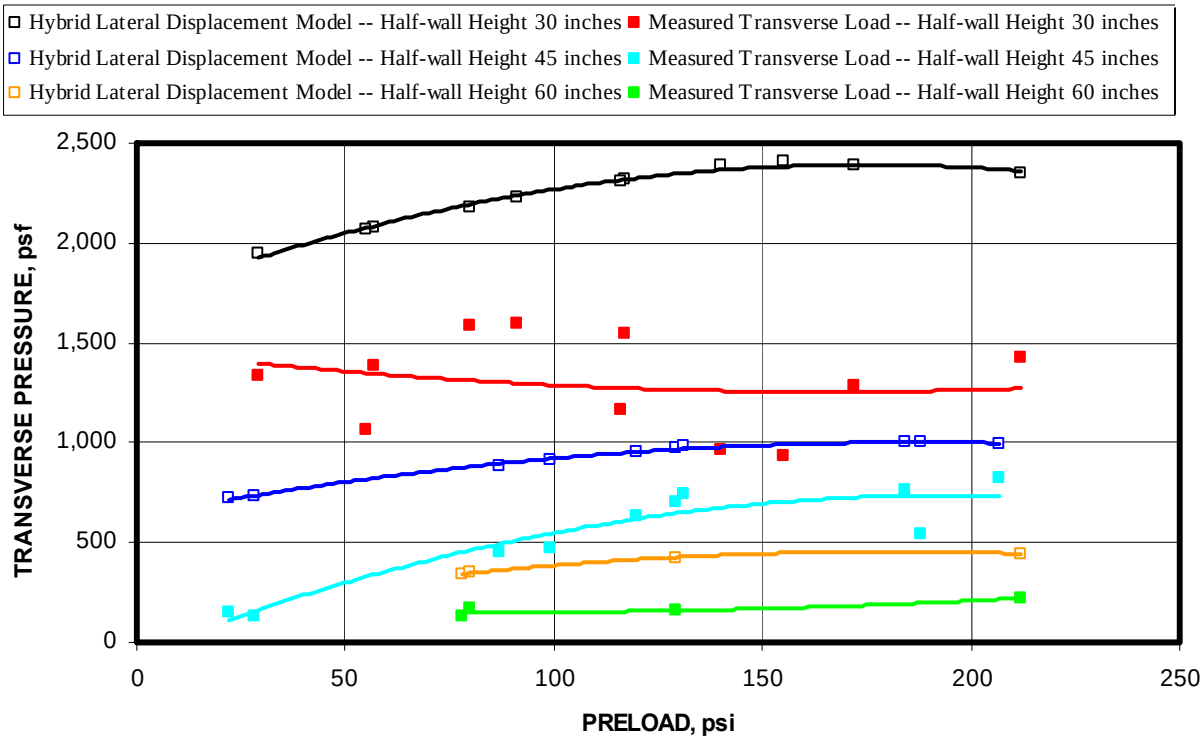

Figure 9-72. Comparison of transverse load capacities from design equations to the measured transverse load from laboratory tests (Hybrid Theoretical Lateral Displacement Model).

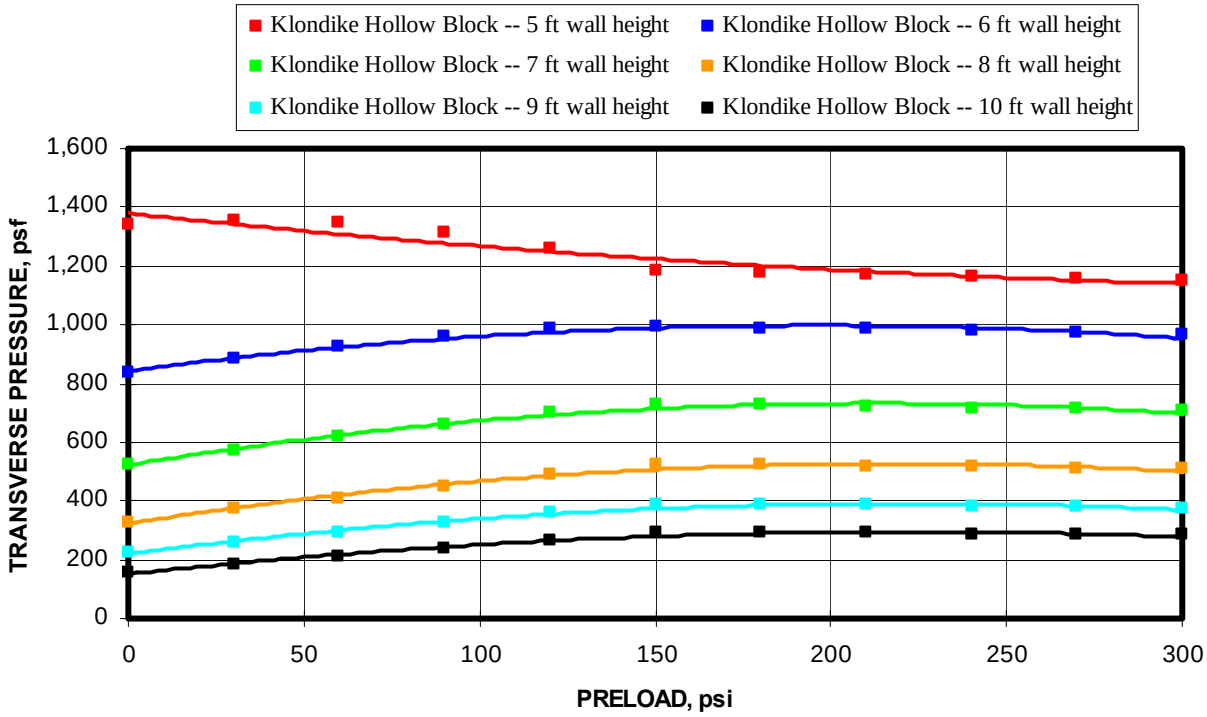

Figure 9-73. Comparison of transverse load capacities from design equations to the measured transverse load from laboratory tests (Hybrid Theoretical Lateral Displacement Model).

9.1.8.2.3 Hybrid Combination Model

The Hybrid Combination Model combines the previous two models by empirically determining both the thrust and lateral displacement. Figure 9-74 compares this model's predictions of transverse load capacity to the measured transverse load capacities from the laboratory testing. The results are considerably more accurate, especially for the short and high walls, than those of the thrust or lateral displacement models. Figure 9-75 is included which displays the transverse load predictions using the hybrid theoretical combination model for 6-in thick walls constructed from Klondike Hollow Core Block ranging in height from 5 to 10 feet in one foot increments with preloads ranging from 0 to 300 psi.

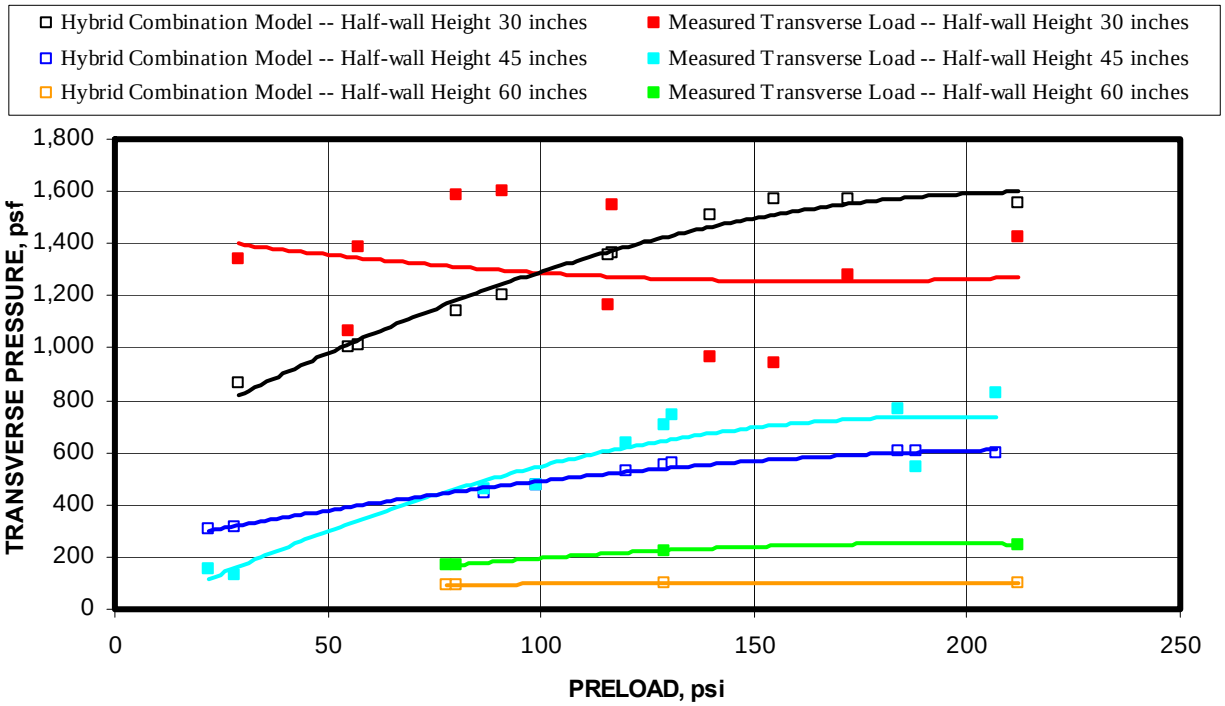

Figure 9-74. Comparison of transverse load capacities from design equations to the measured transverse load from laboratory tests (Hybrid Theoretical Combination Model).

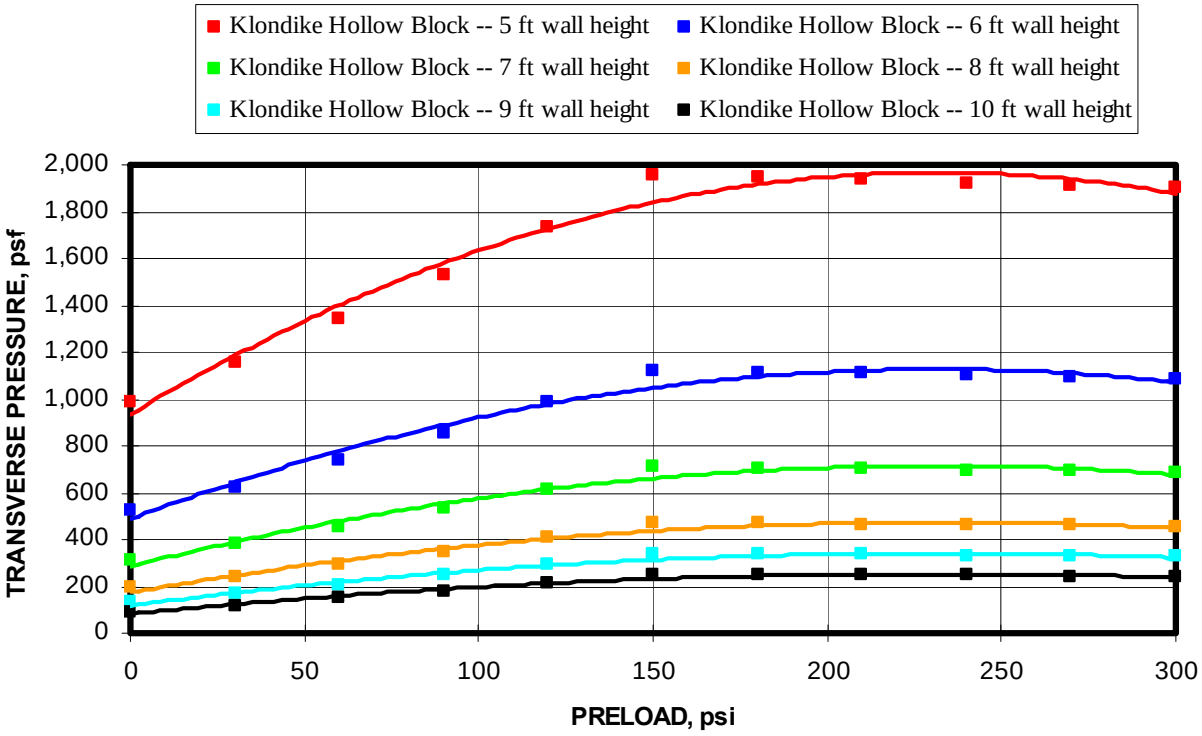

Figure 9-75. Transverse load capacity predictions for 6-in-thick walls constructed from Klondike Hollow Core Block for walls heights ranging from 5 to 10 ft (Hybrid Theoretical Combination Model).

9.1.8.3 Summary of Design Equations for Klondike Hollow Core Block

In summary, a full empirical design model and three hybrid theoretical design models were developed for the Klondike Hollow Core Block stopping constructions. Figure 9-76 displays the calculated transverse load capacities from full empirical model compared to the measured capacities from the MRS tests. The dashed line represents a perfect correlation between the calculated and measured capacities. The red trend line represents the linear regression between the measured and calculated capacities. The regression lines shows that on average the model tends to under predict the transverse load. The regression trend line shows a 4 pct difference between the measured and calculated transverse load. The shaded blue area is a +/- 200 psf variation from the perfect correlation. Examining the chart, it is seen that 52% of the data falls within this variation. Most of the poor predictions occur for the short wall configuration (30-in half-wall height) where the transverse load was inconsistent with premature localized failures occurring in block near the hinge point contact zones. Figure 9-77 displays this same information for the three hybrid theoretical design models. Based on the regression trend line correlating the calculated transverse loads to the measured transverse loads, the combination model, which computes both the thrust and lateral displacement from laboratory test data, is the most accurate of the three, with a 3 pct difference in calculated and measured loads. The least accurate is the lateral displacement model with 12 pct difference. Examining the +/-400 psf variation (blue shading), the thrust model and the combination model have 83% of the data within this variation, while the lateral displacement model has only 35 pct of the data within this variation.

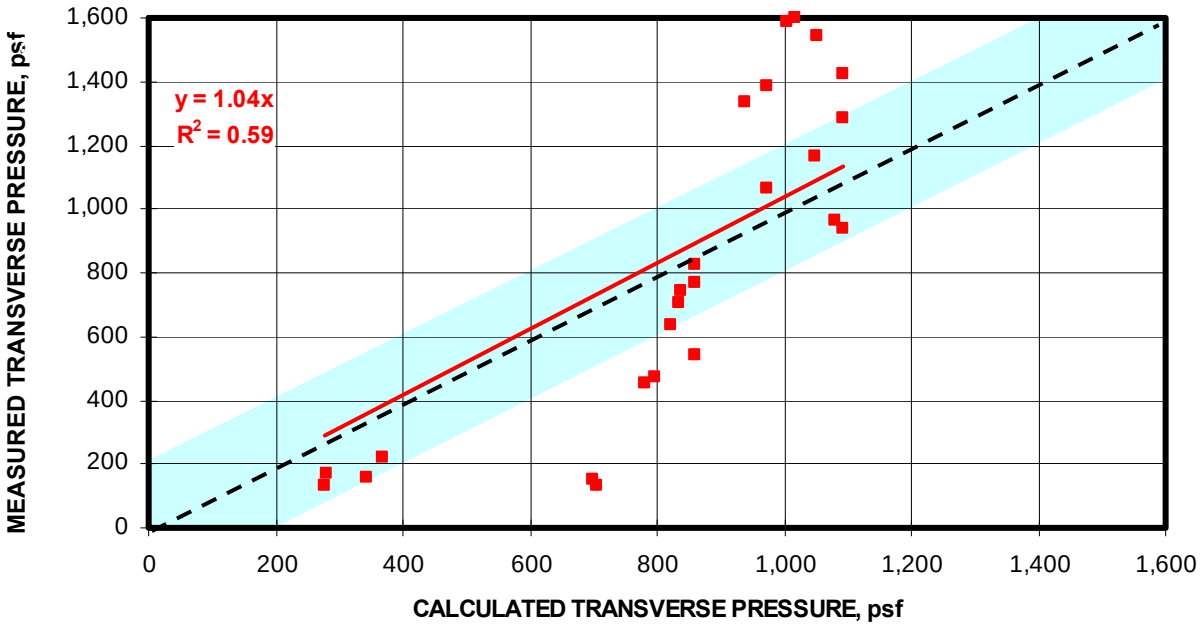

Figure 9-76. Comparison of predicted transverse load capacities compared to the measured capacities for the MRS laboratory tests (Full Empirical Model).

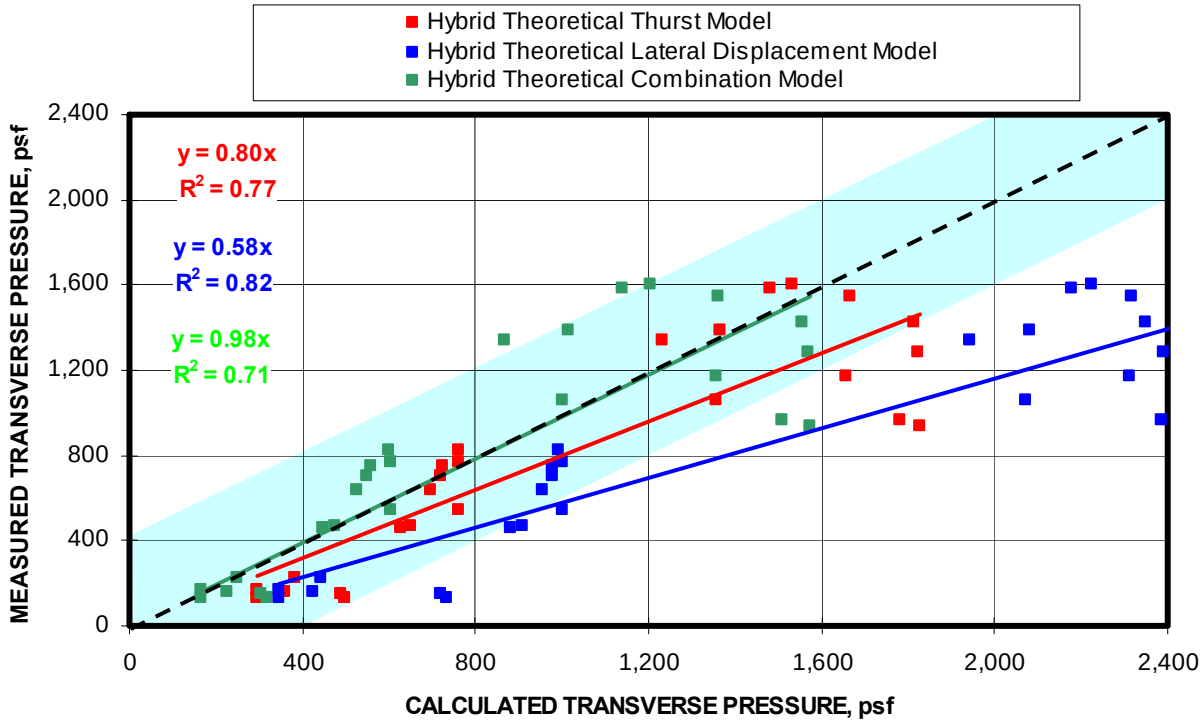

Figure 9-77. Comparison of predicted transverse load capacities compared to the measured capacities for the MRS laboratory tests (Hybrid Theoretical Models).

9.2 GENERIC BLOCK MODELS

The previous section developed models for a specific block. These models will provide the best design information if that particular block is being utilized. The goal of this section is to broaden the design formulations to permit design of stoppings constructed of a different block type. One approach would be to select a specific block model that most closely matches the physical characteristics of the block in question and use that model for design. Another approach is to generalize the specific block models into categories by grouping the performance parameters for similar style block materials. This is the approach that is described in this section. The categories selected for analysis are as follows: (1) standard CMU block with compressive strengths ranging from 1,000 to 2,000 psi, (2) cellular block materials with compressive strengths ranging from 250 to 750 psi, and (3) low strength block materials with compressive strengths less than 100 psi. The approach utilized in developing the specific block models whereby an empirical model and three hybrid theoretical models, is also pursued in the development of these generic models.

9.2.1 Standard CMU Block

Two block materials were evaluated that fit this category: (1) the Klondike block and (2) the Peerless Backsaver block. These blocks were similar in size and density, but the Peerless Backsaver block had a 60 pct higher compressive strength. Also included in this data set was a group of partially cured Peerless Backsaver block, which had a 50 pct reduction in compressive strength. In summary, the compressive strength of these blocks ranged from 1,070 to 2,160 psi.

9.2.1.1 Generic Empirical Model

The Generic Empirical Model is developed from a multivariable regression analysis of the data using the $Ex(t/L)^2$ term and the preload. Equation 9.34 documents the resulting design equation.

$$\text{Transverse pressure} = 5.2021 \times Ex(t/L)^2 + 1.8325 \times \text{Preload} - 962 \quad \textbf{(9.34)}$$

Where E = material modulus, psi,

t = wall thickness, in,

L = full wall height, in, and

Preload = ground pressure preload, psi.

Figure 9-78 compares the measured transverse pressure from the Klondike block tests to the Generic Empirical Model. Based on the regression line comparing the measured and calculated transverse pressures, the Generic Empirical Model predicts the transverse pressure to within 4 pct error. The blue shaded area represents a +/- 400 psf variation. It is seen that 77 pct of the data falls within this load variation.

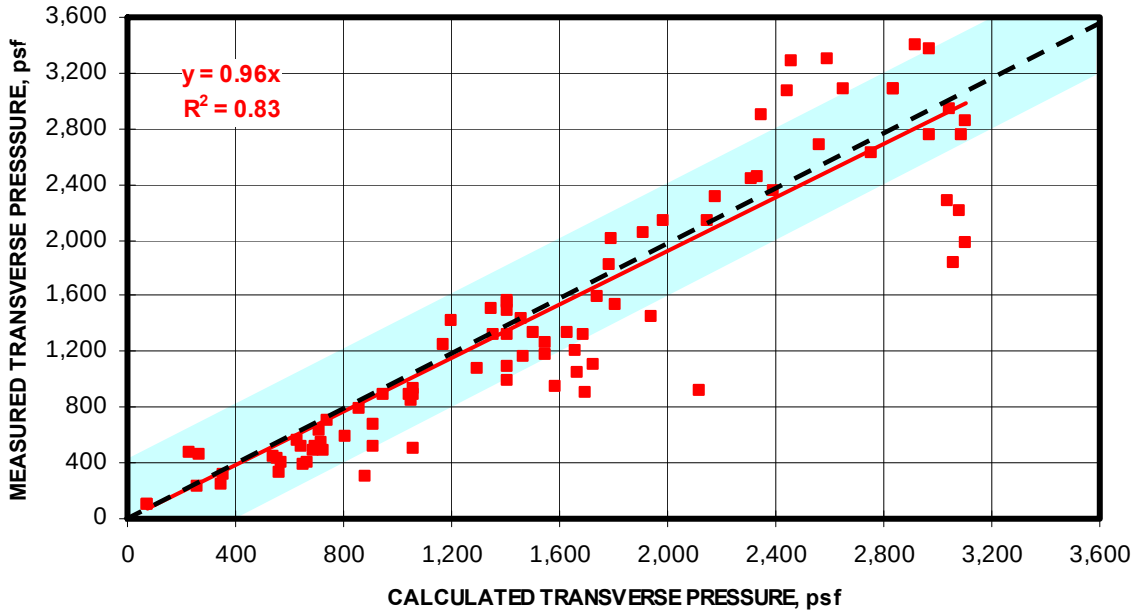

Figure 9-78. Comparison of predicted transverse pressure capacities compared to measured capacities for the MRS laboratory tests for the Klondike block (Generic Empirical Model).

9.2.1.2 Generic Hybrid Theoretical Models

Transverse pressure capacity forecasts will be made using the three hybrid theoretical models developed from the full generic standard CMU data set: (1) Hybrid Thrust Model, (2) Hybrid Lateral Displacement Model, and (3) Hybrid Combination Thrust and Lateral Displacement Model. The design equations and graph showing a comparison of the predicted and measured transverse pressure are included in the next sections.

9.2.1.2.1 Generic Hybrid Thrust Model

The Hybrid Thrust Model determines the normalized thrust force from a multivariable relationship between the thrust force and the $Ex(t/L)^2$ term and preload, both of which are considered to be known parameters. The multivariable linear regression analysis based on 120 laboratory tests of various wall constructions consisting of Klondike and Peerless Backsaver block constructions. Equation 9.35 is used to compute the normalized thrust force per unit width of wall. This can be multiplied by the block length to determine the full thrust on a single column block wall or whatever is appropriate for the analysis being conducted. A multivariable regression analysis results used to determine the resultant thrust position factor (d), which can be computed using equation 9.36. These parameters can then be substituted into the equations shown if the flowchart in figure 9-2 to compute the transverse pressure for that particular stopping construction.

$$P/BL = 0.0023 \times Ex(t/L)^2 + 0.0033 \times Preload + 0.6137 \quad \textbf{(9.35)}$$

Where P/BL = Normalized thrust per unit width of block, kips/in,

E = Elastic modulus, psi,

t = wall thickness, in,

L = height of wall, in, and

Preload = preload pressure, psi.

$$d = -0.0018 \times \text{Half-wall Height} - 0.0031 \times \text{Thrust} + 0.9301 \quad \textbf{(9.36)}$$

Figure 9-79 compares the predicted transverse pressure with the measured transverse pressure for the Klondike block as an example of the accuracy of the model. As seen from the regression trend line in the figure, the Generic Thrust Model predicts the transverse pressure to within a 9 pct error, however 87 pct of the data was within the +/- 400 psf variation compared to only 77 pct for the empirical model shown in figure 9-78.

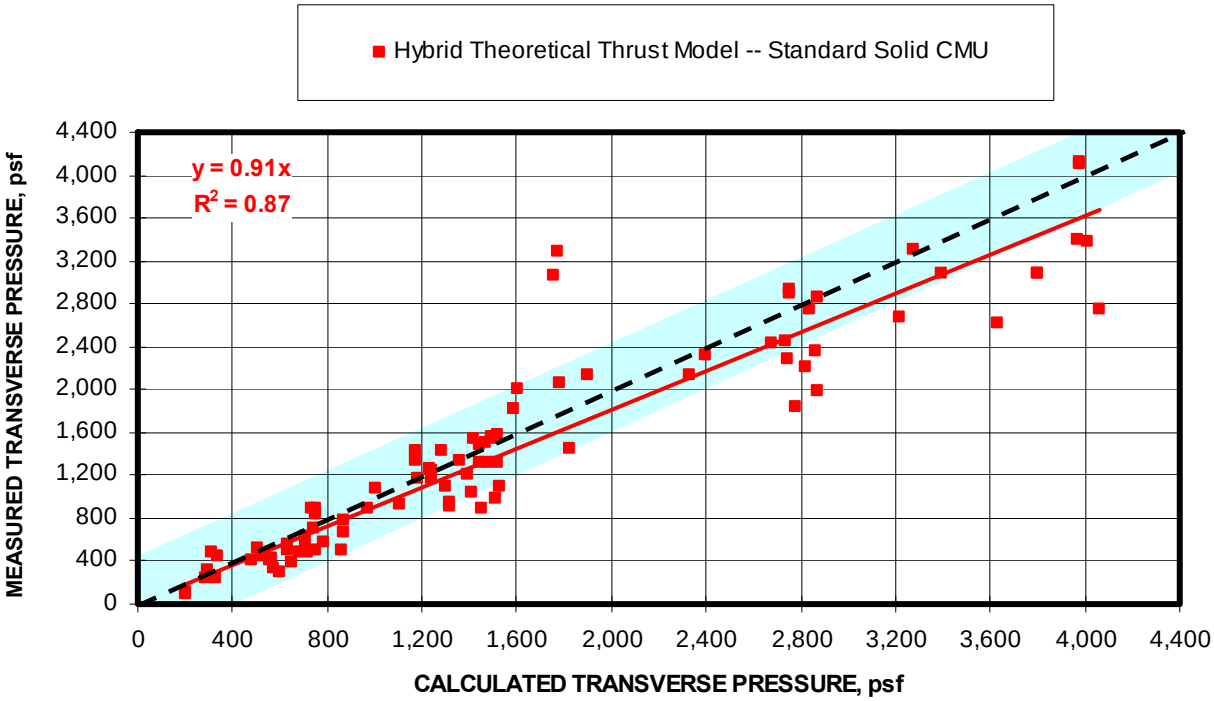

Figure 9-79. Comparison of predicted transverse pressure capacities compared to measured capacities for the MRS laboratory tests for the Klondike block (Generic Thrust Model).

9.2.1.2.2 Generic Hybrid Lateral Displacement Model

The Hybrid Lateral Displacement Model determines the lateral displacement from a multivariable relationship between the lateral displacement and the $Ex(t/L)^2$ term and preload, both of which are considered to be known parameters. The multivariable linear regression analysis based on 120 laboratory tests of various wall constructions consisting of Klondike and Peerless Backsaver block constructions. Equation 9.37 is used to compute the lateral displacement of wall. The same multivariable regression analysis that was used in the thrust model is also used to determine the resultant thrust position factor (d), which can be computed using equation 9.36. These parameters can then be substituted into the equations shown if the flowchart in figure 9-3 to compute the transverse pressure for that particular stopping construction.

$$\text{Lateral Displacement} = -0.0012 \times Ex(t/L)^2 - 0.0024 \times \text{Preload} + 2.0058 \quad \textbf{(9.37)}$$

Figure 9-80 compares the predicted transverse pressure with the measured transverse pressure for the Klondike block as an example of the accuracy of the model. As seen from the regression trend line in the figure, the Generic Lateral Displacement Model predicts the transverse pressure to within a 10 pct error. In this example, 85 pct of the data was within the +/- 400 psf variation.

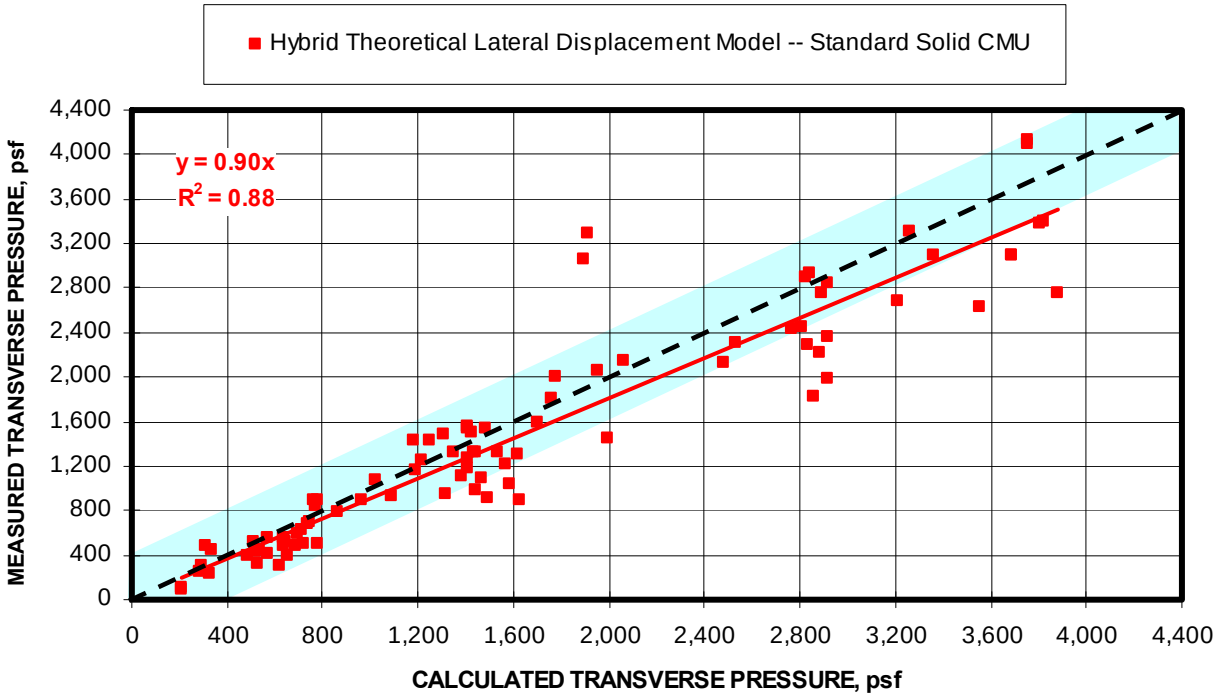

Figure 9-80. Comparison of predicted transverse pressures capacities compared to measured capacities for the MRS laboratory tests for the Klondike block (Generic Lateral Displacement Model).

9.2.1.2.3 Generic Hybrid Combination Thrust and Lateral Displacement Model

The Hybrid Combination Model determines both the lateral displacement and the thrust from a multivariable relationship between these parameters and the $Ex(t/L)^2$ term and preload using the equations presented in the previous sections. The same multivariable regression analysis that was used in the thrust model is also used to determine the resultant thrust position factor (d), which can be computed using equation 9.36, is also used in this model. These parameters can then be substituted into the equations shown if the flowchart in figure 9-4 to compute the transverse pressure for that particular stopping construction. Figure 9-81 compares the predicted and measured transverse pressures using this model for the Klondike

tests. The regression line indicates that the transverse pressure can be predicted to within an 8 pct difference with this model. The chart also shows that 90 pct of the data falls within the +/- 400 psf variation as illustrated by the shaded blue area.

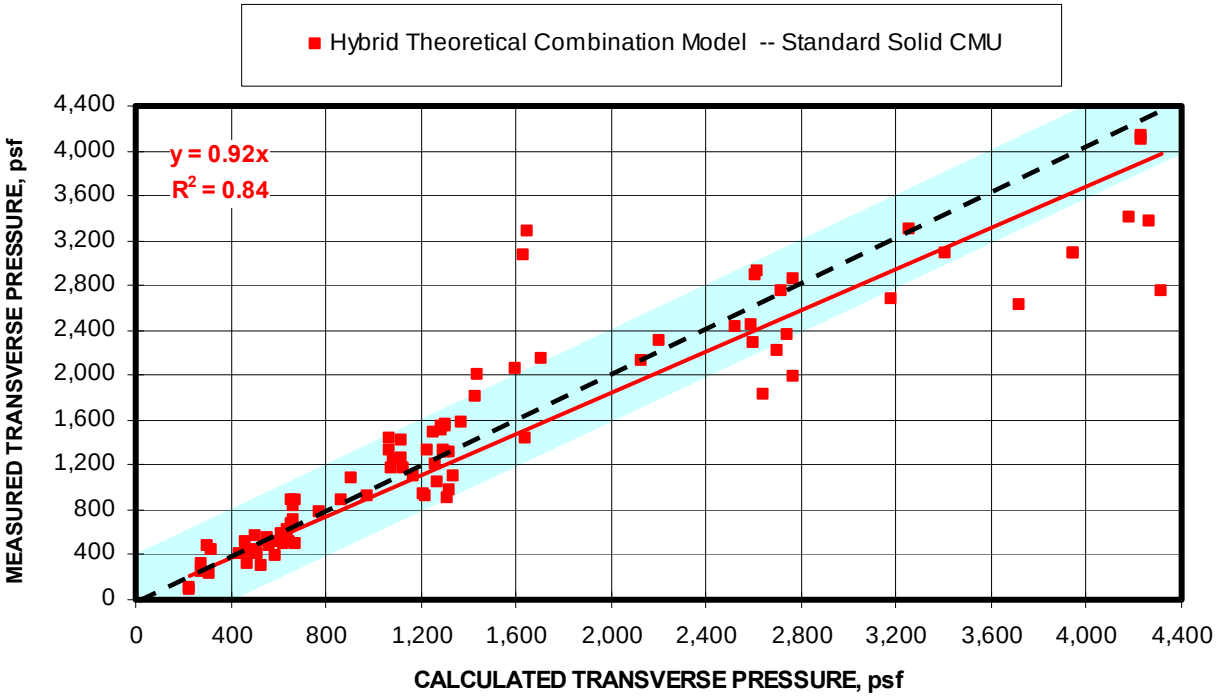

Figure 9-81. Comparison of predicted transverse pressure capacities compared to measured capacities for the MRS laboratory tests for the Klondike block (Generic Combination Model).

9.2.2 Cellular Concrete Block Materials

All of the lightweight block materials examined in this study utilized air-entrained concrete to provide a low density material that can effectively reduce the weight of the block per unit volume, or by taking advantage of the lower density material, allow larger blocks to be fabricated within an acceptable weight limit. Three blocks fit into this category: (1) Ytong, (2) ACCOA, and (3) Kingsway. The blocks vary in size and compressive strength, which ranges from 446 to 705 psi.

9.2.2.1 Generic Empirical Model

The Generic Empirical Model is developed from a multivariable regression analysis of the data using the $Ex(t/L)^2$ term and the preload from the Ytong, ACCOA, and Kingsway block performance data. Equation 9.38 documents the resulting design equation.

Transverse pressure = 3.5096 x Ex(t/L)^2 + 1.0386 x Preload – 100.9456 **(9.38)**

Where E = material modulus, psi,

t = wall thickness, in,

L = full wall height, in, and

Preload = ground pressure preload, psi.

Figure 9-82 compares the measured transverse pressure from the Ytong block tests to the Generic Empirical Model. Based on the regression line comparing the measured and calculated transverse pressures, the Generic Empirical Model predicts the transverse pressure to within 1 pct error. The blue shaded area represents a +/- 200 psf variation. It is seen that 100 pct of the data falls within this load variation.

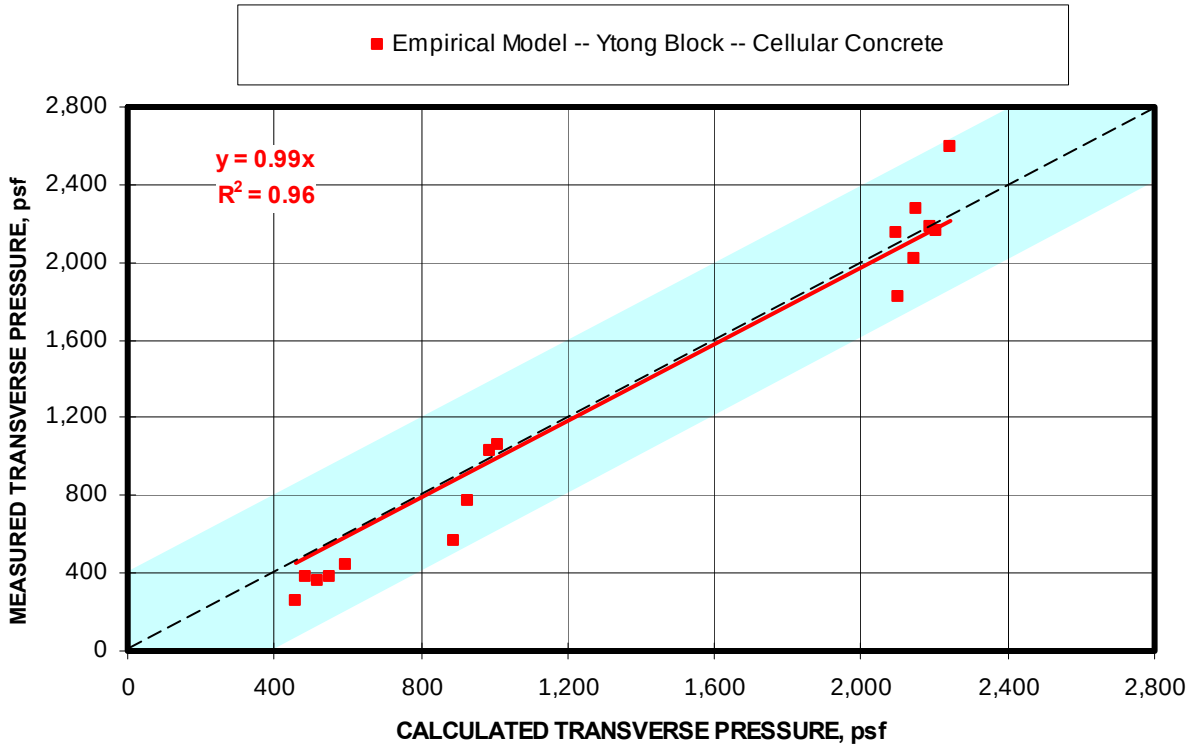

Figure 9-82. Comparison of predicted transverse pressure capacities compared to measured capacities for the MRS laboratory tests for the Ytong block (Generic Empirical Model).

9.2.2.2 Generic Hybrid Theoretical Models

Transverse pressure capacity forecasts will be made using the three hybrid theoretical models developed from the full generic Cellular Concrete data set: (1) Hybrid Thrust Model,

(2) Hybrid Lateral Displacement Model, and (3) Hybrid Combination Thrust and Lateral Displacement Model. The design equations and graph showing a comparison of the predicted and measured transverse pressure are included in the next sections.

9.2.2.2.1 Hybrid Thrust Model

The Hybrid Thrust Model determines the normalized thrust force from a multivariable relationship between the thrust force and the $Ex(t/L)^2$ term and preload, both of which are considered to be known parameters. The multivariable linear regression analysis based on 43 laboratory tests of various wall constructions consisting of Ytong, ACCOA, and Kingsway block constructions. Equation 9.39 is used to compute the normalized thrust force per unit width of wall. This can be multiplied by the block length to determine the full thrust on a single column block wall or whatever is appropriate for the analysis being conducted. A multivariable regression analysis results used to determine the resultant thrust position factor (d), which can be computed using equation 9.40. These parameters can then be substituted into the equations shown if the flowchart in figure 9-2 to compute the transverse pressure for that particular stopping construction.

$$P/BL = 0.0019 \times Ex(t/L)^2 + 0.0044 \times Preload + 0.3257 \quad \textbf{(9.39)}$$

Where P/BL = Normalized thrust per unit width of block, kips/in,
E = Elastic modulus, psi,
t = wall thickness, in,
L = height of wall, in, and
Preload = preload pressure, psi.

$$d = -0.0028 \times Half\text{-}wall\ Height - 0.0076 \times Thrust + 1.0181 \quad \textbf{(9.40)}$$

Figure 9-83 compares the predicted transverse pressure with the measured transverse pressure for the Ytong block as an example of the accuracy of the model. As seen from the regression trend line in the figure, the Generic Thrust Model predicts the transverse pressure to within a 1 pct error, however 100 pct of the data was within the +/- 400 psf variation compared to only 77 pct for the empirical model shown in figure 9-82.

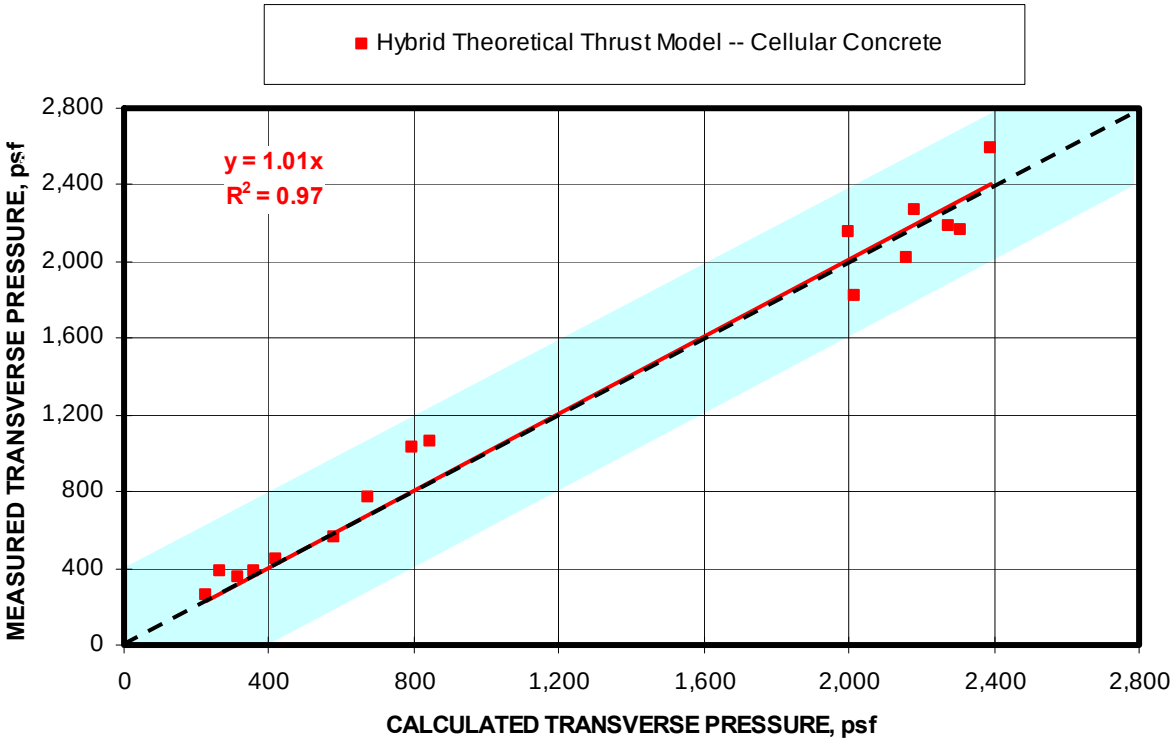

Figure 9-83. Comparison of predicted transverse pressure capacities compared to measured capacities for the MRS laboratory tests for the Ytong block (Generic Thrust Model).

9.2.2.2.2 Generic Hybrid Lateral Displacement Model

The Hybrid Lateral Displacement Model determines the lateral displacement from a multivariable relationship between the thrust force and the $Ex(t/L)^2$ term and preload, both of which are considered to be known parameters. The multivariable linear regression analysis based on 43 laboratory tests of various wall constructions consisting of Ytong, ACCOA, and Kingsway. Equation 9.41 is used to compute the lateral displacement of wall. The same multivariable regression analysis that was used in the thrust model is also used to determine the resultant thrust position factor (d), which can be computed using equation 9.40. These parameters can then be substituted into the equations shown if the flowchart in figure 9-3 to compute the transverse pressure for that particular stopping construction.

$$\text{Lateral Displacement} = -0.0004 \times Ex(t/L)^2 - 0.0045 \times \text{Preload} + 1.4303 \qquad \textbf{(9.41)}$$

Figure 9-84 compares the predicted transverse pressure with the measured transverse pressure for the Ytong block as an example of the accuracy of the model. As seen from the regression trend line in the figure, the Generic Lateral Displacement Model predicts the

transverse pressure to within a 6 pct error. In this example, 85 pct of the data was within the +/- 400 psf variation.

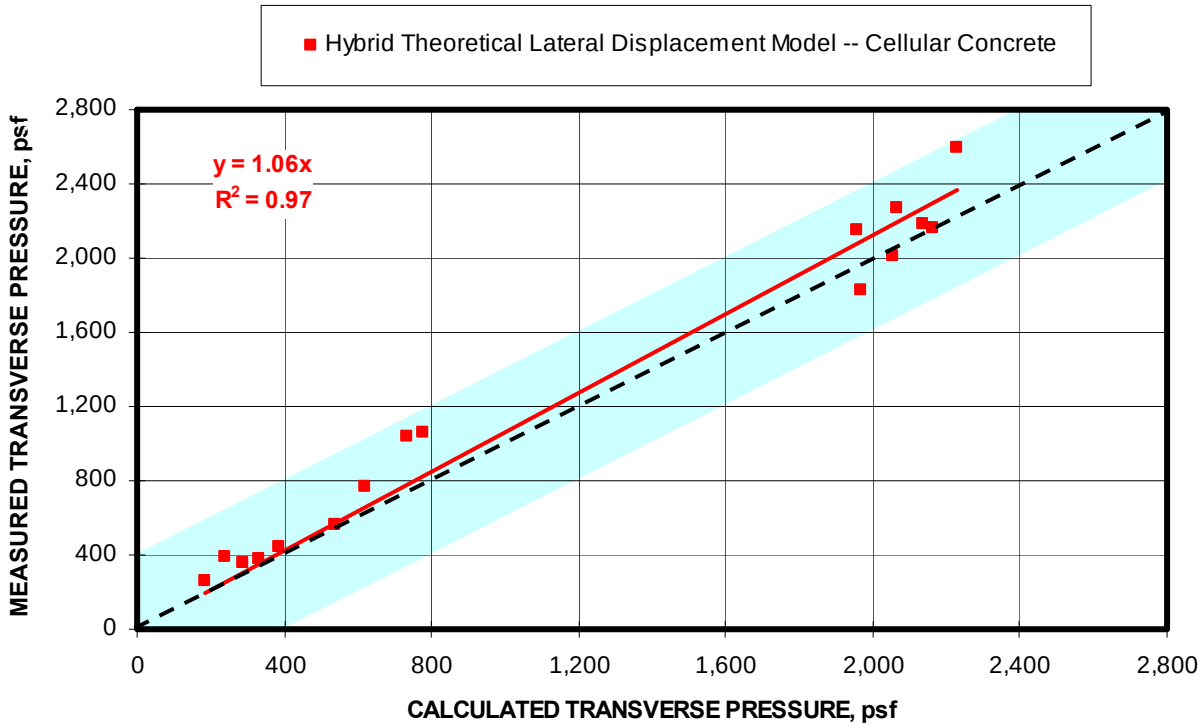

Figure 9-84. Comparison of predicted transverse pressure capacities compared to measured capacities for the MRS laboratory tests for the Ytong block (Generic Lateral Displacement Model).

9.2.2.2.3 Generic Hybrid Combination Thrust and Lateral Displacement Model

The Hybrid Combination Model determines both the lateral displacement and the thrust from a multivariable relationship between these parameters and the $Ex(t/L)^2$ term and preload using the equations presented in the previous sections. The same multivariable regression analysis that was used in the thrust model is also used to determine the resultant thrust position factor (d), which can be computed using equation 9.40, is also used in this model. These parameters can then be substituted into the equations shown if the flowchart in figure 9-4 to compute the transverse pressure for that particular stopping construction. Figure 9-85 compares the predicted and measured transverse pressures using this model for the Ytong tests. The regression line indicates that the transverse pressure can be predicted to within a 9 pct difference with this model. The chart also shows that 90 pct of the data falls within the +/- 400 psf variation as illustrated by the shaded blue area.

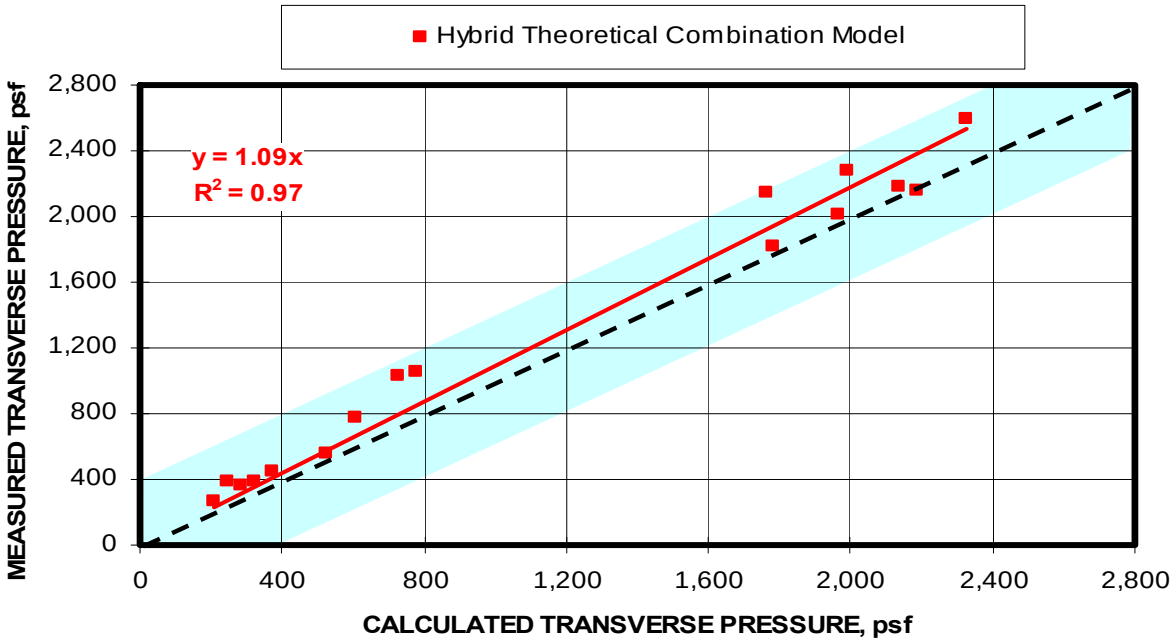

Figure 9-85. Comparison of predicted transverse pressure capacities compared to measured capacities for the MRS laboratory tests for the Ytong block (Generic Combination Model).

9.2.3 Low Strength Block Materials

A separate model is made for blocks with compressive strengths less than 100 psi. These relatively very weak materials behave differently than the other block materials examined in this study. Two blocks fell into this category: (1) Omega Block and (2) Peerless Super Block. Both of these are cellular type concrete materials, but they are much weaker than the cellular materials examined in the Cellular Concrete Models in the previous section. The Peerless Super Block incorporates small Styrofoam pellets into the mix to provide additional yield capabilities. As noted in the previous chapters, the performance of these two block materials was the least consistent of all materials examined.

9.2.3.1 Generic Empirical Model

The Generic Empirical Model is developed from a multivariable regression analysis of the data using the $Ex(t/L)^2$ term and the preload from the Omega and Super Block performance data. Equation 9.42 documents the resulting design equation.

$$\text{Transverse pressure} = -8.8762 \times Ex(t/L)^2 + 0.2252 \times \text{Preload} + 221 \quad \textbf{(9.42)}$$

Where E = material modulus, psi,

t = wall thickness, in,

L = full wall height, in, and

Preload = ground pressure preload, psi.

Figure 9-86 compares the measured transverse pressure from the Omega block tests to the Generic Empirical Model. Based on the regression line comparing the measured and calculated transverse pressures, the Generic Empirical Model predicts the transverse pressure to within 11 pct error. However, it is seen that only 36 pct of the data falls within a +/- 40 psf variation as represented by the blue shaded area, indicating that in this particular case, the generic empirical model is not a well suited to this block.

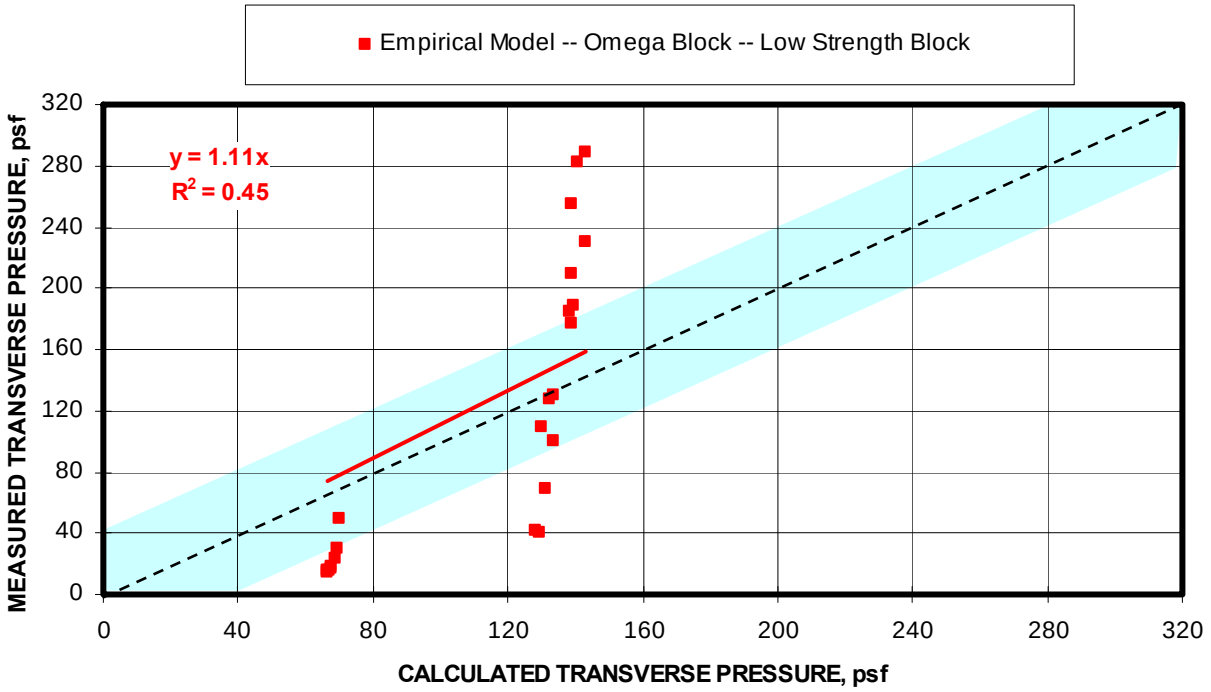

Figure 9-86. Comparison of predicted transverse pressure capacities compared to measured capacities for the MRS laboratory tests for the Omega block (Generic Empirical Model).

9.2.3.2 Generic Hybrid Theoretical Models

Transverse pressure capacity forecasts will be made using the three hybrid theoretical models developed from the full generic low strength block data set: (1) Hybrid Thrust Model, (2) Hybrid Lateral Displacement Model, and (3) Hybrid Combination Thrust and Lateral

Displacement Model. The design equations and graph showing a comparison of the predicted and measured transverse pressure are included in the next sections.

9.2.3.2.1 Hybrid Thrust Model

The Hybrid Thrust Model determines the normalized thrust force from a multivariable relationship between the thrust force and the $Ex(t/L)^2$ term and preload, both of which are considered to be known parameters. The multivariable linear regression analysis based on 53 laboratory tests of various wall constructions consisting of Omega and Peerless Super Block. Equation 9.43 is used to compute the normalized thrust force per unit width of wall. This can be multiplied by the block length to determine the full thrust on a single column block wall or whatever is appropriate for the analysis being conducted. A multivariable regression analysis results used to determine the resultant thrust position factor (d), which can be computed using equation 9.44. These parameters can then be substituted into the equations shown if the flowchart in figure 9-2 to compute the transverse pressure for that particular stopping construction.

$$P/BL = -0.0046 \times Ex(t/L)^2 + 0.0033 \times Preload + 0.1325 \quad \textbf{(9.43)}$$

Where P/BL = Normalized thrust per unit width of block, kips/in,
E = Elastic modulus, psi,
t = wall thickness, in,
L = height of wall, in, and
Preload = preload pressure, psi.

$$d = -0.0060 \times \text{Half-wall Height} - 0.0361 \times \text{Thrust} + 1.0924 \quad \textbf{(9.44)}$$

Figure 9-87 compares the predicted transverse pressure with the measured transverse pressure for the Omega block as an example of the accuracy of the model. As seen from the regression trend line in the figure, the Generic Thrust Model predicts the transverse pressure to within a 8 pct error, however 87 pct of the data was within the +/- 40 psf variation compared to only 36 pct for the empirical model shown in figure 9-86.

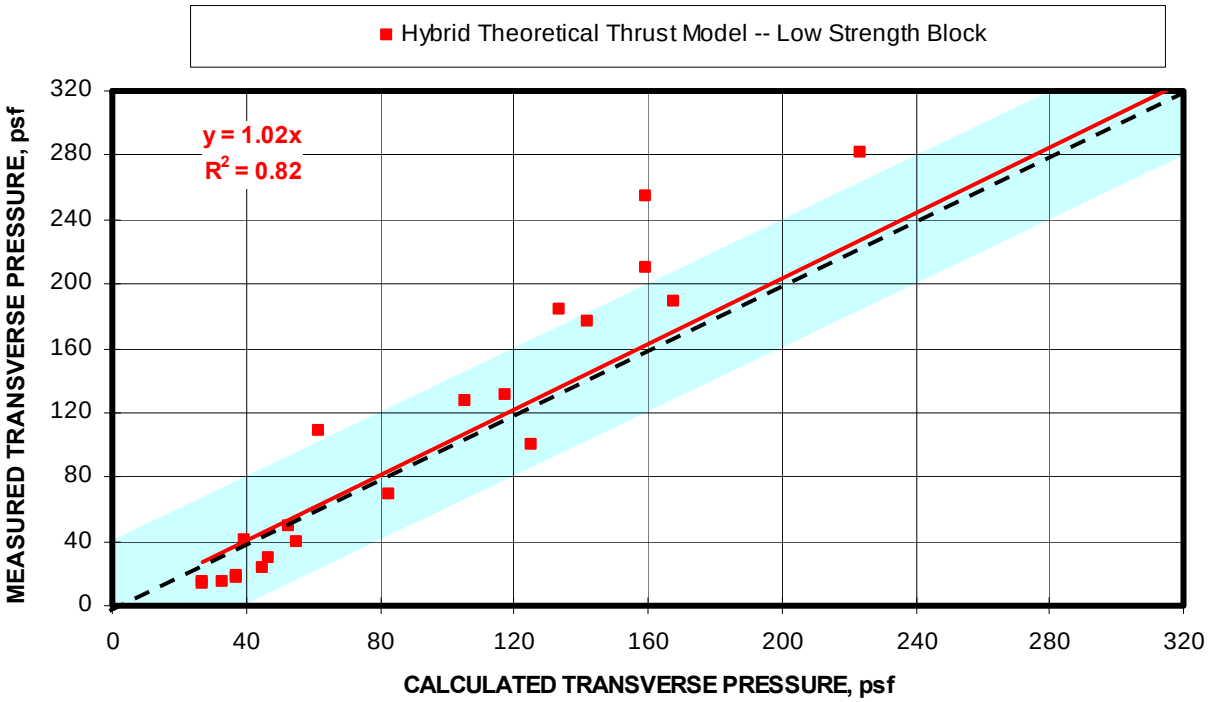

Figure 9-87. Comparison of predicted transverse pressure capacities compared to measured capacities for the MRS laboratory tests for the Omega block (Generic Thrust Model).

9.2.3.2.2 Generic Hybrid Lateral Displacement Model

The Hybrid Lateral Displacement Model determines the lateral displacement from a multivariable relationship between the thrust force and the $Ex(t/L)^2$ term and preload, both of which are considered to be known parameters. The multivariable linear regression analysis based on 53 laboratory tests of various wall constructions consisting of Omega and Peerless Super Block. Equation 9.45 is used to compute the lateral displacement of wall. The same multivariable regression analysis that was used in the thrust model is also used to determine the resultant thrust position factor (d), which can be computed using equation 9.44. These parameters can then be substituted into the equations shown if the flowchart in figure 9-3 to compute the transverse pressure for that particular stopping construction.

$$\text{Lateral Displacement} = -0.0114 \times Ex(t/L)^2 - 0.0204 \times \text{Preload} + 2.0080 \qquad \textbf{(9.45)}$$

Figure 9-88 compares the predicted transverse pressure with the measured transverse pressure for the Omega block as an example of the accuracy of the model. As seen from the regression trend line in the figure, the Generic Lateral Displacement Model predicts the transverse pressure to within a 21 pct error. In this example, 68 pct of the data was within the +/- 40 psf variation.

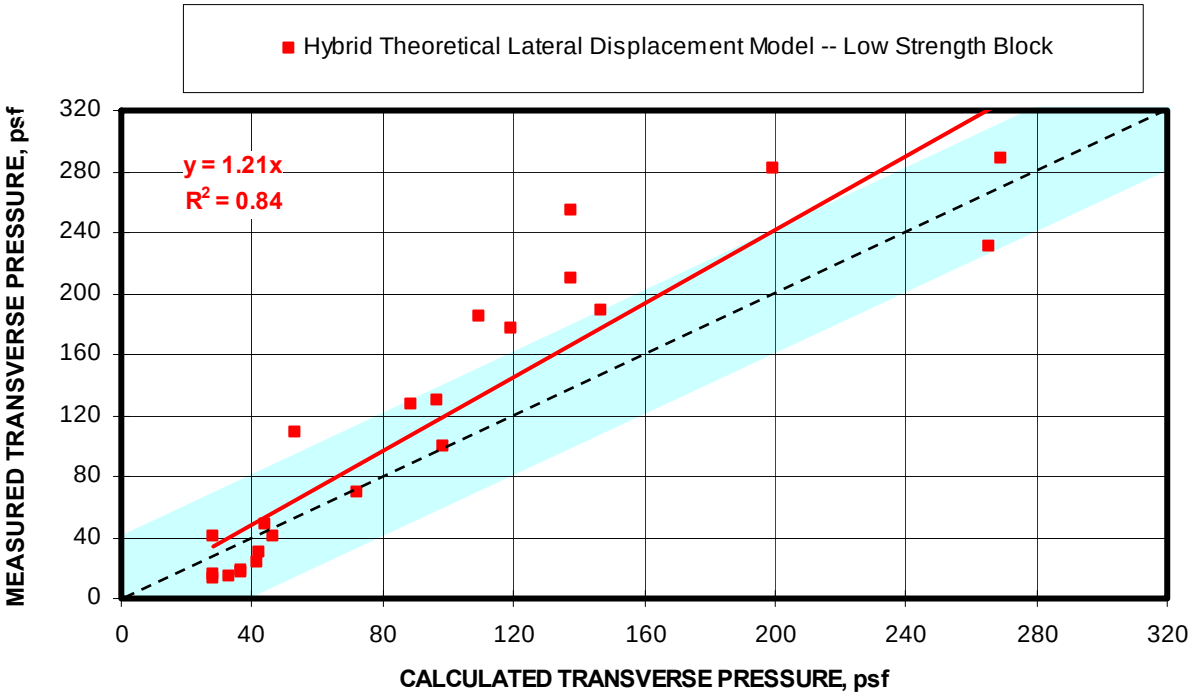

Figure 9-88. Comparison of predicted transverse pressure capacities compared to measured capacities for the MRS laboratory tests for the Omega block (Generic Lateral Displacement Model).

9.2.3.2.3 Generic Hybrid Combination Thrust and Lateral Displacement Model

The Hybrid Combination Model determines both the lateral displacement and the thrust from a multivariable relationship between these parameters and the $Ex(t/L)^2$ term and preload using the equations presented in the previous sections. The same multivariable regression analysis that was used in the thrust model is also used to determine the resultant thrust position factor (d), which can be computed using equation 9.44, is also used in this model. These parameters can then be substituted into the equations shown if the flowchart in figure 9-4 to compute the transverse pressure for that particular stopping construction. Figure 9-89 compares the predicted and measured transverse pressures using this model for the Omega

tests. The regression line indicates that the transverse pressure can be predicted to within a 32 pct difference with this model. The chart also shows that 65 pct of the data falls within the +/- 40 psf variation as illustrated by the shaded blue area.

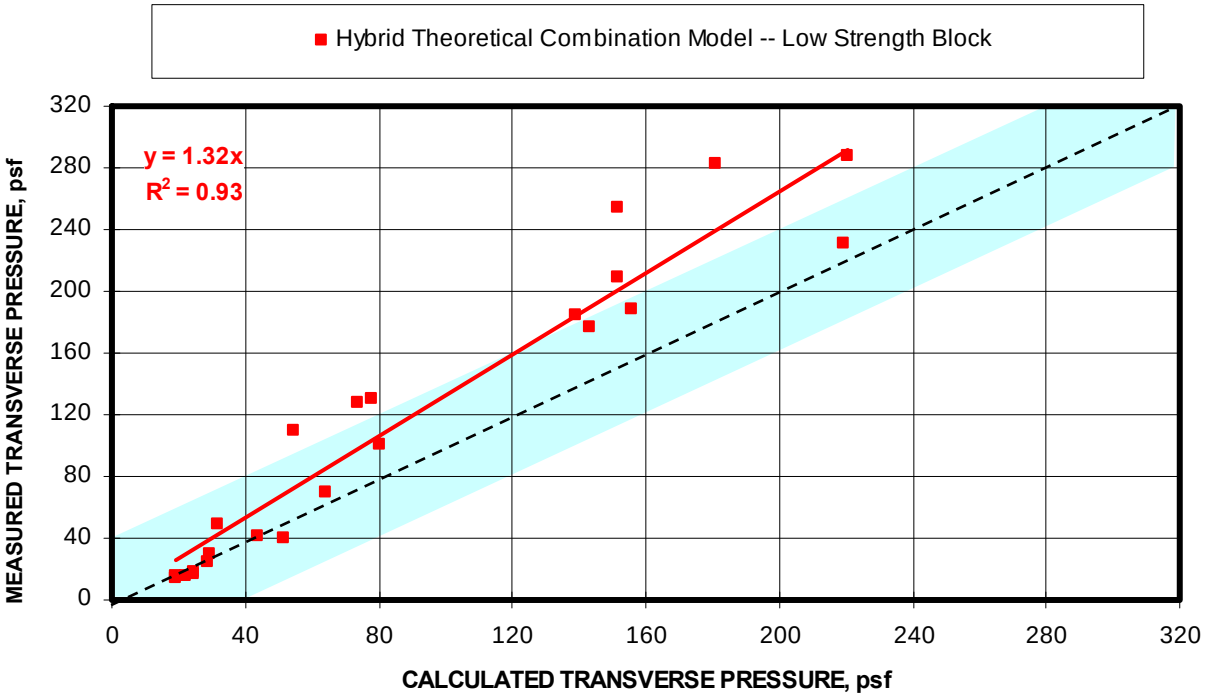

Figure 9-89. Comparison of predicted transverse pressure capacities compared to measured capacities for the MRS laboratory tests for the Omega block (Generic Combination Model).

CHAPTER 10: RECOMMENDED DESIGN FORMULATIONS FOR STOPPING BLOCK WALLS

The previous chapter documented the development of several design models for evaluating the transverse pressure capacity of mine ventilation stoppings. The purpose of this chapter is to recommend one model that provides the best potential for accurately predicting the transverse pressure capacity of a particular stopping construction. This information can also be used to design a stopping using the appropriate block materials and construction geometry to meet specific design criteria for a particular application. Design formulations for each of the specific block materials evaluated in this study are presented.

In addition, models that are more generic are provided. These allow approximation of the transverse load capacity of any block construction to be determined, providing the material modulus is known. However, a word of caution about the modulus values. The effective modulus as used in this design formulation is based on testing of a column of block representing the half-wall height of the stopping wall. Furthermore, the wall is rotated by a few degrees to provide a one-inch offset between the top and bottom edge of the column prior to vertical load application. The modulus is then determined by the initial load-deformation response. Values should be comparable to the block materials examined in this study.

10.1 SPECIFIC BLOCK DESIGN FORMULATIONS

Charts depicting the transverse pressure determinations at 1 foot height increments for the most common block thickness construction are presented in this section. The design formulation from which this chart was derived is also indicated. Four formulations were considered: (1) Full Empirical, (2) Hybrid Theoretical Thrust, (3) Hybrid Theoretical Lateral Displacement, (4) Hybrid Theoretical Combination Thrust and Lateral Displacement. Reference is made to chapter 9 if the user wants to examine the particular formulation in detail. The flowcharts presented in figures 9-2, 9-3, and 9-4 can be used to compute the transverse pressure directly using either the Hybrid Theoretical Thrust, Hybrid Theoretical Lateral Displacement, or Hybrid Theoretical Combination Thrust and Lateral Displacement respectively.

10.1.1 Klondike Block Constructions

Klondike is a conventional concrete block made from Portland cement with a moderate compressive strength ranging from 1,300 to 1,700 psi. The block measures nominally 5-5/8 x 7-1/2 x 16 inches. The best model for this block was the Hybrid Theoretical Combination Thrust and Lateral Displacement model. Figure 10-1 shows the transverse pressure estimates for 6-in-thick walls constructed at heights ranging from 5 to 10 ft in one ft height increments with preload pressures ranging from 0 to 600 psi. These graphs can then be used to approximate the transverse pressure capacity for a particular set of conditions. For example, the transverse pressure capacity of a 6-ft-high wall with 200 psi of ground pressure would be approximately 1,600 psf.

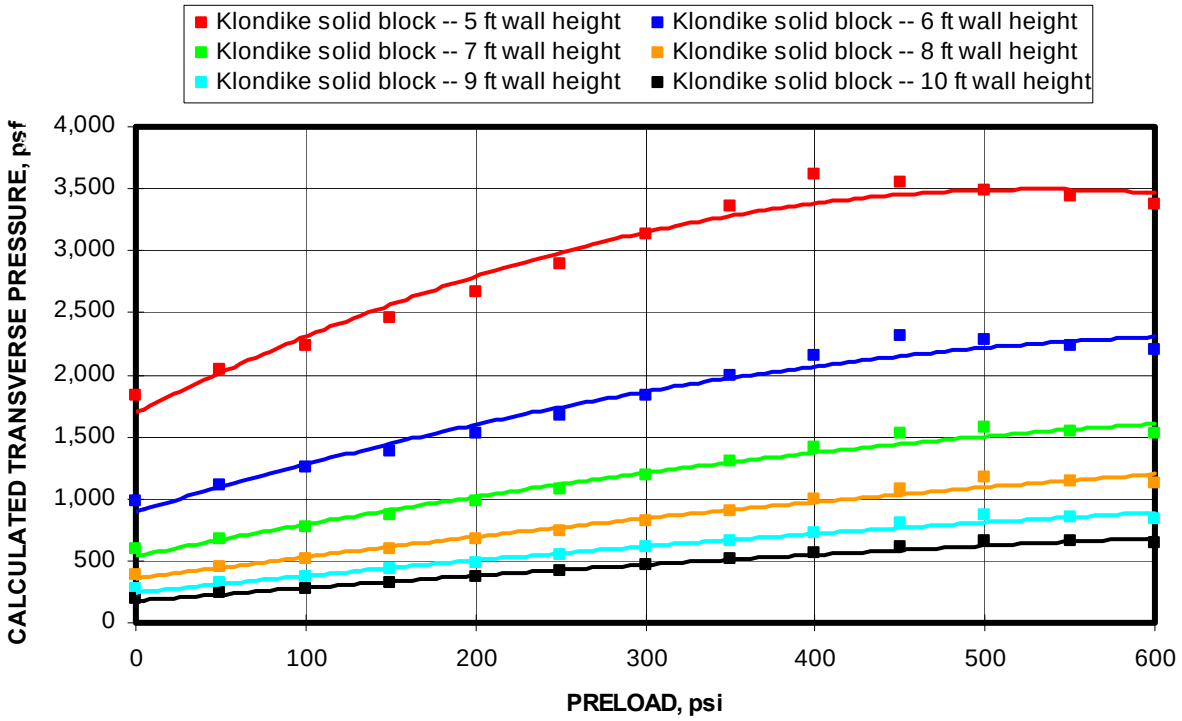

Figure 10-1. Design chart for Klondike solid block showing transverse load as a function of preload for wall heights ranging from 5-10 ft (Hybrid Combination Model).

The transverse pressure for any condition can also be calculated using the formulation documented in chapter 9 and outlined in the flowchart in figure 9-4. Using the previous example, the following calculations are made to determine the transverse pressure capacity of the stopping using the narrow block dimension to establish the wall thickness with a 6-ft

height and a preload of 200 psi. A parametric analysis can also be made and a regression line fitted to the resulting data to provide a chart similar to that shown in figure 10-1.

Normalized thrust load (P/BL) = 0.0025 x Ex(t/L)^2 + 0.0034 x Preload + 0.6100

P/BL = 0.0025 x 60,000 x (5.625/72)^2 + 0.0034 x 200 + 0.6100 = 2.21 kips/in

Thrust (P_m) = 2.21 x 16 = 35.38 kips

Thrust resultant position factor (d) = -.0021 x Half-wall Height - .00361 x Thrust + 0.9547

Thrust resultant position factor (d) = -.0021 x 36 - .00361 x 35.38 + 0.9547 = 0.75

Lateral Displacement (δ_h) = -0.0009 x Ex(t/L)^2 - 0.0023 x Preload + 1.8776

(δ_h) = -0.0009 x 60,000 x (5.625/72)^2 - 0.0023 x 200 + 1.8776 = 1.10 in

$$\textbf{Horizontal Force (HF)} = \frac{P_m \times (d \times t - \delta_h)}{L/2} = \frac{35.38 \times 1000 \times (0.75 \times 5.625 - 1.10)}{72/2} = 3{,}065 \text{ lbs}$$

$$\textbf{Transverse Pressure} = \frac{2 \times HF}{w \times L/2} = \frac{2 \times 3{,}065}{16 \times 72/2} \times 144 = 1{,}532 \text{ psf}$$

10.1.2 Peerless Backsaver Block Constructions

Peerless Backsaver is also a conventional concrete block made from Portland cement. One set of blocks tested as part of this study were fully cured for over a year and had a high compressive strength of 2,169 psi. Partially cured blocks (two-week cure) were also tested, and these had a compressive strength of only 1,070 psi. The block measures nominally 5-7/8 x 7-1/2 x 15-1/2 inches. The best model for this block was the Hybrid Theoretical Thrust model. Figure 10-2 shows the transverse pressure estimates for 6-in-thick walls constructed at heights ranging from 5 to 10 ft in one ft height increments with preload pressures ranging from 0 to 500 psi. These graphs can then be used to approximate the transverse pressure capacity for a particular set of conditions. For example, the transverse pressure capacity of an 8-ft-high wall with 200 psi of ground pressure would be approximately 800 psf.

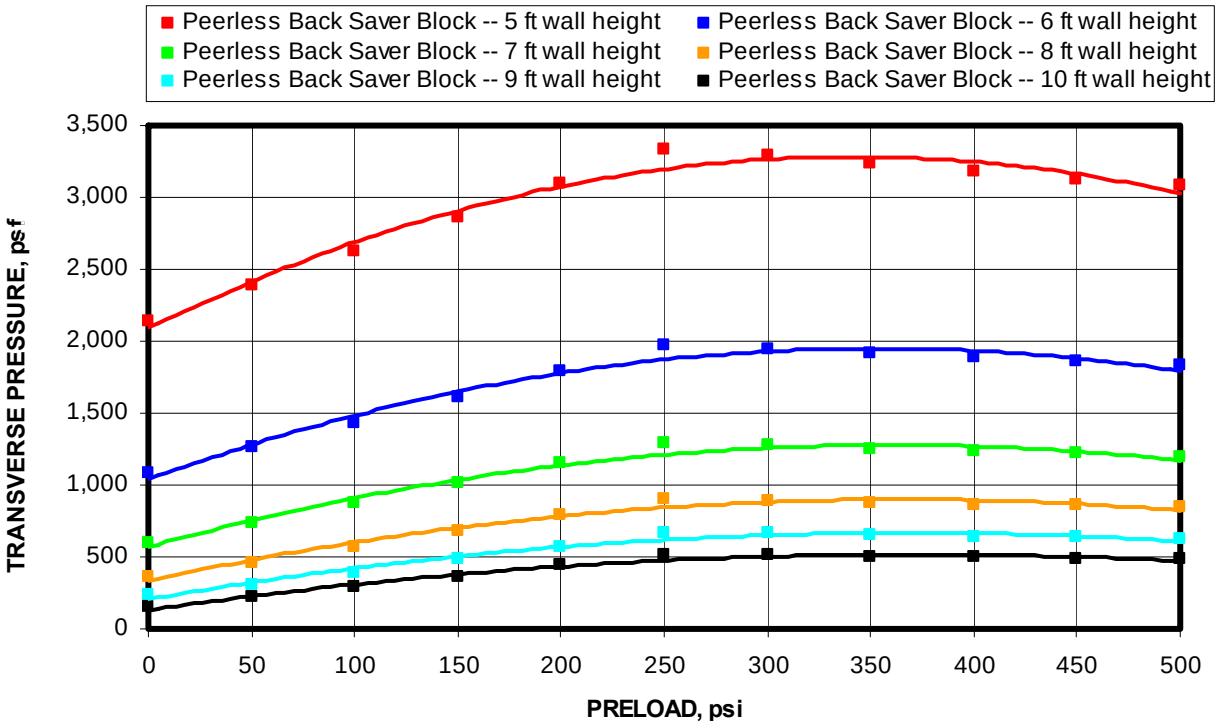

Figure 10-2. Design chart for Peerless Backsaver Block showing transverse load as a function of preload for wall heights ranging from 5-10 ft (Hybrid Thrust Model).

The transverse pressure capacity for any condition can also be calculated using the formulation documented in chapter 9 and outlined in the flowchart in figure 9-2. Using the previous example, the following calculations are made to determine the transverse pressure capacity of the stopping using the narrow block dimension to establish the wall thickness with an 8-ft height and a preload of 200 psi. A parametric analysis can also be made and a regression line fitted to the resulting data to provide a chart similar to that shown in figure 10-2.

Normalized thrust load (P/BL) = 0.0041 x Ex$(t/L)^2$ + 0.0045 x Preload + 0.2142

P/BL = 0.0041 x 45,000 x $(5.875/96)^2$ + 0.0045 x 200 + 0.2142 = 1.80 kips/in

Thrust (P_m) = 1.80 x 15.5= 27.90 kips

Preload (PL) = (200 x 15.5 x 5.875)/1000 = 18.21

Arch Thrust (P_{arch}) = 27.90 – 18.21 = 9.69

Hinge Point Deformation (y) $= \frac{P_{arch} \times L/2}{2 \times A \times E} = \frac{9.69 \times 1000 \times 96/2}{2 \times 15.5 \times 5.875 \times 45{,}000} = 0.0568$ inches

$$\textbf{Lateral Displacement } (\delta_h) = \frac{2\times t - \sqrt{4\times t^2 - 4\times\left(2\times 1\times y - 4\times y^2\right)}}{2}$$

$$\textbf{Lateral Displacement } (\delta_h) = \frac{2\times 5.875 - \sqrt{4\times 5.875^2 - 4\times\left(2\times 96\times .0562 - 4\times .0562^2\right)}}{2} = 1.003 \text{ in}$$

Thrust resultant position factor (d) = -.0017 x Half-wall Height - .0026 x Thrust + 0.9222

Thrust resultant position factor (d) = -.0017 x 48 - .0026 x 27.90 + 0.9222 = 0.768

$$\textbf{Horizontal Force (HF)} = \frac{P_m \times \left(d\times t - \delta_h\right)}{L/2} = \frac{27.90\times 1000\times\left(0.768\times 5.875 - 1.003\right)}{96/2} = 2{,}040 \text{ lbs}$$

$$\textbf{Transverse Pressure} = \frac{2\times HF}{w\times L/2} = \frac{2\times 2{,}040}{15.5\times 96/2}\times 144 = 790 \text{ psf}$$

10.1.3 Klondike Hollow Core Block Constructions

Klondike Hollow Core Block is the same material as the solid block except that three 3.5 x 3.5-in hollow cores are created to reduce the material volume and cost of the block. Obviously, this also reduces the weight of the block since the overall size is the same as the solid block. Although the concrete mix is similar, the effective block strength is less because the webs are not as strong as the solid structure. The unit block compressive strength was measured at 907 psi. The best model for this block was the Hybrid Theoretical Combination Thrust and Lateral Displacement model. Figure 10-3 shows the transverse pressure estimates for 6-in-thick walls constructed at heights ranging from 5 to 10 ft in one ft height increments with preload pressures ranging from 0 to 300 psi. These graphs can then be used to approximate the transverse pressure capacity for a particular set of conditions. Using the same example as was used for the solid block construction, the transverse pressure capacity of a 6-ft-high wall with 200 psi of ground pressure would be approximately 1,110 psf.

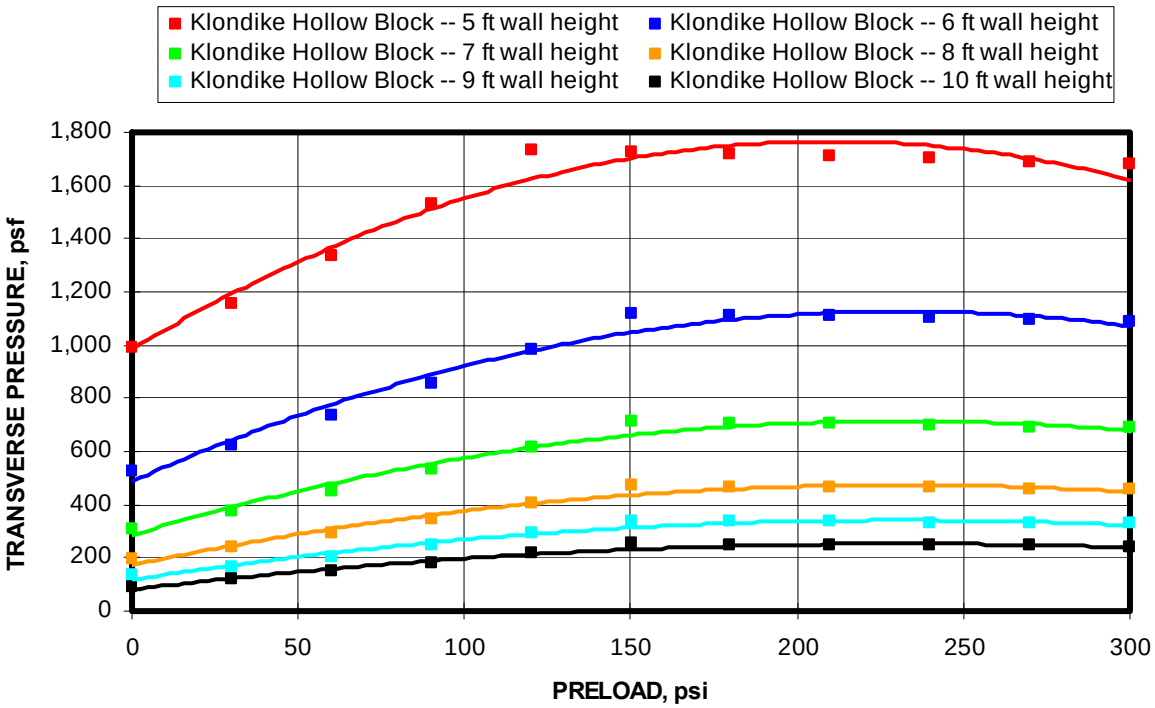

Figure 10-3. Design chart for Klondike Hollow Core block showing transverse load as a function of preload for wall heights ranging from 5-10 ft (Hybrid Combination Model).

The transverse pressure for any condition can also be calculated using the formulation documented in chapter 9 and outlined in the flowchart in figure 9-4. Using the previous example, the following calculations are made to determine the transverse pressure capacity of the stopping using the narrow block dimension to establish the wall thickness with a 6-ft height and a preload of 200 psi. A parametric analysis can also be made and regression line fitted to the resulting data to provide a chart similar to that shown in figure 10-3. Two additional factors need to be considered when analyzing the Klondike Hollow Core Block. First, the effective modulus was adjusted as a function of wall height. Second, the preload limit is set at 150 psi for this particular block.

Effective Modulus (E) = 1,491 x Half-wall height – 5,263 = 1,491 x 36 - 5,263 = 48,420 psi

Normalized thrust load (P/BL) = 0.0015 x Ex$(t/L)^2$ + 0.0028 x Preload + 0.2936

P/BL – 0.0015 x 48,420 x $(5.625/72)^2$ + 0.0028 x 150 + 0.2936 = 1.16 kips/in

Thrust (P_m) = 1.16 x 15.5 = 17.98 kips

Thrust resultant position factor (d) = -.0013 x Half-wall Height - .0033 x Thrust + 1.0272

Thrust resultant position factor (d) = -.0013 x 36 - .0033 x 17.98 + 1.0272 = 0.921

Lateral Displacement (δ_h) = -0.0095 x Ex$(t/L)^2$ + 0.0085 x Preload + 4.9588

(δ_h) = -0.0095 x 48420 x $(5.625/72)^2$ - 0.0085 x 150 + 4.9588 = 0.88 in

$$\textbf{Horizontal Force (HF)} = \frac{P_m \times (d \times t - \delta_h)}{L/2} = \frac{17.98 \times 1000 \times (0.921 \times 5.625 - 0.88)}{72/2} = 2{,}148 \text{ lbs}$$

$$\textbf{Transverse Pressure} = \frac{2 \times HF}{w \times L/2} = \frac{2 \times 2{,}148}{15.56 \times 72/2} \times 144 = 1{,}108 \text{ psf}$$

10.1.4 ACCOA Block Constructions

ACCOA Block is a cellular concrete block. The autoclaved aerated concrete is made from sand, flyash, and copper mine tailings as a source for the silica, which reacts with the aluminum to form a chemical reaction which creates millions of tiny air cells within the concrete matrix. The block has a compressive strength of 421 psi. The block measures nominally 6 x 12 x 24 inches. An 8-in-thick block is also manufactured. The best model for this block was the Hybrid Cellular Thrust Model, meaning that due to the limited test data, all cellular block materials were analyzed to produce a design model for this block. Figure 10-4 shows the transverse pressure estimates for 6-in-thick walls constructed at heights ranging from 5 to 10 ft in one ft height increments with preload pressures ranging from 0 to 200 psi. These graphs can then be used to approximate the transverse pressure capacity for a particular set of conditions. For example, the transverse pressure capacity of a 6-ft-high wall with 100 psi of ground pressure would be approximately 800 psf.

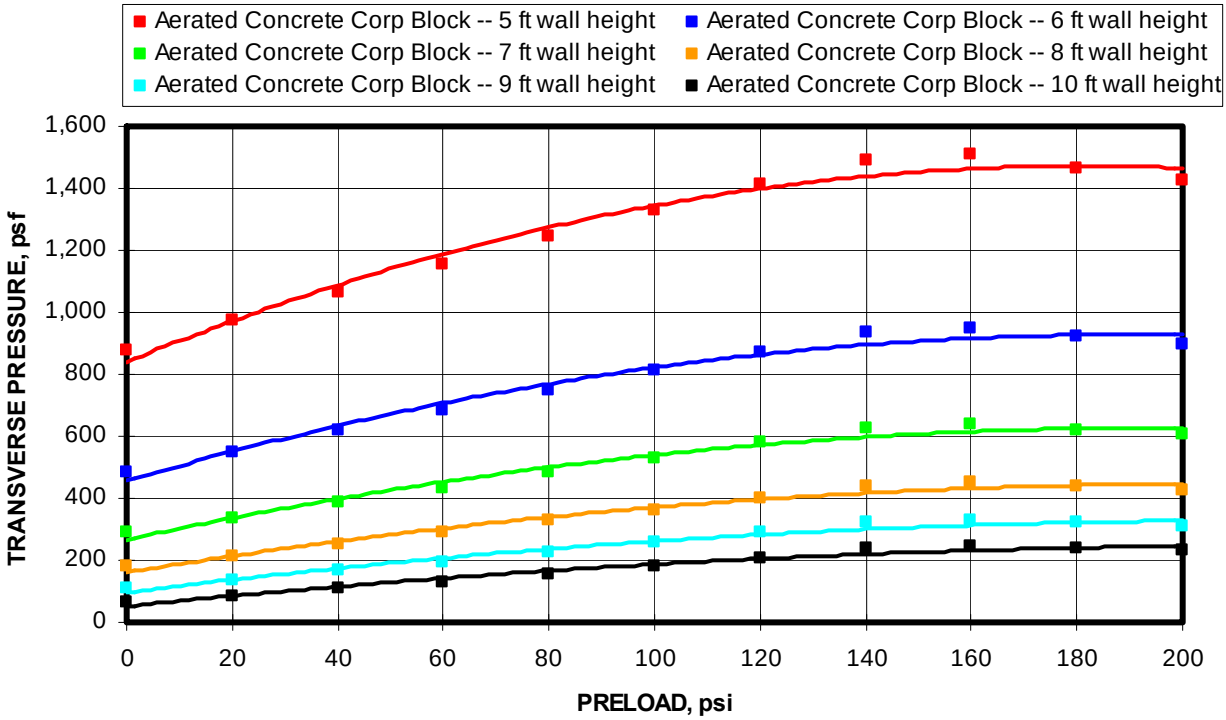

Figure 10-4. Design chart for ACCOA block showing transverse load as a function of preload for wall heights ranging from 5-10 ft (Hybrid Thrust Model).

The transverse pressure for any condition can also be calculated using the formulation documented in chapter 9 and outlined in section 9.2.3.2.1 and the flowchart in figure 9-2. Using the previous example, the following calculations are made to determine the transverse pressure capacity of the stopping using the narrow block dimension to establish the wall thickness with a 6-ft height and a preload of 100 psi. A parametric analysis can also be made and a regression line fitted to the resulting data to provide a chart similar to that shown in figure 10-4.

Normalized thrust load (P/BL) = 0.0019 x Ex$(t/L)^2$ + 0.0044 x Preload + 0.3257

P/BL = 0.0019 x 20,000 x $(6/72)^2$ + 0.0044 x 100 + 0.3257 = 1.03 kips/in

Thrust (P_m) = 1.03 x 24 = 24.72 kips

Preload (PL) = (100 x 24 x 6)/1000 = 14.40 kips

Arch Thrust (P_{arch}) = 24.72 – 14.40 = 10.32 kips

$$\textbf{Hinge Point Deformation (y)} = \frac{P_{arch} \times L/2}{2 \times A \times E} = \frac{10.32 \times 1000 \times 72/2}{2 \times 24 \times 6 \times 20{,}000} = 0.065 \text{ inches}$$

$$\textbf{Lateral Displacement } (\delta_h) = \frac{2 \times t - \sqrt{4 \times t^2 - 4 \times \left(2 \times L \times y - 4 \times y^2\right)}}{2}$$

$$\textbf{Lateral Displacement } (\delta_h) = \frac{2 \times 6 - \sqrt{4 \times 6^2 - 4 \times \left(2 \times 72 \times .065 - 4 \times .065^2\right)}}{2} = 0.837 \text{ inches}$$

Thrust resultant position factor (d) = -.0028 x Half-wall Height - .0076 x Thrust + 1.0181

Thrust resultant position factor (d) = -.0028 x 36 - .0076 x 24.72 + 1.0181 = 0.729

$$\textbf{Horizontal Force (HF)} = \frac{P_m \times \left(d \times t - \delta_h\right)}{L/2} = \frac{24.72 \times 1000 \times \left(0.729 \times 6 - 0.837\right)}{72/2} = 2{,}429 \text{ lbs}$$

$$\textbf{Transverse Pressure} = \frac{2 \times HF}{w \times L/2} = \frac{2 \times 2{,}429}{24 \times 72/2} \times 144 = 810 \text{ psf}$$

10.1.5 Ytong Block Constructions

Ytong is another cellular concrete block, similar to the ACCOA block. The Ytong block has a compressive strength of 705 psi. The block measures nominally 8 x 8 x 24 inches. The best model for this block was the Hybrid Theoretical Combination Thrust and Lateral Displacement model. Figure 10-5 shows the transverse pressure estimates for 8-in-thick walls constructed at heights ranging from 5 to 10 ft in one ft height increments with preload pressures ranging from 0 to 200 psi. These graphs can then be used to approximate the transverse pressure capacity for a particular set of conditions. For example, the transverse pressure capacity of an 8-ft-high wall with 80 psi of ground pressure would be approximately 800 psf.

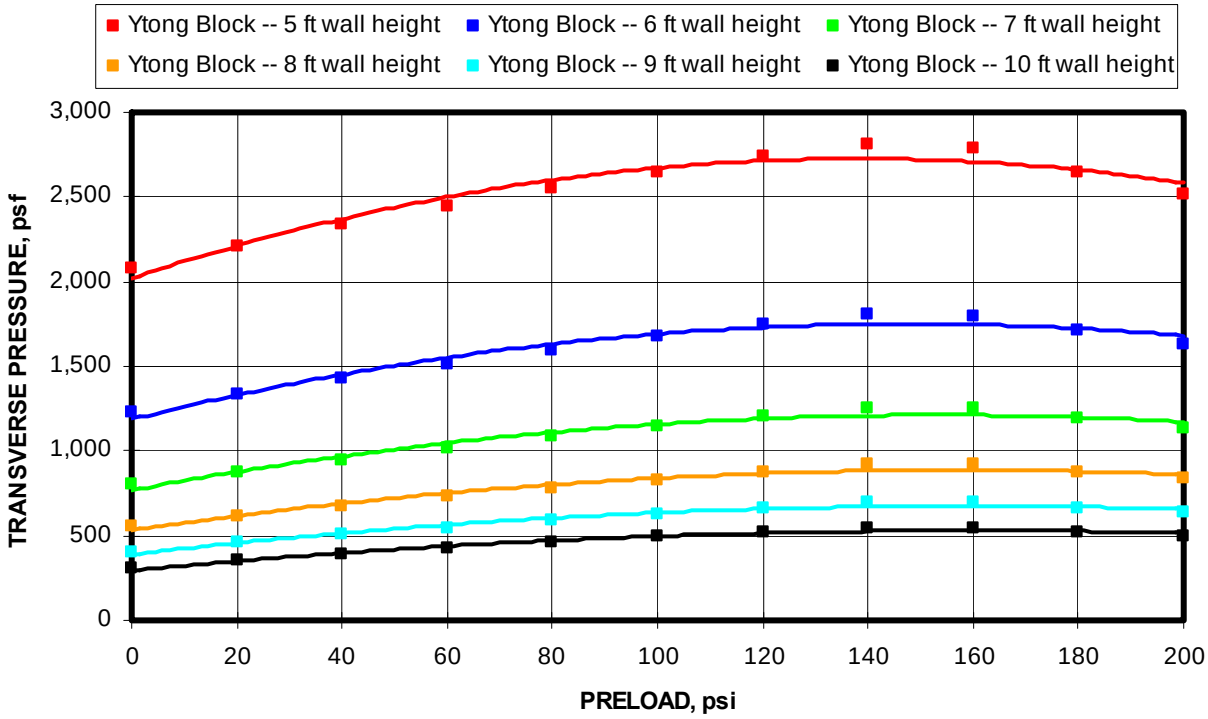

Figure 10-5. Design chart for Ytong Block showing transverse load as a function of preload for wall heights ranging from 5-10 ft (Hybrid Combination Model).

The transverse load for any condition can also be calculated using the formulation documented in chapter 9 and outlined in the flowchart in figure 9-4. Using the previous example, the following calculations are made to determine the transverse load capacity of the stopping which the narrow block dimension to establish the wall thickness with an 8-ft height and a preload of 80 psi. A parametric analysis can also be made and regression line fitted to the resulting data to provide a chart similar to that shown in figure 10-5.

Normalized thrust load (P/BL) = 0.0012 x Ex(t/L)^2 + 0.0061 x Preload + 0.5809

P/BL = 0.0012 x 40,000 x (7.875/96)^2 + 0.0061 x 80 + 0.5809 = 1.39 kips/in

Thrust (P_m) = 1.39 x 24 = 33.36 kips

Thrust resultant position factor (d) = -.0011 x Half-wall Height - .0080 x Thrust + 1.0308

Thrust resultant position factor (d) = -.0011 x 48 - .0080 x 33.36 + 1.0308 = 0.711

Lateral Displacement (δ_h) = -0.00075 x Ex(t/L)^2 - 0.0037 x Preload + 1.5578

(δ_h) = -0.00075 x 40,000 x (7.875/96)^2 - 0.0037 x 80 + 1.5578 = 1.06 in

$$\textbf{Horizontal Force (HF)} = \frac{P_m \times (d \times t - \delta_h)}{L/2} = \frac{33.36 \times 1000 \times (0.711 \times 7.875 - 1.06)}{96/2} = 3{,}154 \text{ lbs}$$

$$\textbf{Transverse Pressure} = \frac{2 \times HF}{w \times L/2} = \frac{2 \times 3{,}154}{24 \times 96/2} \times 144 = 788 \text{ psf}$$

10.1.6 Kingsway Block Constructions

Kingsway is another cellular concrete block, similar to the ACCOA block. The Kingsway block has a compressive strength of 546 psi. The block measures nominally 5-7/8 x 8-3/8 x 17-1/4 inches. The best model for this block was the Hybrid Theoretical Combination Thrust and Lateral Displacement model. Figure 10-6 shows the transverse pressure estimates for 8-in-thick walls constructed at heights ranging from 5 to 10 ft in one ft height increments with preload pressures ranging from 0 to 140 psi. These graphs can then be used to approximate the transverse pressure capacity for a particular set of conditions. For example, the transverse pressure capacity of a 9-ft-high wall with 80 psi of ground pressure would be approximately 200 psf.

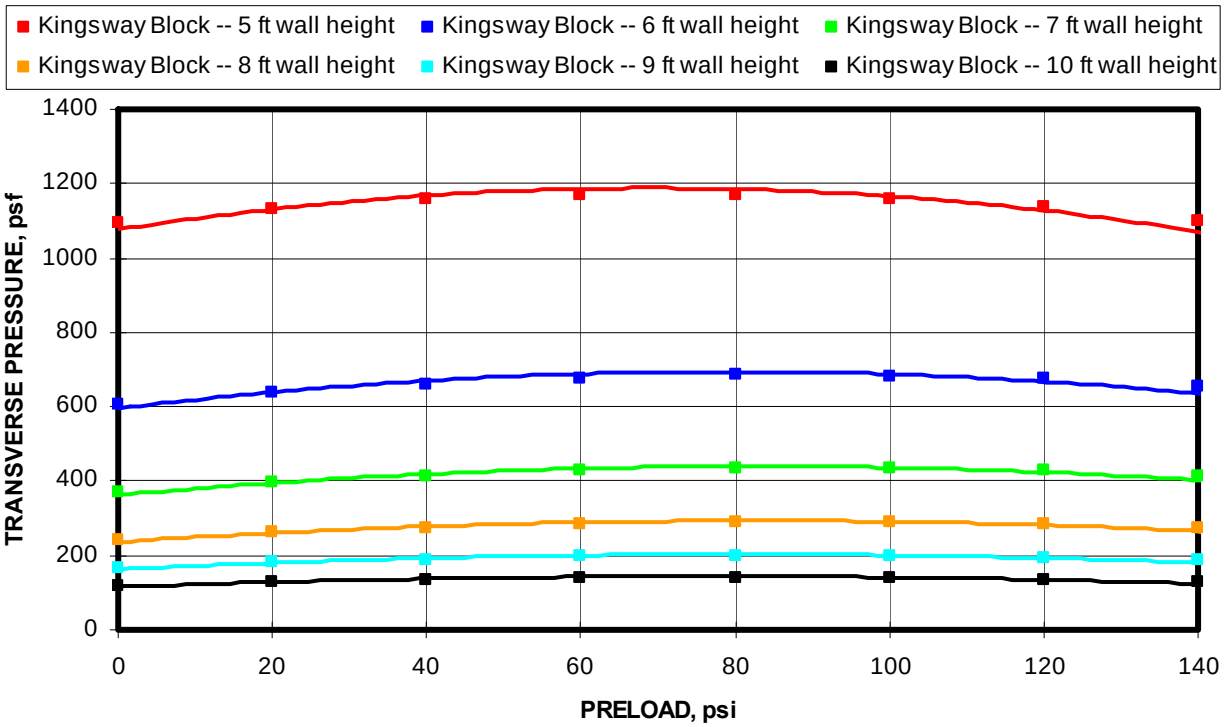

Figure 10-6. Design chart for Kingsway Block showing transverse load as a function of preload for wall heights ranging from 5-10 ft (Hybrid Combination Model).

The transverse pressure for any condition can also be calculated using the formulation documented in chapter 9 and outlined in the flowchart in figure 9-4. Using the previous example, the following calculations are made to determine the transverse pressure capacity of the stopping using the narrow block dimension to establish the wall thickness with a 9-ft height and a preload of 80 psi. A parametric analysis can also be made and regression line fitted to the resulting data to provide a chart similar to that shown in figure 10-6.

Normalized thrust load (P/BL) = 0.0018 x Ex(t/L)^2 + 0.0034 x Preload + 0.2850

P/BL = 0.0018 x 24,000 x (5.875/108)^2 + 0.0034 x 80 + 0.2850 = 0.69 kips/in

Thrust (P_m) = 0.69 x 17.25 = 11.90 kips

Thrust resultant position factor (d) = -.0087 x Half-wall Height - .0453 x Thrust + 1.7532

Thrust resultant position factor (d) = -.0087 x 54 - .0453 x 11.90 + 1.7532 = 0.744

Lateral Displacement (δ_h) = -0.0057 x Ex(t/L)^2 - 0.0020 x Preload + 2.0018

(δ_h) = -0.0057 x 24,000 x (5.875/108)^2 - 0.0020 x 80 + 2.0018 = 1.44 in

$$\textbf{Horizontal Force (HF)} = \frac{P_m \times (d \times t - \delta_h)}{L/2} = \frac{11.90 \times 1000 \times (0.744 \times 5.875 - 1.44)}{108/2} = 646 \text{ lbs}$$

$$\textbf{Transverse Pressure} = \frac{2 \times HF}{w \times L/2} = \frac{2 \times 646}{17.25 \times 108/2} \times 144 = 200 \text{ psf}$$

10.1.7 Omega Block Constructions

Omega is also a cellular concrete block, but with a compressive strength of only 84 psi, it is much weaker than any of the other cellular block materials. The low density material allows the block to be fabricated in an 8 x 16 x 24 inch size, which is also the largest of any stopping block evaluated in this study. The low strength of the block leads to inconsistent transverse pressure behavior, making models also more difficult to develop. The best model for this block was the Hybrid Theoretical Combination Thrust and Lateral Displacement model. Figure 10-7 shows the transverse pressure estimates for 8-in-thick walls constructed at heights ranging from 5 to 10 ft in one ft height increments with preload pressures ranging from 0 to 30 psi. These graphs can then be used to approximate the transverse pressure capacity for a particular set of conditions. For example, the transverse pressure capacity of an 8-ft-high wall with 15 psi of ground pressure would be approximately 80 psf.

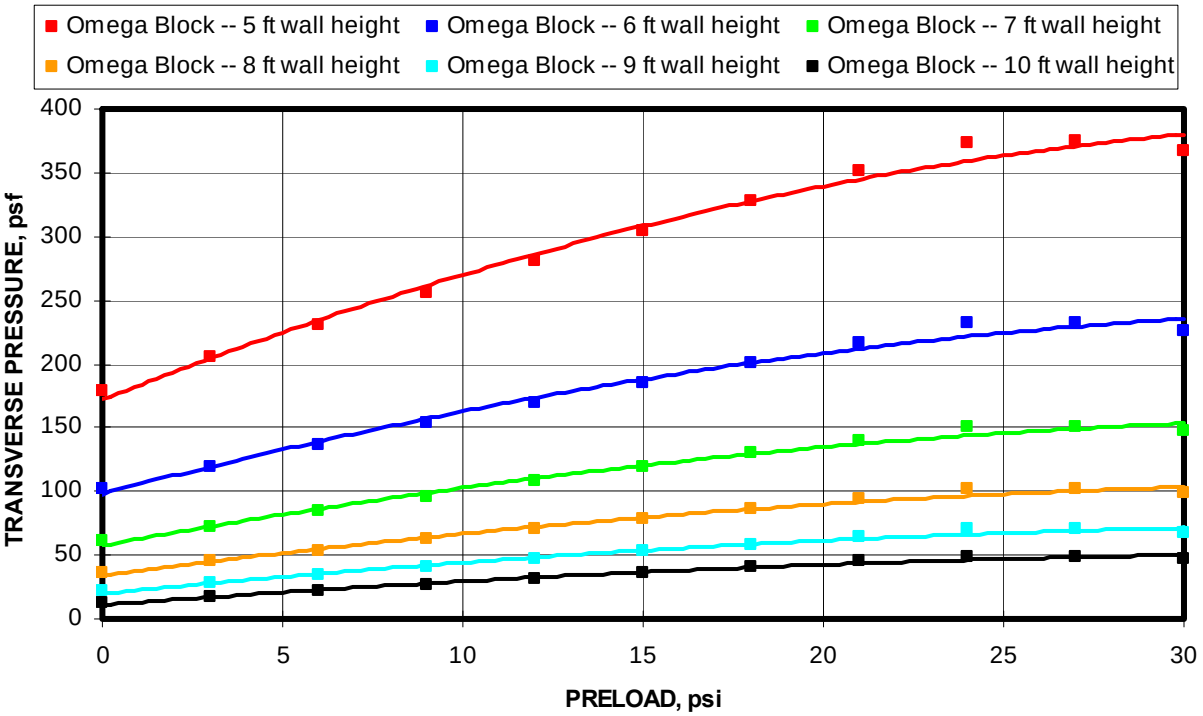

Figure 10-7. Design chart for Omega Block showing transverse load as a function of preload for wall heights ranging from 5-10 ft (Hybrid Combination Model).

The transverse pressure for any condition can also be calculated using the formulation documented in chapter 9 and outlined in the flowchart in figure 9-4. Using the previous example, the following calculations are made to determine the transverse pressure capacity of the stopping using the narrow block dimension to establish the wall thickness with a 8-ft height and a preload of 15 psi. A parametric analysis can also be made and regression line fitted to the resulting data to provide a chart similar to that shown in figure 10-7.

Effective Modulus (E) = .027 x Half-wall height$^{2.87}$ = 1,805 psi

Normalized thrust load (P/BL) = -0.0083 x Ex(t/L)^2 + 0.0046 x Preload + 0.1590

P/BL = -0.0083 x 1,805 x (8/96)^2 + 0.0046 x 15 + 0.1590 = 0.12 kips/in

Thrust (P_m) = 0.12 x 24 = 2.88 kips

Thrust resultant position factor (d) = -.0080 x Half-wall Height - .0524 x Thrust + 1.3723

Thrust resultant position factor (d) = -.0080 x 48 - .0524 x 2.88 + 1.3723 = 0.837

Lateral Displacement (δ_h) = 0.0333 x Ex(t/L)^2 - 0.0293 x Preload + 1.6449

(δ_h) = 0.0333 x 1805 x (8/96)^2 - 0.0293 x 15 + 1.6449 = 1.62 in

$$\textbf{Horizontal Force (HF)} = \frac{P_m \times (d \times t - \delta_h)}{L/2} = \frac{2.88 \times 1000 \times (0.837 \times 8 - 1.62)}{96/2} = 305 \text{ lbs}$$

$$\textbf{Transverse Pressure} = \frac{2 \times HF}{w \times L/2} = \frac{2 \times 305}{24 \times 96/2} \times 144 = 76\,\text{psf}$$

10.1.8 Peerless Super Block Constructions

Peerless Super Block is a unique block design. Styrofoam pellets are imbedded in a weak cement to provide a very low density material. The measured compressive strength is 86 psi, about the same as the Omega block. The low-density material allows the block to be fabricated in a 6 x 16 x 24 inch size, second only to the Omega block in physical size. The low strength of the block and non-uniform distribution of the Styrofoam pellets leads to inconsistent transverse pressure behavior, making models also more difficult to develop. The best model for this block was the Hybrid Theoretical Combination Thrust and Lateral Displacement model. Figure 10-8 shows the transverse pressure estimates for 6-in-thick walls constructed at heights ranging from 5 to 10 ft in with preload pressures ranging from 0 to 100 psi. These graphs can then be used to approximate the transverse pressure capacity for a particular set of conditions.

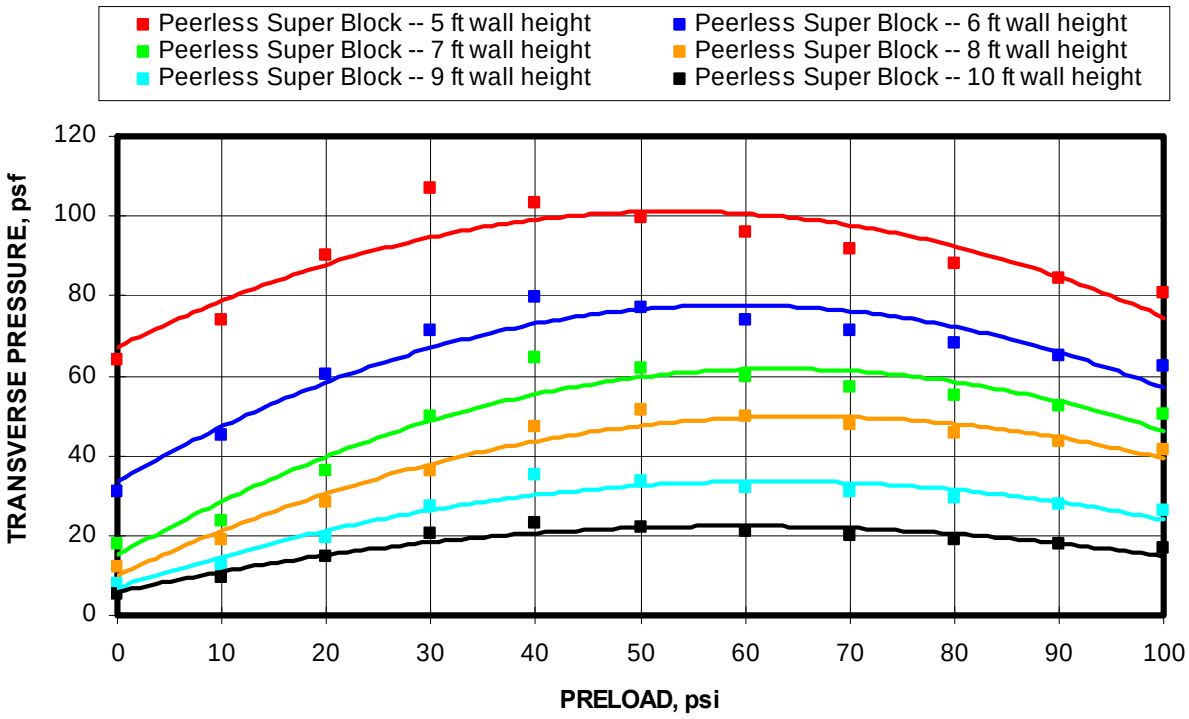

Figure 10-8. Design chart for Peerless Super Block showing transverse load as a function of preload for wall heights ranging from 5-10 ft (Hybrid Combination Model).

The transverse pressure for any condition can also be calculated using the formulation documented in chapter 9 and outlined in the flowchart in figure 9-4. Using the previous example, the following calculations are made to determine the transverse pressure capacity of the stopping using the narrow block dimension to establish the wall thickness with a 10-ft height and a preload of 30 psi. A parametric analysis can also be made and regression line fitted to the resulting data to provide a chart similar to that shown in figure 10-8.

Effective Modulus (E) = 5.51 x Half-wall height$^{1.78}$ = 8,058 psi

Normalized thrust load (P/BL) =- 0.0018 x Ex(t/L)^2 + 0.0034 x Preload + 0.0603

P/BL = -0.0018 x 8058 x (5.8/120)^2 + 0.0034 x 30 + 0.0603 = 0.13 kips/in

Thrust (P_m) = 0.13 x 24 = 3.12 kips

Thrust resultant position factor (d) = -.0036 x Half-wall Height - .0188 x Thrust + 0.7892

Thrust resultant position factor (d) = -.0036 x 60 - .0188 x 3.12 + 0.7892 = 0.515

Lateral Displacement (δ_h) = 0.0038 x Ex(t/L)^2 + 0.0177 x Preload + 1.5636

(δ_h) = 0.0038 x 8058 x (5.8/120)^2 - 0.0177 x 30 + 1.5636 = 1.10 in

$$\textbf{Horizontal Force (HF)} = \frac{P_m \times (d \times t - \delta_h)}{L/2} = \frac{3.12 \times 1000 \times (0.515 \times 5.8 - 1.10)}{120/2} = 98 \text{ lbs}$$

$$\textbf{Transverse Pressure} = \frac{2 \times HF}{w \times L/2} = \frac{2 \times 98}{24 \times 120/2} \times 144 = 19.6 \text{ psf}$$

10.2 GENERIC BLOCK DESIGN FORMULATIONS

The same suite of models that was developed for the specific block constructions was also developed by categorizing the blocks into groups with similar material properties. Specifically, the categories were defined as follows: (1) standard CMU block with compressive strengths ranging from 1,000 to 2,000 psi, (2) cellular block materials with compressive strengths ranging from 250 to 750 psi, and (3) low strength block materials with compressive strengths less than 100 psi. These models were discussed in detail in Chapter 9. When compared with actual test data, the hybrid combination thrust and lateral displacement model generally provides the most accurate predictions of the transverse pressure capacities of the stopping. This model uses a combination of empirical formulations from multivariable regression analysis of test data and theoretical calculations of various parameters affecting

the transverse loading capacity of the stopping. The formulations are presented in figures 10-9, 10-10, and 10-11 for the three block categories.

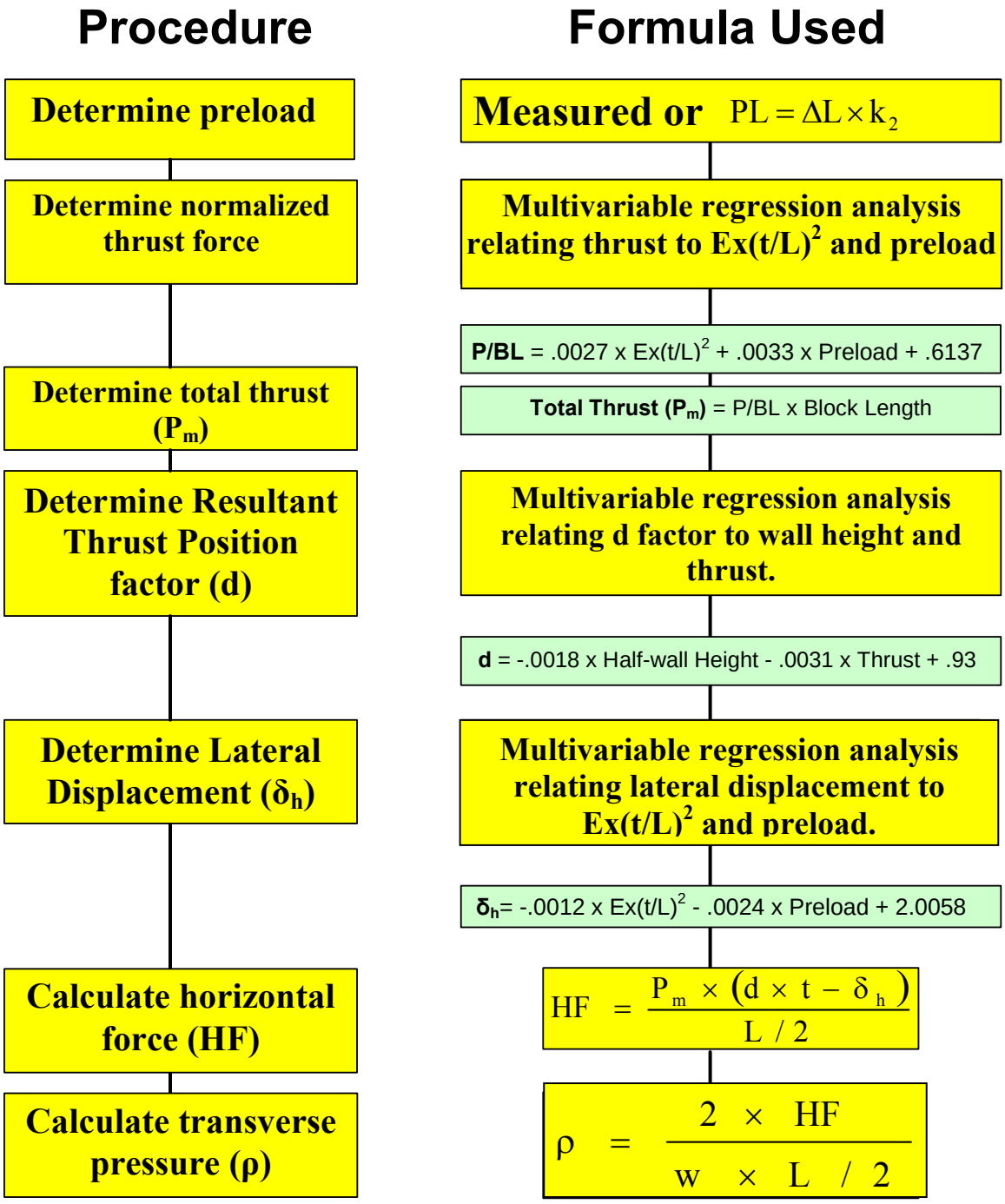

Figure 10-9. Flowchart for Standard CMU model.

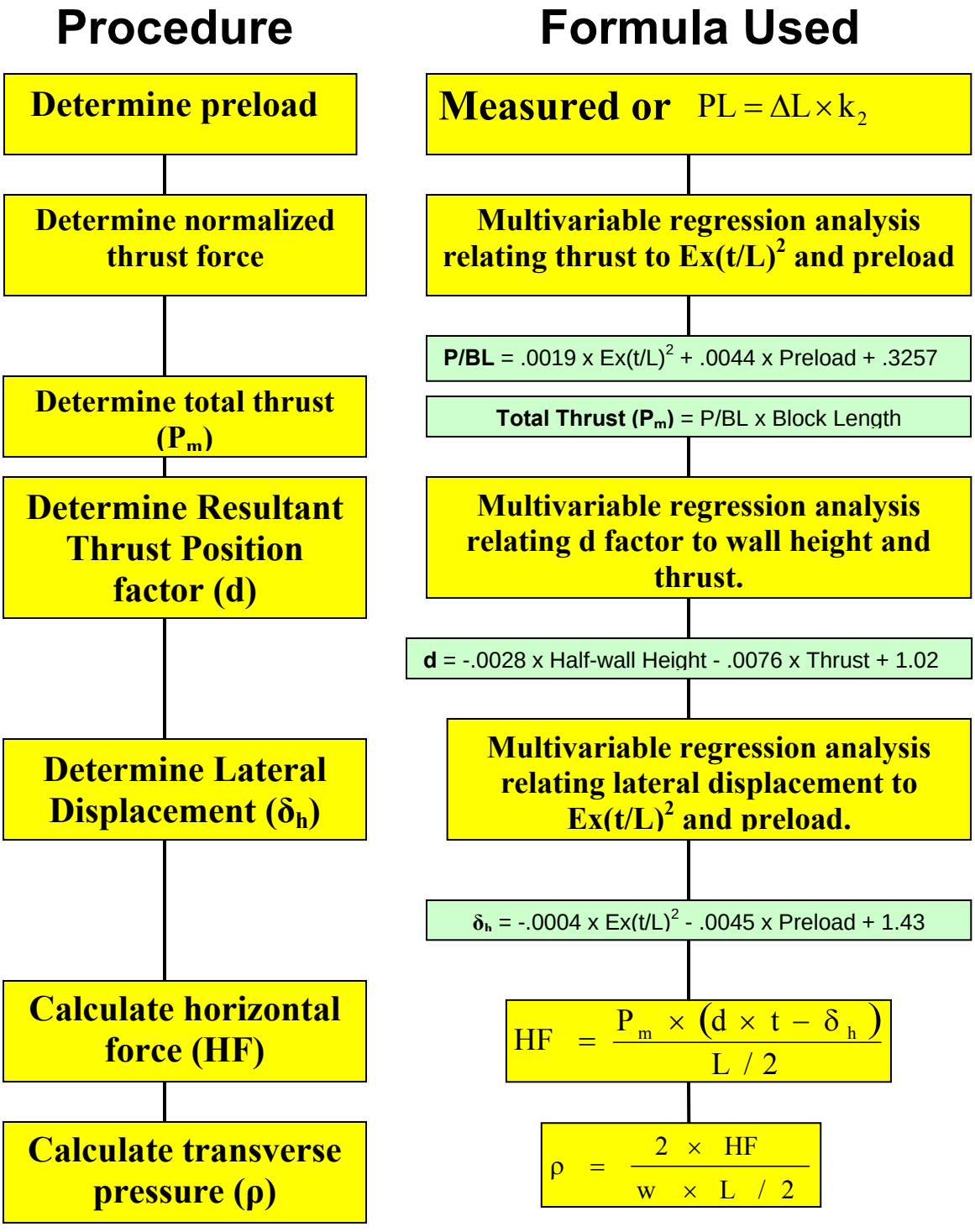

Figure 10-10. Flowchart for the Cellular Concrete Model.

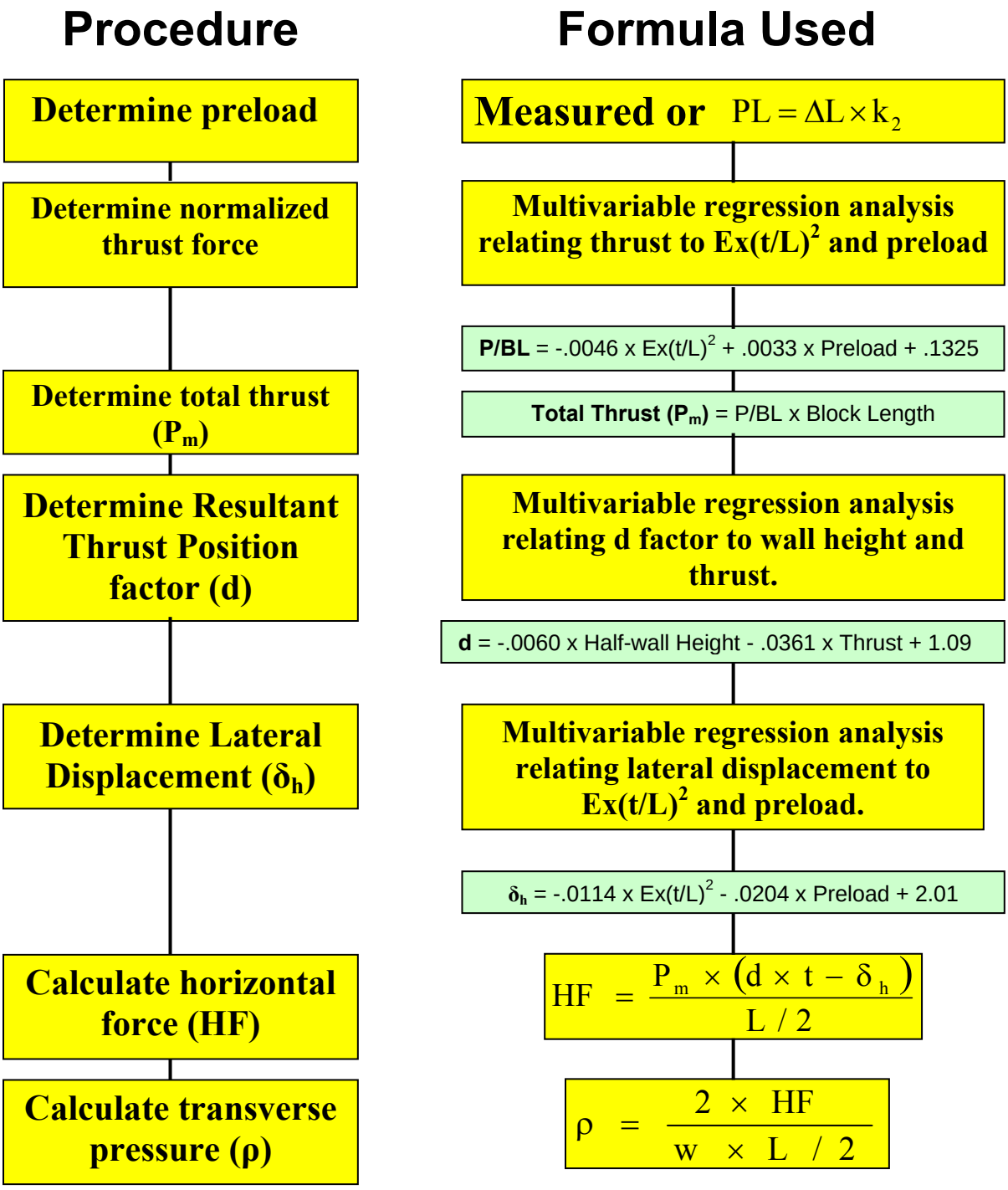

Figure 10-11. Flowchart for the Low Strength Specialty Block Model.

SUMMARY AND CONCLUSIONS

Stoppings are an integral part of any underground mine ventilation system. In coal mines, stoppings may be either classified as temporary or permanent structures. Permanent stoppings are generally constructed from some form of concrete block, typically dry-stacked to form a wall, equal in thickness to the narrow dimension of the block, and bridging between the mine roof and floor and pillar ribs. The CFR specifies that stoppings must be able to withstand 39 psf of transverse loading on the face of the stopping in a freestanding loading condition to be suitable for coal mine use in the United States. This specification is based on ASTM E 72 testing requirements, which is intended for building construction of masonry panels and walls. The author does not believe that this testing requirement provides an accurate representation of the loading conditions that occur in mining situations. For dry-stacked stopping constructions, the transverse load capacity under the CFR criteria, as studies clearly show, is primarily determined by the tensile strength of the sealant. Any block material, regardless of its physical properties, can be made to pass the acceptance test for use in underground coal mines provided the sealant is strong enough and can adhere to the surface of the block. As such, the 39-psf transverse load requirement is an irrelevant, arbitrary, and a misleading performance measure that does not accurately correspond to the true transverse loading capability of stoppings in the mine.

The restraint provided by the mine roof and floor and coal pillars allow the stopping wall to arch between these abutments as the wall bends from the application of transverse loading. Arching has long been recognized as a valid loading mechanism that can dramatically improve the capability of jointed structures to resist loading induced by bending. Arching relies on compressive forces within the wall structure to offset the bending moment induced by the deflection of the wall from the application of transverse loading. For dry-stacked stopping constructions, which have no tensile strength across the joints except for the sealant on the face of the joint, these compressive forces can increase the transverse load capacity of a stopping by an order of magnitude or more. Transverse loading theoretically causes a three-hinge arch to form in a stopping wall as the joint running horizontally across the wall opens at the mid vertical span between the mine roof and floor. This creates two half-sections of wall, one above and one below the middle joint. Hinges also form at the mine roof and floor interface as the half-wall sections remain together as

unit, but also try to rotate at the roof and floor interface. Vertical compressive forces are developed in the wall as it is restrained from horizontal rotation by the mine roof and floor. These compressive forces allow powerful force couples to be developed that control the transverse loading capacity of a jointed structure that otherwise would have very little capability to resist bending induced by transverse loading.

A lab testing protocol to simulate arching of stopping walls by biaxial loading in the NIOSH Mine Roof Simulator was developed. This process is simulated in the MRS by testing a half-height section of wall. The wall is restrained vertically by the fixed vertical position of the load frame platens, thereby acting as rigid end restraints simulating the mine roof and floor. The lower platen is then moved laterally, causing the base of the wall to displace with the platen and causing the wall to rotate accordingly, similar to the three-hinge theory. Deformation zones are created at the face edges of the half-wall in the areas where these two hinges would occur in a full-height wall. By measuring the lateral load applied to the wall by the simulator, the transverse load capacity of the wall can be determined. This load is normalized to the area of the wall to determine a transverse pressure in psf units equivalent to that used in the CFR specifications.

The MRS arch testing protocol was validated through two full-scale tests of stopping walls in the NIOSH Experimental Coal Mine at the Pittsburgh Research Laboratory. In these tests, two different block types with different physical characteristics were evaluated. One block was made from a low density, autoclaved concrete material with a compressive strength of 540 psi, while the other block was made from more conventional materials including Portland cement, sand, and aggregate and had a compressive strength of 1,330 psi. Half-walls equivalent to the seam height in the Experimental Coal Mine were constructed in the MRS using these block materials and tested in accordance with the arch testing protocol. Transverse pressure capacities from the laboratory tests were computed and compared to the in-mine tests with full-scale stoppings of the same construction, which were conducted in a fabricated air pressure chamber in a remote cross section of the mine. The laboratory test results closely matched the full-scale mine tests. The peak transverse pressure measured in the laboratory for the lower strength cellular concrete block (Kingsway) was 417 psf compared to 400 psf for the full-scale mine tests, an error of only 4 pct. For the stronger conventional block, the laboratory measured transverse pressure (1.067 psf) was within 6 pct

of the measured transverse pressure on the full-scale mine stopping (975 psf). Additional verification of the laboratory model was provided to develop a mathematical relationship based on the arching mechanics between the compressive strength of the block and the wall geometry, namely the wall thickness (t) and the wall height (L). It was postulated, based on a static analysis of the arching mechanics, that the transverse pressure should be related to the product of the block compressive strength (f_c) and the squared ratio of the wall thickness and length, mathematically expressed by the term $f_c \times (t/L)^2$. Using this relationship, the transverse pressure of an untested wall construction at the NIOSH Lake Lynn facility was predicted to within a 10 pct error.

Further examination of the arching mechanics indicated that the transverse load capacity of a stopping is also related to the lateral displacement of the wall in addition to the arching thrust that is developed. The following formulation was used to describe the arching mechanics and would serve to provide a mathematical basis for developing various design models to define the transverse load capacity of any hypothetical stopping construction.

$$\rho = \frac{\dfrac{2 \times P \times (0.8 \times t - \delta_h)}{L/2}}{w \times L/2} \times 144 = \frac{2 \times P \times (0.8 \times t - \delta_h)}{w \times (L/2)^2} \times 144$$

Where

ρ	=	transverse load, psf,
P	=	arching force, lbs,
T	=	wall thickness, in,
δ_h	=	lateral displacement of wall at the mid span, in,
w	=	width of the wall, in, and
L/2	=	half-wall height, in.

From this formulation, it is seen that several parameters will affect the transverse load response of a mine ventilation stopping, none of which are included in the current CFR criteria. The impacts of these parameters are summarized as follows:

- **Wall height** – Wall height is a critical parameter in controlling the transverse load capacity of a stopping. An increase in wall height will significantly reduce the transverse load capacity, since the transverse load varies inversely with the square of the half-wall height. Hence, the transverse load capacity of a 10-ft-high stopping wall will be reduced

by a factor of 4 for a 5-ft-high stopping wall of the same construction. From a mechanics perspective, the wall height controls the horizontal force couple upon which the arching is dependent for moment equilibrium requirements.

- **Wall thickness –** The transverse load capacity of a stopping is directly related to the thickness of the stopping. Ultimately, the thickness of the wall determines the arch moment arm (distance between the resultant thrust forces at the hinge points as represented by the factor 0.8 x t - δ_h term). Since most blocks are dimensionally anisotropic, the orientation of the block (wide-side-down or wide-side-up) during wall construction can have a significant impact on the transverse load capacity of the stopping. The thicker the wall, the greater the transverse load capacity will be.
- **Wall Width --** The wall width does not affect the transverse pressure capability of the stopping, despite the width generally being greater than the height of the stopping. Since the blocks are dry-stacked, the joints have no tensile strength and create a hinge line causing the arch to form from the mine floor to the mine roof instead of from coal pillar to coal pillar, as is generally the case in seal behavior.
- **Arch Thrust --** The compressive arch thrust force is the key to the how much transverse capacity a stopping of a given geometry can develop. The development of arching thrust depends on several factors including the geometry of the wall (i.e. height and thickness). However, it is primarily determined by the material properties of the block and boundary stiffness of the roof and floor, both of which control how much lateral displacement of the wall will occur as the transverse pressure is applied to the face of the stopping.
- **Lateral Displacement** -- The lateral displacement also plays a big role in determining the transverse capacity of a block stopping. The width of the arch thrust, represented by the distance between the resultant thrust forces and mathematically expressed as 0.8 x t-δ_h, will decrease as the lateral deflection of the wall increases. The decrease in the width of the arch will cause a proportional decrease in the transverse load capacity of the wall, since the force couple produced by the arch thrust will decrease. The lateral displacement will increase as the boundary stiffness decreases, thereby reducing the transverse load capacity of the stopping. Likewise, walls constructed from a lower modulus block material will also have reduced transverse load potential, since the thrust force developed, as a function of the lateral displacement will be reduced.

The transverse load capacity of a stopping wall is limited even if the material strength has not been exceeded, because the rotation of the wall impacts the development of the arching thrust and moment equilibrium requires that the force couple developed with the arching thrust and the transverse loading must balance. This indicates that there is an optimum block strength that is needed to ensure that the full transverse load potential is realized. Beyond this, the transverse loading will be controlled by the arching mechanics and the benefit of the higher block strength will not be realized in the transverse load development of the stopping. Due to the arching mechanics, the optimum block strength will also depend on the material modulus, since the modulus controls the deformation from the thrust forces in the hinge areas. The lower the modulus, the higher the optimum compressive strength requirement for a particular block geometry.

The full arching potential for any stopping will be realized for rigid boundary conditions, which will then establish the maximum transverse loading capacity for the stopping. Under rigid arching conditions, the lateral displacement of the wall is controlled by the stiffness and elastic response of the block wall. The transverse load capacity will decreases as the block modulus decreases since more lateral displacement of the wall will occur. The increase in lateral displacement reduces the force couple provided by the arching thrust and this causes a decrease in the transverse load capacity of the stopping. If the abutments are not rigid, then the lateral displacement will increase further, resulting in a further reduction in the transverse load capacity of the stopping. Therefore, a small change in the abutment stiffness can cause significant changes in the arching capacity and transverse load capacity of a stopping. A theoretical assessment of the impact of the boundary stiffness was made by varying the system modulus, which is the equivalent stiffness of the wall and the roof and floor acting in series with one another. The system stiffness was reduced to 75, 50, and 25 pct of the rigid boundary condition, and the transverse load capacity determined using the arching mechanics formulations. To put this in perspective, if the boundary stiffness was equal to the wall stiffness, the system stiffness would be reduced by 50 pct. Likewise, if the boundary stiffness were three times that of the wall, the system stiffness would be 75 pct of the rigid boundary condition, and if the boundary stiffness were one third of the wall stiffness, the system stiffness would be 25 pct of the rigid boundary condition. The percent reduction in transverse pressure remains the same for all wall heights, but the

absolute reductions in transverse pressure for shorter walls than it will for taller walls. As an example, the transverse pressure for a 30-in half-wall height is reduced from 1,128 psf for the rigid boundary condition to 470 psf when the boundary modulus is one third of the wall modulus thereby reducing the system modulus to 25 pct of the rigid boundary condition. This represents a 58 pct decrease in the transverse pressure capacity of the stopping.

Another important factor in considering the transverse load capacity of a stopping is the axial loading induced from the ground pressures. Even without arching, a superimposed axial or vertical load acting on a stopping wall can greatly increase the transverse load capacity of the stopping by resisting the moment induced by the transverse pressure. For arching conditions, the superimposed axial loading will act to strengthen the force couple created by the arching thrust. The result of the superimposed axial pressure will be that the transverse load development will occur at smaller lateral displacements of the wall, which results in higher transverse loading capacities. Increases in transverse loading by a factor of 5 can be attained with an 8-ft wall constructed from conventional solid concrete block materials when the ground pressure is increased from 0 to 600 psi. The ground pressure can also help to offset the impact of reductions in boundary stiffness. Using the previous example which indicated a 58 pct reduction in transverse loading due to a reduction in system modulus to 25 pct of the rigid boundary condition, a theoretical analysis indicates that this would drop to a 7 pct reduction if an axial preload pressure of 567 psi was applied to the same stopping.

A systematic study of various stopping constructions using the arch testing protocol was conducted for the following different block materials. The block materials fall into three basic categories, which characterize their material properties and physical characteristics:

(1) **Standard concrete masonry units or CMU's --** These blocks made from conventional Portland cement and various aggregate fillers. Historically, these have been the most commonly used concrete block materials for stopping construction. They can be fabricated in either solid or hollow core fashion. They have compressive strengths ranging from 1,000 to 2,000 psi, dependent primarily on how much Portland cement is used in the mix. Generally, the blocks measure nominally 6x8x16 inches and weigh approximately 50 lbs. Three specific blocks were evaluated in this study: (a) Klondike solid block, (b) Peerless Backsaver block, (c) Klondike hollow core block.

(2) **Cellular concrete materials --** These blocks utilize autoclaved aerated concrete where entrained air is cured in an autoclaved oven to formulate air pockets within the concrete structure that provides a very low-density material that is lightweight, durable, and easy to cut, making it attractive for mine ventilation stoppings. Silica is the largest dry raw material. Sand, flyash, and copper mine tailings are often used for the silica source. The silica reacts with aluminum incorporated into the mix to form a chemical reaction that creates millions of tiny air cells, which give AAC its unique properties. Only about 20 pct of the material is cement. Due to the low material density, the block size is enlarged to block thicknesses of 8 inches and lengths to 24 inches. Compressive strengths range from 464 to 705 psi for the products tested in this study. Three specific blocks were evaluated from this category in this study: (a) Ytong block, (b) ACCOA block, and (c) Kingsway block.

(3) Low strength specialty type materials – These blocks have relatively low strengths and material modulus such that they behave differently than the products in the other two categories. The Omega block has been used for over a decade and was the first cellular type material to gain acceptance for use in stopping construction. The block is separated from the cellular category due to its weaker strength (84 psi). Another unique block is the Peerless Super Block. This block is characterized by styrofoam pellets that are imbedded in the concrete mix to provide a low density material. Included in the mix is polypropelene fibers to help hold the weak material together during failure. It has a compressive strength of 86 psi comparable to that of the Omega block.

A series of tests were conducted in the Mine Roof Simulator using these block materials. The experimental design was to evaluate 3 different heights, typically 30, 48, and 60-in half-walls representing full wall heights of 5, 8, and 10 ft. Preloading to evaluate the impact of ground pressures was varied in 50 to 100 psi increments to the limit of the block strength. Generally, a minimum of two tests were conducted for each configuration to evaluate consistency in the wall response. Additional tests were conducted as needed if the data was inconsistent.

Several predictive models were developed to define the transverse load capacity of mine ventilation stoppings. Chapter 7 presented two models, which utilized either the measured arch thrust or the measured lateral displacement to predict the laboratory arch test results. The procedures are summarized in the flowcharts below, first for the lateral displacement method and second for the arch thrust method.

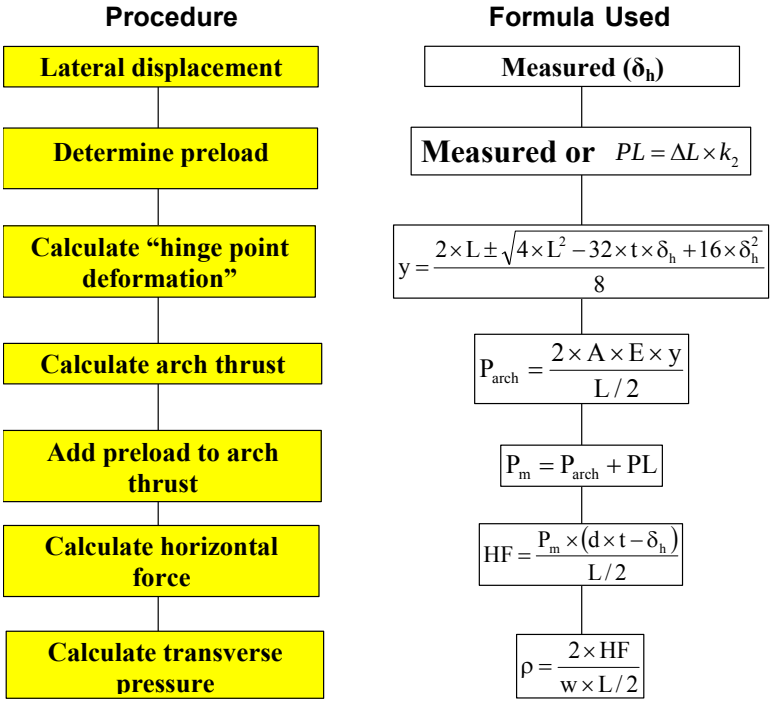

Chapter 8 utilized these models to evaluate the test results for each of the block materials and examine parametric trends in the transverse load performance of the various stopping constructions. It was clearly shown in the analysis that if either the lateral wall displacement or the arching thrust is known, the transverse load capacity of the stopping could be predicted to within a few percent error. One or both of the models predicted the

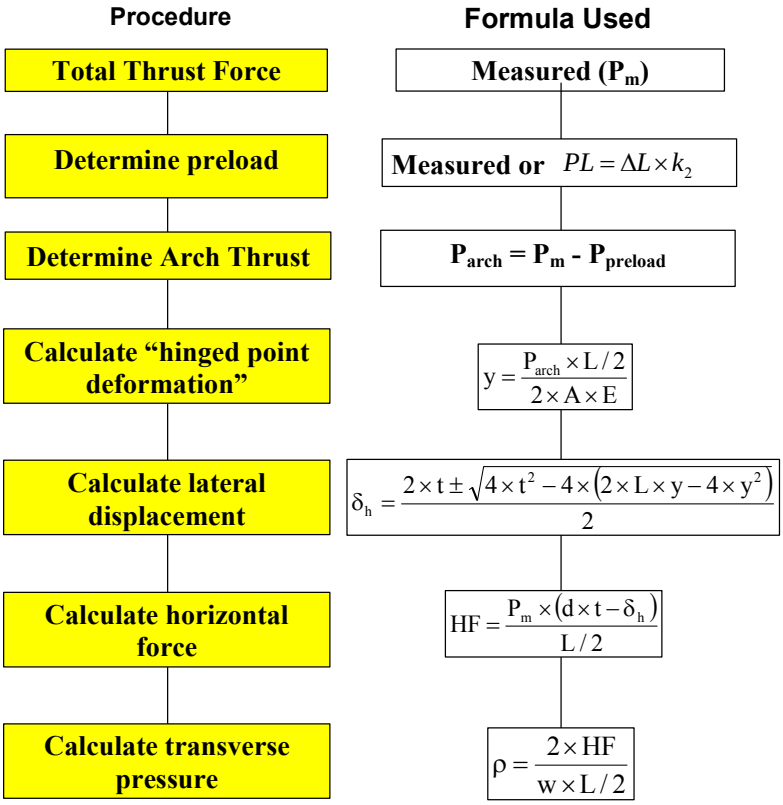

transverse load to within 5 pct error for all but the Omega and Peerless Super Block constructions. The performance of these blocks was much less consistent than all the other blocks due to the low strength and inconsistent material properties. The Omega block transverse loading was predicted to within 16 pct accuracy and the Peerless Super Block error prediction was 21 pct.

Chapter 9 took this analysis one-step further. Instead of using measured lateral displacement or thrust information, methods were developed that would allow these measures to be estimated and then utilized in the models for transverse load prediction. Four formulations were developed: (1) Full Empirical, (2) Hybrid Theoretical Thrust, (3) Hybrid Theoretical Lateral Displacement, (4) Hybrid Theoretical Combination Thrust and Lateral Displacement. These models were constructed for each particular block that was examined in the study. A more generic model was constructed using data grouped into the three categories previously described: (1) Standard CMU, (2) Cellular Concrete, and (3) Specialty Block. The generic models allow transverse load approximations to be developed for any hypothetical block material that fits within these broad criteria.

- **Full Empirical Model –** This model uses empirical data from the laboratory half-wall tests to construct a multivariable regression analysis correlating the term $Ex(t/L)^2$ and preload to the transverse pressure. In this formulation, E is the material modulus, t is the wall thickness, and L is the height of the wall.
- **Hybrid Theoretical Thrust Model –** This model uses a multivariable regression analysis of test data to correlate the thrust force to the $Ex(t/L)^2$ term and preload pressure. Once this is determined, the formulation previously shown is used to compute the hinge area deformation and lateral displacement. Then using the moment equilibrium requirements for arching, the horizontal force and transverse pressure is determined.
- **Hybrid Theoretical Lateral Displacement Model –** This model is similar to the Hybrid Theoretical Thrust Model except the empirical data is use to estimate the lateral displacement instead of the thrust force. Once the lateral displacement is determined, the hinge area deformation and arch thrust is computed using the previously described formulation. Then using the moment equilibrium requirements for arching, the horizontal force and transverse pressure is determined as is done in the thrust model.

- **Hybrid Theoretical Combination Model –** This model essentially combines the thrust model and lateral displacement models. In the Hybrid Combination Model, both the thrust and lateral displacement are estimated from a multivariable regression analysis of the laboratory test data, again correlating these measures to the $Ex(t/L)^2$ term and preload pressure. The transverse pressure is then computed using the moment equilibrium requirements that satisfy the arching mechanics.

Finally, chapter 10 examines each of these design formulations and recommends a specific design formulation, which provides the most accurate approximation of the transverse load capacity of the stopping. Design formulations are recommended for the specific block materials examined in this study as well as for the three generic categories. For the most part, the Hybrid Theoretical Combination Model was the recommended design formulation. The transverse load capacities for all blocks were predicted to within a 4 pct error using the recommended design models.

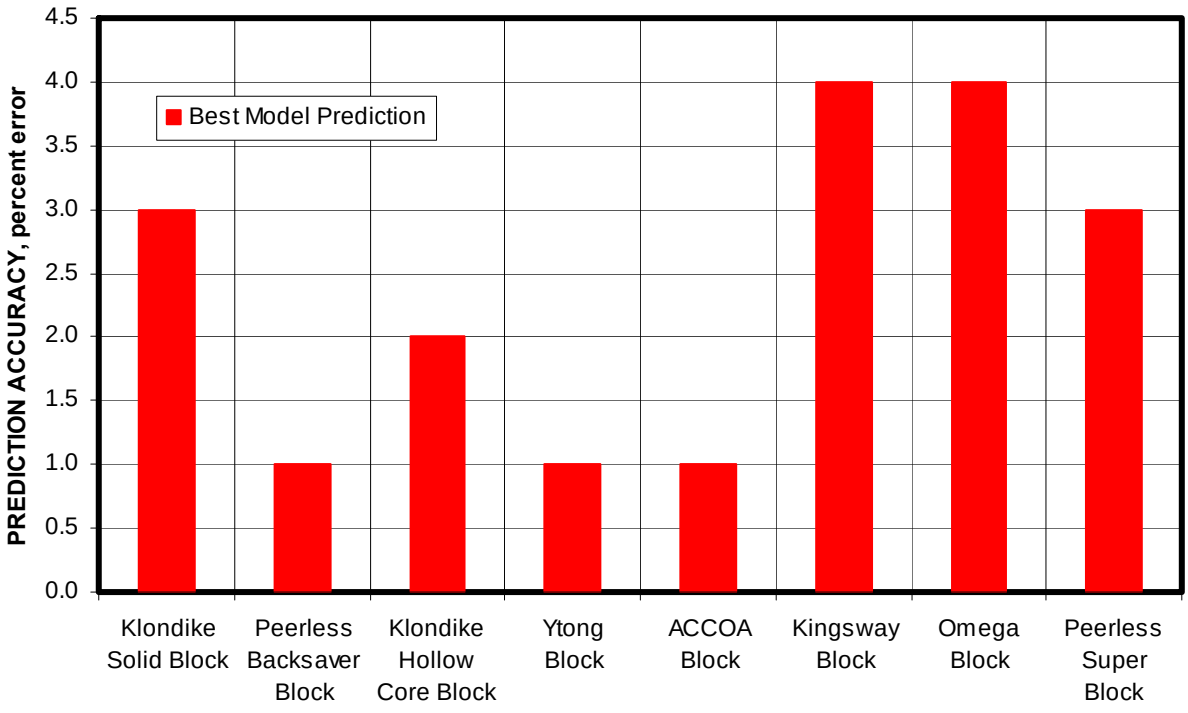

In conclusion, arching stopping design would be a radical departure from the current freestanding wall design required by the CFR. The physical properties of the block and the size of the mine opening would need to be examined to determine the proper design for a stopping application. The sealant would no longer be considered to affect the transverse load

capability of the stopping. Since the actual transverse load capacity of the stopping can be determined, the stopping can be designed based on the required transverse load capacity for a specific set of conditions in the mine, as opposed to the current system that permits stoppings of widely ranging transverse loading capabilities to be employed in the same environment. This approach should lead to a safer mine environment for the tens of thousands of mineworkers in underground coal mines.

FUTURE RESEARCH RECOMMENDATIONS

This study conducted a comprehensive evaluation of arching in laboratory conditions for dry-stacked mine ventilation stoppings. The laboratory test protocol was verified with some full-scale testing of stoppings including two tests in a coal mine environment. The results of these underground trials did confirm the laboratory test procedure and experimental design, but the overriding question remains the issue significance of the abutment stiffness and its impact on arching. It is clear that arching can occur in a mine environment as was demonstrated by the full-scale in mine testing. An extensive theoretical analysis of the impact of the abutment stiffness was also conducted as part of this research. That analysis indicates that the abutment stiffness can significantly affect the arching capability and degrade the transverse load capacity of a stopping, but it also indicates that arching will continue to occur even under relatively soft boundary conditions. It was also shown by the analysis that the superimposed axial loading from the ground pressures can do much to offset the impact of lower stiffness boundary conditions. Nonetheless, additional data needs to be acquired on actual roof and floor stiffness relative to a stopping construction to further define the range of boundary conditions that actually exist in the mine. It is proposed that some in mine studies of ground stiffness be conducted relative to stopping block contact conditions to further define this problem.

Although this study was comprehensive in scope, the current industry practice of using strain softening materials to absorb ground deformation and thereby extend the service life of the stopping, remains a major detriment to preserving the arching and transverse load capacity of stoppings. First, the industry needs to be made aware of the impact of the strain softening materials relative to transverse loading to avoid creating hazardous ventilation conditions with poor stopping construction. Research needs to be done to develop a material

that is more compatible to the block physical properties so that a reasonable compromise can be made to preserve both the service life and transverse load capacity of the stopping. Additional approaches could also be pursued in which the hinge element would be removed while still allowing vertical deformation to occur. This could be some sort of mechanical device or some form of membrane control that would provide this function.

Finally, the very weak block materials taxed the limits of the laboratory system to accurately evaluate the arching thrust and transverse loading. Some additional testing with a higher resolution of measurement should be conducted to improve the accuracy of the design formulations for these materials.

BIBLIOGRAPHY

1. Anderson C. 1984. Arching Action in Transverse Laterally Loaded Masonry Wall Panels. The Structural Engineer, vol. 62B, no. 1, March, 12 pp.
2. ASTM Designation E 72-80. 1981. Standard Methods of Conducting Strength Tests for Building Construction. Annual Book of ASTM Standards, Vol. 04.07, March, pp. 283, 293.
3. Barczak, T. M. Development Of New Protocols To Evaluate The Transverse Loading Of Mine Ventilation Stoppings. Master's Thesis, West Virginia University, Morgantown, WV, November, 2004, 86 pp.
4. British Standards Institution. 1978. Code of Practice for Use of Masonry: Part 1 – Structural Use of Unreinforced Masonry. BS 5628, BSI, London.
5. Code of Federal Regulations, Title 30 Mineral Resources, Part 75 Mandatory Safety Standards – Underground Coal Mines, Subpart D – Ventilation, Section 75.333 Ventilation Controls, pp. 471-473.
6. Cranston, W. B. and J. J. Roberts. 1976. The Structural Behavior of Concrete Masonry –Reinforced and Unreinforced. The Structural Engineer, vol. 54, no. 11, November, pp. 423-436.
7. Drysdale, R. G., A. A. Hamid and L. R Baker. 1994. Masonry Structures: Behavior and Design. Englewood Cliffs, NJ, Prentice Hall, ISBN: 0135620260.
8. Gillies, A. D. S., R. D. Pearson, R. Day, P. Dux and A. R. Green. 2001. Testing and Usage of Ventilation Control Devices within the Australian Coal Mining Industry. Proceedings of the 7th International Mine Ventilation Congress, Chapter 80, Cracow, Poland, June 17-22, pp. 565-572.
9. Kawenski, E. M. and D. W. Mitchell. 1966. Evaluation of Materials for Ventilation Structures. Mining Congress Journal, March, pp. 49-53.
10. Masonry Designer's Guide: Based on Building Code Requirements for Masonry Structures (ACI 530-92/ASCE, 5-92/TMS 402-92) and Specifications for Masonry Structures (ACI 530.1-92/ASCE 6-93/TMS 602-92). John H. Matthys editor.
11. Massachusetts Institute of Technology. 1954. Behavior of Wall Panels Under Static and Dynamic Loads II. Department of Civil and Sanitary Engineering, January.

12. McDowell, E. L., K. E. McKee and E. Sevin. 1956. Arching Action Theory of Masonry Walls. Journal of the Structural Division, Proceedings of the American Society of Civil Engineers, vol. 82, no ST2, Paper 915, March, pp. 915-1 - 915-18.
13. Perloff, W. H. and Baron, W. Soil Mechanics: Principles and Applications. John Wiley and Sons, 1976, ISBN: 047106671-0, pp. 178-186.
14. Sapko, M. J, E. S. Weiss and S. P. Harteis. 2003. Alternative Methodologies for Evaluating Explosion-Resistant Mine Ventilation Seals. Published in the 30th International Conference of Safety in Mines Research Institutes, South African Institute of Mining and Metallurgy.
15. Tien, J. 1996. Air Leakage Costs. A Strong Stopping Maintenance Program Saves Money and Gets More Air to the Face. Coal Age, Sept., pp. 88-121.
16. Weiss, E. S., S. P. Harteis and K. L. Cashdollar. 2003. NIOSH-PRL Evaluation of the Kennedy and Solid-Concrete-Block Stopping Designs for MSHA during LLEM Explosion Tests, September-November 2003. NIOSH Internal Report, March, 13 pp.
17. Weiss, E. S., S. P. Harteis and K. L. Cashdollar. 2004. NIOSH-PRL Evaluation of the Kennedy and Solid-Concrete-Block Stopping Designs for MSHA during LLEM Explosion Tests, Sept., 40 pp.

APPENDIX A: DESCRIPTION OF THE MINE ROOF SIMULATOR

The Mine Roof Simulator (MRS) is a servo-controlled hydraulic press custom built by MTS Systems Corporation to U.S. Bureau of Mines (USBM) specifications. The simulator was built in 1979 at a cost of $7.5 million. It was designed specifically for longwall shield testing, and is the only active load frame in the United States that can accommodate full-size shields. However, its size and unique capabilities provides a facility for testing a wide variety of large-scale structures, including various forms of standing roof support structures and mine ventilation stoppings.

A functional diagram of the load frame is shown in figure A-1. The load frame has several distinctive characteristics. The size of the upper and lower platen is 20 ft x 20 ft. The upper platen can be moved up or down and hydraulically clamped into a fixed position on the directional columns to establish a height for testing. With a maximum vertical opening between the upper and lower platen of 16-ft, the load frame can accommodate the largest shields currently in use. Load application is provided by controlled movement of the lower platen, operating in either force of displacement control. The load frame is a biaxial frame, capable of applying both vertical and horizontal loads. Load actuators are equipped with special hydrostatic slip bearings to permit simultaneous load and travel. This allows vertical and horizontal loads to be applied simultaneously. The capability to provide controlled loading simultaneously in two orthogonal directions is unique at this scale.

Vertical loading is provided by a set of four actuators, one on each of the corners of the lower platen. Loads of up to 3 million pounds can be applied in the vertical direction by upward movement of the lower platen. Each actuator is capable of applying the full 3 million pounds of force, so that the specimen can be placed anywhere on the platen surface and the full 3 million pound capacity can be provided. The vertical (upward) range of motion of the lower platen is 24 inches.

Horizontal loading is also provided by four actuators, with two actuators located on both the left and right side of the load frame just below the floor level. These actuators act in pairs to provide horizontal displacement of the lower platen in either a positive or a

negative (x) direction, reacting off the corner columns of the load frame. The horizontal range of motion of the lower platen is 16 in.

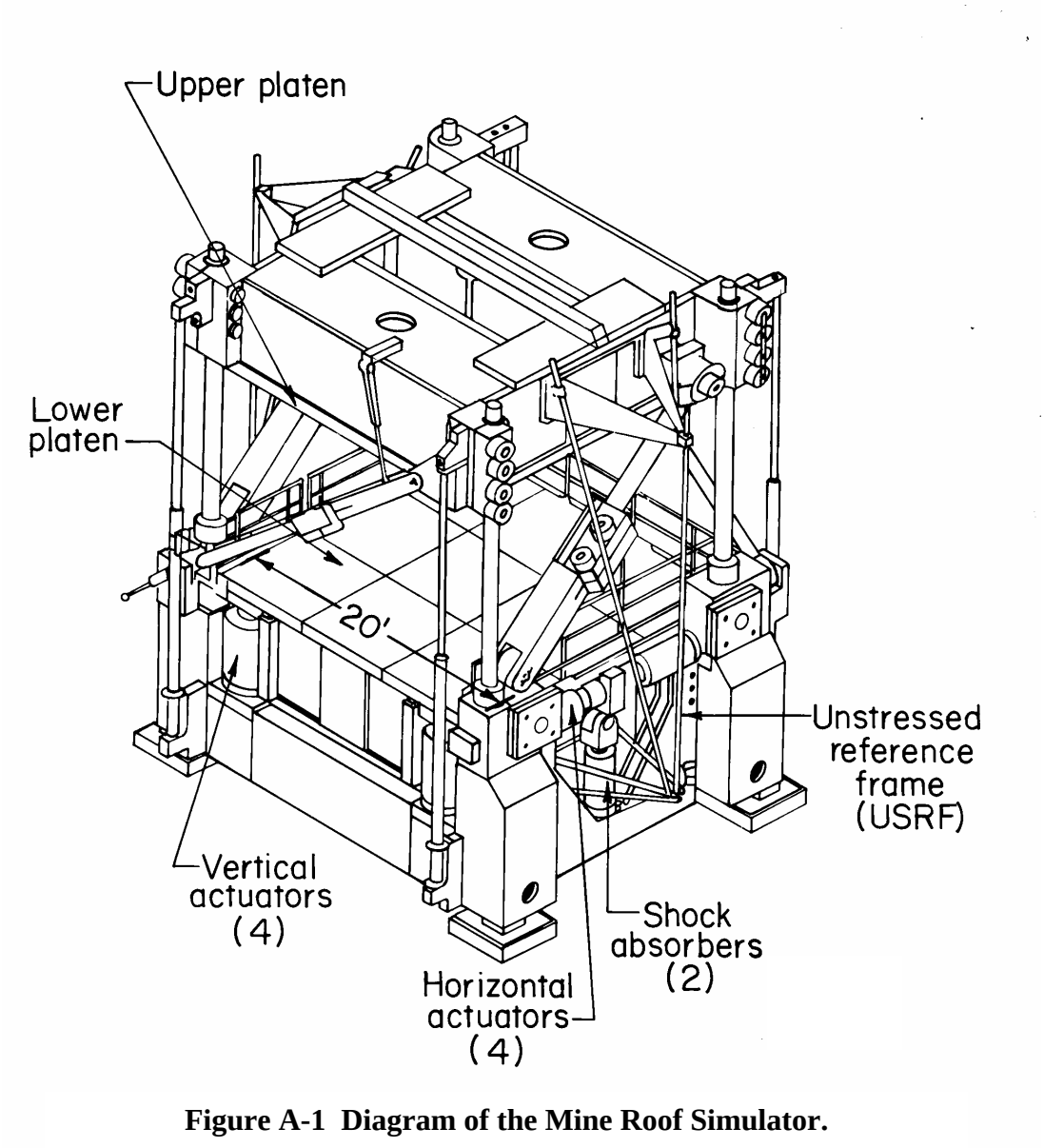

Figure A-1 Diagram of the Mine Roof Simulator.

There is no programmable control of the lower platen in the lateral horizontal axis (y-direction). The load frame has a reactive capacity of 1.6 million pounds in this direction, but loads cannot be applied in the lateral direction. The range of motion of the lower platen in this direction is $\pm$ 0.5 in.

Six degrees of freedom control of the lower platen are provided by the unstressed reference frame, which provides feedback on platen displacements and rotations to the closed-loop control system. Pitch, yaw, and roll of the lower platen are controlled to keep the lower and upper platens parallel during load application.

A shock absorber actuator is positioned on the left and right side of the lower platen. These shock absorbers will control the displacement of the lower platen to less than 0.1 in in the event of sudden failure of the support specimen. This system absorbs energy stored in the load frame to maintain control of the platen and to avoid releasing stored energy into the specimen immediately following an abrupt specimen failure.

Two hydraulic pumps provide up to 3,000 psi of pressure to the vertical and horizontal actuators during load application. The rate of movement of the lower platen is limited by the 140-gpm capacity of the hydraulic pumps. The maximum platen velocity assuming simultaneous vertical and horizontal displacement is 5.0 inches per minute.

APPENDIX B: MRS HALF-WALL TEST DATA

KLONDIKE BLOCK

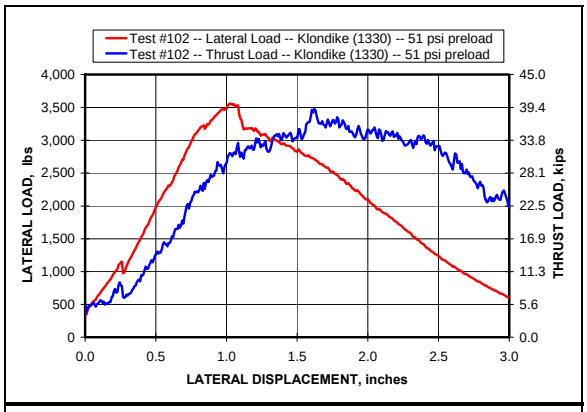

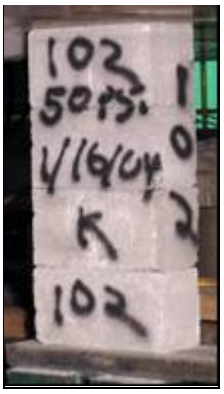

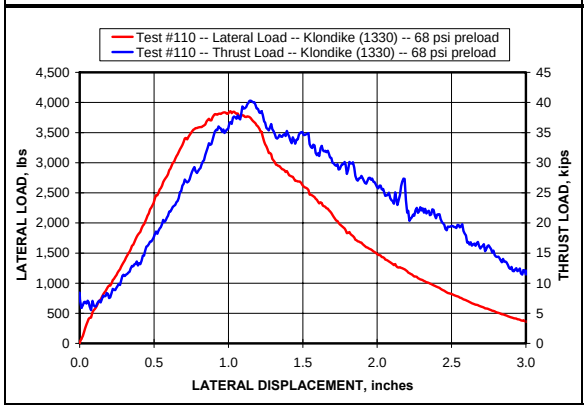

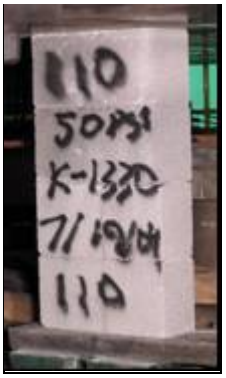

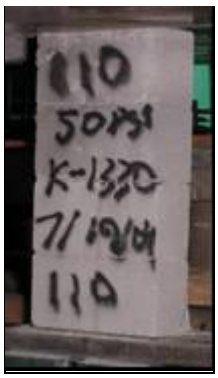

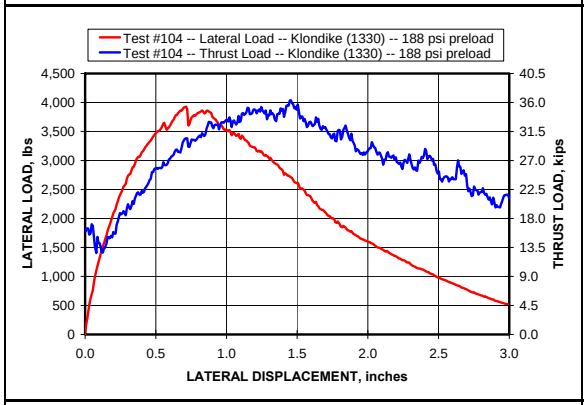

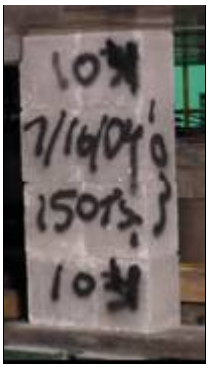

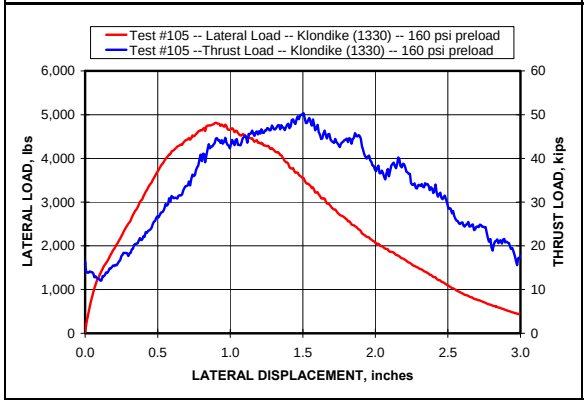

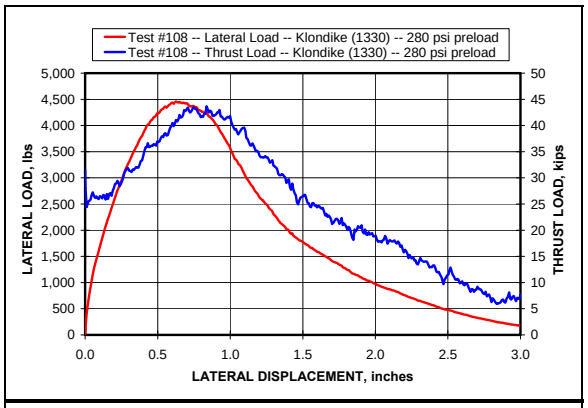
Test #108 -- Lateral Load -- Klondike (1330) -- 280 psi preload
Test #108 -- Thrust Load -- Klondike (1330) -- 280 psi preload
LATERAL LOAD, lbs
THRUST LOAD, kips
LATERAL DISPLACEMENT, inches


108
300PSI
7/19/04
K
108


108
300PSI
7/19/04
K
108

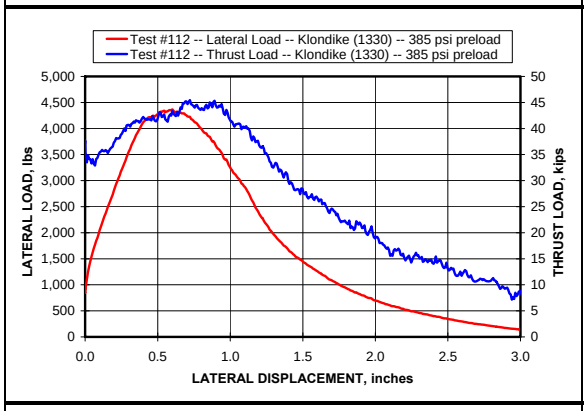
Test #112 -- Lateral Load -- Klondike (1330) -- 385 psi preload
Test #112 -- Thrust Load -- Klondike (1330) -- 385 psi preload
LATERAL LOAD, lbs
THRUST LOAD, kips
LATERAL DISPLACEMENT, inches


112
400
PSI
K1330
7/19/04
112


400
PSI
K1330
7/19/04
112

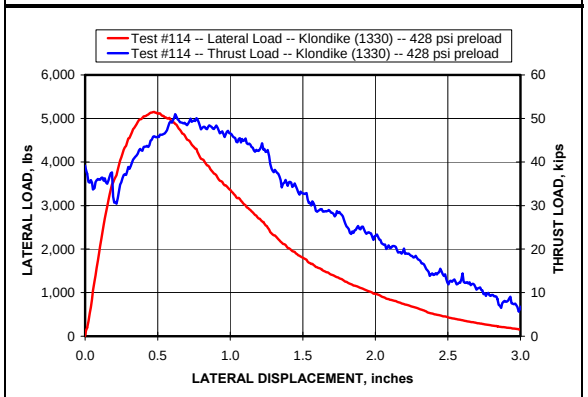
Test #114 -- Lateral Load -- Klondike (1330) -- 428 psi preload
Test #114 -- Thrust Load -- Klondike (1330) -- 428 psi preload
LATERAL LOAD, lbs
THRUST LOAD, kips
LATERAL DISPLACEMENT, inches


114
400PSI
K 1330
7/20/04
114


114
400PSI
K 1330
7/20/04
114

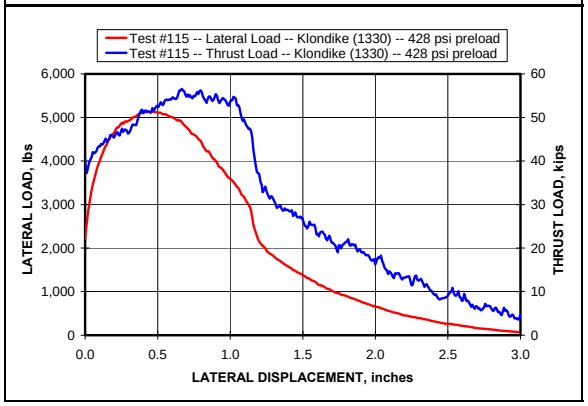
Test #115 -- Lateral Load -- Klondike (1330) -- 428 psi preload
Test #115 -- Thrust Load -- Klondike (1330) -- 428 psi preload
LATERAL LOAD, lbs
THRUST LOAD, kips
LATERAL DISPLACEMENT, inches

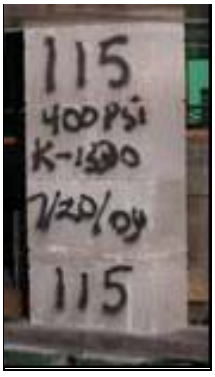
115
400PSI
K-1330
7/20/04
115


115
400PSI
K-1330
7/20/04
115

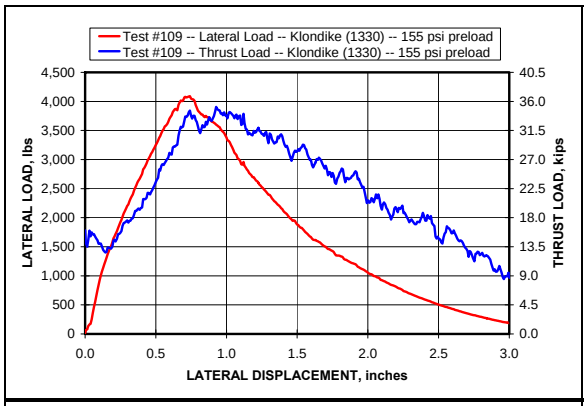
Test #109 -- Lateral Load -- Klondike (1330) -- 155 psi preload
Test #109 -- Thrust Load -- Klondike (1330) -- 155 psi preload
LATERAL LOAD, lbs
THRUST LOAD, kips
LATERAL DISPLACEMENT, inches

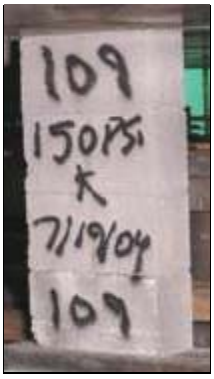
109
150PSI
K
7/19/04
109

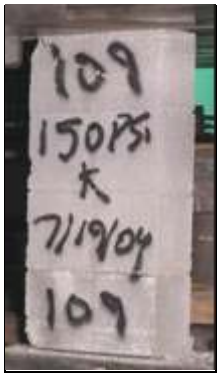
109
150PSI
K
7/19/04
109

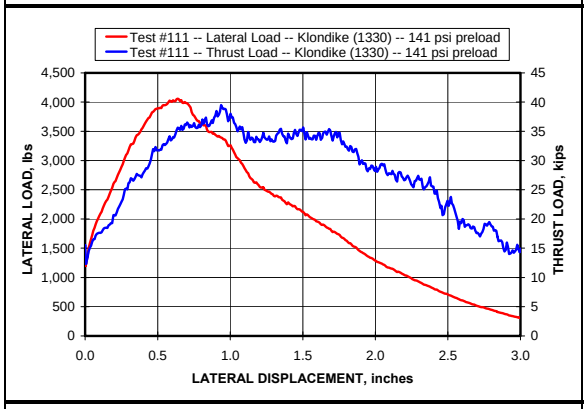
Test #111 -- Lateral Load -- Klondike (1330) -- 141 psi preload
Test #111 -- Thrust Load -- Klondike (1330) -- 141 psi preload
LATERAL LOAD, lbs
THRUST LOAD, kips
LATERAL DISPLACEMENT, inches


111
150PSI
K130
7/19/04
111


111
150PSI
K130
7/19/04
111

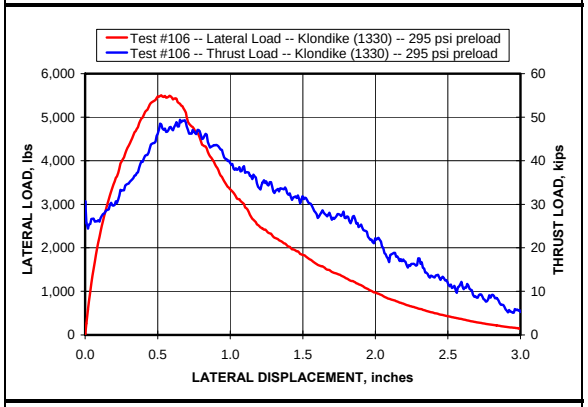
Test #106 -- Lateral Load -- Klondike (1330) -- 295 psi preload
Test #106 -- Thrust Load -- Klondike (1330) -- 295 psi preload
LATERAL LOAD, lbs
THRUST LOAD, kips
LATERAL DISPLACEMENT, inches

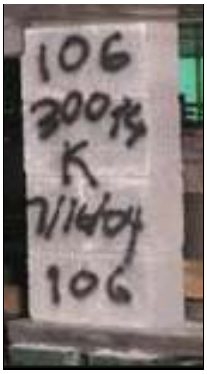
106
300PSI
K
7/16/04
106


106
300PSI
K
7/16/04
106

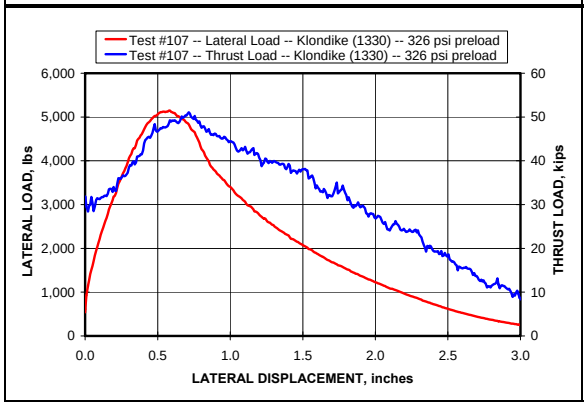
Test #107 -- Lateral Load -- Klondike (1330) -- 326 psi preload
Test #107 -- Thrust Load -- Klondike (1330) -- 326 psi preload
LATERAL LOAD, lbs
THRUST LOAD, kips
LATERAL DISPLACEMENT, inches


107
300PSI
7/17/04
K
107


107
300PSI
7/17/04
K
107

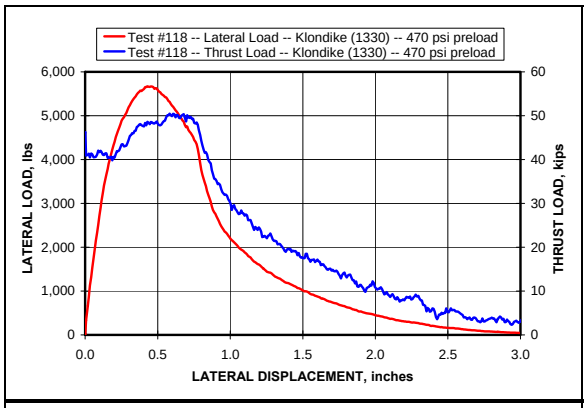
Test #118 -- Lateral Load -- Klondike (1330) -- 470 psi preload
Test #118 -- Thrust Load -- Klondike (1330) -- 470 psi preload
LATERAL LOAD, lbs
THRUST LOAD, kips
LATERAL DISPLACEMENT, inches


118
500
psi
7/20/04
118


500
psi
7/20/04
118

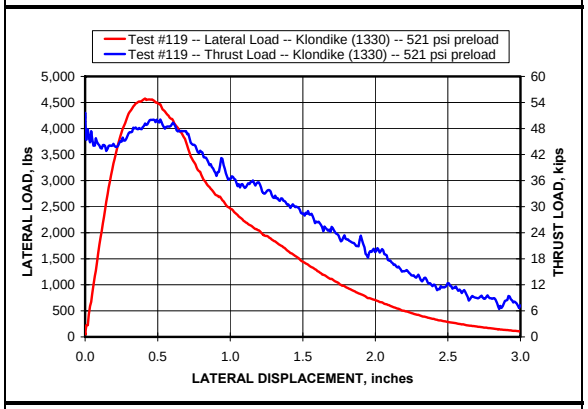
Test #119 -- Lateral Load -- Klondike (1330) -- 521 psi preload
Test #119 -- Thrust Load -- Klondike (1330) -- 521 psi preload
LATERAL LOAD, lbs
THRUST LOAD, kips
LATERAL DISPLACEMENT, inches


119
500psi
K1330
7/21/04
119


500psi
K1330
7/21/04
119

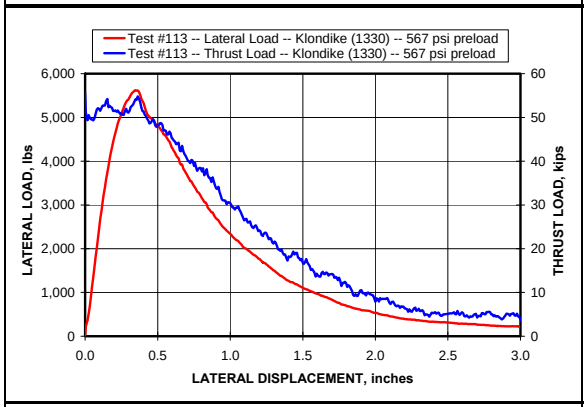
Test #113 -- Lateral Load -- Klondike (1330) -- 567 psi preload
Test #113 -- Thrust Load -- Klondike (1330) -- 567 psi preload
LATERAL LOAD, lbs
THRUST LOAD, kips
LATERAL DISPLACEMENT, inches


113
600psi
K1330
7/19/04
113


600psi
K1330
7/19/04
113

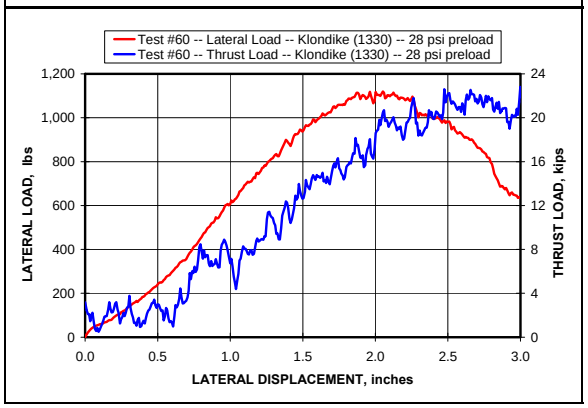
Test #60 -- Lateral Load -- Klondike (1330) -- 28 psi preload
Test #60 -- Thrust Load -- Klondike (1330) -- 28 psi preload
LATERAL LOAD, lbs
THRUST LOAD, kips
LATERAL DISPLACEMENT, inches


60
60


60
60

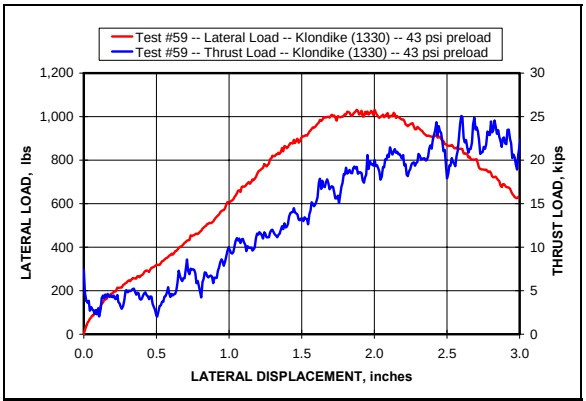

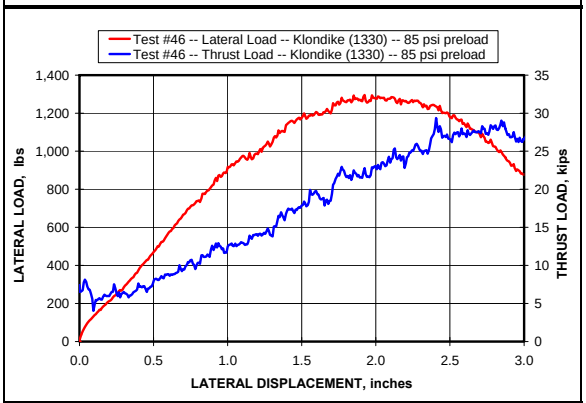

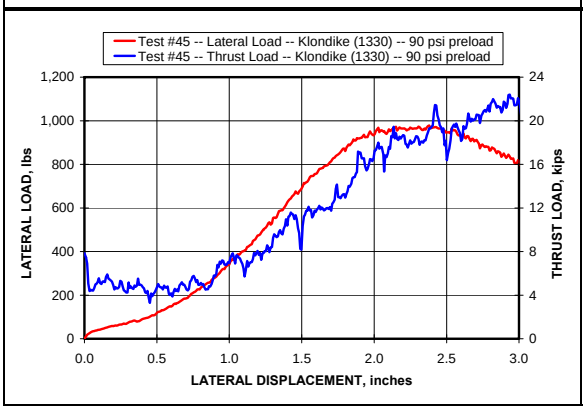

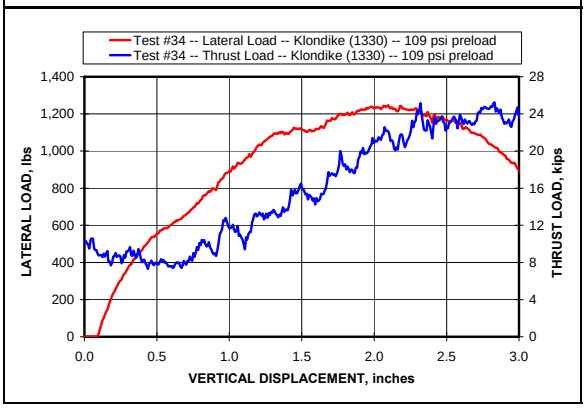

Photo Not Available

Photo Not Available

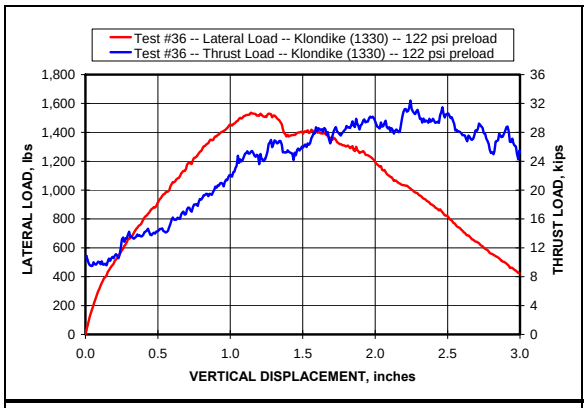

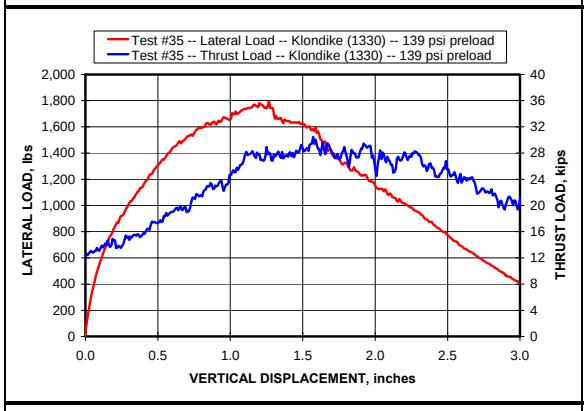

Photo Not Available

Photo Not Available

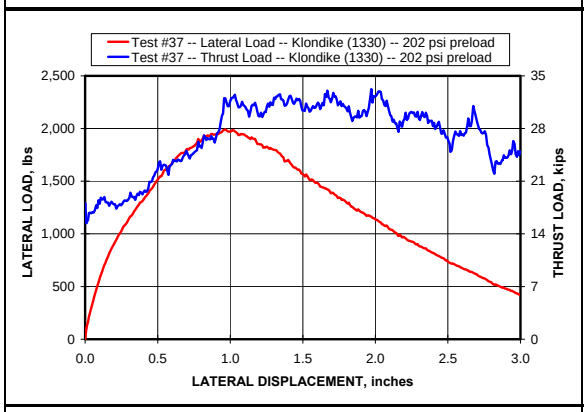

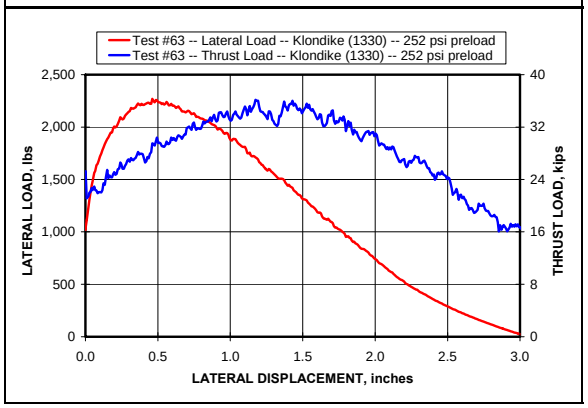

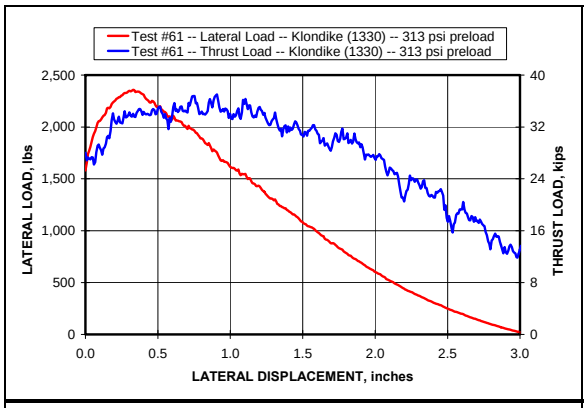
Test #61 -- Lateral Load -- Klondike (1330) -- 313 psi preload
Test #61 -- Thrust Load -- Klondike (1330) -- 313 psi preload
LATERAL LOAD, lbs
THRUST LOAD, kips
LATERAL DISPLACEMENT, inches

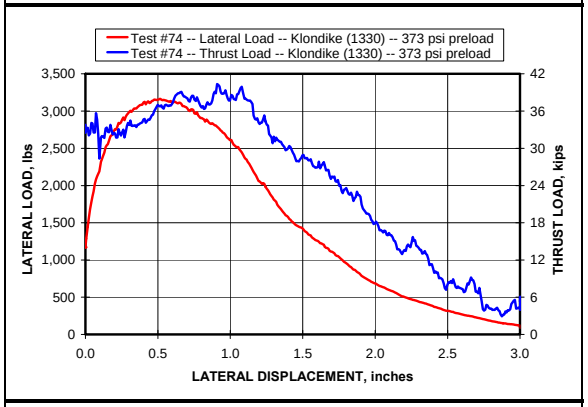
Test #74 -- Lateral Load -- Klondike (1330) -- 373 psi preload
Test #74 -- Thrust Load -- Klondike (1330) -- 373 psi preload
LATERAL LOAD, lbs
THRUST LOAD, kips
LATERAL DISPLACEMENT, inches

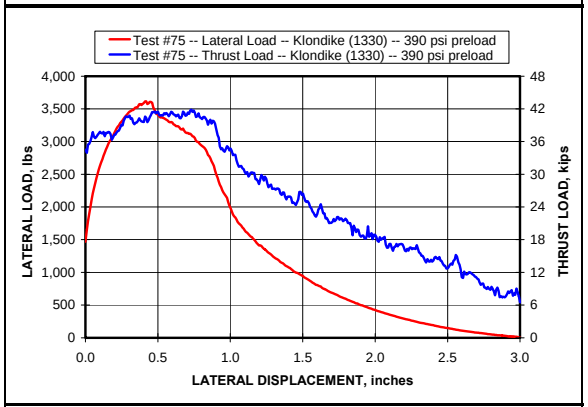
Test #75 -- Lateral Load -- Klondike (1330) -- 390 psi preload
Test #75 -- Thrust Load -- Klondike (1330) -- 390 psi preload
LATERAL LOAD, lbs
THRUST LOAD, kips
LATERAL DISPLACEMENT, inches

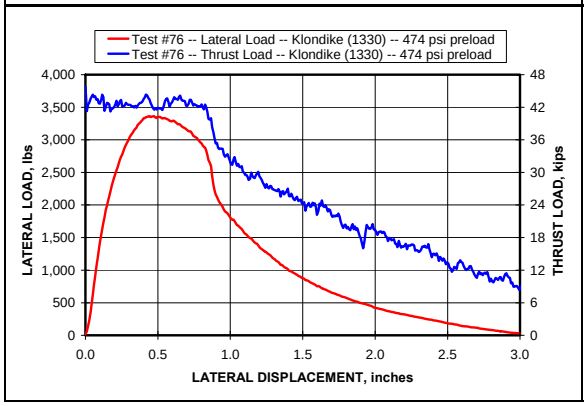
Test #76 -- Lateral Load -- Klondike (1330) -- 474 psi preload
Test #76 -- Thrust Load -- Klondike (1330) -- 474 psi preload
LATERAL LOAD, lbs
THRUST LOAD, kips
LATERAL DISPLACEMENT, inches

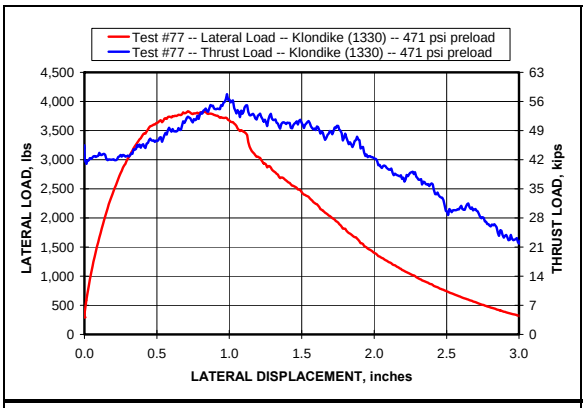
Test #77 -- Lateral Load -- Klondike (1330) -- 471 psi preload
Test #77 -- Thrust Load -- Klondike (1330) -- 471 psi preload
LATERAL LOAD, lbs
THRUST LOAD, kips
LATERAL DISPLACEMENT, inches

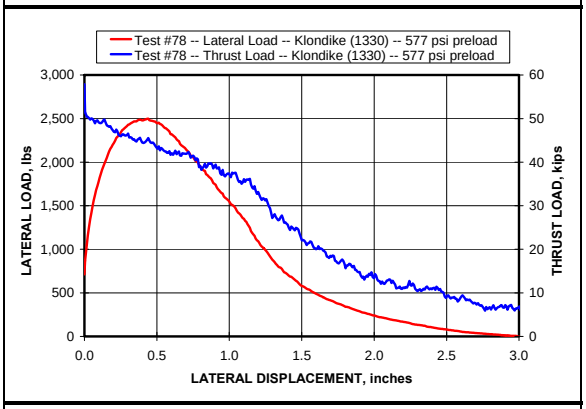
Test #78 -- Lateral Load -- Klondike (1330) -- 577 psi preload
Test #78 -- Thrust Load -- Klondike (1330) -- 577 psi preload
LATERAL LOAD, lbs
THRUST LOAD, kips
LATERAL DISPLACEMENT, inches

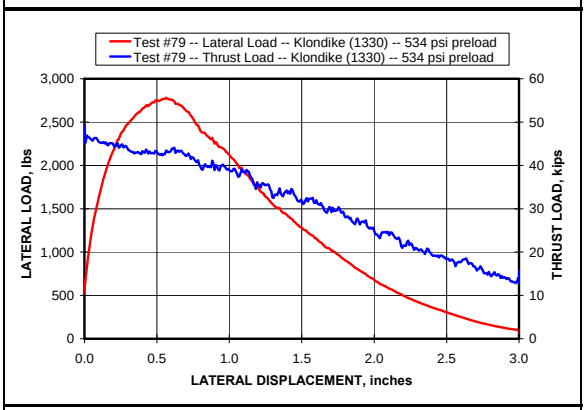
Test #79 -- Lateral Load -- Klondike (1330) -- 534 psi preload
Test #79 -- Thrust Load -- Klondike (1330) -- 534 psi preload
LATERAL LOAD, lbs
THRUST LOAD, kips
LATERAL DISPLACEMENT, inches

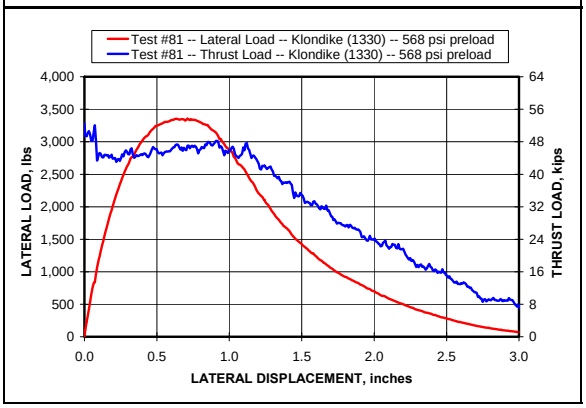
Test #81 -- Lateral Load -- Klondike (1330) -- 568 psi preload
Test #81 -- Thrust Load -- Klondike (1330) -- 568 psi preload
LATERAL LOAD, lbs
THRUST LOAD, kips
LATERAL DISPLACEMENT, inches

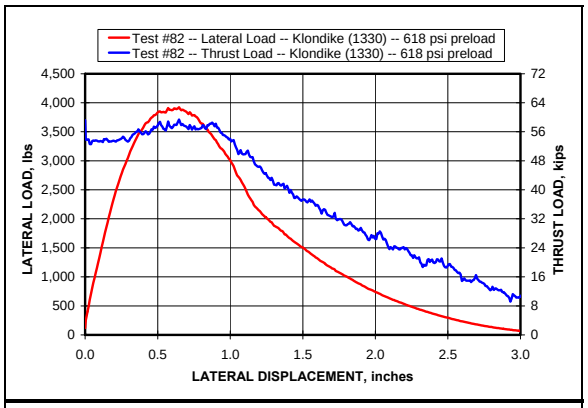

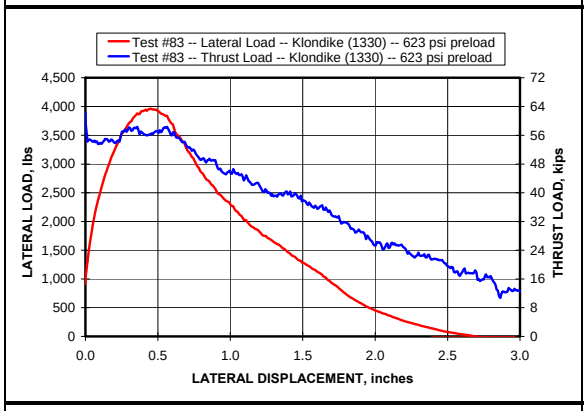

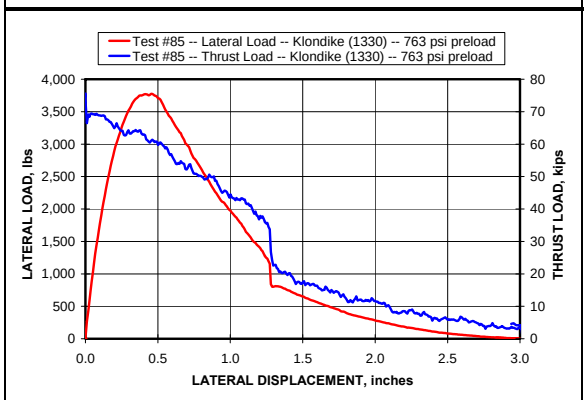

Photo Not Available

Photo Not Available

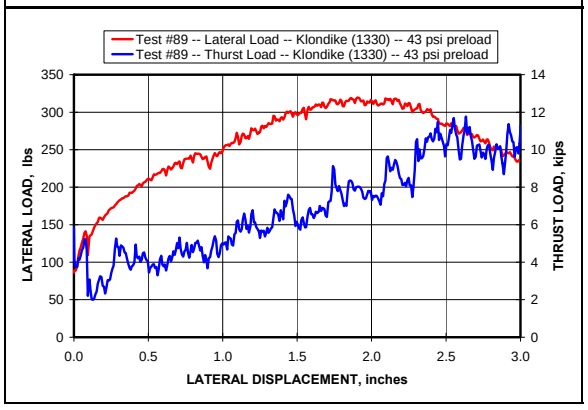

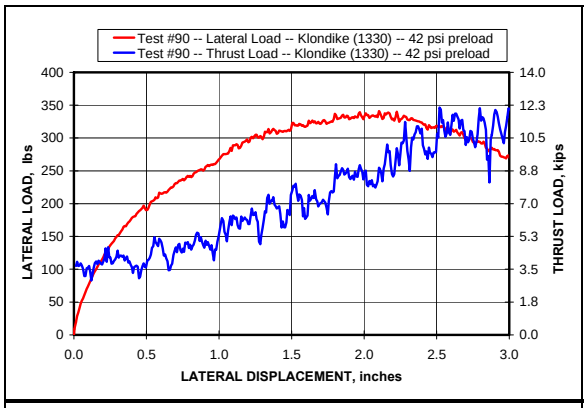
Test #90 -- Lateral Load -- Klondike (1330) -- 42 psi preload
Test #90 -- Thrust Load -- Klondike (1330) -- 42 psi preload
LATERAL LOAD, lbs
THRUST LOAD, kips
LATERAL DISPLACEMENT, inches

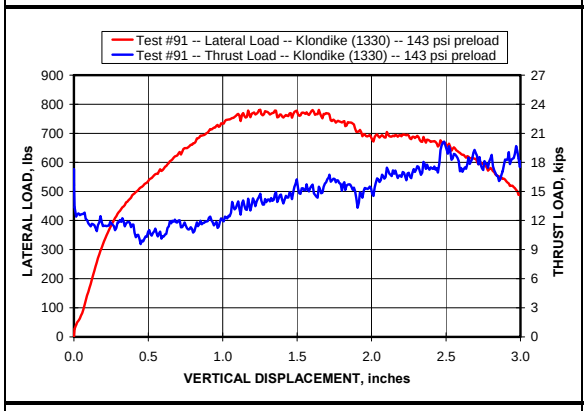
Test #91 -- Lateral Load -- Klondike (1330) -- 143 psi preload
Test #91 -- Thrust Load -- Klondike (1330) -- 143 psi preload
LATERAL LOAD, lbs
THRUST LOAD, kips
VERTICAL DISPLACEMENT, inches

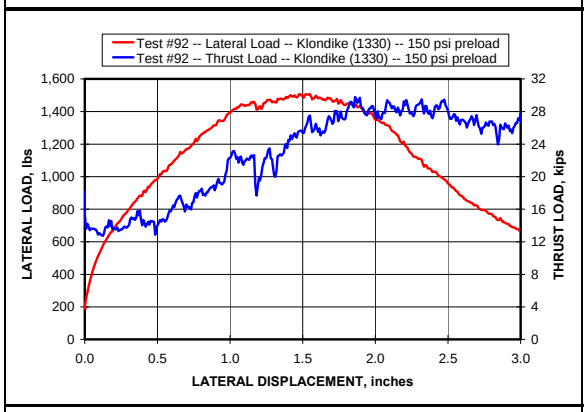
Test #92 -- Lateral Load -- Klondike (1330) -- 150 psi preload
Test #92 -- Thrust Load -- Klondike (1330) -- 150 psi preload
LATERAL LOAD, lbs
THRUST LOAD, kips
LATERAL DISPLACEMENT, inches

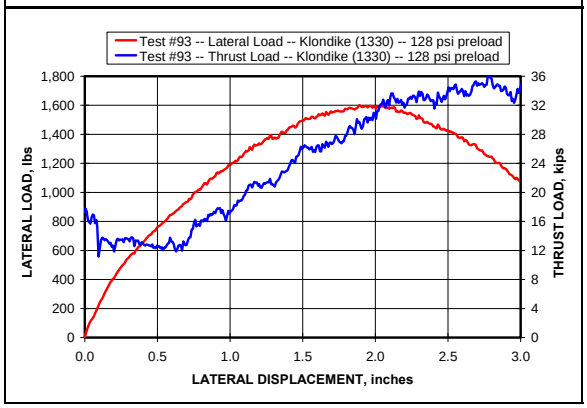
Test #93 -- Lateral Load -- Klondike (1330) -- 128 psi preload
Test #93 -- Thrust Load -- Klondike (1330) -- 128 psi preload
LATERAL LOAD, lbs
THRUST LOAD, kips
LATERAL DISPLACEMENT, inches


93
7/12/04
150 PSI
K
1330
93


93
7/12/04
150 PSI
K
1330
93

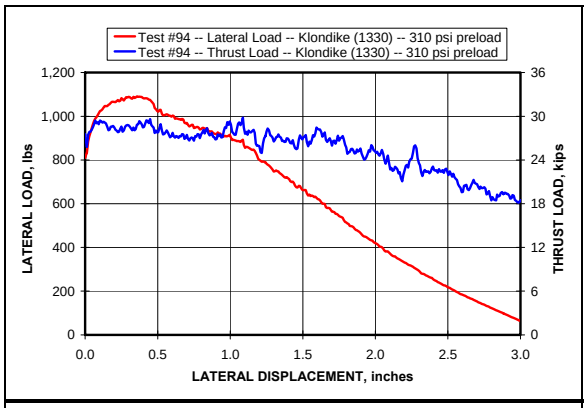
Test #94 -- Lateral Load -- Klondike (1330) -- 310 psi preload
Test #94 -- Thrust Load -- Klondike (1330) -- 310 psi preload
LATERAL LOAD, lbs
THRUST LOAD, kips
LATERAL DISPLACEMENT, inches


94
K
1330
94


94
K
1330
94

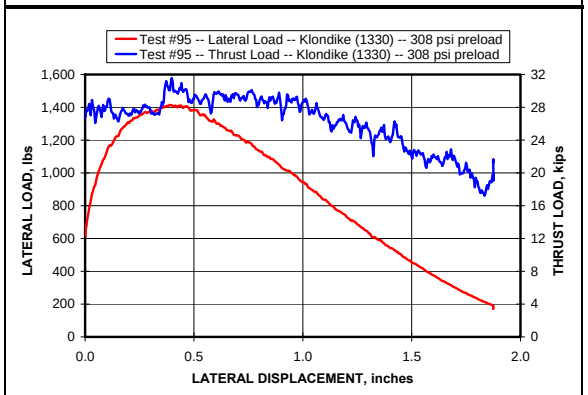
Test #95 -- Lateral Load -- Klondike (1330) -- 308 psi preload
Test #95 -- Thrust Load -- Klondike (1330) -- 308 psi preload
LATERAL LOAD, lbs
THRUST LOAD, kips
LATERAL DISPLACEMENT, inches


95
K
1330
95


95
K
1330
95

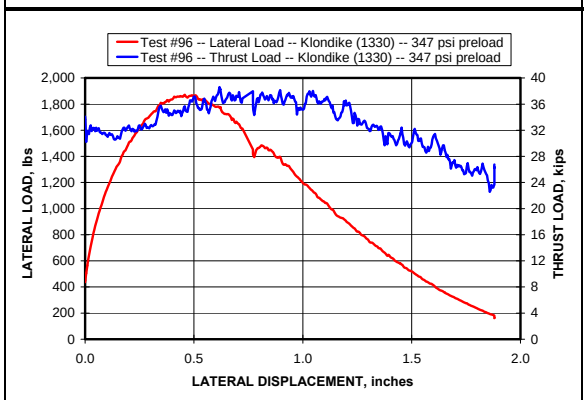
Test #96 -- Lateral Load -- Klondike (1330) -- 347 psi preload
Test #96 -- Thrust Load -- Klondike (1330) -- 347 psi preload
LATERAL LOAD, lbs
THRUST LOAD, kips
LATERAL DISPLACEMENT, inches


96
K
1330
96


96
K
1330
96

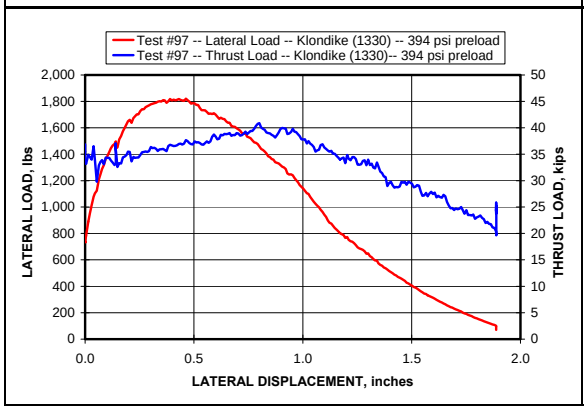
Test #97 -- Lateral Load -- Klondike (1330) -- 394 psi preload
Test #97 -- Thrust Load -- Klondike (1330)-- 394 psi preload
LATERAL LOAD, lbs
THRUST LOAD, kips
LATERAL DISPLACEMENT, inches


97
K
1330
97


97
K
1330
97

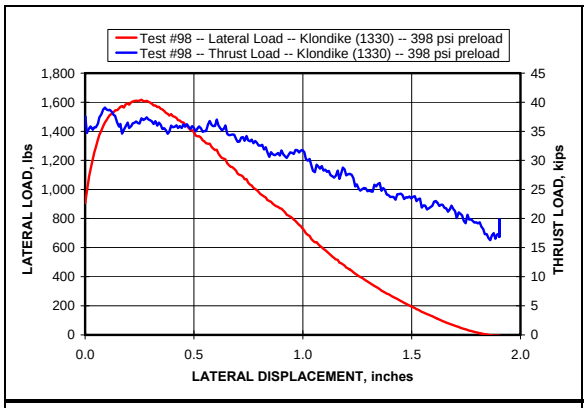
Test #98 -- Lateral Load -- Klondike (1330) -- 398 psi preload
Test #98 -- Thrust Load -- Klondike (1330) -- 398 psi preload
LATERAL LOAD, lbs
THRUST LOAD, kips
LATERAL DISPLACEMENT, inches


98


98

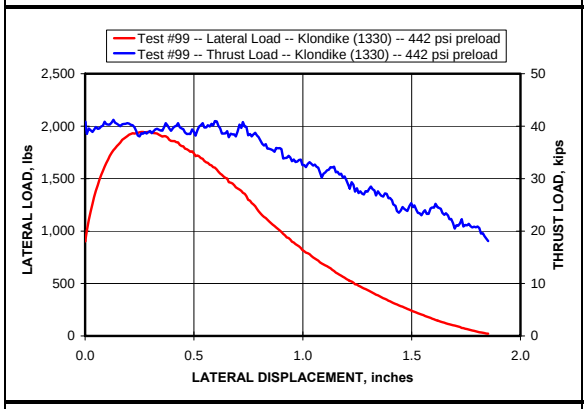
Test #99 -- Lateral Load -- Klondike (1330) -- 442 psi preload
Test #99 -- Thrust Load -- Klondike (1330) -- 442 psi preload
LATERAL LOAD, lbs
THRUST LOAD, kips
LATERAL DISPLACEMENT, inches


99


99

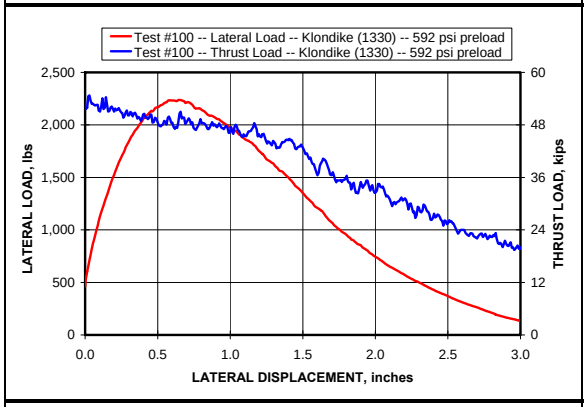
Test #100 -- Lateral Load -- Klondike (1330) -- 592 psi preload
Test #100 -- Thrust Load -- Klondike (1330) -- 592 psi preload
LATERAL LOAD, lbs
THRUST LOAD, kips
LATERAL DISPLACEMENT, inches

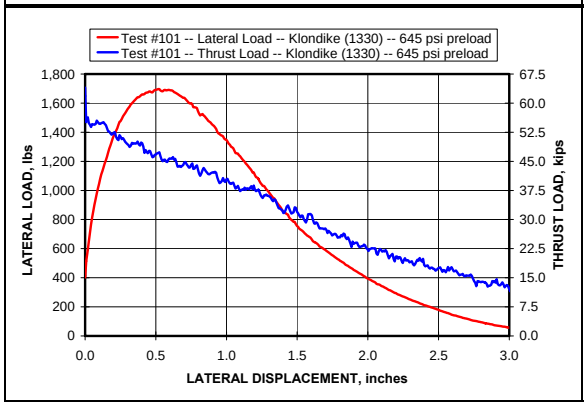
Test #101 -- Lateral Load -- Klondike (1330) -- 645 psi preload
Test #101 -- Thrust Load -- Klondike (1330) -- 645 psi preload
LATERAL LOAD, lbs
THRUST LOAD, kips
LATERAL DISPLACEMENT, inches

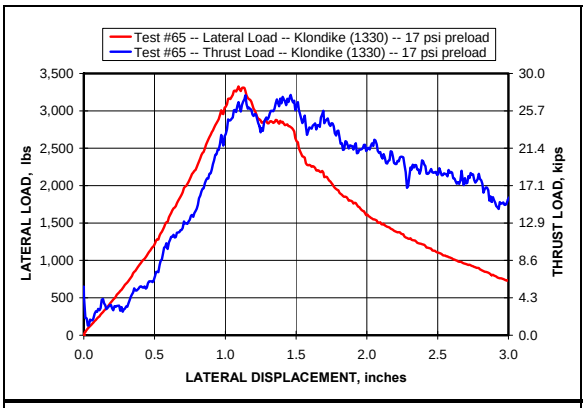
Test #65 -- Lateral Load -- Klondike (1330) -- 17 psi preload
Test #65 -- Thrust Load -- Klondike (1330) -- 17 psi preload
LATERAL LOAD, lbs
THRUST LOAD, kips
LATERAL DISPLACEMENT, inches

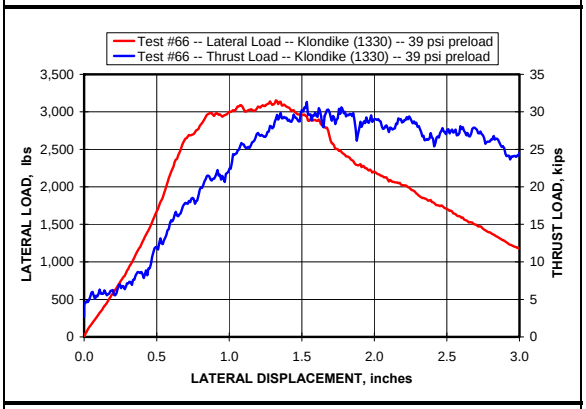
Test #66 -- Lateral Load -- Klondike (1330) -- 39 psi preload
Test #66 -- Thrust Load -- Klondike (1330) -- 39 psi preload
LATERAL LOAD, lbs
THRUST LOAD, kips
LATERAL DISPLACEMENT, inches

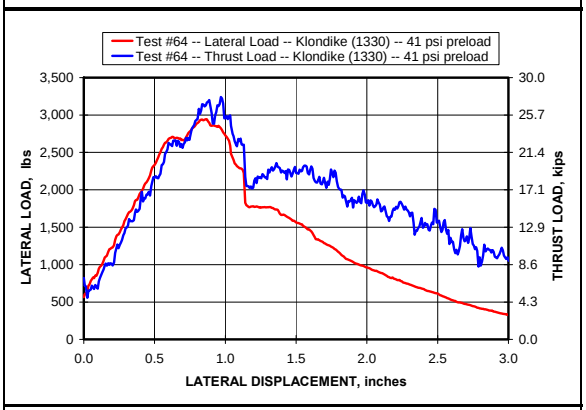
Test #64 -- Lateral Load -- Klondike (1330) -- 41 psi preload
Test #64 -- Thrust Load -- Klondike (1330) -- 41 psi preload
LATERAL LOAD, lbs
THRUST LOAD, kips
LATERAL DISPLACEMENT, inches

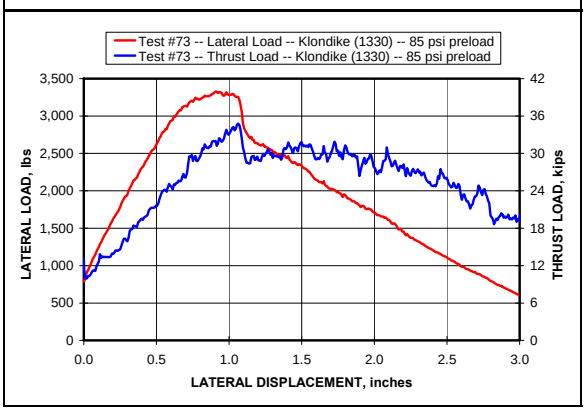
Test #73 -- Lateral Load -- Klondike (1330) -- 85 psi preload
Test #73 -- Thrust Load -- Klondike (1330) -- 85 psi preload
LATERAL LOAD, lbs
THRUST LOAD, kips
LATERAL DISPLACEMENT, inches

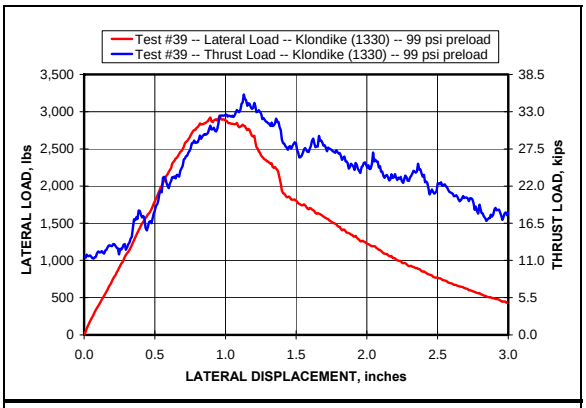
Test #39 -- Lateral Load -- Klondike (1330) -- 99 psi preload
Test #39 -- Thrust Load -- Klondike (1330) -- 99 psi preload
LATERAL LOAD, lbs
THRUST LOAD, kips
LATERAL DISPLACEMENT, inches

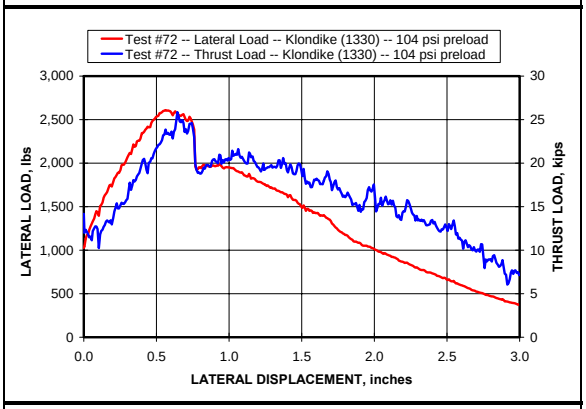
Test #72 -- Lateral Load -- Klondike (1330) -- 104 psi preload
Test #72 -- Thrust Load -- Klondike (1330) -- 104 psi preload
LATERAL LOAD, lbs
THRUST LOAD, kips
LATERAL DISPLACEMENT, inches

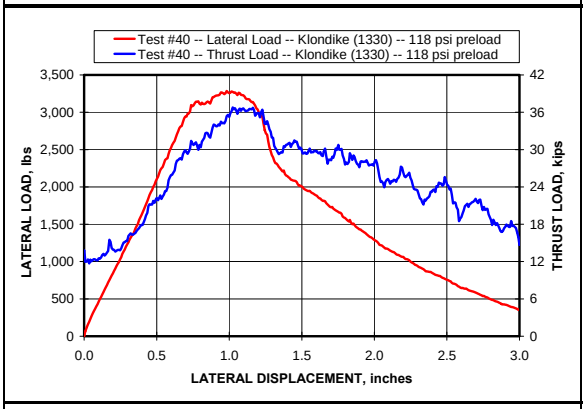
Test #40 -- Lateral Load -- Klondike (1330) -- 118 psi preload
Test #40 -- Thrust Load -- Klondike (1330) -- 118 psi preload
LATERAL LOAD, lbs
THRUST LOAD, kips
LATERAL DISPLACEMENT, inches

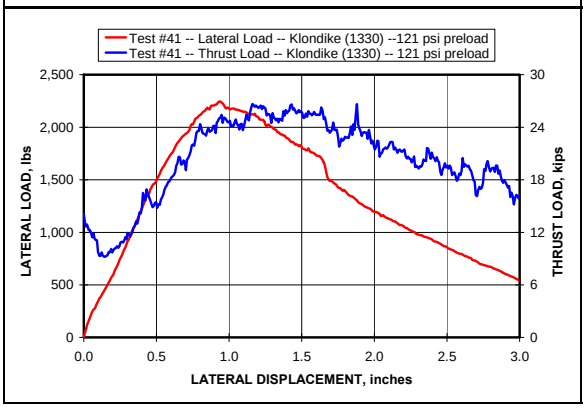
Test #41 -- Lateral Load -- Klondike (1330) --121 psi preload
Test #41 -- Thrust Load -- Klondike (1330) -- 121 psi preload
LATERAL LOAD, lbs
THRUST LOAD, kips
LATERAL DISPLACEMENT, inches

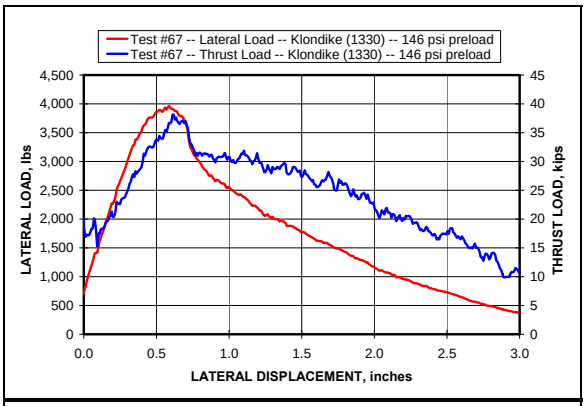
Test #67 -- Lateral Load -- Klondike (1330) -- 146 psi preload
Test #67 -- Thrust Load -- Klondike (1330) -- 146 psi preload
LATERAL LOAD, lbs
THRUST LOAD, kips
LATERAL DISPLACEMENT, inches

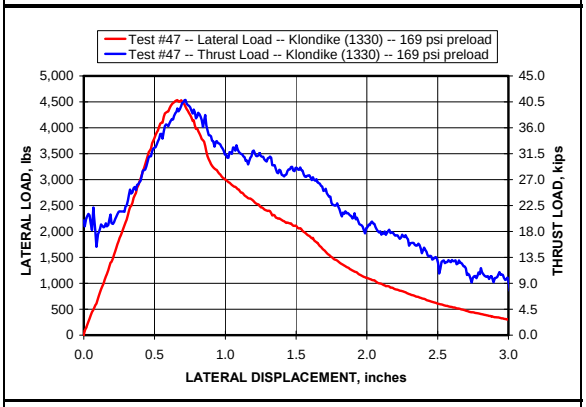
Test #47 -- Lateral Load -- Klondike (1330) -- 169 psi preload
Test #47 -- Thrust Load -- Klondike (1330) -- 169 psi preload
LATERAL LOAD, lbs
THRUST LOAD, kips
LATERAL DISPLACEMENT, inches

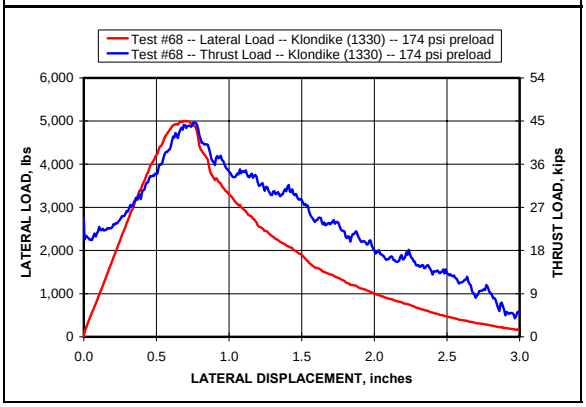
Test #68 -- Lateral Load -- Klondike (1330) -- 174 psi preload
Test #68 -- Thrust Load -- Klondike (1330) -- 174 psi preload
LATERAL LOAD, lbs
THRUST LOAD, kips
LATERAL DISPLACEMENT, inches

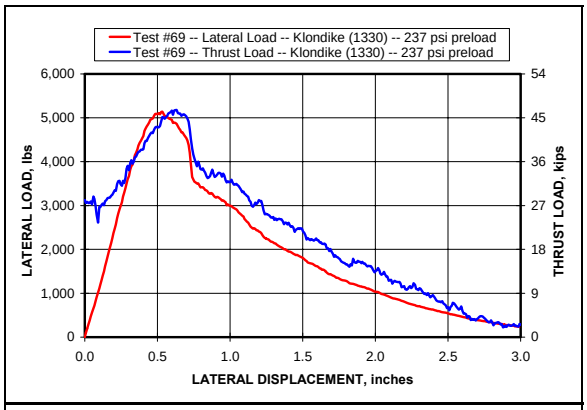
Test #69 -- Lateral Load -- Klondike (1330) -- 237 psi preload
Test #69 -- Thrust Load -- Klondike (1330) -- 237 psi preload
LATERAL LOAD, lbs
THRUST LOAD, kips
LATERAL DISPLACEMENT, inches

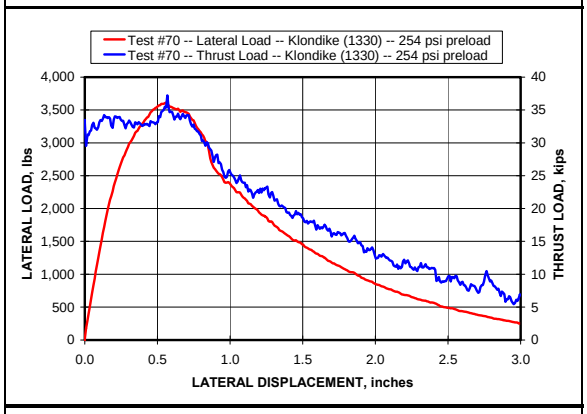
Test #70 -- Lateral Load -- Klondike (1330) -- 254 psi preload
Test #70 -- Thrust Load -- Klondike (1330) -- 254 psi preload
LATERAL LOAD, lbs
THRUST LOAD, kips
LATERAL DISPLACEMENT, inches

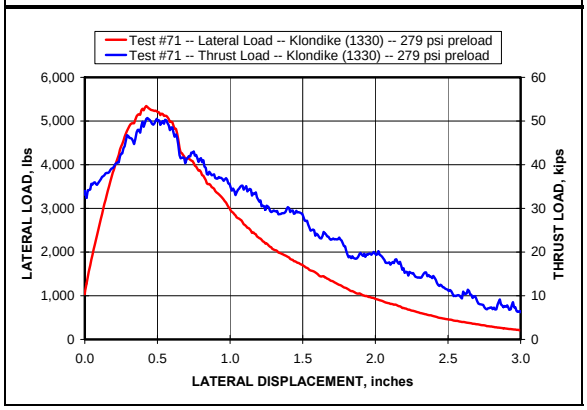
Test #71 -- Lateral Load -- Klondike (1330) -- 279 psi preload
Test #71 -- Thrust Load -- Klondike (1330) -- 279 psi preload
LATERAL LOAD, lbs
THRUST LOAD, kips
LATERAL DISPLACEMENT, inches

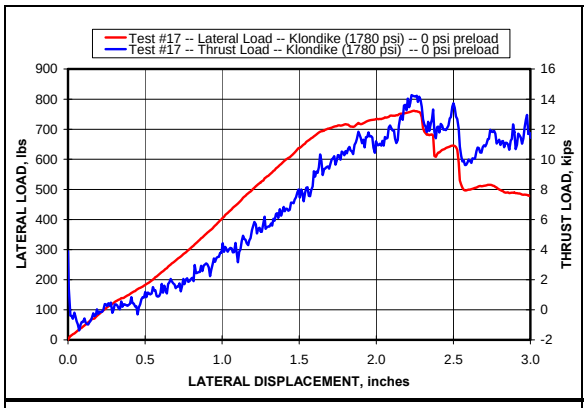

Photo Not Available

Photo Not Available

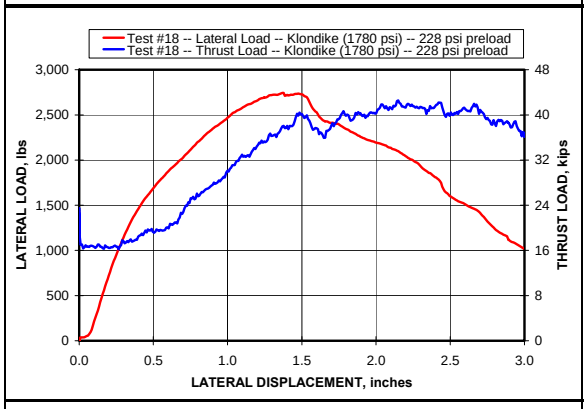

Photo Not Available

Photo Not Available

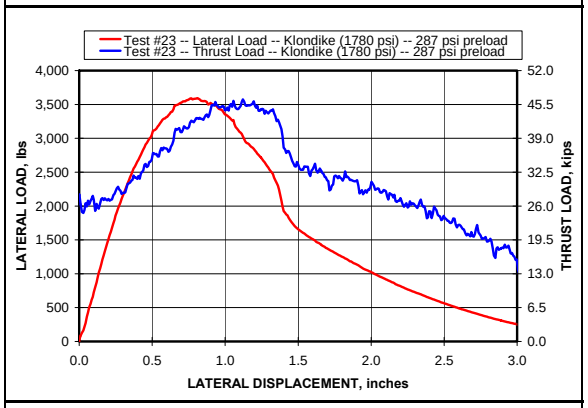

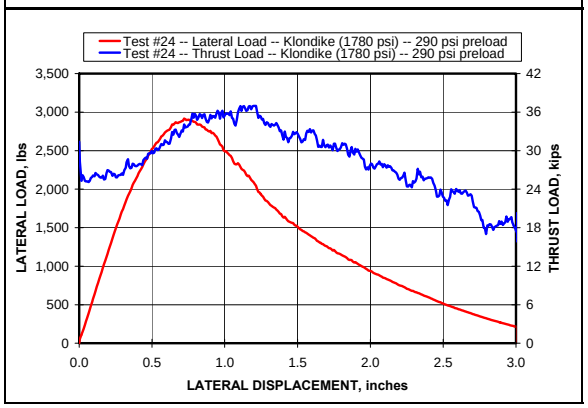

Photo Not Available

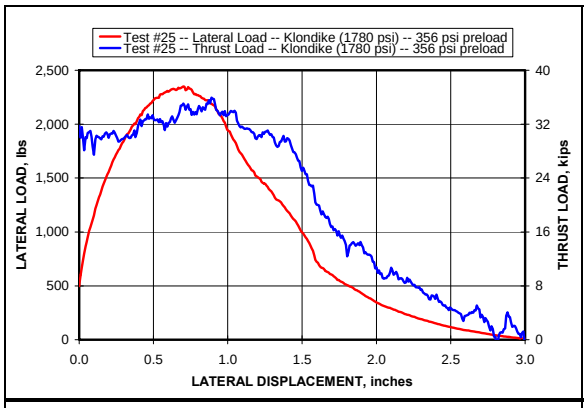

Photo Not Available

Photo Not Available

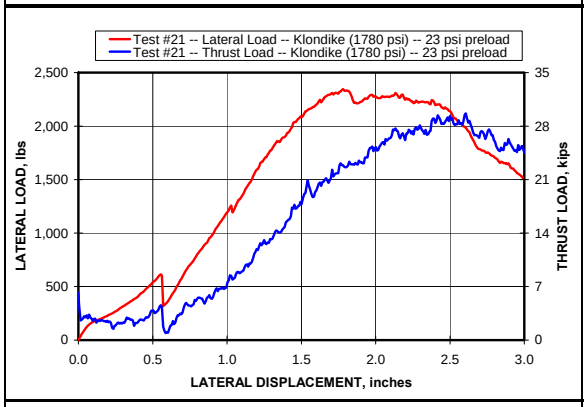

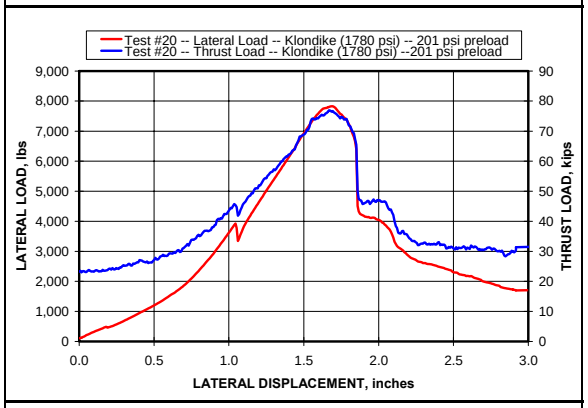

Photo Not Available

Photo Not Available

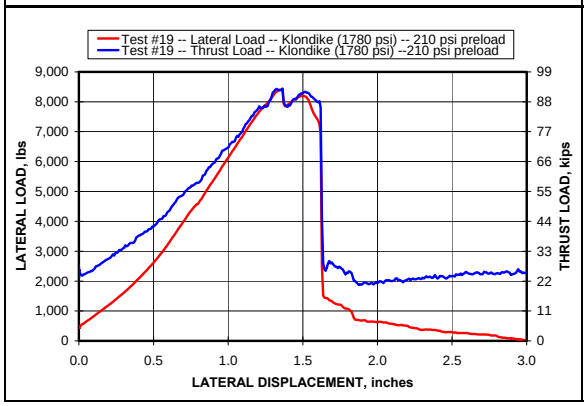

Photo Not Available

Photo Not Available

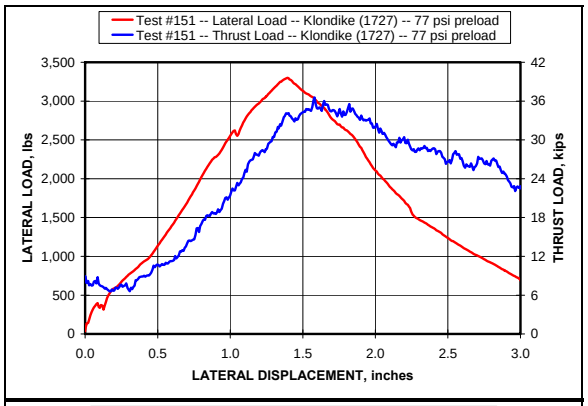
Test #151 -- Lateral Load -- Klondike (1727) -- 77 psi preload
Test #151 -- Thrust Load -- Klondike (1727) -- 77 psi preload
LATERAL LOAD, lbs
THRUST LOAD, kips
LATERAL DISPLACEMENT, inches


151
220kN
50kip
9/17/09
151


151
220kN
50kip
9/17/09
151

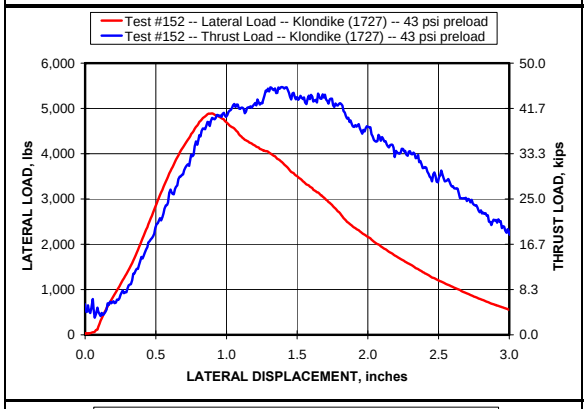
Test #152 -- Lateral Load -- Klondike (1727) -- 43 psi preload
Test #152 -- Thrust Load -- Klondike (1727) -- 43 psi preload
LATERAL LOAD, lbs
THRUST LOAD, kips
LATERAL DISPLACEMENT, inches


152
220kN
9/17/09
152

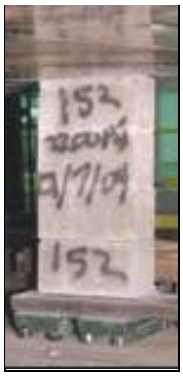
152
220kN
9/17/09
152

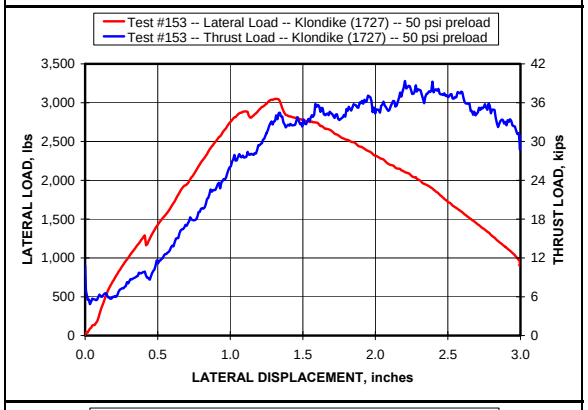
Test #153 -- Lateral Load -- Klondike (1727) -- 50 psi preload
Test #153 -- Thrust Load -- Klondike (1727) -- 50 psi preload
LATERAL LOAD, lbs
THRUST LOAD, kips
LATERAL DISPLACEMENT, inches


153
220kN
50kip
7/9/09
153


153
220kN
50kip
7/9/09
153

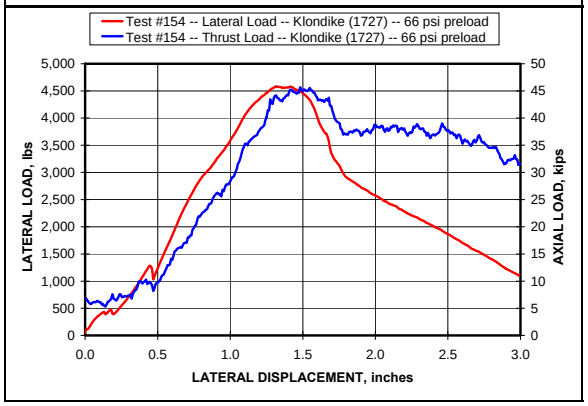
Test #154 -- Lateral Load -- Klondike (1727) -- 66 psi preload
Test #154 -- Thrust Load -- Klondike (1727) -- 66 psi preload
LATERAL LOAD, lbs
AXIAL LOAD, kips
LATERAL DISPLACEMENT, inches

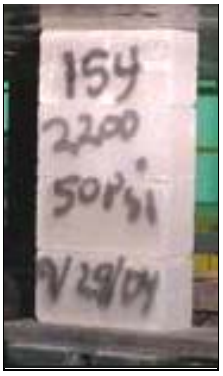
154
2200
50kip
9/29/09

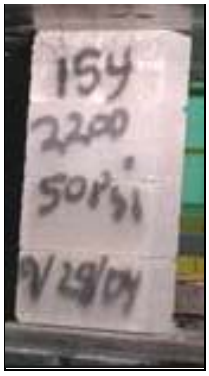
154
2200
50kip
9/29/09

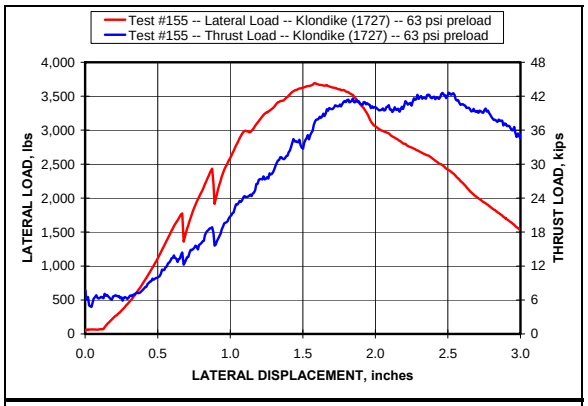
Test #155 -- Lateral Load -- Klondike (1727) -- 63 psi preload
Test #155 -- Thrust Load -- Klondike (1727) -- 63 psi preload
LATERAL LOAD, lbs
THRUST LOAD, kips
LATERAL DISPLACEMENT, inches

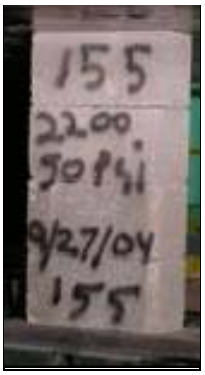
155
2200
50 psi
9/27/04
155


155
2200
50 psi
9/27/04
155

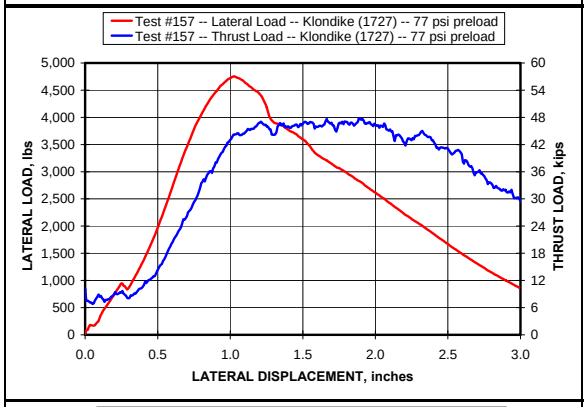
Test #157 -- Lateral Load -- Klondike (1727) -- 77 psi preload
Test #157 -- Thrust Load -- Klondike (1727) -- 77 psi preload
LATERAL LOAD, lbs
THRUST LOAD, kips
LATERAL DISPLACEMENT, inches


157
2200
50 psi
9/30/04
157


157
2200
50 psi
9/30/04
157

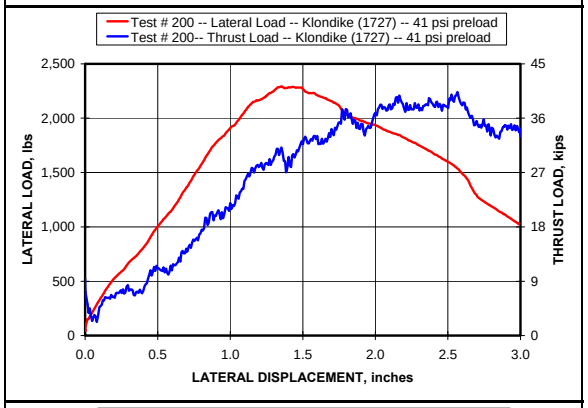
Test # 200 -- Lateral Load -- Klondike (1727) -- 41 psi preload
Test # 200-- Thrust Load -- Klondike (1727) -- 41 psi preload
LATERAL LOAD, lbs
THRUST LOAD, kips
LATERAL DISPLACEMENT, inches


200
1727
50psi
200


200
1727
50psi
200

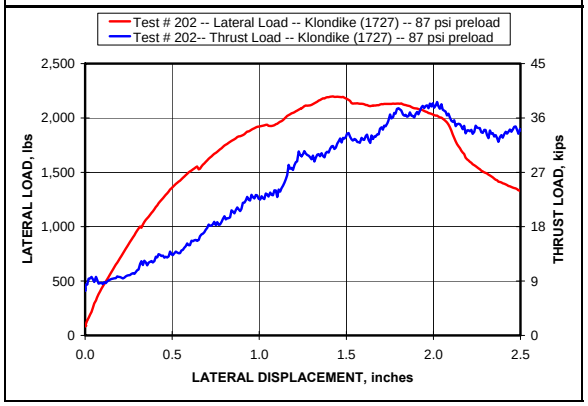
Test # 202 -- Lateral Load -- Klondike (1727) -- 87 psi preload
Test # 202-- Thrust Load -- Klondike (1727) -- 87 psi preload
LATERAL LOAD, lbs
THRUST LOAD, kips
LATERAL DISPLACEMENT, inches


202
1727
50psi
202


202
1727
50psi
202

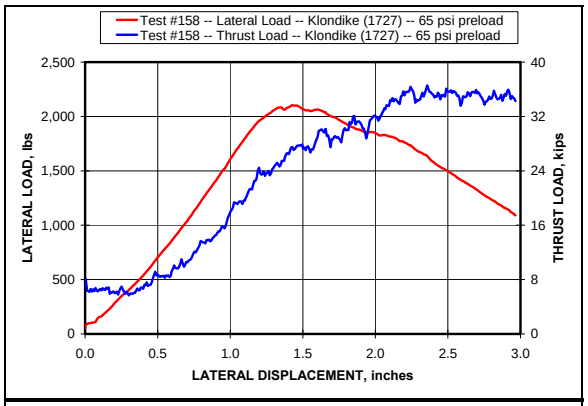
Test #158 -- Lateral Load -- Klondike (1727) -- 65 psi preload
Test #158 -- Thrust Load -- Klondike (1727) -- 65 psi preload
LATERAL LOAD, lbs
THRUST LOAD, kips
LATERAL DISPLACEMENT, inches

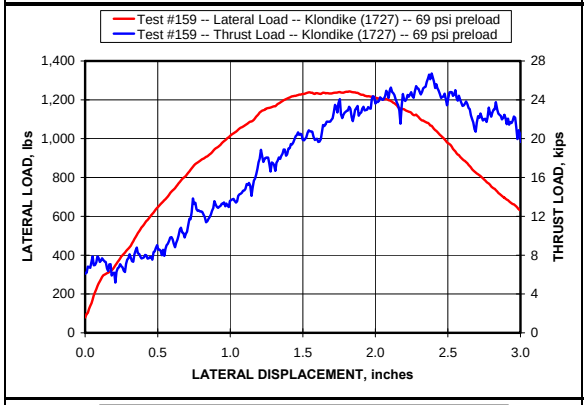
Test #159 -- Lateral Load -- Klondike (1727) -- 69 psi preload
Test #159 -- Thrust Load -- Klondike (1727) -- 69 psi preload
LATERAL LOAD, lbs
THRUST LOAD, kips
LATERAL DISPLACEMENT, inches

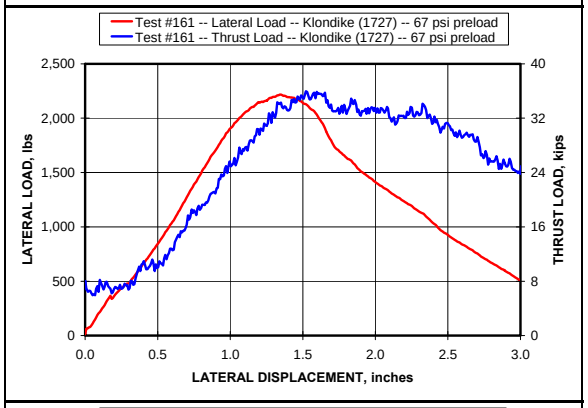
Test #161 -- Lateral Load -- Klondike (1727) -- 67 psi preload
Test #161 -- Thrust Load -- Klondike (1727) -- 67 psi preload
LATERAL LOAD, lbs
THRUST LOAD, kips
LATERAL DISPLACEMENT, inches

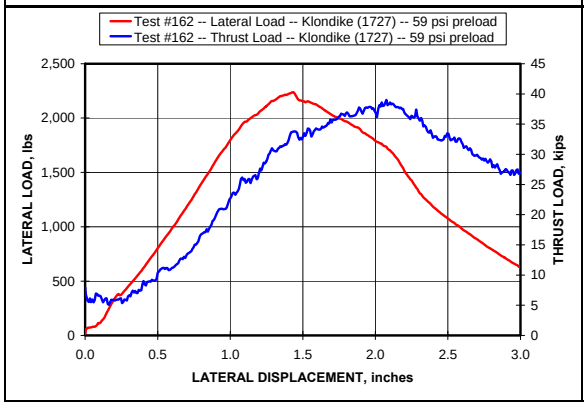
Test #162 -- Lateral Load -- Klondike (1727) -- 59 psi preload
Test #162 -- Thrust Load -- Klondike (1727) -- 59 psi preload
LATERAL LOAD, lbs
THRUST LOAD, kips
LATERAL DISPLACEMENT, inches

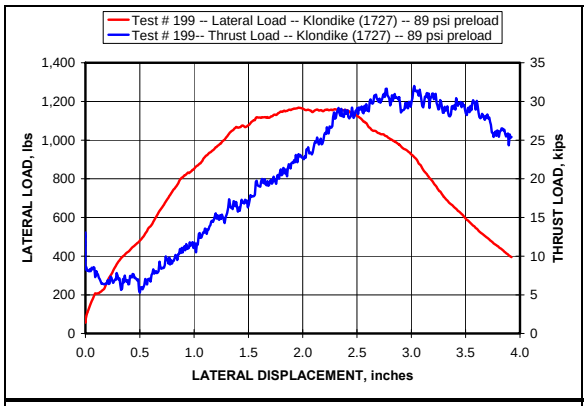
Test # 199 -- Lateral Load -- Klondike (1727) -- 89 psi preload
Test # 199-- Thrust Load -- Klondike (1727) -- 89 psi preload
LATERAL LOAD, lbs
THRUST LOAD, kips
LATERAL DISPLACEMENT, inches

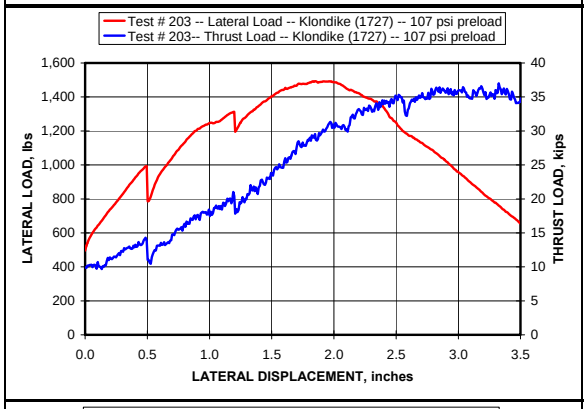
Test # 203 -- Lateral Load -- Klondike (1727) -- 107 psi preload
Test # 203-- Thrust Load -- Klondike (1727) -- 107 psi preload
LATERAL LOAD, lbs
THRUST LOAD, kips
LATERAL DISPLACEMENT, inches

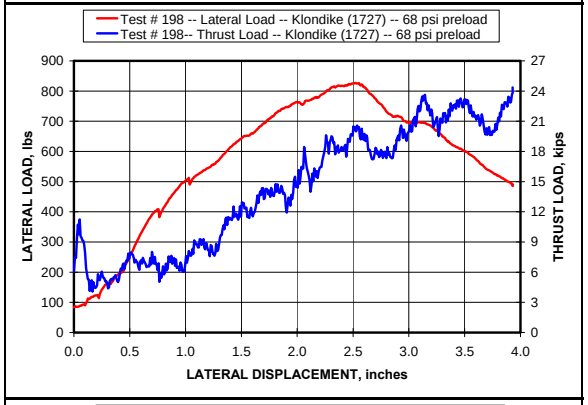
Test # 198 -- Lateral Load -- Klondike (1727) -- 68 psi preload
Test # 198-- Thrust Load -- Klondike (1727) -- 68 psi preload
LATERAL LOAD, lbs
THRUST LOAD, kips
LATERAL DISPLACEMENT, inches

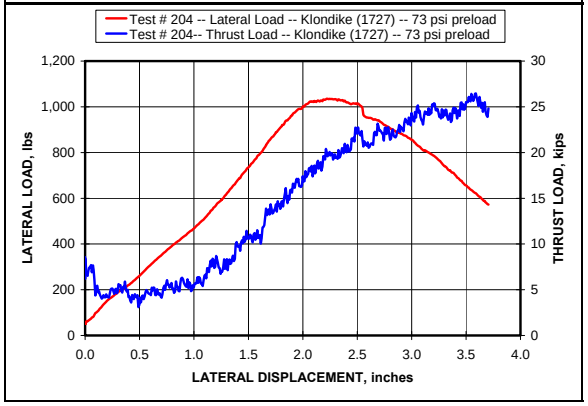
Test # 204 -- Lateral Load -- Klondike (1727) -- 73 psi preload
Test # 204-- Thrust Load -- Klondike (1727) -- 73 psi preload
LATERAL LOAD, lbs
THRUST LOAD, kips
LATERAL DISPLACEMENT, inches

PEERLESS BACKSAVER

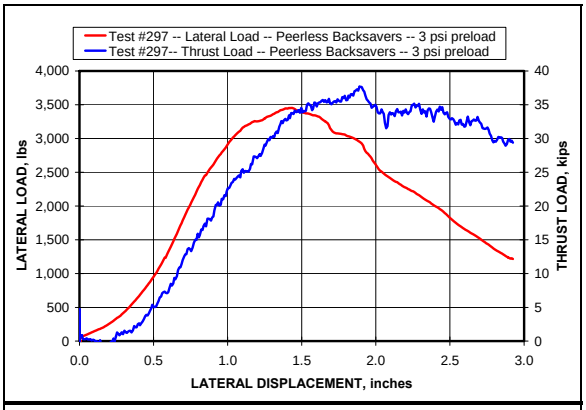

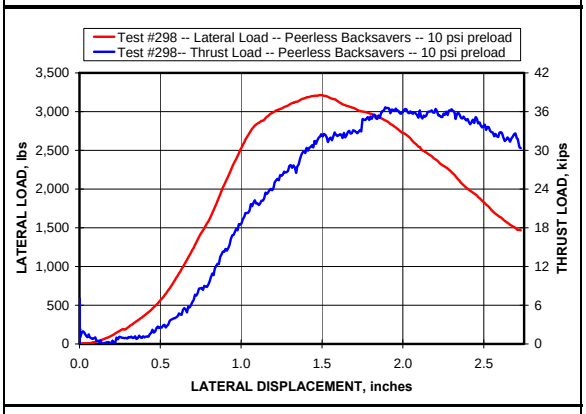

Photo Not Available

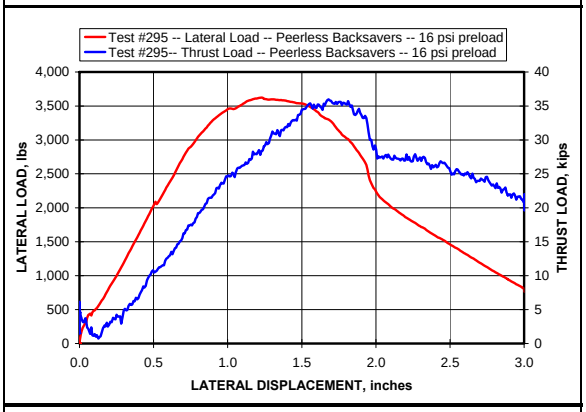

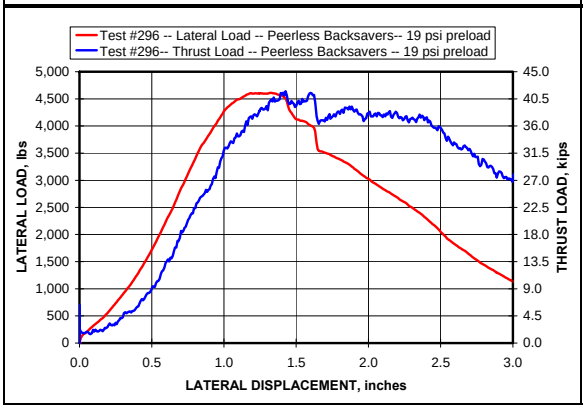

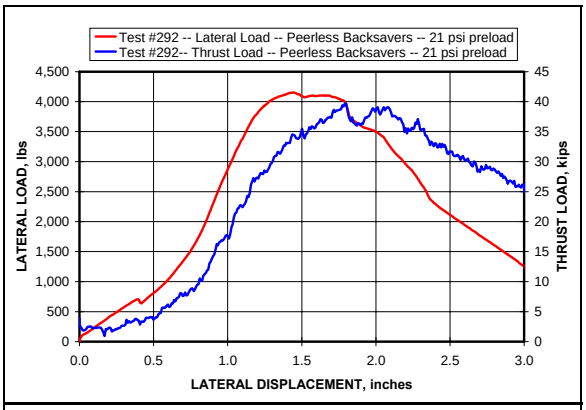
Test #292 -- Lateral Load -- Peerless Backsavers -- 21 psi preload
Test #292-- Thrust Load -- Peerless Backsavers -- 21 psi preload
LATERAL LOAD, lbs
THRUST LOAD, kips
LATERAL DISPLACEMENT, inches

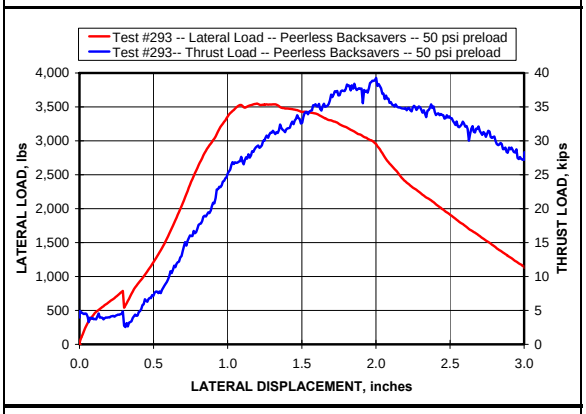
Test #293 -- Lateral Load -- Peerless Backsavers -- 50 psi preload
Test #293-- Thrust Load -- Peerless Backsavers -- 50 psi preload
LATERAL LOAD, lbs
THRUST LOAD, kips
LATERAL DISPLACEMENT, inches

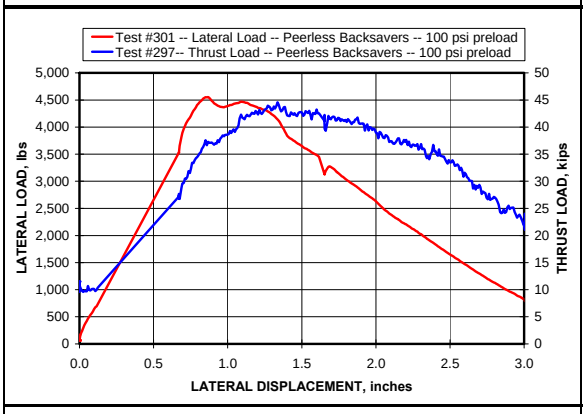
Test #301 -- Lateral Load -- Peerless Backsavers -- 100 psi preload
Test #297-- Thrust Load -- Peerless Backsavers -- 100 psi preload
LATERAL LOAD, lbs
THRUST LOAD, kips
LATERAL DISPLACEMENT, inches

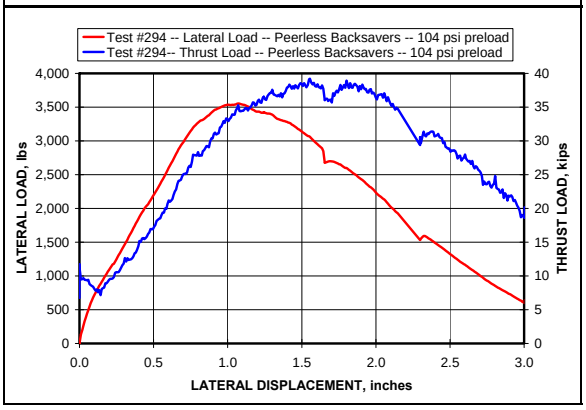
Test #294 -- Lateral Load -- Peerless Backsavers -- 104 psi preload
Test #294-- Thrust Load -- Peerless Backsavers -- 104 psi preload
LATERAL LOAD, lbs
THRUST LOAD, kips
LATERAL DISPLACEMENT, inches

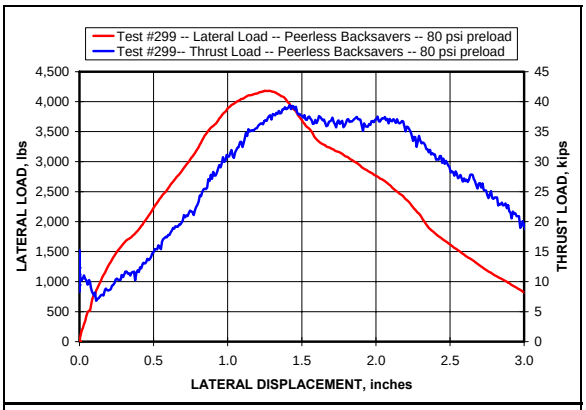
Test #299 -- Lateral Load -- Peerless Backsavers -- 80 psi preload
Test #299-- Thrust Load -- Peerless Backsavers -- 80 psi preload
LATERAL LOAD, lbs
THRUST LOAD, kips
LATERAL DISPLACEMENT, inches

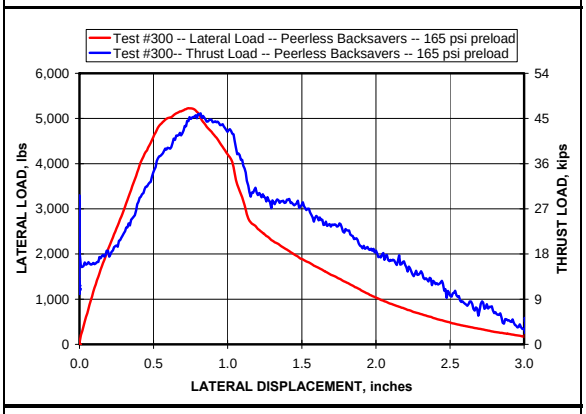
Test #300 -- Lateral Load -- Peerless Backsavers -- 165 psi preload
Test #300-- Thrust Load -- Peerless Backsavers -- 165 psi preload
LATERAL LOAD, lbs
THRUST LOAD, kips
LATERAL DISPLACEMENT, inches

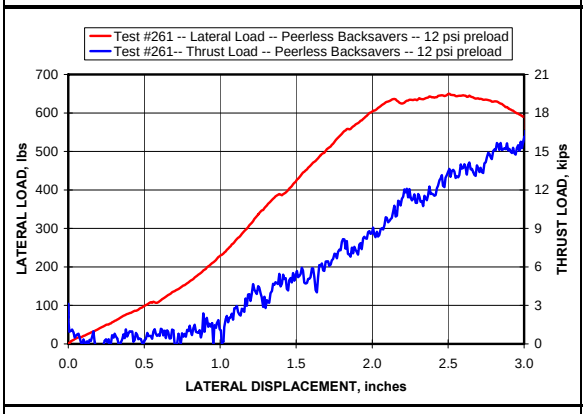
Test #261 -- Lateral Load -- Peerless Backsavers -- 12 psi preload
Test #261-- Thrust Load -- Peerless Backsavers -- 12 psi preload
LATERAL LOAD, lbs
THRUST LOAD, kips
LATERAL DISPLACEMENT, inches

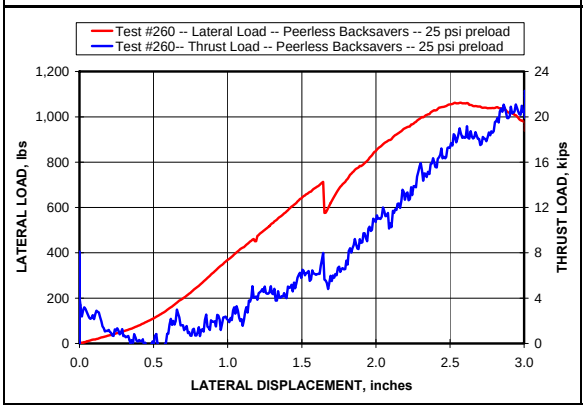
Test #260 -- Lateral Load -- Peerless Backsavers -- 25 psi preload
Test #260-- Thrust Load -- Peerless Backsavers -- 25 psi preload
LATERAL LOAD, lbs
THRUST LOAD, kips
LATERAL DISPLACEMENT, inches

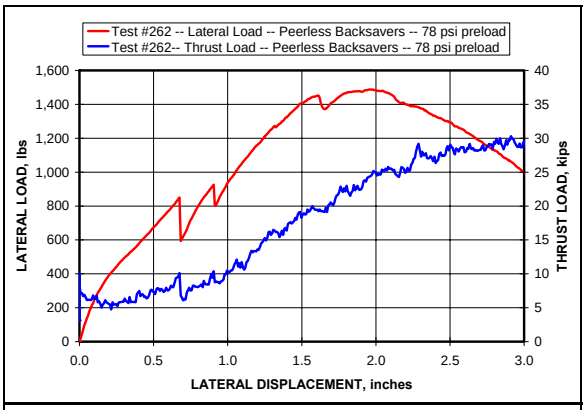
Test #262 -- Lateral Load -- Peerless Backsavers -- 78 psi preload
Test #262-- Thrust Load -- Peerless Backsavers -- 78 psi preload
LATERAL LOAD, lbs
THRUST LOAD, kips
LATERAL DISPLACEMENT, inches

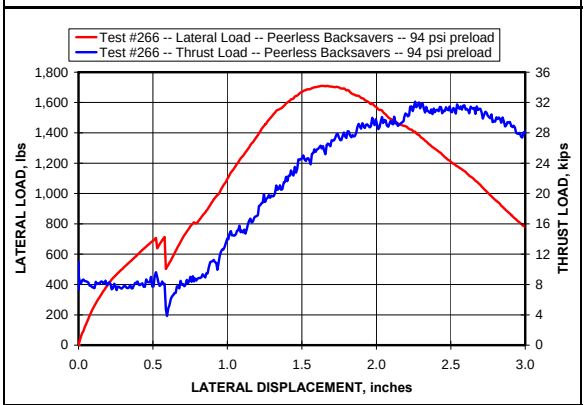
Test #266 -- Lateral Load -- Peerless Backsavers -- 94 psi preload
Test #266 -- Thrust Load -- Peerless Backsavers -- 94 psi preload
LATERAL LOAD, lbs
THRUST LOAD, kips
LATERAL DISPLACEMENT, inches

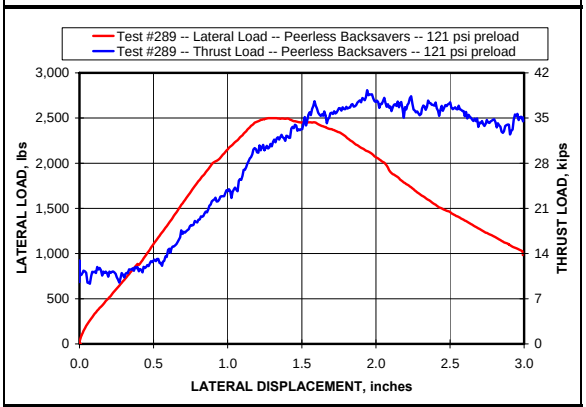
Test #289 -- Lateral Load -- Peerless Backsavers -- 121 psi preload
Test #289 -- Thrust Load -- Peerless Backsavers -- 121 psi preload
LATERAL LOAD, lbs
THRUST LOAD, kips
LATERAL DISPLACEMENT, inches

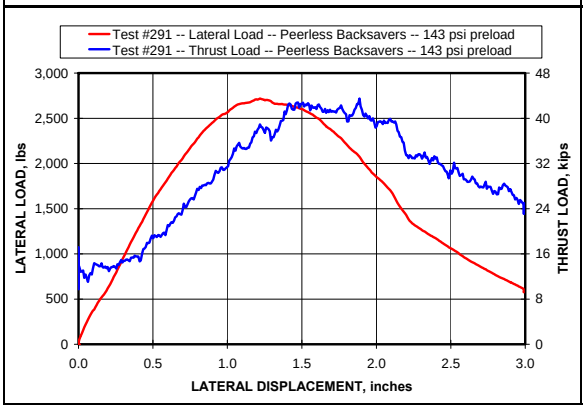
Test #291 -- Lateral Load -- Peerless Backsavers -- 143 psi preload
Test #291 -- Thrust Load -- Peerless Backsavers -- 143 psi preload
LATERAL LOAD, lbs
THRUST LOAD, kips
LATERAL DISPLACEMENT, inches

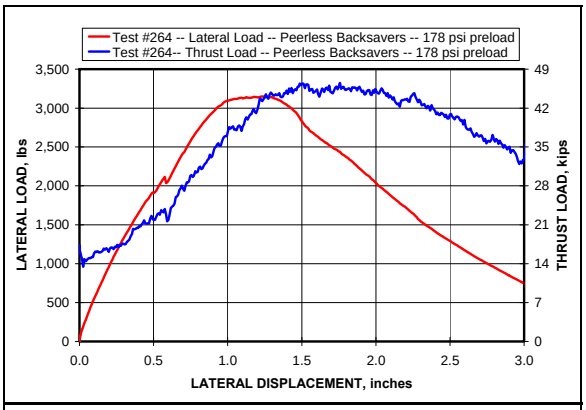
Test #264 -- Lateral Load -- Peerless Backsavers -- 178 psi preload
Test #264-- Thrust Load -- Peerless Backsavers -- 178 psi preload
LATERAL LOAD, lbs
THRUST LOAD, kips
LATERAL DISPLACEMENT, inches

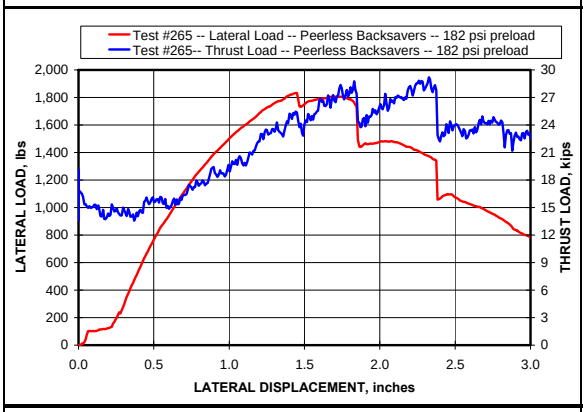
Test #265 -- Lateral Load -- Peerless Backsavers -- 182 psi preload
Test #265-- Thrust Load -- Peerless Backsavers -- 182 psi preload
LATERAL LOAD, lbs
THRUST LOAD, kips
LATERAL DISPLACEMENT, inches

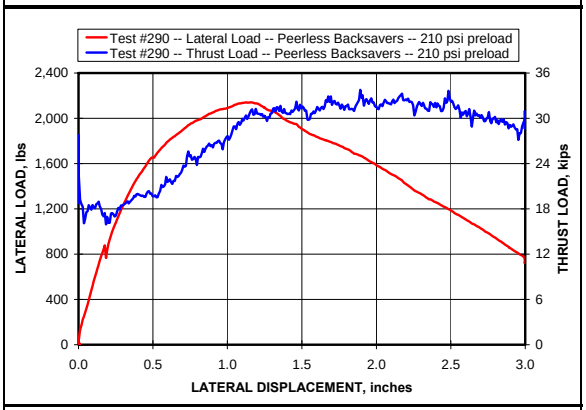
Test #290 -- Lateral Load -- Peerless Backsavers -- 210 psi preload
Test #290 -- Thrust Load -- Peerless Backsavers -- 210 psi preload
LATERAL LOAD, lbs
THRUST LOAD, kips
LATERAL DISPLACEMENT, inches

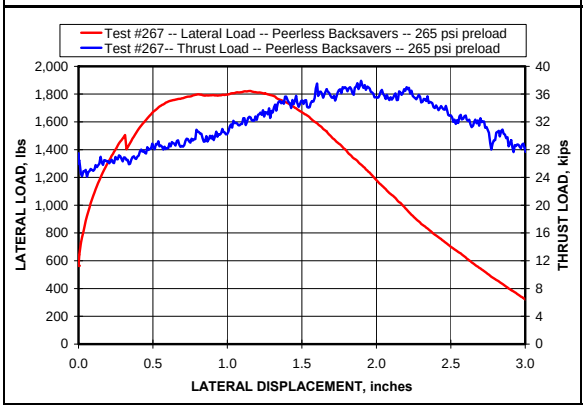
Test #267 -- Lateral Load -- Peerless Backsavers -- 265 psi preload
Test #267-- Thrust Load -- Peerless Backsavers -- 265 psi preload
LATERAL LOAD, lbs
THRUST LOAD, kips
LATERAL DISPLACEMENT, inches

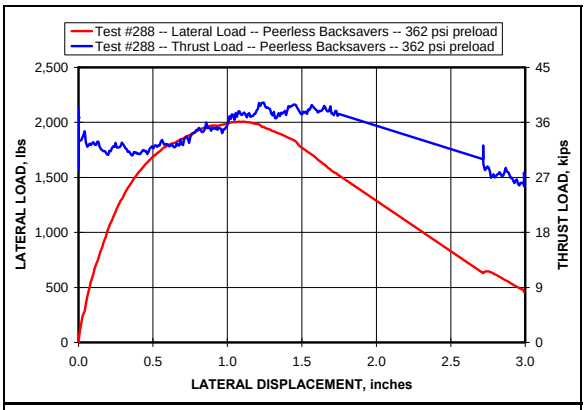
Test #288 -- Lateral Load -- Peerless Backsavers -- 362 psi preload
Test #288 -- Thrust Load -- Peerless Backsavers -- 362 psi preload
LATERAL LOAD, lbs
THRUST LOAD, kips
LATERAL DISPLACEMENT, inches

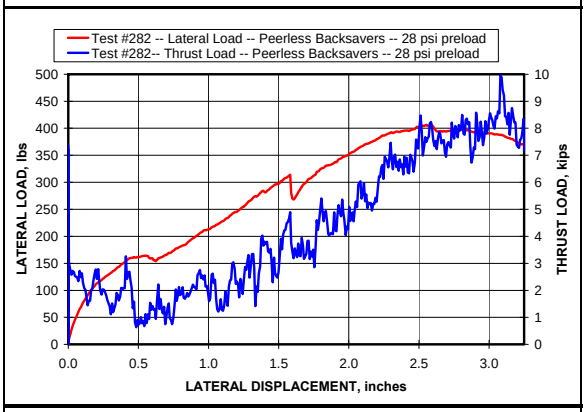
Test #282 -- Lateral Load -- Peerless Backsavers -- 28 psi preload
Test #282-- Thrust Load -- Peerless Backsavers -- 28 psi preload
LATERAL LOAD, lbs
THRUST LOAD, kips
LATERAL DISPLACEMENT, inches

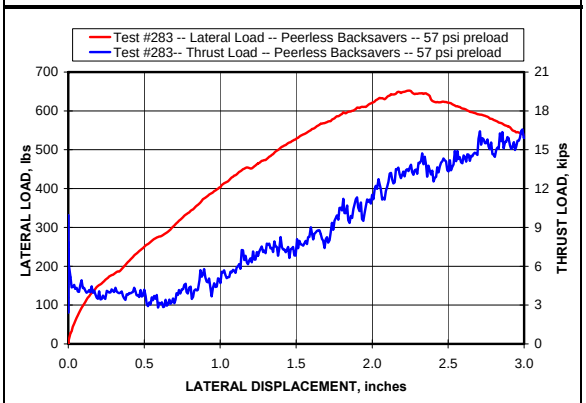
Test #283 -- Lateral Load -- Peerless Backsavers -- 57 psi preload
Test #283-- Thrust Load -- Peerless Backsavers -- 57 psi preload
LATERAL LOAD, lbs
THRUST LOAD, kips
LATERAL DISPLACEMENT, inches

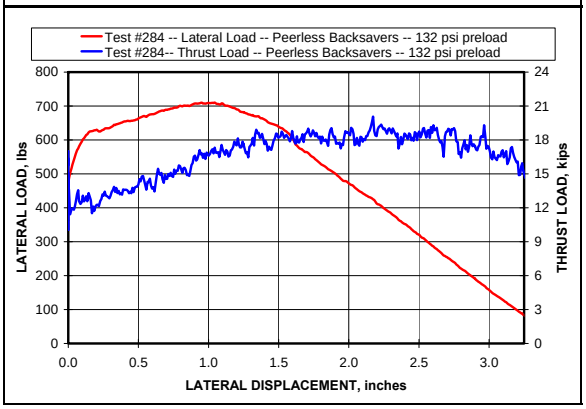
Test #284 -- Lateral Load -- Peerless Backsavers -- 132 psi preload
Test #284-- Thrust Load -- Peerless Backsavers -- 132 psi preload
LATERAL LOAD, lbs
THRUST LOAD, kips
LATERAL DISPLACEMENT, inches

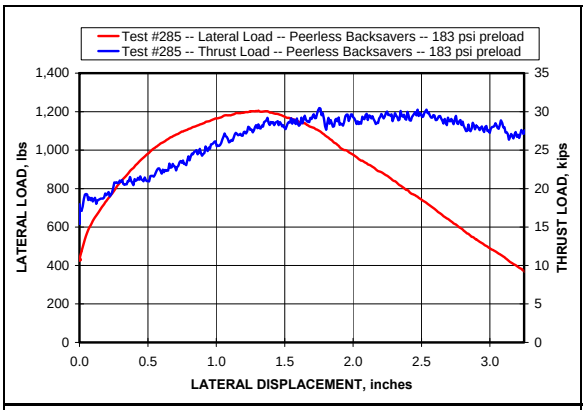
Test #285 -- Lateral Load -- Peerless Backsavers -- 183 psi preload
Test #285 -- Thrust Load -- Peerless Backsavers -- 183 psi preload
LATERAL LOAD, lbs
THRUST LOAD, kips
LATERAL DISPLACEMENT, inches

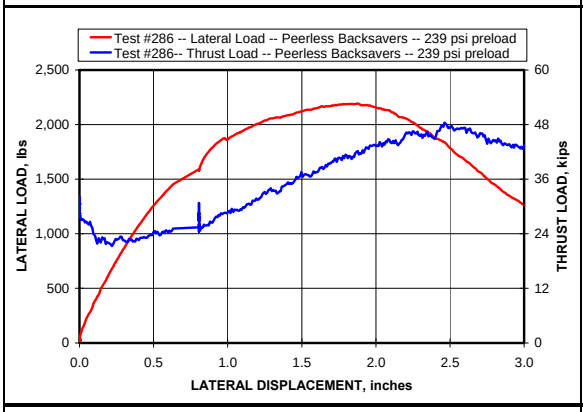
Test #286 -- Lateral Load -- Peerless Backsavers -- 239 psi preload
Test #286-- Thrust Load -- Peerless Backsavers -- 239 psi preload
LATERAL LOAD, lbs
THRUST LOAD, kips
LATERAL DISPLACEMENT, inches

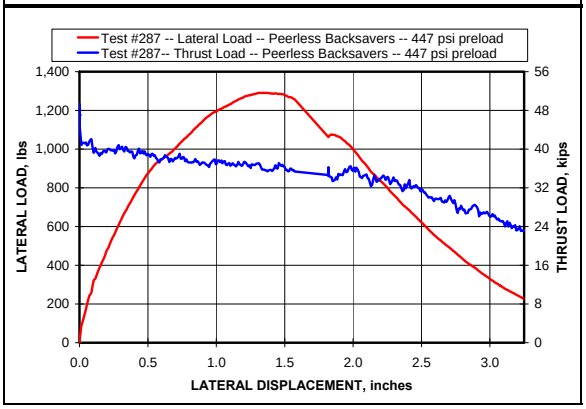
Test #287 -- Lateral Load -- Peerless Backsavers -- 447 psi preload
Test #287-- Thrust Load -- Peerless Backsavers -- 447 psi preload
LATERAL LOAD, lbs
THRUST LOAD, kips
LATERAL DISPLACEMENT, inches

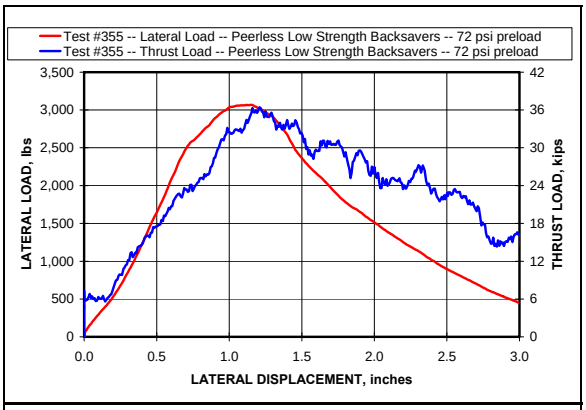
Test #355 -- Lateral Load -- Peerless Low Strength Backsavers -- 72 psi preload
Test #355 -- Thrust Load -- Peerless Low Strength Backsavers -- 72 psi preload
LATERAL LOAD, lbs
THRUST LOAD, kips
LATERAL DISPLACEMENT, inches

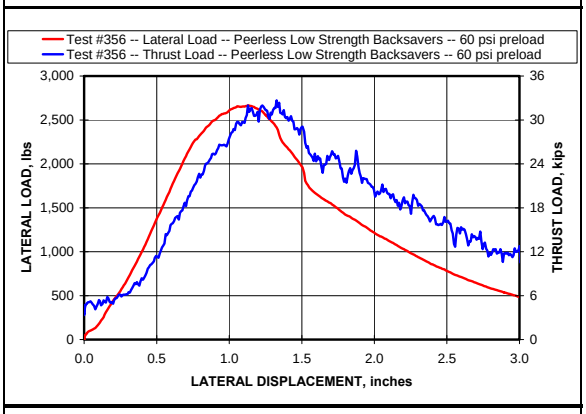
Test #356 -- Lateral Load -- Peerless Low Strength Backsavers -- 60 psi preload
Test #356 -- Thrust Load -- Peerless Low Strength Backsavers -- 60 psi preload
LATERAL LOAD, lbs
THRUST LOAD, kips
LATERAL DISPLACEMENT, inches

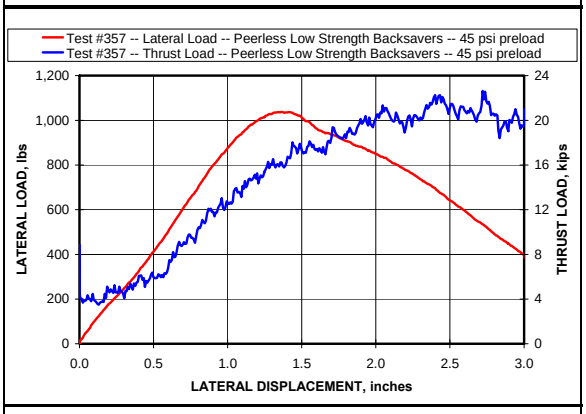
Test #357 -- Lateral Load -- Peerless Low Strength Backsavers -- 45 psi preload
Test #357 -- Thrust Load -- Peerless Low Strength Backsavers -- 45 psi preload
LATERAL LOAD, lbs
THRUST LOAD, kips
LATERAL DISPLACEMENT, inches

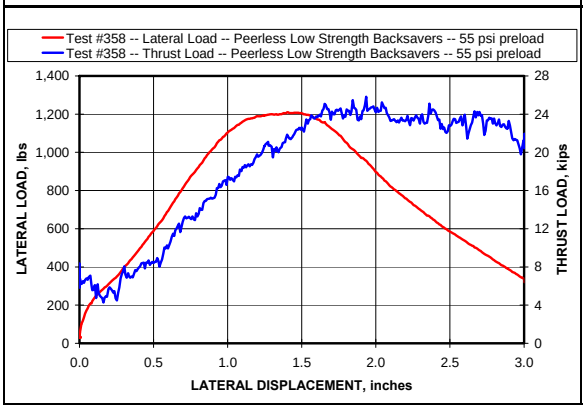
Test #358 -- Lateral Load -- Peerless Low Strength Backsavers -- 55 psi preload
Test #358 -- Thrust Load -- Peerless Low Strength Backsavers -- 55 psi preload
LATERAL LOAD, lbs
THRUST LOAD, kips
LATERAL DISPLACEMENT, inches

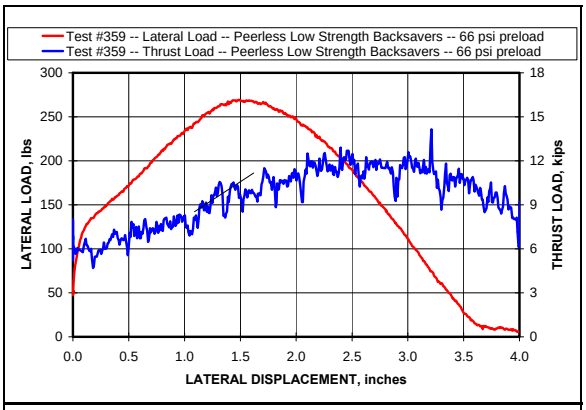
Test #359 -- Lateral Load -- Peerless Low Strength Backsavers -- 66 psi preload
Test #359 -- Thrust Load -- Peerless Low Strength Backsavers -- 66 psi preload
LATERAL LOAD, lbs
THRUST LOAD, kips
LATERAL DISPLACEMENT, inches

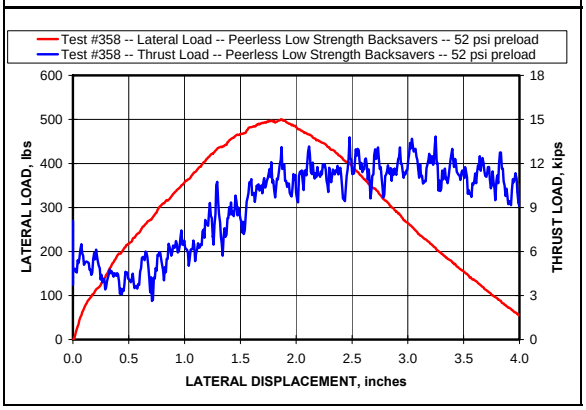
Test #358 -- Lateral Load -- Peerless Low Strength Backsavers -- 52 psi preload
Test #358 -- Thrust Load -- Peerless Low Strength Backsavers -- 52 psi preload
LATERAL LOAD, lbs
THRUST LOAD, kips
LATERAL DISPLACEMENT, inches

ACCOA BLOCK

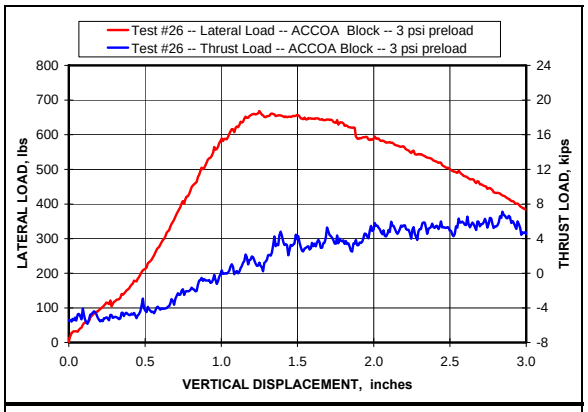

Photo Not Available

Photo Not Available

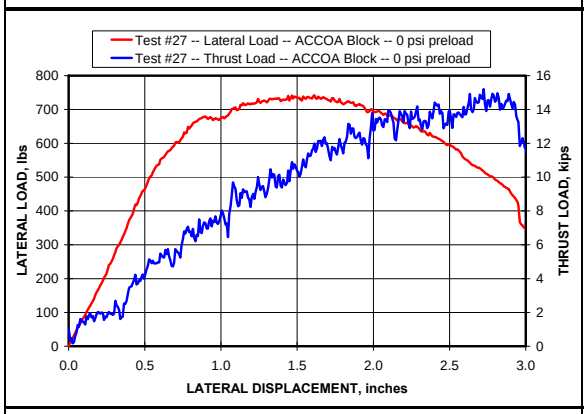

Photo Not Available

Photo Not Available

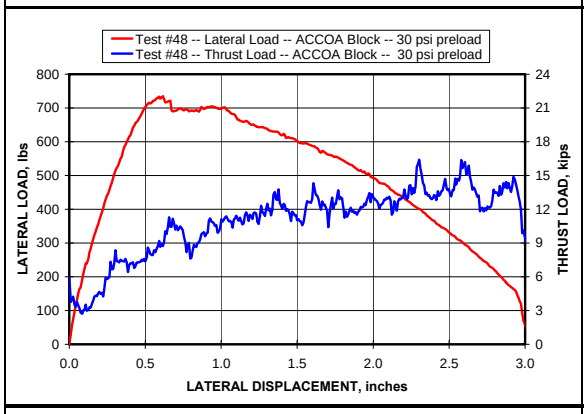

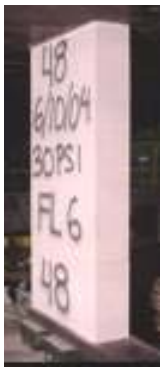

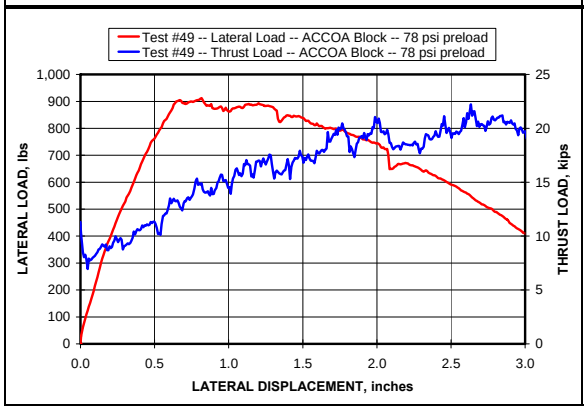

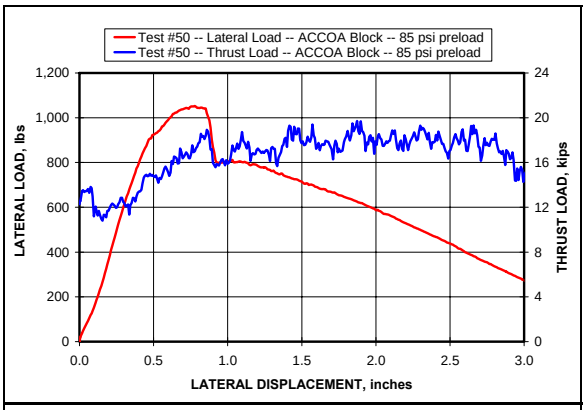

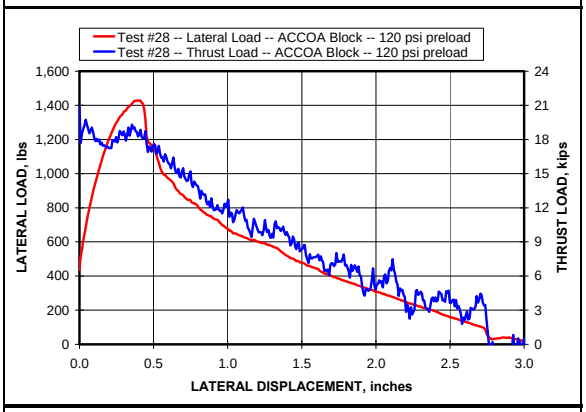

Photo Not Available

Photo Not Available

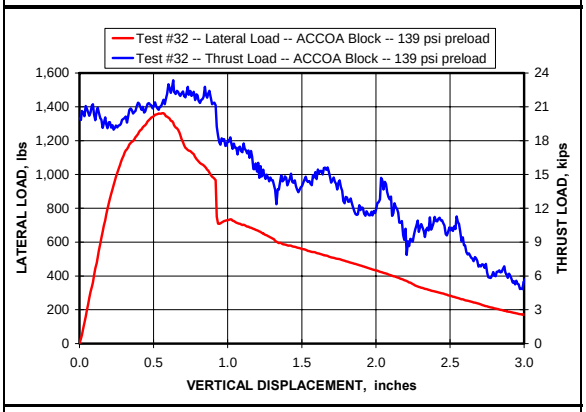

Photo Not Available

Photo Not Available

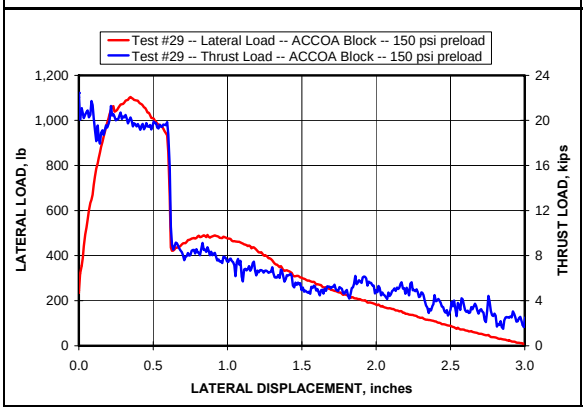

Photo Not Available

Photo Not Available

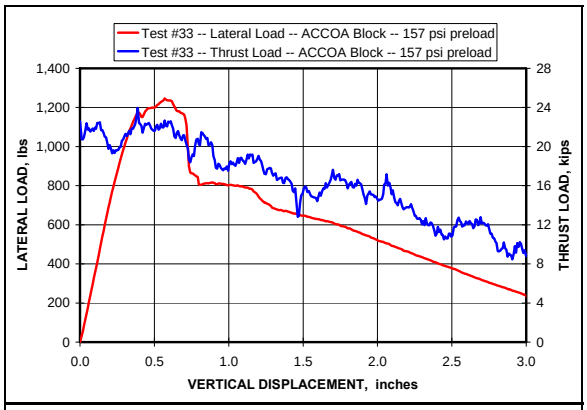

Photo Not Available

Photo Not Available

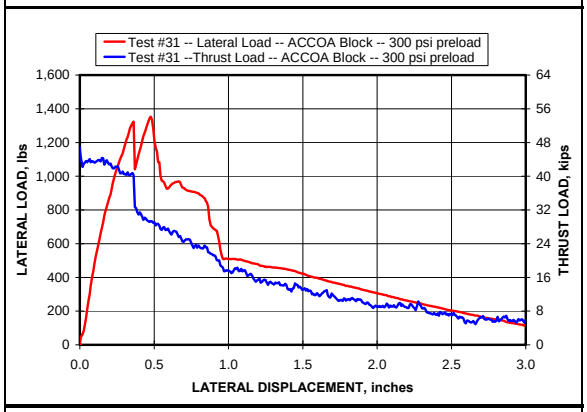

Photo Not Available

Photo Not Available

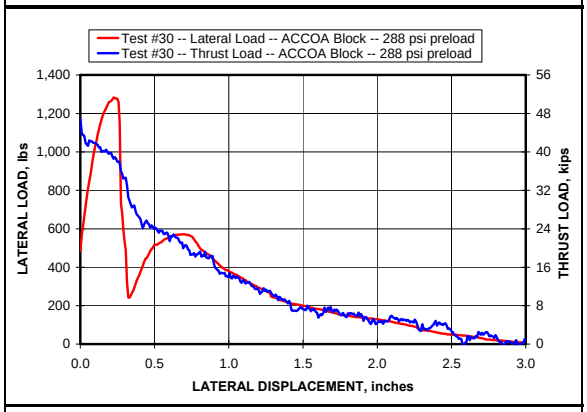

Photo Not Available

Photo Not Available

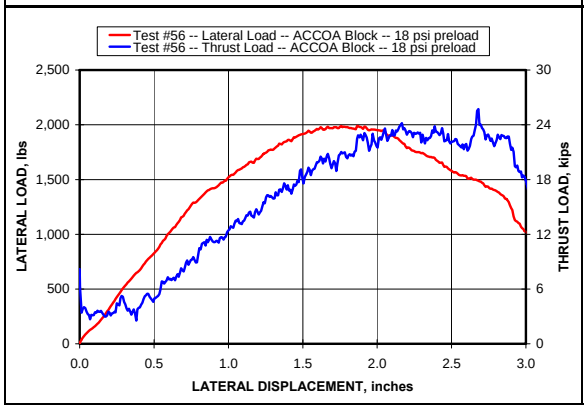

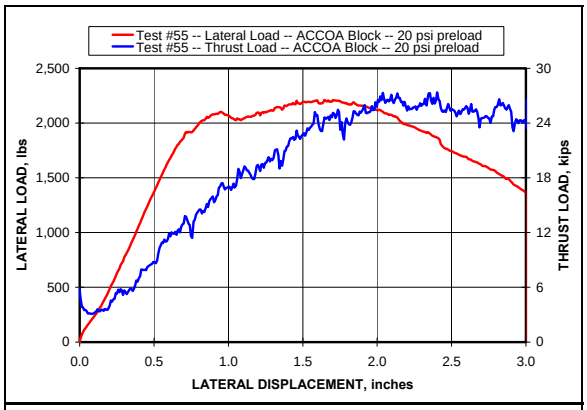
Test #55 -- Lateral Load -- ACCOA Block -- 20 psi preload
Test #55 -- Thrust Load -- ACCOA Block -- 20 psi preload
LATERAL LOAD, lbs
THRUST LOAD, kips
LATERAL DISPLACEMENT, inches


55
6/22/04
30 PSI
FL8
55


55
6/22/04
30 PSI
FL8
55

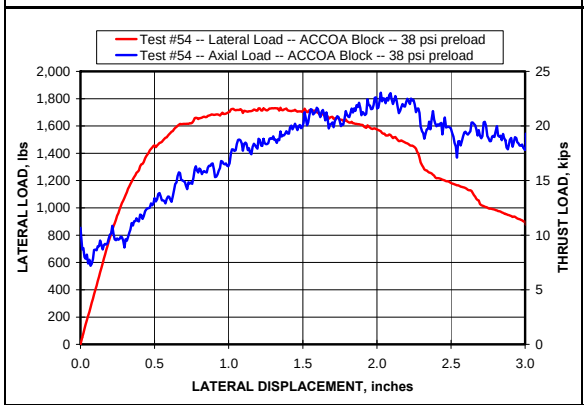
Test #54 -- Lateral Load -- ACCOA Block -- 38 psi preload
Test #54 -- Axial Load -- ACCOA Block -- 38 psi preload
LATERAL LOAD, lbs
THRUST LOAD, kips
LATERAL DISPLACEMENT, inches


54
6/22/04
75 PSI
FL8
54


54
6/22/04
75 PSI
FL8
54

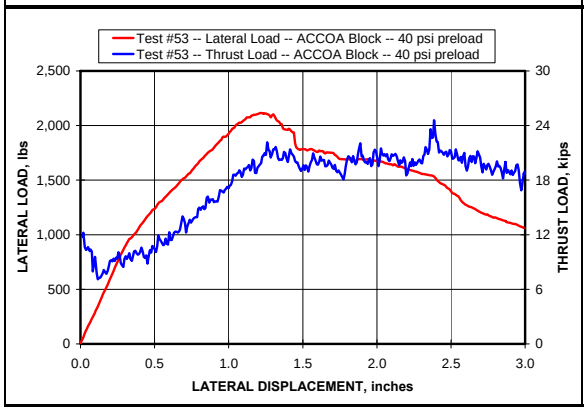
Test #53 -- Lateral Load -- ACCOA Block -- 40 psi preload
Test #53 -- Thrust Load -- ACCOA Block -- 40 psi preload
LATERAL LOAD, lbs
THRUST LOAD, kips
LATERAL DISPLACEMENT, inches


53
6/23/04
75 PSI
FL8
53


53
6/23/04
75 PSI
FL8
53

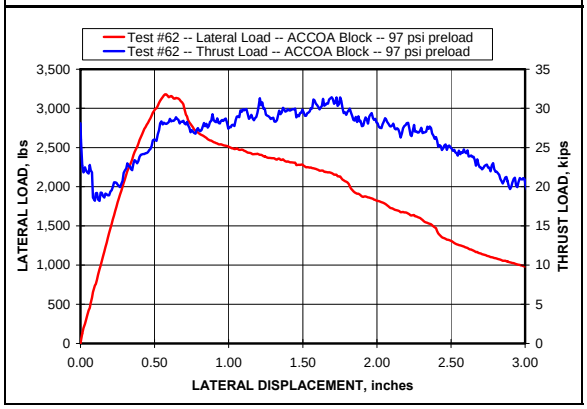
Test #62 -- Lateral Load -- ACCOA Block -- 97 psi preload
Test #62 -- Thrust Load -- ACCOA Block -- 97 psi preload
LATERAL LOAD, lbs
THRUST LOAD, kips
LATERAL DISPLACEMENT, inches


62
6/28/04
150 PSI
FL8
62


62
6/28/04
150 PSI
FL8
62

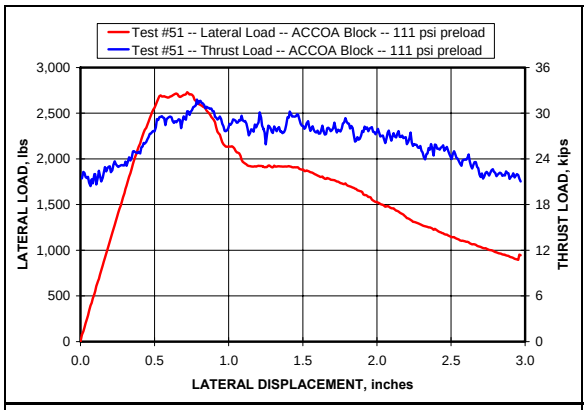
Test #51 -- Lateral Load -- ACCOA Block -- 111 psi preload
Test #51 -- Thrust Load -- ACCOA Block -- 111 psi preload
LATERAL LOAD, lbs
THRUST LOAD, kips
LATERAL DISPLACEMENT, inches
3,000
2,500
2,000
1,500
1,000
500
0
36
30
24
18
12
6
0
0.0
0.5
1.0
1.5
2.0
2.5
3.0


51
5
1
FL8
51


51
5
1
FL8
51

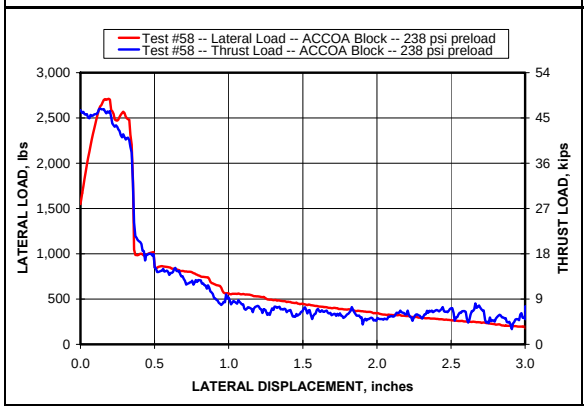
Test #58 -- Lateral Load -- ACCOA Block -- 238 psi preload
Test #58 -- Thrust Load -- ACCOA Block -- 238 psi preload
LATERAL LOAD, lbs
THRUST LOAD, kips
LATERAL DISPLACEMENT, inches
3,000
2,500
2,000
1,500
1,000
500
0
54
45
36
27
18
9
0
0.0
0.5
1.0
1.5
2.0
2.5
3.0


58
5
8
FL8
58


58
5
8
FL8
58

YTONG BLOCK

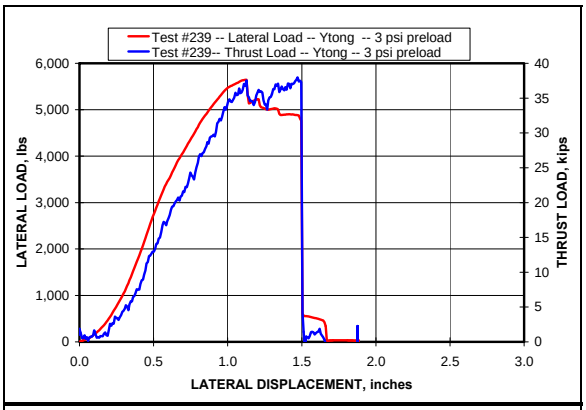
Test #239 -- Lateral Load -- Ytong -- 3 psi preload
Test #239-- Thrust Load -- Ytong -- 3 psi preload
LATERAL LOAD, lbs
THRUST LOAD, kips
LATERAL DISPLACEMENT, inches


239
0 psi
7-28-05
YTONG
239

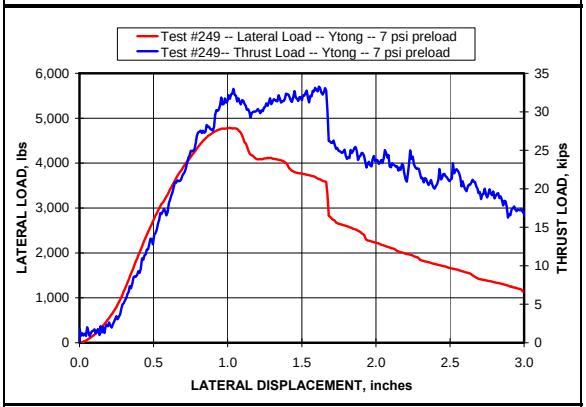
Test #249 -- Lateral Load -- Ytong -- 7 psi preload
Test #249-- Thrust Load -- Ytong -- 7 psi preload
LATERAL LOAD, lbs
THRUST LOAD, kips
LATERAL DISPLACEMENT, inches


249
0 psi
3-30-05
YTONG
249


249
0 psi
3-30-05
YTONG
249

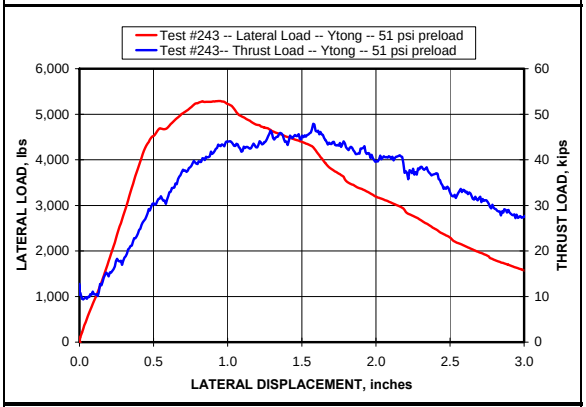
Test #243 -- Lateral Load -- Ytong -- 51 psi preload
Test #243-- Thrust Load -- Ytong -- 51 psi preload
LATERAL LOAD, lbs
THRUST LOAD, kips
LATERAL DISPLACEMENT, inches

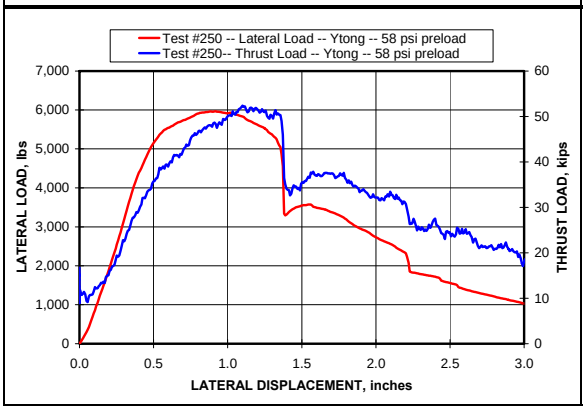
Test #250 -- Lateral Load -- Ytong -- 58 psi preload
Test #250-- Thrust Load -- Ytong -- 58 psi preload
LATERAL LOAD, lbs
THRUST LOAD, kips
LATERAL DISPLACEMENT, inches

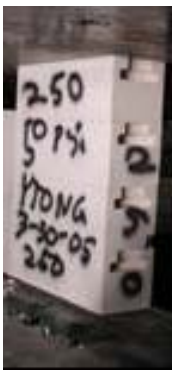
250
50 psi
YTONG
3-30-05
250


250
50 psi
YTONG
3-30-05
250

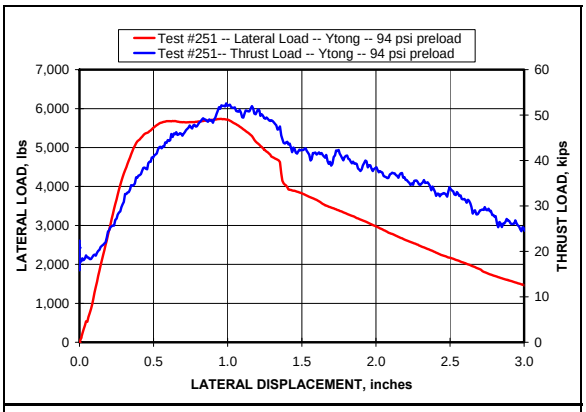

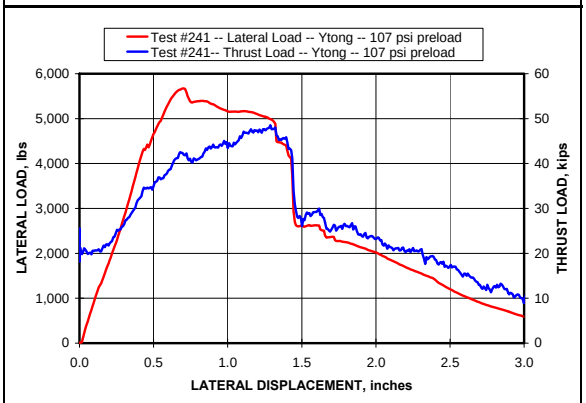

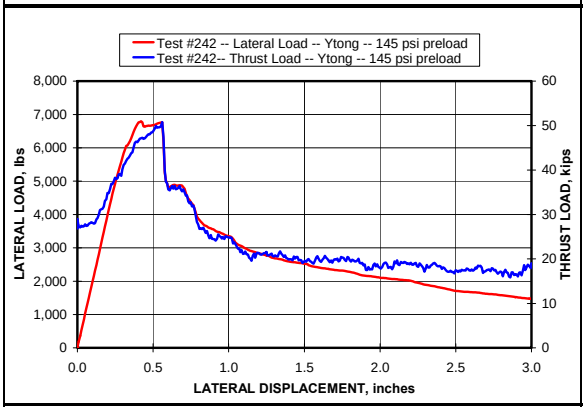

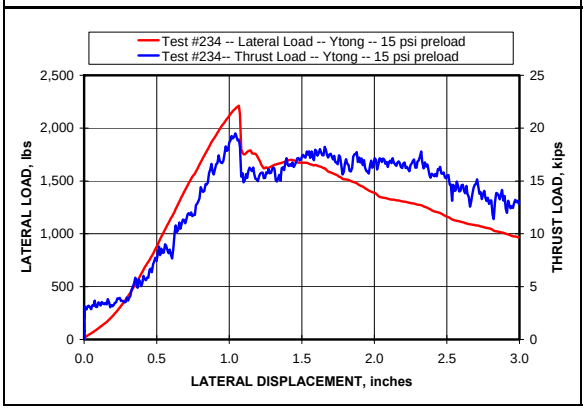

Photo Not Available

Photo Not Available

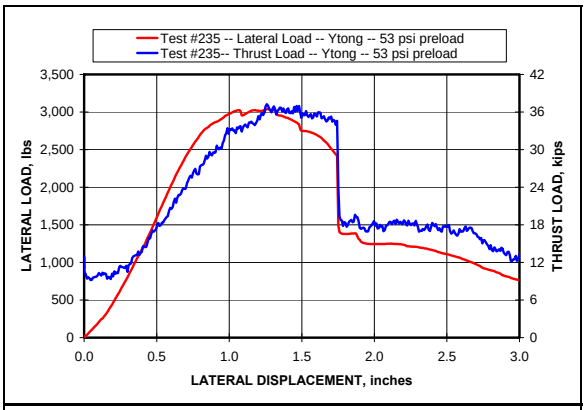
Test #235 -- Lateral Load -- Ytong -- 53 psi preload
Test #235-- Thrust Load -- Ytong -- 53 psi preload
LATERAL LOAD, lbs
THRUST LOAD, kips
LATERAL DISPLACEMENT, inches

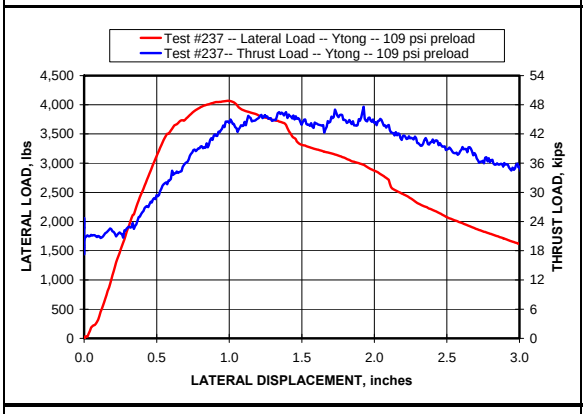
Test #237 -- Lateral Load -- Ytong -- 109 psi preload
Test #237-- Thrust Load -- Ytong -- 109 psi preload
LATERAL LOAD, lbs
THRUST LOAD, kips
LATERAL DISPLACEMENT, inches

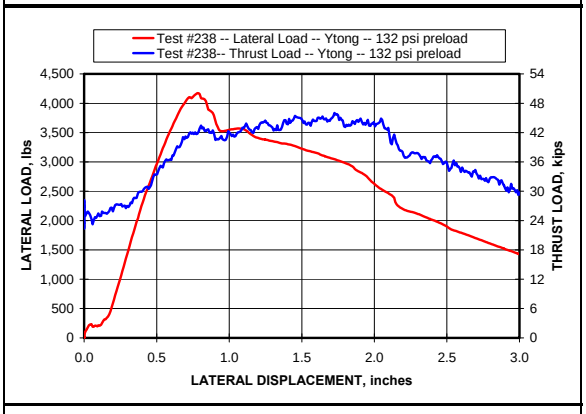
Test #238 -- Lateral Load -- Ytong -- 132 psi preload
Test #238-- Thrust Load -- Ytong -- 132 psi preload
LATERAL LOAD, lbs
THRUST LOAD, kips
LATERAL DISPLACEMENT, inches

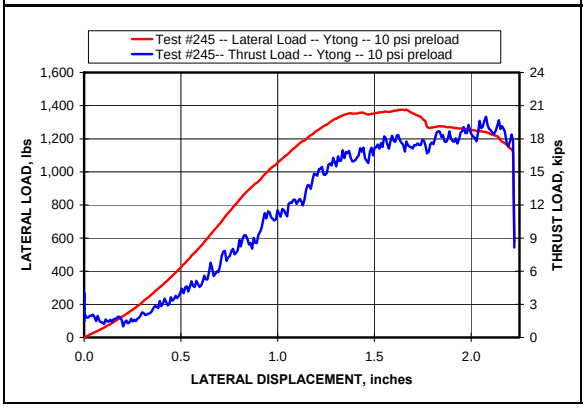
Test #245 -- Lateral Load -- Ytong -- 10 psi preload
Test #245-- Thrust Load -- Ytong -- 10 psi preload
LATERAL LOAD, lbs
THRUST LOAD, kips
LATERAL DISPLACEMENT, inches

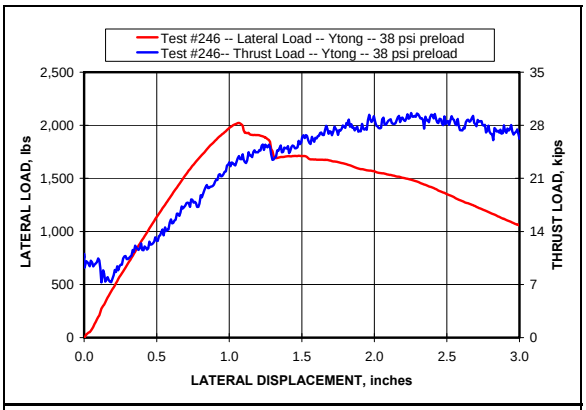
Test #246 -- Lateral Load -- Ytong -- 38 psi preload
Test #246-- Thrust Load -- Ytong -- 38 psi preload
LATERAL LOAD, lbs
THRUST LOAD, kips
LATERAL DISPLACEMENT, inches

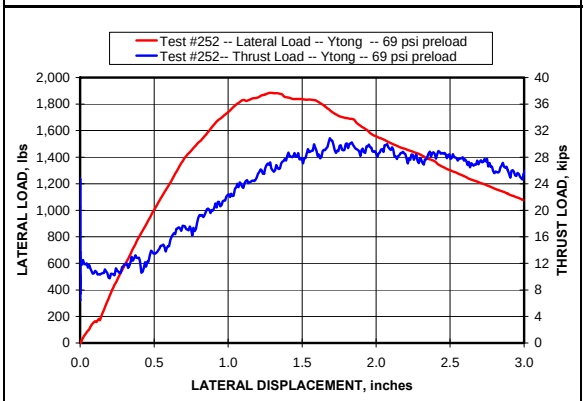
Test #252 -- Lateral Load -- Ytong -- 69 psi preload
Test #252-- Thrust Load -- Ytong -- 69 psi preload
LATERAL LOAD, lbs
THRUST LOAD, kips
LATERAL DISPLACEMENT, inches

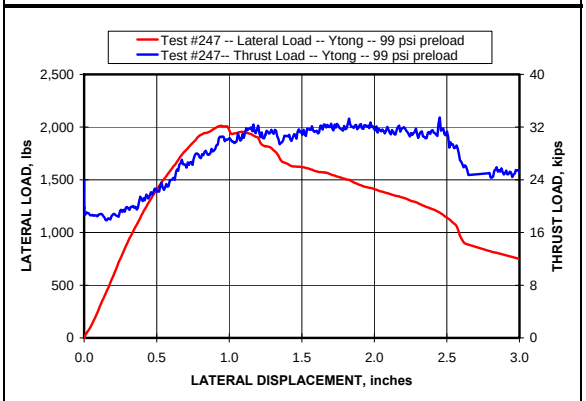
Test #247 -- Lateral Load -- Ytong -- 99 psi preload
Test #247-- Thrust Load -- Ytong -- 99 psi preload
LATERAL LOAD, lbs
THRUST LOAD, kips
LATERAL DISPLACEMENT, inches

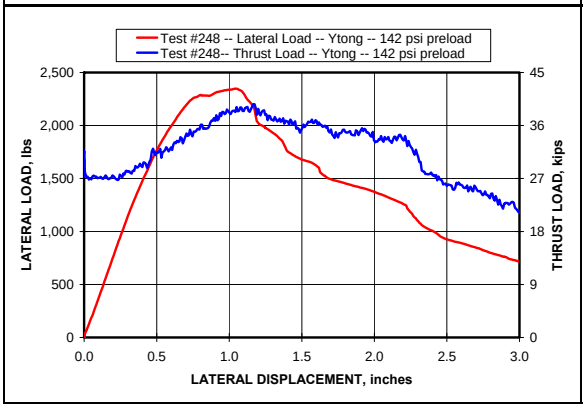
Test #248 -- Lateral Load -- Ytong -- 142 psi preload
Test #248-- Thrust Load -- Ytong -- 142 psi preload
LATERAL LOAD, lbs
THRUST LOAD, kips
LATERAL DISPLACEMENT, inches

KINGSWAY BLOCK

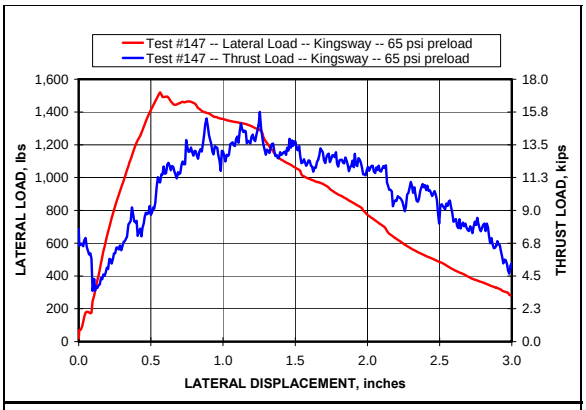

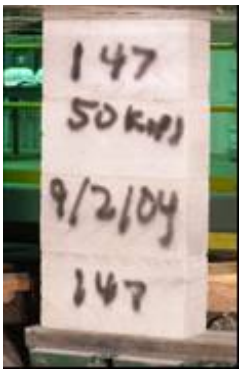

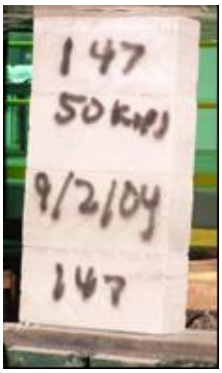

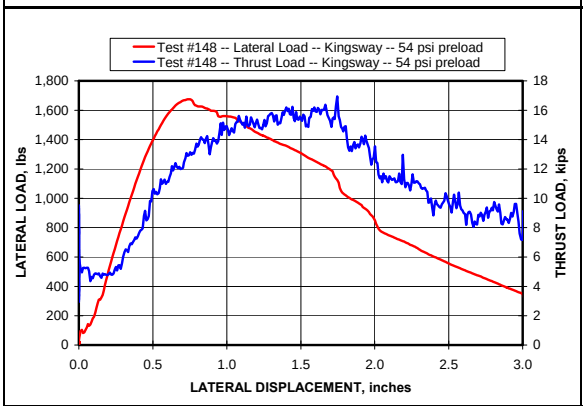

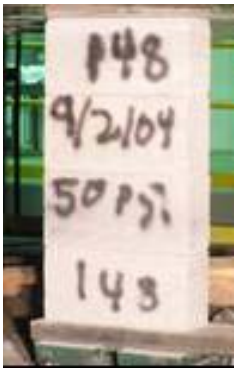

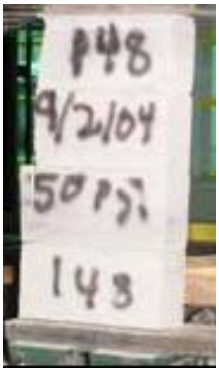

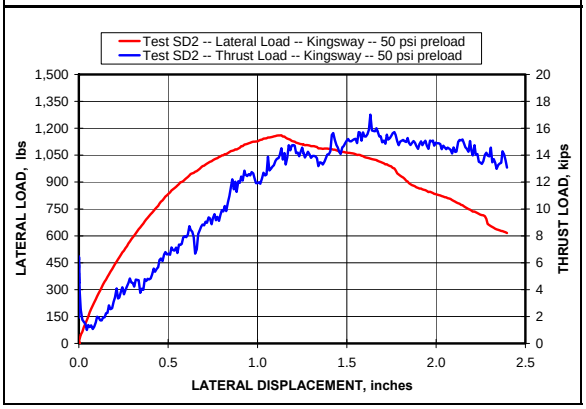

Photo Not Available

Photo Not Available

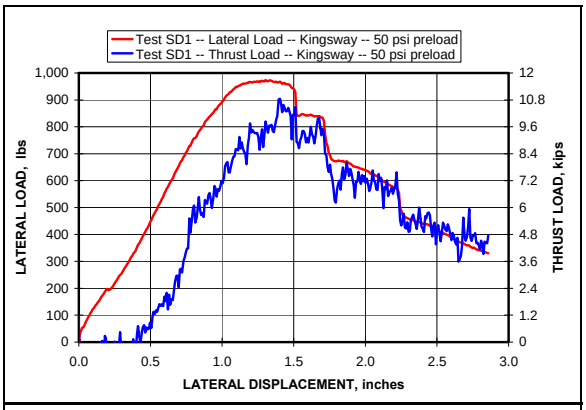

Photo Not Available

Photo Not Available

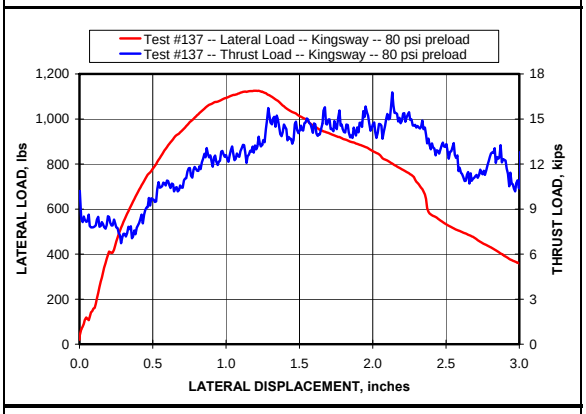

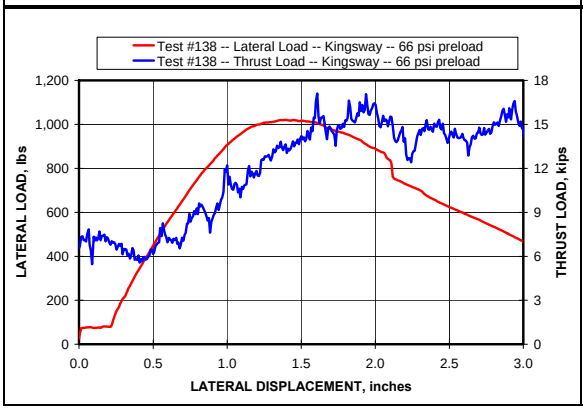

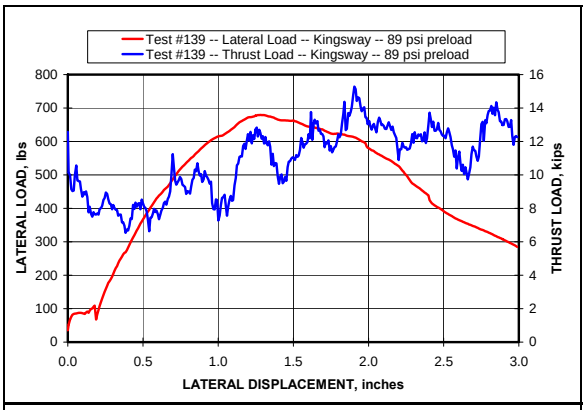
Test #139 -- Lateral Load -- Kingsway -- 89 psi preload
Test #139 -- Thrust Load -- Kingsway -- 89 psi preload
LATERAL LOAD, lbs
THRUST LOAD, kips
LATERAL DISPLACEMENT, inches

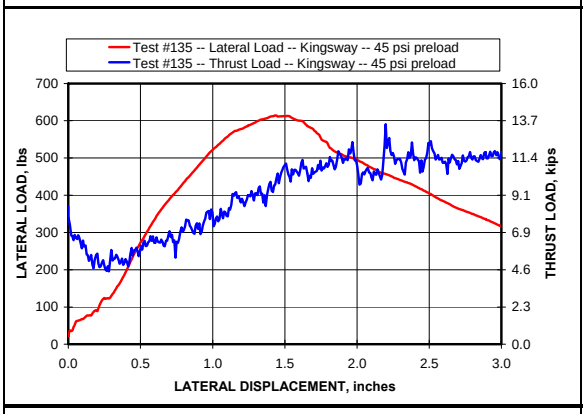
Test #135 -- Lateral Load -- Kingsway -- 45 psi preload
Test #135 -- Thrust Load -- Kingsway -- 45 psi preload
LATERAL LOAD, lbs
THRUST LOAD, kips
LATERAL DISPLACEMENT, inches

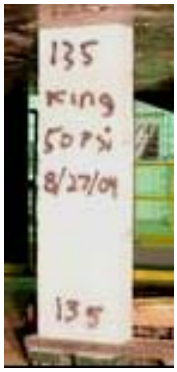
135
King
50 psi
8/27/04
135


135
King
50 psi
8/27/04
135

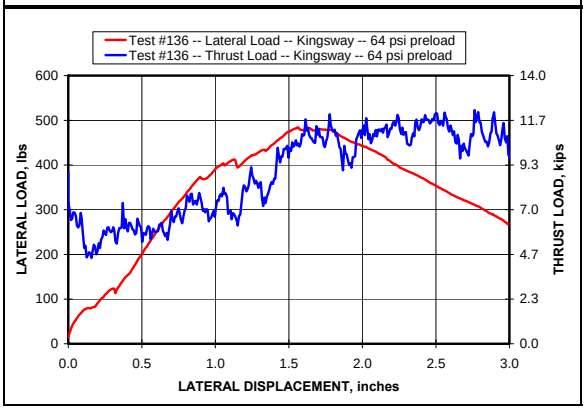
Test #136 -- Lateral Load -- Kingsway -- 64 psi preload
Test #136 -- Thrust Load -- Kingsway -- 64 psi preload
LATERAL LOAD, lbs
THRUST LOAD, kips
LATERAL DISPLACEMENT, inches

OMEGA BLOCK

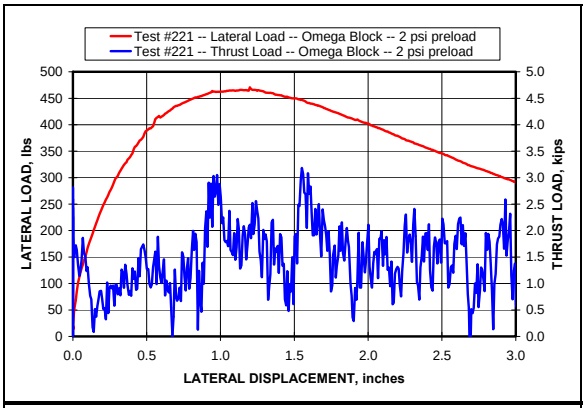
Test #221 -- Lateral Load -- Omega Block -- 2 psi preload
Test #221 -- Thrust Load -- Omega Block -- 2 psi preload
LATERAL LOAD, lbs
THRUST LOAD, kips
LATERAL DISPLACEMENT, inches

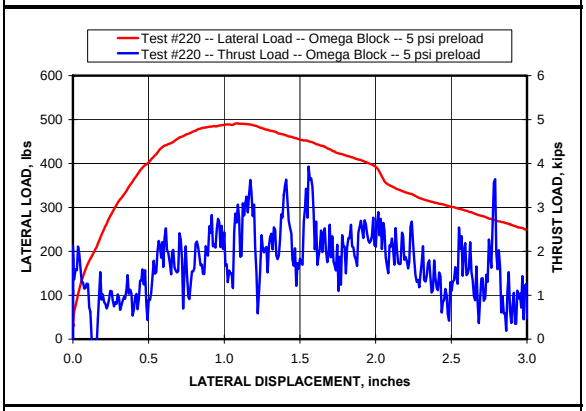
Test #220 -- Lateral Load -- Omega Block -- 5 psi preload
Test #220 -- Thrust Load -- Omega Block -- 5 psi preload
LATERAL LOAD, lbs
THRUST LOAD, kips
LATERAL DISPLACEMENT, inches

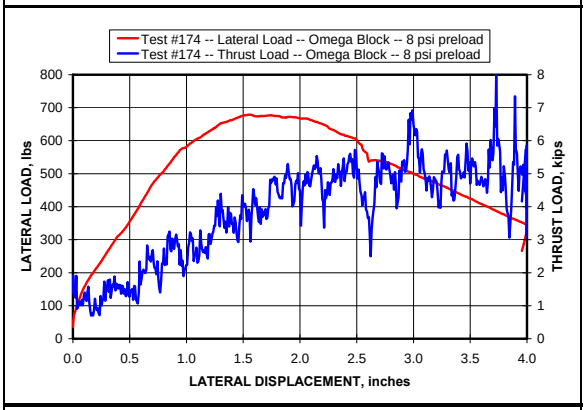
Test #174 -- Lateral Load -- Omega Block -- 8 psi preload
Test #174 -- Thrust Load -- Omega Block -- 8 psi preload
LATERAL LOAD, lbs
THRUST LOAD, kips
LATERAL DISPLACEMENT, inches

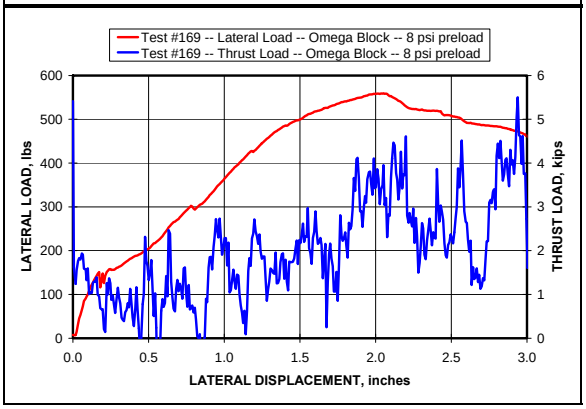
Test #169 -- Lateral Load -- Omega Block -- 8 psi preload
Test #169 -- Thrust Load -- Omega Block -- 8 psi preload
LATERAL LOAD, lbs
THRUST LOAD, kips
LATERAL DISPLACEMENT, inches

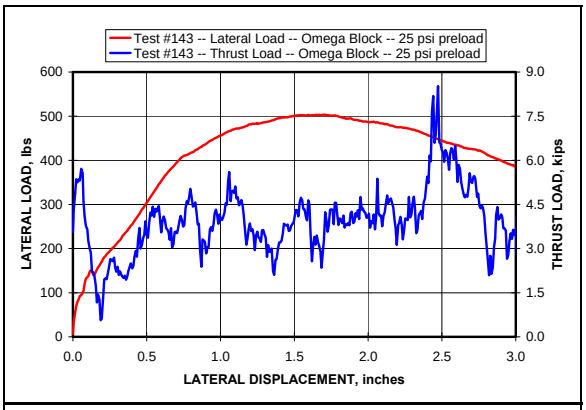
Test #143 -- Lateral Load -- Omega Block -- 25 psi preload
Test #143 -- Thrust Load -- Omega Block -- 25 psi preload
LATERAL LOAD, lbs
THRUST LOAD, kips
LATERAL DISPLACEMENT, inches

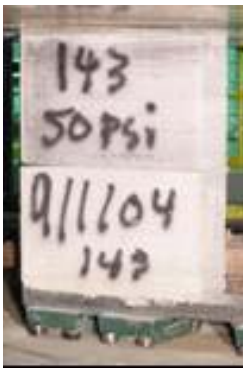
143
50psi
9/1/04
143


143
50psi
9/1/04
143

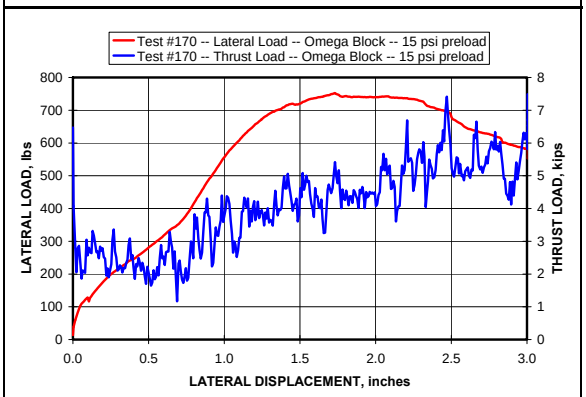
Test #170 -- Lateral Load -- Omega Block -- 15 psi preload
Test #170 -- Thrust Load -- Omega Block -- 15 psi preload
LATERAL LOAD, lbs
THRUST LOAD, kips
LATERAL DISPLACEMENT, inches

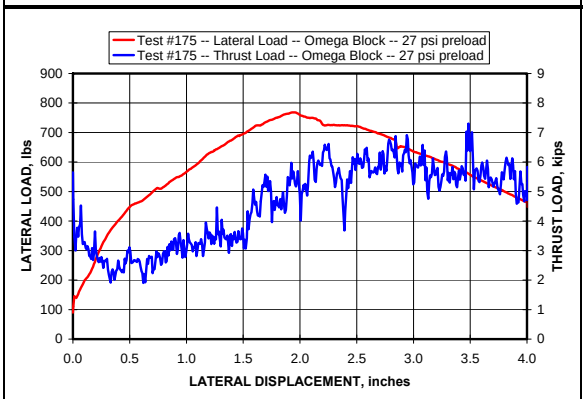
Test #175 -- Lateral Load -- Omega Block -- 27 psi preload
Test #175 -- Thrust Load -- Omega Block -- 27 psi preload
LATERAL LOAD, lbs
THRUST LOAD, kips
LATERAL DISPLACEMENT, inches

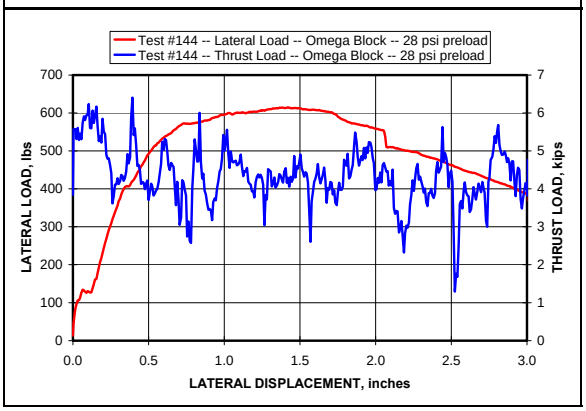
Test #144 -- Lateral Load -- Omega Block -- 28 psi preload
Test #144 -- Thrust Load -- Omega Block -- 28 psi preload
LATERAL LOAD, lbs
THRUST LOAD, kips
LATERAL DISPLACEMENT, inches


144
9/1/04
30psi
144


144
9/1/04
30psi
144

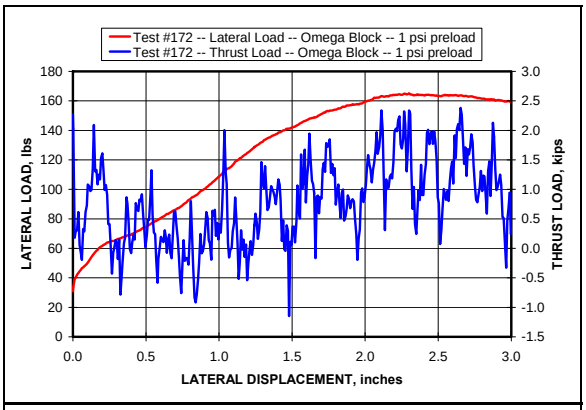
Test #172 -- Lateral Load -- Omega Block -- 1 psi preload
Test #172 -- Thrust Load -- Omega Block -- 1 psi preload
LATERAL LOAD, lbs
THRUST LOAD, kips
LATERAL DISPLACEMENT, inches

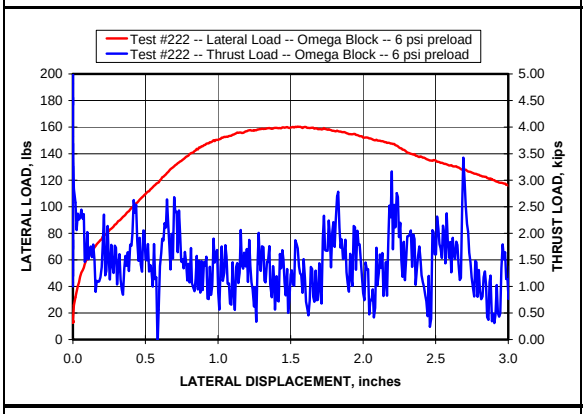
Test #222 -- Lateral Load -- Omega Block -- 6 psi preload
Test #222 -- Thrust Load -- Omega Block -- 6 psi preload
LATERAL LOAD, lbs
THRUST LOAD, kips
LATERAL DISPLACEMENT, inches

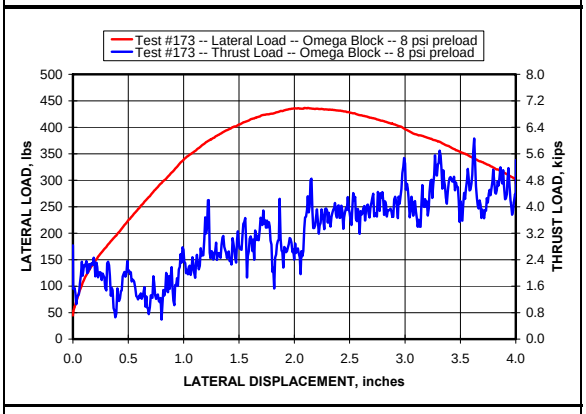
Test #173 -- Lateral Load -- Omega Block -- 8 psi preload
Test #173 -- Thrust Load -- Omega Block -- 8 psi preload
LATERAL LOAD, lbs
THRUST LOAD, kips
LATERAL DISPLACEMENT, inches

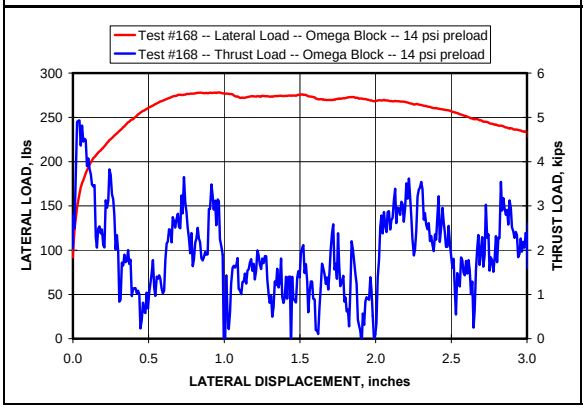
Test #168 -- Lateral Load -- Omega Block -- 14 psi preload
Test #168 -- Thrust Load -- Omega Block -- 14 psi preload
LATERAL LOAD, lbs
THRUST LOAD, kips
LATERAL DISPLACEMENT, inches

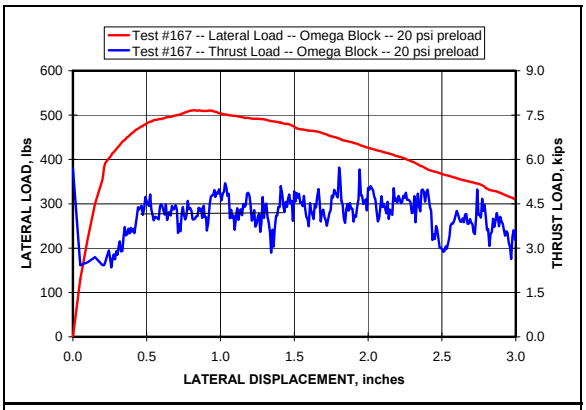
Test #167 -- Lateral Load -- Omega Block -- 20 psi preload
Test #167 -- Thrust Load -- Omega Block -- 20 psi preload
LATERAL LOAD, lbs
THRUST LOAD, kips
LATERAL DISPLACEMENT, inches

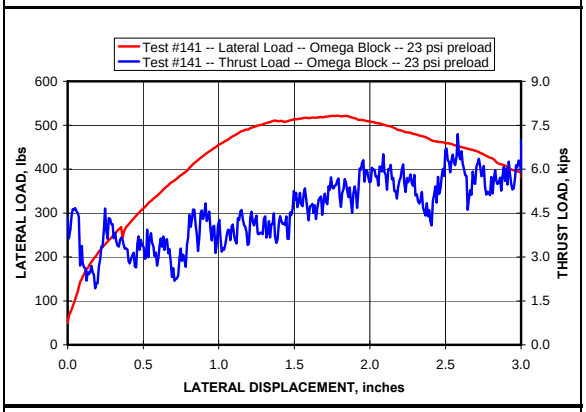
Test #141 -- Lateral Load -- Omega Block -- 23 psi preload
Test #141 -- Thrust Load -- Omega Block -- 23 psi preload
LATERAL LOAD, lbs
THRUST LOAD, kips
LATERAL DISPLACEMENT, inches

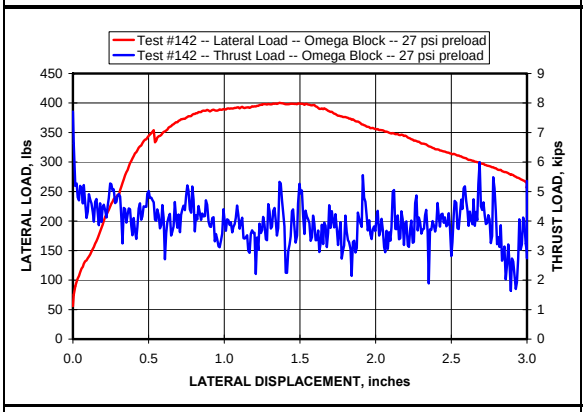
Test #142 -- Lateral Load -- Omega Block -- 27 psi preload
Test #142 -- Thrust Load -- Omega Block -- 27 psi preload
LATERAL LOAD, lbs
THRUST LOAD, kips
LATERAL DISPLACEMENT, inches

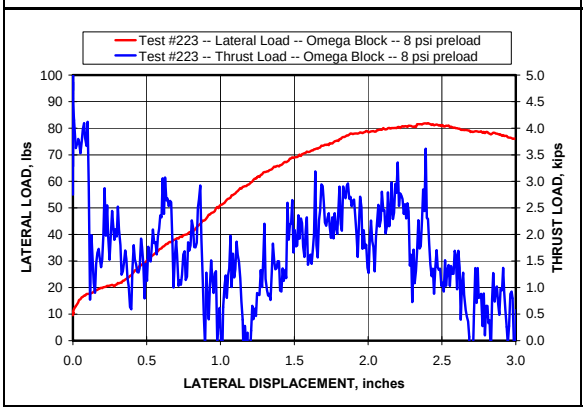
Test #223 -- Lateral Load -- Omega Block -- 8 psi preload
Test #223 -- Thrust Load -- Omega Block -- 8 psi preload
LATERAL LOAD, lbs
THRUST LOAD, kips
LATERAL DISPLACEMENT, inches

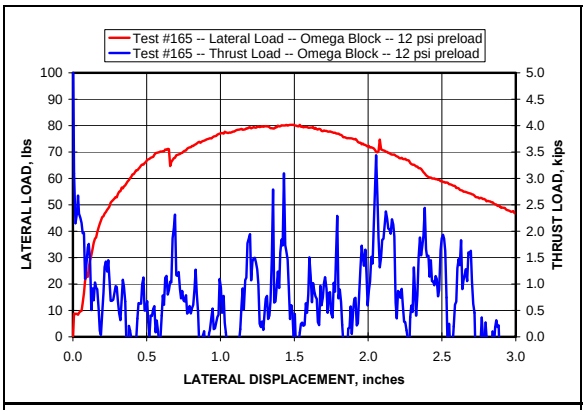
Test #165 -- Lateral Load -- Omega Block -- 12 psi preload
Test #165 -- Thrust Load -- Omega Block -- 12 psi preload
LATERAL LOAD, lbs
THRUST LOAD, kips
LATERAL DISPLACEMENT, inches

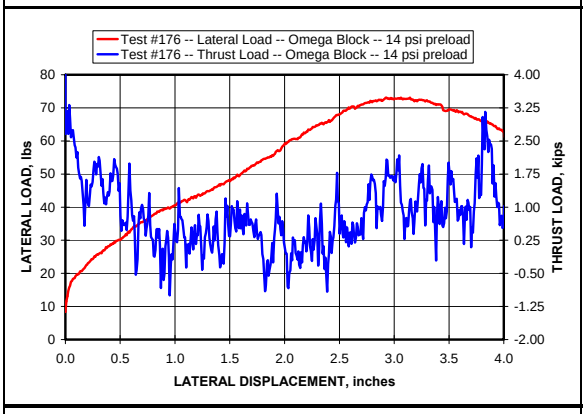
Test #176 -- Lateral Load -- Omega Block -- 14 psi preload
Test #176 -- Thrust Load -- Omega Block -- 14 psi preload
LATERAL LOAD, lbs
THRUST LOAD, kips
LATERAL DISPLACEMENT, inches

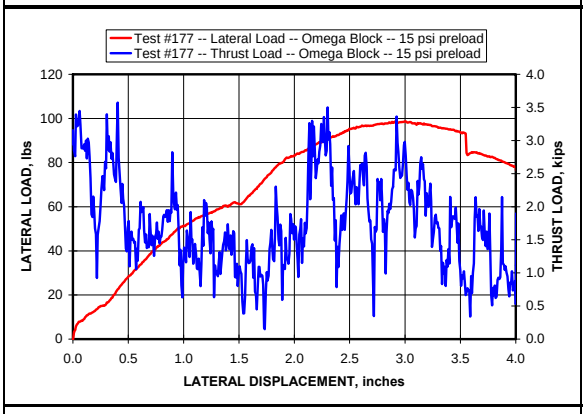
Test #177 -- Lateral Load -- Omega Block -- 15 psi preload
Test #177 -- Thrust Load -- Omega Block -- 15 psi preload
LATERAL LOAD, lbs
THRUST LOAD, kips
LATERAL DISPLACEMENT, inches

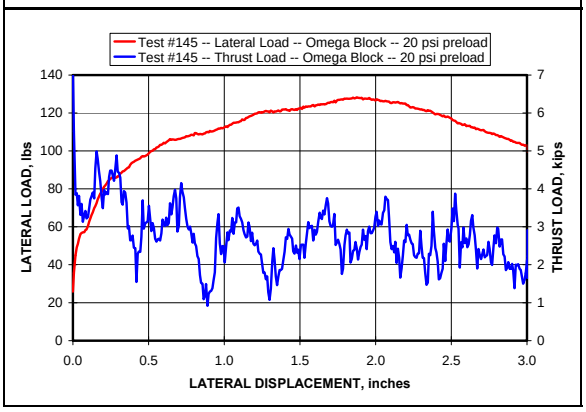
Test #145 -- Lateral Load -- Omega Block -- 20 psi preload
Test #145 -- Thrust Load -- Omega Block -- 20 psi preload
LATERAL LOAD, lbs
THRUST LOAD, kips
LATERAL DISPLACEMENT, inches

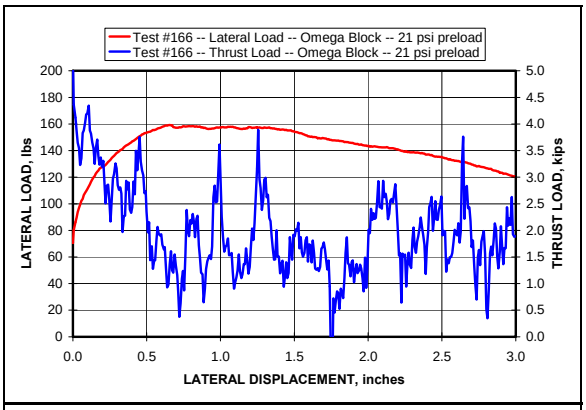
Test #166 -- Lateral Load -- Omega Block -- 21 psi preload
Test #166 -- Thrust Load -- Omega Block -- 21 psi preload
LATERAL LOAD, lbs
THRUST LOAD, kips
LATERAL DISPLACEMENT, inches

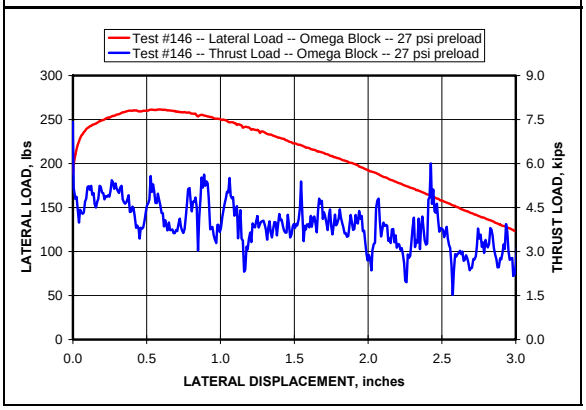
Test #146 -- Lateral Load -- Omega Block -- 27 psi preload
Test #146 -- Thrust Load -- Omega Block -- 27 psi preload
LATERAL LOAD, lbs
THRUST LOAD, kips
LATERAL DISPLACEMENT, inches

PEERLESS SUPER BLOCK

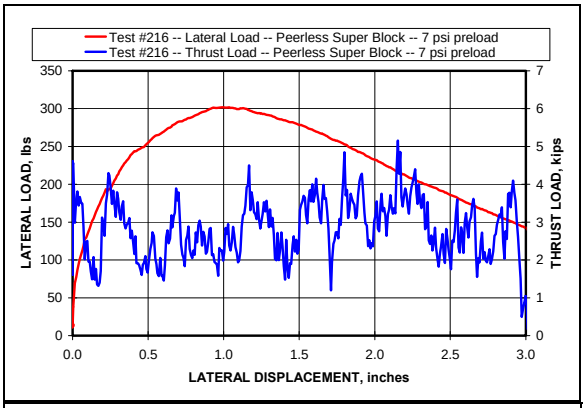

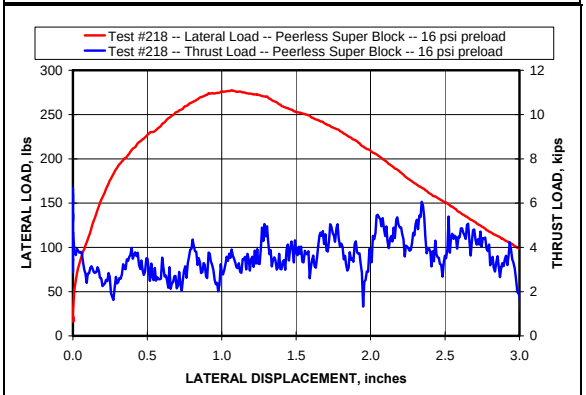

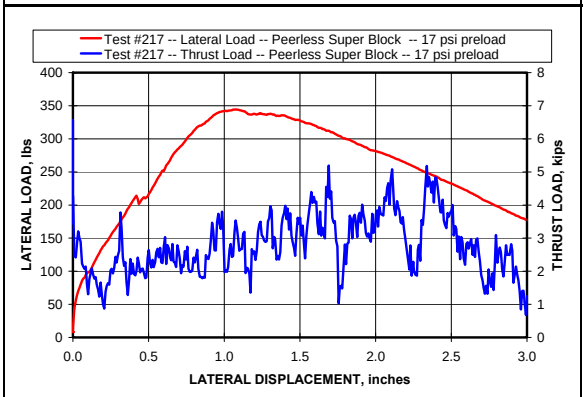

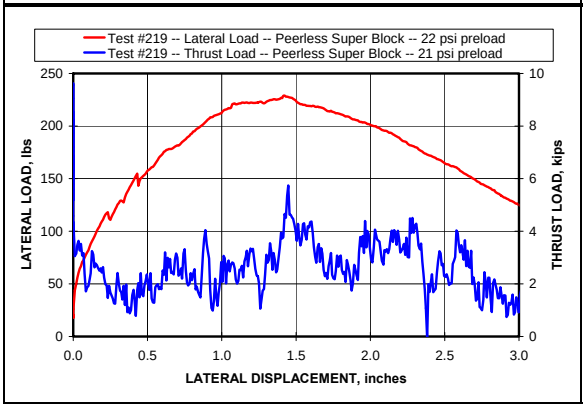

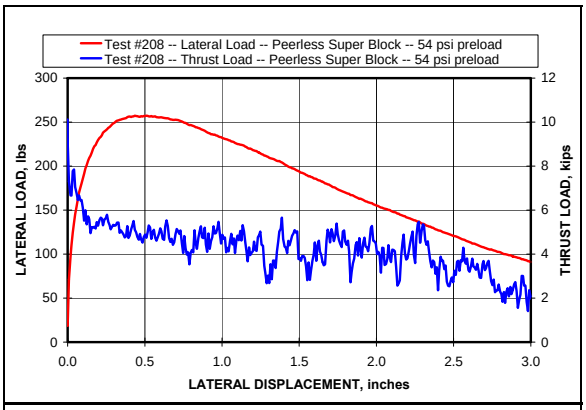

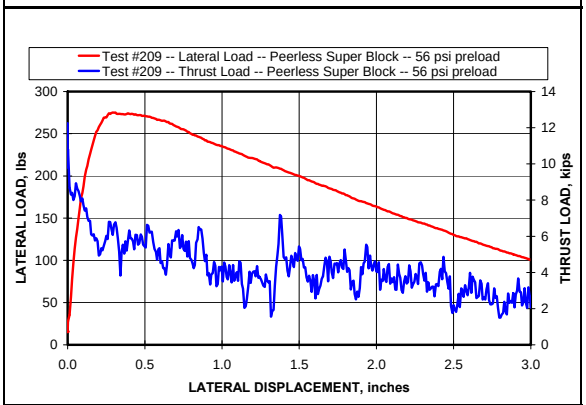

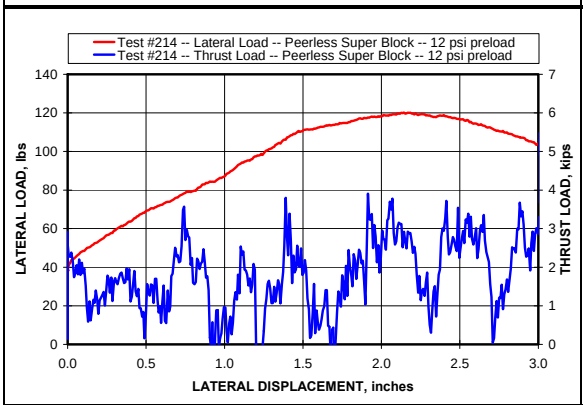

Photo Not Available

Photo Not Available

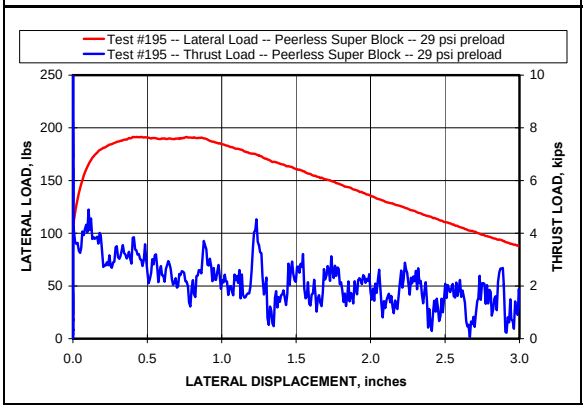

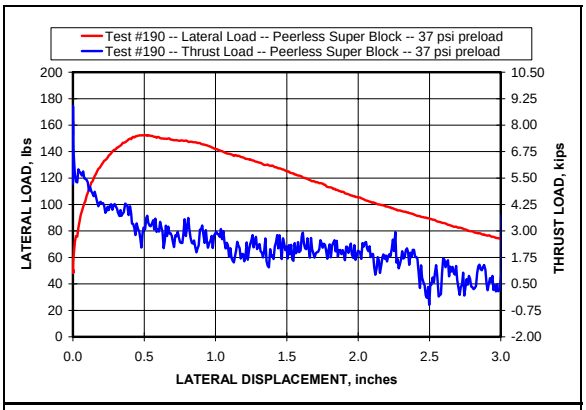
Test #190 -- Lateral Load -- Peerless Super Block -- 37 psi preload
Test #190 -- Thrust Load -- Peerless Super Block -- 37 psi preload
LATERAL LOAD, lbs
THRUST LOAD, kips
LATERAL DISPLACEMENT, inches


190
P
2-17-05
190


190
P
2-17-05
190

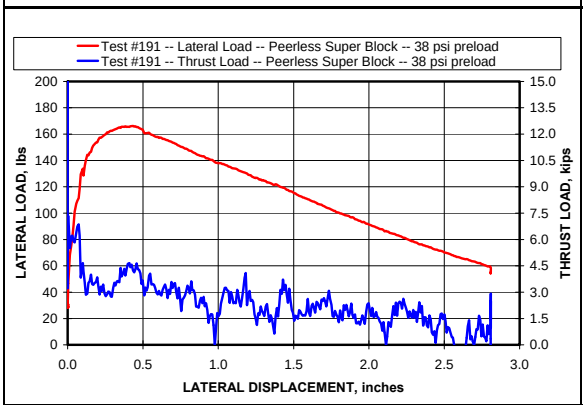
Test #191 -- Lateral Load -- Peerless Super Block -- 38 psi preload
Test #191 -- Thrust Load -- Peerless Super Block -- 38 psi preload
LATERAL LOAD, lbs
THRUST LOAD, kips
LATERAL DISPLACEMENT, inches


191
2-18-05
Peerless
191


191
2-18-05
Peerless
191

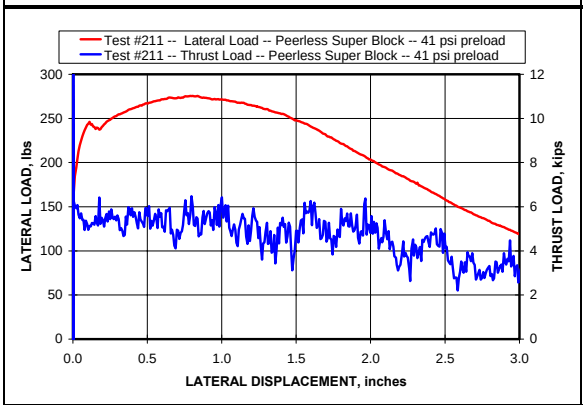
Test #211 -- Lateral Load -- Peerless Super Block -- 41 psi preload
Test #211 -- Thrust Load -- Peerless Super Block -- 41 psi preload
LATERAL LOAD, lbs
THRUST LOAD, kips
LATERAL DISPLACEMENT, inches


211
2-14-05
Peerless
211


211
2-14-05
Peerless
211

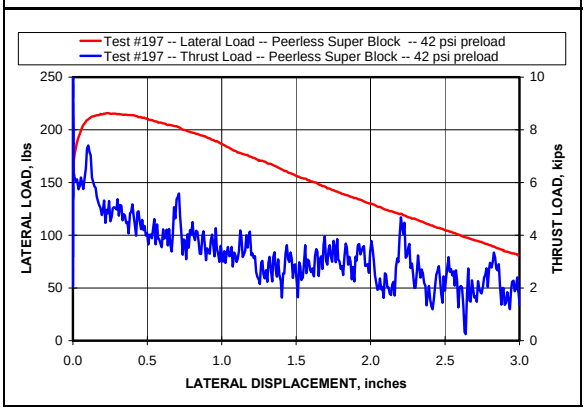
Test #197 -- Lateral Load -- Peerless Super Block -- 42 psi preload
Test #197 -- Thrust Load -- Peerless Super Block -- 42 psi preload
LATERAL LOAD, lbs
THRUST LOAD, kips
LATERAL DISPLACEMENT, inches


197
2.5 inch
Peep
2-23-05
197


197
2.5 inch
Peep
2-23-05
197

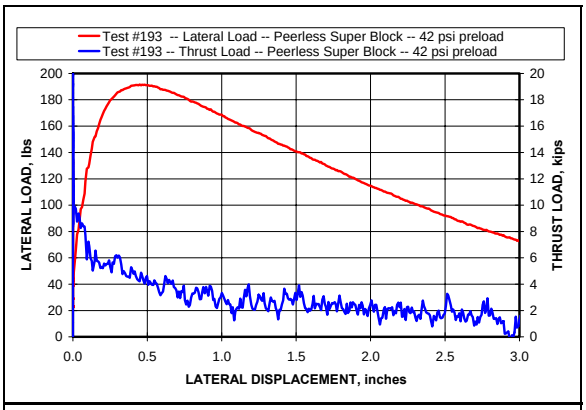

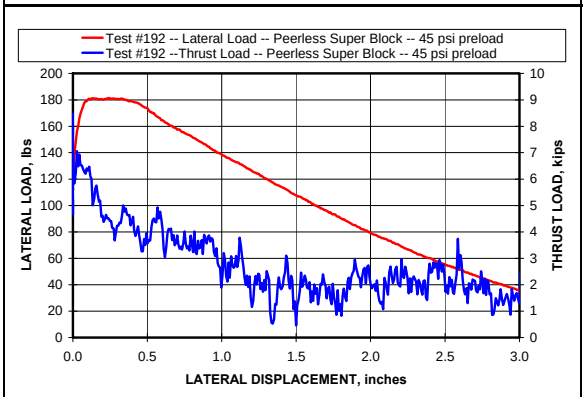

Photo Not Available

Photo Not Available

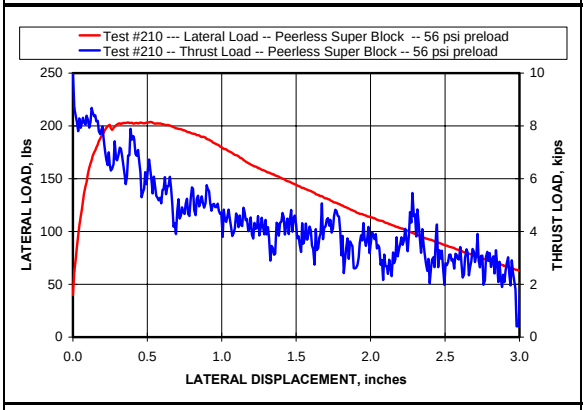

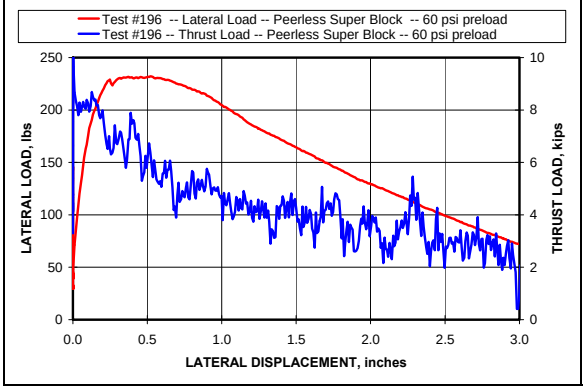

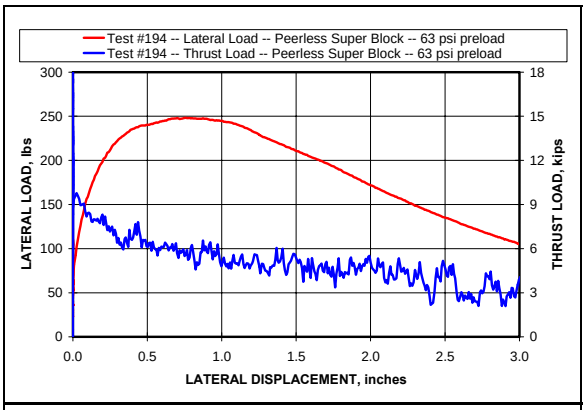

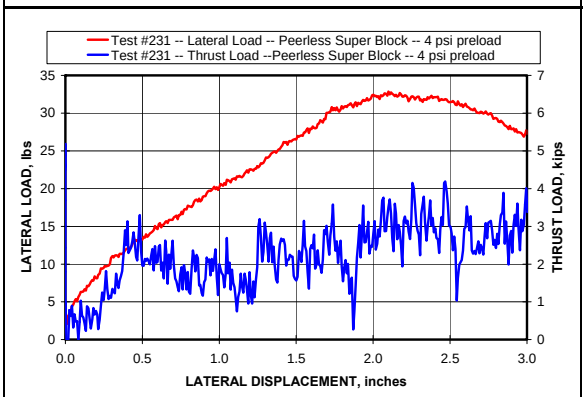

Photo Not Available

Photo Not Available

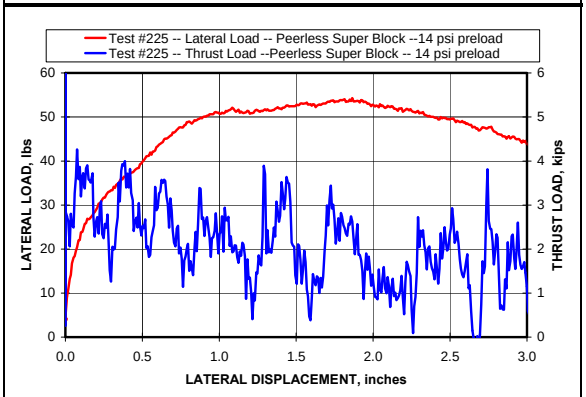

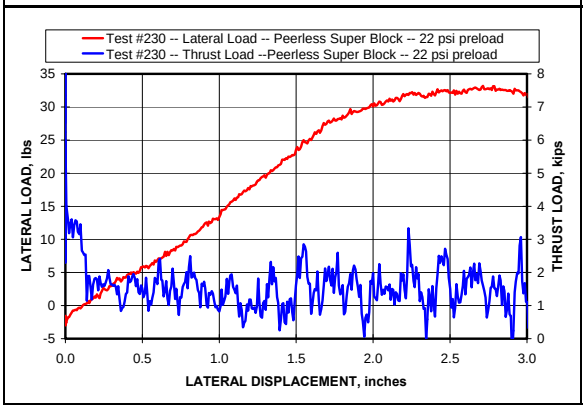

Photo Not Available

Photo Not Available

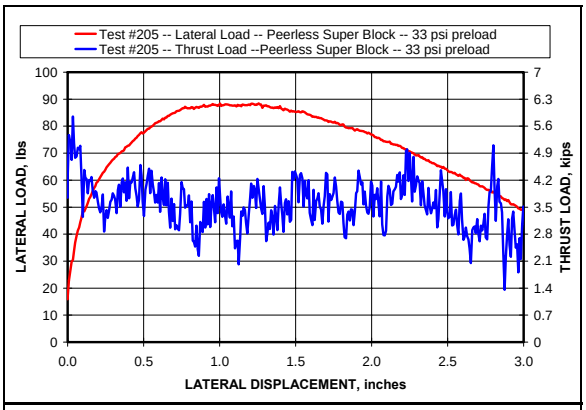

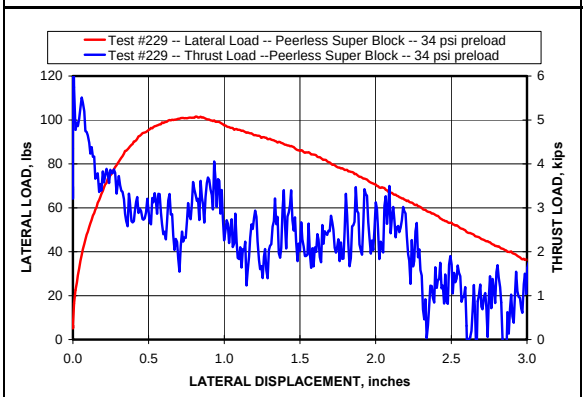

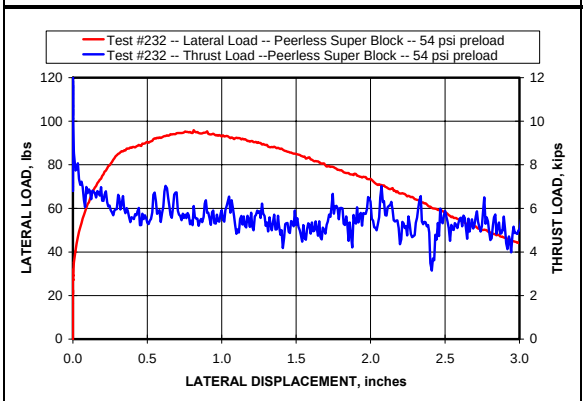

Photo Not Available

Photo Not Available

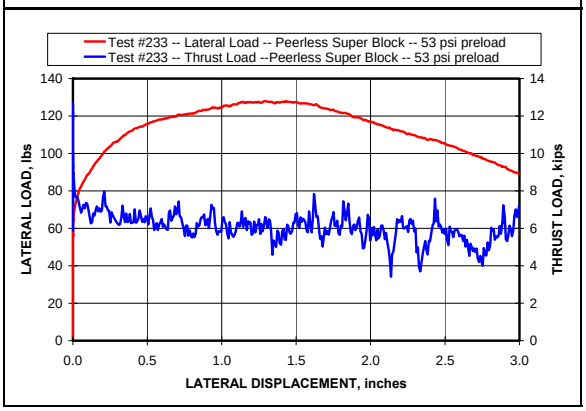

Photo Not Available

Photo Not Available

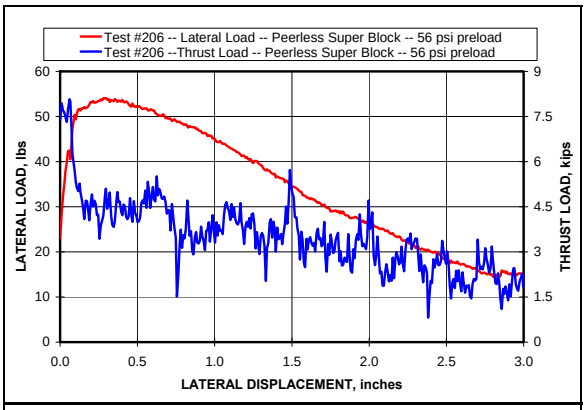
Test #206 -- Lateral Load -- Peerless Super Block -- 56 psi preload
Test #206 --Thrust Load -- Peerless Super Block -- 56 psi preload
LATERAL LOAD, lbs
THRUST LOAD, kips
LATERAL DISPLACEMENT, inches


206
PEER
50PSI
3-10-05
206


206
PEER
50PSI
3-10-05
206

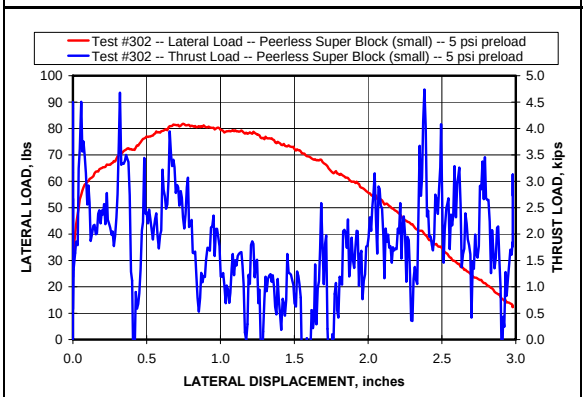
Test #302 -- Lateral Load -- Peerless Super Block (small) -- 5 psi preload
Test #302 -- Thrust Load -- Peerless Super Block (small) -- 5 psi preload
LATERAL LOAD, lbs
THRUST LOAD, kips
LATERAL DISPLACEMENT, inches


302
6-2-05
0PSI
302


302
6-2-05
0PSI
302

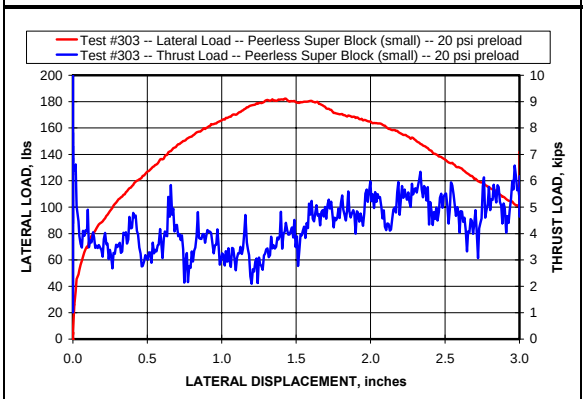
Test #303 -- Lateral Load -- Peerless Super Block (small) -- 20 psi preload
Test #303 -- Thrust Load -- Peerless Super Block (small) -- 20 psi preload
LATERAL LOAD, lbs
THRUST LOAD, kips
LATERAL DISPLACEMENT, inches


303
20PSI
6-2-05
303


303
20PSI
6-2-05
303

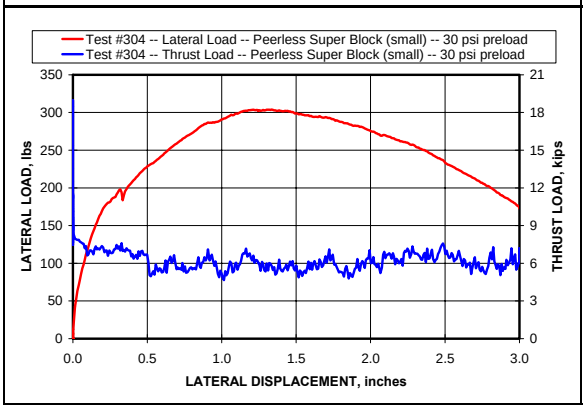
Test #304 -- Lateral Load -- Peerless Super Block (small) -- 30 psi preload
Test #304 -- Thrust Load -- Peerless Super Block (small) -- 30 psi preload
LATERAL LOAD, lbs
THRUST LOAD, kips
LATERAL DISPLACEMENT, inches


304
90PSI
6-2-05
304


304
90PSI
6-2-05
304

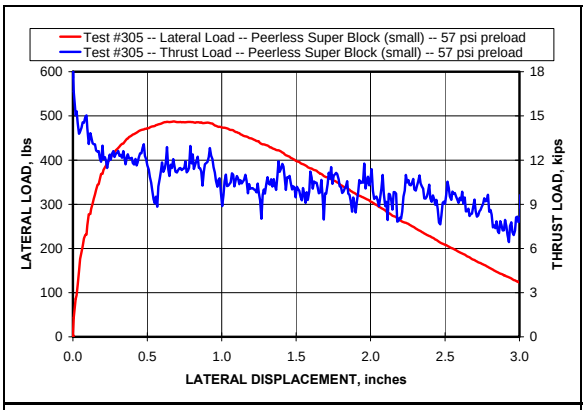

Photo Not Available

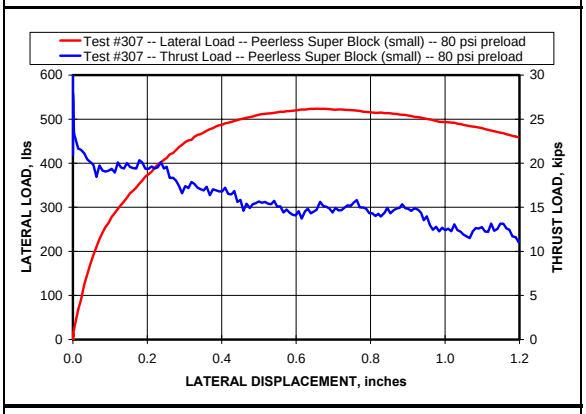

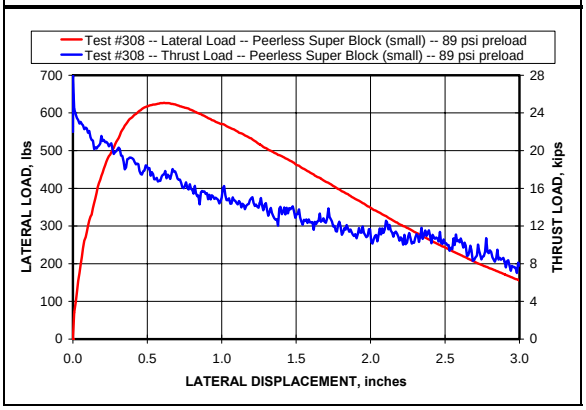

APPENDIX C: MRS TABULAR HALF-WALL TEST DATA

KLONDIKE BLOCK

Block Type	Test No.	Half Wall Height (in)	Preload (psi)	Peak Thrust Force (kips)	Displ at Peak Thrust Force (in)	Peak Horz. Load (lbs)	Displ at Peak Horz. Load (in)	Thrust Load at Peak Horz Load (kips)
Klondike 1330	102	30	51	39.13	1.62	3559	1.02	31.54
Klondike 1330	110	30	68	40.29	1.15	3855	1.01	36.77
Klondike 1330	104	30	188	36.35	1.46	3929	0.71	30.44
Klondike 1330	105	30	160	50.34	1.51	4818	0.90	44.54
Klondike 1330	109	30	155	35.15	0.927	4090	0.74	34.60
Klondike 1330	111	30	141	39.49	0.937	4059	0.64	35.63
Klondike 1330	106	30	295	49.42	0.654	5506	0.53	48.34
Klondike 1330	107	30	326	51.09	0.714	5151	0.59	49.27
Klondike 1330	108	30	280	43.66	0.837	4459	0.63	41.04
Klondike 1330	112	30	385	45.45	0.722	4368	0.60	43.41
Klondike 1330	114	30	428	51.00	0.621	5150	0.48	45.93
Klondike 1330	115	30	428	56.57	0.666	5148	0.47	52.18
Klondike 1330	118	30	471	50.48	0.583	5675	0.42	48.63
Klondike 1330	119	30	521	50.10	0.518	4578	0.41	49.17
Klondike 1330	113	30	567	54.83	0.363	5625	0.35	54.10
Klondike 1330	116	30	600	63.71	0.574	6882	0.49	61.24
Klondike 1330	121	30	599	68.97	0.458	6830	0.41	66.99
Klondike 1330	60	45.75	28	22.80	2.99	1120	2.05	20.48
Klondike 1330	59	45.75	43	25.08	2.6	1032	1.88	19.23
Klondike 1330	46	45.75	85	29.38	2.41	1296	1.92	22.79
Klondike 1330	45	45.75	90	22.40	2.94	978	2.38	19.30
Klondike 1330	34	45.75	109	25.24	2.83	1246	2.10	22.11
Klondike 1330	36	45.75	122	32.40	2.26	1597	1.15	25.33
Klondike 1330	35	45.75	139	30.47	1.59	1795	1.27	28.87
Klondike 1330	37	45.75	202	33.24	1.97	1992	0.97	32.01
Klondike 1330	63	45.75	252	36.16	1.18	2268	0.46	29.52
Klondike 1330	61	45.75	313	37.01	0.909	2359	0.33	34.02
Klondike 1330	74	45.75	373	40.35	0.909	3166	0.52	37.76
Klondike 1330	75	45.75	390	41.87	0.731	3617	0.41	40.59
Klondike 1330	76	45.75	474	45.76	0.418	3365	0.44	43.47
Klondike 1330	77	45.75	471	57.76	0.984	3831	0.72	52.38
Klondike 1330	78	45.75	577	57.87	0.005	2499	0.44	45.54
Klondike 1330	79	45.75	534	49.17	0.017	2779	0.56	43.48
Klondike 1330	81	45.75	568	52.05	0.072	3358	0.71	47.02
Klondike 1330	82	45.75	618	59.35	0.647	3922	0.65	59.35
Klondike 1330	83	45.75	623	58.36	0.563	3960	0.45	56.30
Klondike 1330	85	45.75	763	69.46	0.044	3776	0.45	61.08
Klondike 1330	89	60	43	12.70	3.02	320	1.90	8.02
Klondike 1330	90	60	42	13.06	3.05	341	2.10	8.91
Klondike 1330	91	60	143	20.14	2.49	781	1.25	14.78
Klondike 1330	92	60	150	29.79	1.86	1507	1.55	27.51
Klondike 1330	93	60	128	36.42	2.78	1601	1.89	29.71
Klondike 1330	94	60	310	29.90	1.086	1091	0.36	26.00
Klondike 1330	95	60	308	31.57	0.398	1415	0.39	30.09
Klondike 1330	96	60	347	38.60	0.617	1871	0.46	35.66
Klondike 1330	97	60	394	40.89	0.801	1821	0.46	37.68
Klondike 1330	98	60	398	39.08	0.091	1618	0.26	37.25
Klondike 1330	99	60	442	41.23	0.13	1946	0.26	38.64
Klondike 1330	100	60	592	54.73	0.03	2239	0.65	50.59
Klondike 1330	101	60	645	56.29	0.019	1698	0.52	47.16

Block Type	Test No.	Half Wall Height (in)	Preload (psi)	Peak Thrust Force (kips)	Displ at Peak Thrust Force (in)	Peak Horz. Load (lbs)	Displ at Peak Horz. Load (in)	Thrust Load at Peak Horz Load (kips)
Klondike 1330	65	45	17	27.54	1.46	3327	1.09	26.71
Klondike 1330	66	45	39	31.33	1.53	3154	1.32	29.11
Klondike 1330	64	45	41	27.78	0.969	2944	0.87	27.14
Klondike 1330	73	45	85	34.78	1.06	3329	0.91	31.99
Klondike 1330	39	45	99	35.56	1.14	3028	0.98	32.34
Klondike 1330	72	45	104	25.86	0.645	2610	0.56	23.86
Klondike 1330	40	45	118	36.77	1.02	3285	0.98	35.35
Klondike 1330	41	45	121	26.67	1.16	2245	0.93	25.01
Klondike 1330	67	45	146	38.17	0.619	3964	0.59	36.70
Klondike 1330	47	45	169	40.84	0.719	4536	0.66	39.34
Klondike 1330	68	45	174	44.74	0.754	5002	0.70	44.12
Klondike 1330	69	45	237	46.59	0.632	5139	0.53	45.16
Klondike 1330	70	45	254	37.21	0.568	3611	0.56	35.37
Klondike 1330	71	45	279	50.68	0.43	5345	0.42	54.48

Block Type	Test No.	Half Wall Height (in)	Preload (psi)	Peak Thrust Force (kips)	Displ at Peak Thrust Force (in)	Peak Horz. Load (lbs)	Displ at Peak Horz. Load (in)	Thrust Load at Peak Horz Load (kips)
Klondike 1780	17	45.75	0	14.27	2.23	761	2.25	14.20
Klondike 1780	18	45.75	228	42.55	2.15	2744	1.38	38.04
Klondike 1780	23	45	287	46.48	1.12	3595	0.81	42.88
Klondike 1780	24	45	290	36.98	1.20	2917	0.72	34.09
Klondike 1780	25	45	356	35.93	0.890	2350	0.70	35.05
Klondike 1780	21	46	23	29.67	2.61	2346	1.78	22.89
Klondike 1780	20	46	201	76.93	1.67	7826	1.69	76.66
Klondike 1780	19	46	210	92.87	1.36	8400	1.35	92.40
Klondike 1727	151	30	77	36.55	1.58	3300	1.39	34.07
Klondike 1727	152	30	43	45.60	1.3922	4892	0.90	39.93
Klondike 1727	153	30	50	39.35	2.204	3050	1.32	34.03
Klondike 1727	154	30	66	45.66	1.482	4585	1.32	44.18
Klondike 1727	155	30	63	42.64	2.504	3693	1.58	37.53
Klondike 1727	156	30	40	44.76	1.875	3811	1.55	38.68
Klondike 1727	157	30	77	47.87	1.887	4752	1.02	44.22
Klondike 1727	200	37.5	41	40.35	2.566	2294	1.35	31.15
Klondike 1727	202	37.5	87	38.63	2.021	3198	1.42	31.35
Klondike 1727	158	45	65	36.56	2.357	2104	1.43	27.51
Klondike 1727	159	45	69	26.71	2.388	1243	1.82	23.28
Klondike 1727	161	45	67	35.97	1.521	2218	1.35	34.30
Klondike 1727	162	45	59	39.03	2.076	2239	1.44	33.81
Klondike 1727	199	52.5	89	32.01	3.027	1169	1.96	23.18
Klondike 1727	203	52.5	107	37.01	3.325	1493	1.85	29.54
Klondike 1727	198	60	68	23.64	3.144	828	2.55	20.31
Klondike 1727	204	60	73	26.48	3.59	1036	2.22	20.05

PEERLESS BACKSAVER

Block Type	Test No.	Half Wall Height (in)	Preload (psi)	Peak Thrust Force (kips)	Displ at Peak Thrust Force (in)	Peak Horz. Load (lbs)	Displ at Peak Horz. Load (in)	Thrust Load at Peak Horz Load (kips)
Peerless Backsavers	297	30	3	37.66	1.89	3452	1.41	33.43
Peerless Backsavers	298	30	10	36.65	1.89	3213	1.50	32.51
Peerless Backsavers	295	30	16	35.99	1.68	3625	1.23	28.33
Peerless Backsavers	296	30	69	41.77	1.43	4611	1.33	40.39
Peerless Backsavers	292	30	21	39.68	1.80	4154	1.45	34.44
Peerless Backsavers	293	30	50	39.26	2.00	3549	1.20	29.19
Peerless Backsavers	301	30	100	44.57	1.34	4553	0.87	37.28
Peerless Backsavers	294	30	89	39.22	1.55	3554	1.07	35.28
Peerless Backsavers	299	30	80	39.42	1.42	4181	1.28	37.58
Peerless Backsavers	300	30	165	46.02	0.82	5227	0.73	44.48
Peerless Backsavers	261	45	12	15.77	2.98	650	2.51	13.64
Peerless Backsavers	260	45	25	21.09	2.94	1063	2.57	18.56
Peerless Backsavers	262	45	78	30.30	2.91	1487	1.96	24.35
Peerless Backsavers	266	45	94	32.13	2.26	1710	1.67	26.58
Peerless Backsavers	289	45	128	39.33	1.94	2499	1.29	30.99
Peerless Backsavers	291	45	188	43.52	1.89	2719	1.22	38.92
Peerless Backsavers	265	45	182	29.19	2.33	1832	1.45	25.37
Peerless Backsavers	290	45	210	33.78	1.89	2142	1.13	30.40
Peerless Backsavers	267	45	265	37.92	1.90	1823	1.15	32.73
Peerless Backsavers	288	45	362	39.24	1.24	2007	1.08	37.82
Peerless Backsavers	282	60	22	13.62	3.26	406	2.55	7.49
Peerless Backsavers	283	60	57	17.74	3.62	652	2.24	13.35
Peerless Backsavers	284	60	132	20.07	2.17	710	1.04	17.32
Peerless Backsavers	285	60	183	30.45	1.75	1205	1.31	28.35
Peerless Backsavers	286	60	344	48.41	2.46	2000	1.53	42.20
Peerless Backsavers	287	60	447	49.21	0.00	1291	1.35	35.78
Peerless Backsavers (partially cured)	355	30	72	36.44	1.21	3069	1.12	32.00
Peerless Backsavers (partially cured)	356	30	60	32.69	1.33	2667	1.29	31.97
Peerless Backsavers (partially cured)	357	45	60	22.63	2.72	1038	1.36	16.22
Peerless Backsavers (partially cured)	358	45	54	25.81	1.93	1209	1.40	21.84
Peerless Backsavers (partially cured)	359	60	66	14.16	3.21	269	1.49	8.00
Peerless Backsavers (partially cured)	360	60	52	13.84	3.25	501	1.87	13.13

KLONDIKE HOLLOW CORE BLOCK

Block Type	Test No.	Half Wall Height (in)	Preload (psi)	Peak Thrust Force (kips)	Displ at Peak Thrust Force (in)	Peak Horz. Load (lbs)	Displ at Peak Horz. Load (in)	Thrust Load at Peak Horz Load (kips)
Klondike Hollow Block	330	30	29	18.21	1.39	2160	1.39	18.21
Klondike Hollow Block	334	30	80	18.84	1.63	2561	1.50	20.00
Klondike Hollow Block	338	30	91	22.53	1.94	2583	1.50	22.53
Klondike Hollow Block	339	30	117	16.84	0.70	2494	0.72	16.66
Klondike Hollow Block	340	30	57	13.69	1.14	2235	1.16	16.20
Klondike Hollow Block	335	30	172	15.53	1.52	2071	1.00	14.47
Klondike Hollow Block	333	30	212	19.63	0.55	2300	0.50	18.43
Klondike Hollow Block	336	30	155	9.25	0.54	1515	0.54	9.25
Klondike Hollow Block	337	30	140	12.75	1.08	1559	1.08	12.75
Klondike Hollow Block	331	30	55	12.80	1.12	1716	1.13	12.46
Klondike Hollow Block	332	30	116	14.35	1.35	1886	1.35	14.35
Klondike Hollow Block	314	45	28	9.32	3.98	313	2.86	5.48
Klondike Hollow Block	321	45	22	7.09	3.81	364	2.50	5.31
Klondike Hollow Block	315	45	99	20.20	3.18	1145	1.87	15.85
Klondike Hollow Block	323	45	87	19.41	3.07	1106	2.36	16.82
Klondike Hollow Block	320	45	120	26.82	3.14	1535	2.12	22.77
Klondike Hollow Block	322	45	129	19.77	1.30	1713	1.32	18.89
Klondike Hollow Block	318	45	131	25.16	1.77	1805	1.66	24.33
Klondike Hollow Block	317	45	188	13.28	0.66	1309	0.60	12.97
Klondike Hollow Block	319	45	184	25.47	1.73	1859	1.73	25.47
Klondike Hollow Block	324	45	207	19.71	0.82	2005	0.81	19.70
Klondike Hollow Block	325	60	78	13.80	4.14	434	3.01	11.00
Klondike Hollow Block	327	60	80	15.34	4.64	543	2.75	12.00
Klondike Hollow Block	328	60	129	14.65	3.24	511	2.33	12.99
Klondike Hollow Block	329	60	212	17.18	2.05	715	1.54	15.78

ACCOA BLOCK

Block Type	Test No.	Half Wall Height (in)	Preload (psi)	Peak Thrust Force (kips)	Displ at Peak Thrust Force (in)	Peak Horz. Load (lbs)	Displ at Peak Horz. Load (in)	Thrust Load at Peak Horz Load (kips)
AAC 6	26	48	3	12.81	3.22	668	1.25	7.20
AAC 6	27	48	3	15.2	2.72	742	1.61	10.40
AAC 6	48	48	30	22.26	2.58	735	0.62	9.6
AAC 6	49	48	60	22.26	2.63	912	0.82	12.5
AAC 6	50	48	75	19.76	1.87	1052	0.78	17.01
AAC 6	32	48	132	23.35	0.63	1363	0.57	21.63
AAC 6	29	48	136	24.43	0.00	1104	0.35	20.00
AAC 6	33	48	136	26.27	0.00	1302	0.57	22.66
AAC 6	28	48	120	26.38	0.00	1429	0.39	24.20
AAC 6	31	48	293	46.85	0.00	1353	0.48	40.20
AAC 6	30	48	300	48.83	0.00	1283	0.22	38.00
AAC 8	56	48	18	25.73	2.68	1990	1.86	22.48
AAC 8	55	48	20	27.36	2.40	2210	1.65	24.59
AAC 8	54	48	38	23.06	2.03	1733	1.35	19.51
AAC 8	53	48	40	24.58	2.39	2115	1.22	19.87
AAC 8	51	48	111	31.79	0.79	2730	0.39	30.25
AAC 8	62	48	97	31.42	1.69	3179	0.58	28.02
AAC 8	58	48	238	46.88	0.13	2710	0.19	46.03

YTONG BLOCK

Block Type	Test No.	Half Wall Height (in)	Preload (psi)	Peak Thrust Force (kips)	Displ at Peak Thrust Force (in)	Peak Horz. Load (lbs)	Displ at Peak Horz. Load (in)	Thrust Load at Peak Horz Load (kips)
Ytong	239	31.5	3	37.97	1.47	5645	1.13	37.53
Ytong	249	31.5	7	33.27	1.62	4785	1.02	31.70
Ytong	243	31.5	51	47.93	1.58	5292	0.94	41.00
Ytong	250	31.5	58	52.40	1.10	5966	0.92	45.00
Ytong	251	31.5	94	52.60	0.99	5737	0.95	46.00
Ytong	241	31.5	107	48.54	1.29	5672	0.63	42.32
Ytong	242	31.5	145	50.79	0.56	6797	0.42	47.17
Ytong	234	47.25	15	19.51	1.04	2212	1.07	18.92
Ytong	235	47.25	53	37.25	1.26	3040	1.27	33.70
Ytong	237	47.25	109	47.61	1.93	4068	0.99	44.57
Ytong	238	47.25	132	46.02	1.73	4172	0.78	41.77
Ytong	245	63	10	20.00	2.08	1376	1.65	17.46
Ytong	246	63	38.5	29.62	2.25	2023	1.07	23.94
Ytong	252	63	69	30.86	1.69	1885	1.28	27.21
Ytong	247	63	99	33.47	2.45	2012	0.94	30.50
Ytong	248	63	142	39.63	1.17	2349	1.05	39.15

KINGSWAY BLOCK

Block Type	Test No.	Half Wall Height (in)	Preload (psi)	Peak Thrust Force (kips)	Displ at Peak Thrust Force (in)	Peak Horz. Load (lbs)	Displ at Peak Horz. Load (in)	Thrust Load at Peak Horz Load (kips)
Kingsway	147	33.5	65	15.75	1.26	1520	0.56	10.92
Kingsway	148	33.5	54	16.95	0.74	1675	0.74	12.93
Kingsway	SD2	41.875	50	17.01	1.63	1161	1.13	14.51
Kingsway	SD1	41.875	50	10.86	1.40	973	1.34	9.63
Kingsway	137	41.875	80	16.78	2.13	1126	1.22	13.83
Kingsway	138	41.875	66	17.11	1.61	1021	1.39	13.64
Kingsway	139	50.25	89	15.28	1.91	679	1.28	12.53
Kingsway	135	58.625	65	13.51	2.20	614	1.43	9.78
Kingsway	136	58.625	64	12.20	2.76	484	1.56	10.45

OMEGA BLOCK

Block Type	Test No.	Half Wall Height (in)	Preload (psi)	Peak Thrust Force (kips)	Displ at Peak Thrust Force (in)	Peak Horz. Load (lbs)	Displ at Peak Horz. Load (in)	Thrust Load at Peak Horz Load (kips)
Omega Block	143	32	9	8.53	2.47	504	1.70	3.00
Omega Block	144	32	28	6.41	0.39	615	1.42	4.00
Omega Block	169	32	8	5.50	2.94	559	2.05	3.60
Omega Block	170	32	15	7.49	3.00	753	1.73	4.50
Omega Block	174	32	8	8.08	3.73	679	1.57	3.75
Omega Block	175	32	27	7.30	3.48	769	1.94	5.20
Omega Block	220	32	5	5.60	1.56	491	1.09	2.50
Omega Block	221	32	6	7.24	1.55	471	1.20	2.50
Omega Block	141	48	23	7.20	2.58	522	1.78	5.00
Omega Block	142	48	27	6.00	2.69	400	1.37	4.00
Omega Block	167	48	20	7.03	1.80	511	0.83	4.00
Omega Block	168	48	14	4.93	0.04	278	0.96	2.00
Omega Block	222	48	6	5.17	2.69	160	1.55	1.25
Omega Block	172	48	1	2.38	2.65	165	2.30	1.30
Omega Block	173	48	8	6.06	3.62	436	2.09	3.50
Omega Block	145	64	20	4.99	0.16	128	1.88	2.70
Omega Block	146	64	27	6.01	2.43	262	0.58	4.65
Omega Block	165	64	12	3.43	2.06	80	1.45	1.00
Omega Block	166	64	21	3.89	1.26	159	0.66	2.00
Omega Block	176	64	8	3.16	3.83	73	2.92	1.75
Omega Block	177	64	15	3.57	0.41	99	3.00	2.00
Omega Block	223	64	8	7.98	0.10	82	2.41	1.25
Omega Block	224	64	15	7.30	0.11	90	1.29	1.25

PEERLESS SUPER BLOCK

Block Type	Test No.	Half Wall Height (in)	Preload (psi)	Peak Thrust Force (kips)	Displ at Peak Thrust Force (in)	Peak Horz. Load (lbs)	Displ at Peak Horz. Load (in)	Thrust Load at Peak Horz Load (kips)
Peerless Super Block	216	32	7	3.16	2.15	302	0.99	2.70
Peerless Super Block	218	32	16	4.06	2.34	278	1.07	2.60
Peerless Super Block	217	32	17	3.19	1.69	344	1.08	2.80
Peerless Super Block	219	32	21	0.00	0.00	229	1.42	3.20
Peerless Super Block	208	32	54	7.85	0.04	257	0.51	4.40
Peerless Super Block	209	32	56	8.93	0.05	275	0.29	4.50
Peerless Super Block	190	48	37	5.91	0.04	153	0.53	2.50
Peerless Super Block	191	48	38	6.87	0.07	166	0.43	2.75
Peerless Super Block	192	48	45	7.06	0.03	181	0.24	3.8
Peerless Super Block	193	48	42	9.80	0.01	192	0.45	3.90
Peerless Super Block	194	48	63	9.77	0.03	248	0.76	6.30
Peerless Super Block	195	48	29	4.90	0.11	191	0.76	3.20
Peerless Super Block	196	48	60	8.68	0.13	232	0.52	6.00
Peerless Super Block	197	48	42	7.41	0.10	216	0.23	4.50
Peerless Super Block	210	48	56	8.45	0.13	204	0.52	6.00
Peerless Super Block	211	48	41	6.47	0.80	275	0.79	0.79
Peerless Super Block	214	48	12	1.30	1.91	120	2.14	3.00
Peerless Backsavers (small foam)	302	45.75	5	4.74	2.38	82	0.75	0.75
Peerless Backsavers (small foam)	303	45.75	20	6.62	0.02	182	1.42	1.42
Peerless Backsavers (small foam)	304	45.75	30	7.55	0.07	304	1.34	1.34
Peerless Backsavers (small foam)	305	45.75	57	15.04	0.09	488	0.67	0.67
Peerless Backsavers (small foam)	307	45.75	80	22.88	0.01	524	0.67	0.67
Peerless Super Block	205	64	33	5.85	0.03	88	1.26	2.80
Peerless Super Block	206	64	56	8.08	0.06	54	0.30	3.75
Peerless Super Block	225	64	14	5.12	0.00	54	1.86	1.60
Peerless Super Block	229	64	34	5.51	0.00	102	0.81	2.50
Peerless Super Block	230	64	22	3.33	0.00	33	2.71	1.60
Peerless Super Block	231	64	4	4.19	0.00	33	2.10	2.50
Peerless Super Block	232	64	54	12.74	0.00	96	0.81	5.60
Peerless Super Block	233	64	53	12.67	0.00	128	1.29	6.00